Neural Plasticity

Hearing Loss: Reestablish the Neural Plasticity in Regenerated Spiral Ganglion Neurons and Sensory Hair Cells 2018

Lead Guest Editor: Renjie Chai
Guest Editors: Geng-lin Li, Jian Wang, Jing Zou, and Hai Huang

Hearing Loss: Reestablish the Neural Plasticity in Regenerated Spiral Ganglion Neurons and Sensory Hair Cells 2018

Neural Plasticity

Hearing Loss: Reestablish the Neural Plasticity in Regenerated Spiral Ganglion Neurons and Sensory Hair Cells 2018

Lead Guest Editor: Renjie Chai
Guest Editors: Geng-lin Li, Jian Wang, and Hai Huang

Editorial Board

Contents

Hindawi
Neural Plasticity
Volume 2018, Article ID 4759135, 3 pages
https://doi.org/10.1155/2018/4759135

Editorial

Hearing Loss: Reestablish the Neural Plasticity in Regenerated Spiral Ganglion Neurons and Sensory Hair Cells 2018

Renjie Chai,[1,2] **Geng-Lin Li**,[3] **Jian Wang**,[4] **and Hai Huang**[5]

[1]*MOE Key Laboratory of Developmental Genes and Human Disease, Institute of Life Sciences, Southeast University, Nanjing 210096, China*
[2]*Co-Innovation Center of Neuroregeneration, Nantong University, Nantong 226001, China*
[3]*Biology Department, University of Massachusetts Amherst, Amherst, MA 01003, USA*
[4]*School of Communication Science & Disorders, Dalhousie University, 5850 College Street, Halifax, NS, Canada B3J1Y6*
[5]*Department of Cell and Molecular Biology, Tulane University, New Orleans, LA 70118, USA*

Correspondence should be addressed to Renjie Chai; renjiec@seu.edu.cn

Received 29 October 2018; Accepted 6 December 2018; Published 17 December 2018

Hearing loss is a common sensory disorder that has been a serious concern globally. It is recently estimated that around 466 million people worldwide have disabling hearing loss, including 34 million children, and this number will increase to over 900 million by 2050 (according to WHO report 2018). The majority of hearing disorders occur due to the death of either inner ear hair cells (HCs) or spiral ganglion neurons (SGNs), thus leading to sensorial neural hearing loss (SNHL). SNHL is known as the most common form of hearing disorder that comprises about 85% of all hearing loss cases. This type of damage is induced by a variety of reasons such as inner ear trauma, ischemia, ototoxic drugs, noise exposure, inflammation, viral infections, genetic deficits, autoimmunologic reaction, and aging. SNHL is generally not reversible due to the lack of regeneration capacity of HCs and SGNs. However, various recent studies have determined that the HCs and SGNs hold a regenerative potential and it is possible to find the cure for SNHL in the near future. This is supported by the clear understanding of the genetical control and signaling pathways involved in the development of HCs and SGNs and their functions, the regenerative potential of residing adult stem cells, and the development of gene therapy and the clinical trials of new pharmaceutical compounds on damaged cochleae. Last year, we have published the first special issue of "Hearing Loss: Reestablish the Neural Plasticity in Regenerated Spiral Ganglion Neurons and Sensory Hair Cells", and this year in this second special issue, we are presenting a new series of articles to report the most recent advances in several major areas as summarized below: HC development, HC damage and protection, HC regeneration, SGN development and protection, inherited hearing loss, and inner ear drug delivery.

1. Hair Cell Development

A. Chang et al. ("Specific influences of early acoustic environments on cochlear HCs in postnatal mice") report that the early environmental sounds promote functional maturation of HCs. Acoustic environment significantly decreases the ABR threshold, increases prestin expression in outer HCs, and enhance maturation of ribbon synapses in the postnatal mouse cochleae. P. Chen et al. ("Postnatal Development of Microglial like Cells in Mouse Cochlea") demonstrate that the microglial-like cells are present in the developing mouse cochlea, and these cells go through the drastic morphological and distributional changes during the postnatal cochlear development. Also, these cells might participate in the maturation and remodeling of the cochlea. F. Chen et al. ("Hydromechanical Structure of the Cochlea Supports the Backward Traveling Wave in the Cochlea *In Vivo*") for the first time experimentally demonstrate the backward traveling wave theory by measuring the phase spectra of the basilar

membrane vibration at multiple longitudinal locations along the cochlea. X. Cheng et al. ("Modulation of Glucose Takeup by Glucose Transport on the Isolated OHCs") report that glucose is transported into OHCs via glucose transporter 1 and 4, which are mainly expressed on the lateral wall of OHCs and the glucose antagonist and ATP regulate this energy transport mechanism. S. Liu et al. ("The Key Transcription Factor Expression in the Developing Vestibular and Auditory Sensory Organs: A Comprehensive Comparison of Spatial and Temporal Patterns") determine that Pax2, Sox2, and Prox1 have differential and overlapping temporospatial expression patterns during the development of vestibular and auditory sensory organs in mice.

2. Hair Cell Damage and Protection

B. Tong et al. ("Mechanisms of Hearing Loss in a Guinea Pig Model of Superior Semicircular Canal Dehiscence") explore the pathogenesis of superior semicircular canal dehiscence (SSCD) in the guinea pig model and report that the bony fenestration of the superior semicircular canal mimics the hearing loss pattern of SSCD patients. J. Hong et al. ("N-Methyl-D-Aspartate Receptors Involvement in the Gentamicin-Induced Hearing Loss and Pathological Changes of Ribbon Synapse in the Mouse Cochlear Inner Hair Cells") investigate that the N-methyl-D-aspartate receptors regulate the number and distribution of inner HC ribbon synapses after gentamicin-induced ototoxicity and their inhibition by antagonist minimized the drug-induced ototoxicity, and thus maintain the integrity of ribbon synapses. L. Xia et al. ("Comparison of Acceptable Noise Level Generated Using Different Transducers and Response Modes") compare the acceptable noise level (ANL) in 20 mandarin subjects with normal hearing. The author obtained ANL through different methods and determined that the ANL in normal hearing listeners may not be affected by different modes of presentation. M. Waqas et al. ("Inner Ear Hair Cell Protection in Mammals against the Noise-Induced Cochlear Damage") provide a brief review about the mechanisms involved in the HC loss after noise-induced trauma and discuss the recent HC protection strategies to prevent and recover hearing function in mammals after noise-induced damage. X. Cheng et al. ("The Benefits of Residual Hair Cell Function for Speech and Music Perception in Pediatric Bimodal Cochlear Implant Listeners") report that the combination of electric and acoustic hearing significantly improves the perception of music and Mandarin tones in pediatric cochlear implant patients. X. Ding et al. ("The Characteristic and Short-Term Prognosis of Tinnitus Associated with Sudden Sensorineural Hearing Loss") determine the association between tinnitus and sudden sensorineural hearing loss (SSNHL). The authors found that tinnitus can be ameliorated by the successful treatment of SSNHL. G. Li et al. ("The Role of Autoimmunity in the Pathogenesis of Sudden Sensorineural Hearing Loss") provide a brief review on the autoimmune mechanisms involved in SSHL and discuss the role of immunosuppressive drugs in immune therapy. N. Zhao et al. ("Functional Change in the Caudal Pontine Reticular Nucleus Induced by Age-Related Hearing Loss") report that the age-related hearing loss causes an increase in PnC sensitivity that in turn enhances acoustic startle responses in C57 mice. B. Li et al. ("Effects of Various Extents of High-Frequency Hearing Loss on Speech Recognition and Gap Detection at Low Frequencies in Patients with Sensorineural Hearing Loss") investigate the extent of SNHL at high frequencies influences the ability to recognize compressed speech of lower frequencies in hearing loss patients.

3. Hair Cell Regeneration

M. Tang et al. ("Potential Application of Electrical Stimulation in Stem Cell-Based Treatment against Hearing Loss") provide a comprehensive review to address the current challenges and problems in stem cell transplant-based treatments in the inner ear against deafness and present a critical viewpoint about electrical stimulations as a physical factor to modulate stem cell behavior and promote stem cell therapy to treat hearing loss.

4. Spiral Ganglion Neuron Development and Protection

J. Li et al. ("Contralateral Suppression of DPOAEs in Mice after Ouabain Treatment") determine that the type II SGNs participate in the contralateral suppression of the medial olivocochlear reflex after selectively inducing apoptosis in the type I SGNs using ouabain treatment.

5. Inherited Hearing Loss

H. Du et al. ("Identification of Binding Partners of Deafness-Related Protein PDZD7") determine the eleven novel PDZD7-binding proteins through yeast two-hybrid screening that are expressed in the inner ear. Most of the new PDZD7-binding partners such as TRIM35, CADM1, AMOT, BLZF1, Numb, KCDT10, CCDC27, and TRIP11 have not been reported before and will help to understand the role of PDZD7 in hearing transduction. P. Li et al. ("Knock-In Mice with Myo3a Y137C Mutation Displayed Progressive Hearing Loss and Hair Cell Degeneration in the Inner Ear") report that Myo3a kinase domain Y137C mutant mice have an elevated hearing threshold, degenerated inner ear HCs, and structural abnormality in HCs stereocilia after 6 months of age, thus Myo3a is essential for maintaining the intact structure of HC and normal hearing function. S. Hu et al. ("Genetic Etiology Study of Ten Chinese Families with Nonsyndromic Hearing Loss") identify novel pathogenic variants in six Chinese families with a hereditary hearing loss by targeted next generation sequencing. F. Zhang et al. ("Three *MYO15A* Mutations Identified in One Chinese Family with Autosomal Recessive Nonsyndromic Hearing Loss") report three MYO15A variants c.3971C>A (p.A1324D), c.4011insA (p.Q1337Qfs*22), and c.9690+1G>A. These variants are absent in 200 normal controls and cosegregated with hearing disability in this family. X. Wang et al. ("A Novel p.G141R Mutation in *ILDR1* Leads to Recessive Nonsyndromic Deafness DFNB42 in Two Chinese Han Families") identify a novel p.G141R homozygous mutation in ILDR1 gene that

may be the genetic cause of deafness in two unrelated Chinese Han families. X. Wu et al. ("Autosomal Recessive Congenital Sensorineural Hearing Loss Due to a Novel Compound Heterozygous PTPRQ Mutation in a Chinese Family") report that the novel compound heterozygous missense mutation c.4472C>T p.T1491M and c.1973T>C p.V658A in PTPRQ gene is the genetic cause of recessively inherited sensorineural hearing loss in a Chinese family.

6. Inner Ear Drug Delivery System

X. Xu et al. ("Hollow Mesoporous Silica@Zeolitic Imidazolate Framework Capsules and Their Applications for Gentamicin Delivery") synthesize a new nanoparticle capsule that can be used as a drug delivery route for the gentamicin transfer at the specific site in the inner ear. The authors also determine the sustained release capacity of gentamicin from the capsule by *in vitro* and *in vivo* assays.

We believe that the studies included in this second special issue of "Hearing Loss: Reestablish the Neural Plasticity in Regenerated Spiral Ganglion Neurons and Sensory Hair Cells" provide important insights into cochlear physiology and pathology as well as the important progress in technology that can be translated into clinical application of the medical treatment of cochlear damage in SNHL. We wish that this special issue will represent a significant contribution in the effort to achieve effective protection and treatment of hearing loss in the near future.

Conflicts of Interest

The editors declare that they have no conflicts of interest regarding the publication of this special issue.

Renjie Chai
Geng-Lin Li
Jian Wang
Hai Huang

Hindawi
Neural Plasticity
Volume 2018, Article ID 7513258, 9 pages
https://doi.org/10.1155/2018/7513258

Research Article

The Key Transcription Factor Expression in the Developing Vestibular and Auditory Sensory Organs: A Comprehensive Comparison of Spatial and Temporal Patterns

Shaofeng Liu,[1] **Yunfeng Wang**,[2,3] **Yongtian Lu**,[4] **Wen Li**,[2] **Wenjing Liu**,[1] **Jun Ma**,[1] **Fuqin Sun**,[1] **Mao Li**,[1] **Zheng-Yi Chen**,[5] **Kaiming Su**,[6] **and Wenyan Li**[2,3]

[1]*Department of Otolaryngology-Head and Neck Surgery, Yijisan Hospital of Wanan Medical College, Wuhu, Anhui 241001, China*
[2]*ENT Institute and Otorhinolaryngology Department of Affiliated Eye and ENT Hospital, State Key Laboratory of Medical Neurobiology, Fudan University, Shanghai 200031, China*
[3]*Key Laboratory of Hearing Medicine of NHFPC, Shanghai 200031, China*
[4]*Otorhinolaryngology Department of the Shenzhen Second People's Hospital (First Affiliated Hospital of Shenzhen University), Shenzhen, China*
[5]*Department of Otolaryngology and Program in Neuroscience, Harvard Medical School and Eaton Peabody Laboratory, Massachusetts Eye and Ear Infirmary, Boston, MA 02114, USA*
[6]*Department of Otolaryngology, Head and Neck Surgery, Affiliated Sixth People's Hospital, Shanghai Jiao Tong University, Shanghai 200230, China*

Correspondence should be addressed to Shaofeng Liu; liusf_cn@163.com, Kaiming Su; 021china@sina.com, and Wenyan Li; wenyan_li2000@126.com

Received 23 March 2018; Revised 31 July 2018; Accepted 6 September 2018; Published 15 October 2018

Academic Editor: Clive R. Bramham

Inner ear formation requires that a series of cell fate decisions and morphogenetic events occur in a precise temporal and spatial pattern. Previous studies have shown that transcription factors, including Pax2, Sox2, and Prox1, play important roles during the inner ear development. However, the temporospatial expression patterns among these transcription factors are poorly understood. In the current study, we present a comprehensive description of the temporal and spatial expression profiles of Pax2, Sox2, and Prox1 during auditory and vestibular sensory organ development in mice. Using immunohistochemical analyses, we show that Sox2 and Pax2 are both expressed in the prosensory cells (the developing hair cells), but Sox2 is later restricted to only the supporting cells of the organ of Corti. In the vestibular sensory organ, however, the Pax2 expression is localized in hair cells at postnatal day 7, while Sox2 is still expressed in both the hair cells and supporting cells at that time. Prox1 was transiently expressed in the presumptive hair cells and developing supporting cells, and lower Prox1 expression was observed in the vestibular sensory organ compared to the organ of Corti. The different expression patterns of these transcription factors in the developing auditory and vestibular sensory organs suggest that they play different roles in the development of the sensory epithelia and might help to shape the respective sensory structures.

1. Introduction

The inner ear is a complex sensory organ responsible for both hearing and balance in vertebrates. Although the inner ear has an intricate structure and is multifunctional, its origin is quite simple, and both the hair cells and supporting cells of the inner ear arise from common progenitor cells [1, 2]. The formation of the inner ear requires that a series of cell fate decisions and morphogenetic events occur in a precise temporal and spatial pattern in order to subdivide these prosensory cells into their differentiated populations of hair cells and supporting cells [3, 4].

A number of different signaling pathways and transcription factors are known to be necessary for these developmental processes [5–8]. The paired-domain transcription factor Pax2, for example, plays a key role in regulating differential growth within the cochlear duct [9–12]. We also previously showed that Pax2 overexpression strongly promotes the proliferation of supporting cells in vitro [13]. The SRY-related HMG box (Sox) proteins are a group of transcription factors that regulate diverse developmental processes. A recent study demonstrated that Sox2, a member of the SoxB1 group along with Sox1 and Sox3, is required for the development of sensory epithelia, including the organ of Corti [14–17]. *Prox1* is the vertebrate homolog of the homeobox gene *prospero* in *Drosophila melanogaster*. Both *Prox1* and *prospero* play important roles in the development of various embryonic tissues and organs, such as the central nervous system [18, 19] and inner ear [7, 20, 21]. Thus, these three transcription factors are essential during inner ear development and sensory cell differentiation.

In previous study, we have already studied the gene expression in hair cells as well as surrounding cells of inner ear from E16 to P7 by a comprehensive cell type-specific RNA-Seq study [22], which provided a general idea about the expression tendency of Pax2, Sox2, and Prox1 in both hair cells and surrounding cells during the development of inner ear. While the spatial expression Pax2, Sox2, and Prox1 during inner ear development are also particularly important. Notably, the expression of Pax2 is one of the first indicators of otic placode induction, and it continues to be expressed in various regions of the ear throughout subsequent stages of development. In contrast, Sox2 is expressed in the neural tube and dorsolateral regions of murine otocysts at embryonic day 9.5 (E9.5), which is consistent with a role in sensory organ development. Prox1 is very weakly expressed in the most basal region of the developing mouse organ of Corti at E14.5. As the sensory epithelium differentiates, Prox1 becomes restricted to a subset of supporting cells, and this expression is consistent through the duration of embryogenesis and into the second postnatal week [20]. Although the expression patterns of Pax2, Sox2, and Prox1 have been investigated previously, there was no systematic study on the temporal and spatial expression profiles of these transcription factors during the development of cochlea, and the detailed expression pattern will help understand their functions.

In this study, we present a comprehensive description of the temporal and spatial expression profiles of Pax2, Sox2, and Prox1 during auditory and vestibular sensory organ development. Our results demonstrate that Pax2, Sox2, and Prox1 are differentially expressed and overlap in various regions of the developing inner ear. Comparison of their unique expression patterns facilitates our understanding on the individual underlying genes functions as well as the cochlear developmental process, meanwhile provided more clues for further investigating the relationships among those transcriptional factors on the sensory epithelium determination, progenitor cell proliferation, and hair cell differentiation during the inner ear development.

2. Results

2.1. The Expression Patterns of Pax2, Sox2, and Prox1 during the Sensory Epithelium Determination in Mouse Inner Ear (E9.5–E13.5). To better understand the role of Sox2 in mouse inner ear development, we first compared the pattern of Sox2 gene expression with that of Pax2 in specific presumptive sensory tissues by colabeling with antibodies against both proteins. Pax2 transcripts were previously shown to be initially distributed uniformly throughout the epithelium of the otic placode [23]. From E8.5 to E9.5, invagination of the otic placode continues and leads to the formation of the otic vesicle, and we found that during this period Pax2 distribution undergoes reorganization. At E9.5, Pax2 was expressed throughout the epithelium of the otic otocyst, but it was more concentrated in the centro-medial area next to the neural tube. In contrast, Sox2 was found in all sensory regions, with higher expression in the dorsolateral area of the otic vesicle (Figure 1, A1–A3).

The cochlear duct begins to develop as an out-pocketing of the otocyst at E11.5. And we found that two separate Sox2 expression domains were present at this time, a dorsal domain that corresponds to the sensory primordia of the utricle and a more ventral domain that corresponds to the sensory primordia of the saccule and the prosensory domain of the cochlea. Compared to Sox2, Pax2 expression only partially overlapped with the sensory regions of the saccule and the cochlea. Further, there was no obvious overlap of Pax2 expression with the macula of the utricle. At this stage, Pax2 expression was mostly restricted to the posterior region of the cochlear anlage (Figure 1, B1–B3).

Within the cochlear duct at E12.5, Sox2 was expressed in the medial half of the duct that appeared to correspond with the prosensory domain, specifically the population of cells that would give rise to the organ of Corti. This expression pattern partially overlapped with that of Pax2 but had obvious differences in distribution. Pax2 was mainly expressed in both sides of Reissner's membrane. Notably, Pax2 expression gradually weakened in the prosensory domain of the saccule at this developmental stage (Figure 1, C1–C3).

At E13.5, Pax2 was mainly located in the nonsensory domains of the vestibular organ and the cochlea. In contrast, Sox2 was gradually restricted to the prosensory domain, primarily in the medial half of the cochlear duct at the apex. A band of Sox2 expression was also observed within the basal region of the cochlear duct, which is correlated with the position of the developing organ of Corti and Kolliker's organ (Figure 1, D1–D3). At this stage, Prox1 expression was weakly detected in the sensory epithelia of the vestibular organ, but not in the cochlea (data not shown).

2.2. The Expression Patterns of Pax2, Sox2, and Prox1 during the Hair Cell Development in Mouse Inner Ear (E15.5-E18.5). To relate Pax2, Sox2, and Prox1 expression to hair cell development, we colabeled the cells with the hair cell marker myosin7a. At E15.5, myosin7a was clearly expressed in developing inner hair cells, but not in the developing outer hair cells (OHCs) at the basal end of the cochlea (Figure 2, A4–A5). However, at E16.5, this expression expanded to

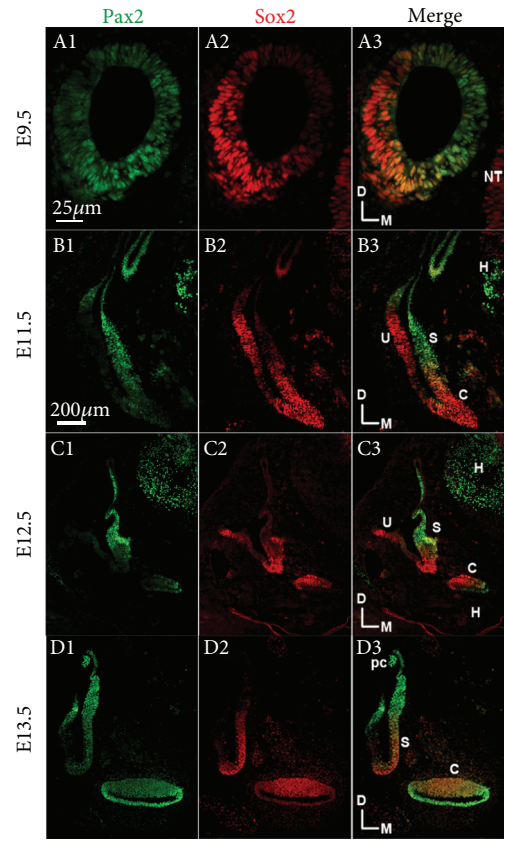

Figure 1: Comparison of Pax2, Sox2 expression in the inner ear from E9.5 to E13.5. Immunofluorescence staining of Sox2 (red), Pax2 (green), and Prox1 (green) in the mouse inner ear at E9.5, E11.5, E12.5, and E13.5. S: saccule; U: utricle; C: cochlea; D: dorsal; M: medial; pc: posterior crista; H: hindbrain; NT: neural tube. Scale bars = 25 μm (A1–A3); 200 μm (B1–B3, C1–C3, and D1–D3).

include some of the OHCs (Figure 2, B4–B5), and at E18.5, expression was seen in all hair cells (Figure 2, C4–C5).

We observed an interesting phenomenon regarding Pax2 expression, whereby it was still expressed in Reissner's membrane and the stria vascularis, but it was not expressed in the hair cells when they began to express myosin7a at E15.5 (Figure 2, A1–A5). At later time points, Pax2 expression was upregulated in the hair cells of the organ of Corti and was stably expressed in these hair cells by E18.5 (Figure 2, B1–B5 and C1–C5).

At E15.5, Sox2 was still expressed in the medial half of the cochlear duct at the apex as well as within the basal region of the cochlear duct that is correlated with the position of the developing organ of Corti and Kolliker's organ (Figure 2, A1–A5). At later stages, Sox2 was expressed in both immature hair cells and supporting cells, and this expression was maintained in hair cells through E18.5 (Figure 2, B1–B5 and C1–C5).

Expression of Pax2 in the utricle, saccule, and three cristae of the vestibular organ differed from the expression in the organ of Corti. At E16.5, Pax2 was still expressed in immature hair cells and supporting cells of the sensory epithelia of the saccule, but only in the hair cells of the crista ampullaris at E15.5 (Figure 3, A1–A3) and of the macula utriculi at E16.5 (Figure 3, B1–B3). After E18.5, Pax2 expression was restricted to the hair cells of the saccule (Figure 3, C1–C3).

To determine the expression pattern of Prox1 during the hair cell differentiation of the inner ear, we colabeled embryonic sections using antibodies against Prox1 and Myo7a or Prox1 and Sox2. Prox1 was detected in the precursor cells in the most basal region of the developing cochlea until E15.5, including in the future outer hair cells (OHCs), Dieter's cells, and pillar cells (Figure 4, A1–A3 and B1–B3), consistent with an earlier description [20].

Prox1 induction also followed a base-to-apex gradient along the length of the cochlear duct, which is similar to Pax2 and Sox2. By E16.5, Prox1 was expressed in Dieters' cells and pillar cells of the basal region of the developing cochlea but could not be detected in the apical region. Kirjavainen et al. previously showed Prox1 expression in OHCs of the basal coil at postnatal day 0 (P0) [24]; however, we found that Prox1 was only transiently expressed in OHCs and was rapidly downregulated in OHCs while expression of Prox1 was sustained in the supporting cells through E18.5 (Figure 4, C1–C4). At this stage, the morphological distinction between the supporting cells and the hair cells was clear throughout the cochlea, and the supporting cells underlying the hair cells expressed high levels of Prox1. This was distinct from the Sox2 expression, which was found in all of the supporting cells and in a group of cells within Kolliker's organ (Figure 4, C1–C4). Notably, the inner phalangeal cells, border cells, and Hensen's cells did not express Prox1 at this stage (Figure 4, C1–C4). The supporting cells underlying the inner hair cells did not express Prox1, thus distinguishing these two adjacent populations of supporting cells.

Prox1 was not detected in the utricle after E16.5 (Figure 5, A1–A3 and C1–C3). These data differ from an earlier study [24] in which the expression of Prox1 was maintained until P1, but they are consistent with the results of Bermingham-McDonogh et al. [20]. In contrast, Prox1 was still expressed in the saccule at E18.5 (Figure 5, A1–A3 and C1–C3).

2.3. The Expression Patterns of Pax2, Sox2, and Prox1 in Neonatal Mouse Inner Ear (P0-P7). Pax2 expression was maintained in hair cells at P0, but the expression was notably weaker in the inner hair cells in the basal region of the cochlea (Figure 6, A1–A4). By P7, this protein was no longer detectable in any of the hair cells (Figure 6, B1–B2). Compared with Pax2, Sox2 expression was restricted to the supporting cells—including the inner phalangeal cells, inner pillar cells, outer pillar cells, Dieter's cells, and Hensen's cells—in the basal region of the cochlea by P0 as well as in a group of cells within Kolliker's organ (Figure 6, A1–A4). Furthermore, Pax2 was still expressed in the hair cells of the vestibular sensory epithelia at P7 (Figure 6, C1–C4), while Sox2 was found in both the hair cells and supporting cells (Figure 6, C1–C4).

Prox1 expression continued in Dieters' cell and pillar cell nuclei after birth, but the intensity gradually weakened over the course of development (Figure 7, A1–A4). At P7, Prox1

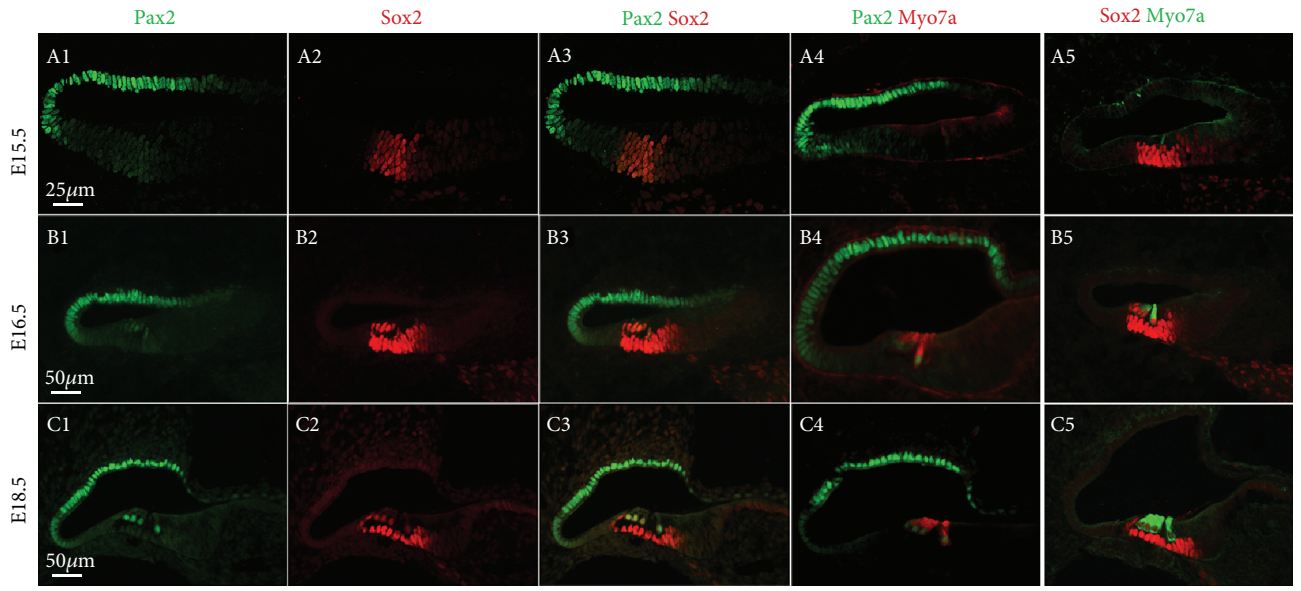

Figure 2: Comparison of Pax2, Sox2 expression in the cochlea. Immunofluorescence of Sox2, Pax2, and myosin7a expression in the cochlear duct at E15.5, E16.5, and E18.5. Scale bars = 25 μm (A1–A5); 50 μm (B1–B5 and C1–C5).

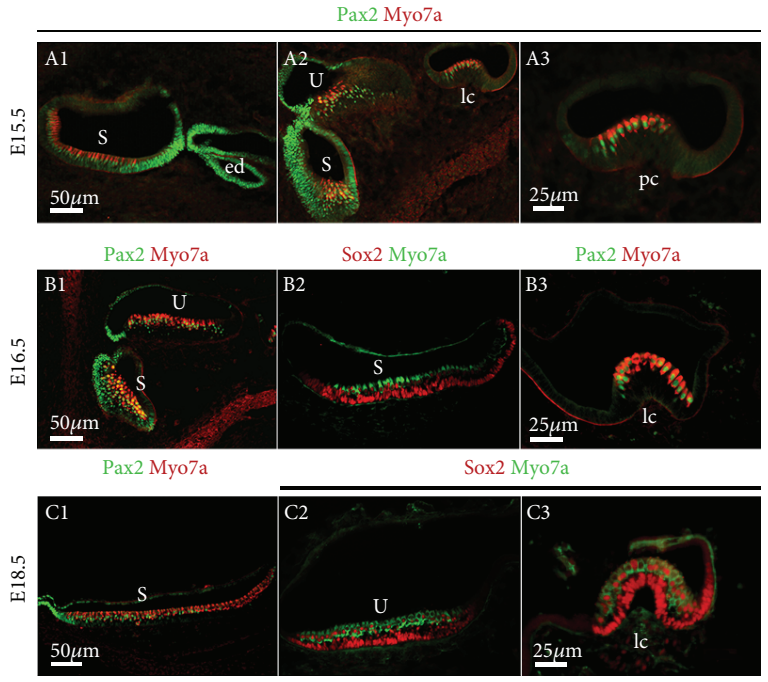

Figure 3: Comparison of Pax2 and Sox2 gene expression in the vestibule. Immunofluorescence of Pax2, Sox2, and myosin7a in the vestibule from E15.5 to 18.5. S: saccule; U: utricle; ed: endolymphatic duct; pc: posterior crista; lc: lateral crista. Scale bars = 50 μm (A1–A2, B1–B2, and C1–C2); 25 μm (A3, B3, and C3).

immunoreactivity was noticeably reduced in subsets of supporting cells, particularly those in the first and second rows of Dieters' cells and in outer pillar cells in the apical region of the organ of Corti, and Prox1 was even more weakly expressed in the basal region (Figure 7, B1–B4 and C1–C4). This is similar to cProx1 expression in the basilar papilla in chicken where nuclear cProx1 expression is downregulated in most hair cells by stage 37 and in many supporting cells by stage 40 [25]. Prox1 was not detected in the saccule or ampulla after birth.

3. Discussion

3.1. Distinct Temporospatial Expression Patterns of Pax2 and Sox2 during the Development of Mouse Cochlea. It has been reported that Pax-2 is one of the earliest markers of the

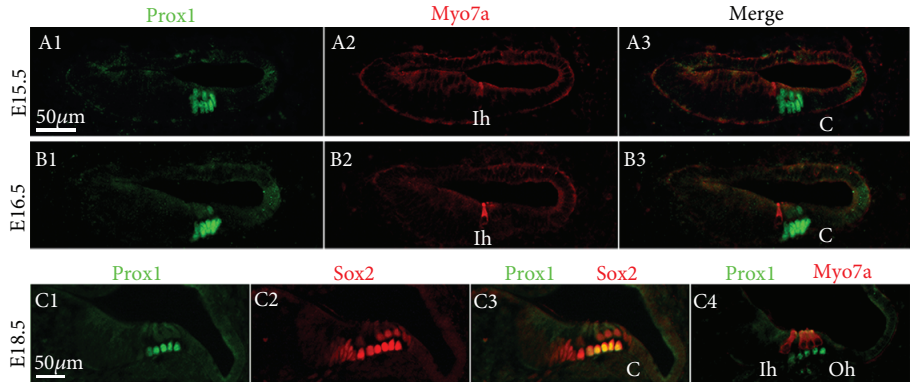

Figure 4: Prox1 gene expression patterns in the cochlea. Immunofluorescence of Prox1 (green) and myosin7a (red) in the cochlea at E15.5, E16.5, and E18.5. Scale bar = 25 μm.

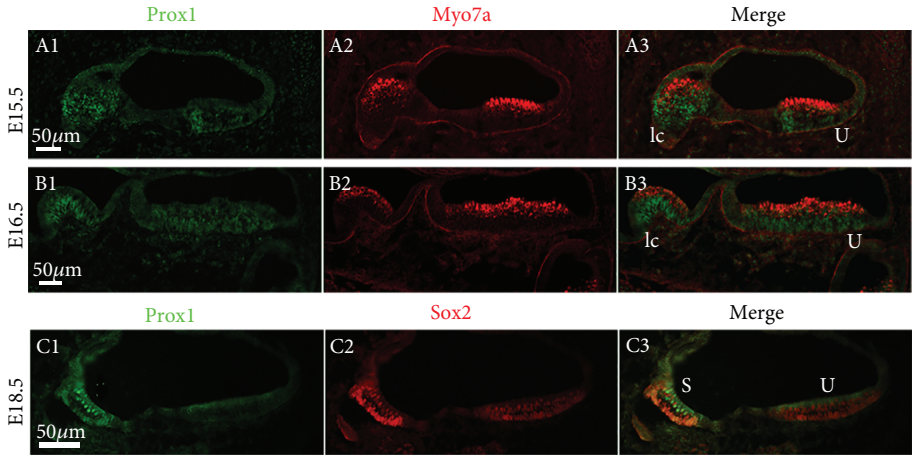

Figure 5: Prox1 expression in the prosensory domain of the developing vestibule. Immunofluorescence of Prox1 (green) and myosin7a/Sox2 (red) in the macula sacculi, macula utriculi, and crista ampullaris from E13.5 to E18.5. S: saccule; U: utricle; pc: posterior crista; lc: lateral crista. Scale bars = 50 μm.

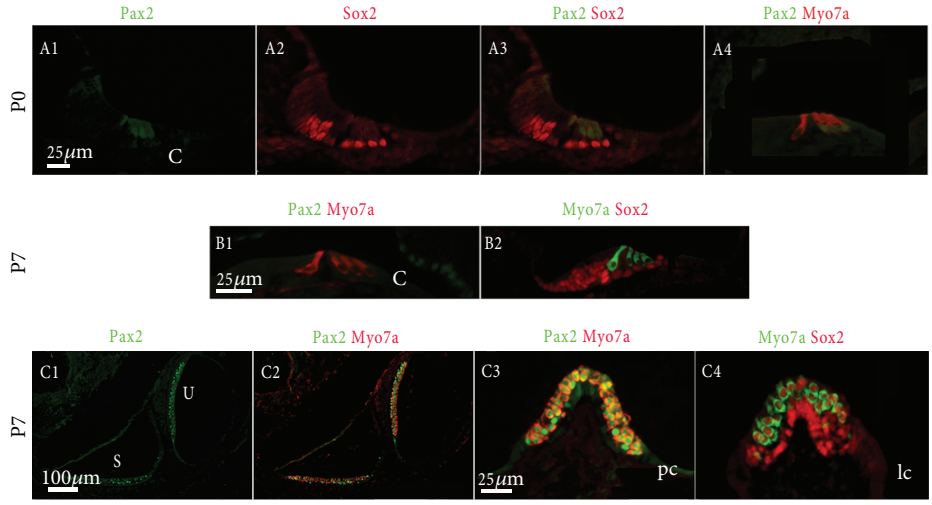

Figure 6: Pax2 and Sox2 gene expression patterns in the neonatal mouse inner ear (P0-P7). Scale bars = 25 μm (A1–A4, B1–B2, and C3–C4); 100 μm (C1–C2).

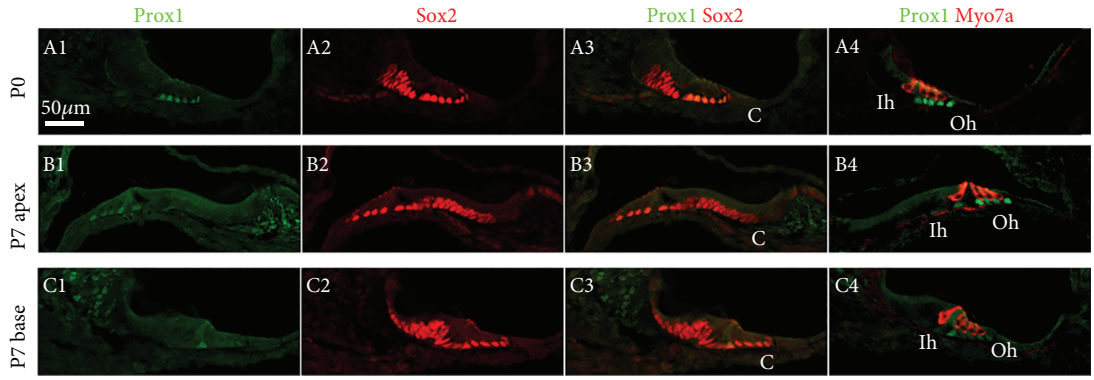

Figure 7: Prox1 is expressed in the neonatal mouse cochleae. Immunohistochemistry of Prox1, Sox2, and anti-myosin7a from P0 to P7. Scale bars = 50 μm.

developing inner ear, which was expressed in the auditory and vestibular sensory primordia [26, 27] and related to the highly proliferative potential of progenitor cells in developing sensory patches of chicken [28]. Mutations in the Pax2 gene result in defects of the auditory and vestibular organs [9, 29]. Meanwhile, Sox2 is another earliest and critical gene for the development of the inner ear, which defined the prosensory domain during the development of the cochlea. The absence or reduced expression of Sox2 within the developing inner ear resulted the impaired development of sensory epithelium and followed hearing loss [15, 30].

One of the primary goals of this study was to determine the temporal and spatial relationships in the expression profiles of Pax2 and Sox2 in order to gain further insight into their possible functions. Our results demonstrate that Pax2 and Sox2 have a reciprocal relationship. In early development, they, respectively, define the medial and lateral sides of the otocyst, and as the sensory patches are innervated, Pax2 is downregulated in the prosensory domain. However, it is selectively upregulated in the hair cells when they begin to express myosin7a, and this expression is maintained in the cochlea until at least P0. This expression pattern suggests that Pax2 might have diverse roles in sensory cell development within the cochlea.

Sox2 expression in the mammalian inner ear initially correlates with the formation of prosensory domains before ultimately becoming restricted to the supporting cells [14–17]. The downregulation of Sox2 in the developing hair cells is required in order for a subset of these cells to differentiate into hair cells. While Sox2 has been shown to activate *Atoh1* by directly binding to consensus sequences in the *Atoh1* enhancer [14], Puligilla and Kelley found that Sox2 plays a dual role in inner ear formation [31]. Their work showed that Sox2 is initially required to specify prosensory competence, but the subsequent downregulation of Sox2 must occur in order to allow Atoh1 expression.

Using Pax2 as a marker for the prosensory cells, the initial overlap and subsequent differential expression of Sox2 suggests that these two proteins likely function in different molecular pathways that act to direct cells towards different cell fates. Thus, Sox2 might be used as a marker of prosensory cells/supporting cells in the cochlea.

3.2. Differential Expression of Sox2 and Prox1 during Cochlear Development. It has been reported that the Prox1 expressed during the development of vertebrate inner ear [25]. In the current study, we characterize the temporal and spatial expression of the mouse developing organ of Corti as well as the vestibular organs, as compared with the distribution of Sox2 and Myo7a. As shown, Sox2 is expressed in prosensory cells and subsequently in immature hair cells and the developing supporting cells before ultimately becoming restricted only to the supporting cells in the auditory epithelia, which suggests that this protein is involved in hair cell differentiation. Notably, the duration of Prox1 expression was shorter than that of Sox2, as it began later in development and was only transiently expressed in the presumptive hair cells and developing supporting cells. Furthermore, Prox1 was only expressed in a subset of developing supporting cells, and not in any mature supporting cells, suggesting that Prox1 might play different roles in supporting cell development depending on the stage of embryonic development. Prox1 has also been proposed to be a marker for the developing supporting cells [21]. Unfortunately, we cannot speculate on the interactions between Prox1 and Sox2 because their expression patterns did not overlap significantly in the presumptive hair cells and developing supporting cells. In addition to being a downstream target of Sox2, Prox1 also upregulates its own expression, which likely plays a role in hair cell development. Similarly, using cotransfection of Prox1 and Atoh1 in cochlear prosensory cells, Prox1 was shown to inhibit Atoh1-induced expression of Myo6, a hair cell marker, in nonsensory cells [30].

3.3. Differential Roles of Pax2, Sox2, and Prox1 during Vestibular and Auditory Organ Development. We found that Pax2 was expressed in all of the immature auditory hair cells in the mouse, but its expression gradually decreased and had completely disappeared by P7. In contrast, Pax2 protein expression was still evident in hair cells of the vestibular organ at P7. Similarly, Sox2 was not only expressed in prosensory cells but also expressed in the supporting cells and nascent hair cells of both the auditory and vestibular organs at very early stages of development. At P7, however, Sox2 was only expressed in the supporting cells of the organ of

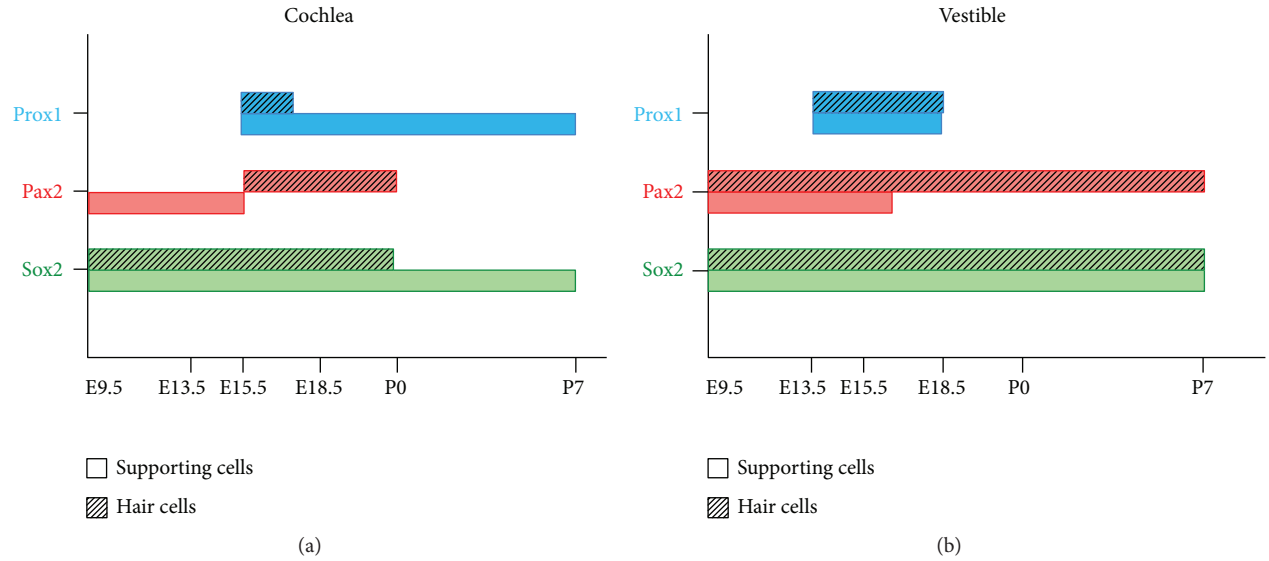

Figure 8: Schematic diagram of Sox2, Pax2, and Prox1 gene expression during mouse inner ear development.

Corti, but it was still present in both hair cells and supporting cells of the vestibular sensory organ. Prox1 was transiently expressed in both presumptive hair cells and developing supporting cells, but it had a much shorter time course of expression compared to the total time for the cochlea to fully develop and mature, and it had much lower expression intensity in the sensory epithelia of the vestibular organ compared to the auditory organ.

The different expression patterns of Pax2 and Sox2 in the vestibular versus the auditory organs suggest that the expression of these proteins might be associated with different requirements in vestibular hair cell specialization [9, 32]. Both auditory and vestibular hair cells have similar functions and appear morphologically similar, but they have clear differences in terms of detailed structures such as ion channels, cilium structures, and innervation [33, 34].

The data presented here suggest that Pax2, Sox2, and Prox1 expression might be involved in this cell fate choice, and the different expression patterns of these proteins in the developing auditory and vestibular sensory organs might help to shape each respective sensory structure.

4. Conclusions

Pax2, Sox2, and Prox1 have differential and overlapping expression patterns during auditory and vestibular sensory organ development. Sox2 and Pax2 are both expressed in the prosensory cell/developing hair cells, but Pax2 expression eventually disappear and Sox2 expression is subsequently restricted to the supporting cells of the organ of Corti. In contrast, in the vestibular organ, Pax2 is still clearly expressed in hair cells at P7, and Sox2 is still expressed in both hair cells and supporting cells. Prox1 is only transiently expressed in presumptive hair cells and developing supporting cells in the organ of Corti, and Prox1 has a weaker expression in the vestibular sensory organ compared to the auditory organ. The different expression patterns in the developing auditory and vestibular sensory organs suggest that Sox2 and Pax2 play different roles in the development of the sensory epithelia and might help to shape the corresponding sensory structures (Figure 8).

5. Materials and Methods

5.1. Animals. Pregnant C57/6 mice (Department of Laboratory Animal Science, Medical College of Fudan University) were time-mated and checked for plugs the following day to verify that they were pregnant. The plug date was designated as E0.5, and the day of birth was defined as P0. Pregnant mice were euthanized on E9.5, E11.5, E12.5, E13.5, E15.5, E16.5, and E18.5, according to the Guide of the Care and Use of Laboratory Animals. All animal procedures were performed according to the protocols approved by the Animal Care and Use Committee of Fudan University and were consistent with the National Institutes of Health Guide for the Care and Use of Laboratory Animals.

5.2. Cryosectioning. The embryonic mice were removed and decapitated, and the whole heads from E9.5 to E16.6 mice or otic bullae from E18.5 to P7 were fixed in 4% paraformaldehyde (Sigma-Aldrich) in 0.01 M phosphate-buffered saline (PBS, PH7.4) at 4°C. For P7 and older mice, decalcification was performed with 10% EDTA for 1-2 days at 4°C. Tissues were washed three times in phosphate-buffered saline (PBS), cryoprotected in successive changes of increasing sucrose concentrations (from 15% sucrose to 30% sucrose in PBS), and embedded in optimal cutting temperature compound (Sakura Finetek) at 4°C overnight. Sections with a thickness of 10 μm were made with a Leica CM3050 cryostat (Leica).

5.3. Immunofluorescence. For immunofluorescence, tissue sections were washed in PBS and permeated with PBS/0.1% Triton X-100 for 40 min at 37°C, and subsequently incubated in a solution of 10% normal goat or donkey serum for 30 min

at room temperature. After antigen retrieval in a 97.9°C water-bath with 10 mM Na-Citrate, pH 6.0, the samples were incubated overnight at 4°C with primary antibody. After incubation, samples were rinsed and incubated with an Alexa Fluor 488 donkey anti-goat or donkey anti-rabbit (1 : 200 dilution; Molecular Probes) for 1 h at 37°C. If double immunostaining was performed, Cy3-conjugated AffiniPure Donkey Anti-Goat IgG (H + L) (1 : 200 dilution; Jackson ImmunoResearch) was also used. The samples were then rinsed again, mounted with anti-fade medium (Slowfade Gold Antifade Reagent with DAPI, Molecular Probes), and observed with a Leica microscope. The following primary antibodies were used: Pax2 (1 : 200 dilution), Prox1 (1 : 1000 dilution), Sox2 (1 : 600 dilution) (all from Santa Cruz Biotechnology), and goat anti-myosin7a (1:200 dilution; Proteus Biosciences). Slides were analyzed by conventional fluorescence microscopy using a Nikon Eclipse TE2000-5 Fluorescence Microscope with a Nikon Digital Sight DS-U1 CCD camera. Images were acquired with the Nikon NIS-Elements D2.30 image manager, and Adobe Photoshop CS 2.0 was used to obtain the merged images and to adjust the contrast and brightness. All images were adjusted equally.

Data Availability

The data used to support the findings of this study are available from the corresponding author upon request.

Conflicts of Interest

The authors have no competing interests.

Authors' Contributions

Shaofeng Liu, Yunfeng Wang, and Yongtian Lu contributed equally to this work.

Acknowledgments

The authors thank Yan Chen, Shan Sun, and TianFeng Wang for their excellent technical support. Huawei Li conceived the study. This work was supported by the National Key R&D Program of China (Nos. 2016YFC0905202, 2017YFA0103900), the National Natural Science Foundation of China (Nos. 81371089, 81771011, 81470687, 81620108005), Shanghai Talent Development Fund (No. 2017046), and the Shanghai Health System Talent Training Program (No. 2017Q003).

References

[1] D. M. Fekete, S. Muthukumar, and D. Karagogeos, "Hair cells and supporting cells share a common progenitor in the avian inner ear," *Journal of Neuroscience*, vol. 18, no. 19, pp. 7811–7821, 1998.

[2] J. Xu, H. Ueno, C. Y. Xu, B. Chen, I. L. Weissman, and P. X. Xu, "Identification of mouse cochlear progenitors that develop hair and supporting cells in the organ of Corti," *Nature Communications*, vol. 8, article 15046, 2017.

[3] E. C. Driver, A. Northrop, and M. W. Kelley, "Cell migration, intercalation and growth regulate mammalian cochlear extension," *Development*, vol. 144, no. 20, pp. 3766–3776, 2017.

[4] J. C. Fuchs and A. S. Tucker, "Development and integration of the ear," *Current Topics in Developmental Biology*, vol. 115, pp. 213–232, 2015.

[5] M. Anwar, M. Tambalo, R. Ranganathan, T. Grocott, and A. Streit, "A gene network regulated by FGF signalling during ear development," *Scientific Reports*, vol. 7, no. 1, p. 6162, 2017.

[6] A. E. Hickox, A. C. Y. Wong, K. Pak et al., "Global analysis of protein expression of inner ear hair cells," *Journal of Neuroscience*, vol. 37, no. 5, pp. 1320–1339, 2017.

[7] K. Nishimura, T. Noda, and A. Dabdoub, "Dynamic expression of Sox2, Gata3, and Prox1 during primary auditory neuron development in the mammalian cochlea," *PLoS One*, vol. 12, no. 1, p. e0170568, 2017.

[8] C. N. Paxton, S. B. Bleyl, S. C. Chapman, and G. C. Schoenwolf, "Identification of differentially expressed genes in early inner ear development," *Gene Expression Patterns*, vol. 10, no. 1, pp. 31–43, 2010.

[9] M. Bouchard, D. de Caprona, M. Busslinger, P. Xu, and B. Fritzsch, "Pax2 and Pax8 cooperate in mouse inner ear morphogenesis and innervation," *BMC Developmental Biology*, vol. 10, no. 1, p. 89, 2010.

[10] N. A. D. Christophorou, M. Mende, L. Lleras-Forero, T. Grocott, and A. Streit, "Pax2 coordinates epithelial morphogenesis and cell fate in the inner ear," *Developmental Biology*, vol. 345, no. 2, pp. 180–190, 2010.

[11] S. Freter, Y. Muta, P. O'Neill, V. S. Vassilev, S. Kuraku, and R. K. Ladher, "Pax2 modulates proliferation during specification of the otic and epibranchial placodes," *Developmental Dynamics*, vol. 241, no. 11, pp. 1716–1728, 2012.

[12] E. J. Pechriggl, M. Bitsche, R. Glueckert et al., "Development of the innervation of the human inner ear," *Developmental Neurobiology*, vol. 75, no. 7, pp. 683–702, 2015.

[13] Y. Chen, H. Yu, Y. Zhang et al., "Cotransfection of Pax2 and Math1 promote in situ cochlear hair cell regeneration after neomycin insult," *Scientific Reports*, vol. 3, no. 1, 2013.

[14] J. S. Kempfle, J. L. Turban, and A. S. B. Edge, "Sox2 in the differentiation of cochlear progenitor cells," *Scientific Reports*, vol. 6, no. 1, 2016.

[15] A. E. Kiernan, A. L. Pelling, K. K. H. Leung et al., "Sox2 is required for sensory organ development in the mammalian inner ear," *Nature*, vol. 434, no. 7036, pp. 1031–1035, 2005.

[16] J. Neves, A. Kamaid, B. Alsina, and F. Giraldez, "Differential expression of Sox2 and Sox3 in neuronal and sensory progenitors of the developing inner ear of the chick," *Journal of Comparative Neurology*, vol. 503, no. 4, pp. 487–500, 2007.

[17] A. R. Steevens, D. L. Sookiasian, J. C. Glatzer, and A. E. Kiernan, "SOX2 is required for inner ear neurogenesis," *Scientific Reports*, vol. 7, no. 1, p. 4086, 2017.

[18] A. Lavado and G. Oliver, "Prox1 expression patterns in the developing and adult murine brain," *Developmental Dynamics*, vol. 236, no. 2, pp. 518–524, 2007.

[19] A. Pistocchi, G. Gaudenzi, S. Carra, E. Bresciani, L. del Giacco, and F. Cotelli, "Crucial role of zebrafish prox1 in hypothalamic catecholaminergic neurons development," *BMC Developmental Biology*, vol. 8, no. 1, p. 27, 2008.

[20] O. Bermingham-McDonogh, E. C. Oesterle, J. S. Stone, C. R. Hume, H. M. Huynh, and T. Hayashi, "Expression of Prox1

during mouse cochlear development," *Journal of Comparative Neurology*, vol. 496, no. 2, pp. 172–186, 2006.

[21] B. Fritzsch, M. Dillard, A. Lavado, N. L. Harvey, and I. Jahan, "Canal cristae growth and fiber extension to the outer hair cells of the mouse ear require Prox1 activity," *PLoS One*, vol. 5, no. 2, article e9377, 2010.

[22] D. I. Scheffer, J. Shen, D. P. Corey, and Z. Y. Chen, "Gene expression by mouse inner ear hair cells during development," *The Journal of Neuroscience*, vol. 35, no. 16, pp. 6366–6380, 2015.

[23] G. Lawoko-Kerali, M. N. Rivolta, and M. Holley, "Expression of the transcription factors GATA3 and Pax2 during development of the mammalian inner ear," *Journal of Comparative Neurology*, vol. 442, no. 4, pp. 378–391, 2002.

[24] A. Kirjavainen, M. Sulg, F. Heyd et al., "Prox1 interacts with Atoh1 and Gfi1, and regulates cellular differentiation in the inner ear sensory epithelia," *Developmental Biology*, vol. 322, no. 1, pp. 33–45, 2008.

[25] J. S. Stone, J. L. Shang, and S. Tomarev, "Expression of Prox1 defines regions of the avian otocyst that give rise to sensory or neural cells," *Journal of Comparative Neurology*, vol. 460, no. 4, pp. 487–502, 2003.

[26] M. R. Hutson, J. E. Lewis, D. Nguyen-Luu, K. H. Lindberg, and K. F. Barald, "Expression of Pax2 and patterning of the chick inner ear," *Journal of Neurocytology*, vol. 28, no. 10/11, pp. 795–807, 1999.

[27] S. Rinkwitz-Brandt, A. Hans-Henning, and E. Bober, "Regionalized expression of *Nkx5-1*, *Nkx5-2*, *Pax2* and *sek* genes during mouse inner ear development," *Hearing Research*, vol. 99, no. 1-2, pp. 129–138, 1996.

[28] H. Li, H. Liu, C. E. Corrales, H. Mutai, and S. Heller, "Correlation of Pax-2 expression with cell proliferation in the developing chicken inner ear," *Journal of Neurobiology*, vol. 60, no. 1, pp. 61–70, 2004.

[29] J. Favor, R. Sandulache, A. Neuhauser-Klaus et al., "The mouse *Pax2*^{1Neu} mutation is identical to a human *PAX2* mutation in a family with renal-coloboma syndrome and results in developmental defects of the brain, ear, eye, and kidney," *Proceedings of the National Academy of Sciences of the United States of America*, vol. 93, no. 24, pp. 13870–13875, 1996.

[30] A. Dabdoub, C. Puligilla, J. M. Jones et al., "Sox2 signaling in prosensory domain specification and subsequent hair cell differentiation in the developing cochlea," *Proceedings of the National Academy of Sciences of the United States of America*, vol. 105, no. 47, pp. 18396–18401, 2008.

[31] C. Puligilla and M. W. Kelley, "Dual role for Sox2 in specification of sensory competence and regulation of Atoh1 function," *Developmental Neurobiology*, vol. 77, no. 1, pp. 3–13, 2017.

[32] M. E. Warchol and G. P. Richardson, "Expression of the Pax2 transcription factor is associated with vestibular phenotype in the avian inner ear," *Developmental Neurobiology*, vol. 69, no. 2-3, pp. 191–202, 2009.

[33] J. R. A. Wooltorton, S. Gaboyard, K. M. Hurley et al., "Developmental changes in two voltage-dependent sodium currents in utricular hair cells," *Journal of Neurophysiology*, vol. 97, no. 2, pp. 1684–1704, 2007.

[34] W. J. McLean, D. T. McLean, R. A. Eatock, and A. S. B. Edge, "Distinct capacity for differentiation to inner ear cell types by progenitor cells of the cochlea and vestibular organs," *Development*, vol. 143, no. 23, pp. 4381–4393, 2016.

Hindawi
Neural Plasticity
Volume 2018, Article ID 1970150, 5 pages
https://doi.org/10.1155/2018/1970150

Research Article

Postnatal Development of Microglia-Like Cells in Mouse Cochlea

Penghui Chen,[1,2,3] Yongchuan Chai,[1,2,3] Haijin Liu,[4] Gen Li,[1,2,3] Longhao Wang,[1,2,3] Tao Yang,[1,2,3] and Hao Wu[1,2,3]

[1]*Department of Otorhinolaryngology-Head and Neck Surgery, Shanghai Ninth People's Hospital, Shanghai Jiao Tong University School of Medicine, Shanghai, China*
[2]*Ear Institute, Shanghai Jiao Tong University School of Medicine, Shanghai, China*
[3]*Shanghai Key Laboratory of Translational Medicine on Ear and Nose Diseases, Shanghai, China*
[4]*Department of Pediatric Surgery, The First Affiliated Hospital of Gannan Medical University, Jiangxi Province, China*

Correspondence should be addressed to Tao Yang; yangtfxl@sina.com and Hao Wu; wuhao622@sina.cn

Received 26 January 2018; Revised 9 May 2018; Accepted 9 July 2018; Published 31 July 2018

Academic Editor: Hai Huang

Microglial cells are involved in surveillance and cleaning of the central nervous system. Recently, microglial-like cells (MLC) have been found in an adult cochlea and investigated for their role in cochlear inflammation. The presence and potential roles of MLCs during the development of the cochlea, however, remain unclear. In this study, immunostaining was performed using the MLC-specific marker IBA1 to characterize the presence, distribution, and morphology of MLCs in the developing cochlea. From P0 to P14, MLCs were present in a variety of cochlear regions including the modiolus, spiral lamina, spiral ganglion, spiral ligament, and the organ of Corti. Interestingly, the overall number of MLCs in a mouse cochlea steadily increased since P0, peaks at P5, then gradually decreased from P5 to P14. In the spiral ligament, the distribution of the MLCs trends to shift from the type I/II fibrocyte-rich regions to the type III/IV fibrocyte-rich regions during the course of cochlear development, accompanied by the morphological changes of MLCs from the amoeboid, activated form to the ramified, quiescent form. Our results suggested that MLCs experience drastic morphological and distributional changes during postnatal cochlear development, which may play a role in the maturing and remodeling of the cochlea.

1. Introduction

Microglia-like cells (MLC) are bone marrow-derived cells that act as tissue-resident macrophage in the inner ear. The cochlear labyrinth was used to be thought of as immune-privileged, free of macrophage. More recently, increasing studies demonstrated the existence of both resident cochlear macrophages and recruitment of inflammatory macrophages to the cochlea [1–4].

Observation of MLCs has been originally reported in the avian and murine inner ear [5, 6]. In 2008, Okano et al. found that bone marrow-derived cells expressing the microglia-specific marker IBA1 are present as tissue-resident macrophages in the mouse inner ear [1, 3]. Recently, O'Malley et al. reported the existence of IBA1+, CD68+, and CD163+ macrophages/microglia in the adult human cochlea [7]. Seigel et al. isolated and enriched the population of CD11b+ cells from the cochlea and immortalized these cells to derive a novel microglial cell line named Mocha (microglia of the cochlea) [8].

Microglial cells function as the resident immune cells of the central nervous system (CNS), retina, and inner ear and are primary mediators of inflammations [9]. Many studies indicate that excessive microglial activation is deleterious for the neuron, while microglial inhibition may reduce neural damage. In the inner ear, deactivation of MLC minimizes hair cell loss and improves hearing after cochlear damage [10, 11]. However, other studies showed that microglial activation may also have some neuroprotective effects [6].

Microglia in the CNS originates from cells of mesodermal lineage. In the cochlea, the MLCs originate from bone marrow-derived cells [2, 4]. To date, the distribution of MLCs was mostly studied in the adult cochlea, where the presence of MLCs was detected in the stria vascularis,

spiral ligament, basilar membrane, and 8th nerve [1, 7]. On the other hand, the microglial morphology and distribution during cochlear development have been far less investigated. This paper aimed at exploring the origins and distribution of the resident MLCs in the mouse cochlea during development.

2. Materials and Methods

2.1. Animals. C57BL/6 mice were bought from Shanghai SLAC Laboratory Animal Co. All animal procedures were performed following protocols that were approved by the Institutional Authority for Laboratory Animal Care of Ninth People's Hospital, School of Medicine, Shanghai Jiao Tong University. All possible efforts were made to minimize the number of animals used and their suffering. In our experiments, P0 was defined as the day of birth.

2.2. Immunohistochemistry. Cochleae were quickly extracted and immersion fixed in 4% paraformaldehyde overnight at 4°C. Decalcification was performed for cochleae of P7 and later for 24 hours. The specimens were then dehydrated with a graded series of ethanol and embedded in paraffin wax. Paraffin sections in 3 um thickness were deparaffinized, rehydrated, antigen retrieved, and blocked with 10% normal rabbit serum at room temperature for 30 min. Slides were incubated with a primary antibody (IBA1, Abcam, Ab178846 1 : 500 diluted with PBS) overnight at 4°C, washed three times with PBS (pH 7.4) for 5 min each, and then incubated with a secondary antibody (secondary antibody: HRP-goat anti-rabbit 1 : 300) labelled with HRP at room temperature for 50 min. Freshly prepared DAB chromogenic reagent was added to the dry sections. Nuclei were stained blue with hematoxylin while the nuclei of IBA1+ cells were stained brown-yellow with DAB reagent.

2.3. Transmission Electron Microscopy (TEM). Cochleae were perfused with ice-cold 2.5% glutaraldehyde and immersion fixed overnight at 4°C. After postfixing in 2% osmium tetroxide at 4°C for 1 h, cochleae were dehydrated and embedded in 812 resin. The ultrathin sections were stained with lead citrate and uranyl acetate and observed under a Philips CM-120 transmission electron microscope (Philips, Amsterdam, Netherlands).

2.4. Quantification and Statistical Analysis. The number of IBA1+ cells was counted for the overall section of the cochlea (Figure 1, left column) and for sections of the basal turn lateral wall (Figure 1, right column) in three continuous immunohistochemistry slices. The statistical significance of different IBA1+ cell numbers among adjacent observation time points was analyzed using Student's *t*-test. *P* values of 0.05 or less were deemed as statistically significant.

3. Results

3.1. Presence of MLCs in Mouse Cochlea during Development. In P0–P14 mouse cochleae, IBA1+ cells were mainly observed in the modiolus, spiral lamina, spiral ganglion, spiral ligament, and the organ of Corti (Figure 1). Spots of

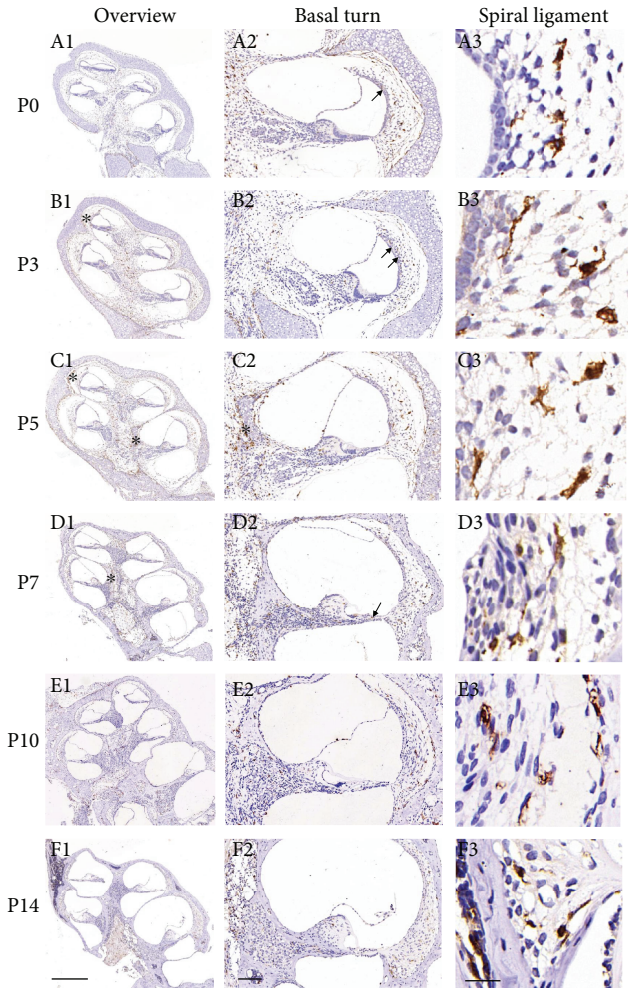

Figure 1: Distribution and morphology of IBA1+ cells in the postnatal development of a mouse cochlea. Left column: overview, 5x, scale bar = 400 um. Middle column: basal turn, 10x, scale bar = 100 um. Right column: spiral ligament at basal turn, 90x, scale bar = 20 um. Rows A–F: P0, P3, P5, P7, P10, and P14, respectively. Arrows: IBA1+ cells on the undersurface of the basilar membrane in the scala tympani and the stria vascularis. Asterisks: IBA1+ cells in the endosteal layer of the cochlea.

IBA1+ cells were detected on the undersurface of the basilar membrane in the scala tympani and the stria vascularis (Figure 1, arrows) and were abundantly present at the endosteal layer of the cochlea, especially at the early postnatal stages (Figure 1, asterisks). At P5, the IBA1+ cells clustered at the modiolus around the cartilage (Figure 1, C2), which disappeared after P7. Some IBA1+ cells can be occasionally identified in close vicinity to the large vessels of the organ of Corti (Figure 2).

The total number of IBA1+ cells changed significantly during the postnatal development of the mouse cochlea, increasing from P1 to P5 by nearly 2-fold and then decreased to the original level from P5 to P14 (Figures 1 and 3).

3.2. Distribution and Morphology Change of MLCs in the Spiral Ligament of Mouse Cochlea during Development. In this study, we observed a significant change of the distribution

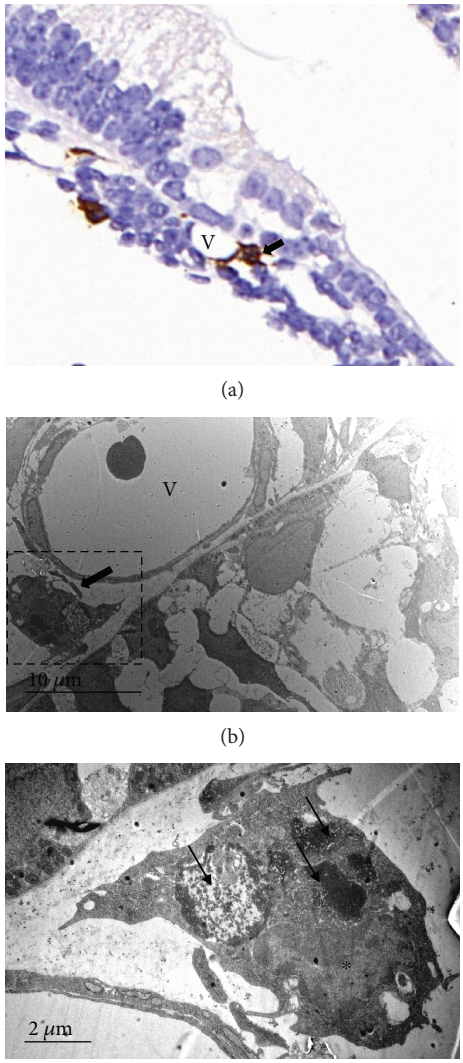

Figure 2: Perivascular resident MLC at basal membrane of P3 mouse cochlea. (a) Immunohistochemistry images. Arrow: MLC; V: vessel. (b) TEM images. Arrow: MLC; V: vessel. (c) Magnification of the dashed box of B. Asterisk: nuclei of MLC. Arrows: engulfing and digesting of the cellular debris.

and morphology of the MLCs in the spiral ligament during the development of the mouse cochlea. At P0, MLCs mainly inhabited the peripheral and central regions of the spiral ligament that are filled with type I and type II fibrocytes. From P0 to P14, MLCs gradually migrated towards the subcentral region and marginal region that are filled with type III and IV fibrocytes (Figure 1, right column; see Supplementary Figure 1 for the localization of type I, II, III, and IV fibrocytes in the lateral wall of the cochlea).

A significant morphological change of the MLCs was also observed in the spiral ligament during mouse cochlear development. Representative shapes of the different types of MLCs are shown in Supplementary Figure 2. At P0, most MLCs in the spiral ligament were in a round, amoeboid shape (Figure 1, A3), indicative of the activated form of MLCs [12]. At P3, some extended, bipolar-like MLCs

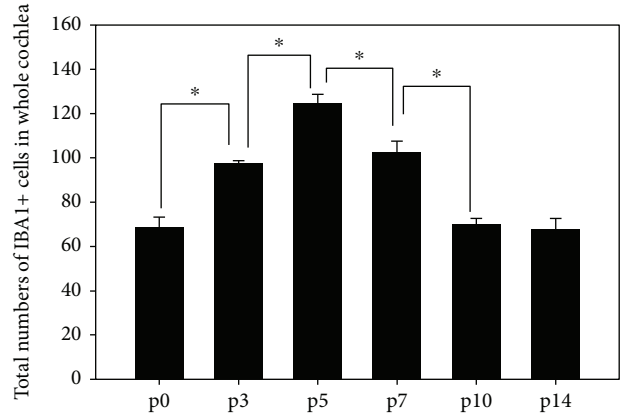

Figure 3: Number counts of IBA1+ cells at midmodiolar sections of P0–P14 mouse cochleae. Asterisks: statistical significance ($P < 0.05$).

appeared in the spiral ligament (Figure 1, B3) and at P5 this form of MLCs became the majority (Figure 1, C3). At P7, the MLCs were further extended and arborized (Figure 1, D3). At P14, most MLCs have a ramified shape, characterized by long branching processes and a small cellular body (Figure 1, E3) and indicative of the quiescent form of MLCs.

4. Discussion

The current study investigated the presence, distribution, and morphology of MLCs in a developing mouse cochlea. Consistent with previous findings in the adult mouse cochlea [1, 7], MLCs were identified in similar regions including the modiolus, spiral lamina, spiral ganglion, spiral ligament, and the organ of Corti from P0 to P14 (Figure 1). The abundance, distribution, and morphology of MLCs, however, underwent a significant change during the postnatal development of the cochlea.

In the current study, we observed a change of the overall abundance of MLCs in the mouse cochlea between P0 and P14. The total number of the IBA1+ cells steadily increased from P0 to P5 and then decreased back to the original level from P5 to P14 (Figure 3). In the CNS, microglia play a critical role in tissue homeostasis and innate immunity by constantly removing infectious agents or unwanted cells. Activated microglial cells are also capable of producing both neurotrophic factors and antioxidants that can improve the neuronal function as well as neurotoxic cell signal factors [12–15]. Between P0 and P14, as the hearing function is gradually maturing, a great variety of cells in the cochlea will undergo different cell fates [16, 17]. Some cells such as glial cells and supporting cells may undergo extensive differentiation and proliferation, while other cells in regions such as the greater epithelial ridge (GER) and the lesser epithelial ridge (LER) may enter programmed apoptosis [16]. Therefore, it is conceivable that during the postnatal cochlear development, MLCs may assist in cleaning and removing the dead or dying cells and its abundance may change accordingly during the process.

In the spiral ligament of the developing cochlea, we also observed a significant change of the distribution and morphology of MLCs. Between P0 and P14, MLCs migrated from the type I/II fibrocyte-rich regions to the type III/IV fibrocyte-rich regions with a morphological shift from the amoeboid, activated form to the ramified, quiescent form (Figure 1). In the CNS, ramified, resting microglia surveys and assesses the microenvironment by the extension and retraction of its processes. In response to physiological changes, it can de-ramify into the phagocytic amoeboid form [9]. The spiral ligament of the cochlea consists of connective tissue cells, epithelial cells, blood vessels, and extracellular matrix material. We speculated that MLCs may help in remodeling the extracellular matrix of collagen fibers at different developmental stages.

Based on our observations, we speculated that for cells entering programmed apoptosis during postnatal cochlear development, removal of dead or dying cell debris may require the assist of activated MLCs. Accordingly, the disruption of MLCs may interfere with the normal development and maturing of the mouse cochlea. Due to limited technical solutions to directly deactivate the MLCs, however, it is difficult to prove this point experimentally at the current stage. A drug specifically targeting the MLCs in the developmental cochlea is needed for this purpose.

5. Conclusions

MLCs are present in the developing mouse cochlea and change in distribution and morphology during the process, suggesting a key role in cochlear development.

Data Availability

Readers can access additional experimental data in optional supplementary materials.

Conflicts of Interest

The authors declare no competing financial interests.

Authors' Contributions

Penghui Chen, Yongchuan Chai, and Haijin Liu contributed equally to this work.

Acknowledgments

This research was supported by grants from the National Science Foundation of China (81570930 to Tao Yang and 81600815 to Yongchuan Chai), Science and Technology Commission of Shanghai Municipality (14DZ2260300 to Hao Wu), and Shanghai Municipal Education Commission—Gaofeng Clinical Medicine Grant (20152519 to Tao Yang).

Supplementary Materials

Supplementary 1. Supplementary Figure 1: localization of type I, II, III, and IV fibrocytes in the lateral wall of the cochlea.

Supplementary 2. Supplementary Figure 2: representative shapes of the different types of MLCs. (A) round, amoeboid; (B) extended, bipolar-like; (C) further extended and arborized; and (D) ramified.

References

[1] S. Ladrech, J. Wang, L. Simonneau, J. L. Puel, and M. Lenoir, "Macrophage contribution to the response of the rat organ of Corti to amikacin," *Journal of Neuroscience Research*, vol. 85, no. 9, pp. 1970–9, 2007.

[2] H. Lang, Y. Ebihara, R. A. Schmiedt et al., "Contribution of bone marrow hematopoietic stem cells to adult mouse inner ear: mesenchymal cells and fibrocytes," *The Journal of Comparative Neurology*, vol. 496, no. 2, pp. 187–201, 2006.

[3] T. Okano, T. Nakagawa, T. Kita et al., "Bone marrow-derived cells expressing Iba1 are constitutively present as resident tissue macrophages in the mouse cochlea," *Journal of Neuroscience Research*, vol. 86, no. 8, pp. 1758–1767, 2008.

[4] E. Sato, H. E. Shick, R. M. Ransohoff, and K. Hirose, "Repopulation of cochlear macrophages in murine hematopoietic progenitor cell chimeras: the role of CX3CR1," *The Journal of Comparative Neurology*, vol. 506, no. 6, pp. 930–942, 2008.

[5] S. A. Bhave, E. C. Oesterle, and M. D. Coltrera, "Macrophage and microglia-like cells in the avian inner ear," *The Journal of Comparative Neurology*, vol. 398, no. 2, pp. 241–256, 1998.

[6] Z. Wang and H. Li, "Microglia-like cells in rat organ of Corti following aminoglycoside ototoxicity," *NeuroReport*, vol. 11, no. 7, pp. 1389–1393, 2000.

[7] J. T. O'Malley, J. B. Nadol Jr., and M. J. McKenna, "Anti $CD163^+$, $Iba1^+$, and $CD68^+$ cells in the adult human inner ear – normal distribution of an unappreciated class of macrophages/microglia and implications for inflammatory otopathology in humans," *Otology & Neurotology*, vol. 37, no. 1, pp. 99–108, 2016.

[8] G. M. Seigel, S. Manohar, Y. Y. Bai, D. Ding, and R. Salvi, "An immortalized microglial cell line (Mocha) derived from rat cochlea," *Molecular and Cellular Neurosciences*, vol. 85, pp. 202–210, 2017.

[9] M. Prinz and J. Priller, "Microglia and brain macrophages in the molecular age: from origin to neuropsychiatric disease," *Nature Reviews Neuroscience*, vol. 15, no. 5, pp. 300–312, 2014.

[10] S. Sun, H. Yu, H. Yu et al., "Inhibition of the activation and recruitment of microglia-like cells protects against neomycin-induced ototoxicity," *Molecular Neurobiology*, vol. 51, no. 1, pp. 252–267, 2015.

[11] Z. He, L. Guo, Y. Shu et al., "Autophagy protects auditory hair cells against neomycin-induced damage," *Autophagy*, vol. 13, no. 11, pp. 1884–1904, 2017.

[12] S. G. Torres-Platas, S. Comeau, A. Rachalski et al., "Morphometric characterization of microglial phenotypes in human cerebral cortex," *Journal of Neuroinflammation*, vol. 11, no. 1, p. 12, 2014.

[13] M. Hinwood, R. J. Tynan, J. L. Charnley, S. B. Beynon, T. A. Day, and F. R. Walker, "Chronic stress induced remodeling of the prefrontal cortex: structural re-organization of microglia

and the inhibitory effect of minocycline," *Cerebral Cortex*, vol. 23, no. 8, pp. 1784–1797, 2013.

[14] A. Nimmerjahn, F. Kirchhoff, and F. Helmchen, "Resting microglial cells are highly dynamic surveillants of brain parenchyma in vivo," *Science*, vol. 308, no. 5726, pp. 1314–1318, 2005.

[15] M. Waqas, S. Sun, C. Xuan et al., "Bone morphogenetic protein 4 promotes the survival and preserves the structure of flow-sorted Bhlhb5+ cochlear spiral ganglion neurons in vitro," *Scientific Reports*, vol. 7, no. 1, p. 3506, 2017.

[16] M. C. Kelly and P. Chen, "Development of form and function in the mammalian cochlea," *Current Opinion in Neurobiology*, vol. 19, no. 4, pp. 395–401, 2009.

[17] L. Liu, Y. Chen, J. Qi et al., "Wnt activation protects against neomycin-induced hair cell damage in the mouse cochlea," *Cell Death & Disease*, vol. 7, no. 3, article e2136, 2016.

Hindawi
Neural Plasticity
Volume 2018, Article ID 7502648, 11 pages
https://doi.org/10.1155/2018/7502648

Research Article

Hydromechanical Structure of the Cochlea Supports the Backward Traveling Wave in the Cochlea *In Vivo*

Fangyi Chen,[1,2] **Dingjun Zha**,[2,3] **Xiaojie Yang**,[1] **Allyn Hubbard**,[4] **and Alfred Nuttall**[2,5]

[1]*Department of Biomedical Engineering, Southern University of Science and Technology, Shenzhen, Guangdong 518055, China*
[2]*Oregon Hearing Research Center, Department of Otolaryngology and Head and Neck Surgery, Oregon Health and Science University, Portland, OR 97239, USA*
[3]*Department of Otolaryngology-Head and Neck Surgery, Xijing Hospital, Fourth Military Medical University, Xi'an, Shaanxi 710032, China*
[4]*Department of Electrical & Computer Engineering, Boston University, Boston, MA 02215, USA*
[5]*Kresge Hearing Research Institute, The University of Michigan, Ann Arbor, MI 48109, USA*

Correspondence should be addressed to Fangyi Chen; chenfy@sustc.edu.cn and Dingjun Zha; zhadjun@fmmu.edu.cn

Received 21 March 2018; Accepted 12 May 2018; Published 17 July 2018

Academic Editor: Jian Wang

The discovery that an apparent forward-propagating otoacoustic emission (OAE) induced basilar membrane vibration has created a serious debate in the field of cochlear mechanics. The traditional theory predicts that OAE will propagate to the ear canal via a backward traveling wave on the basilar membrane, while the opponent theory proposed that the OAE will reach the ear canal via a compression wave. Although accepted by most people, the basic phenomenon of the backward traveling wave theory has not been experimentally demonstrated. In this study, for the first time, we showed the backward traveling wave by measuring the phase spectra of the basilar membrane vibration at multiple longitudinal locations of the basal turn of the cochlea. A local vibration source with a unique and precise location on the cochlear partition was created to avoid the ambiguity of the vibration source in most previous studies. We also measured the vibration pattern at different places of a mechanical cochlear model. A slow backward traveling wave pattern was demonstrated by the time-domain sequence of the measured data. In addition to the wave propagation study, a transmission line mathematical model was used to interpret why no tonotopicity was observed in the backward traveling wave.

1. Introduction

Ears not only hear sound but also generate sound, which is called the otoacoustic emission (OAE) and was discovered in 1978 [1]. There are currently two competing theories established to explain the propagation of sound from the place where it is produced inside the cochlea towards the exit of the cochlea. The backward traveling wave theory, which postulates that OAE-induced waves travel slowly along the basilar membrane (BM), is widely accepted as an explanation of the propagation of the OAE [1, 2]. However, this predominant backward slow-wave theory cannot explain some experimental phenomena [3–6] favoring the fast compression wave theory that would exist in the lymph fluids surrounding the BM. In the compression wave theory, the slow-speed propagation of the backward transversal wave motion of the BM is replaced by a fast-fluidic compression wave and experimental time/phase differences are accounted for by mechanisms independent of the wave. To date, it is still an open question about the OAE path. Resolving this question is important because the OAE has become a useful and noninvasive clinical tool for hearing screening. To utilize the OAE for more precise diagnoses, it is necessary to understand how it propagates backward to the ear canal. In relation to the backward propagation of the OAE, von Békésy discovered that the wave on the BM always traveled from the base to the apex, even the stimulus (the stapes vibration) was placed at the apex of the cochlea. This so-called paradoxical wave was a hurdle that prevented people from believing that the OAE can propagate along the BM backward at the time

when OAE was just discovered. In a few years since then, the seeming contradiction to the paradoxical phenomena was explained by stating that the vibration source of OAE was on the BM rather than in the fluid by the stapes as in the paradoxical wave. Hence, the theory of backward traveling wave was widely accepted.

One critical issue that causes the uncertainty in determining the wave propagation mechanism is that the actual location of the OAE source is uncertain. Most of the previous studies used nonlinear, intrinsic vibration to the organ of Corti to generate organ vibration at the intermodulation frequency of two tones. This intrinsic vibration initializes the backward wave propagation, but the spatial location of the vibration along the BM is still debated. This caused the analysis of the experimental data to be difficult because the generation mechanism of the OAE is complicated [2], and the origin of the OAE could be multiple sites. Although the width and location of the generation site are so important, they cannot be ascertained. The uncertainty of the source location also makes it difficult to estimate the wave propagation speed, which is a critical data for distinguishing the propagation forms and testing which theory explains the sound propagation mechanisms. Such an uncertainty has often resulted in interpretations of the same experimental results [6–8] using both competing theories. Thus, it is critical to study the backward wave propagation from a vibration source at a unique and precise location in the cochlea.

In addition, although as a widely accepted theory, the backward traveling wave theory has not been validated directly using an experiment where the vibration on the BM is measured [3]. The evidence used to support this theory is mostly from mathematical modeling [7, 9–14] and indirect measurements [15, 16]. Attempts have been made to experimentally generate local vibration on the BM via optical [17] and direct mechanical [18] methods but with limited success. The optical method [17] does not provide enough mechanical vibration until the light is strong enough to cause damage to the organ of Corti. The mechanical stimulation in Richter et al. [18] did provide an accurate vibration source with enough energy, but the hemicochlea preparation in this study destroyed the integrity of the basic hydromechanical structure of the cochlea. Also, the poor sensitivity (~10 nm) of the vibration measurement method limited its capability to detect the small vibration on the BM.

Since the hypothesized backward traveling wave is a transverse vibration on the BM, these indirect measurements [15, 16] have also been criticized to not truly represent the BM vibration [19, 20]. Moreover, other structures (e.g., tectorial membrane and Reissner's membrane) in the cochlea have also been suggested to be capable of supporting wave propagation inside the cochlea [21, 22], but their contribution to the cochlear mechanical dynamics has not been thoroughly studied and determined. Therefore, a direct measurement of the BM vibration using an experiment is necessary to determine the wave propagation mechanism of OAE in cochlea.

In the present study, we designed a novel method using a mechanical/piezoelectric stimulator to drive the BM at a precisely known location; thus, the location of the vibration source initiating the backward wave was accurately known. The BM vibration was then directly measured at multiple locations in an *in vivo* cochlear preparation. We found that the phase of the measured BM motion showed a consistent lag with the increase of the distance from the vibration source. The speed of the wave propagation was shown in the order of tens of meters per second, much less than the speed of a compression wave in water. This study, for the first time, used directly an experiment to prove that there was a slow backward traveling wave on the BM of the cochlea *in vivo*. The computer simulation of the experimental results in a mechanical model, termed "artificial cochlea," also confirmed that the hydromechanical structure of the cochlea supported the backward traveling wave.

2. Methods

2.1. Specimens. A total of 6 young guinea pigs weighted at 250 g–400 g were used in this study. After an animal was anesthetized by intramuscular injection of a mixture of ketamine (30 mg/kg) and xylazine (20 mg/kg), the temporal bone was opened using the dorsal-ventricle approach as described by Zheng et al. [23]. During the experiment, the animal was anesthetized with regular supplements of anesthetics. Tracheotomy was performed, and a ventilation tube was inserted into the trachea for natural breathing. The guinea pig's head was then mounted on a heated head holder. A surgical operation was performed to expose the left bulla, which was then opened for access to the cochlea. During the experiment, the core temperature of the animal was maintained at 37°C-38°C by a heating blanket and a rectal thermometer, which was controlled by a servo temperature controller (FHC, Bowdoinham, ME, USA) [23]. After the bulla was opened to expose the cochlea, an oblong window of about 2 mm long and 0.5 mm wide was opened on the bony wall at the cochlear basal turn to expose the BM. As shown in Figure 1(a), the basal turn of the cochlea was cut to open and the BM was exposed over almost the whole basal turn. Reflective beads assigned names of basal, middle, and apical were placed on the BM along the longitudinal direction. The tip of stimulator touched the BM at the apical end of the basal turn and delivered the vibration to initiate the backward wave. The wave propagation along the BM was recorded by focusing the laser of the vibrometer onto the reflective beads.

In the preparation, the joint between the incus and stapes was dislocated so that the middle ear chain was disrupted, significantly reducing any possible middle-ear-conducted acoustic stimulation. The ossicular dislocation was done because the piezo stack used to stimulate the BM also radiates acoustic energy. This sound will propagate to the adjacent tympanic membrane, initiating a normal acoustic stimulus to the cochlea and thus producing a forward traveling wave in the cochlea if the ossicular chain is intact. That forward traveling wave would interfere with the backward wave initiated by the stimulation probe on the BM. The fluid level of the perilymph in the scala tympani was carefully lowered using cotton wicks so that only a very small amount of fluid (~30 μm thick based on visual comparison with the

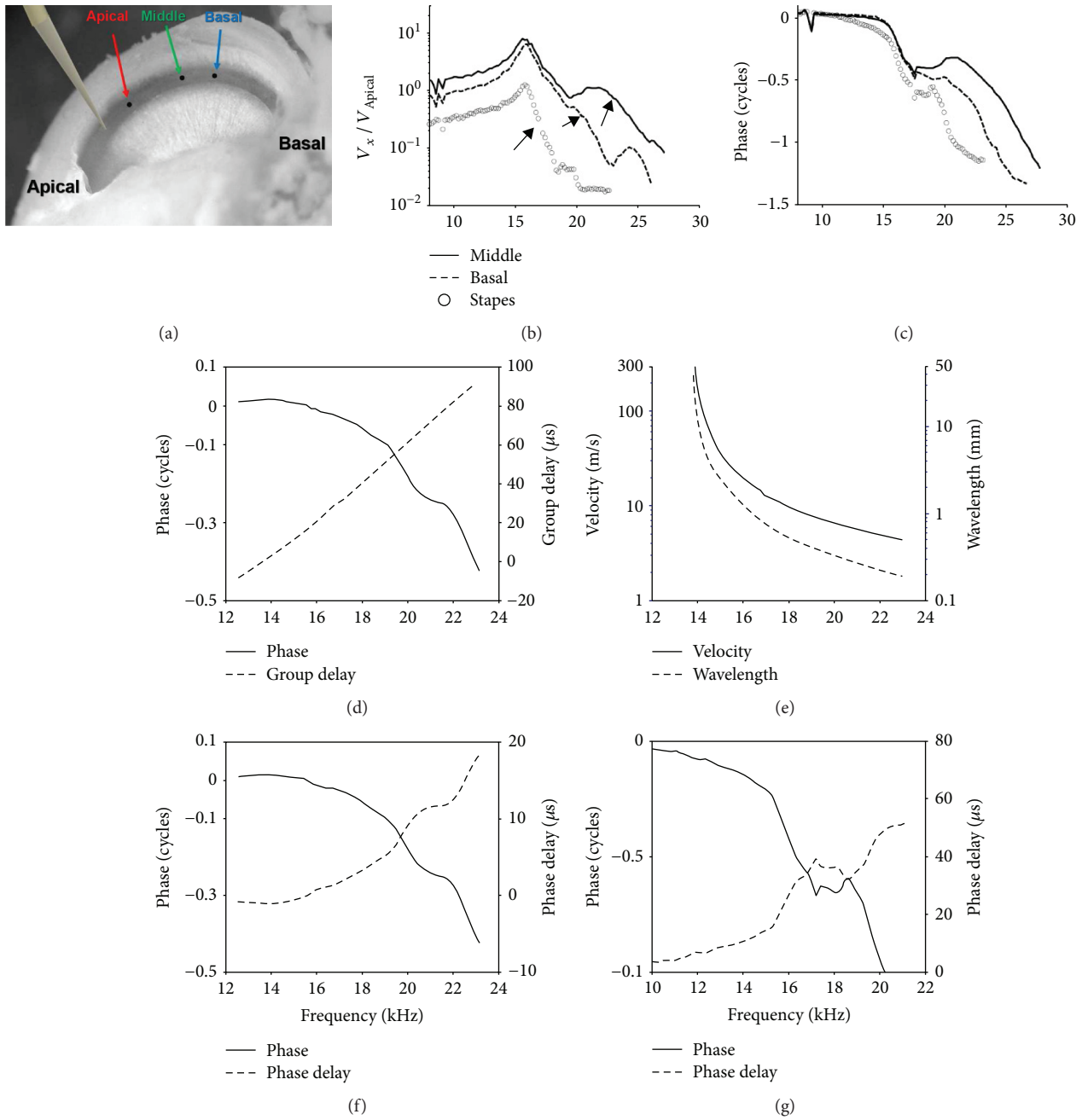

Figure 1: BM and stapes vibration spectra induced by a point stimulation of the BM. (a) The opened cochlea with stimulator and reflective beads in place. The stimulator probe is a blunt pipette driven by a piezoelectric stack. Reflective beads are placed on the BM, labeled as apical, middle, or basal, in the direction away from the stimulator. A bead was also placed on the stapes for recording its vibration. Vibration amplitude (b) and phase (c) of the middle (solid), basal (dash), and the stapes (circle) beads, relative to that of the apical bead. (d) Phase difference (solid) between the middle and basal beads and the calculated group delay (dash). (e) Wave velocity and the wavelength, calculated from the phase difference in *D*. The negative delay value at lower frequencies (<14 kHz) in both (d) and (e) is likely due to a local disturbance, such as the local reflection with the insertion of the stimulator. The wave speed is high at lower frequencies, and the distance between these two beads is small. Both effects make it vulnerable to the disturbance. For a wider range, apical to stapes, this small negative delay is absent (g). (f) Phase difference (solid) between the middle and basal beads and the calculated phase delay (dash). (g) Phase of the stapes vibration (solid) relative to the apical bead and the calculated phase delay (dash).

known diameter of the probe tip) was left to moisten the exposed BM.

The study was approved by the Institutional Animal Care and Use Committee of Oregon Health and Science University.

2.2. Piezo Stimulator Design and Mounting. The accurate location of the vibration source was a problem in almost all of the previous studies designed to measure the backward wave propagation in the cochlea. In our study, the direct mechanical driving method was adopted with a different

design. The tip of a pulled pipette when heated with an electrical cautery, melted into a sphere of about 50 μm in diameter. This rounded tip was appropriate in size compared to the BM width for the delivery of a local vibration. Then a ~2 cm piece from the tip end of the pipette was cut off and attached to a piezo stack (AE0203D04F from Thorlabs, Newton, New Jersey) using cyanoacrylate cement. The driver was then cemented onto a steel bar, which was mounted on a micromanipulator. Figure 2 shows a view of the assembled probe. The overall size of the piezo stimulator allowed it to fit under the objective lens of the laser Doppler vibrometer (LDV). During the experiment, the piezo stimulator was advanced in about a 60-degree (relative to the horizon) angle by the micromanipulator into the opened scala tympani and to get contact with the BM by the tip. This process is visually guided under a surgical microscope. Careful attention was taken to avoid significant deformation or perforation on the BM. After placing the stimulator, the surgical microscope was moved away and the LDV with the objective lens was then moved in for vibration measurement. The piezo stack and the steel bar were held in such a way as to reduce interference caused by the laser beam of the velocimeter. The contact of the probe tip to the BM was also verified by measuring the vibration of the bead that is closest to the probe on the BM.

2.3. Calculation of the Delays. Two kinds of delays, group delay and phase delay, were calculated from the phase spectra in this study. The group delay is the derivative of the phase difference. To avoid the influence of the noise, the phase data was firstly fitted with a 4th-order polynomial to smooth the curve before performing the differentiation.

$$\text{Group delay} = -\frac{d\varphi}{2\pi df}, \tag{1}$$

where d is the differential operator, φ is the phase in radius, and f is the frequency.

Group delay has been used in most OAE studies [2, 5, 15, 16, 24] to quantify the delay for determining the direction of the wave propagation.

Besides group delay, another method to quantify the delay from the phase response is to calculate the phase delay by

$$\text{Phase delay} = -\frac{\varphi}{2\pi f}. \tag{2}$$

This method has been adopted in previous studies by Ren and his colleagues [3–6, 17, 19].

2.4. The Mechanical Cochlear Model. In this study, a mechanical model of the cochlea was used to verify the backward wave propagation. This mechanical device consisted of a fluid channel, a membrane section, and an artificial BM to simulate the basic hydromechanical structure of the cochlea [25]. The artificial BM was constructed from a polymer membrane with 32 copper beams deposited on it. The lengths of the copper slots increased gradually from one (basal) end to the other (apical) and resulted in a stiffness gradient for simulating that in the cochlea. Vibration measurement on this mechanical model demonstrated the traveling wave-like features, that is, tonotopicity, the frequency-to-place map, unsymmetrical filtering (the shallow slope at the low-frequency side of the peak but steep slope at the high-frequency side), and slow traveling wave phase. Therefore, it is a valid model of the cochlear hydromechanical structure for verifying the backward wave propagation.

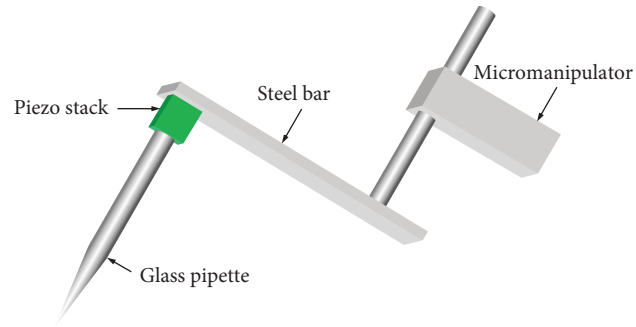

Figure 2: Construction of the piezo stimulator. Glass pipette with melted tip was glued on a piezo stack and then on a steel bar, which was fixed on a micromanipulator.

2.5. Transmission Line Model of the Cochlea. A mathematical model, lumped transmission line model, was created and simulated in a circuit simulator LTSPICE (Linear Technology, Milpitas, CA) based on acoustic-electrical analogy. The basic structure of the model is shown in Figure 3(a) and reviewed by Ni et al. [26]. This circuit model was firstly developed by Peterson and Bogert [27] and represented the basic hydromechanical property of the cochlea. Rather than a one-dimensional structure, our model includes a two-dimensional matrix of mass and dampers to represent the fluid channel. The cochlear partition was modeled as 400 sections of dampened mass-spring resonators and coupled with the fluid channel. No active component (outer hair cell) was included since the experimental preparation was passive. By placing a vibration source at the very basal end of the fluid channel, we simulated the stapes driving the cochlea; by placing the source inside a more apical section on the BM, we simulated the backward wave case where the glass probe stimulates the BM directly. The BM stiffness was taken from Puria and Steele [28], and the cochlear tonotopicity was taken from Greenwood [29].

3. Results

3.1. In Vivo Data Demonstrated a Slow Backward Wave on the BM. For this experiment, the cochlea of a young guinea pig was surgically exposed and the basal turn of the cochlea was widely opened. Reflective beads were placed on the BM at different longitudinal locations and on the head of stapes, as shown in Figure 1(a). In a typical experiment, vibration spectra were measured from three beads (named apical, middle, and basal, according to their relative longitudinal locations) and from the stapes. Vibration spectra measured at the middle and basal beads were scaled by the spectra measured at the apical bead, the closest one to the vibration

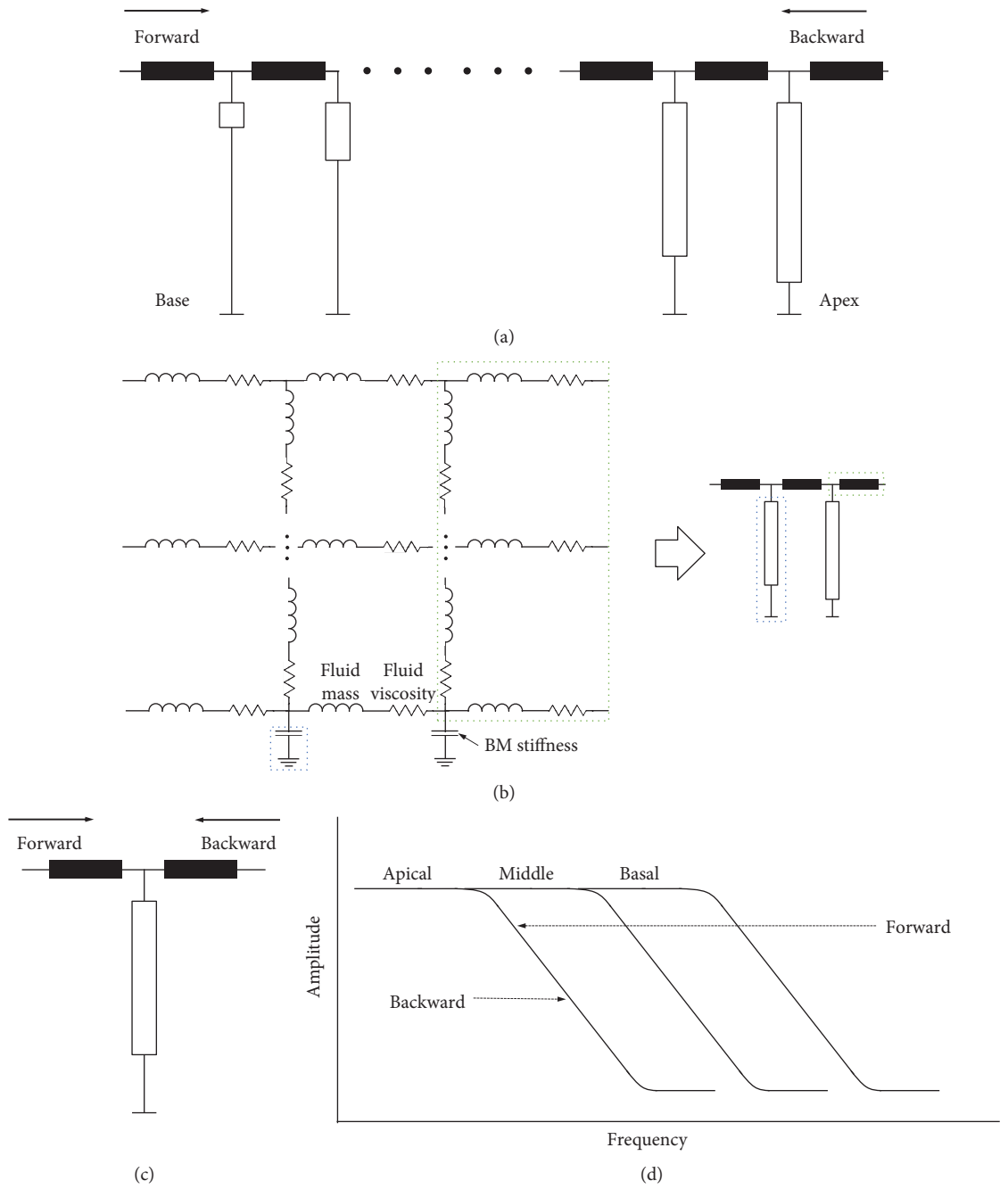

Figure 3: Model of the cochlear passive hydromechanical structure. (a) Schematic of the model structure. The thick solid lines represent the fluid channel and the open rectangles represent the cochlear partition, or simply BM. In this lumped model, the fluid channel and the cochlear partition (or simply BM) were divided into a series of sections. The rectangle is wider and shorter at the base and thinner and longer at the apex, representing the BM stiffness gradient: stiffer at the base and softer at the apex. (b) Circuit analogy of each section. The fluid mass is analogous to a series of inductors; the fluid viscosity is analogous to a series of resistors; the stiffness of the partition is analogous to a capacitor. (c) At each section, the forward and backward waves experience the same low-pass filtering. (d) Schematic shows the low-pass filters that the traveling wave experiences during the forward and backward propagation. Note that the forward direction is towards the low frequency. The roll-off frequency at the basal, middle, and apical locations decreases.

source, in order to calculate the transfer functions. Figure 1(b) shows the amplitude responses. In this plot, the amplitude of all the transfer functions demonstrated peaks at about 16 kHz and a gradually decreasing roll-off frequency in the direction away from the stimulus. This peak is likely due to the standing wave that was introduced by inserting the probe. In absolute units, the maximum vibration velocity magnitudes are 1.3 mm/s, which correspond to a displacement of 12 nm at the 16 kHz peak of the middle location response. As indicated by the arrows in Figure 1(b), in addition to the 16 kHz peak and the roll-off after, the amplitude responses showed higher-frequency roll-offs from about

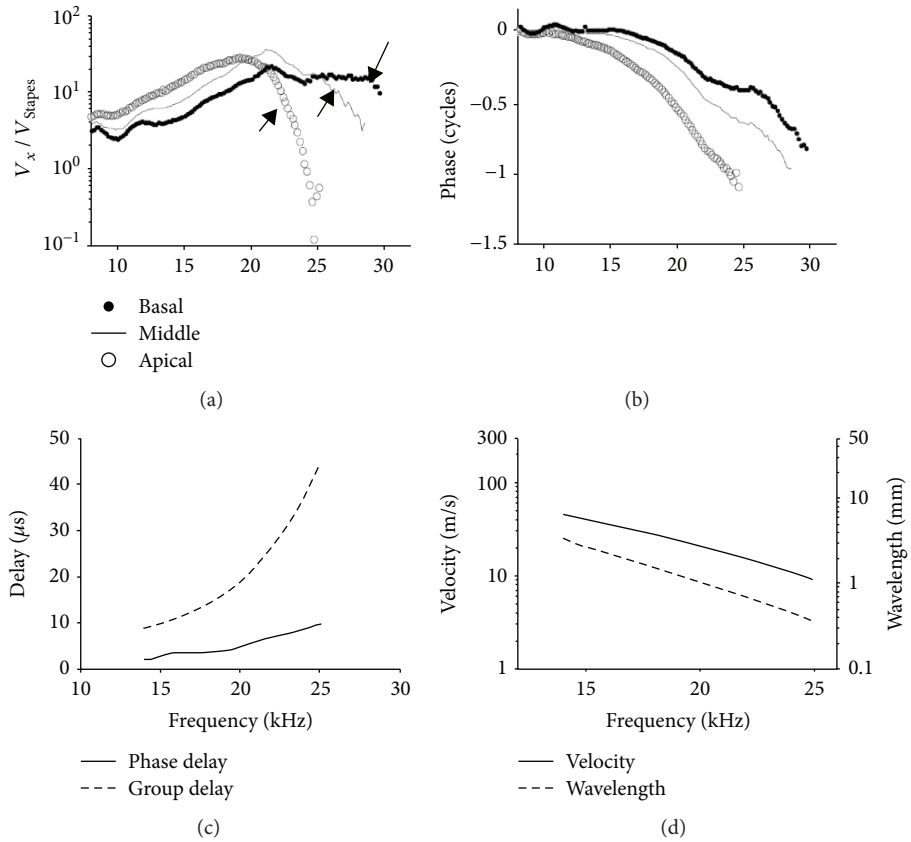

Figure 4: BM responses induced by normal acoustic stimulation at the ear drum. Vibration amplitude (a) and phase (b) of the beads on the BM. They are labeled as basal (dotted), middle (solid line), and apical (open cycle). Arrows in (a) indicates the roll-off of the amplitude responses. (c) Calculated phase and group delay between basal (dotted) and middle (solid line). (d) Calculated velocity (solid line) and wavelength (dashed line).

23 kHz for the middle location to about 20 kHz for the basal location and about 17 kHz at the stapes. Corresponding to the gradually decreasing roll-off frequencies, the phase of the spectra demonstrates a significant phase lag from the middle to the basal bead and then the stapes, indicating a slow wave propagating backward in the cochlea. The phase lag from the apical location to the stapes is more than one cycle (Figure 1(c)).

Phase difference between two neighboring—middle and basal—beads was used to calculate values of the wave propagation parameters: delay, wave velocity, and wavelength. The phase data were smoothed and fitted with polynomial before calculating the delay and velocity, as stated in Methods. The group delay between the middle and basal beads gradually increased with an increasing vibration frequency. It amounted to 62 μs at 20 kHz (Figure 1(d)). Correspondingly, the wave velocity and wavelength decreased. The wave velocity was about 6.4 m/s at 20 kHz for the distance of 400 μm between the two beads (Figure 1(e)).

Another method used to estimate the delay from the phase response was to calculate the phase delay. In Figure 1(f), we show that the phase delay value also increases with increasing frequencies but was smaller than the group delay, about 10 μs at 20 kHz. This resulted in a higher estimated speed of 38 m/s, as compared with using group delay. However, both speed values were much smaller than the estimated compression wave speed of approximately 1500 m/s. The calculated phase delay from the apical bead to the stapes is about 40 μs at 20 kHz.

3.2. BM Vibrations from Conventional Acoustic Stimulation Validated the Preparation. In this preparation, the sound-conduction system (i.e., the tympanic membrane and the ossicular chain) inside the middle ear was maintained to be intact and functional. The basal turn of the cochlea was widely opened, and the fluid at the scala tympani of the basal turn was maintained only at a level to moisten the BM. The cochlea thus became a single-channel hydrodynamic structure. To verify that this single-channel preparation preserved the forward traveling wave feature of the normal cochlea, the BM vibration was measured at the same longitudinal locations under normal acoustic conditions, that is, the sound was delivered to the ear drum. Rather than scaled by the vibration spectrum of the apical bead, here, the vibration spectra of three beads were scaled by the stapes vibration to obtain the forward cochlear-transfer functions. The amplitude plotted in Figure 4(a) shows a tonotopic map. The vibration spectrum rolled off at 28 kHz at the basal location; it rolled off at about 25 kHz at the middle location and at about 20 kHz at the apical location. Correspondingly, the phase

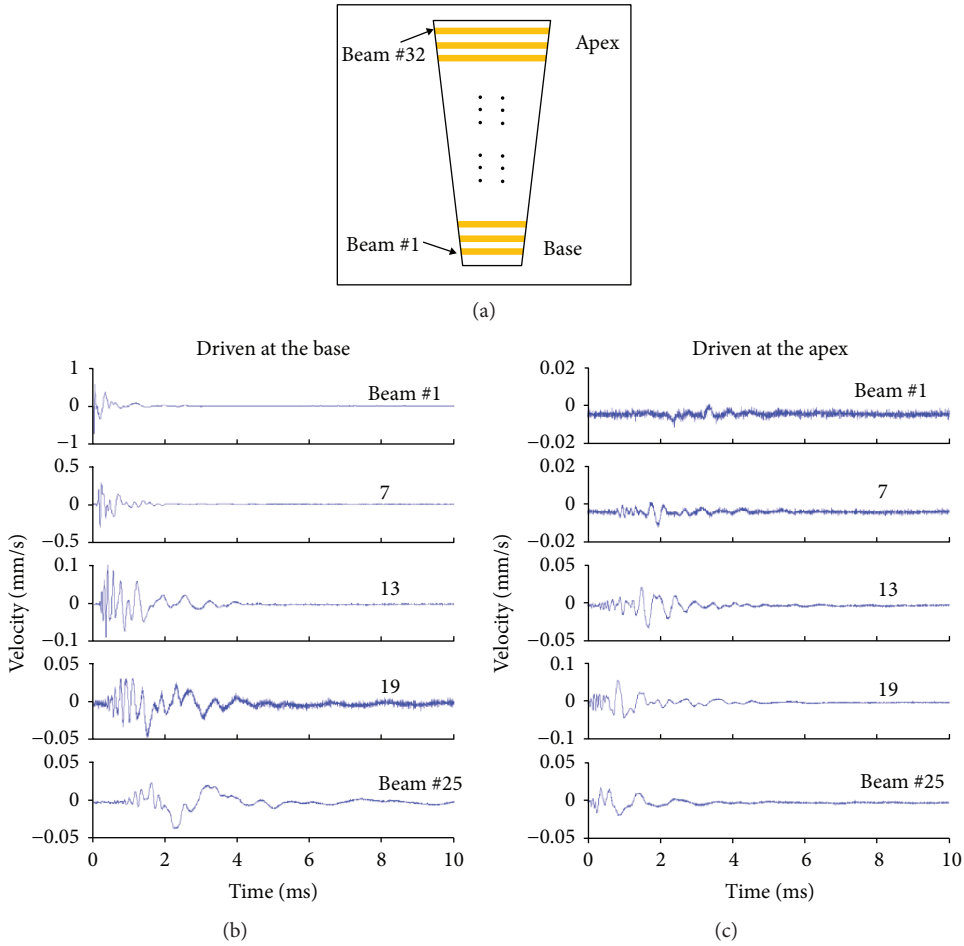

Figure 5: Vibration responses of a mechanical model of the cochlea. (a) Schematic view of the artificial BM. The length of the copper beam varies from 4 mm at the base (narrower) to 8 mm at the apex (wider). A total of 32 beams are placed on a membrane. The distance between beam #1 and #32 is about 20 mm. (b) BM vibration of the model while it was driven at the base, the narrowest, and thus the stiffest end. The driver was placed on the membrane right next to beam #1 at the base. Note that the scale of y-axis decreases from the top to the bottom, showing that the vibration amplitude was attenuated during the propagation. (c) BM vibration while it was driven at the apex. The driver was placed on the membrane at beam #29, close to the apex.

plotted in Figure 4(b) shows gradually the increasing phase lag from the basal to the middle and then to the apical locations. These are expected traveling wave-like features under conventional acoustic stimulation. The phase and group delay increased with the increasing frequency (Figure 4(c)). The phase delay amounted to about 1/5 of the group delay, similar to what they were in the backward direction as shown in Figures 1(d) and 1(f). The velocity and wavelength decreased with the increasing frequency (Figure 4(d)). The velocity ranged from about 10 m/s to 40 m/s. Correspondingly, the wavelength ranged from 0.3 mm to 2 mm. The trend and the values of the delay, velocity, and the wavelength all indicated a slow forward traveling wave. This experimentally verifies the wave propagation function of the single-channel cochlea.

3.3. Forward and Backward Traveling Waves Were Observed in the Mechanical Model of the Cochlea. To better understand the role of the hydromechanical structure of the cochlea in the backward wave propagation, we studied a mechanical model of the cochlea. This artificial device was composed of a fluid channel to simulate the scala vestibuli and a membrane to simulate the BM. Figure 5(a) shows the top schematic view of the device. Thirty-two copper beams are deposited on a membrane to form an artificial BM. The beam length varies gradually from beam #1 to beam #32, simulating the BM stiffness gradient from the base to the apex. The single fluid channel is underneath the BM (detailed construction of the device can be found in Chen et al. [25]). In a previous study, we showed that this hydromechanical structure could demonstrate cochlea-like features and its capability to support the forward cochlear traveling wave [25].

Figure 5(b) shows the time-domain response of the beam vibration, when the artificial cochlea was driven at the base, just before beam #1. About 1 ms delay was demonstrated between the onset responses of beam #1 and beam #25. The distance of these two beams was about 15 mm, so the speed of the wave propagation was about 15 m/s. Figure 5(c) shows the results when the device was driven at the apex, on Beam #32. A clear

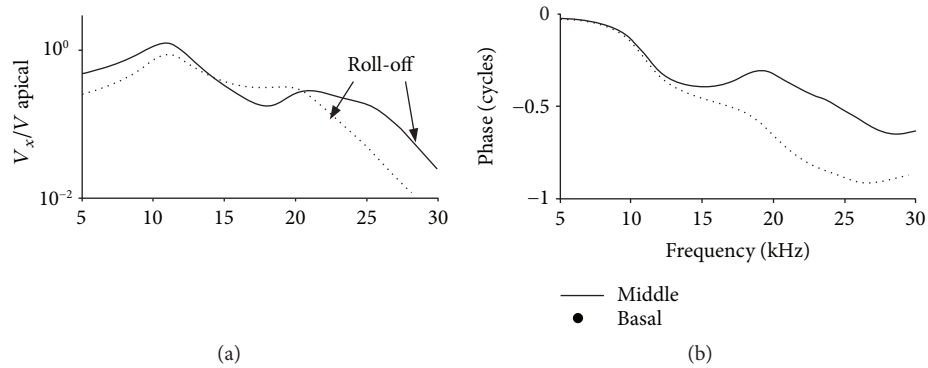

Figure 6: BM vibration responses of a mathematical model of the cochlea under backward driving. (a) Amplitude responses of BM vibration at two longitudinal locations. Solid line, labeled as middle, is at a more apical location; dotted line, labeled as basal, is at a more basal location. The arrows marked the roll-off points. (b) Phase responses.

backward delay was demonstrated in the plots. The amount of the delay was similar to its forward counterpart and so as the speed. This slow wave propagation implies that a backward traveling wave exists in this artificial device.

3.4. Simulation Results from a Mathematical Cochlear Model Where a Point Vibration Source Reproduced Features of the Experimental Data. In addition to the *in vivo* data and the experimental results from the mechanical model, we also studied the backward traveling wave in a mathematical model. This model has a traditional transmission line structure for simulating the hydromechanical structure of the cochlea. With this model, we simulated the backward responses. This was done by placing a vibration source at about 1/3 of the length of the cochlear model from the base and computing the BM vibration responses at more basal places towards to the stapes. BM vibration at three locations was computed to simulate the measured results at the apical, middle, and basal beads. As in the experimental results, the vibration spectra of the middle and basal beads were scaled by that of the apical bead, as shown in Figure 6. Features in the experimental results, as shown in Figures 1(b) and 1(c), were also demonstrated in the simulation results. The spectra can be viewed at two different frequency ranges. At lower frequencies (about <15 kHz), the amplitude response in Figure 6(a) shows a peak at about 12 kHz for both middle and basal locations. Correspondingly, the phase plotted in Figure 6(b) shows a steep roll off at the peak frequency. This could be due to reflection between the point source and the stapes. At frequencies lower than the peak, the phase responses of both locations almost overlap. This can be interpreted as a fast traveling wave at lower frequencies. The amplitude response rolled off at about 25 kHz for the middle location and at about 20 kHz for the basal location. Correspondingly, the phase response showed a clear delay from the middle to the basal location. This indicates a slow backward wave.

4. Discussion

4.1. Direction of the Wave Propagation. It has been hypothesized [1] that the OAE, generated as vibration at the organ of Corti, will propagate backward toward the stapes via a traveling wave on the BM. Although this theory is widely accepted and used to interpret the OAEs [2], the backward traveling wave has never been demonstrated with direct evidence of the BM vibration. Analysis of the OAE phase [9, 15] and cochlear microphonic signal that were measured at the round window [16] was used as indirect evidence of backward propagation. In this present study, the organ of Corti was set into vibration at a specific point location. This produced the first directly observed *in vivo* backward wave propagating on the BM. The phase plotted in Figure 1(c) has a gradual increase of phase lag at the vibration spectra measured at the apical (used as the reference; not shown) to the middle, the basal bead, and then the stapes. The velocity and delay calculated from the phase plot were within the same order of magnitude of their forward counterpart (Figure 4). These results are also evidence of a slow transverse wave propagating backward on the BM. In addition, we found a slow reverse wave propagation in a mechanical model of the cochlea (Figure 5). Since the cochlea prepared through the surgical procedure became a passive one (surgical damage removes the amplification by cochlear outer hair cells), this wave propagation appears to be a fundamental property of the hydromechanical structure of the cochlea. The artificial cochlea, which mimics the basic hydromechanical structure of the cochlea, confirms and supports the essential nature of the slow transverse waves, that is, they exhibit bidirectional propagation.

4.2. Interpretation of No Tonotopicity in Backward Wave Propagation. Although the experimental results in Figure 1 demonstrated the correct phase in reverse propagation, the amplitude response did not show the expected cochlear tonotopicity: the peak-frequency-to-place map [29]. In contrast, there was a slight inversion or reversal of the map, that is, the roll-off frequency is higher at the more apical location and lower at the more basal location. These seemly controversial reverse wave features are simulated by the transmission line model of the cochlea, as shown schematically in Figure 3.

The hydromechanical theory of the cochlea asserts that tonotopicity is achieved with the combination of fluid coupling in the scalae and a local resonance at the BM,

the so-called critical-layer resonance [30]. For a passive cochlea, as used in this study, the hydromechanical structure is the dominant contributor [31]. The passive responses lack sharp tuning and diminish at high frequencies. Therefore, the local resonance is simplified in the model to a capacitor because the resonator is stiffness dominant at the lower frequencies. Acoustic energy in the fluid couples to the BM, whose stiffness decreases from the base to the apex.

Although the stiffness gradient is the most important feature for the tonotopicity [32], a small amount of frequency selectivity can be achieved without it. This process is most easily explained with an electric circuit analogy. The cochlear hydromechanical structure is analogous to a lossy transmission line, as originally proposed by Zwislocki [31]. In a lumped model, the cochlea is divided into a series of connected repeating sections (Figure 3(a)). At each section (Figure 3(b)), the fluid coupling effect was modeled as a series of inductors and resistors, representing the fluid mass and viscosity, respectively [33]; the mechanical impedance of the cochlear partition was modeled as a capacitor, representing the stiffness of the BM. Although the BM is usually modeled as a second-order resonator to account for the sharp tuning of the cochlea, generality is maintained with the simplification to a spring (capacitor in a circuit analogy) to model the passive responses. This simplification is fundamental to Zwislocki's transmission line theory [31] to interpret the passive vibration data observed by von Békésy [34]. With this simplification, the propagation of the BM vibration was described using a wave equation [31]. Each section of the structure applies a low-pass filtering effect onto the vibration of the BM, attenuating the high-frequency components and producing propagation delay. Vibration, originated from either a basal or apical location, will experience the same low-pass filtering sections (Figure 3(c)), but from different directions. Therefore, the high-frequency components of the BM vibration are continuously attenuated, and the phase delay is continuously accumulated during the propagation, no matter which end the wave originates.

Figure 3(d) explains why no cochlear tonotopicity is achieved in reverse propagation. In the forward direction, the stiffness of the cochlear partition decreases in the direction of the propagation. Therefore, the roll-off frequency of the low-pass filtering, implemented by the fluid mass and the stiffness of the partition, becomes lower and lower. Therefore, the high-frequency components of the traveling wave are cut off gradually during the propagation, resulting in the passive cochlear tonotopicity. In the reverse direction, the traveling wave encounters the low-pass section with the lowest roll-off first. Most of the high-frequency components are attenuated at this early section. During the propagation, although the traveling wave will still experience low-pass sections, its already low-passed components will not be further cut off because the roll-off frequencies of the later sections are all higher. The result is that no clear tonotopicity is produced, but the high-frequency components are still slightly attenuated along the direction of propagation.

Despite the significant difference in the amplitude responses, the transmission line-like structure of the cochlea produces a propagation delay in the direction of away from the vibration source, no matter where the vibration source is located. This is shown in both the experimental data in Figure 1(c) and the simulation results in Figure 6(b).

4.3. Validation of the Preparation. Since we opened the cochlea widely and drained the fluid in the scala tympani at the base, we need to ensure that this preparation can still support the wave propagation as a normal cochlea. The single-channel preparation for the measurement of basilar membrane vibration has been used previously [35, 36] and has theoretically been proven to be able to produce forward traveling wave features [37]. LePage [36] used a capacitive probe to measure the BM motion, which required the fluid in the scala tympani to be removed. It was shown that the BM vibration showed similar responses as its dual-channel counterpart. The acoustic driving results in Figure 4 also showed traveling wave features. Therefore, this preparation still maintains the basic hydromechanical structure of the cochlea. The *in vivo* physiological environment in the cochlea is maintained stably so that the mechanical properties provided by the cellular structure of the organ of Corti do not deteriorate during the experiments. Although this preparation is designed to verify the backward traveling wave, it does not preclude the existence of the compression wave, as the intact scala vestibule can still support the compression wave propagation. The open channel at the scala tympani could influence the speed of the compression wave. However, this influence is minimal considering that the speed of the compression wave is two orders of magnitude higher than that of the traveling wave. The BM vibration measurement method used in this study is also essentially the same as that used by He et al. and Ren et al. [3–5]. Therefore, if the compression wave does exist in this preparation, we should be able to observe its effect, as a transverse wave in the forward direction in our experiments.

To ensure that the vibration source in this study is on the BM, we drained the perilymph at the opened portion of the scala tympani and then maintained the fluid at a very low level (~30 μm) with a cotton wick. According to the current theory, it is the vibration generated in the organ of Corti on the BM that initiates the backward traveling wave. The OAE is also generated in the organ of Corti. The stimulus in the fluid may result in a similar effect as the stimulation by the stapes, producing a forward wave. This phenomenon has been demonstrated by von Békésy [38] and termed as the *paradoxical wave*, where even if the stapes is placed at the apex of the cochlea, a forward traveling wave was still observed, moving towards the source.

4.4. Passive or Active Preparation. In this study, the extensive surgery on the cochlea resulted in a loss of sensitivity, so that the preparation was essentially passive. Although loss of cochlear amplification would influence the generation of the OAE, the passive preparation is an advantage in studying the wave propagation. The wave propagation inside the cochlea is mostly determined by the hydromechanical structure, and our preparation preserves the basic hydromechanical components of the cochlea.

The advantage in the use of the passive preparation is that it avoids any phase delay introduced by the active tuning of the cochlea. In a sensitive preparation, active tuning of the cochlea contributes strongly to the measured group delay [20]. Tuning-induced group delay is primarily responsible for the enhancement of the propagation delay in the forward-propagation condition, because the tuning frequency of the cochlea decreases in the forward direction and this frequency gradient produces a phase lag in the same direction. In a sensitive cochlea, artificially driven to produce a backward wave, tuning-induced forward delay may mask the possible backward traveling wave delay. The propagation delay increases while traveling away from the source. However, the tuning delay is determined by the cochlear frequency map and it always increases from the base to the apex, no matter where the source is. Therefore, in the measured phase responses in a backward-traveling-wave study, there are two components that can contribute oppositely to the total delay. This tuning-induced delay could be one way to explain the results of He et al., Ren et al., and Ren [3–6], in which the measured phase delay increased from the base to the apex and thus indicated the absence of a detectable backward traveling wave. In those experiments, however, a very sensitive preparation was usually required by the vibration-source-generation method (acoustically produced distortion product or electrically stimulated emission). The tuning delay may be significant, especially when the vibration at two close locations is compared to determine the direction of the wave propagation [3]. In their study, the measurement range was narrow, and thus, the propagation delay was relatively small, compared to the tuning delay.

5. Conclusions

In this study, we investigated the backward wave propagation inside the cochlea. By creating a vibration source at a precise location, we avoided the uncertainty of the place where the vibration was originated in most previous studies. With measurements at multiple longitudinal locations along the cochlea, we, for the first time, demonstrated a slow backward traveling wave towards the stapes. This result was also confirmed in a mechanical model of the cochlea and interpreted with a traditional transmission line mathematical model.

Data Availability

The data used to support the findings of this study are available from the corresponding author upon request.

Conflicts of Interest

The authors declare that they have no conflicts of interest.

Authors' Contributions

Fangyi Chen and Dingjun Zha designed the experiments; Fangyi Chen analyzed the data; Fangyi Chen, Xiaojie Yang, Allyn Hubbard, and Alfred Nuttall wrote the paper; and all authors helped with the manuscript preparation and revision.

Acknowledgments

The authors would like to thank Drs. Egbert DeBoer, Anders Fridberger, and Sripriya Ramamoorthy for their comments on the manuscript. This work was funded by the National Natural Science Foundation of China (Grant nos. 81470701 and 81771882), the Fundamental Research (Discipline Layout) Foundation from Shenzhen Committee of Science, Technology and Innovation (Grant no. JCYJ20170817111912585), and Deafness Research Foundation for Fangyi Chen; the National Natural Science Foundation of China (Grant nos. 81271077 and 81470695) for Dingjun Zha; and NIDCDR01 (Grant nos. DC000141 and DC010399) for Alfred Nuttall.

References

[1] D. T. Kemp, "Stimulated acoustic emissions from within the human auditory system," *The Journal of the Acoustical Society of America*, vol. 64, no. 5, pp. 1386–1391, 1978.

[2] C. A. Shera and J. J. Guinan Jr, "Evoked otoacoustic emissions arise by two fundamentally different mechanisms: a taxonomy for mammalian OAEs," *The Journal of the Acoustical Society of America*, vol. 105, no. 2, pp. 782–798, 1999.

[3] W. He, A. Fridberger, E. Porsov, K. Grosh, and T. Ren, "Reverse wave propagation in the cochlea," *Proceedings of the National Academy of Sciences of the United States of America*, vol. 105, no. 7, pp. 2729–2733, 2008.

[4] W. He, A. Fridberger, E. Porsov, and T. Ren, "Fast reverse propagation of sound in the living cochlea," *Biophysical Journal*, vol. 98, no. 11, pp. 2497–2505, 2010.

[5] T. Ren, W. He, M. Scott, and A. L. Nuttall, "Group delay of acoustic emissions in the ear," *Journal of Neurophysiology*, vol. 96, no. 5, pp. 2785–2791, 2006.

[6] T. Ren, "Reverse propagation of sound in the gerbil cochlea," *Nature Neuroscience*, vol. 7, no. 4, pp. 333-334, 2004.

[7] C. A. Shera, A. Tubis, and C. L. Talmadge, *Four Counter-Arguments for Slow-Wave OAEs in 9th International Symposium*, A. L. Nuttall, Ed., pp. 449–457, 2015.

[8] H. Zhang and D. C. Mountain, *Concepts and Challenges in the Biophysics of Hearing*, N. P. Cooper and D. T. Kemp, Eds., World Scientific, Singapore, 2009.

[9] E. de Boer, J. Zheng, E. Porsov, and A. L. Nuttall, "Inverted direction of wave propagation (IDWP) in the cochlea," *The Journal of the Acoustical Society of America*, vol. 123, no. 3, pp. 1513–1521, 2008.

[10] Y. Li and K. Grosh, "Direction of wave propagation in the cochlea for internally excited basilar membrane," *The Journal of the Acoustical Society of America*, vol. 131, no. 6, pp. 4710–4721, 2012.

[11] C. A. Shera, "Mechanisms of mammalian otoacoustic emission and their implications for the clinical utility of otoacoustic emissions," *Ear and Hearing*, vol. 25, no. 2, pp. 86–97, 2004.

[12] A. Vetešník and A. W. Gummer, "Transmission of cochlear distortion products as slow waves: a comparison of experimental and model data," *The Journal of the Acoustical Society of America*, vol. 131, no. 5, pp. 3914–3934, 2012.

[13] R. Sisto, A. Moleti, T. Botti, D. Bertaccini, and C. A. Shera, "Distortion products and backward-traveling waves in nonlinear active models of the cochlea," *The Journal of the Acoustical Society of America*, vol. 129, no. 5, pp. 3141–3152, 2011.

[14] S. J. Elliott, G. Ni, B. R. Mace, and B. Lineton, "A wave finite element analysis of the passive cochlea," *The Journal of the Acoustical Society of America*, vol. 133, no. 3, pp. 1535–1545, 2013.

[15] W. Dong and E. S. Olson, "Supporting evidence for reverse cochlear traveling waves," *The Journal of the Acoustical Society of America*, vol. 123, no. 1, pp. 222–240, 2008.

[16] S. W. F. Meenderink and M. van der Heijden, "Reverse cochlear propagation in the intact cochlea of the gerbil: evidence for slow traveling waves," *Journal of Neurophysiology*, vol. 103, no. 3, pp. 1448–1455, 2010.

[17] A. Fridberger and T. Ren, "Local mechanical stimulation of the hearing organ by laser irradiation," *Neuroreport*, vol. 17, no. 1, pp. 33–37, 2006.

[18] C.-P. Richter, B. N. Evans, R. Edge, and P. Dallos, "Basilar membrane vibration in the gerbil hemicochlea," *Journal of Neurophysiology*, vol. 79, no. 5, pp. 2255–2264, 1998.

[19] T. Ren and E. Porsov, "Reverse propagation of sounds in the intact cochlea," *Journal of Neurophysiology*, vol. 104, no. 6, p. 3732, 2010.

[20] M. A. Ruggero and A. N. Temchin, "Similarity of traveling-wave delays in the hearing organs of humans and other tetrapods," *Journal of the Association for Research in Otolaryngology*, vol. 8, no. 2, pp. 153–166, 2007.

[21] R. Ghaffari, A. J. Aranyosi, and D. M. Freeman, "Longitudinally propagating traveling waves of the mammalian tectorial membrane," *Proceedings of the National Academy of Sciences of the United States of America*, vol. 104, no. 42, pp. 16510–16515, 2007.

[22] T. Reichenbach, A. Stefanovic, F. Nin, and A. J. Hudspeth, "Waves on Reissner's membrane: a mechanism for the propagation of otoacoustic emissions from the cochlea," *Cell Reports*, vol. 1, no. 4, pp. 374–384, 2012.

[23] J. Zheng, N. Deo, Y. Zou, K. Grosh, and A. L. Nuttall, "Chlorpromazine alters cochlear mechanics and amplification: in vivo evidence for a role of stiffness modulation in the organ of Corti," *Journal of Neurophysiology*, vol. 97, no. 2, pp. 994–1004, 2007.

[24] M. A. Ruggero, "Comparison of group delays of 2f1−f2 distortion product otoacoustic emissions and cochlear travel times," *Acoustics Research Letters Online*, vol. 5, no. 4, pp. 143–147, 2004.

[25] F. Chen, H. I. Cohen, T. G. Bifano et al., "A hydromechanical biomimetic cochlea: experiments and models," *The Journal of the Acoustical Society of America*, vol. 119, no. 1, pp. 394–405, 2006.

[26] G. Ni, S. J. Elliott, M. Ayat, and P. D. Teal, "Modelling cochlear mechanics," *BioMed Research International*, vol. 2014, no. 7, Article ID 150637, 42 pages, 2014.

[27] L. C. Peterson and B. P. Bogert, "A dynamical theory of the cochlea," *The Journal of the Acoustical Society of America*, vol. 22, no. 3, pp. 369–381, 1950.

[28] S. Puria and C. R. Steele, *The Senses: A Comprehensive Reference*, A. I. Bassbaum, A. Kaneko, G. M. Shepherd, and G. Westheimer, Eds., vol. 3, Ch. Audition, Academic Press, 2008.

[29] D. D. Greenwood, "A cochlear frequency-position function for several species—29 years later," *The Journal of the Acoustical Society of America*, vol. 87, no. 6, pp. 2592–2605, 1990.

[30] J. Lighthill, "Energy flow in the cochlea," *Journal of Fluid Mechanics*, vol. 106, no. 1, pp. 149–213, 1981.

[31] J. Zwislocki, "Theory of the acoustical action of the cochlea," *The Journal of the Acoustical Society of America*, vol. 22, no. 6, pp. 778–784, 1950.

[32] G. Ni, L. Sun, and S. J. Elliott, "A linearly tapered box model of the cochlea," *The Journal of the Acoustical Society of America*, vol. 141, no. 3, pp. 1793–1803, 2017.

[33] G. Ni and S. J. Elliott, "Comparing methods of modeling near field fluid coupling in the cochlea," *The Journal of the Acoustical Society of America*, vol. 137, no. 3, pp. 1309–1317, 2015.

[34] G. V. Békésy, "The variation of phase along the basilar membrane with sinusoidal vibrations," *The Journal of the Acoustical Society of America*, vol. 19, no. 3, pp. 452–460, 1947.

[35] J. P. Wilson and J. R. Johnstone, "Basilar membrane and middle-ear vibration in guinea pig measured by capacitive probe," *The Journal of the Acoustical Society of America*, vol. 57, no. 3, pp. 705–723, 1975.

[36] E. L. LePage, "The application of a capacitive probe technique for direct observation of electromechanical processes in the guinea pig cochlea," *The Journal of the Acoustical Society of America*, vol. 82, no. 1, pp. 126–138, 1987.

[37] R. Patuzzi, "Springer Handbook of Auditory Research," in *The Cochlea*, P. Dallos, Ed., vol. 8, Springer, New York, 1996.

[38] G. v. Békésy, "Paradoxical direction of wave travel along the cochlear partition," *The Journal of the Acoustical Society of America*, vol. 27, no. 1, pp. 137–145, 1955.

Hindawi
Neural Plasticity
Volume 2018, Article ID 3170801, 9 pages
https://doi.org/10.1155/2018/3170801

Review Article

Inner Ear Hair Cell Protection in Mammals against the Noise-Induced Cochlear Damage

Muhammad Waqas,[1,2] Song Gao,[3] Iram-us-Salam,[1] Muhammad Kazim Ali,[1,4] Yongming Ma,[3] and Wenyan Li[5]

[1]*Department of Biotechnology, Federal Urdu University of Arts, Science and Technology, Gulshan-e-Iqbal Campus, Karachi, Pakistan*
[2]*Key Laboratory for Developmental Genes and Human Disease, Ministry of Education, Institute of Life Sciences, Southeast University, Nanjing 210096, China*
[3]*Department of Otolaryngology, Affiliated People's Hospital of Jiangsu University, Zhenjiang 212002, China*
[4]*Karachi Institute of Biotechnology and Genetic Engineering (KIBGE), University of Karachi, Karachi 72570, Pakistan*
[5]*ENT Institute and Department of Otorhinolaryngology of the Affiliated Eye and ENT Hospital, State Key Laboratory of Medical Neurobiology, Fudan University, Shanghai 200031, China*

Correspondence should be addressed to Yongming Ma; maym121@163.com and Wenyan Li; wenyan_li2000@126.com

Received 24 January 2018; Revised 11 April 2018; Accepted 7 May 2018; Published 15 July 2018

Academic Editor: Geng-lin Li

Inner ear hair cells are mechanosensory receptors that perceive mechanical sound and help to decode the sound in order to understand spoken language. Exposure to intense noise may result in the damage to the inner ear hair cells, causing noise-induced hearing loss (NIHL). Particularly, the outer hair cells are the first and the most affected cells in NIHL. After acoustic trauma, hair cells lose their structural integrity and initiate a self-deterioration process due to the oxidative stress. The activation of different cellular death pathways leads to complete hair cell death. This review specifically presents the current understanding of the mechanism exists behind the loss of inner ear hair cell in the auditory portion after noise-induced trauma. The article also explains the recent hair cell protection strategies to prevent the damage and restore hearing function in mammals.

1. Introduction

The inner ear is the most incredible and sophisticated organ of the body. It connects the personnel with the outer world in the form of hearing. The hearing loss is referred to as the most common sensory disorder that affects all age groups of the world population. The complex architecture of the mammalian organ of Corti makes it more susceptible to damage and is difficult to revert back into its native form [1, 2]. Although the neonatal cochlea holds the potential to form new hair cells by transforming the supporting cells (such as Lgr5+ cells) into the hair cells in the apical till basal region [3–6]. This capability completely sheds off in the adult sensory epithelium. Lack of understanding of the mechanical sound voice has a massive impact on a person's ability to communicate and deal with the normal and emergency life situations. It badly affects the patient's mental and physical health as well as makes their life isolated and depressed [7–10]. Such people are more in danger of accidental injuries than others and are completely relying on their attendant [11].

Sensorineural hearing loss (SNHL) is referred to as the most common type of hearing disorder occurs due to the damage or loss of the hair cells, the neuron-hair cell synapses, and/or degeneration of neurons. The SNHL is not completely recoverable due to the lack of self-regenerative capacity of HCs and SGNs. The patients having SNHL may be provided with the hearing aids, and in case of severe to profound hearing loss, the patients have the only option of cochlear implants [12]. However, besides the advancements in the

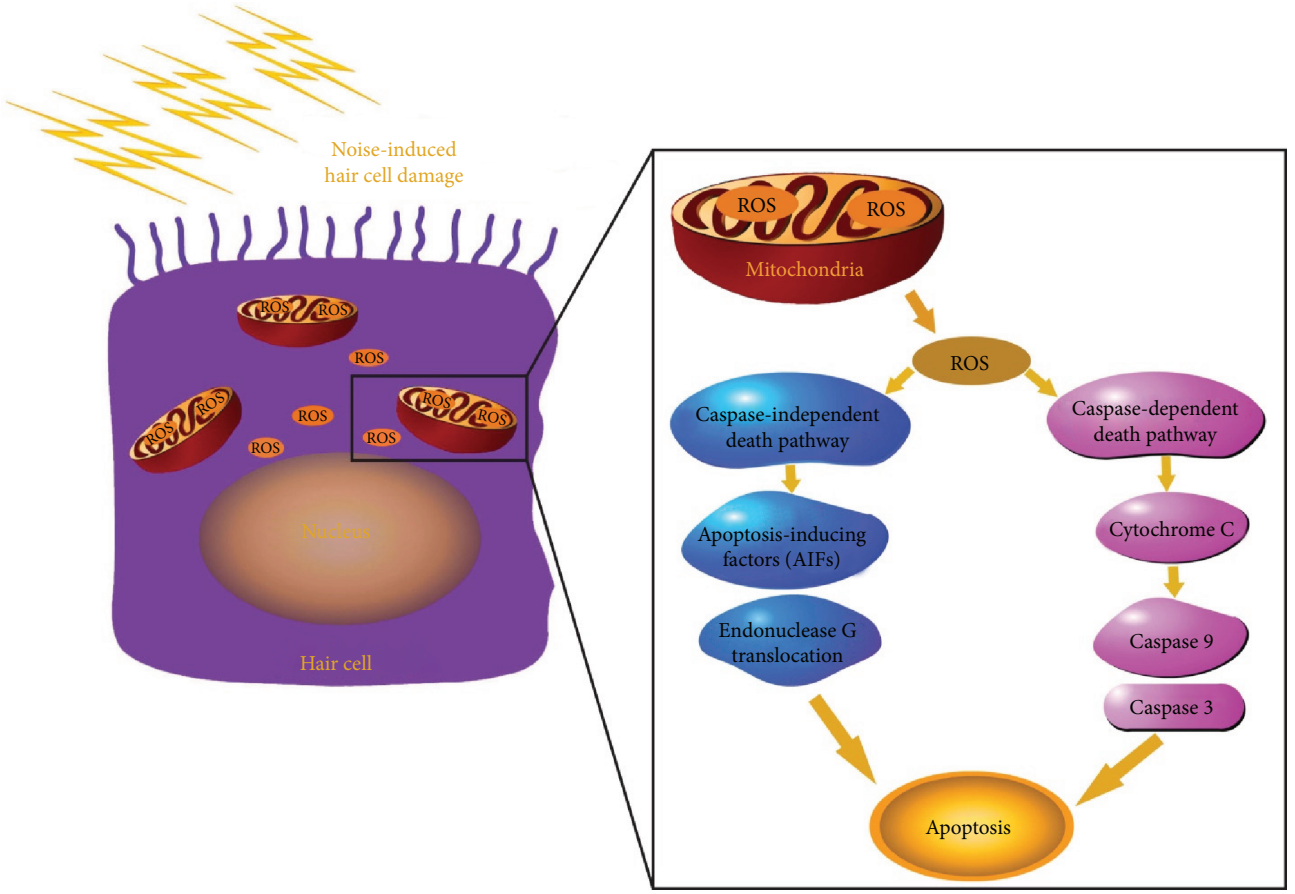

Figure 1: Schematic of the generation of reactive oxygen species (ROS) along with the activation of caspase-mediated and independent death pathways in hair cell after noise-induced oxidative stress.

engineering, surgical, and pharmaceutical operations, normal hearing function yet not completely be restored using hearing devices.

There are multiple etiologies of SNHL. At any age, the foremost reasons for hearing loss are genetic and the environmental factors. The main causes of SNHL are degenerative processes associated with aging, gene mutations, noise exposure, and the use of therapeutic drugs that have ototoxic side effects [13–16]. Interestingly, the noise and the ototoxicity are actually the consequences of men made technological advancements and do not really exist in nature. Other etiologies include the autoimmune disorder, head injury, and the hair cell overstimulation [17–21]. Exposure to intense noise results in the irreversible damage to hair cells via different cellular mechanisms. In this review, we aim to discuss the different mechanisms of hair cell damage and highlight the recent findings as well as possible strategies for hair cell protection against the noise-induced hearing loss.

2. Mechanism of Hair Cell Loss in Mammals after Noise-Induced Trauma

Stereociliary bundles found on the surface of hair cells are more susceptible to mechanical damage. The exposure to intense noise causes direct mechanical disruption of stereociliary structure and disrupts the normal cellular organization of the organ of Corti [22–24]. However, the deepest level of damage is not only because of intense mechanical sound but also depends on different cellular pathways involved in hair cell growth.

2.1. Noise-Induced Oxidative Stress. The reactive oxygen species (ROS) are observed in the hair cells after the acoustic overexposure and exist there for about 10 days [25]. The ROS are produced in the cell mitochondria, and disturbance in the integrity of mitochondria may result in the production and continuous release of ROS in the cell cytoplasm [26, 27]. The generation of reactive oxygen species and the increased metabolic activity in the hair cells after noise-induced ototoxicity have been reported to create hair cell loss (Figure 1) [28–31]. The reactive nitrogen species (RNS) also accumulate in the hair cells after being exposed to loud voices [32, 33]. Both the ROS and RNS have stimulated caspase-mediated apoptotic cell death pathways in the cochlea [30, 34]. Besides, ROS formation also promotes inflammation and generates proinflammatory cytokines such as interleukin (IL) 6 and [35, 36], tumor necrosis factor-α (TNF-α) [37, 38].

2.2. Caspase- and JNK-Dependent Hair Cell Death Pathways. Two complex signaling pathways are commonly involved in

noise-induced hair cell loss that are known as intrinsic and extrinsic cell death signaling pathways. In the cochlea exposed to intense noise, the extracellular stimuli initiate the extrinsic cell death signaling pathway by inducing the transmembrane death receptors. These receptors activate the caspase 8, which further triggers the distinct downstream signaling pathway leading to the activation of caspase 3 that mediates apoptosis in the outer hair cells [39]. The intrinsic death pathway starts in the outer hair cells due to the modifications in the permeability of mitochondrial membrane that stimulates the caspase 9 and releases cytochrome c from mitochondria, thus induces programmed cell death [39, 40]. Together with caspases, the receptor-interacting protein kinase (RIP) is also implicated in the activation of necrotic cell death pathways in the outer hair cells of adult mice exposed to loud noise [41]. Another study has shown that after noise trauma, the c-Jun *N*-terminal kinase (JNK)/mitogen-activated protein kinase (MAPK) also induces a mitochondrial cell death pathway through the stimulation and translocation of Bax and procaspases, release of cytochrome c from mitochondria into the damage cell cytoplasm, and lastly, the cleavage of fodrin by activating caspases [42]. A recent work of Fuentes-Santamaría et al. also determined the permanent hearing threshold shift in response to loud noise overexposure. This shift simultaneously occurred with the outer hair cell loss, upregulation of prestin, and microglial activation. The authors also observed that the TNF-α and interleukin 1β were upregulated by the microglia, fibrocytes, and neuronal cells at different time points in the noise-exposed cochlea [43] suggesting that there is an involvement of complex interplay among the different cytokine-producing cells that might be responsible for cochlear pathophysiology in the noise-exposed cochlea.

2.3. Caspase-Independent Cell Death Pathway. Caspase-independent apoptotic pathway is also involved in the hair cell loss. After the exposure to loud noise, the mitochondria participate in the apoptosis by releasing the apoptosis-inducing factors (AIFs) and endonuclease G (EndoG) through the outer mitochondrial membrane into the hair cell cytoplasm. EndoG translocates to cell nucleus in order to initiate apoptosis while the AIFs may not directly be involved in apoptosis but act as a redox factor in return to noise-induced oxidative stress [44]. However, Han et al. reported that both AIF and EndoG were translocated to the nuclei and participated in the hair cell death [45]. The tumor necrosis factor-α (TNF-α) pathway has also been activated in the noise-induced damage model [34]; however, it is still unclear whether the pathway activation is specifically in the hair cells. According to the study of Bohne et al., three different death pathways were observed in the outer hair cells on the basis of their morphological characteristics after noise-induced auditory damage. Among them, two were the oncotic (swollen cell following rupture) and apoptotic (programmed cell death) pathways whereas in the third death pathway, the outer hair cells lose their basolateral cell membrane but maintain their cytoplasm with cellular debris intact in a cylindrical frame structure [46].

2.4. Excessive Calcium Accumulation in Hair Cells. The acoustic overexposure results in an increase accumulation of free calcium ions in the outer hair cells that enter through the L-type calcium channels and cell intracellular stores such as the mitochondria and endoplasmic reticulum [47, 48]. These free calcium ions independently activate both the necrotic and apoptotic pathways in outer hair cells without any ROS formation [48, 49]. However, the accumulation of calcium after acoustic overexposure in the outer hair cells stimulates the mitochondria-mediated cell death pathways through activation of Bcl-2-associated death promoters (BAD) by calcium-dependent phosphatase calcineurin [50]. This study suggests that the translocation of BAD to the mitochondria of diminishing outer hair cells is an indicator of the activation of its proapoptotic activity.

These studies highlight the possible mechanisms of hair cell loss in a noise-induced cochlear damage model. Besides the fact that the oxidative stress and the activated death pathways after acoustic overexposure detrimentally affect the cochlea, it takes a longer duration to degenerate hair cells after acoustic injury, suggesting that there is a possibility to interrupt this diminishing process in the mammalian cochlea.

2.5. The Genetics of NIHL and the Noise-Induced Synaptopathy. Genetic factors may contribute to the development of noise-induced hearing loss. The individual humans and animals displayed a variation in the susceptibility to noise-induced damage even under controlled conditions. This difference in susceptibility may be influenced by the genetic factors. For the last two decades, several genetic studies were performed to identify the NIHL susceptibility genes and among them various NIHL susceptibility genes have been known to involved in different cellular pathways such as the genes involved in the potassium recycling pathway (Kcnq1, Kcnq4, kcne1, Kcnj10, Gjb1, Gjb2, and Gjb4) [51, 52], oxidative stress gene (Sod2, Cat, Gstm1, and Pon2) [53, 54], heat shock protein genes (Hsp70) [55], and monogenic deafness genes (Myh14 and Pcdh15) [56]. The variation in these genes has shown to be associated with the susceptibility to noise-induced hearing loss in different populations [57]. Similarly, several studies in the transgenic mice model showed that the deficit in different cellular pathway genes increases the susceptibility of the inner ear to acoustic overexposure. Many homozygous and heterozygous mice, including Cdh23 [58], Pmca2 [59], Sod1 [60], Gpx1 [61], Trpv4 [62], and Hsf1 [63, 64] knockout mice, have been shown to be more sensitive to noise-induced hearing loss than the other wild-type strains.

Apart from this, recent studies also highlight that the synapse degeneration in the inner ear is another key contributor of NIHL. The synapsis between the inner hair cells and spiral ganglion neurons is more prone to cellular damage [65]. Glutamate excitotoxicity and calcium signaling pathways are considered as a candidate in cochlear synaptopathy. The excessive release of glutamate results in a synaptic destruction between inner hair cells and spiral ganglion neurons [66]. This excessive glutamate concentration further leads to the huge influx of calcium, sodium, and

potassium ions into the spiral ganglion neurons that ultimately swell and damage the synaptic structures [67–69]. Moreover, L-type and T-type calcium channels also participated to excessive calcium influx after noise-induced damage [70, 71]. However, the role of different signaling pathways and the exact mechanism of cochlear synaptopathy are not completely understood yet and need further investigations in the future.

3. Strategies for Hair Cell Protection in Mammals against the Noise-Induced Hearing Loss

Various strategies have been defined to protect inner ear hair cells from acoustic damage. Some of the useful external protective measures are to reduce the exposure of loud noise by eliminating the basic source of the noise. However, it is not possible to take this measure in all the conditions, particularly in the areas of high noise pollution such as in the industrial world. Therefore, the use of hearing protection devices is recommended and in somewhat effective to reduce the acoustic damage. Multiple studies have suggested the use of hearing protection devices that significantly reduce the loud noise exposure, thus minimizing the risk of hearing loss in the industrial workers [72–74]. However, the use of hearing protection devices sometimes creates a barrier in the communication and discomfort for the user if the device is not completely fit externally.

Besides the external measures of hearing protection, the otoprotective treatment on a cellular level is mainly focused for the prevention of hair cell loss and induction of the self-repair mechanism to restore auditory function. The most effective strategies used to prevent hair cell loss after noise-induced damage are: (1) use of antioxidants, (2) inhibition of programmed cell death pathways, (3) anti-inflammatory therapies, and (4) neurotrophic factors.

3.1. Antioxidant Treatment. Antioxidants are the potential therapeutics used to protect inner ear hair cells from acoustic damage. The oral administration of antioxidant drugs such as 4-hydroxy-alpha-phenyl-*tert*-butylnitrone (4-OHPBN) and N-acetyl-L-cysteine (NAC) after acoustic overexposure significantly reduces the noise-induced hearing loss [75]. Another study reported the use of two antioxidants (disodium 2,4-disulfophenyl-N-*tert*-butylnitrone and NAC) in combination that also protected the hair cells and afferent neurites from noise-induced damage and preserved the cochlear structural components [76]. In addition, the prior studies also reported that the NAC is an effective antioxidant that provides otoprotection against the noise-induced hearing loss in animal models [77–81]. Similarly, multiple studies in humans also reported the little significant and protective effects of NAC on hearing preservation [82–84]. The oral administration of NAC during the continuous acoustic overexposure prevents the noise-induced temporary threshold shift (TTS) following 14 days of treatment as compared to the control group [82–84]. However, Kramer et al. demonstrated that before the loud noise exposure, the oral administration of NAC alone does not have any significant otoprotective effects on the inner ear [83]. Kopke et al. worked on a large military group exposed to loud noise for 16 days and observed 6-7% reduction in the hearing threshold shift after daily oral administration of NAC [85]. Collectively, these studies highlight the beneficiary effects of NAC against the noise-induced hearing loss. Moreover, some other antioxidants are also effective to prevent the noise-induced trauma, such as synthetic organoselenium drug ebselen [86], coenzyme Q10 [87], resveratrol [88], glutathione [89], ginseng [82], D-methionine [90], and vitamins A, C, E, and B12 [91–95]. The detailed clinical trials of different pharmaceutical agents including antioxidant, against the noise-induced hearing loss, are thoroughly reviewed recently [96, 97]. These antioxidants are still in their preliminary trial phases and must subjected to further investigation in the future.

3.2. Inhibition of Programmed Cell Death Pathways. Manipulation of intrinsic cell death cascades using different antiapoptotic inhibitors is also a promising strategy to protect hair cells after the noise-induced hearing loss. Multiple studies have shown the activation of MAPK/JNK pathways in cellular stress response. The blocking of this pathway using the JNK inhibitory molecules in the animal model provides significant protection against the acoustic trauma [98, 99]. Similarly, the administration of the JNK inhibitor through the round window prevents hair cell death caused by the acoustic overexposure and restores hearing in an animal model in a dose dependent manner [42]. The sound trauma could potentially be minimized by the otoprotective peptide AM-111 that is also a JNK inhibitor [100, 101]. The systemic or local administration of AM-111 after impulse noise exposure provides significant protection against the noise-induced hearing loss [102]. Likewise, the subcutaneous administration of CEP-1347 (a derivative of indolocarbazole K252a and a JNK pathway inhibitor) has shown the less hearing threshold shift in the guinea pig exposed to noise [103]. The post sound exposure treatment of retinoic acid (a potent JNK pathway inhibitor) for five days in mice showed a reduced hearing threshold shift and hearing deterioration [91]. Together, these studies suggested that the use of apoptotic inhibitor is a potential therapeutic intervention in noise-induced hearing loss; however, further clinical trials are needed to form a combinative antiapoptotic strategy to treat noise-induced hearing loss.

3.3. Anti-Inflammatory Agents. Several types of anti-inflammatory drugs have been reported to rescue the hearing deterioration in the inner ear induced by the sound overexposure. Particularly, the use of steroids such as dexamethasone and dehydroepiandrosterone reduces the noise-induced trauma in the guinea pig and mice models [104–107]. The higher intratympanic dose administration of dexamethasone efficiently preserves the hearing in mice than the intraperitoneal administration against the noise trauma. The intratympanic administration is more effective for the efferent terminal outer hair cell synapses, while intraperitoneal administration protects the organ of Corti in a mouse model suggesting that the otoprotective effects

are different if the route and dose of administration are changed [108]. As compared to intratympanic administration of steroids alone, the early concurrent administration of intratympanic steroid injections and systemic steroids preserves the hearing capability of patients more appropriately after sound trauma caused by the gunshot noise [109]. Overall, these studies highlight the effective concurrent intratympanic and systemic steroid treatment against the acoustic damage that protects the hearing and structural integrity of the cochlea. However, the long-term use of steroids may cause several adverse effects on human body.

3.4. Neurotrophin-3 (NT-3) and Brain-Derived Neurotrophic Factor (BDNF). Although the neurotrophins are the key regulators for differentiation, survival, and maintenance of neuronal cells, several studies have reported their otoprotective role against the noise-induced hearing loss [110–113]. Neurotrophin-3 (NT3) and brain-derived neurotrophic factor (BDNF) are well known to participate in the development and establishment of hair cell ribbon synapses in the inner ear [111]. After noise-induced damage, NT3 expression by associated supporting cells promotes the ribbon synapse regeneration and restores their function in the cochlea [110, 111]. Surprisingly, a single dose of neurotrophins (NT3 + BDNF) delivers through the round window protects the hair cell and lessens the synaptopathy after the noise-induced trauma in guinea pigs [112]. In summary, these studies explain the potential therapeutic use of neurotrophins in the animal model. However, further research is still required to explore the potential and study the long-term effects of neurotrophins in the human model.

4. Future Perspective

It is very fascinating to observe that several strategies and drugs have been discovered to protect the inner ear hair cells from acoustic damage. A common strategy in recent years appears to target and manipulate the programmed cell death pathways and involves the use of antioxidants to control the oxidative stress in hair cells. After noise-induced ototoxic damage, there are different signaling pathways activated in the cochlea that induce hair cell death. The interruption in one of these death signaling cascades by specific inhibitor might not be that effective to rescue the auditory function until the multiple drugs or molecular inhibitors are not used in combination. The cellular cascades are interlinked with each other, and there is a possibility that the inhibition of one pathway with specific inhibitor might result in the activation of other cell death pathways in hair cells. Thus, a synergistic approach would be more beneficial to restore the hearing loss.

As reviewed above, to study the noise-induced hearing loss in the animal model, the researchers used various approaches such as different animal species, sound intensity, frequency spectrum, and continuous or impulse noise. This sometime creates a conflict among the results of some drug studies that have found to be otoprotective by one group while reported as ineffective by the other group. The most probable reason for these conflicts is the difference between genetic backgrounds of different animal species that have different sensitivities to intense sound; thus, there is a possibility for different responses of same drug in different animal models. It is important to understand that the majority of animal studies showed a statistically significant impact when the protective drug reduces the hearing loss by 2-3 decibels (dB). However, in humans, this shift should be more than 10 dB to be effective for the auditory performance, and the hearing below this level may have a very less impact on person hearing capability. Therefore, in the future, it is important to first perform the otoprotective therapeutic experiments in different animal models with different acoustic exposure conditions before taking it into the clinical trials.

5. Conclusion

In recent years, research on the noise-induced hearing loss is focused in order to develop various therapeutic strategies for appropriate protection of hair cells from any damage and to restore the auditory function after acoustic trauma. The momentum builts up by these studies on the effectiveness of different otoprotective agents such as the antioxidants, anti-inflammatory agents, and neurotrophic factors, and manipulation of the intrinsic cell death pathways in hair cells will likely drive the complete development of therapeutic interventions for restoring the noise-induced hearing loss in the future. However, identification of the optimal conditions such as the dose regimen, effective route of administration, and timings for new drugs and their synergistic plans to treat sound-induced hearing loss in patients is important to be focused in the future experiments.

Conflicts of Interest

The authors declare that they have no competing interests.

Authors' Contributions

Muhammad Waqas and Song Gao contributed equally to this work.

Acknowledgments

The authors appreciate the Higher Education Commission (HEC) of Pakistan for their support and valuable assistance to the institute.

References

[1] T. Moser and A. Starr, "Auditory neuropathy—neural and synaptic mechanisms," *Nature Reviews Neurology*, vol. 12, no. 3, pp. 135–149, 2016.

[2] R. Mittal, D. Nguyen, A. P. Patel et al., "Recent advancements in the regeneration of auditory hair cells and hearing restoration," *Frontiers in Molecular Neuroscience*, vol. 10, p. 236, 2017.

[3] R. Chai, B. Kuo, T. Wang et al., "Wnt signaling induces proliferation of sensory precursors in the postnatal mouse cochlea," *Proceedings of the National Academy of Sciences*, vol. 109, no. 21, pp. 8167–8172, 2012.

[4] M. Waqas, L. Guo, S. Zhang et al., "Characterization of Lgr5+ progenitor cell transcriptomes in the apical and basal turns of the mouse cochlea," *Oncotarget*, vol. 7, no. 27, pp. 41123–41141, 2016.

[5] B. C. Cox, R. Chai, A. Lenoir et al., "Spontaneous hair cell regeneration in the neonatal mouse cochlea *in vivo*," *Development*, vol. 141, no. 4, pp. 816–829, 2014.

[6] M. Waqas, S. Zhang, Z. He, M. Tang, and R. Chai, "Role of Wnt and notch signaling in regulating hair cell regeneration in the cochlea," *Frontiers of Medicine*, vol. 10, no. 3, pp. 237–249, 2016.

[7] C. C. Tseng, L. Y. Hu, M. E. Liu, A. C. Yang, C. C. Shen, and S. J. Tsai, "Risk of depressive disorders following sudden sensorineural hearing loss: a nationwide population-based retrospective cohort study," *Journal of Affective Disorders*, vol. 197, pp. 94–99, 2016.

[8] N. C. Homans, R. M. Metselaar, J. G. Dingemanse et al., "Prevalence of age-related hearing loss, including sex differences, in older adults in a large cohort study," *Laryngoscope*, vol. 127, no. 3, pp. 725–730, 2017.

[9] A. M. Goman, N. S. Reed, and F. R. Lin, "Addressing estimated hearing loss in adults in 2060," *JAMA Otolaryngology Head & Neck Surgery*, vol. 143, no. 7, pp. 733-734, 2017.

[10] L. W. Sun, R. D. Johnson, C. S. Langlo et al., "Assessing photoreceptor structure in retinitis pigmentosa and Usher syndrome," *Investigative Ophthalmology & Visual Science*, vol. 57, no. 6, pp. 2428–2442, 2016.

[11] S. L. Smith and M. K. Pichora-Fuller, "Associations between speech understanding and auditory and visual tests of verbal working memory: effects of linguistic complexity, task, age, and hearing loss," *Frontiers in Psychology*, vol. 6, 2015.

[12] G. M. Sprinzl and H. Riechelmann, "Current trends in treating hearing loss in elderly people: a review of the technology and treatment options–a mini-review," *Gerontology*, vol. 56, no. 3, pp. 351–358, 2010.

[13] V. A. McHaney, G. Thibadoux, F. A. Hayes, and A. A. Green, "Hearing loss in children receiving cisplatin chemotherapy," *The Journal of Pediatrics*, vol. 102, no. 2, pp. 314–317, 1983.

[14] L. P. Rybak, "Drug ototoxicity," *Annual Review of Pharmacology and Toxicology*, vol. 26, no. 1, pp. 79–99, 1986.

[15] J. Schacht, "Molecular mechanisms of drug-induced hearing loss," *Hearing Research*, vol. 22, no. 1–3, pp. 297–304, 1986.

[16] L. L. Cunningham and D. L. Tucci, "Hearing loss in adults," *The New England Journal of Medicine*, vol. 377, no. 25, pp. 2465–2473, 2017.

[17] M. B. Said, M.'h. Grati, T. Ishimoto et al., "A mutation in *SLC22A4* encoding an organic cation transporter expressed in the cochlea strial endothelium causes human recessive non-syndromic hearing loss DFNB60," *Human Genetics*, vol. 135, no. 5, pp. 513–524, 2016.

[18] D. N. Furness, "Molecular basis of hair cell loss," *Cell and Tissue Research*, vol. 361, no. 1, pp. 387–399, 2015.

[19] A. F. Goodall and M. A. Siddiq, "Current understanding of the pathogenesis of autoimmune inner ear disease: a review," *Clinical Otolaryngology*, vol. 40, no. 5, pp. 412–419, 2015.

[20] T. Mijovic, A. Zeitouni, and I. Colmegna, "Autoimmune sensorineural hearing loss: the otology–rheumatology interface," *Rheumatology*, vol. 52, no. 5, pp. 780–789, 2013.

[21] R. Mittal, C. V. Lisi, R. Gerring et al., "Current concepts in the pathogenesis and treatment of chronic suppurative otitis media," *Journal of Medical Microbiology*, vol. 64, no. 10, pp. 1103–1116, 2015.

[22] M. C. Liberman and D. G. Beil, "Hair cell condition and auditory nerve response in normal and noise-damaged cochleas," *Acta Oto-Laryngologica*, vol. 88, no. 1–6, pp. 161–176, 1979.

[23] N. Slepecky, "Overview of mechanical damage to the inner ear: noise as a tool to probe cochlear function," *Hearing Research*, vol. 22, no. 1–3, pp. 307–321, 1986.

[24] R. B. Patuzzi, G. K. Yates, and B. M. Johnstone, "Outer hair cell receptor current and sensorineural hearing loss," *Hearing Research*, vol. 42, no. 1, pp. 47–72, 1989.

[25] H. Yamane, Y. Nakai, M. Takayama et al., "The emergence of free radicals after acoustic trauma and strial blood flow," *Acta Oto-Laryngologica*, vol. 115, Supplement 519, pp. 87–92, 1995.

[26] C. Batandier, X. Leverve, and E. Fontaine, "Opening of the mitochondrial permeability transition pore induces reactive oxygen species production at the level of the respiratory chain complex I," *Journal of Biological Chemistry*, vol. 279, no. 17, pp. 17197–17204, 2004.

[27] T. Huang, A. G. Cheng, H. Stupak et al., "Oxidative stress-induced apoptosis of cochlear sensory cells: otoprotective strategies," *International Journal of Developmental Neuroscience*, vol. 18, no. 2-3, pp. 259–270, 2000.

[28] Y. Ohinata, J. M. Miller, R. A. Altschuler, and J. Schacht, "Intense noise induces formation of vasoactive lipid peroxidation products in the cochlea," *Brain Research*, vol. 878, no. 1-2, pp. 163–173, 2000.

[29] A. R. Fetoni, P. de Bartolo, S. L. M. Eramo et al., "Noise-induced hearing loss (NIHL) as a target of oxidative stress-mediated damage: cochlear and cortical responses after an increase in antioxidant defense," *The Journal of Neuroscience*, vol. 33, no. 9, pp. 4011–4023, 2013.

[30] B. H. Hu, D. Henderson, and T. M. Nicotera, "Involvement of apoptosis in progression of cochlear lesion following exposure to intense noise," *Hearing Research*, vol. 166, no. 1-2, pp. 62–71, 2002.

[31] D. Henderson, E. C. Bielefeld, K. C. Harris, and B. H. Hu, "The role of oxidative stress in noise-induced hearing loss," *Ear and Hearing*, vol. 27, no. 1, pp. 1–19, 2006.

[32] D. Yamashita, H. Y. Jiang, J. Schacht, and J. M. Miller, "Delayed production of free radicals following noise exposure," *Brain Research*, vol. 1019, no. 1-2, pp. 201–209, 2004.

[33] D. Yamashita, H. Y. Jiang, C. G. le Prell, J. Schacht, and J. M. Miller, "Post-exposure treatment attenuates noise-induced hearing loss," *Neuroscience*, vol. 134, no. 2, pp. 633–642, 2005.

[34] B. H. Hu, Q. Cai, S. Manohar et al., "Differential expression of apoptosis-related genes in the cochlea of noise-exposed rats," *Neuroscience*, vol. 161, no. 3, pp. 915–925, 2009.

[35] K. Wakabayashi, M. Fujioka, S. Kanzaki et al., "Blockade of interleukin-6 signaling suppressed cochlear inflammatory response and improved hearing impairment in noise-damaged mice cochlea," *Neuroscience Research*, vol. 66, no. 4, pp. 345–352, 2010.

[36] M. Fujioka, S. Kanzaki, H. J. Okano, M. Masuda, K. Ogawa, and H. Okano, "Proinflammatory cytokines expression in noise-induced damaged cochlea," *Journal of Neuroscience Research*, vol. 83, no. 4, pp. 575–583, 2006.

[37] E. M. Keithley, X. Wang, and G. C. Barkdull, "Tumor necrosis factor α can induce recruitment of inflammatory cells to the

cochlea," *Otology & Neurotology*, vol. 29, no. 6, pp. 854–859, 2008.

[38] H. Satoh, G. S. Firestein, P. B. Billings, J. P. Harris, and E. M. Keithley, "Tumor necrosis factor-α, an initiator, and etanercept, an inhibitor of cochlear inflammation," *The Laryngoscope*, vol. 112, no. 9, pp. 1627–1634, 2002.

[39] T. M. Nicotera, B. H. Hu, and D. Henderson, "The caspase pathway in noise-induced apoptosis of the chinchilla cochlea," *Journal of the Association for Research in Otolaryngology*, vol. 4, no. 4, pp. 466–477, 2003.

[40] T. R. Van De Water, F. Lallemend, A. A. Eshraghi et al., "Caspases, the enemy within, and their role in oxidative stress-induced apoptosis of inner ear sensory cells," *Otology & Neurotology*, vol. 25, no. 4, pp. 627–632, 2004.

[41] H.-W. Zheng, J. Chen, and S.-H. Sha, "Receptor-interacting protein kinases modulate noise-induced sensory hair cell death," *Cell Death & Disease*, vol. 5, no. 5, article e1262, 2014.

[42] J. Wang, J. Ruel, S. Ladrech, C. Bonny, T. van de Water, and J. L. Puel, "Inhibition of the c-Jun N-terminal kinase-mediated mitochondrial cell death pathway restores auditory function in sound-exposed animals," *Molecular Pharmacology*, vol. 71, no. 3, pp. 654–666, 2007.

[43] V. Fuentes-Santamaría, J. C. Alvarado, P. Melgar-Rojas, M. C. Gabaldón-Ull, J. M. Miller, and J. M. Juiz, "The role of glia in the peripheral and central auditory system following noise overexposure: contribution of TNF-α and IL-1β to the pathogenesis of hearing loss," *Frontiers in Neuroanatomy*, vol. 11, 2017.

[44] D. Yamashita, J. M. Miller, H. Y. Jiang, S. B. Minami, and J. Schacht, "AIF and EndoG in noise-induced hearing loss," *Neuroreport*, vol. 15, no. 18, pp. 2719–2722, 2004.

[45] W. Han, X. Shi, and A. L. Nuttall, "AIF and endoG translocation in noise exposure induced hair cell death," *Hearing Research*, vol. 211, no. 1-2, pp. 85–95, 2006.

[46] B. A. Bohne, G. W. Harding, and S. C. Lee, "Death pathways in noise-damaged outer hair cells," *Hearing Research*, vol. 223, no. 1-2, pp. 61–70, 2007.

[47] A. Fridberger, A. Flock, M. Ulfendahl, and B. Flock, "Acoustic overstimulation increases outer hair cell Ca^{2+} concentrations and causes dynamic contractions of the hearing organ," *Proceedings of the National Academy of Sciences*, vol. 95, no. 12, pp. 7127–7132, 1998.

[48] S. Orrenius, B. Zhivotovsky, and P. Nicotera, "Regulation of cell death: the calcium-apoptosis link," *Nature Reviews Molecular Cell Biology*, vol. 4, no. 7, pp. 552–565, 2003.

[49] J. E. Gale, V. Piazza, C. D. Ciubotaru, and F. Mammano, "A mechanism for sensing noise damage in the inner ear," *Current Biology*, vol. 14, no. 6, pp. 526–529, 2004.

[50] M. A. Vicente-Torres and J. Schacht, "A BAD link to mitochondrial cell death in the cochlea of mice with noise-induced hearing loss," *Journal of Neuroscience Research*, vol. 83, no. 8, pp. 1564–1572, 2006.

[51] M. Pawelczyk, L. van Laer, E. Fransen et al., "Analysis of gene polymorphisms associated with K ion circulation in the inner ear of patients susceptible and resistant to noise-induced hearing loss," *Annals of Human Genetics*, vol. 73, no. 4, pp. 411–421, 2009.

[52] L. Van Laer, P. I. Carlsson, N. Ottschytsch et al., "The contribution of genes involved in potassium-recycling in the inner ear to noise-induced hearing loss," *Human Mutation*, vol. 27, no. 8, pp. 786–795, 2006.

[53] P. M. Rabinowitz, J. Pierce Wise Sr., B. Hur Mobo, P. G. Antonucci, C. Powell, and M. Slade, "Antioxidant status and hearing function in noise-exposed workers," *Hearing Research*, vol. 173, no. 1-2, pp. 164–171, 2002.

[54] G. Fortunato, E. Marciano, F. Zarrilli et al., "Paraoxonase and superoxide dismutase gene polymorphisms and noise-induced hearing loss," *Clinical Chemistry*, vol. 50, no. 11, pp. 2012–2018, 2004.

[55] M. Yang, H. Tan, Q. Yang et al., "Association of hsp70 polymorphisms with risk of noise-induced hearing loss in Chinese automobile workers," *Cell Stress & Chaperones*, vol. 11, no. 3, pp. 233–239, 2006.

[56] A. Konings, L. van Laer, A. Wiktorek-Smagur et al., "Candidate gene association study for noise-induced hearing loss in two independent noise-exposed populations," *Annals of Human Genetics*, vol. 73, no. 2, pp. 215–224, 2009.

[57] M. Sliwinska-Kowalska and M. Pawelczyk, "Contribution of genetic factors to noise-induced hearing loss: a human studies review," *Mutation Research/Reviews in Mutation Research*, vol. 752, no. 1, pp. 61–65, 2013.

[58] R. H. Holme and K. P. Steel, "Progressive hearing loss and increased susceptibility to noise-induced hearing loss in mice carrying a *Cdh23* but not a *Myo7a* mutation," *Journal of the Association for Research in Otolaryngology*, vol. 5, no. 1, pp. 66–79, 2004.

[59] P. J. Kozel, R. R. Davis, E. F. Krieg, G. E. Shull, and L. C. Erway, "Deficiency in plasma membrane calcium ATPase isoform 2 increases susceptibility to noise-induced hearing loss in mice," *Hearing Research*, vol. 164, no. 1-2, pp. 231–239, 2002.

[60] K. K. Ohlemiller, S. L. McFadden, D. L. Ding et al., "Targeted deletion of the cytosolic Cu/Zn-superoxide dismutase gene (*Sod1*) increases susceptibility to noise-induced hearing loss," *Audiology and Neurotology*, vol. 4, no. 5, pp. 237–246, 1999.

[61] K. K. Ohlemiller, S. L. McFadden, D. L. Ding, P. M. Lear, and Y. S. Ho, "Targeted mutation of the gene for cellular glutathione peroxidase (*Gpx1*) increases noise-induced hearing loss in mice," *Journal of the Association for Research in Otolaryngology*, vol. 1, no. 3, pp. 243–254, 2000.

[62] K. Tabuchi, M. Suzuki, A. Mizuno, and A. Hara, "Hearing impairment in TRPV4 knockout mice," *Neuroscience Letters*, vol. 382, no. 3, pp. 304–308, 2005.

[63] D. A. Fairfield, M. I. Lomax, G. A. Dootz et al., "Heat shock factor 1-deficient mice exhibit decreased recovery of hearing following noise overstimulation," *Journal of Neuroscience Research*, vol. 81, no. 4, pp. 589–596, 2005.

[64] K. Sugahara, S. Inouye, H. Izu et al., "Heat shock transcription factor HSF1 is required for survival of sensory hair cells against acoustic overexposure," *Hearing Research*, vol. 182, no. 1-2, pp. 88–96, 2003.

[65] M. Kobel, C. G. le Prell, J. Liu, J. W. Hawks, and J. Bao, "Noise-induced cochlear synaptopathy: past findings and future studies," *Hearing Research*, vol. 349, pp. 148–154, 2017.

[66] G. Wan, M. E. Gómez-Casati, A. R. Gigliello, M. C. Liberman, and G. Corfas, "Neurotrophin-3 regulates ribbon synapse density in the cochlea and induces synapse regeneration after acoustic trauma," *eLife*, vol. 3, 2014.

[67] J. L. Puel, R. Pujol, F. Tribillac, S. Ladrech, and M. Eybalin, "Excitatory amino acid antagonists protect cochlear auditory

neurons from excitotoxicity," *Journal of Comparative Neurology*, vol. 341, no. 2, pp. 241–256, 1994.

[68] J.-L. Puel, J. Ruel, C. G. d'Aldin, and R. Pujol, "Excitotoxicity and repair of cochlear synapses after noise-trauma induced hearing loss," *Neuroreport*, vol. 9, no. 9, pp. 2109–2114, 1998.

[69] C. G. Le Prell, M. Yagi, K. Kawamoto et al., "Chronic excitotoxicity in the guinea pig cochlea induces temporary functional deficits without disrupting otoacoustic emissions," *The Journal of the Acoustical Society of America*, vol. 116, no. 2, pp. 1044–1056, 2004.

[70] J. Bao, M. Hungerford, R. Luxmore et al., "Prophylactic and therapeutic functions of drug combinations against noise-induced hearing loss," *Hearing Research*, vol. 304, pp. 33–40, 2013.

[71] B. J. Kopecky, R. Liang, and J. Bao, "T-type calcium channel blockers as neuroprotective agents," *Pflügers Archiv-European Journal of Physiology*, vol. 466, no. 4, pp. 757–765, 2014.

[72] T. W. Frederiksen, C. H. Ramlau-Hansen, Z. A. Stokholm et al., "Noise-induced hearing loss–a preventable disease? Results of a 10-year longitudinal study of workers exposed to occupational noise," *Noise & Health*, vol. 19, no. 87, pp. 103–111, 2017.

[73] J. H. Verbeek, E. Kateman, T. C. Morata, W. A. Dreschler, and C. Mischke, "Interventions to prevent occupational noise-induced hearing loss: a Cochrane systematic review," *International Journal of Audiology*, vol. 53, Supplement 2, pp. S84–S96, 2014.

[74] R. P. el Dib, J. L. Mathew, and R. H. Martins, "Interventions to promote the wearing of hearing protection," *Cochrane Database of Systematic Reviews*, vol. 4, 2012.

[75] J. Lu, W. Li, X. du et al., "Antioxidants reduce cellular and functional changes induced by intense noise in the inner ear and cochlear nucleus," *Journal of the Association for Research in Otolaryngology*, vol. 15, no. 3, pp. 353–372, 2014.

[76] C.-H. Choi, X. Du, R. A. Floyd, and R. D. Kopke, "Therapeutic effects of orally administrated antioxidant drugs on acute noise-induced hearing loss," *Free Radical Research*, vol. 48, no. 3, pp. 264–272, 2014.

[77] E. C. Bielefeld, R. D. Kopke, R. L. Jackson, J. K. M. Coleman, J. Liu, and D. Henderson, "Noise protection with N-acetyl-L-cysteine (NAC) using a variety of noise exposures, NAC doses, and routes of administration," *Acta Oto-Laryngologica*, vol. 127, no. 9, pp. 914–919, 2007.

[78] J. Coleman, X. Huang, J. Liu, R. Kopke, and R. Jackson, "Dosing study on the effectiveness of salicylate/N-acetylcysteine for prevention of noise-induced hearing loss," *Noise and Health*, vol. 12, no. 48, pp. 159–165, 2010.

[79] A. R. Fetoni, R. Piacentini, A. Fiorita, G. Paludetti, and D. Troiani, "Water-soluble coenzyme Q10 formulation (Q-ter) promotes outer hair cell survival in a guinea pig model of noise induced hearing loss (NIHL)," *Brain Research*, vol. 1257, pp. 108–116, 2009.

[80] G. Lorito, P. Giordano, J. Petruccelli, A. Martini, and S. Hatzopoulos, "Different strategies in treating noise-induced hearing loss with N-acetylcysteine," *Medical Science Monitor*, vol. 14, no. 8, pp. BR159–BR164, 2008.

[81] R. P. Hamernik, W. Qiu, and B. Davis, "The effectiveness of N-acetyl-L-cysteine (L-NAC) in the prevention of severe noise-induced hearing loss," *Hearing Research*, vol. 239, no. 1-2, pp. 99–106, 2008.

[82] A. Doosti, Y. Lotfi, A. Moossavi, E. Bakhshi, A. H. Talasaz, and A. Hoorzad, "Comparison of the effects of N-acetylcysteine and ginseng in prevention of noise induced hearing loss in male textile workers," *Noise and Health*, vol. 16, no. 71, pp. 223–227, 2014.

[83] S. Kramer, L. Dreisbach, J. Lockwood et al., "Efficacy of the antioxidant N-acetylcysteine (NAC) in protecting ears exposed to loud music," *Journal of the American Academy of Audiology*, vol. 17, no. 4, pp. 265–278, 2006.

[84] A.-C. Lindblad, Å. Olofsson, U. Rosenhall, and B. Hagerman, "The efficacy of N-acetylcysteine to protect the human cochlea from subclinical hearing loss caused by impulse noise: a controlled trial," *Noise and Health*, vol. 13, no. 55, pp. 392–401, 2011.

[85] R. Kopke, M. D. Slade, R. Jackson et al., "Efficacy and safety of N-acetylcysteine in prevention of noise induced hearing loss: a randomized clinical trial," *Hearing Research*, vol. 323, pp. 40–50, 2015.

[86] A. Pourbakht and T. Yamasoba, "Ebselen attenuates cochlear damage caused by acoustic trauma," *Hearing Research*, vol. 181, no. 1-2, pp. 100–108, 2003.

[87] P. Staffa, J. Cambi, C. Mezzedimi, D. Passali, and L. Bellussi, "Activity of coenzyme Q_{10} (Q-Ter multicomposite) on recovery time in noise-induced hearing loss," *Noise and Health*, vol. 16, no. 72, pp. 265–269, 2014.

[88] M. Seidman, S. Babu, W. Tang, E. Naem, and W. S. Quirk, "Effects of resveratrol on acoustic trauma," *Otolaryngology—-Head and Neck Surgery*, vol. 129, no. 5, pp. 463–470, 2003.

[89] T. Yamasoba, C. Harris, F. Shoji, R. J. Lee, A. L. Nuttall, and J. M. Miller, "Influence of intense sound exposure on glutathione synthesis in the cochlea," *Brain Research*, vol. 804, no. 1, pp. 72–78, 1998.

[90] K. C. M. Campbell, R. P. Meech, J. J. Klemens et al., "Prevention of noise- and drug-induced hearing loss with D-methionine," *Hearing Research*, vol. 226, no. 1-2, pp. 92–103, 2007.

[91] H. J. Shim, H. H. Kang, J. H. Ahn, and J. W. Chung, "Retinoic acid applied after noise exposure can recover the noise-induced hearing loss in mice," *Acta Oto-Laryngologica*, vol. 129, no. 3, pp. 233–238, 2009.

[92] S. L. McFadden, J. M. Woo, N. Michalak, and D. Ding, "Dietary vitamin C supplementation reduces noise-induced hearing loss in guinea pigs," *Hearing Research*, vol. 202, no. 1-2, pp. 200–208, 2005.

[93] N. Kapoor, R. Shyam, A. P. Singh, K. V. Mani, R. K. Sharma, and W. Selvamurthy, "Effect of vitamin E supplementation on carbogen-induced amelioration of noise induced hearing loss in man," *Noise and Health*, vol. 13, no. 55, pp. 452–458, 2011.

[94] F. Hou, S. Wang, S. Zhai, Y. Hu, W. Yang, and L. He, "Effects of α-tocopherol on noise-induced hearing loss in guinea pigs," *Hearing Research*, vol. 179, no. 1-2, pp. 1–8, 2003.

[95] A. Quaranta, A. Scaringi, R. Bartoli, M. A. Margarito, and N. Quaranta, "The effects of 'supra-physiological' vitamin B12 administration on temporary threshold shift. Efectos de la administración "supra-fisiológica" de vitamina B12 sobre el cambio temporal de umbrales," *International Journal of Audiology*, vol. 43, no. 3, pp. 162–165, 2004.

[96] S.-H. Sha and J. Schacht, "Emerging therapeutic interventions against noise-induced hearing loss," *Expert Opinion on Investigational Drugs*, vol. 26, no. 1, pp. 85–96, 2017.

[97] M. G. Crowson, R. Hertzano, and D. L. Tucci, "Emerging therapies for sensorineural hearing loss," *Otology & Neurotology*, vol. 38, no. 6, pp. 792–803, 2017.

[98] J. Wang, T. R. van de Water, C. Bonny, F. de Ribaupierre, J. L. Puel, and A. Zine, "A peptide inhibitor of c-Jun N-terminal kinase protects against both aminoglycoside and acoustic trauma-induced auditory hair cell death and hearing loss," *The Journal of Neuroscience*, vol. 23, no. 24, pp. 8596–8607, 2003.

[99] A. A. Eshraghi and T. R. Van De Water, "Cochlear implantation trauma and noise-induced hearing loss: apoptosis and therapeutic strategies," *The Anatomical Record*, vol. 288A, no. 4, pp. 473–481, 2006.

[100] M. Suckfuell, M. Canis, S. Strieth, H. Scherer, and A. Haisch, "Intratympanic treatment of acute acoustic trauma with a cell-permeable JNK ligand: a prospective randomized phase I/II study," *Acta Oto-Laryngologica*, vol. 127, no. 9, pp. 938–942, 2007.

[101] M. Suckfuell, G. Lisowska, W. Domka et al., "Efficacy and safety of AM-111 in the treatment of acute sensorineural hearing loss: a double-blind, randomized, placebo-controlled phase II study," *Otology & Neurotology*, vol. 35, no. 8, pp. 1317–1326, 2014.

[102] J. K. M. Coleman, C. Littlesunday, R. Jackson, and T. Meyer, "AM-111 protects against permanent hearing loss from impulse noise trauma," *Hearing Research*, vol. 226, no. 1-2, pp. 70–78, 2007.

[103] U. Pirvola, L. Xing-Qun, J. Virkkala et al., "Rescue of hearing, auditory hair cells, and neurons by CEP-1347/KT7515, an inhibitor of c-Jun N-terminal kinase activation," *The Journal of Neuroscience*, vol. 20, no. 1, pp. 43–50, 2000.

[104] K. Takemura, M. Komeda, M. Yagi et al., "Direct inner ear infusion of dexamethasone attenuates noise-induced trauma in guinea pig," *Hearing Research*, vol. 196, no. 1-2, pp. 58–68, 2004.

[105] K. Tabuchi, H. Murashita, T. Tobita et al., "Dehydroepiandrosterone sulfate reduces acoustic injury of the guinea-pig cochlea," *Journal of Pharmacological Sciences*, vol. 99, no. 2, pp. 191–194, 2005.

[106] L. Chen, C. Dean, M. Gandolfi, E. Nahm, L. Mattiace, and A. H. Kim, "Dexamethasone's effect in the retrocochlear auditory centers of a noise-induced hearing loss mouse model," *Otolaryngology–Head and Neck Surgery*, vol. 151, no. 4, pp. 667–674, 2014.

[107] S. S. Gumrukcu, İ. Topaloglu, Z. Salturk et al., "Effects of intratympanic dexamethasone on noise-induced hearing loss: an experimental study," *American Journal of Otolaryngology*, vol. 39, no. 1, pp. 71–73, 2018.

[108] M. A. Han, S. A. Back, H. L. Kim, S. Y. Park, S. W. Yeo, and S. N. Park, "Therapeutic effect of dexamethasone for noise-induced hearing loss: systemic versus intratympanic injection in mice," *Otology & Neurotology*, vol. 36, no. 5, pp. 755–762, 2015.

[109] Y.-S. Chang, K. H. Bang, B. Jeong, and G. G. Lee, "Effects of early intratympanic steroid injection in patients with acoustic trauma caused by gunshot noise," *Acta Oto-Laryngologica*, vol. 137, no. 7, pp. 716–719, 2017.

[110] L. L. Cunningham and D. L. Tucci, "Restoring synaptic connections in the inner ear after noise damage," *New England Journal of Medicine*, vol. 372, no. 2, pp. 181-182, 2015.

[111] G. Wan, M. E. Gómez-Casati, A. R. Gigliello, M. C. Liberman, and G. Corfas, "Neurotrophin-3 regulates ribbon synapse density in the cochlea and induces synapse regeneration after acoustic trauma," *eLife*, vol. 3, article e03564, 2014.

[112] D. J. Sly, L. Campbell, A. Uschakov, S. T. Saief, M. Lam, and S. J. O'Leary, "Applying neurotrophins to the round window rescues auditory function and reduces inner hair cell synaptopathy after noise-induced hearing loss," *Otology & Neurotology*, vol. 37, no. 9, pp. 1223–1230, 2016.

[113] F. Shoji, A. L. Miller, A. Mitchell, T. Yamasoba, R. A. Altschuler, and J. M. Miller, "Differential protective effects of neurotrophins in the attenuation of noise-induced hair cell loss," *Hearing Research*, vol. 146, no. 1-2, pp. 134–142, 2000.

Hindawi
Neural Plasticity
Volume 2018, Article ID 3989201, 16 pages
https://doi.org/10.1155/2018/3989201

Research Article

N-Methyl-D-Aspartate Receptors Involvement in the Gentamicin-Induced Hearing Loss and Pathological Changes of Ribbon Synapse in the Mouse Cochlear Inner Hair Cells

Juan Hong,[1,2] Yan Chen,[1,3] Yanping Zhang,[1,3] Jieying Li,[1,3] Liujie Ren,[1,3] Lin Yang,[1,3] Lusen Shi,[4] Ao Li,[4] Tianyu Zhang,[1,3] Huawei Li,[1,3,5,6] and Peidong Dai[1,3]

[1]*ENT Institute and Otorhinolaryngology Department of Affiliated Eye and ENT Hospital, State Key Laboratory of Medical Neurobiology, Fudan University, Shanghai 200031, China*
[2]*Department of Otorhinolaryngology-Head and Neck Surgery, Huashan Hospital, Fudan University, Shanghai 200040, China*
[3]*NHC Key Laboratory of Hearing Medicine, Fudan University, Shanghai 200031, China*
[4]*Department of Otolaryngology Head and Neck Surgery, Affiliated Drum Tower Hospital of Nanjing University Medical School, Jiangsu Provincial Key Medical Discipline (Laboratory), Nanjing 210008, China*
[5]*Institutes of Biomedical Sciences, The Institutes of Brain Science and the Collaborative Innovation Center for Brain Science, Fudan University, Shanghai 200032, China*
[6]*Shanghai Engineering Research Centre of Cochlear Implant, Shanghai 200031, China*

Correspondence should be addressed to Huawei Li; hwli@shmu.edu.cn and Peidong Dai; daipeidongent@163.com

Received 12 March 2018; Accepted 17 May 2018; Published 15 July 2018

Academic Editor: Geng-lin Li

Cochlear inner hair cell (IHC) ribbon synapses play an important role in sound encoding and neurotransmitter release. Previous reports show that both noise and aminoglycoside exposures lead to reduced numbers and morphologic changes of synaptic ribbons. In this work, we determined the distribution of N-methyl-D-aspartate receptors (NMDARs) and their role in the gentamicin-induced pathological changes of cochlear IHC ribbon synaptic elements. In normal mature mouse cochleae, the majority of NMDARs were distributed on the modiolar side of IHCs and close to the IHC nuclei region, while most of synaptic ribbons and α-amino-3-hydroxy-5-methyl-4-isoxazolepropionic acid receptor (AMPAR) were located on neural terminals closer to the IHC basal poles. After gentamicin exposure, the NMDARs increased and moved towards the IHC basal poles. At the same time, synaptic ribbons and AMPARs moved toward the IHC bundle poles on the afferent dendrites. The number of ribbon synapse decreased, and this was accompanied by increased auditory brainstem response thresholds and reduced wave I amplitudes. NMDAR antagonist MK801 treatment reduced the gentamicin-induced hearing loss and the pathological changes of IHC ribbon synapse, suggesting that NMDARs were involved in gentamicin-induced ototoxicity by regulating the number and distribution of IHC ribbon synapses.

1. Introduction

Cochlear inner hair cell (IHC) ribbon synapses play an important role in sound encoding and glutamate release. The IHC ribbon synapses are the first afferent synaptic connection in the hearing pathway, and they are located between the IHCs and the terminals of spiral ganglion neurons (SGNs). Bursts of synaptic activity are induced through periodic excitation of IHCs by mechanisms that are intrinsic to the cochlea [1], resulting in IHC Ca^{2+} spikes, glutamate release, and ultimately bursts of action potentials in SGNs that are carried to the brain by auditory nerve fibers. Cochlear synaptic ribbon pairs consist of presynaptic ribbons, to which many synaptic vesicles are connected, and postsynaptic α-amino-3-hydroxy-5-methyl-4-isoxazolepropionic acid receptors (AMPARs), which are glutamate receptors that mediate the excitatory postsynaptic currents of the SGNs' afferent dendrites [2].

Cochlear ribbon synapses are very sensitive to aminoglycoside and noise-induced injury [3–6]. Liberman et al. reported the reorganization of synaptic ribbon locations, the loss of synaptic ribbons, and the downregulation of AMPAR expression in the peripheral terminals after noise exposure [7]. Liu et al. found that moderate ototoxicity in mice leads to reduced numbers and morphologic changes in the synaptic ribbons, which are accompanied by mild hearing loss but no significant loss of HCs or SGNs in the cochlea [8]. However, the mechanism behind these pathological changes in cochlear IHC ribbon synapse remains unclear.

In the mammalian inner ear, almost all SGNs express another glutamate receptor, N-methyl-D-aspartate receptor (NMDAR), in addition to AMPAR [9–12]. In the developing cochlea, NMDARs in the IHC-SGN synapses enhance the spontaneous activity and promote the survival of SGNs [13]. NMDARs have also been shown to be involved in regulating the number of surface AMPARs on the cell membrane of auditory neurons in cultured neurons and to be involved in the response to acoustic stimulation [14]. However, the function of NMDARs was not clear in the IHC-SGN synapses of the mature cochlea.

Several studies suggest that NMDARs play a role in ototoxicity in the cochlea [15–17]. Aminoglycosides generate excess free radicals in the cochlea that damage both sensory HCs and SGNs, resulting in permanent hearing loss [18]. By using a severe hearing loss model with a large dose of aminoglycoside, in which both HCs and SGNs were severely injured, Basile et al. demonstrated that the NMDA antagonist dizocilpine maleate (MK801) could attenuate aminoglycoside-induced damage to SGNs and IHCs [15]. However, in this severe hearing loss model, the detailed pathological changes in the afferent synaptic connection between the IHCs and SGNs could not be evaluated due to the extensive injury to the HCs and SGNs. In this study, we used a low dose of gentamicin (100 mg/kg bodyweight) [3, 8, 19] to obtain a mild hearing loss model in which most of the HCs survived. We systematically analyzed the detailed morphological configuration, distribution, and number of presynaptic ribbons, postsynaptic AMPARs, and NMDARs in the cochlear IHC-SGN synapses of adult mice. To determine the role of NMDARs in the IHC-SGN synaptic plasticity in response to ototoxicity, we used the NMDAR antagonist MK801, which prevented gentamicin-induced injury to the IHC ribbon synapse and thus prevented hearing loss *in vivo*.

2. Materials and Methods

2.1. Animals. In total, 30 female C57BL/6J mice with documented dates of birth (5 weeks old) were obtained from the Chinese Academy of Medical Sciences Animal Center (Shanghai, China). All mice were housed with free access to food and water at the Experimental Animal Center, Shanghai Medical College of Fudan University, China. No outer or middle ear pathologies were observed. The animals were divided randomly into three groups. The first group was injected daily with a low dose of gentamicin (100 mg/kg, Sigma-Aldrich, USA) in saline intraperitoneally (i.p.) for 4 or 7 consecutive days [3, 8, 19, 20]. The second group of animals received daily i.p. injections of gentamicin (100 mg/kg in saline) and the NMDAR antagonist MK801 (0.2 mg/kg in saline, Sigma-Aldrich, USA) for 4 or 7 consecutive days [17, 21, 22]. The mice in the third group served as the control group and received daily injections of equivalent volumes of normal saline. This study was carried out in strict accordance with the "Guiding Directive for Humane Treatment of Laboratory Animals" issued by the Chinese National Ministry of Science and Technology in September 2006. We performed all animal procedures according to protocols that were approved by the Shanghai Medical Experimental Animal Administrative Committee and were consistent with the National Institute of Health's Guide for the Care and Use of Laboratory Animals. All efforts were made to minimize suffering and reduce the number of animals used [23].

2.2. Assessment of Auditory Function. Auditory brainstem response (ABR) tests were performed in a sound-attenuating chamber to determine auditory thresholds. Animals were anesthetized via i.p. injections with ketamine (100 mg/kg) and xylazine (25 mg/kg). Specific auditory stimuli (clicks and 4, 8, 16, and 24 kHz tone bursts) were measured using a Tucker-Davis Technology System 3 (Tucker-Davis Technologies, Gainesville, FL, USA) as described previously [23, 24]. ABR stimuli consisted of 5 ms tone pips with a 0.5 ms rise-fall time delivered at 30 stimuli. The ABR threshold was defined as the lowest stimulus level at which a repeatable morphology could be identified in the response waveform (at least two consistent peaks). The ABR wave I peak-to-peak amplitude was computed by off-line analysis of stored waveforms as previous studies [12, 25]. All ABR tests were performed on mice on the following day after the injections with gentamicin alone or in combination with MK-801 (i.e., ABR was performed on day 5 or day 8).

2.3. Cochlear Tissue Processing and Immunostaining. After the ABR recordings, the mice were sacrificed by cervical dislocation and then decapitated. The temporal bone was removed, and the cochlea was quickly separated. The round and oval windows were opened and perfused with 4% paraformaldehyde in phosphate-buffered saline (PBS) at pH 7.4 and postfixed in the same solution for 2 h at room temperature. All cochleae were decalcified in 10% ethylene diamine tetraacetic acid (EDTA) solution. As quickly as possible, the cochlear shell and spiral ligament were removed under a dissecting microscope in 0.01 mM PBS solution. The vestibular membrane and tectorial membrane were removed from the basal membrane. The apical, middle, and basal turns from the cochlear basilar membrane were processed for immunofluorescent staining with antibodies against myosin 7a. Considering the fact that ribbon synapses near the basal turn of the cochlea are most susceptible to ototoxicity exposure [3, 8, 19], in this paper, only the synaptic elements of the cochlear middle-basal turn (51%–75% of the cochlear length from the apex) were quantified to determine the gentamicin-induced synaptic pathology.

Specimens were blocked with 10% donkey serum in 10 mM PBS with 0.3% Triton X-100 for 1 h at room temperature and then incubated with primary antibody for 48 h at

4°C. The primary antibodies included mouse anti-C-terminal-binding protein-2 (CtBP2) (612044; BD Biosciences, USA) at 1 : 500 dilution; mouse anti-glutamate receptor 2, extracellular, clone 6C4 (GluA2) (MAB397; Millipore, Germany) at 1 : 2000 dilution; rabbit anti-NMDAR1 (GluN1) (AB9864R; Millipore, Germany) at 1 : 1000 dilution; chicken anti-200 kD neurofilament heavy chain (NF) (cat. number ab72996; Abcam, UK) at 1 : 1500 dilution; and rabbit anti-myosin 7a polyclonal (Proteus BioSciences, USA) at 1 : 500 dilution. On the following day, the appropriate Alexa Fluor-conjugated secondary antibodies were incubated overnight at 4°C. Nuclear staining was performed with DAPI (1 : 800 dilution; Sigma-Aldrich, USA). Negative controls were performed by omitting the primary antibodies [26–28].

2.4. Confocal Microscopy Imaging. For confocal microscopy imaging, a laser scanning confocal microscope was used (SP5; Leica Microsystems, Biberach, Germany) with a 63x oil immersion objective lens. Excitation wavelengths were 488, 568, and 647 nm, and local images were magnified digitally by 2.74-fold. In each region, 10 to 12 IHCs were typically assessed. Sequence scanning was performed at an interval of 0.50 μm [27]. The laser excitation power and microscope emission and detection settings were maintained across different observations. The resulting confocal image series (z-stack) contained a three-dimensional (3D) record of the imaged information in the entire volume of the explant. The 3D-reconstructed z-stack was viewed, rotated, and "sliced" to provide final images and movies as necessary using the software from a TCS SP8 confocal laser-scanning microscope (Leica, Heidelberg, Germany).

2.5. Synapse Counts and Positioning Analysis. The contrast and brightness of the images were processed using Adobe Photoshop CS6. Synapse counts from the confocal images were performed using ImageJ (NIH, USA). The ribbon pairs were identified by the positive colocalization for double staining with CtBP2 and GluA2. Immunofluorescently identified AMPAR patches and NMDAR patches were counted at afferent nerve fibers (ANFs). All IHCs observed in 2 or 3 image fields were counted [26, 27]. The total numbers of puncta and patches were divided by the total numbers of IHC nuclei to obtain the average number of ribbons and glutamate receptors for each IHC. To describe the distribution of ribbons in IHCs and glutamate receptors (AMPARs and NMDARs) in afferent dendritic terminals, the concepts of basal and bundle poles of IHCs were introduced [29]. To count the number of synaptic elements, we drew one line along the top of the IHC nuclei and another line along the bottom of the inner spiral bundles (ISBs). Then the field between these two lines was divided into two parts, the "IHC nuclei region" and "IHC basal pole region." As shown in Figure 1(d), the IHC nuclei region was defined as the half region proximal to the nuclei and the bundle poles of the IHCs, and the IHC basal pole region was defined as the half region proximal to the ISBs and the basal poles of IHCs. The synaptic elements located between the IHC nuclei region and IHC bundle pole were also counted within the IHC nuclei region for convenience.

2.6. Statistical Analysis. All data are shown as means ± SE. Statistical analyses were conducted using Microsoft Excel and GraphPad Prism® 6 software. In all experiments, n represents the number of replicates. Two-tailed, unpaired Student's t-tests were used to determine statistical significance when comparing two groups, and one-way ANOVA followed by Dunnett's multiple comparisons test was used when comparing more than two groups. A value of $p < 0.05$ was considered to indicate statistical significance.

3. Results

3.1. The Distributions of Ribbons, NMDARs, and AMPARs at the IHC-SGN Synaptic Connection in the Mature Cochlea under Physiological Conditions. We first evaluated the morphological features, distribution, and numbers of ribbons, NMDARs, and AMPARs in the IHC-SGN synaptic connection of the adult mouse cochlea. CtBP2 was used as a marker of presynaptic ribbons. GluN1 and GluA2 were used as markers of NMDARs and AMPARs, respectively. Consistent with a previous study [2], in normal mature cochleae, the CtBP2-positive IHC ribbons were distributed on the cell membrane at the basal poles of IHCs, close to the ISBs (Figures 2(a)–2(e)). The ISBs appeared as a dense meshwork of neuronal processes around the basal poles of the IHCs (Figures 2(b)–2(e)), and these mostly included radially directed dendritic terminals of afferent type I ANFs and the efferent fibers [27, 30].

We observed different distributions of NMDARs and AMPARs at the IHC-SGN synapses in normal mature cochleae. In order to quantify these synaptic elements, we defined the IHC nuclei region and IHC basal pole region (see Figures 1(a) and 1(d) and Materials and Methods). The majority of GluA2-positive AMPAR patches were observed in ISBs, which were found in the basal pole region of IHCs (Figures 1(a)–1(e)), while most of GluN1-positive NMDAR patches were distributed on the neural dendritic terminals that were closer to the IHC nuclei region (Figures 1(c) and 1(e)). In the IHC nuclei region, some NMDARs colocalized with GluA2-positive AMPAR puncta, which were smaller than the AMPAR patches in the IHC basal pole region. Counts of NMDARs in the mature mouse cochlear middle-basal turn yielded averages of 1.00 ± 0.22 and 5.40 ± 0.27 per IHC in the IHC basal pole region and the IHC nuclei region, respectively (Supplementary Table 2). The average numbers of AMPARs were 13.70 ± 0.42 and 1.20 ± 0.13 per IHC in the IHC basal pole region and the IHC nuclei region, respectively (Supplementary Table 1). The 3D-reconstructed images showed that in normal mature mouse cochleae, the majority of NMDARs were distributed on the modiolar side of IHCs and close to the IHC nuclei region, while the AMPARs were distributed at the IHC basal pole region, on the modiolar and pillar sides of IHCs (Figures 1(f) and 1(g) and Supplemental video 1).

3.2. A Low Dose of Gentamicin-Induced Moderate Hearing Loss and the Rearrangement of Cochlear IHC-SGN Synaptic Elements. In order to determine the mechanisms of synaptic pathology, the same dose of gentamicin (100 mg/kg) as

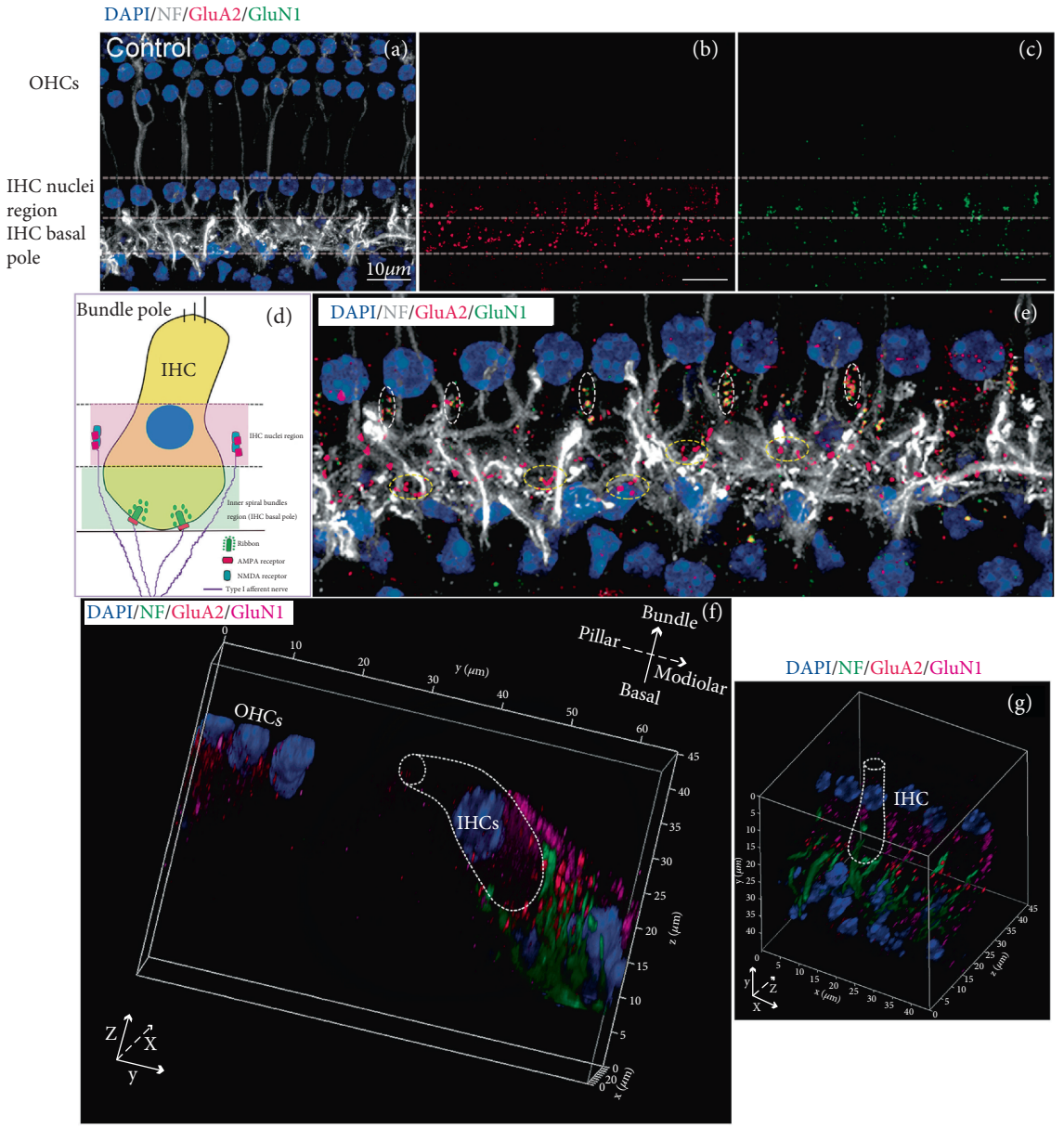

Figure 1: The different distributions of NMDARs and AMPARs at afferent dendritic terminals around IHCs in the normal mature cochlea. Postsynaptic AMPARs, NMDARs, and nerve fibers were identified by immunostaining for GluA2 (red), GluN1 (green), and neurofilament (NF) (grey), respectively. Nuclei were labeled with DAPI (blue). (a) The ISBs appeared as a dense meshwork of neuronal processes at the basal pole region of the IHCs. (b) AMPAR patches were mostly distributed among the ISBs around the basal poles of the IHCs. (c) Most of the NMDAR patches were distributed on the neural dendritic terminals, which were near the IHC nuclei region. (d) A diagram of the different locations of NMDARs and AMPARs at type I ANFs under physiological conditions. To count the number of synaptic elements, we drew one line along the top of the IHC nuclei and another line along the bottom of the ISBs. Then the field between these two lines was divided into two parts, the "IHC nuclei region" and the "IHC basal pole region." The IHC nuclei region was defined as the half region proximal to the nuclei and the bundle poles of the IHCs, and the IHC basal pole region was defined as the half region proximal to the ISBs and the basal poles of the IHCs. (e) Enlarged view of merged images (a), (b), and (c). Most of the NMDAR patches were distributed on the neural dendritic terminals between the adjoining IHCs and closer to the IHC nuclei region, while most of the AMPAR patches were observed among the ISBs around the basal poles of the IHCs. In the IHC nuclei region, some NMDARs colocalized with GluA2-positive AMPAR puncta (the dashed white circles), which were smaller than AMPAR patches in the IHC basal pole region (the dashed yellow circles). (f, g) The 3D-reconstructed images showing spatial distributions of AMPARs and NMDARs in SGN fibers around the IHCs. Postsynaptic AMPARs, NMDARs, and nerve fibers were identified by immunostaining for GluA2 (red), GluN1 (magenta), and NF (green), respectively. Nuclei were labeled with DAPI (blue). IHC: inner hair cell; OHC: outer hair cell; ISBs: inner spiral bundles; ANFs: afferent nerve fibers. Scale bar = 10 μm.

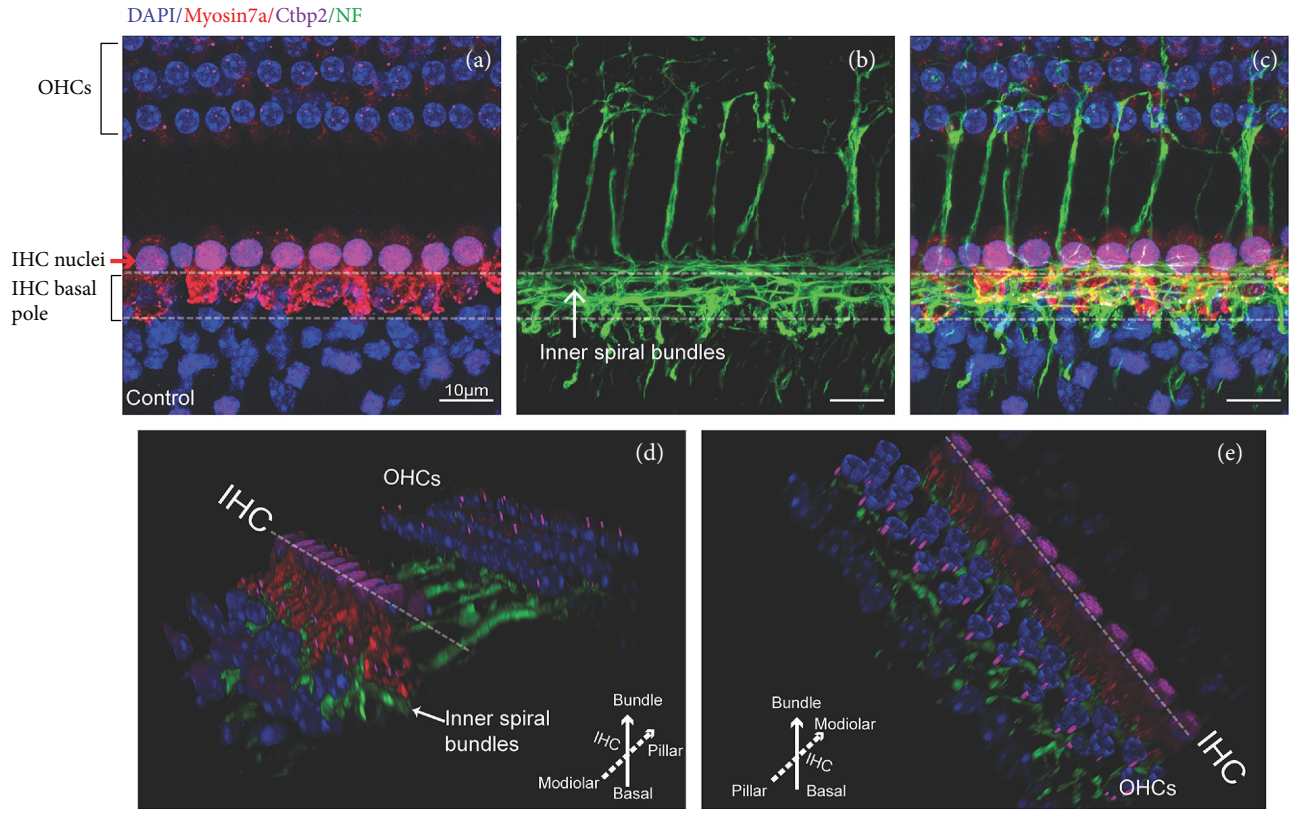

Figure 2: Spatial distribution of cochlear ribbons in IHCs and their relationship with inner spiral bundles in the normal mouse mature cochlea. The HCs, presynaptic ribbons, and nerve fibers were identified by immunostaining for myosin 7a (red), Ctbp2 (magenta), and neurofilament (NF) (green), respectively. Nuclei were labeled with DAPI (blue). (a) Ctbp2-positive ribbons (magenta puncta) were distributed at the basal poles of the IHCs and below the IHC nuclei. The IHC nuclei are marked with a red arrow. (b) NF staining showed that the ISBs appeared as nets of nerve fibers that include radially directed dendritic terminals of type I ANFs and efferent fibers of the olivocochlear system. (c) Merged images of (a) and (b). The IHC basal poles were surrounded by ISBs. (d, e) The 3D-reconstructed images showing the spatial relation among IHCs, presynaptic ribbons, and ISBs. (d) View from the modiolar side to the pillar side. (e) View from the pillar side to the modiolar side. IHC: inner hair cell; OHC: outer hair cell; ISBs: inner spiral bundles; ANFs: afferent nerve fibers. Scar bar = 10 μm.

used in previous studies was applied to the mice in this study [3, 8, 19]. Briefly, mice were injected daily with gentamicin (100 mg/kg) for 4 or 7 consecutive days, and mice receiving injections of normal saline served as controls. ABR tests were performed on the following day after gentamicin injections for 4 or 7 days. The mice were sacrificed, and the cochleae were isolated for immunostaining. Consistent with these previous reports [3, 8], we also found that a low dose of ototoxic gentamicin (100 mg/kg) led to moderate hearing loss and that this was associated with pathological changes in the presynaptic ribbons but with intact HCs and SGNs. Myosin 7a staining showed no obvious HC loss in any of the three turns after gentamicin treatment; however, moderate elevations in ABR thresholds for clicks and tone bursts at 4, 8, 16, and 24 kHz were found in the gentamicin-treated group ($p < 0.05$, Figures 3(a)–3(f)). The amplitude of ABR wave I, reflecting the synchronous summated neural activity of the auditory nerve and functional level of IHC synapses between IHCs and terminals of SGNs [25, 31], was significantly reduced in gentamicin-treated mice (Figure 3(g), $p < 0.05$).

In normal mature cochleae, CtBP2-positive presynaptic ribbons were paired to GluA2-positive postsynaptic AMPARs, and the paired CtBP2/GluA2 double-positive patches were defined as "ribbon synaptic pairs." In undamaged mouse cochleae, most of the ribbon synaptic pairs were distributed around the basal poles of the IHCs (Figure 4(a)). The average numbers of ribbon synaptic pairs were 13.30 ± 0.37 and 0.80 ± 0.10 per IHC in the IHC basal pole region and the IHC nuclei region, respectively, in the control group (Supplementary Table 1). In the gentamicin-treated group, the number of ribbon synaptic pairs was significantly decreased. Moreover, presynaptic ribbons and postsynaptic AMPARs were relocated toward the IHC bundle poles, some of which reached to or across the IHC nuclei region (Figures 4(b) and 4(c) and Supplemental Videos 3 and 4).

In the IHC basal pole region, gentamicin treatment induced a significant decrease in the number of ribbons (13.30 ± 0.37, 6.40 ± 0.37, and 4.20 ± 0.23 in the control, 4-day gentamicin, and 7-day gentamicin groups, resp.) (Figure 4(e) and Supplementary Table 1). The average number of AMPARs was also significantly decreased in the IHC basal pole region in gentamicin-treated cochleae compared with the control group (13.70 ± 0.42, 7.20 ± 0.39, and 5.50 ± 0.37 in the control, 4-day gentamicin, and 7-day

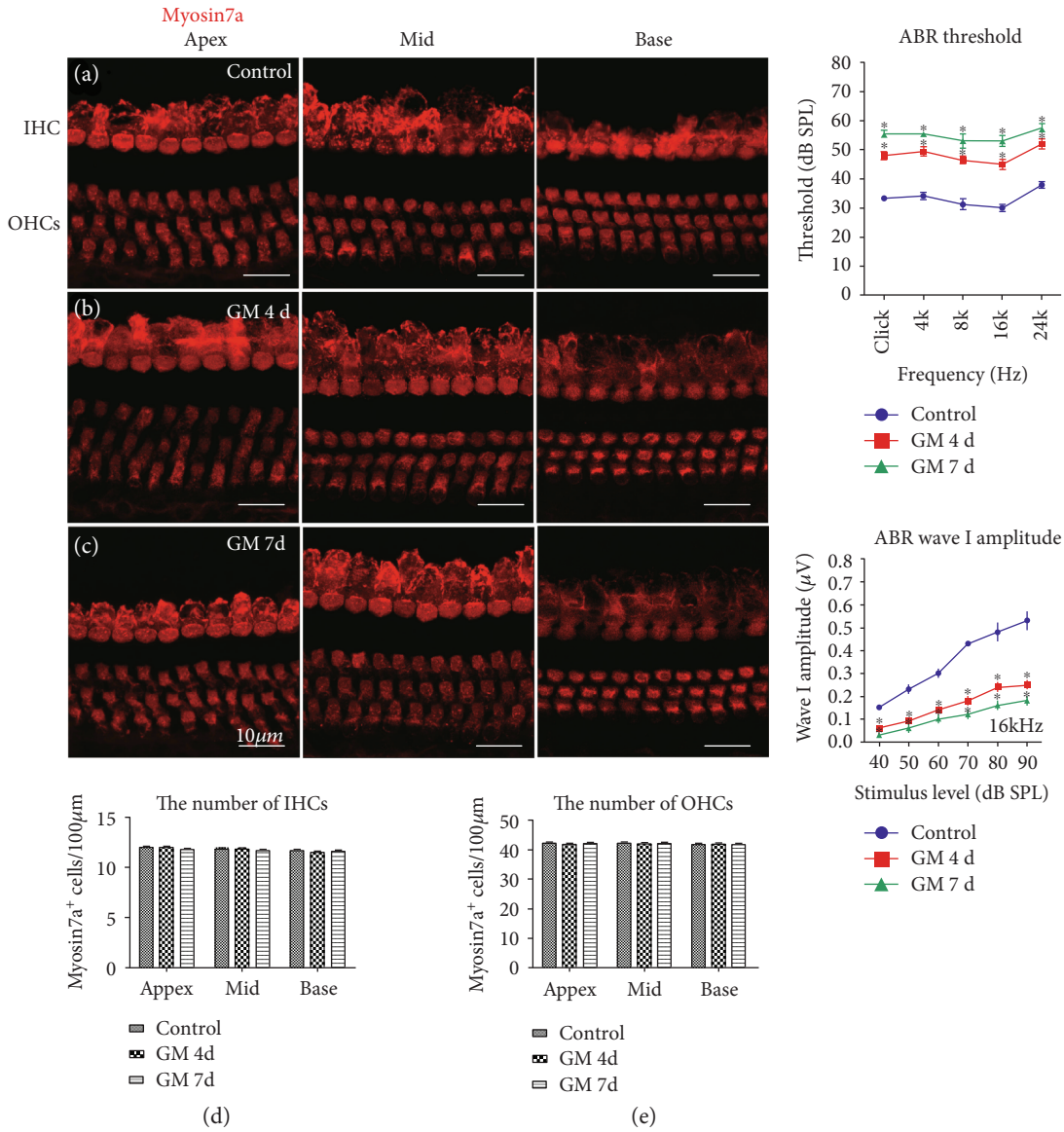

Figure 3: A low dose of gentamicin-induced moderate hearing loss with no obvious HC loss. The HCs were identified by immunostaining for myosin 7a (red) in the three turns of the cochlea. (a–c) After gentamicin treatment for 4 and 7 days, the morphology and arrangement of cochlear HCs were similar to the control group. (d-e) Quantitative data showed no HC loss in any of the three turns after gentamicin treatment. No significant difference was found in the number of IHCs or the three rows of OHCs among the control group and the gentamicin-treatment groups for 4 days or 7 days ($p > 0.05$). (f) A significant increase was observed in the ABR thresholds for clicks and for tone bursts at 4, 8, 16, and 24 kHz in the gentamicin-treated groups ($^*p < 0.05$, versus the control group). (g) A significant decline was observed in the ABR wave I amplitudes at 16 kHz in the gentamicin-treated groups ($^*p < 0.05$, *versus* the control group). GM 4 d, 7 d: gentamicin treatment for 4 days or 7 days; IHC: inner hair cell; OHC: outer hair cell. Scale bar = 10 μm. $^*p < 0.05$.

gentamicin groups, resp.) (Figure 4(f) and Supplementary Table 1). These results indicate that there was a significant decrease in the number of presynaptic ribbons and postsynaptic AMPARs at the basal poles of the IHCs (Figures 4(e)–4(g)), and thus the number of ribbon synaptic pairs significantly decreased at the basal poles of the IHCs in the gentamicin-treated group compared with the control group ($p < 0.05$) (Figure 4(g)). We also observed some anomalously aggregated ribbons and/or AMPARs at the IHC basal pole region in the gentamicin-treated cochleae (Figure 4(c)), which is consistent with a previous report [8].

In the IHC nuclei region in normal cochleae, the average number of AMPARs, ribbons, and ribbon synaptic pairs were 1.20 ± 0.13, 0.80 ± 0.10, and 0.80 ± 0.10 per IHC, respectively. After gentamicin treatment, there was a significant increase in the number of relocated AMPARs, ribbons, and ribbon synaptic pairs in the IHC nuclei region ($p < 0.05$). After gentamicin treatment for 4 days, the numbers of AMPARs, ribbons, and ribbon synaptic pairs were 3.80 ± 0.28, 2.20 ± 0.32, and 1.90 ± 0.32 per IHC in the IHC nuclei region, respectively. After gentamicin treatment for 7 days, the numbers of AMPARs, ribbons, and ribbon synaptic pairs

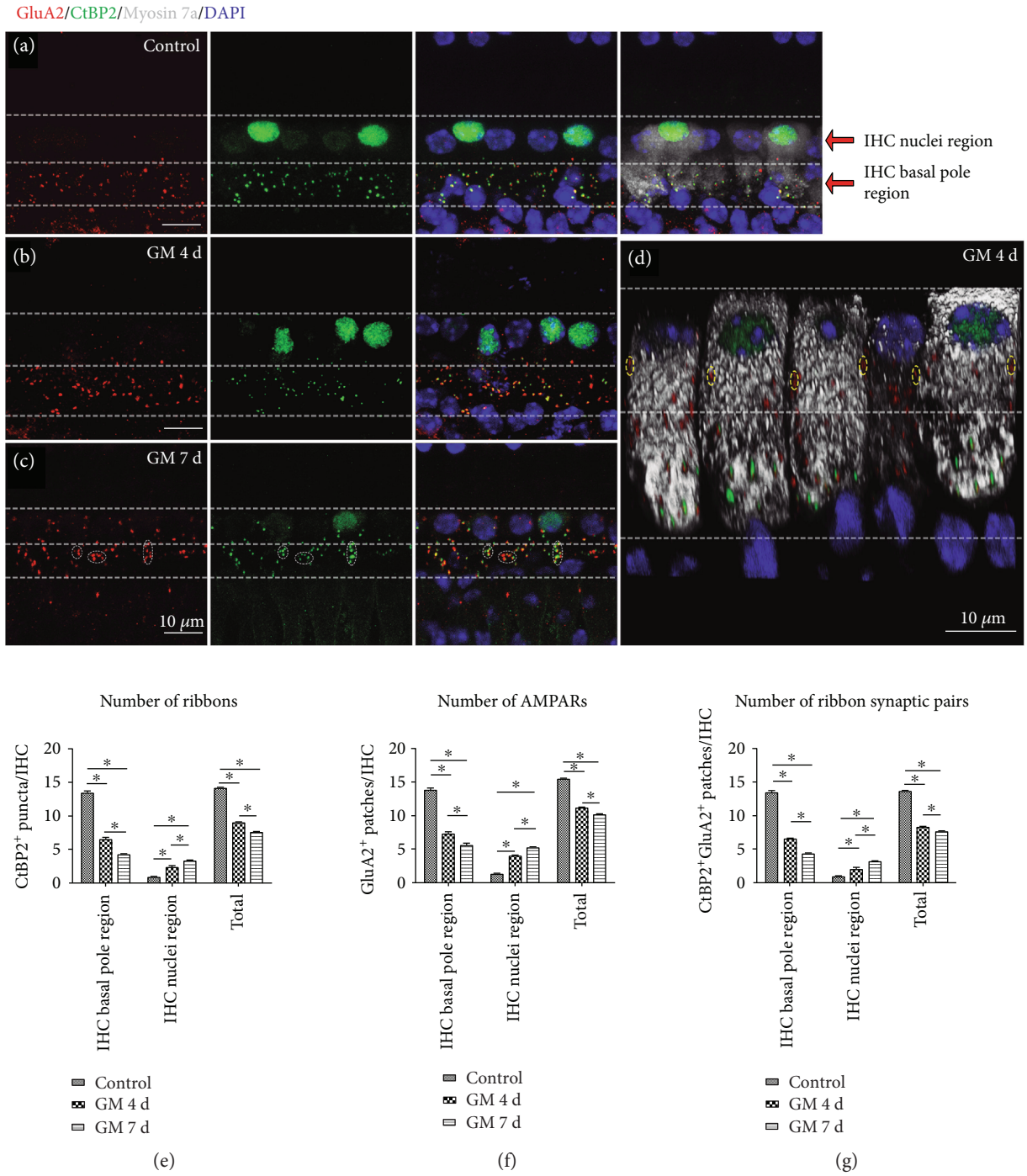

FIGURE 4: The number of cochlear ribbon synapses decreased and their locations changed from the basal pole region toward the nuclei region of the IHCs after gentamicin treatment. The IHCs were outlined by myosin 7a fluorescence in the cytoplasm (grey), and the nuclei were stained with DAPI (blue). The afferent synapses on the IHCs were labeled by immunostaining presynaptic ribbons with anti-CtBP2 (green) and the postsynaptic AMPARs with anti-GluA2 (red). (a) Ribbons and AMPARs were almost perfectly paired at the basal poles of the IHCs under physiological conditions. (b) After gentamicin treatment for 4 days, the ribbons and AMPARs moved towards the bundle poles of the IHCs. (c) After gentamicin treatment for 7 days, ribbons and AMPARs migrated towards the bundle poles of the IHCs, and some of them reached to or across the IHC nuclei region. The dashed white circles indicate some variegated ribbons and/or AMPARs at the IHC basal pole region. (d) The 3D-reconstructed image. The dashed yellow circles show orphan AMPARs near the bundle poles of the IHCs after 4 days of gentamicin treatment. (e) The numbers of CtBP2-positive ribbons. (f) The numbers of GluA2-positive AMPARs. (g) The numbers of CtBP2 and GluA2 double-positive ribbon synaptic pairs. GM 4 d, 7 d: gentamicin treatment for 4 days or 7 days; IHC: inner hair cell. Scale bar = 10 μm. $^{*}p < 0.05$.

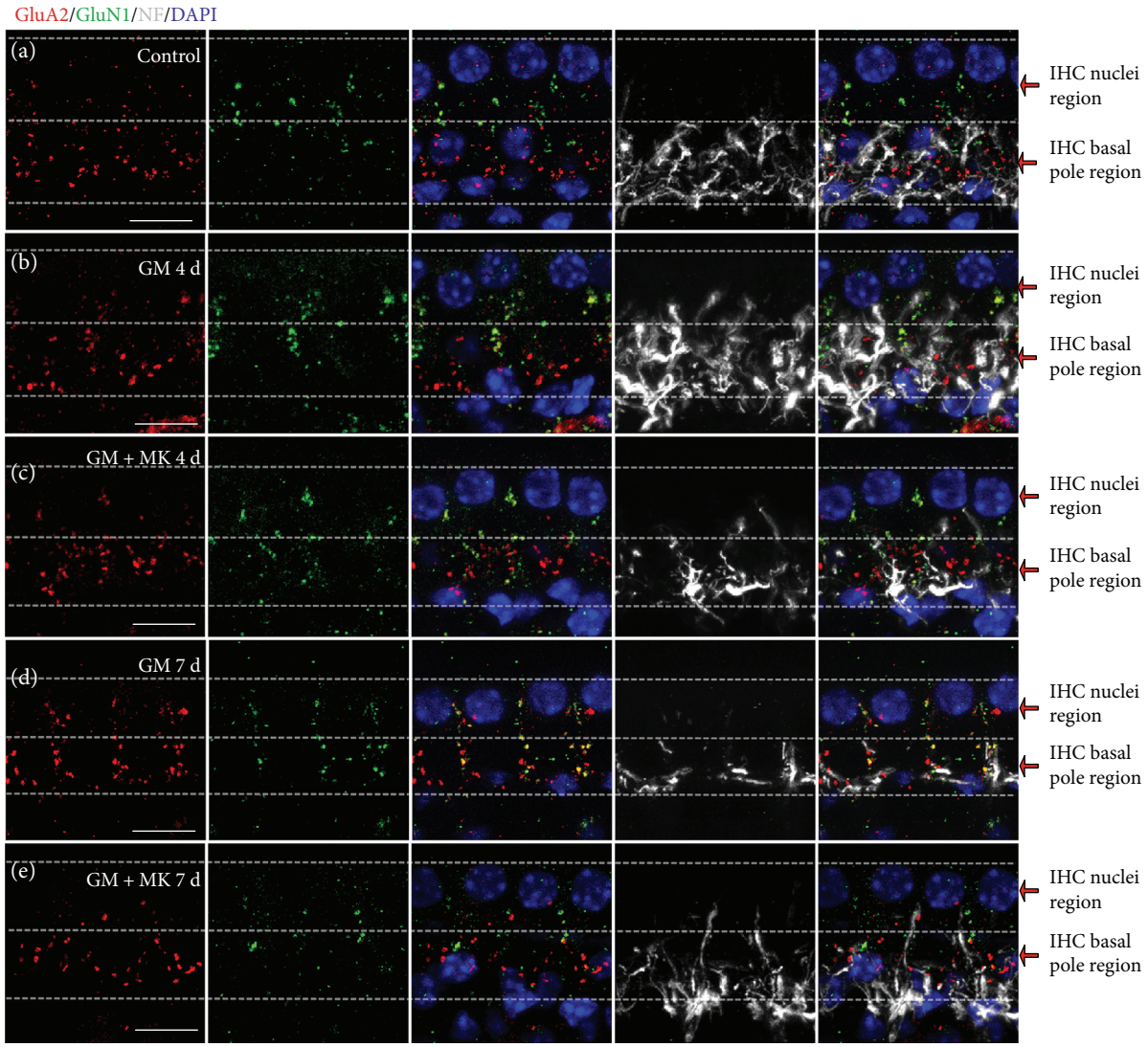

Figure 5: AMPARs and NMDARs were relocated on SGN dendrites after gentamicin exposure, and this was blocked by coinjection of the NMDAR antagonist MK801. Postsynaptic AMPARs, NMDARs, and nerve fibers were identified by immunostaining for GluA2 (red), GluN1 (green), and neurofilament (NF) (grey), respectively. Nuclei were labeled with DAPI (blue). (a) The different locations of NMDARs and AMPARs at afferent dendritic terminals in the normal mature cochlea. AMPAR patches were mostly observed on the ISBs around the basal poles of the IHCs, while NMDAR patches were almost all distributed on nerve terminals between the adjoining IHCs and closer to the IHC nuclei region. (b) After gentamicin treatment for 4 days, the AMPARs migrated upwards towards the bundle poles of the IHCs, while NMDARs migrated downwards towards the basal poles of the IHCs. (c) After the combined treatment with MK801 and gentamicin for 4 days, AMPARs and NMDARs were prevented from delocalizing to the dendritic terminals around the IHCs. (d) After gentamicin treatment for 7 days, the AMPARs and NMDARs had essentially switched locations along the dendritic terminals. Many colocalized AMPARs and NMDARs were observed laterally between the adjoining IHCs. (e) After the combined treatment with gentamicin and MK801 for 7 days, the gentamicin-induced rearrangements of AMPARs and NMDARs at the afferent dendritic terminals were partly blocked. GM 4 d, 7 d: gentamicin treatment for 4 days or 7 days; GM + MK 4d, 7d: combined treatment with gentamicin and MK801 for 4 days or 7 days; IHC: inner hair cell; ISBs: inner spiral bundles. Scale bar = 10 μm.

were 5.00 ± 0.31, 3.10 ± 0.28, and 3.00 ± 0.28 per IHC, respectively, in the IHC nuclei region (Figures 4(e)–4(g) and Supplementary Table 1). Moreover, many orphan AMPARs, which lack closely apposed presynaptic ribbons in the IHC, were observed in the IHC nuclei region after gentamicin treatment for 4 days (Figure 4(d)). More relocated ribbon synaptic pairs were found in the IHC nuclei region in the 7-day gentamicin group than the 4-day gentamicin group (Figure 4(g)), suggesting that the IHC ribbons matched up again with the earlier relocated postsynaptic AMPARs in the 7-day gentamicin group.

3.3. A Low Dose of Gentamicin-Induced Rearrangement of NMDARs at Nerve Terminals Innervating the IHCs. We next explored the changes in NMDARs and its relationship with AMPARs after gentamicin injury. First, we found that the number of NMDARs was significantly increased in the SGN-IHC synapses after gentamicin treatment ($p < 0.05$)

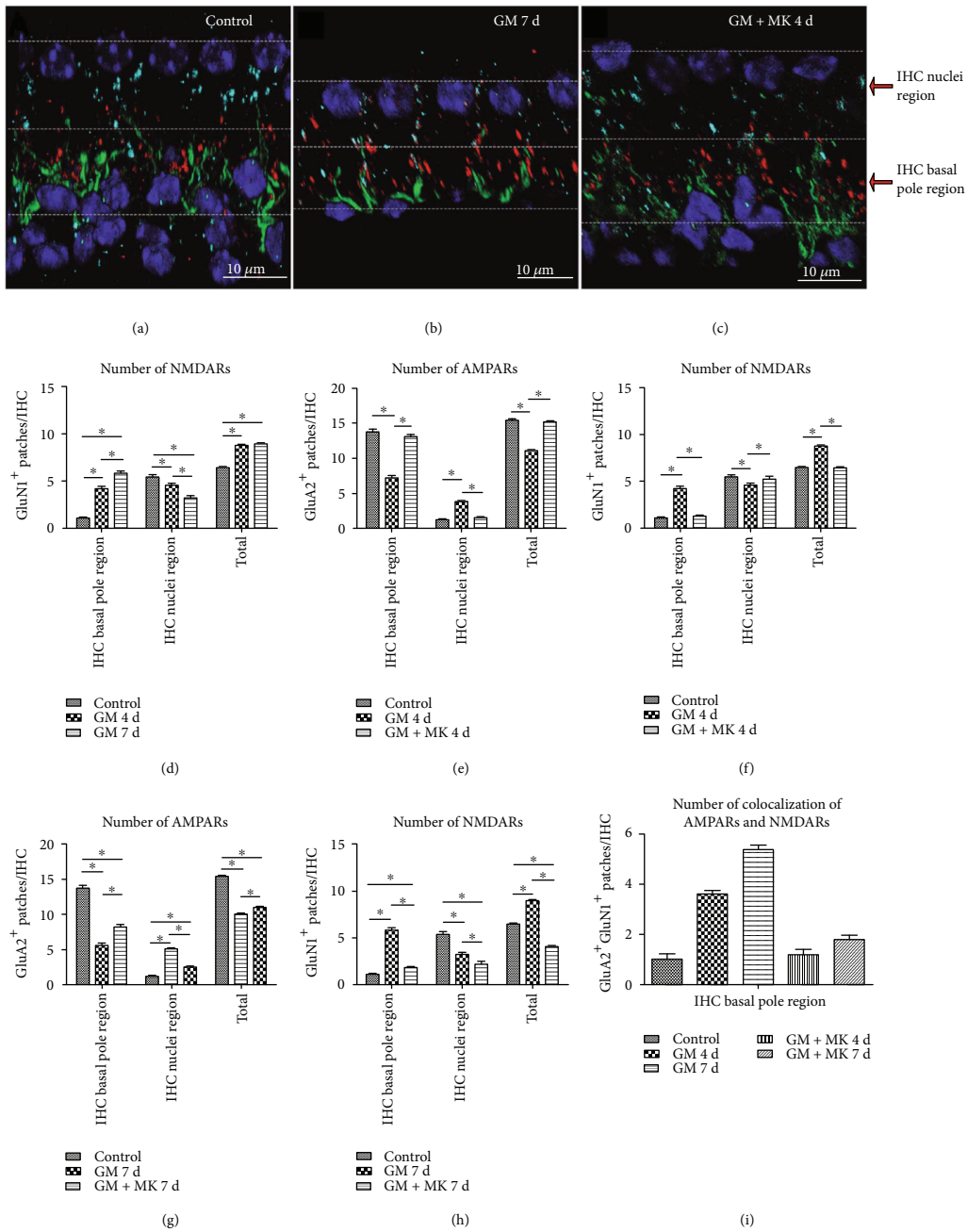

Figure 6: The 3D-reconstructed images and the numbers of NMDARs and AMPARs at the nerve fibers around the IHCs. Postsynaptic AMPARs, NMDARs, and nerve fibers around the IHCs were identified by immunostaining for GluA2 (red), GluN1 (cyan), and neurofilament (NF) (green). Nuclei were labeled with DAPI (blue). (a, b, c) In the study, we define the "IHC basal pole region" and the "IHC nuclei region" in every single IHC. The changed tendency in location of AMPARs and NMDARs was observed at the afferent dendrites around the adjacent IHC in the 3D-reconstructed images. (a) The locations of NMDARs and AMPARs at the afferent dendritic terminals in the normal cochlea. (b) AMPARs and NMDARs essentially switched locations on SGN dendrites after gentamicin treatment for 7 days. (c) The gentamicin-induced translocation of AMPARs and NMDARs was almost completely blocked after coinjection of MK801 and gentamicin for 4 days. (d, f, h) The numbers of GluN1-positive NMDARs. (e, g) The numbers of GluA2-positive AMPARs. (i) The numbers of colocalized AMPARs and NMDARs at the basal poles of the IHCs. GM 4 d, 7 d: gentamicin treatment for 4 days or 7 days; GM + MK 4d, 7d: combined treatment of gentamicin and MK801 for 4 days or 7 days; IHC: inner hair cell. $^{*}p < 0.05$.

(Figures 5(b), 5(d), 6(b), and 6(d)). Second, we observed the rearrangement of NMDARs at afferent dendritic terminals. NMDAR patches migrated towards the basal poles of the IHCs, closer to the ISBs. After gentamicin treatment, compared with the control group, the number of NMDAR patches significantly increased in the IHC basal pole region ($p < 0.05$) and significantly decreased in the IHC nuclei region ($p < 0.05$) (Figures 5(b), 5(d), 6(b), and 6(d) and 4 days, the numbers of NMDARs were 4.50 ± 0.30 and 4.20 ± 0.31 per IHC in the IHC nuclei region and the IHC basal

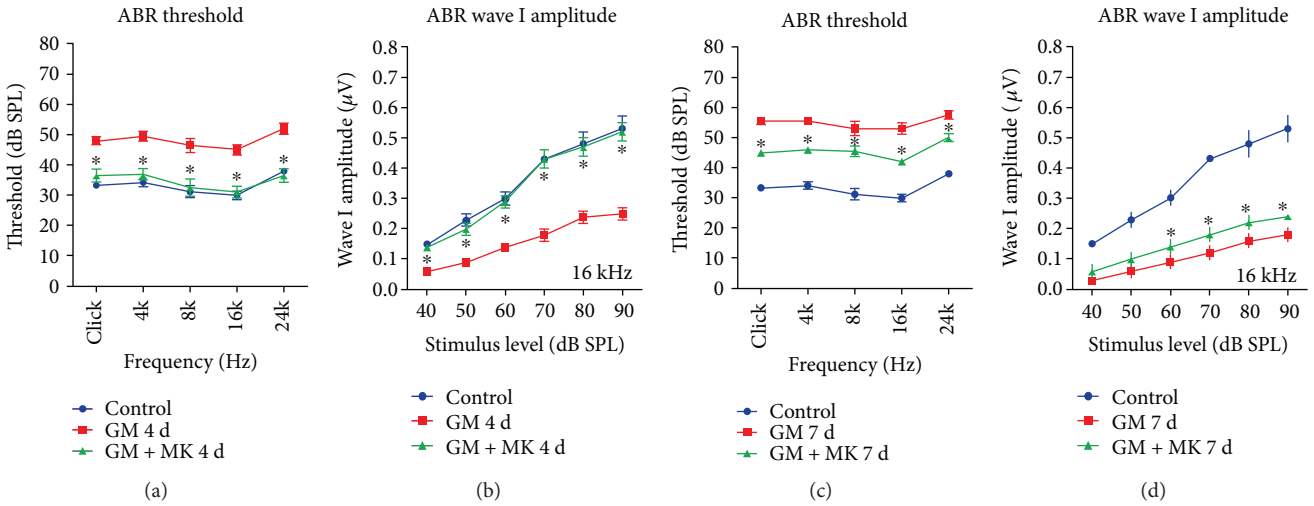

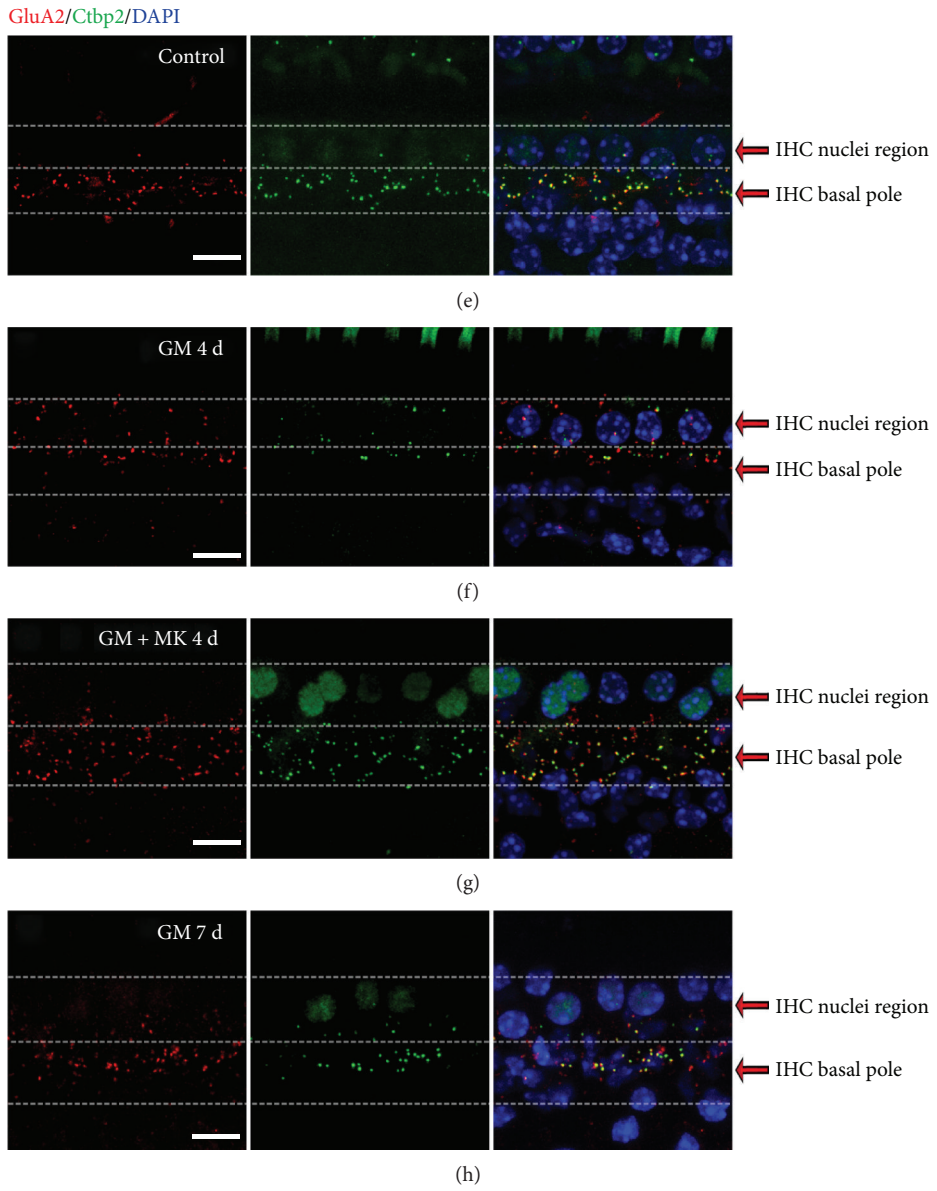

Figure 7: Continued.

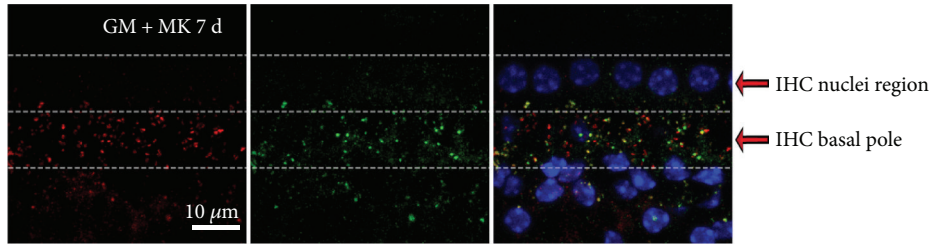

(i)

Figure 7: Cochlear ribbon synapses were maintained when MK801 was coinjected with gentamicin. (a-b) The elevation of ABR thresholds and the decline of ABR wave I amplitudes induced by gentamicin injury were successfully rescued by MK801 treatment in the 4-day treatment group ($^*p < 0.05$, *versus* gentamicin-only group). (c-d) The elevation of ABR thresholds and the decline of ABR wave I amplitudes induced by gentamicin injury were partly blocked by MK801 treatment in the 7-day treatment group ($^*p < 0.05$, *versus* gentamicin-only group). (e–i) Afferent ribbon synaptic pairs were observed by immunostaining presynaptic ribbons with anti-CtBP2 (green) and postsynaptic AMPARs with anti-GluA2 (red). Nuclei were labeled by DAPI (blue). (e) Ribbons and AMPARs were paired at the basal poles of the IHCs in the undamaged cochlea. (f) After gentamicin treatment for 4 days, AMPARs and ribbons moved upwards towards the bundle poles of the IHCs. The translocation of AMPARs occurred earlier than that of the presynaptic ribbons. (g) After the combined treatment with gentamicin and MK801 for 4 days, the ribbon synaptic pairs had similar location, morphology, and distribution as undamaged controls. (h) After gentamicin treatment for 7 days, AMPARs and ribbons were further relocated towards the bundle poles of the IHCs. Some large ribbons and/or AMPARs were also observed at the basal poles of the IHCs. (i) After the combined treatment with gentamicin and MK801 for 7 days, the quantity of the ribbon synaptic pairs was significantly increased in the IHC basal pole region compared with that in gentamicin-only treatment. GM 4 d, 7 d: gentamicin treatment for 4 days or 7 days; GM + MK 4d, 7d: combined treatment with gentamicin and MK801 for 4 days or 7 days; IHC: inner hair cell. Scale bar = 10 μm. $^*p < 0.05$.

pole region, respectively (Figures 5(b) and 6(d), and Supplementary Table 2). After gentamicin treatment for 7 days, the numbers of NMDARs were 3.20 ± 0.25 and 5.80 ± 0.25 per IHC in the IHC nuclei region and the IHC basal pole region, respectively (Figures 5(d), 6(b), and 6(d) and Supplementary Table 2). Moreover, the number of colocalized AMPARs and NMDARs per IHC was also significantly increased in the IHC basal pole region after gentamicin treatment (Figure 6(i) and Supplementary Table 2).

3.4. Treatment with the NMDAR Antagonist MK801 Prevented the Gentamicin-Induced Rearrangement of AMPARs and NMDARs at the IHC-SGN Synaptic Connection. MK801 is a noncompetitive NMDA receptor antagonist that is thought to protect neurons in the brain against excitotoxicity induced by excessive glutamate activity [17, 32]. MK801 was used as a NMDAR antagonist with the dose range from 0.2 to 1.0 (mg/kg) in previous studies [17, 21, 22].To explore the role of NMDARs in synaptic plasticity during ototoxicity, MK801 (0.2 mg/kg, i.p.) was used to rescue the gentamicin-induced damage. Briefly, mice were injected daily with MK801 and/or gentamicin for 4 or 7 consecutive days, and mice receiving injections of normal saline served as controls. ABR tests were performed on the following day after injections for 4 or 7 days.

GluN1 staining showed that MK801 treatment clearly prevented the gentamicin-induced movement of NMDARs toward the IHC basal poles (Figures 5 and 6). The number, morphology, and distribution of GluN1-positive patches in MK801-treated cochleae were similar to normal cochleae (Figure 6). Compared with the gentamicin-only group, the number of NMDARs in the IHC nuclei region increased significantly in the MK801 rescue group in both the 4-day and 7-day treatment groups (Figures 6(f) and 6(h)). There was no significant difference in the number of NMDARs in the IHC nuclei region between the undamaged control group and the MK801 rescue group in the 4-day treatment group (Figure 6(f)).

GluA2 staining showed that the gentamicin-induced movement toward the IHC bundle poles and the pathological changes of postsynaptic AMPARs were blocked by coinjection of MK801 (Figures 5–8). Moreover, compared with the gentamicin-only group, the number of colocalized AMPARs and NMDARs significantly decreased in the IHC basal pole region in the MK801 rescue group in both the 4-day and 7-day treatment groups ($p < 0.05$, Figures 6(f), 6(h), and 6(i)). These results suggested that MK801 treatment blocked the gentamicin-induced activation of NMDARs and the pathological changes of AMPARs in the SGN terminals.

3.5. NMDAR Antagonist MK801 Treatment Protects against Gentamicin-Induced Hearing Loss by Preventing the Disruption of Ribbon Synapses. We next explored whether gentamicin-induced hearing loss and disruption of ribbon synaptic pairs could be affected by the NMDAR antagonist MK801. In this experiment, we found that gentamicin-induced hearing loss was successfully rescued by MK801 treatment (Figures 7(a)–7(d)). Compared with the undamaged group, the ABR thresholds were significantly increased while ABR wave I amplitudes were significantly reduced after gentamicin injury. However, the elevation of ABR thresholds and reduction of wave I amplitudes induced by gentamicin injury was successfully rescued by MK801 treatment in both the 4-day and 7-day treatment groups. Indeed, no significant differences were seen in the ABR thresholds and wave I amplitude between the undamaged control group and the MK801 rescue group in the 4-day treatment group (Figures 7(a) and 7(b)), suggesting that MK801 treatment could attenuate the gentamicin-induced hearing loss.

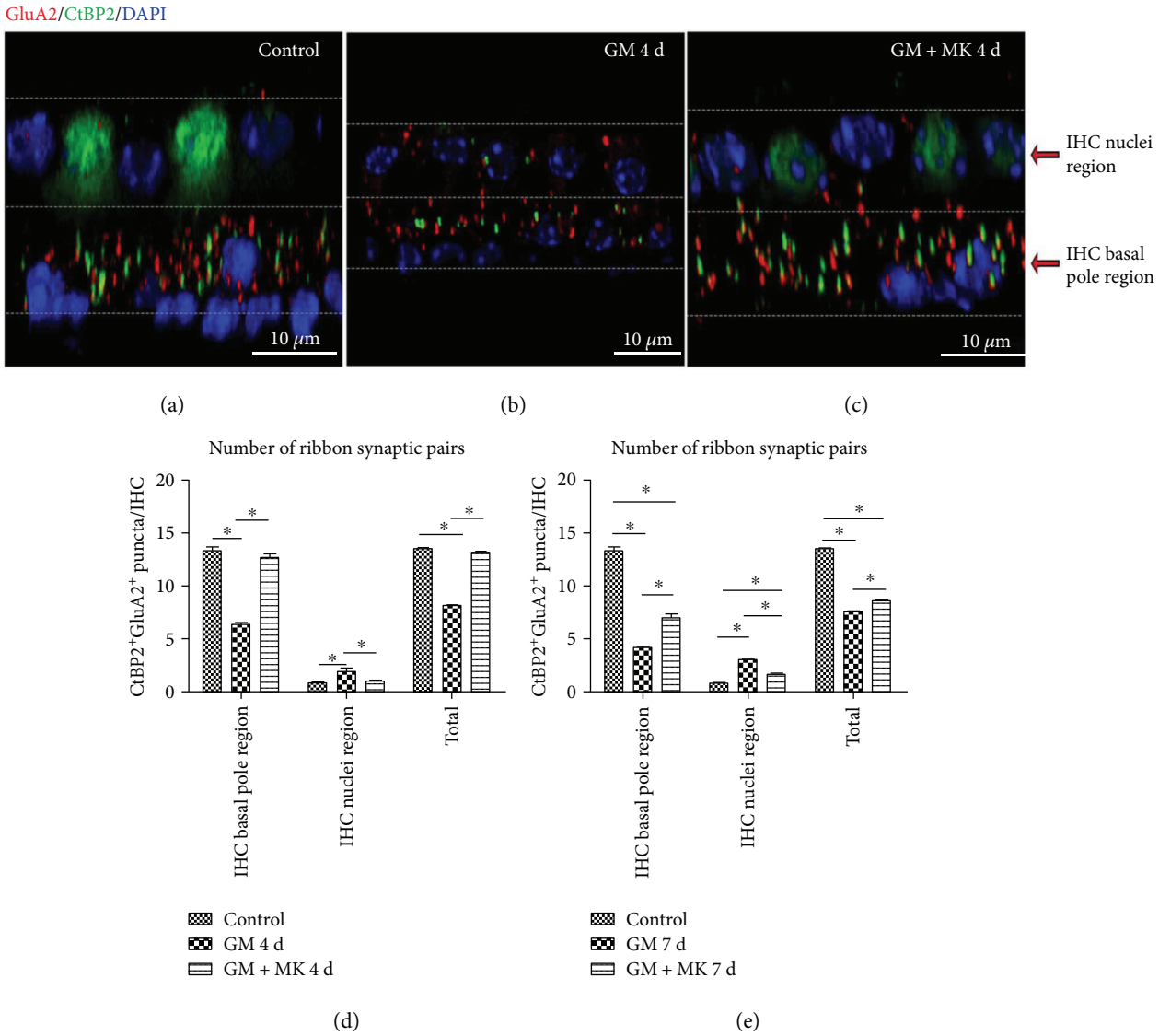

Figure 8: The 3D-reconstructed images and numerical data for the ribbon pairs after different treatments. Afferent synapses on IHCs are seen by immunostaining presynaptic ribbons with anti-CtBP2 (green) and postsynaptic AMPARs with anti-GluA2 (red). Nuclei were labeled with DAPI (blue). (a, b, c) In the study, we define the "IHC basal pole region" and the "IHC nuclei region" in every single IHC. The changed tendency in location of AMPARs and ribbons was observed around the IHC in the 3D-reconstructed images. (a) Ribbons and AMPARs were paired at the basal poles of the IHCs in the control cochlea. (b) After gentamicin treatment for 4 days, the presynaptic ribbons and postsynaptic AMPARs were relocated towards the bundle poles of the IHCs. The number of ribbons and AMPARs was decreased at the basal pole of IHCs. (c) After combined treatment with gentamicin and MK801 for 4 days, most of the IHC ribbons and postsynaptic AMPARs remained at the basal poles of the IHCs, but a few AMPARs were still observed near the IHC nuclei region. (d) The number of ribbon synaptic pairs among the control group, gentamicin treatment group for 4 days, and combined treatment group with gentamicin and MK801 for 4 days. (e) The number of ribbon synaptic pairs among the control group, gentamicin treatment group for 7 days, and combined treatment group with gentamicin and MK801 for 7 days. GM 4 d, 7 d: gentamicin treatment for 4 days or 7 days; GM + MK 4d, 7d: combined treatment with gentamicin and MK801 for 4 days or 7 days; IHC: inner hair cell $^{*}p < 0.05$.

CtBP2 staining showed that the movement of presynaptic ribbons toward the IHC bundle poles in response to gentamicin was blocked by coinjection with MK801 (Figures 7 and 8). Not only the location but also the quantity, morphology, and distribution of presynaptic ribbons in the MK801-treated cochlea were comparable to normal undamaged cochleae (Figures 7(e)–7(i), and Supplemental Video 5). Compared with the gentamicin-only group, the numbers of ribbon synaptic pairs at the IHC basal pole region were significantly increased in the MK801 rescue groups at both 4 and 7 days (Figures 8(d) and 8(e)). There was no significant difference in the number of ribbon synaptic pairs in the IHC basal pole region between the control and the MK801 rescue group in the 4-day treatment group (Figure 8(d)). These results suggested that the rearrangement of NMDARs is a primary element of the injury in IHC-SGNs synapses induced by gentamicin and early interruption of NMDAR activation protected against gentamicin-induced

pathological changes in the IHC synapses. Together, these results suggest that inhibition of NMDARs protected against gentamicin-induced hearing loss, likely by maintaining the integrity of the ribbon synapses.

4. Discussion

Transmission of nerve impulses at IHC-SGN synapses is mediated by the release of glutamate from ribbon terminals [2, 33]. Patch clamp recordings of the type I SGN afferent dendrite convincingly show that excitatory postsynaptic currents are AMPAR mediated and that NMDARs do not contribute to synaptic transmission at the type I SGN synapse under physiological conditions [34–37]. Although the role of NMDARs in ototoxicity was speculated to be through glutamate excitotoxicity [15–17], there was no direct morphological evidence for this or for the role of NMDARs in cochlear IHC-SGN synapses.

4.1. NMDARs and AMPARs Are Located in Different Regions of ANF Terminals under Physiological Conditions. GluA2, GluA3, and possibly GluA4 subunits of AMPAR are present in SGN afferent dendrites in the adult cochlea [38], and the GluA2 subunit determines the key biophysical properties of GluAs *in vivo* [39]. Under physiological conditions, GluA2-positive AMPAR patches were paired with CtBP2 positive IHC ribbons and were distributed in the ISBs around the basal poles of the IHCs (Figure 4), which was consistent with previous studies [2, 3, 8]. NMDARs are composed of the mandatory GluN1 subunit and a variety of GluN2A, B, C, and D subunits [38, 40]. In this paper, we found that the majority of NMDARs were distributed on the modiolar side and close to the nuclei region of IHCs. However, the AMPARs are mainly distributed at the IHC basal pole region, on the modiolar and pillar sides of IHCs. Some NMDARs were colocalized with small GluA2-positive puncta, which might be regarded as a "resting state" of small-puncta AMPARs in the central nervous system (Figure 1) [38, 41]. This study reported the different characteristics of the distribution of AMPARs and NMDARs at type I ANFs contacting IHCs in the adult mouse cochlea (Figures 1 and 5).

4.2. NMDARs Are Involved in AMPAR Rearrangement in the Cochlear IHC-SGN Synapse Connection as Part of the Ototoxic Mechanism of Gentamicin Treatment. Reorganization of postsynaptic AMPARs and NMDARs was observed after gentamicin treatment. Rows of NMDARs moved towards the IHC basal poles, while AMPAR patches moved towards the IHC bundle poles and reached to or across the IHC nuclei region on the afferent dendrites contacting the IHCs (Figures 5, 6, and 9). As a result, the spatial distribution AMPARs and NMDARs was different from the distribution under physiological conditions. The number of NMDARs in the ISBs was significantly increased in response to gentamicin treatment (Figures 5 and 6). In the central nervous system, calcium overload and cell death are mediated by NMDARs through glutamate excitotoxicity [40, 42–44], and our data suggest that rearrangement of AMPARs and NMDARs might be involved in the glutamate excitotoxicity observed in cochlear IHC-SGN synapses after gentamicin treatment.

In the brain, NMDARs are required for the control of synaptic rearrangement and axonal remodeling [45]. Activation of synaptic NMDARs induces the membrane insertion of new AMPARs in cultured hippocampal neurons [46], and NMDAR agonists can regulate the expression of surface AMPARs on the cell membrane of cultured SGNs [14]. In the present study, coinjection of the NMDAR antagonist MK801 and gentamicin prevented the rearrangement of AMPARs and NMDARs at the dendritic terminals (Figures 5–8), suggesting that NMDAR activation is involved in the AMPAR rearrangement in IHC-SGN synapses in response to gentamicin. Furthermore, cotreatment with MK801 prevented gentamicin-induced damage of the IHC ribbon synapse (Figure 7) and reduced gentamicin-induced hearing loss (Figure 8), suggesting that NMDARs are involved in ototoxicity by regulating the number and distribution of ribbon synapses in the IHC-SGN afferent synapse connection.

4.3. Ribbons in IHCs Might Follow the Rearrangement of AMPARs at Afferent Dendritic Terminals in Response to Gentamicin Treatment. Studies of both noise-induced hearing loss and drug-induced hearing loss have shown reduced numbers and abnormal distributions of ribbons, which were found to be isolated in the cytoplasm and proximal to the IHC nuclei region [7, 8]. However, the mechanism and implications of this abnormal distribution of ribbons has remained unclear.

Under physiological conditions, presynaptic ribbons were paired to postsynaptic AMPARs. In gentamicin-induced ototoxicity, AMPARs on the SGN dendrites moved quickly toward the bundle poles of the IHCs, some of which reached to or across the IHC nuclei region. Orphan AMPARs lacking opposed ribbons were often observed in the IHC nuclei region of SGN afferent dendritic terminals in the 4-day gentamicin group. However, in the 7-day gentamicin group, the IHC ribbons were increasingly relocated and matched up again with postsynaptic AMPARs in the IHC nuclei region. These results suggest that the relocation of AMPARs takes place earlier than the relocation of the presynaptic ribbons and that the presynaptic ribbons in the IHC membrane might follow the movement of postsynaptic AMPARs at type I SGN afferent dendritic terminals in response to gentamicin treatment (Figure 4).

The expression of mature ribbons on the membrane of IHCs requires several intracellular processes, including the synthesis of glutamate vesicles, transportation, assembly, and final localization of ribbons at the membrane [2]. Sobkowicz et al. studied the distribution of synaptic ribbons in the developing organ of Corti and found that nerve fibers appear to be critical in influencing the location of the synaptic ribbon [47]. It has been suggested that nitric oxide, as a neuronal messenger, might be involved in transferring signals between presynaptic and postsynaptic elements and regulating the excitability at glutamatergic synapses. In the brain, neuronal nitric oxide synthase is broadly expressed

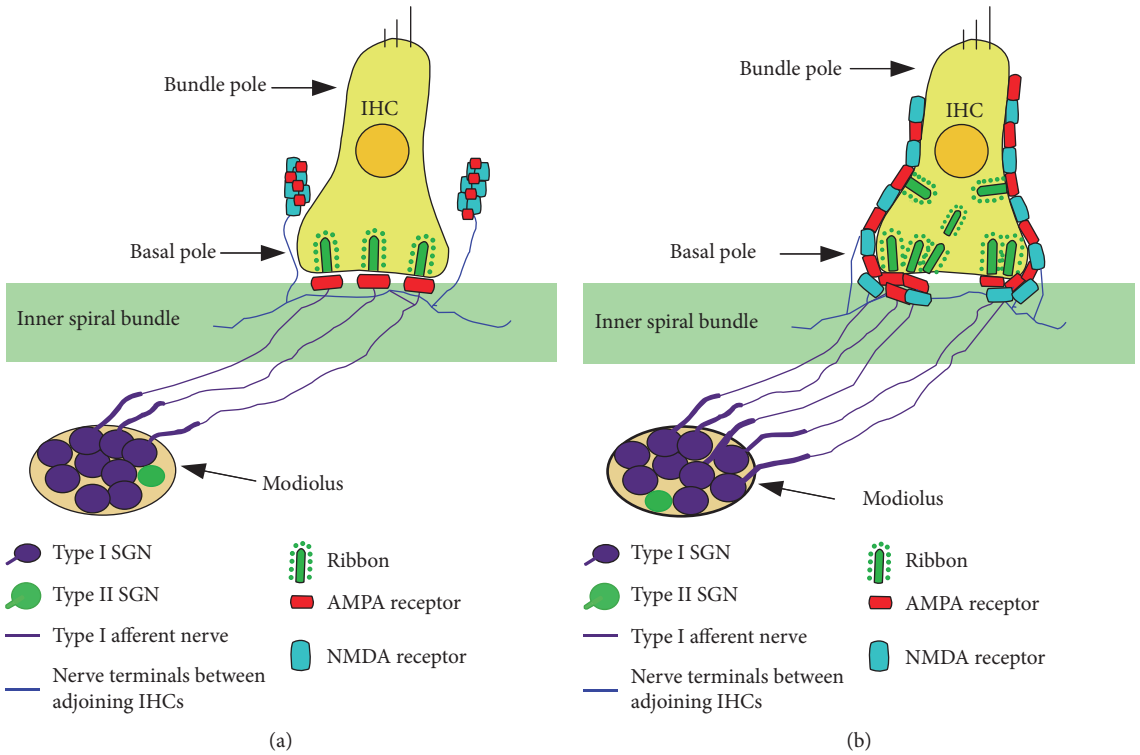

Figure 9: Diagrams illustrating the gentamicin-induced changes in ribbons, NMDARs, and AMPARs at the IHC-SGN synapse in the mouse cochlea. (a) In the normal mouse adult cochlea, presynaptic ribbons and postsynaptic AMPARs show a nearly one-to-one relationship. The ribbon synaptic pairs (double staining for CtBP2-positive puncta and GluA2-positive patches) are distributed around the basal poles of the IHCs. Most of the AMPARs are observed in the ISBs, but most NMDARs are distributed on the neural dendritic terminals between the adjoining IHCs and closer to the IHC nuclei region. In IHC nuclei region, some NMDARs colocalize with GluA2-positive AMPAR puncta, which are smaller than AMPAR patches in the IHC basal pole region. In the mouse cochlea, each IHC is contacted by roughly 10–20 ANFs depending on cochlear location. Each cochlear neuron is excited by a single ribbon synapse with a single IHC. (b) After gentamicin treatment, AMPARs and NMDARs are relocated at nerve fiber terminals around IHCs, and their locations are essentially reversed. AMPARs move upwards towards the bundle poles of the IHCs, and NMDARs migrate downwards towards the basal poles of the IHCs. The number of colocalized AMPARs and NMDARs gradually increases in the IHC basal pole region. Some anomalously aggregated ribbons and/or AMPARs in the IHC basal pole region are observed. IHC: inner hair cell; SGN: spiral ganglion neuron; ISBs: inner spiral bundles; ANFs: afferent nerve fibers.

and is associated with synaptic plasticity through NMDAR-mediated calcium influx [48]. The role of nitric oxide and synaptic plasticity in the progression of ototoxicity requires further study.

5. Conclusions

This study showed that NMDARs are involved in cochlear ribbon synaptic rearrangement in gentamicin-induced ototoxicity. The postsynaptic arrangement of AMPARs on the dendrites of SGNs might affect the number and location of presynaptic ribbons. Inhibition of NMDARs successfully prevented gentamicin-induced ototoxicity by preventing the relocation of AMPARs and NMDARs on the dendrites of the SGNs and thus maintaining the integrity of the ribbon synapses and preserving hearing function.

Data Availability

The data used to support the findings of this study are available from the corresponding author upon request.

Conflicts of Interest

The authors declare that they have no conflict of interest.

Authors' Contributions

Juan Hong, Peidong Dai, and Huawei Li conceived and designed the experiments. Juan Hong, Yan Chen, Yanping Zhang, Jieying Li, Liujie Ren, Lin Yang, Tianyu Zhang, Lusen Shi, and Ao Li performed the experiments. Juan Hong and Yan Chen analyzed the data. Juan Hong, Yan Chen, Huawei Li, and Peidong Dai drafted and revised the manuscript. Juan Hong and Yan Chen contributed equally to this work.

Acknowledgments

The authors wish to thank Dan You, Xiaoling Lu, Dongmei Tang, Wenli Ni, and Chenlong Li of the Eye and ENT Hospital of Fudan University for help in the experiment. The authors also thank Jin Li and Yalin Huang of the Institutes of Biomedical Sciences of Fudan University for

providing technical support with the confocal microscope. This work was supported by grants from the National Science and Technology Support Program, China (Grant no. 2015BAK31B01), the National Key R&D Program of China (Grant nos. 2017YFA0103900, 2016YFC0905200), the National Natural Science Foundation of China (Grant nos. 81620108005, 81230019, 81570911, 81470687, and 81771010), the Natural Science Foundation of Zhejiang Province of China (Grant no. LY14H130002), and the Science and Technology Plan Project of Wenzhou City of China (Grant no. Y20130223).

Supplementary Materials

Supplementary Table 1: the number of presynaptic ribbons, postsynaptic AMPARs, and ribbon synaptic pairs in different groups. Supplementary Table 2: the number of the AMPARs and NMDARs at the IHC-SGN synapse in different groups. Legends of supplemental videos: Supplemental Video 1: spatial distribution of NMDARs and AMPARs in the IHC-SGN synapse of normal mouse mature cochlea. Supplemental Video 2: spatial distribution of NMDARs and AMPARs in the IHC-SGN synapse of gentamicin treated mouse cochlea (GM 7d). Supplemental Video 3: spatial distribution of ribbons and AMPARs in the IHC-SGN synapse of normal mouse mature cochlea. Supplemental Video 4: spatial distribution of ribbons and AMPARs in the IHC-SGN synapse of gentamicin-treated mouse cochlea (GM 4d). Supplemental Video 5: spatial distribution of ribbons and AMPARs in the IHC-SGN synapse of gentamicin and MK801-treated mouse cochlea (GM + MK 4d). *(Supplementary Materials)*

References

[1] S. L. Johnson, T. Eckrich, S. Kuhn et al., "Position-dependent patterning of spontaneous action potentials in immature cochlear inner hair cells," *Nature Neuroscience*, vol. 14, no. 6, pp. 711–717, 2011.

[2] R. Nouvian, D. Beutner, T. D. Parsons, and T. Moser, "Structure and function of the hair cell ribbon synapse," *The Journal of Membrane Biology*, vol. 209, no. 2-3, pp. 153–165, 2006.

[3] K. Liu, X. Jiang, C. Shi et al., "Cochlear inner hair cell ribbon synapse is the primary target of ototoxic aminoglycoside stimuli," *Molecular Neurobiology*, vol. 48, no. 3, pp. 647–654, 2013.

[4] S. G. Kujawa and M. C. Liberman, "Adding insult to injury: cochlear nerve degeneration after "temporary" noise-induced hearing loss," *The Journal of Neuroscience*, vol. 29, no. 45, pp. 14077–14085, 2009.

[5] S. G. Kujawa and M. C. Liberman, "Synaptopathy in the noise-exposed and aging cochlea: primary neural degeneration in acquired sensorineural hearing loss," *Hearing Research*, vol. 330, Part B, pp. 191–199, 2015.

[6] M. Lafon-Cazal, S. Pietri, M. Culcasi, and J. Bockaert, "NMDA-dependent superoxide production and neurotoxicity," *Nature*, vol. 364, no. 6437, pp. 535–537, 1993.

[7] L. D. Liberman, J. Suzuki, and M. C. Liberman, "Dynamics of cochlear synaptopathy after acoustic overexposure," *Journal of the Association for Research in Otolaryngology*, vol. 16, no. 2, pp. 205–219, 2015.

[8] K. Liu, D. Chen, W. Guo et al., "Spontaneous and partial repair of ribbon synapse in cochlear inner hair cells after ototoxic withdrawal," *Molecular Neurobiology*, vol. 52, no. 3, pp. 1680–1689, 2015.

[9] S. Usami, A. Matsubara, S. Fujita, H. Shinkawa, and M. Hayashi, "NMDA (NMDAR1) and AMPA-type (GluR2/3) receptor subunits are expressed in the inner ear," *Neuroreport*, vol. 6, no. 8, pp. 1161–1164, 1995.

[10] E. Soto, A. Flores, C. Ero´stegui, and R. Vega, "Evidence for NMDA receptor in the afferent synaptic transmission of the vestibular system," *Brain Research*, vol. 633, no. 1-2, pp. 289–296, 1994.

[11] J. Ruel, C. Chabbert, R. Nouvian et al., "Salicylate enables Cochlear arachidonic-acid-sensitive NMDA receptor responses," *The Journal of Neuroscience*, vol. 28, no. 29, pp. 7313–7323, 2008.

[12] M. Knipper, P. Van Dijk, I. Nunes, L. Ruttiger, and U. Zimmermann, "Advances in the neurobiology of hearing disorders: recent developments regarding the basis of tinnitus and hyperacusis," *Progress in Neurobiology*, vol. 111, pp. 17–33, 2013.

[13] Y. Zhang-Hooks, A. Agarwal, M. Mishina, and D. E. Bergles, "NMDA receptors enhance spontaneous activity and promote neuronal survival in the developing cochlea," *Neuron*, vol. 89, no. 2, pp. 337–350, 2016.

[14] Z. Chen, S. G. Kujawa, and W. F. Sewell, "Auditory sensitivity regulation via rapid changes in expression of surface AMPA receptors," *Nature Neuroscience*, vol. 10, no. 10, pp. 1238–1240, 2007.

[15] A. S. Basile, J. M. Huang, C. Xie, D. Webster, C. Berlin, and P. Skolnick, "N-methyl-D-aspartate antagonists limit aminoglycoside antibiotic-induced hearing loss," *Nature Medicine*, vol. 2, no. 12, pp. 1338–1343, 1996.

[16] J. A. Segal, B. D. Harris, Y. Kustova, A. Basile, and P. Skolnick, "Aminoglycoside neurotoxicity involves NMDA receptor activation," *Brain Research*, vol. 815, no. 2, pp. 270–277, 1999.

[17] M. Duan, K. Agerman, P. Ernfors, and B. Canlon, "Complementary roles of neurotrophin 3 and a N-methyl-D-aspartate antagonist in the protection of noise and aminoglycoside-induced ototoxicity," *Proceedings of the National Academy of Sciences of the United States of America*, vol. 97, no. 13, pp. 7597–7602, 2000.

[18] E. Selimoglu, "Aminoglycoside-induced ototoxicity," *Current Pharmaceutical Design*, vol. 13, no. 1, pp. 119–126, 2007.

[19] L. Chen, S. Xiong, Y. Liu, and X. Shang, "Effect of different gentamicin dose on the plasticity of the ribbon synapses in cochlear inner hair cells of C57BL/6J mice," *Molecular Neurobiology*, vol. 46, no. 2, pp. 487–494, 2012.

[20] H. Li and P. S. Steyger, "Systemic aminoglycosides are trafficked via endolymph into cochlear hair cells," *Scientific Reports*, vol. 1, no. 1, p. 159, 2011.

[21] P. Singer, D. Boison, H. Mohler, J. Feldon, and B. K. Yee, "Modulation of sensorimotor gating in prepulse inhibition by conditional brain glycine transporter 1 deletion in mice," *European Neuropsychopharmacology*, vol. 21, no. 5, pp. 401–413, 2011.

[22] A. S. de Miranda, F. Brant, L. B. Vieira et al., "A neuroprotective effect of the glutamate receptor antagonist MK801 on long-term cognitive and behavioral outcomes secondary to experimental cerebral malaria," *Molecular Neurobiology*, vol. 54, no. 9, pp. 7063–7082, 2017.

[23] L. Liu, Y. Chen, J. Qi et al., "Wnt activation protects against neomycin-induced hair cell damage in the mouse cochlea," *Cell Death & Disease*, vol. 7, no. 3, article e2136, 2016.

[24] S. Sun, H. Yu, H. Yu et al., "Inhibition of the activation and recruitment of microglia-like cells protects against neomycin-induced ototoxicity," *Molecular Neurobiology*, vol. 51, no. 1, pp. 252–267, 2015.

[25] E. Lobarinas, C. Spankovich, and C. G. le Prell, "Evidence of "hidden hearing loss" following noise exposures that produce robust TTS and ABR wave-I amplitude reductions," *Hearing Research*, vol. 349, pp. 155–163, 2017.

[26] W. Ni, C. Lin, L. Guo et al., "Extensive supporting cell proliferation and mitotic hair cell generation by *in vivo* genetic reprogramming in the neonatal mouse cochlea," *The Journal of Neuroscience*, vol. 36, no. 33, pp. 8734–8745, 2016.

[27] Y. Yuan, F. Shi, Y. Yin et al., "Ouabain-induced cochlear nerve degeneration: synaptic loss and plasticity in a mouse model of auditory neuropathy," *Journal of the Association for Research in Otolaryngology*, vol. 15, no. 1, pp. 31–43, 2014.

[28] X. Lu, S. Sun, J. Qi et al., "Bmi1 regulates the proliferation of cochlear supporting cells via the canonical Wnt signaling pathway," *Molecular Neurobiology*, vol. 54, no. 2, pp. 1326–1339, 2017.

[29] M. C. Liberman, "Noise-induced and age-related hearing loss: new perspectives and potential therapies," *F1000Res*, vol. 6, p. 927, 2017.

[30] D. O. J. Reijntjes and S. J. Pyott, "The afferent signaling complex: regulation of type I spiral ganglion neuron responses in the auditory periphery," *Hearing Research*, vol. 336, pp. 1–16, 2016.

[31] D. Bing, S. C. Lee, D. Campanelli et al., "Cochlear NMDA receptors as a therapeutic target of noise-induced tinnitus," *Cellular Physiology and Biochemistry*, vol. 35, no. 5, pp. 1905–1923, 2015.

[32] P. E. Schauwecker, "Neuroprotection by glutamate receptor antagonists against seizure-induced excitotoxic cell death in the aging brain," *Experimental Neurology*, vol. 224, no. 1, pp. 207–218, 2010.

[33] A. C. Meyer, T. Frank, D. Khimich et al., "Tuning of synapse number, structure and function in the cochlea," *Nature Neuroscience*, vol. 12, no. 4, pp. 444–453, 2009.

[34] J. Ruel, C. Chen, R. Pujol, R. P. Bobbin, and J. L. Puel, "AMPA-preferring glutamate receptors in cochlear physiology of adult guinea-pig," *The Journal of Physiology*, vol. 518, no. 3, pp. 667–680, 1999.

[35] E. Glowatzki and P. A. Fuchs, "Transmitter release at the hair cell ribbon synapse," *Nature Neuroscience*, vol. 5, no. 2, pp. 147–154, 2002.

[36] J. Ruel, J. Wang, G. Rebillard et al., "Physiology, pharmacology and plasticity at the inner hair cell synaptic complex," *Hearing Research*, vol. 227, no. 1-2, pp. 19–27, 2007.

[37] L. Grant, E. Yi, and E. Glowatzki, "Two modes of release shape the postsynaptic response at the inner hair cell ribbon synapse," *The Journal of Neuroscience*, vol. 30, no. 12, pp. 4210–4220, 2010.

[38] S. F. Traynelis, L. P. Wollmuth, C. J. McBain et al., "Glutamate receptor ion channels: structure, regulation, and function," *Pharmacological Reviews*, vol. 62, no. 3, pp. 405–496, 2010.

[39] J. T. R. Isaac, M. C. Ashby, and C. J. McBain, "The role of the GluR2 subunit in AMPA receptor function and synaptic plasticity," *Neuron*, vol. 54, no. 6, pp. 859–871, 2007.

[40] J. T. Sanchez, S. Ghelani, and S. Otto-Meyer, "From development to disease: diverse functions of NMDA-type glutamate receptors in the lower auditory pathway," *Neuroscience*, vol. 285, pp. 248–259, 2015.

[41] D. Liao, N. A. Hessler, and R. Malinow, "Activation of postsynaptically silent synapses during pairing-induced LTP in CA1 region of hippocampal slice," *Nature*, vol. 375, no. 6530, pp. 400–404, 1995.

[42] C. G. D'Aldin, J. Ruel, R. Assie, R. Pujol, and J. L. Puel, "Implication of NMDA type glutamate receptors in neural regeneration and neoformation of synapses after excitotoxic injury in the guinea pig cochlea," *International Journal of Developmental Neuroscience*, vol. 15, no. 4-5, pp. 619–629, 1997.

[43] I. J. Reynolds and T. G. Hastings, "Glutamate induces the production of reactive oxygen species in cultured forebrain neurons following NMDA receptor activation," *The Journal of Neuroscience*, vol. 15, no. 5, pp. 3318–3327, 1995.

[44] Y. Wang and Z. H. Qin, "Molecular and cellular mechanisms of excitotoxic neuronal death," *Apoptosis*, vol. 15, no. 11, pp. 1382–1402, 2010.

[45] R. C. Ewald and H. T. Cline, "NMDA receptors and brain development," in *Biology of the NMDA Receptor*, A. M. Dongen, Ed., pp. 1–29, CRC Press/Taylor & Francis, Boca Raton, FL, USA, 2009.

[46] W.-Y. Lu, H.-Y. Man, W. Ju, W. S. Trimble, J. F. MacDonald, and Y. T. Wang, "Activation of synaptic NMDA receptors induces membrane insertion of new AMPA receptors and LTP in cultured hippocampal neurons," *Neuron*, vol. 29, no. 1, pp. 243–254, 2001.

[47] H. M. Sobkowicz, J. E. Rose, G. L. Scott, and C. V. Levenick, "Distribution of synaptic ribbons in the developing organ of Corti," *Journal of Neurocytology*, vol. 15, no. 6, pp. 693–714, 1986.

[48] J. R. Steinert, C. Kopp-Scheinpflug, C. Baker et al., "Nitric oxide is a volume transmitter regulating postsynaptic excitability at a glutamatergic synapse," *Neuron*, vol. 60, no. 4, pp. 642–656, 2008.

Hindawi
Neural Plasticity
Volume 2018, Article ID 4920980, 7 pages
https://doi.org/10.1155/2018/4920980

Research Article

Genetic Etiology Study of Ten Chinese Families with Nonsyndromic Hearing Loss

Songqun Hu, Feifei Sun, Jie Zhang, Yan Tang, Jinhong Qiu, Zhixia Wang, and Luping Zhang

Department of Otolaryngology, Affiliated Hospital of Nantong University, Nantong, Jiangsu Province, China

Correspondence should be addressed to Luping Zhang; zhanglp910@126.com

Received 24 January 2018; Revised 28 April 2018; Accepted 13 May 2018; Published 5 July 2018

Academic Editor: Hai Huang

Nonsyndromic hearing loss has been shown to have high genetic heterogeneity. In this report, we aimed to disclose the genetic causes of the subjects from the ten Chinese deaf families who did not have pathogenic common genes/mutation. Next-generation sequencing (NGS) of 142 known deafness genes was performed in the probands of ten families followed by cosegregation analysis of all family members. We identified novel pathogenic variants in six families including p.D1806E/p.R1588W, p.R964W/p.R1588W, and p.G17C/p.G1449D in *CDH23*; p.T584M/p.D1939N in *LOXHD1*; p.P1225L in *MYO7A*; and p.K612X in *EYA4*. Sanger sequencing confirmed that these mutations segregated with the hearing loss of each family. In four families, no pathogenic variants were identified. Our study provided better understanding of the mutation spectrum of hearing loss in the Chinese population.

1. Introduction

Hearing loss (HL) is the most common sensory disorder in humans, affecting one in every 500 newborns. Genetic causes account for at least 50% to 60% of childhood HL [1]. An accurate genetic diagnosis provides many immediate and long-term advantages to patients and their families [2]. Hereditary HL, however, is a highly heterogenous disorder. To date, over 90 genes have been identified as responsible for nonsyndromic sensorineural hearing loss (NSHL, http://hereditaryhearingloss.org/). In China, mutations in many genes have been found associated with hereditary HL, and the mutation spectrums were broad and diverse [3].Genetic heterogeneity and the small size of families with hereditary HL have hindered the unravelling of the genetic causes. Recently, the advent of targeted DNA capturing and next-generation sequencing (NGS) may make it possible to analyze most, if not all, deafness genes, as opposed to screening of each individual gene by conventional Sanger sequencing [2–4]. Using this strategy, we analyzed ten Chinese families with hereditary hearing loss and disclose their genetic causes.

2. Methods

2.1. Family Description and Clinical Evaluations. The ten families (NT-1~10) were recruited from the Department of Otolaryngology, Affiliated Hospital of Nantong University, Nantong, China. The pedigrees of those hearing loss-affected families of Han origin are shown in Figures 1 and 2. All patients had bilateral, symmetrical sensorineural hearing loss (SNHL). They received comprehensive medical history inquiry and thorough exams of auditory sense, vestibular function, and ophthalmic function, to rule out any possible environmental factors or syndromic hearing loss. All affected individuals were evaluated through detailed audiological evaluations including otoscopy, pure-tone audiometry, auditory brainstem response (ABR), distortion product otoacoustic emissions (DPOAEs), and auditory steady-state response (ASSR) test in subjects with very young age. The hearing loss level was classified as described previously [3]. Computed tomography (CT) scans were performed in the ten probands. This study was approved by the Ethics Committee of the Affiliated Hospital of Nantong University. All subjects gave

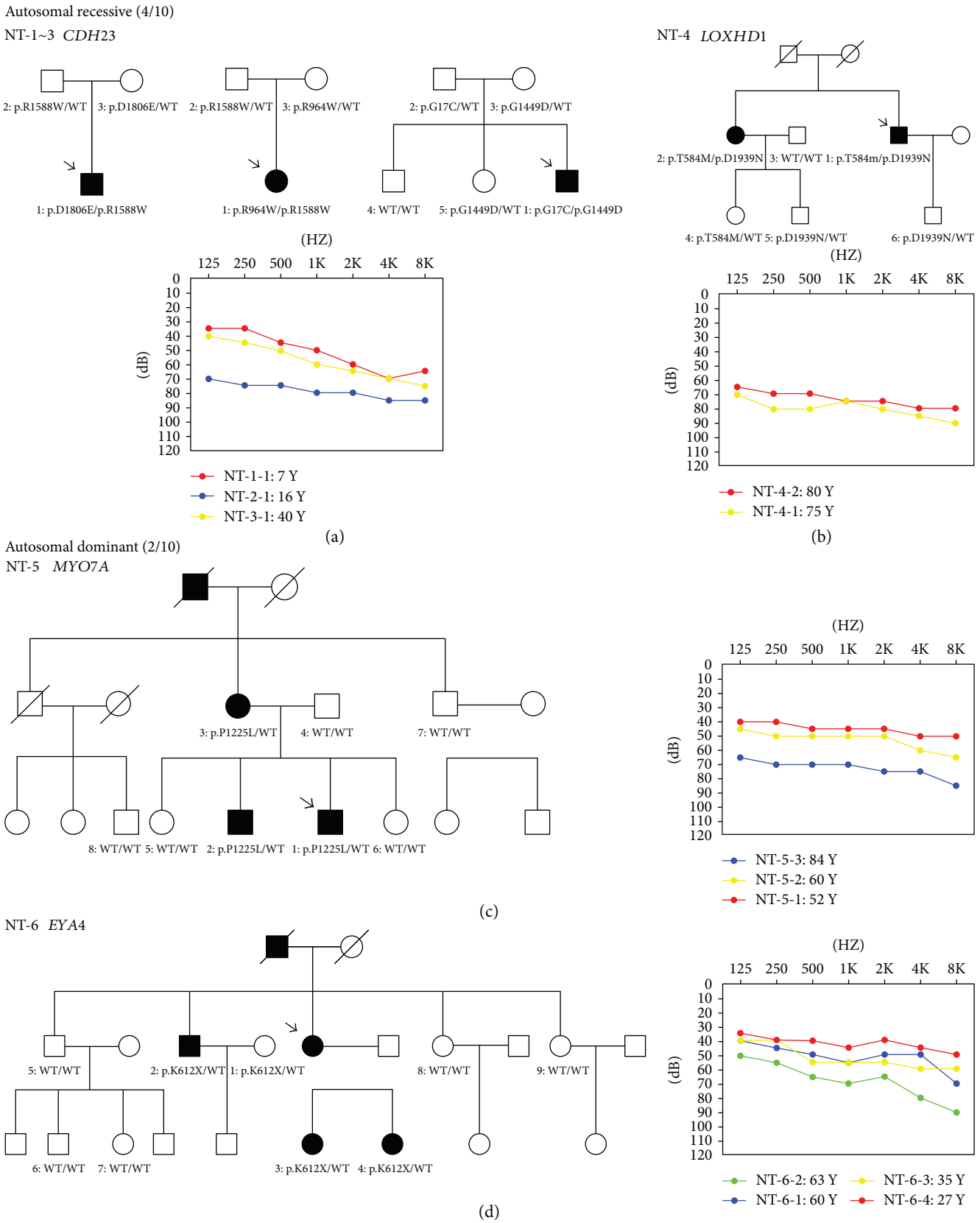

Figure 1: Pedigrees, genetic findings, and audiograms for NT-1~3 (a), NT-4 (b), NT-5 (c), and NT-6 (d). The arrow shows the probands in each family.

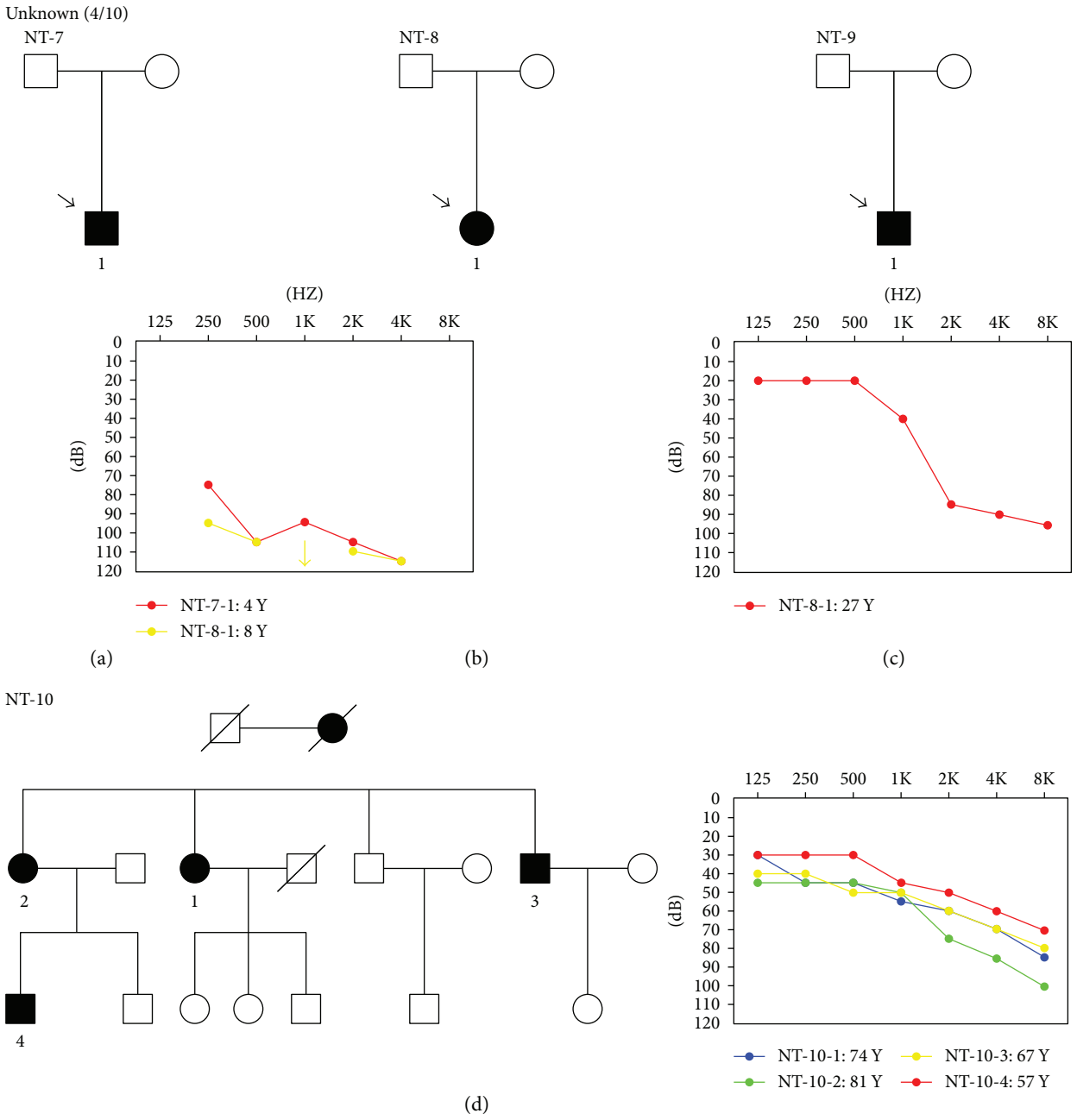

Figure 2: Pedigrees and audiometric features of family NT-7 (a), NT-8 (b), NT-9 (c), and NT-10 (d).

written informed consent to participate in this study from October 1, 2014, to December 31, 2017.

2.2. Targeted Massively Parallel Sequencing. Genomic DNAs from all the family members available were extracted from whole peripheral blood leukocytes using a DNA extraction kit (Tiangen Biotech, China). Mutation screening of *GJB2*, *SLC26A4*, and the mitochondrial 12S rRNA was conducted first in ten probands using polymerase chain reaction (PCR) amplification, and exons were sequenced directly. All 10 probands of the deaf families were subjected to a gene panel containing 142 deafness-related genes by NGS (Supplementary 1). Targeted gene capturing, data processing, bioinformatic analysis, and filtering against multiple databases for SNPs were performed as reported in detail previously [3]. Potential causative variants detected by targeted massively parallel sequencing were confirmed by Sanger sequencing in each proband. Cosegregation analysis was also performed for multiplex probands in all family individuals if available.

3. Results

3.1. Clinical Manifestations. All the patients in the ten Chinese families showed bilateral, symmetrical, nonsyndromic, sensorineural hearing impairment. The age of the affected family members ranged from 4 to 84 years. The age at onset of hearing loss in these patients ranged from

congenital to 42 years old. The hearing loss was symmetric while there was a wide range of different degrees of HL including moderate, severe, and profound. The patients, who carried compound heterozygous mutations in *CDH23* (NT-1-1, NT-2-1, and NT-3-1) and *MYO7A* (NT-5-1), two genes associated with both nonsyndromic deafness and Usher syndrome type 1, did not show any degenerative symptoms of retinitis pigmentosa. No inner ear malformation was observed by CT scanning.

3.2. Mutation Analysis. The results of screening of the three common genes in the probands of the 10 families were all negative. Targeted NGS of 142 hearing loss-related genes was carried out in the ten probands. Briefly, to detect possible causative mutations, variants meeting the criteria were filtered out as previously described [3]. Possible causative variants were summarized in Supplementary 2. The novel compound heterozygous variants were verified in four recessive families, including p.R1588W/p.D1806E of *CDH23* in NT-1-1, p.R964W/p.R1588W of *CDH23* in NT-2-1, p.G17C/p.G1449D of *CDH23* in NT-3-1, and p.T584M/p.D1939N of *LOXHD1* in NT-4-1. In addition, we identified two heterozygous candidate mutations p.P1225L in *MYO7A* and p.K612X in *EYA4* in two dominant probands NT-5-1 and NT-6-2, respectively. Sanger sequencing of available family members revealed that these mutations were present in all affected family individuals but not in the normal individuals (Supplementary 3).

Among the nine candidate mutations, p.R1588W, p.D1806E, and p.G1449D in *CDH23* have been reported to be pathogenic in previous reports [4–6]. As for the other six novel variants, p.K612X in *EYA4* was predicted to result in EYA4 eyaHR deletion, while p.G17C and p.R964W in *CDH23*, p.T584M and p.D1939N in *LOXHD1*, and p.P1225L in *MYO7*A were unanimously evaluated to be possibly damaging or disease-causing by more than two of the bioinformatic programs, such as the Mutation Taster, SIFT, and PolyPhen2. Our data indicated that six variants in *CDH23*, *LOXHD1*, *MYO7A*, and *EYA4* were likely to be pathogenic rather than a polymorphism. (Table 1, Supplementary 4). No disease-causing variants were identified in families NT-7, NT-8, NT-9, and NT-10.

4. Discussion

In this study, biallelic mutations in *CDH23* were identified by targeted NGS in 3 of the 10 families. Mutations in *CDH23* are the pathogenic cause for both Usher syndrome 1D (USH1D) and autosomal recessive nonsyndromic hearing loss (DFNB12). Patients with DFNB12 usually carry *CDH23* missense mutations in any domain, whereas individuals with USH1D usually have nonsense, splice-site, and frameshift mutations [5–7]. To date, at least 80 pathogenic variants of the *CDH23* have been reported in familial or sporadic patients of USH1D and DFNB12 worldwide. Ethnic diversity of genetic variance has been reported in deafness gene *CDH23* [4-8]. However, few of these mutations were detected in the Chinese population [3]. In this study, three compound heterozygous mutations (p.R1588W/p.D1806E, p.G17C/p.G1449D, and p.R964W/p.R1588W) in *CDH23* were identified by targeted NGS in two patients with moderate HL and one with severe HL. At the time of this report, the patients NT-1-1, NT-2-1, and NT-3-1 who carried the compound heterozygous *CDH23* mutations were 7, 16, and 43 years, respectively. No visual problems and vestibular dysfunction were revealed in any of them. Nevertheless, especially for young probands NT-1-1 and NT-2-1, we cannot definitely rule out that they would develop retinopathy later in their life. In previous studies, audiological phenotypes of *CDH23* compound heterozygotes seemed to be highly variable [8, 9]. Similarly in our study, NT-1-1 and NT-2-1 manifested prelingual-onset SNHL, while NT-3-1 showed adult-onset progressive SNHL that was not noticeable until age 30. The two probands (NT-1-1, NT-2-1) both used a hearing aid with satisfactory effect. They have normal conversations and are enrolled in regular school. In addition, we identified a relatively high prevalence (3/10) of *CDH23* mutations in Chinese Han population, and our report of the two novel mutations expanded the *CDH23* mutation spectrum.

LOXHD1 mutations have been highly rare, which are known to be the cause of DFNB77. Up to date, there have been only six studies [10]. In the present study, we identified c.1751C>T (p.T584M) and c.5815G>A (p.D1939N) as novel, possibly pathogenic *LOXHD1* mutations, which cosegregated with the disease. It was predicted as possibly pathogenic by PolyPhen2, SIFT, and Mutation Taster. This is the first reported *LOXHD1* mutation causing hearing loss in China. In family NT-4, two affected siblings (NT-4-1, male, 75 years old; NT-4-2, female, 80 years old) had experienced bilateral slowly progressive hearing loss with onset of 35–40 yrs. Additionally, they both reported troublesome tinnitus. Phenotype-wise, compared to the previous reports [10, 11], our cases had milder and progressive hearing impairment.

The *MYO7A* gene mutations have been reported as the cause of Usher syndrome type 1B (USH1B), a syndromic deafness combined with retinitis pigmentosa and vestibular abnormalities [12]. *MYO7A* is also associated with nonsyndromic hearing loss (DFNB2, DFNA11) [13–15]. More recently, only eight mutations in the *MYO7A* gene have been identified associated with DFNA11 [15]. Here, we identify a novel missense variants (c.3674C>T, p.P1225L) in a Chinese family with progressive SNHL affecting all frequencies. In this study, three affected subjects from family NT-5, who had the p.P1225L heterozygous mutation in *MYO7A*, were 84, 60, and 52 years at the test. The genetic defect segregating in this family shows autosomal dominant inheritance. The absence of vestibular and retinal defects and less severe hearing loss is consistent with the phenotype of a recently reported Chinese family [15]. Thus, we speculate this family has nonsyndromic hearing loss (DFNA11).

Another novel causative variant identified in the present study is p.K612X of *EYA4* segregating with dominant hearing loss in family NT-6. The *EYA4* gene is known to be responsible for both nonsyndromic deafness DFNA10 and syndromic deafness with dilated cardiomyopathy [16–18]. The novel

Table 1: Mutations detected in six Chinese Han families.

Family ID	Gene	Mutation type	Nucleotide change (transcript version)	Amino acid change	Phylop score	Mutation taster	PROVEAN (score)	SIFT (score)	Allele frequency in controls	Novel or HGMD
Recessive										
NT-1	CDH23	Missense	c.4762C>T (NM_022124)	p.R1588W	3.822	DC	Deleterious (−3.136)	Damaging −0.001	0/400	HGMD
	CDH23	Missense	c.5418C>G (NM_022124)	p.D1806E	−1.832	DC	Neutral (−0.778)	Damaging −0.007	0/400	HGMD
NT-2	CDH23	Missense	c.2890C>T (NM_022124)	p.R964W	0.855	DC	Deleterious (−2.783)	Damaging −0.005	0/400	Novel
	CDH23	Missense	c.4762C>T (NM_022124)	p.R1588W	3.822	DC	Deleterious (−3.136)	Damaging −0.001	0/400	HGMD
NT-3	CDH23	Missense	c.49G>T NM_001171935	p.G17C	0.8	—	Deleterious (−4.405)	—	0/400	Novel
	CDH23	Missense	c.4346G>A (NM_022124)	p.G1449D	5.967	*DC*	Deleterious (−2.886)	Tolerated −0.233	0/400	HGMD
NT-4	LOXHD1	Missense	c.1751C>T (NM_144612)	p.T584 M	9.151	DC	Deleterious (−4.6)	Damaging −0.001	0/600	Novel
	LOXHD1	Missense	c.5815G>A (NM_144612)	p.D1939N	7.672	DC	Deleterious (−2.51)	Damaging −0.01	0/600	Novel
Dominant										
NT-5	MYO7A	Missense	c.3674C>T (NM_000260)	p.P1225L	5.846	DC	Deleterious (−7.82)	Damaging −0.03	0/600	Novel
NT-6	EYA4	nonsense	c.1834A>T (NM_004100)	p.K612X	7.21	DC	—	—	0/600	Novel

p.K612X truncating mutation changed Lys612 to a stop codon, which was predicted to lead to a premature termination prior to the EYA homolog domains. It suggests that this nonsense mutation may inhibit normal development and maintenance of the organ of Corti and cause SNHL. The postlingual, progressive SNHL phenotype in family NT-6 is similar to what has been reported for four unrelated Chinese DFNA10 families [19–22]. Combining with previous studies, our study suggests that mutations in *EYA4* are not a relatively rare cause for autosomal dominant NSHL in the Chinese population, and our data provide more insights into the genotype-phenotype correlation between the truncating mutation of *EYA4* and the DFNA10 phenotype.

In this study, we were not able to obtain a genetic diagnosis for the other four families using the current NGS panel (Figure 2). Further studies including the whole-exome sequencing in the negative families could be useful to discover potential novel NSHL genes and to draw a complete molecular epidemiology picture.

5. Conclusions

In conclusion, we successfully identified novel and likely pathogenic mutations in six Chinese families by targeted NGS. Our result demonstrates that this new method is a highly effective molecular diagnostic tool for this heterogeneous disorder.

Data Availability

The data used to support the findings of this study are available from the corresponding author upon request.

Conflicts of Interest

The authors declare no competing financial interests.

Authors' Contributions

Songqun Hu and Feifei Sun contributed equally to this work.

Acknowledgments

The authors thank the families for their participation and support in this study. This investigation was supported by grants from Nantong Science and Technology Plan Frontier and Key Technology Innovation Fund (MS22015048 to Luping Zhang), National Science Foundation of China (81641155 to Luping Zhang), and the Postgraduate Innovation Program from Nantong University (SJLX16_0570 to Feifei Sun).

Supplementary Materials

Supplementary 1. Table S1: 142 genes targeted for the next-generation sequencing.

Supplementary 2. Table S2: all variants identified by targeted NGS.

Supplementary 3. Figure 1: validation of candidate mutations by PCR-Sanger sequencing.

Supplementary 4. Function analysis on candidate mutations.

References

[1] C. C. Morton and W. E. Nance, "Newborn hearing screening — a silent revolution," *New England Journal of Medicine*, vol. 354, no. 20, pp. 2151–2164, 2006.

[2] L. P. Zhang, Y. C. Chai, T. Yang, and H. Wu, "Identification of novel *OTOF* compound heterozygous mutations by targeted next-generation sequencing in a Chinese patient with auditory neuropathy spectrum disorder," *International Journal of Pediatric Otorhinolaryngology*, vol. 77, no. 10, pp. 1749–1752, 2013.

[3] T. Yang, X. Wei, Y. Chai, L. Li, and H. Wu, "Genetic etiology study of the non-syndromic deafness in Chinese Hans by targeted next-generation sequencing," *Orphanet Journal of Rare Diseases*, vol. 8, no. 1, p. 85, 2013.

[4] M. Miyagawa, T. Naito, S. Nishio, N. Kamatani, and S. I. Usami, "Targeted exon sequencing successfully discovers rare causative genes and clarifies the molecular epidemiology of Japanese deafness patients," *PLoS One*, vol. 8, no. 8, p. e71381, 2013.

[5] B. J. Kim, A. R. Kim, C. Lee et al., "Discovery of *CDH23* as a significant contributor to progressive postlingual sensorineural hearing loss in Koreans," *PLoS One*, vol. 11, no. 10, article e0165680, 2016.

[6] W. J. Kimberling, M. S. Hildebrand, A. E. Shearer et al., "Frequency of usher syndrome in two pediatric populations: implications for genetic screening of deaf and hard of hearing children," *Genetics in Medicine*, vol. 12, no. 8, pp. 512–516, 2010.

[7] L. M. Astuto, J. M. Bork, M. D. Weston et al., "CDH23 mutation and phenotype heterogeneity: a profile of 107 diverse families with usher syndrome and nonsyndromic deafness," *American Journal of Human Genetics*, vol. 71, no. 2, pp. 262–275, 2002.

[8] K. Mizutari, H. Mutai, K. Namba et al., "High prevalence of *CDH23* mutations in patients with congenital high-frequency sporadic or recessively inherited hearing loss," *Orphanet Journal of Rare Diseases*, vol. 10, no. 1, p. 60, 2015.

[9] M. Miyagawa, S. Nishio, and S. Usami, "Prevalence and clinical features of hearing loss patients with CDH23 mutations: a large cohort study," *PLoS One*, vol. 7, no. 8, p. e40366, 2012.

[10] S. B. Minami, H. Mutai, K. Namba, H. Sakamoto, and T. Matsunaga, "Clinical characteristics of a Japanese family with hearing loss accompanied by compound heterozygous mutations in LOXHD1," *Auris Nasus Larynx*, vol. 43, no. 6, pp. 609–613, 2016.

[11] N. Grillet, M. Schwander, M. S. Hildebrand et al., "Mutations in LOXHD1, an evolutionarily conserved stereociliary protein, disrupt hair cell function in mice and cause progressive hearing loss in humans," *American Journal of Human Genetics*, vol. 85, no. 3, pp. 328–337, 2009.

[12] D. Well, S. Blanchard, J. Kaplan et al., "Defective myosin VIIA gene responsible for Usher syndrome type IB," *Nature*, vol. 374, no. 6517, pp. 60-61, 1995.

[13] Y. Ma, Y. Xiao, F. Zhang et al., "Novel compound heterozygous mutations in *MYO7A* gene associated with autosomal recessive sensorineural hearing loss in a Chinese family,"

International Journal of Pediatric Otorhinolaryngology, vol. 83, no. 4, pp. 179–185, 2016.

[14] Y. Sun, J. Chen, H. Sun et al., "Novel missense mutations in *MYO7A* underlying postlingual high- or low-frequency non-syndromic hearing impairment in two large families from China," *Journal of Human Genetics*, vol. 56, no. 1, pp. 64–70, 2011.

[15] Q. Sang, X. Yan, H. Wang et al., "Identification and functional study of a new missense mutation in the motor head domain of myosin VIIA in a family with autosomal dominant hearing impairment (DFNA11)," *PLoS One*, vol. 8, no. 1, article e55178, 2013.

[16] J. Schönberger, L. Wang, J. T. Shin et al., "Mutation in the transcriptional coactivator *EYA4* causes dilated cardiomyopathy and sensorineural hearing loss," *Nature Genetics*, vol. 37, no. 4, pp. 418–422, 2005.

[17] E. van Beelen, A. M. M. Oonk, J. M. Leijendeckers et al., "Audiometric characteristics of a Dutch DFNA10 family with mid-frequency hearing impairment," *Ear and Hearing*, vol. 37, no. 1, pp. 103–111, 2016.

[18] H. S. Choi, A. R. Kim, S. H. Kim, and B. Y. Choi, "Identification of a novel truncation mutation of EYA4 in moderate degree hearing loss by targeted exome sequencing," *European Archives of Oto-Rhino-Laryngology*, vol. 273, no. 5, pp. 1123–1129, 2016.

[19] A. Huang, Y. Yuan, Y. Liu, Q. Zhu, and P. Dai, "A novel *EYA4* mutation causing hearing loss in a Chinese DFNA family and genotype-phenotype review of *EYA4* in deafness," *Journal of Translational Medicine*, vol. 13, no. 1, p. 154, 2015.

[20] F. Liu, J. Hu, W. Xia et al., "Exome sequencing identifies a mutation in EYA4 as a novel cause of autosomal dominant non-syndromic hearing loss," *PLoS One*, vol. 10, no. 5, article e0126602, 2015.

[21] Y. Sun, Z. Zhang, J. Cheng et al., "A novel mutation of EYA4 in a large Chinese family with autosomal dominant middle-frequency sensorineural hearing loss by targeted exome sequencing," *Journal of Human Genetics*, vol. 60, no. 6, pp. 299–304, 2015.

[22] M. Tan, X. Shen, J. Yao et al., "Identification of I411K, a novel missense EYA4 mutation causing autosomal dominant non-syndromic hearing loss," *International Journal of Molecular Medicine*, vol. 34, no. 6, pp. 1467–1472, 2014.

Hindawi
Neural Plasticity
Volume 2018, Article ID 4372913, 10 pages
https://doi.org/10.1155/2018/4372913

Research Article

Knock-In Mice with Myo3a Y137C Mutation Displayed Progressive Hearing Loss and Hair Cell Degeneration in the Inner Ear

Peipei Li, Zongzhuang Wen, Guangkai Zhang, Aizhen Zhang, Xiaolong Fu, and Jiangang Gao

School of Life Science, Shandong University, Jinan 250100, China

Correspondence should be addressed to Jiangang Gao; jggao@sdu.edu.cn

Received 21 March 2018; Accepted 28 May 2018; Published 5 July 2018

Academic Editor: Renjie Chai

Myo3a is expressed in cochlear hair cells and retinal cells and is responsible for human recessive hereditary nonsyndromic deafness (DFNB30). To investigate the mechanism of DFNB30-type deafness, we established a mouse model of Myo3a kinase domain Y137C mutation by using CRISPR/Cas9 system. No difference in hearing between 2-month-old Myo3a mutant mice and wild-type mice was observed. The hearing threshold of the ≥6-month-old mutant mice was significantly elevated compared with that of the wild-type mice. We observed degeneration in the inner ear hair cells of 6-month-old Myo3a mutant mice, and the degeneration became more severe at the age of 12 months. We also found structural abnormality in the cochlear hair cell stereocilia. Our results showed that Myo3a is essential for normal hearing by maintaining the intact structure of hair cell stereocilia, and the kinase domain plays a critical role in the normal functions of Myo3a. This mouse line is an excellent model for studying DFNB30-type deafness in humans.

1. Introduction

Deafness presents the highest incidence among sensory defects. One-third of the global population suffer from hearing impairment. Approximately 300 million people currently possess hearing disabilities [1–3]. Presbyacusis, also known as age-related hearing loss (ARHL), refers to the gradual onset of sensorineural hearing loss with age. According to WHO statistics, over one-third of the >65-year-old population are currently affected by senile deafness. The contribution of hearing loss to the general health of individuals during that extended lifespan is of considerable clinical and economic significance [4]. ARHL inevitably causes communication difficulties and is associated with social isolation and depression and decreases physical and cognitive function [5, 6]. Therefore, determining ways to prevent presbyacusis and identifying its pathogenesis have become crucial. Senile deafness is related to environmental factors, such as disease, ear-toxic drugs, noise, and mental trauma, and genetic factors play an important role in this process. Nearly 50% of age-related deafness is determined by genetic factors [7]. Senile deafness is a complex disease that can be affected by a variety of environmental factors, and differences in the genetic background of different populations can interfere with research. Therefore, the use of gene knock-out/knock-in mouse model can strictly control environmental conditions and reduce the influence of genetic background, thereby providing important tools for the validation of age- and deafness-related genes. Therefore, the establishment of presbyacusis animal model has become an important method in studying presbyacusis.

Our hearing depends on hair cells in the inner ear, which can convert the vibrations of sound into electrical signals. At the apical surface of each hair cell, three rows of stereocilium are arranged in high and low orders [8, 9]. When sound is introduced into the inner ear, sound waves cause a slight vibration of the cochlear basilar membrane. The basilar membrane vibration is transduced into an electric signal by a mechanoelectro transduction (MET) protein, which can open the ion channel at the top of the stereocilium and

generate a membrane potential. The mechanical signal transduction that occurs at the top of the hair cell stereocilium may comprise a complex of proteins called MET protein complex [10, 11]. In mammals, Myo3a is mainly expressed in the retina [12] and cochlea [13, 14]. In inner ear hair cells, Myo3a is specifically expressed near the tips of the stereocilium, where the MET protein is located [13]. Myo3a protein localization implies its importance in hearing. Myo3a mutations in humans can cause nonsyndrome-type deafness (DFNB30) [14], where patients experience progressive bilateral hearing loss. Hearing loss usually begins at the second decade and becomes severe by the age of 50. In addition, Myo3a is a candidate gene for the disease Bardet-Biedl syndrome, an important human retinal disease [15].

Based on different C-terminal cargo-binding domains, myosin superfamily members are classified into conventional myosins (class II) and unconventional myosins (classes I and III–XV) [16–18]. Myo3a is a class III myosin. The Myo3a protein contains a kinase domain at the N-terminal, followed by a highly conserved motor region and three IQ motifs. Two of the IQ motifs are located at the conserved neck region, and the third motif is located at the center of the tail domain [19]. Myo3a is special because it is autophosphorylated by a kinase domain [20]. In 2010, Walsh et al. generated the Myo3a knock-out mouse model, which showed the characteristics of senile deafness [21]. The knock-out mouse model converts the 1041th codon of Myo3a into a termination codon, which is located at the 28th exon, allowing the knock-out of the protein after the 27th exon. However, the head kinase domain, motor domain, and the regulatory neck domain still remain. The mutation site of Myo3a in humans frequently appears in the head domain of the protein. Our collaborators and our team found that a Myo3a Y129C mutation within the kinase domain can cause ARHL in humans (data not shown). Mimicking this point mutation, we established knock-in mice by changing the tyrosine (Y137) to cysteine in Myo3a. A series of experiments was conducted on these mutant mice to determine the function of Myo3a in the cochlea. The mutant mice displayed progressive hearing loss and inner ear hair cell degeneration. The mouse we generated is a good model for studying DFNB30-type deafness in human and provides valuable material for the study of ARHL.

2. Materials and Methods

2.1. Ethics Statement. All animal experimental procedures were approved by the Ethics Committee of Shandong University. Animal management was performed strictly in accordance with the standards of the Animal Ethics of Shandong University.

2.2. Generation of Myo3a Y137C Mouse. Myo3a mutant mice were generated using the CRISPR-Cas9 genome-editing technology and maintained on the CBA/CaJ background. pX330 plasmid was obtained from Addgene (plasmid ID number 42230). The CRISPR-Cas9 genome-editing technology in mice was used as previously described [22–26]. In brief, a pair of oligonucleotides for the target sequence (5′-CACCGTGTAAAATATATGCAATTAC-3′ and 5′-AAACGTAATTGCATATATTTTACAC-3′) was annealed and ligated to pX330 that was previously digested with BbsI. The pX330 plasmid containing sgRNA and Cas9 was purified and eluted in RNase-free water. The following repair template, which contained the target mutation and two synonymous mutations, was commercially synthesized as follows: ggatttctgaagaggggagaaagaatgagcgagcctgtaatCgcCtGtattttacac gaagcactaatggtaaggctatttgaactctt.

CBA/CaJ female mice were superovulated and mated with CBA/CaJ male mice. The fertilized eggs were removed from the oviducts on the next day. pX330 plasmid (5 ng/μL) mixed with 10 ng/μL repair template was microinjected into the pronucleus of fertilized eggs. After injection, eggs were incubated for 10 min. The eggs were then transferred into the oviducts of pseudopregnant CD1 female mice.

Genomic DNA was extracted from the tails of newborn pups. The genomic DNA fragment around the gRNA target site was amplified by PCR using the Myo3a forward primer 5′-AGCTGTGACCTTTTTGAAGATAGC-3′ and the Myo3a reverse primer 5′-ATCAACAAACACCAAGCTG CC-3′. The total reaction volume of 40 μL contains Taq DNA polymerase, PCR buffer, 2 μL 10 mM forward primers, 2 μL 10 mM reverse primer, and 1 μL DNA fragment. Amplification was performed for 3 min at 95°C, followed by 33 cycles, with each consisting of 30 S at 95°C, 30 S at 60°C, and 30 S at 72°C, with a final extension step of 10 min at 72°C. The obtained PCR products were directly sequenced or cloned using the T/A cloning method and then sequenced to identify the mutation.

2.3. Measurement of Hearing Thresholds. ABR was measured to determine the hearing thresholds of mice in a sound-isolated room as previously described [27, 28]. Mice were anesthetized with 0.007 g/mL pentobarbital sodium by intraperitoneal injection (50 mg/kg body weight). Three needle electrodes were placed subcutaneously in the anesthetized mice. Ground, active, and reference electrodes were placed at the back near the tail, above the vertex between the eyes, and underneath the ear, respectively. Hearing thresholds were measured using a Tucker-Davis Technologies System (TDT, USA) workstation that runs the SigGen32 software (TDT, USA). Mice were presented with click and tone burst stimuli at frequencies of 4, 8, 16, and 32 kHz. Auditory thresholds (dB SPL) were determined by decreasing the sound intensities from 90 dB to 10 dB until the lowest sound intensity at which waveforms lose their reproducible morphology is reached. Myo3a mutant mice were compared with their wild-type littermates at each age. More than five animals were used in each experiment.

2.4. Paraffin Sectioning and Hematoxylin and Eosin (H&E) Staining. The cochleae from Myo3a mutant and wild-type mice were removed, fixed with 4% formaldehyde in 10 mM phosphate buffer at 4°C overnight, decalcified in 10% EDTA in 10 mM phosphate-buffered saline (PBS) at room temperature for 2 d, dehydrated with 30% to 100% ethanol series, and treated with xylene for transparency. The cochlea was embedded in paraffin, and the specimen was sectioned at 7 mm thickness using a thin semiautomatic microtome.

Sections were deparaffinized using xylene and 100% to 30% ethanol series, stained with H&E, and viewed under a light microscope (Nikon YS100).

2.5. Whole-Mount Staining. Wild-type and Myo3a mutant mice were anesthetized with 0.007 g/mL pentobarbital sodium. The cochleae were removed from anesthetized mice, fixed in 4% formaldehyde in 10 mM PBS at 4°C overnight, and decalcified in 10% EDTA at room temperature for 2 days [24, 26]. We isolated the basilar membrane from the cochlea under the Nikon TE2000 fluorescence microscope. The basilar membrane was washed with 10 mM PBS and blocked in 5% goat serum for 30 min at 37°C. Primary antibodies were diluted in 10 mM PBS and incubated with the basilar membrane at 4°C overnight. After being washed with 10 mM PBS, the basilar membrane was incubated at 37°C for 1 h in anti-rabbit TRITC-conjugated secondary antibody diluted in PBS [29, 30]. The basilar membrane was washed again with PBS, and Alexa Fluor 488-conjugated phalloidin (2 μg/mL, Sigma) was applied to the samples for 30 min and 4,6-diamidino-2-phenylindole (DAPI) for 15 min. Finally, the basilar membrane was washed thrice with 10 mM PBS. Morphologic changes in hair cells and stereocilia were observed in the basilar membrane-stretched preparation, and images were acquired using a Leica LSM 700 laser scanning microscope.

2.6. Scanning Electron Microcopy (SEM). Myo3a mutant mice and wild-type mice were anesthetized using pentobarbital sodium and perfused with 4% PFA. The cochleae from Myo3a mutant and wild-type mice were removed, fixed with 2.5% glutaraldehyde in 0.1 M PBS at 4°C overnight, and decalcified in 10% EDTA [31]. The cochleae were dissected out from the temporal bone, and the stria vascularis, Reissner's membrane, and tectorial membrane were removed [32]. The organ of Corti was exposed and postfixed in 1% osmium tetroxide in 0.1 M phosphate buffer [33] for 2 h before dehydration in an ethanol series and critical drying point in an Autosamdri-815A (Tousimis) [32]. Samples were mounted with carbon tape, coated with gold, and imaged with a JEOL 7000 field emission gun scanning electron microscope.

2.7. FM1-43 Staining Experiments. FM1-43 staining experiments were performed as previously reported [34]. First, the Myo3a mutant and wild-type mice were anesthetized, and their cochleae were removed. Cochlear samples were bathed with 3 mM FM1-43 solution for 20 s. The cochlear samples were treated with 4% PFA at 4°C overnight. On the next day, the cochlear samples were washed with 10 mM PBS for 10 min for several times. The cochleae were then observed under an LSM 780 confocal microscope.

2.8. Noise Exposure. Nine 4.5-month-old Myo3a mutant mice and seven wild-type mice were anesthetized with 0.007 g/mL pentobarbital sodium by intraperitoneal injection (50 mg/kg body weight) and placed in a 24 cm × 24 cm × 18 cm stainless steel cage for full white noise handling. The loudspeaker was located just in front of the cage. Sound intensity was calibrated using a standard sound level meter prior to exposure to noise. The mice were continuously treated with 98 ± 2 dB SPL for 2 h to produce a temporary change in auditory threshold shifts.

2.9. Statistical Analysis. All data were expressed as mean ± SD, and all experiments were repeated at least thrice to ensure the data accuracy and repeatability. Statistical analyses were implemented using Microsoft Excel, and charts were constructed using GraphPad Prism 5 software. Two-tailed, unpaired Student's t-tests were used to determine statistical significance when comparing two groups. $P < 0.05$ was considered statistically significant [35].

3. Results

3.1. Generation of Myo3a Y137C Mice Using CRISPR/Cas9. To mimic Myo3a Y129C mutation in human, we introduced the A410G (Y137C) mutation in mice by using CRISPR/Cas9 technology (Figure 1). To introduce the A410G mutation, we first induced a double-strand break (DSB) near the A410 and then repaired the DSB using the repair template with the point mutation of interest.

The sgRNA containing the 20 bp target sequence complexed with Cas9 protease can introduce DSB into the target sequence near a protospacer-adjacent motif (PAM) sequence. On the basis of this principle, we designed a specific sgRNA targeting the sequence near the A410 and cloned the sgRNA into the Px330 plasmid containing the Cas9 gene sequence. Thereafter, we designed a repair template with the mutation of interest based on the location of the DSB. The two synonymous mutations on the repair template aim to prevent a secondary targeting of sgRNA. The Px330 plasmid (5 ng/μL) and the repair template (10 ng/μL) were injected into the pronucleus of the fertilized mouse eggs. Exactly 113 fertilized eggs with clear pronucleus were injected, and 58 fertilized eggs with normal morphology after injection were transferred to the fallopian tubes of three pseudopregnant CD1 female mice. A total of 17 mice were born at 19 days after the transplantation. According to the PCR analysis results of the 17 mice, the mutation of interest was observed in 2 mice—a homozygous mouse and a heterozygous mouse (Figure 1(c)). We also performed sequencing at easy-off sites and found no off-targets. To obtain homozygous Myo3a KI/KI mice, we mated F0 mice with wild-type CBA/CaJ mice to generate F1 heterozygous mice, which were self-crossed to obtain homozygous Myo3a mutant mice. The Myo3a mutant mice were found to harbor cysteine in 137 rather than tyrosine in WT mice, similar to the mutation observed in humans.

Myo3a mutant mice were viable and fertile with no apparent abnormalities in their gross morphology (Figure 1(d)). We then examined the presence of an abnormal structure in the Myo3a mutant mice cochlea by paraffin sectioning and H&E staining. Structural abnormality was not observed in the Myo3a mutant mouse cochlea (Figure 1(e)).

3.2. Progressive Hearing Loss in Myo3a Mutant Mice. In humans, Myo3a mutation can cause nonsyndrome-type deafness. Thus, we wanted to test whether Myo3a mutant mice show the same symptoms. To determine whether

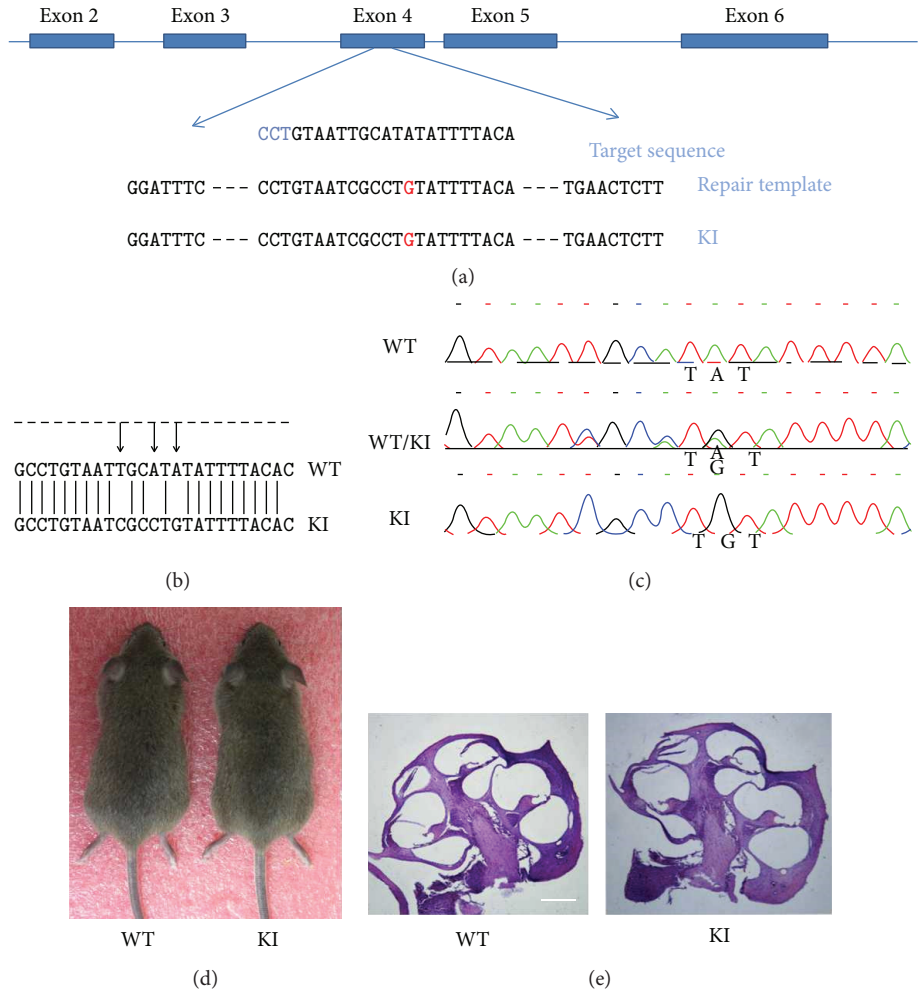

Figure 1: The generation of Myo3a mutant mice using CRISPR/Cas9. (a) Schematic diagram of targeting the mouse myosin IIIA gene. sgRNA was at exon 4 (indicated by the blue rectangles). The point mutation is in red. (b) The comparison of DNA sequences between Myo3a mutant mice (now referred to as Myo3a KI/KI mice) and wild-type mice. (c) Sequence of wild-type mice, heterozygous mice, and homozygous Myo3a KI/KI mutant mice. TAT was changed to TGT, demonstrating the missense mutation at mouse Y137C. (d) Gross morphology of Myo3a KI/KI and wild-type mice at the age of two months. There was no obvious difference. (e) Cochlea morphology is normal in Myo3a mutant mice. Hematoxylin and eosin (HE) staining showed no prominent difference between Myo3a mutant and wide-type mice cochlear at the age of two months. Scale bar = 20 μm.

Myo3a mutant mice demonstrate age-related deafness, we tested the hearing threshold of 2-, 6-, and 12-month-old Myo3a mutant and wild-type mice by ABR measurement. There results indicated no significant difference in the hearing threshold between 2-month-old wild-type ($n = 6$) and Myo3a mutant mice ($n = 7$) (Figure 2(b)). However, by the age of 6 months, Myo3a mutant mice ($n = 7$) exhibited a significantly higher hearing threshold than the wild-type mice ($n = 6$) ($P < 0.05$, Student's t-test) in both the click stimuli and at different frequencies (4, 16, and 32 kHz, Figures 2(a) and 2(c)). Hearing differences between the wild-type and Myo3a mutant mice were increasingly pronounced ($P < 0.01$) at 12 months in the broadband click and tone burst stimuli at frequencies of 4, 8, 16, and 32 kHz (Figures 2(a) and 2(d)). Therefore, we can conclude that Myo3a mutant mice exhibited a gradual hearing loss, which is similar to the characteristics of presbyacusis in humans.

3.3. Progressive Stereocilium Degeneration and Hair Cell Loss in Myo3a Mutant Mice. We investigated the mechanism of senile deafness in Myo3a mutant mice and examined cochlear changes. We dissected the cochleae of 2-, 6-, and 12-month-old wild-type and mutant mice and used phalloidin, DAPI, and Myo7a to stain hair cell stereocilia, hair cell nucleus, and hair cells, respectively. Confocal images of the basilar membrane showed that the stereocilia and hair cells of the wild-type and Myo3a mutant mice were intact at the age of 2 months; by contrast, the stereocilia of the Myo3a mutant mice started to degenerate, and the hair cells began to disappear at 6 months. By the age of 12 months, stereocilium degeneration and hair cell loss became incrementally serious (Figure 3). The confocal image showed that stereocilium degeneration was consistent with hair cell loss.

To further verify the accuracy and reliability of the above result, we used SEM to observe the hair cells of mutant and

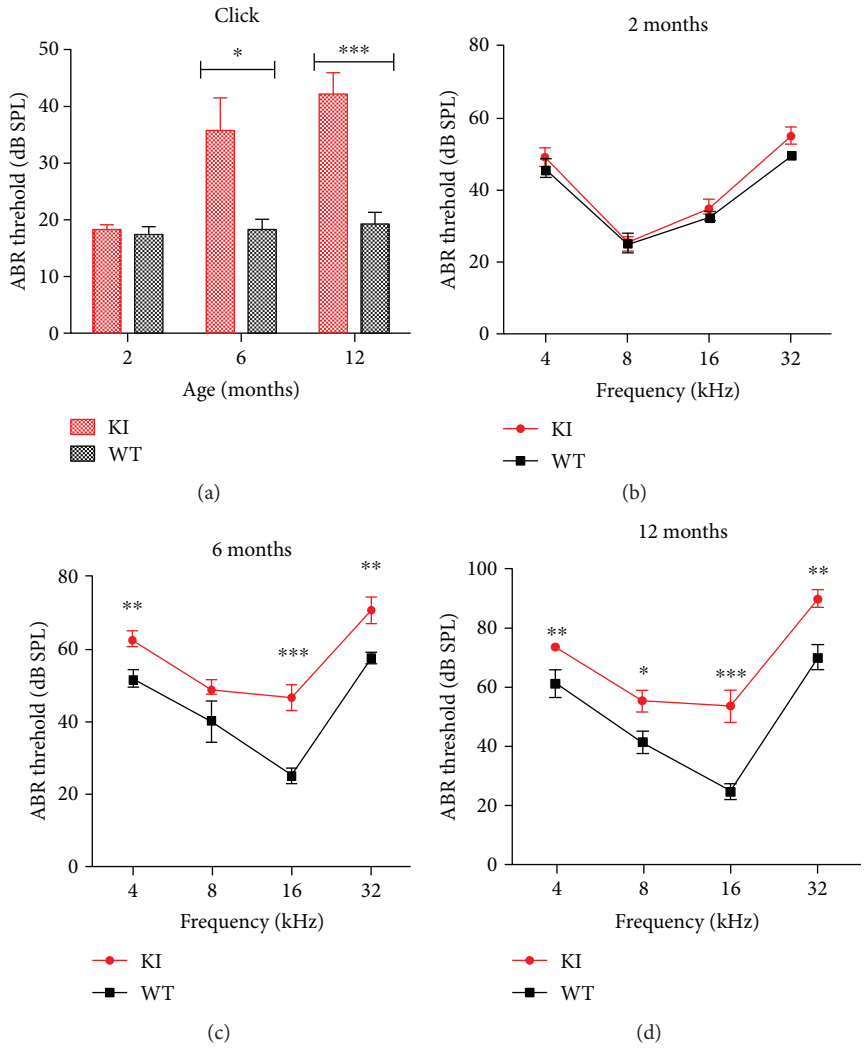

Figure 2: ABR analysis in Myo3a mutant mice (red) and wild-type mice (black) at two months, six months, and twelve months. (a) ABR measurements for broadband click. (b) Frequency-specific pure tone stimulation of Myo3a KI/KI mice and wild-type mice at two months old (b), six months old (c), and twelve months old (d). In contrast to wild-type mice, Myo3a KI/KI mutant mice showed progressive hearing loss. Compared with WT threshold at the corresponding frequency as determined by Student's t-test. $^{*}P < 0.05$; $^{**}P < 0.01$; $^{***}P < 0.001$. Error bars indicate SEM. $n > 5$ for control and mutant mice for each experiment.

wild-type mice in detail. Consistent with the above results, stereocilium degeneration and hair cell loss occurred in 6-month-old Myo3a mutant mice, especially in the stereocilia of inner hair cells (Figure 4(e)), whereas relatively complete hair cells and stereocilia were observed in wild-type mice (Figure 4(b)). By the age of 12 months, Myo3a mutant mice exhibited intensive stereocilium loss (Figure 4(f)), and this finding agreed with the ABR measurement. Through SEM, we also found structural abnormality in the remaining stereocilia in Myo3a mutant mice, in which the stereocilia of certain outer hair cells began to shorten and degenerate from the innermost line of stereocilia (Figure 5(c)). Fusion phenomenon was also noted in certain stereocilia (Figure 5(b)). The results were consistent with the expression location of Myo3a, in which morphological changes were also observed at the tips of the stereocilia in Myo3a mutant mice (Figure 5(d)). Most of the inner hair cells possess cuspidal stereocilia.

During hearing formation, transformation from mechanical energy to electric energy is crucial, and ion channel plays a critical role in this process. The ion channel is located at the tip of the stereocilia where Myo3a is expressed. Thus, we investigated whether the function of the MET activity was affected in Myo3a mutant mice. We used the FM1-43 dye to stain the hair cells of wild-type and Myo3a mutant mice to determine whether the function of the MET activity was affected. The results are shown in Figure 6. Both the wild-type and Myo3a mutant mice showed positive FM1-43 staining in hair cells. This finding indicated that the MET activity of Myo3a mutant mice remained intact and that Myo3a is not a direct component of MET channels.

3.4. No Difference in Noise Resistance between Myo3a Mutant and Wild-Type Mice. Presbyacusis is highly similar to noise-induced deafness in clinical pathology. Numerous senile deaf individuals are extremely sensitive to noise. To verify

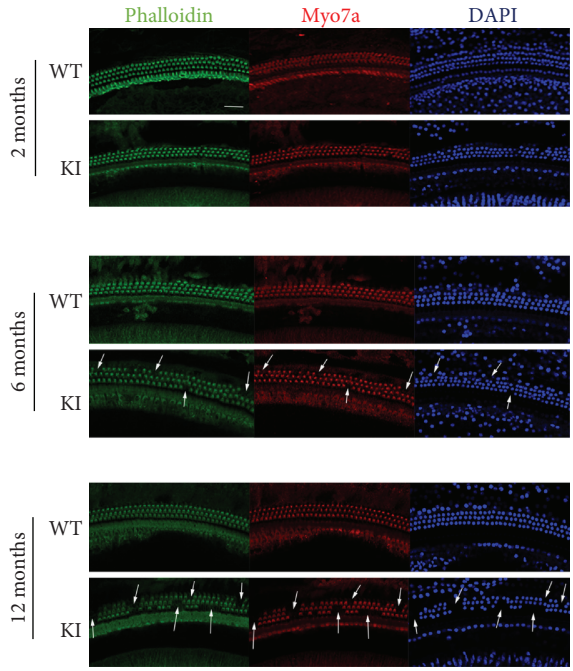

Figure 3: The degeneration of stereocilia and the hair cell loss in the Myo3a mutant mice showed by confocal images. Confocal images of the stereocilia, hair cells, and nucleus in Myo3a mutant and WT mice at two months old, six months old, and 12 months old. Images were taken from the middle turn of the cochlea. Scale bar = 20 μm. The stereocilium degeneration and the loss of hair cells can be seen in the Myo3a mutant mice from 6 months old, and this phenomenon becomes more serious in 12-month-old Myo3a mutant mice.

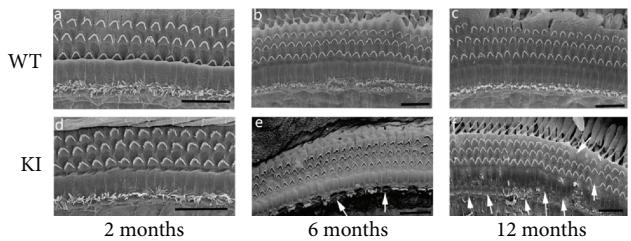

Figure 4: The degeneration of stereocilia in the Myo3a mutant mice showed by SEM. SEM images of the hair cells in Myo3a mutant and WT mice at two months old (a, d), six months old (b, e), and 12 months old (c, f). The inner hair cell stereocilium loss was found in 6-month-old Myo3a mutant mice (e), and this phenomenon becomes more serious in 12-month-old Myo3a mutant mice (f). Scale bar = 20 μm.

whether the noise resistance in the Myo3a mutant mice was affected, we performed continuous white-noise experiment for 2 h in 4.5-month-old wild-type and Myo3a mutant mice. Hearing test was conducted in wild-type and mutant mice before, at 4 h after, and at 1 week after noise treatment. The experimental results are shown in Figure 7; here, the line graph depicts no difference in noise resistance between Myo3a mutant and wild-type mice. The hearing threshold of the wild-type and Myo3a mutant mice significantly increased at 4 h after the white-noise experiment. Statistical analysis showed no difference in hearing between mutant and wild-type mice after the noise treatment. However, no difference in hearing was observed between the wild-type and Myo3a mutant mice. We repeated the noise experiment twice to verify the results. No difference in hearing was determined between the wild-type and Myo3a mutant mice after the noise treatment. Therefore, we conclude that the noise resistance of Myo3a mutant and wild-type mice was similar. However, there remains unanswered question. In our experiments, noise exposure seems to "erase" the initial difference in ABR thresholds between WT and KI, but the mechanism of this phenomenon is still unknown. We will perform further investigation in our future experiments.

4. Discussion

Using CRISPR/Cas9 technology, we generated a model of Myo3a Y137C mice consisting of a mutation in the kinase domain similar to that observed in the human Myo3a Y129C mutation. Through ABR hearing detection in mutant mice and wild-type mice, we found that the mutant mice exhibited progressive hearing loss. In 6 months, the hearing threshold of the mutant mice increased relative to that of the wild-type mice, whereas the hair cells of the 6-month-old mice started to degenerate. At 12 months of age, mutant mice exhibited significantly different hearing threshold and a more severe hair cell degeneration in the inner ear compared with that in the wild-type mice. The increased hearing threshold coincided with the loss of hair cells. This finding shows that kinase activity is crucial for the function of Myo3a and inner hair cells. Progressive hearing loss in Myo3a mutant mice was similar to that observed in human Myo3a mutants. Thus, the Myo3a mutant mouse model that we constructed was not only a good model for presbyacusis but also a satisfactory human disease model.

4.1. Kinase Domain Is Important to Myo3a. As a member of the myosin family, Myo3a transports cargo Espin1 to the top of the stereocilia [36]. In contrast to a previous mouse model that contains a stop codon at 1041 but maintains kinase activity, the mouse model in the current study involves mutation at the kinase domain of Myo3a. Our study has proved that kinase domain is important to the function of Myo3a.

Myo3a retains its motility by using the motor domain and the C-terminal THDII domain in combination with actin. In the wild-type mice, the THDI domain specifically binds to cargo Espin1, ensuring that Myo3a can transport Espin1 to the tip of the stereocilia to stabilize its structure [37]. The phosphorylation-dephosphorylation mechanism plays an essential role in normal Myo3a function [38]. Myo3a concentrates at the tip of the stereocilia, and the kinase domain interacts with and phosphorylates the motor domain because of high Myo3a concentration in the stereocilia; furthermore, motor activity is decreased by phosphorylation, and the phosphorylated motor domain loses its affinity with actin and tends to be transported back to the cell body to bind Espin1 again [39]. In the cell line, wild-type Myo3a localizes along the length of the filopodia, and

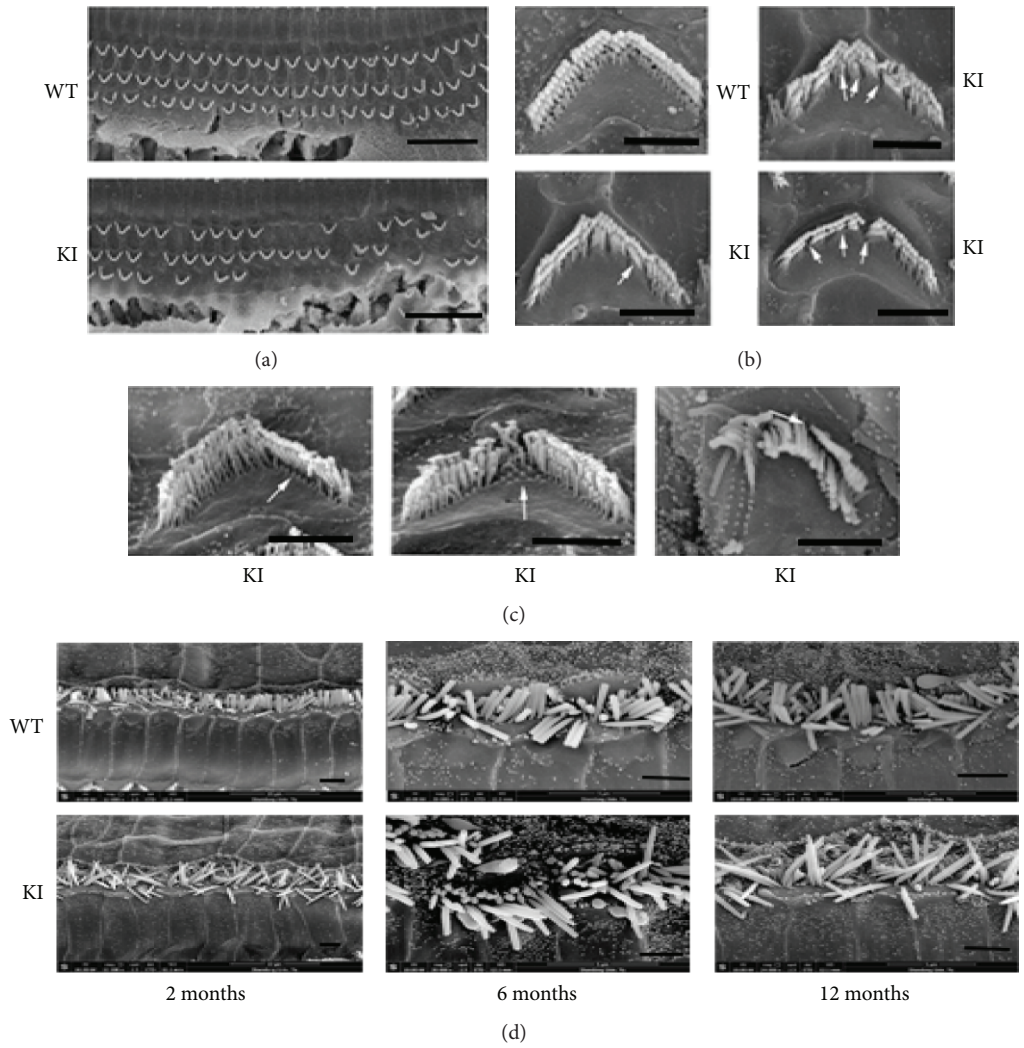

Figure 5: SEM images showed the abnormal structure of the stereocilia in Myo3a mutant mice. (a) The outer hair cell stereocilium loss was serious in 6-month-old Myo3a mutant mice. (b) Fusion phenomenon was observed in some stereocilia of mutant mice. (c) The stereocilia of some outer hair cells were found to be shorter, and the degeneration started from the innermost line of the stereocilia. (d) The stereocilia of inner hair cells become sharp in Myo3a mutant mice at the age of 2 months, 6 months, and 12 months. Scale bar = 10 μm for (a) and 2 μm for (b, c, and d).

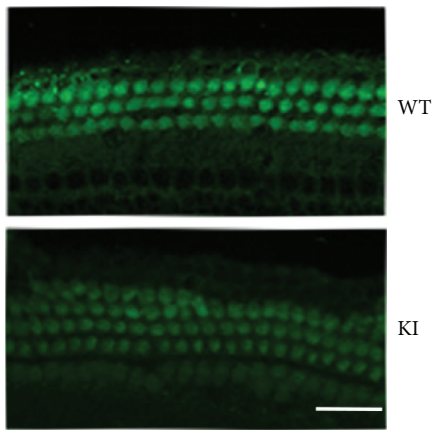

Figure 6: MET activity is not affected in Myo3a mutant mice. FM1-43 staining showed that the MET activity is normal in Myo3a mutant mice. Scale bar = 20 μm.

the kinase-deleted construct present increases tip localization [13]; thus, Myo3a, which does not exhibit kinase activity, may demonstrate difficulty in returning to the cytoplasm to bind with Espin1 again.

Myo3a kinase activity may be disrupted in our mutant mouse model. Myo3a autophosphorylation cannot occur even at high Myo3a concentration at the top of the stereocilia so that the motor domain cannot be phosphorylated. The active motor domain tightly binds with actin and cannot be detached from actin. Thus, Myo3a that is located at the tip of the stereocilia cannot return to the cytoplasm and continue to transport Espin1. Thus, the structure of the top of the stereocilia is abnormal, thereby affecting the normal stereocilia functioning and causing progressive hearing loss.

4.2. Myo3b May Compensate for the Function of Myo3a. We observed normal hearing threshold and normal inner ear hair cell development in the 2-month-old Myo3a mutant

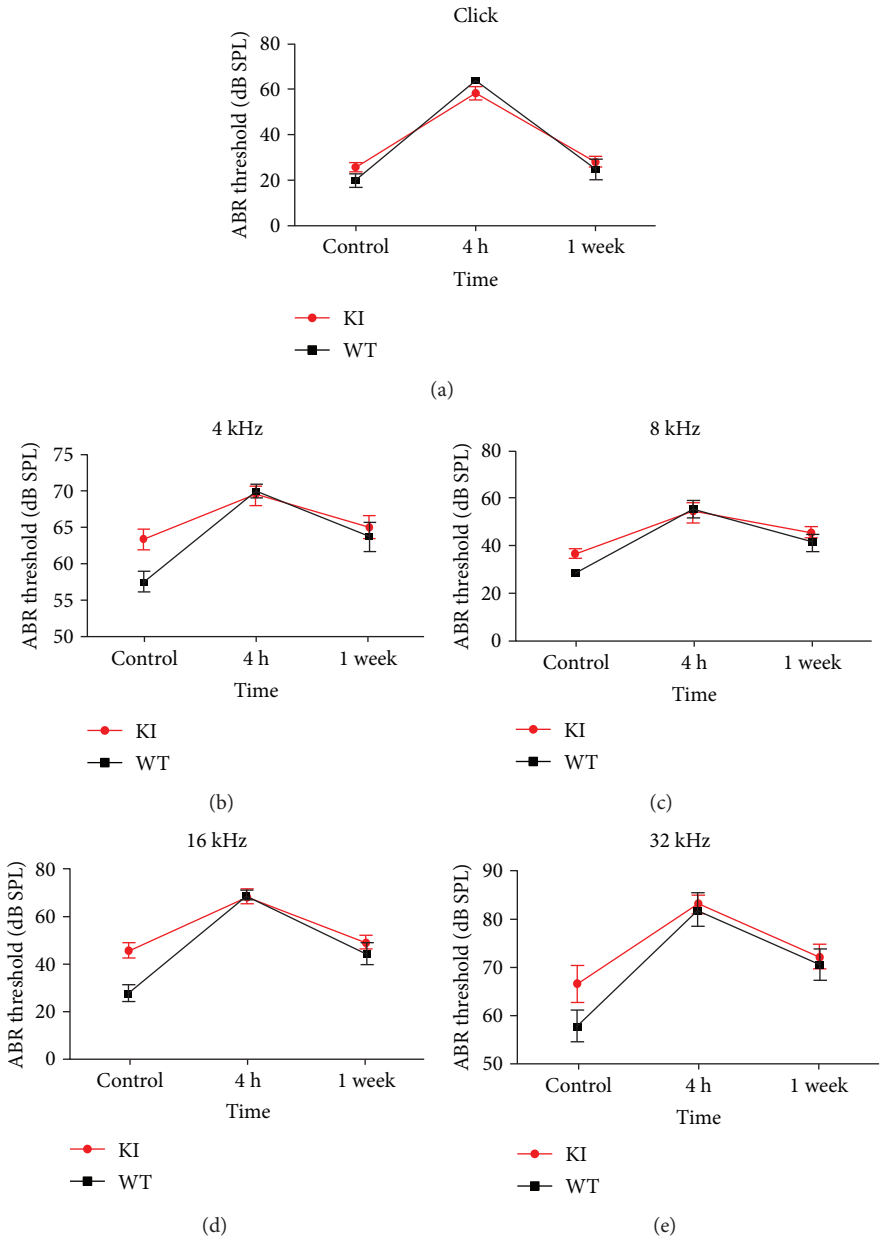

Figure 7: ABR analysis in Myo3a mutant and wide-type mice after noise exposure. ABR threshold was tested for broadband click (a) and frequency-specific pure tone (b, c, d, e) on Myo3a mutant and wide-type mice before (control), 4 h after, and 1 week after noise exposure ($n \geqq 7$); error bars indicate SEM.

mice. The elevated hearing threshold and hair cell degeneration of mutant mice presented at ≥6 months of age. The explanation why mutant mice exhibit progressive rather than profound hearing loss at a young age is unknown. We speculate that Myo3b compensates for the loss of Myo3a.

Compensatory effects in higher organisms are highly common. Myo3b localizes at cochlear hair cell stereocilium tips, similar with the localization of Espin1 and Myo3a [37]. Myo3b contains the motor domain and the THDI domain but lacks the THDII domain, which is contrary to Myo3a, which lacks the ability to "walk along" actin [37]. In COS7 cell line, Myo3a that lacks THDII-actin-binding domain does not localize to filopodial tips but moves toward the tip and promotes filopodial elongation when coexpressed with Espin1 Myo3a. This finding suggests that when lacking the THDII-actin-binding domain, Myo3a can bind to the cargo Espin1 with its THDI domain and then use its motor domain and the Espin1 ABM domain to travel along actin [36]. Similarly, when using the THDI domain combined with Espin1, Myo3b can obtain its capability to "walk along" actin by using its motor domain and the Espin1 ABM domain and perform the function of transporting Espin1 to the tip of stereocilia [37]. In an Espin1 knock-out mouse model, Myo3b is not detectable at the stereocilium tips of extrastriolar hair cells [40], demonstrating that Myo3b can transport Espin1 to the tip of stereocilia only when

combined with Espin1. Nevertheless, Myo3b compensates for Myo3a for Espin1 shipping.

In Myo3a mutant mice, Myo3b can compensate for the loss of function of Myo3a because Myo3b is located at the stereocilium tip of the inner ear hair cells. Thus, we observed normal development of the inner ear hair cells. Myo3a and Myo3b double knock-out mice are profoundly deaf, demonstrating that class III myosins play redundant roles in hearing function [41].

Unlike a previous Myo3a knock-out mouse model [21, 41], the Myo3a mutant mice in the current study were maintained on the CBA/CaJ background. Our mouse model is suitable for studying DFNB30-type deafness in human because the B6 mice exhibit the characteristic of senile deafness.

5. Conclusion

The knock-in mice with Myo3a kinase domain mutation displayed progressive hearing loss and stereocilium degeneration in inner ear hair cells. Our mouse model of Myo3a point mutation made by CRISPR/Cas9 technology can simulate human diseases well and provide a good mouse model for the study of senile deafness.

Data Availability

The data used to support the findings of this study are available from the corresponding author upon request.

Conflicts of Interest

The authors declare no conflict of interests regarding the publication of this paper.

Authors' Contributions

Jiangang Gao and Peipei Li conceived and designed the experiments. Peipei Li and Zongzhuang Wen performed the experiments. Peipei Li analyzed the data. Jiangang Gao contributed reagents/materials/analysis tools. Peipei Li, Zongzhuang Wen, and Jiangang Gao wrote the paper.

Acknowledgments

This work was supported by grants from the Natural Science Foundation of China (31171194), the National 973 Basic Research Program of China (2014CB541703), and Shandong Provincial Science and Technology Key Program (2009GG10002039).

References

[1] T. B. Friedman and A. J. Griffith, "Human nonsyndromic sensorineural deafness," *Annual Review of Genomics and Human Genetics*, vol. 4, no. 1, pp. 341–402, 2003.

[2] C. C. Morton and W. E. Nance, "Newborn hearing screening–a silent revolution," *The New England Journal of Medicine*, vol. 354, no. 20, pp. 2151–2164, 2006.

[3] D. Raviv, A. A. Dror, and K. B. Avraham, "Hearing loss: a common disorder caused by many rare alleles," *Annals of the New York Academy of Sciences*, vol. 1214, no. 1, pp. 168–179, 2010.

[4] G. Stevens, S. Flaxman, E. Brunskill et al., "Global and regional hearing impairment prevalence: an analysis of 42 studies in 29 countries," *European Journal of Public Health*, vol. 23, no. 1, pp. 146–152, 2013.

[5] R. K. Gurgel, P. D. Ward, S. Schwartz, M. C. Norton, N. L. Foster, and J. A. T. Tschanz, "Relationship of hearing loss and dementia: a prospective, population-based study," *Otology & Neurotology*, vol. 35, no. 5, pp. 775–781, 2014.

[6] C. M. Li, X. Zhang, H. J. Hoffman, M. F. Cotch, C. L. Themann, and M. R. Wilson, "Hearing impairment associated with depression in us adults, National Health and Nutrition Examination Survey 2005-2010," *JAMA Otolaryngology. Head & Neck Surgery*, vol. 140, no. 4, pp. 293–302, 2014.

[7] R. J. H. Smith, J. F. Bale Jr, and K. R. White, *Sensorineural Hearing Loss in Children*, Elsevier, 2005.

[8] C. Petit and G. P. Richardson, "Linking genes underlying deafness to hair-bundle development and function," *Nature Neuroscience*, vol. 12, no. 6, pp. 703–710, 2009.

[9] M. Schwander, B. Kachar, and U. Müller, "Review series: the cell biology of hearing," *The Journal of Cell Biology*, vol. 190, no. 1, pp. 9–20, 2010.

[10] P. Kazmierczak, H. Sakaguchi, J. Tokita et al., "Cadherin 23 and protocadherin 15 interact to form tip-link filaments in sensory hair cells," *Nature*, vol. 449, no. 7158, pp. 87–91, 2007.

[11] Z. Xu, A. W. Peng, K. Oshima, and S. Heller, "Magi-1, a candidate stereociliary scaffolding protein, associates with the tip-link component cadherin 23," *Journal of Neuroscience*, vol. 28, no. 44, pp. 11269–11276, 2008.

[12] A. C. Dosé and B. Burnside, "Cloning and chromosomal localization of a human class III myosin," *Genomics*, vol. 67, no. 3, pp. 333–342, 2000.

[13] M. E. Schneider, A. C. Dose, F. T. Salles et al., "A new compartment at stereocilia tips defined by spatial and temporal patterns of myosin IIIa expression," *Journal of Neuroscience*, vol. 26, no. 40, pp. 10243–10252, 2006.

[14] T. Walsh, V. Walsh, S. Vreugde et al., "From flies' eyes to our ears: mutations in a human class III myosin cause progressive nonsyndromic hearing loss DFNB30," *Proceedings of the National Academy of Sciences of the United States of America*, vol. 99, no. 11, pp. 7518–7523, 2002.

[15] A. C. Dose and B. Burnside, "A class III myosin expressed in the retina is a potential candidate for Bardet-Biedl syndrome," *Genomics*, vol. 79, no. 5, pp. 621–624, 2002.

[16] M. J. T. Cope, J. Whisstock, I. Rayment, and J. Kendrick-Jones, "Conservation within the myosin motor domain: implications for structure and function," *Structure*, vol. 4, no. 8, pp. 969–987, 1996.

[17] A. Wang, Y. Liang, R. A. Fridell et al., "Association of unconventional myosin *MYO15* mutations with human nonsyndromic deafness *DFNB3*," *Science*, vol. 280, no. 5368, pp. 1447–1451, 1998.

[18] C. Montell and G. M. Rubin, "The drosophila *ninaC* locus encodes two photoreceptor cell specific proteins with domains homologous to protein kinases and the myosin heavy chain head," *Cell*, vol. 52, no. 5, pp. 757–772, 1988.

[19] T. B. Friedman, J. R. Sellers, and K. B. Avraham, "Unconventional myosins and the genetics of hearing loss," *American Journal of Medical Genetics*, vol. 89, no. 3, pp. 147–157, 1999.

[20] K. P. Ng, T. Kambara, M. Matsuura, M. Burke, and M. Ikebe, "Identification of myosin III as a protein kinase," *Biochemistry*, vol. 35, no. 29, pp. 9392–9399, 1996.

[21] V. L. Walsh, D. Raviv, A. A. Dror et al., "A mouse model for human hearing loss DFNB30 due to loss of function of myosin IIIA," *Mammalian Genome*, vol. 22, no. 3-4, pp. 170–177, 2011.

[22] H. Yang, H. Wang, and R. Jaenisch, "Generating genetically modified mice using CRISPR/CAS-mediated genome engineering," *Nature Protocols*, vol. 9, no. 8, pp. 1956–1968, 2014.

[23] Y. Fujihara and M. Ikawa, "CRISPR/Cas9-based genome editing in mice by single plasmid injection," *Methods in Enzymology*, vol. 546, pp. 319–336, 2014.

[24] K. A. Steigelman, A. Lelli, X. Wu et al., "Polycystin-1 is required for stereocilia structure but not for mechanotransduction in inner ear hair cells," *Journal of Neuroscience*, vol. 31, no. 34, pp. 12241–12250, 2011.

[25] J. Gong, X. Wang, C. Zhu et al., "Insm1a regulates motor neuron development in zebrafish," *Frontiers in Molecular Neuroscience*, vol. 10, p. 274, 2017.

[26] Y. He, X. Lu, F. Qian, D. Liu, R. Chai, and H. Li, "*Insm1a* is required for zebrafish posterior lateral line development," *Frontiers in Molecular Neuroscience*, vol. 10, p. 241, 2017.

[27] X. Fu, L. Zhang, Y. Jin et al., "Loss of myh14 increases susceptibility to noise-induced hearing loss in CBA/CaJ mice," *Neural Plasticity*, vol. 2016, Article ID 6720420, 16 pages, 2016.

[28] Y. Wang, J. Li, X. Yao et al., "Loss of CIB2 causes profound hearing loss and abolishes mechanoelectrical transduction in mice," *Frontiers in Molecular Neuroscience*, vol. 10, p. 401, 2017.

[29] X. Lu, S. Sun, J. Qi et al., "Bmi1 regulates the proliferation of cochlear supporting cells via the canonical Wnt signaling pathway," *Molecular Neurobiology*, vol. 54, no. 2, pp. 1326–1339, 2016.

[30] C. Cheng, L. Guo, L. Lu et al., "Characterization of the transcriptomes of Lgr5+ hair cell progenitors and Lgr5− supporting cells in the mouse cochlea," *Frontiers in Molecular Neuroscience*, vol. 10, p. 122, 2017.

[31] R. Hertzano, E. Shalit, A. K. Rzadzinska et al., "A *Myo6* mutation destroys coordination between the myosin heads, revealing new functions of myosin VI in the stereocilia of mammalian inner ear hair cells," *PLoS Genetics*, vol. 4, no. 10, article e1000207, 2008.

[32] T. Self, M. Mahony, J. Fleming, J. Walsh, S. D. Brown, and K. P. Steel, "Shaker-1 mutations reveal roles for myosin VIIA in both development and function of cochlear hair cells," *Development*, vol. 125, no. 4, pp. 557–566, 1998.

[33] Z. He, L. Guo, Y. Shu et al., "Autophagy protects auditory hair cells against neomycin-induced damage," *Autophagy*, vol. 13, no. 11, pp. 1884–1904, 2017.

[34] A. Lelli, Y. Asai, A. Forge, J. R. Holt, and G. S. G. Géléoc, "Tonotopic gradient in the developmental acquisition of sensory transduction in outer hair cells of the mouse cochlea," *Journal of Neurophysiology*, vol. 101, no. 6, pp. 2961–2973, 2009.

[35] Y. Chen, L. Liu, Y. Zhang, R. Chai, and H. Li, "Wnt activation protects against neomycin-induced hair cell damage in the mouse cochlea," *The Journal of Laryngology & Otology*, vol. 130, no. S3, pp. S105–S105, 2016.

[36] F. T. Salles, R. C. Merritt, U. Manor et al., "Myosin IIIa boosts elongation of stereocilia by transporting espin 1 to the plus ends of actin filaments," *Nature Cell Biology*, vol. 11, no. 4, pp. 443–450, 2009.

[37] R. C. Merritt, U. Manor, F. T. Salles et al., "Myosin IIIB uses an actin-binding motif in its espin-1 cargo to reach the tips of actin protrusions," *Current Biology*, vol. 22, no. 4, pp. 320–325, 2012.

[38] B. C. An, T. Sakai, S. Komaba et al., "Phosphorylation of the kinase domain regulates autophosphorylation of myosin IIIA and its translocation in microvilli," *Biochemistry*, vol. 53, no. 49, pp. 7835–7845, 2014.

[39] O. A. Quintero, W. C. Unrath, S. M. Stevens Jr, U. Manor, B. Kachar, and C. M. Yengo, "Myosin 3A kinase activity is regulated by phosphorylation of the kinase domain activation loop," *Journal of Biological Chemistry*, vol. 288, no. 52, pp. 37126–37137, 2013.

[40] S. Ebrahim, M. R. Avenarius, M.'. Grati et al., "Corrigendum: stereocilia-staircase spacing is influenced by myosin III motors and their cargos espin-1 and espin-like," *Nature Communications*, vol. 8, p. 16133, 2017.

[41] A. Lelli, V. Michel, J. Boutet de Monvel et al., "Class III myosins shape the auditory hair bundles by limiting microvilli and stereocilia growth," *Journal of Cell Biology*, vol. 212, no. 2, pp. 231–244, 2016.

Hindawi
Neural Plasticity
Volume 2018, Article ID 3786489, 9 pages
https://doi.org/10.1155/2018/3786489

Research Article

Comparison of Acceptable Noise Level Generated Using Different Transducers and Response Modes

Liang Xia,[1] Jingchun He,[2] Yuanyuan Sun,[1] Yi Chen,[1] Qiong Luo,[1] Haibo Shi,[1] Yanmei Feng,[1] and Shankai Yin[1]

[1]*Department of Otolaryngology, Shanghai Jiao Tong University Affiliated Sixth People's Hospital, No. 600, Yishan Road, Xuhui District, Shanghai 200233, China*
[2]*Department of Otolaryngology, Shanghai Jiao Tong University Affiliated Xinhua Hospital, No. 1665, Kongjiang Road, Yangpu District, Shanghai 200092, China*

Correspondence should be addressed to Haibo Shi; haibo99@hotmail.com and Yanmei Feng; feng.yanmei@126.com

Received 5 March 2018; Revised 15 May 2018; Accepted 30 May 2018; Published 26 June 2018

Academic Editor: Geng-lin Li

The acceptable noise level (ANL) was defined by subtracting the background noise level (BNL) from the most comfortable listening level (MCL) (ANL = MCL – BNL). This study compared the ANL obtained through different methods in 20 Chinese subjects with normal hearing. ANL was tested with Mandarin speech materials using a loudspeaker or earphones, with each subject tested by himself or by the audiologist. The presentation and response modes were as follows: (1) loudspeaker with self-adjusted noise levels using audiometer controls (LS method); (2) loudspeaker with the subject signaling the audiologist to adjust speech and noise levels (LA method); (3) earphones with self-adjusted noise levels using audiometer controls (ES method); and (4) earphones with the subject signaling the audiologist to adjust speech and noise levels (EA method). ANL was calculated from three measurements with each method. There was no significant difference in the ANL obtained through different presentation modes or response modes sound. The correlations between ANL, MCL, and BNL obtained from each two methods were significant. In conclusion, the ANL in normal-hearing Mandarin listeners may not be affected by presentation modes such as a loudspeaker or earphones nor is it affected by self-adjusted or audiologist-adjusted response modes. Earphone audiometry is as reliable as sound field audiometry and provides an easy and convenient way to measure ANL.

1. Introduction

The acceptable noise level (ANL) test was developed to quantify the critical amount of background noise that subjects could accept while listening to speech [1–6]. ANL is defined as the lowest signal-to-noise ratio (SNR) that a subject could accept when the target speech was presented at the most comfortable listening level (MCL) [6, 7]. ANL is derived by subtracting the background noise level (BNL) that the subject can accept from the MCL. A low ANL indicates that a subject has a high tolerance for background noises, while a subject with high ANL has low tolerance for background noises [7]. According to Nabelek et al. [8], subjects with an ANL below 7 dB are likely to become successful full-time hearing aid users, while subjects with an ANL above 13 dB are likely to become unsuccessful hearing aids users occasionally or not at all. Previous studies have shown that there is a large variation in ANL across normal-hearing subjects [1, 7, 9–13]. This variation seems unrelated to age [1, 11], gender [14], middle-ear function [15], hearing sensitivity [1, 7, 9, 15, 16], outer hair cell function [15], and efferent pathways utilizing the medial olivocochlear bundle [15]. However, it was influenced by speech materials, noise materials, presentation mode, instructions, and working memory capacity [17].

Several types of sensors have been used to present the ANL signal. In most studies, the sound signal was presented in the sound field through a loudspeaker [18]. However, some studies presented the signals used to measure ANL through an earphone [1]. Olsen and Brännström [17] indicated that the values of ANL obtained from an earphone or loudspeaker may be different. If transducers other than a

loudspeaker were used, the ANL data for the specific transducer should be considered. Clinically, audiologists may use ANL data obtained from different transducers. Although most audiologists use a loudspeaker to do ANL, some audiologists could do ANL with earphone when the loudspeaker is not available and predict the ANL results with loudspeaker from the ANL results with earphone. Therefore, it is necessary to contrast different sound presentation modes in ANL tests.

On the other hand, Brannstrom et al. [11] suggested that ANL might be influenced by extrinsic factors such as examiner attitude, instructions, and/or cultural differences in the acceptability of background noise. In most ANL tests, the subject signals the experimenter to adjust the sound volume. However, Nabelek et al. [1] directed subjects to adjust the levels by themselves with visual feedback from the audiometer. The main difference between self-adjusted and audiologist-adjusted measurements is the method to determine the MCL and BNL intensity. During the self-adjusted method, the subjects will determine the MCL and BNL by adjusting the sound levels using the control buttons. During the audiologist-adjusted method, the subjects tell the audiologist the optimal intensity and the maximum intensity signal as the noise level changes continuously; however, there could be a time lag or bias of intensity during this period which can produce differences between the final results and the subjects' true results on ANL tests.

To identify factors that may influence ANL values, this study proposed to investigate and compare the test results of ANL measured through a loudspeaker or earphones and further compared the effect of the self-adjusted or audiologist-adjusted testing method.

2. Methods

The program was approved by the Ethics Committee of Shanghai Jiao Tong University Affiliated Sixth People's Hospital. All participants provided written informed consent prior to the study's commencement.

2.1. Subjects. This study was conducted in twenty adults (10 male, 10 female) with normal hearing whose native language was Mandarin. Their ages ranged from 21 to 30 years and they were all university students. The criterion for normal hearing sensitivity was pure-tone air conduction thresholds for each ear less than or equal to 15 dB HL at each frequency from 0.25 to 8 kHz with an octave step. The subjects reported no recent otologic problems, such as ear infection, draining ears, otalgia, or surgery on or in the ears during the past eight weeks. The equipment set-ups were calibrated before the study started.

2.2. Materials. The test used Mandarin-acceptable noise level material established by Chen et al. [18]. The materials were *The Spring Festival of Beijing* which was chosen from the official textbooks for primary school. The noise signal used to measure BNL was the 12 multitalker babbles routinely used for ANL tests [18]. The ANL signals were a speech signal in one channel and a noise signal in the other channel. In each test condition, the MCL and BNL were tested three measurements, and the average of three measurements for each individual was used as the MCL and BNL of the subjects, and the MCL and BNL of each group were the average values of all the subjects.

2.3. Stimuli and Procedure. In sound field audiometry, listeners were tested individually in an audiometric booth that met ANSI standards for ambient noise levels (ANSI, S 3.1-1991). All the stimuli were generated from a compact disc player and delivered via a clinical audiometer (GN Otometrics, Taastrup, Denmark) connected to a calibrated loudspeaker (GSI) located in a sound-proof room. Both speech and noise were presented from the loudspeaker at zero degrees azimuth 1.5 m away from the subjects. The calibration tone was a 1 kHz pure tone. When calibrating, the two channels were calibrated, respectively, and the readout of the VU table on the audiometer panel should be adjusted to 0. The output levels of the speech stimuli and background noise were calibrated at the position occupied by the listener.

In earphone audiometry, listeners were tested individually in an audiometric booth that met ANSI standards for ambient noise levels (ANSI, S 3.1-1991). All the stimuli were generated from a compact disc player and delivered via clinical audiometer (GN Otometrics, Taastrup, Denmark) connected to a calibrated earphone (Sennheiser HDA 200 circumaural earphones). The calibration tone was a 1 kHz pure tone. The output levels of the speech stimuli and background noise were calibrated using B&K 4134 pressure microphone and B&K 4153 simulation ear. When calibrating, the two channels were calibrated, respectively, and the readout of the VU table on the audiometer panel should be adjusted to 0.

2.4. The Procedure for Audiologist-Adjusted ANL Tests. Both written and oral instructions were given prior to ANL testing. The instructions were Chinese versions of the English instructions. If the subjects had any doubts, the instructions were clarified. Examples of speech and noise were then presented. Subjects' ANLs were obtained as described previously [18].

The initial stimulus level for each repetition was 30 dB HL for both speech and noise signals, and a 2 dB step size was used for all adjustments for both MCL and BNL. Audiologists increased the sound volume until the speech signal became too loud, then decreased it until it became too soft, and finally the subject selected the sound volume that was the most comfortable listening level. The verbal and written instructions for determining the MCL were as follows:

You will listen to a story through a loudspeaker or earphones. After a few moments, select the sound volume level for the story that is most comfortable for you, as if listening to a radio. Hand motions will allow you to signal the audiologist to adjust the signal level up (thumbs up) or down (thumbs down) or to stop adjustments (flat palm; this means that you feel the current level is the most comfortable for you).

Then, BNL was established by adding a noise signal as the speech signal and the subject was instructed to repeat a similar procedure; the speech signal remained fixed at

Table 1: The mean and standard error (SE) of MCL, BNL, and ANL obtained from the three repeated measurements in different methods. MCL: most comfortable listening level; BNL: background noise level; ANL: acceptable noise level; LS: measured through loudspeaker with self-adjusted levels using audiometer controls; LA: measured through loudspeaker with the subject signaling the audiologist to adjust the levels of speech and noise; ES: measured through earphones with self-adjusted levels using audiometer controls; EA: measured through earphones with the subject signaling the audiologist to adjust the levels of speech and noise.

Values	Method	1st measurement		2nd measurement		3rd measurement	
		Mean	SE	Mean	SE	Mean	SE
MCL (dB HL)	LS	35.9	1.54	37.2	1.36	37.4	1.37
	LA	38.1	1.61	38.1	1.32	38.6	1.16
	ES	43.3	1.85	43.8	1.83	45.2	2.01
	EA	44.8	1.45	45.2	1.49	43.8	1.65
BNL (dB HL)	LS	35.8	1.73	37.6	1.46	38.5	1.51
	LA	38.2	1.50	38.7	1.42	39.3	1.23
	ES	43.0	2.02	43.9	1.83	45.5	2.21
	EA	44.2	1.39	45.6	1.72	44.2	1.73
ANL (dB)	LS	0.1	0.76	−0.4	0.54	−1.1	0.62
	LA	−0.1	0.72	−0.6	0.56	−0.9	0.62
	ES	0.4	0.83	−0.1	0.49	−0.3	0.84
	EA	0.6	0.56	−0.5	0.78	−0.4	0.55

the previously established MCL and the subject increased the sound volume of the noise until it became too loud, then decreased it until the speech became very clear, and finally the subject selected the sound volume that he or she could tolerate without becoming tense or tired while following the speech signal for a long period of time. The subject reported when the BNL had been found. The verbal and written instructions for determining the BNL were as follows [18]:

You will now listen to the same story with background noise. After you have listened to this for a few moments, select the maximum level of background noise which you would be willing to tolerate without becoming tense or tired while following the story. Hand motions will also allow you to signal the investigator to adjust the signal level.

2.5. The Procedure of Self-Adjusted ANL Tests. The main steps were the same as those of the audiologist-guided test. After brief instructions to the subjects, they conducted the ANL test by themselves. Instructions for the self-adjusted ANL test were as follows:

You will listen to a story through a loudspeaker or earphones. After a few moments, select the sound volume level for the story that is most comfortable for you, as if you were listening to a radio. You do not need signal the audiologist to adjust the signal level up (thumbs up) or down (thumbs down) or to stop adjustments (flat palm, meaning that you feel the current level is the most comfortable for you). You should regulate the sound volume of sound though the clinical audiometer. When the MCL was found, the multitalker babble was introduced from the loudspeaker or earphones at 30 dB HL. You will now listen to the same story with background noise. After you have listened to this for a few moments, select the maximum level of the background noise which you would be willing to tolerate without becoming tense or tired while following the story. You should regulate the sound volume of the sound though the clinical audiometer too. Both the sound volume level of the 12-talker babble or story are increased in 2 dB steps.

The MCL and BNL were measured three times with a 30 min gap between two measurements. The ANL from each measurement was obtained by subtracting the BNL from the MCL (ANL = MCL − BNL) for each participant and each experimental condition. The average of the three measurements was used to calculate ANL.

2.6. Statistical Analysis. All the statistical analyses were performed using SPSS version 20.0 (IBM Corp., Armonk, NY, USA). Descriptive statistics were calculated for the MCL, BNL, and ANL. The values of different measurements in the same method were compared by paired t-test. Pearson's correlation coefficient was used to evaluate the relationship between ANL, MCL, and BNL among three measurements in each condition. Two-way repeated measures analyses of variance (ANOVA) were used to assess the effects of MCL, BNL, and ANL within each method; Pearson's correlation coefficient was used to examine the relationship between the results of ANL and MCL and between ANL and BNL in each method. Correlations between ANL, MCL, and BNL in each method were investigated by Pearson's correlation. The significance level was set at $p < 0.05$.

3. Results

3.1. MCL, BNL, and ANL Obtained from the Three Measurements with Different Methods. The means and standard error of MCL, BNL, and ANL obtained from the three measurements in different methods are listed in Table 1. The MCL and BNL increased with an increasing number of repetitions in the LS, LA, and ES methods, but the ANL decreased with increasing number of measurements in the LS, LA, and ES methods. However, in the EA method, the MCL and BNL increased first and then decreased with

Table 2: The paired t-tests for MCL, BNL, and ANL obtained from the three measurements in different methods. The significance level was set at $p < 0.05$.

Values	Method	1st versus 2nd measurement		1st versus 3rd measurement		2nd versus 3rd measurement	
		t	p value	t	p value	t	p value
MCL (dB HL)	LS	−1.488	0.153	−1.510	0.148	−0.261	0.797
	LA	−0.469	0.645	1.070	0.298	1.889	0.074
	ES	−0.553	0.587	−1.594	0.127	−1.730	0.100
	EA	−0.469	0.645	1.070	0.298	1.889	0.074
BNL (dB HL)	LS	−1.616	0.122	−2.236	0.038*	−1.917	0.070
	LA	−0.592	0.561	−1.291	0.212	−1.301	0.209
	ES	−0.785	0.442	−1.724	0.101	−1.875	0.076
	EA	−1.453	0.163	0.000	1.000	1.759	0.095
ANL (dB)	LS	0.773	0.449	2.698	0.014*	1.437	0.167
	LA	1.045	0.309	1.506	0.148	0.825	0.419
	ES	0.815	0.425	0.941	0.358	0.335	0.741
	EA	2.604	0.017*	2.517	0.021*	−0.252	0.804

*Values were significantly different from each other.

Table 3: Values of the mean, standard error (SE), and range for MCL, BNL, and ANL averaged across all the subjects for each method. The significance level was set at $p < 0.05$.

Method	MCL value (dB HL)			BNL value (dB HL)			ANL value (dB)		
	Mean	SE	Range	Mean	SE	Range	Mean	SE	Range
LS	36.83*	1.33	25.33~48.00	37.30**	1.47	27.33~55.33	−0.47	0.57	−7.33~3.33
LA	38.27*	1.32	29.33~50.00	38.27**	1.32	30.00~54.67	−0.53	0.58	−4.67~4.00
ES	44.10*	1.81	31.33~60.67	44.13#	1.91	29.33~64.00	0.00	0.63	−4.67~6.00
EA	44.60*	1.45	36.67~58.67	44.67#	1.54	35.33~63.33	−0.10	0.60	−5.33~4.00

*Values of MCL were significantly different from each other. **Values of BNL were significantly different between the ES and EA methods. #Values of BNL were significantly different between the LS and LA methods.

increasing number of repetitions; the ANL decreased first and then increased with increasing number of repetitions. The statistical results comparing the values obtained from the three measurements by paired t-tests within each method are shown in Table 2. The significant difference did not exist in most situations except the BNL in the first measurement versus the third measurement with the LS method, ANL in the first measurement versus the second measurement with the EA method, and ANL in the first measurement versus the third measurement with the LS and EA methods.

The correlations of ANL, MCL, and BNL among three measurements within each method indicated that the correlation coefficient of ANL, MCL, and BNL between any two measurements was significant for each method. The range of correlation coefficients was 0.548 to 0.951 with all $p < 0.05$.

3.2. MCL, BNL, and ANL Averaged from the Three Measurements with Different Methods. MCL, BNL, and ANL values averaged across three repeated measurements were calculated for the four test methods and were shown in Table 3. A two-way repeated measurement analysis of variance was used to assess the effects of different test methods of on MCL, BNL, and ANL. The dependent variable was MCL, BNL, or ANL. The within-subject factor was response modes, with two levels (self-adjusted or audiologist-adjusted), and the between-subject factor was presentation modes, with two factors (loudspeaker or earphones). First, the results show that the main effect of response modes and presentation modes was statistically significant for MCL (response modes [$F = 4.364$; $p = 0.043$] and presentation modes [$F = 10.875$; $p = 0.002$]). However, the interaction effect of response modes × presentation modes was not significant [$F = 1.017$; $p = 0.320$]. These outcomes indicated

Table 4: The correlations between MCL and ANL and between BNL and ANL within each method. The significance level was set at $p < 0.05$.

Method	MCL-ANL		BNL-ANL	
	r	p value	r	p value
LS	−0.033	0.890	−0.4173	0.067
LA	0.207	0.381	0.207	0.327
ES	0.038	0.875	0.298	0.202
EA	0.075	0.753	0.325	0.162

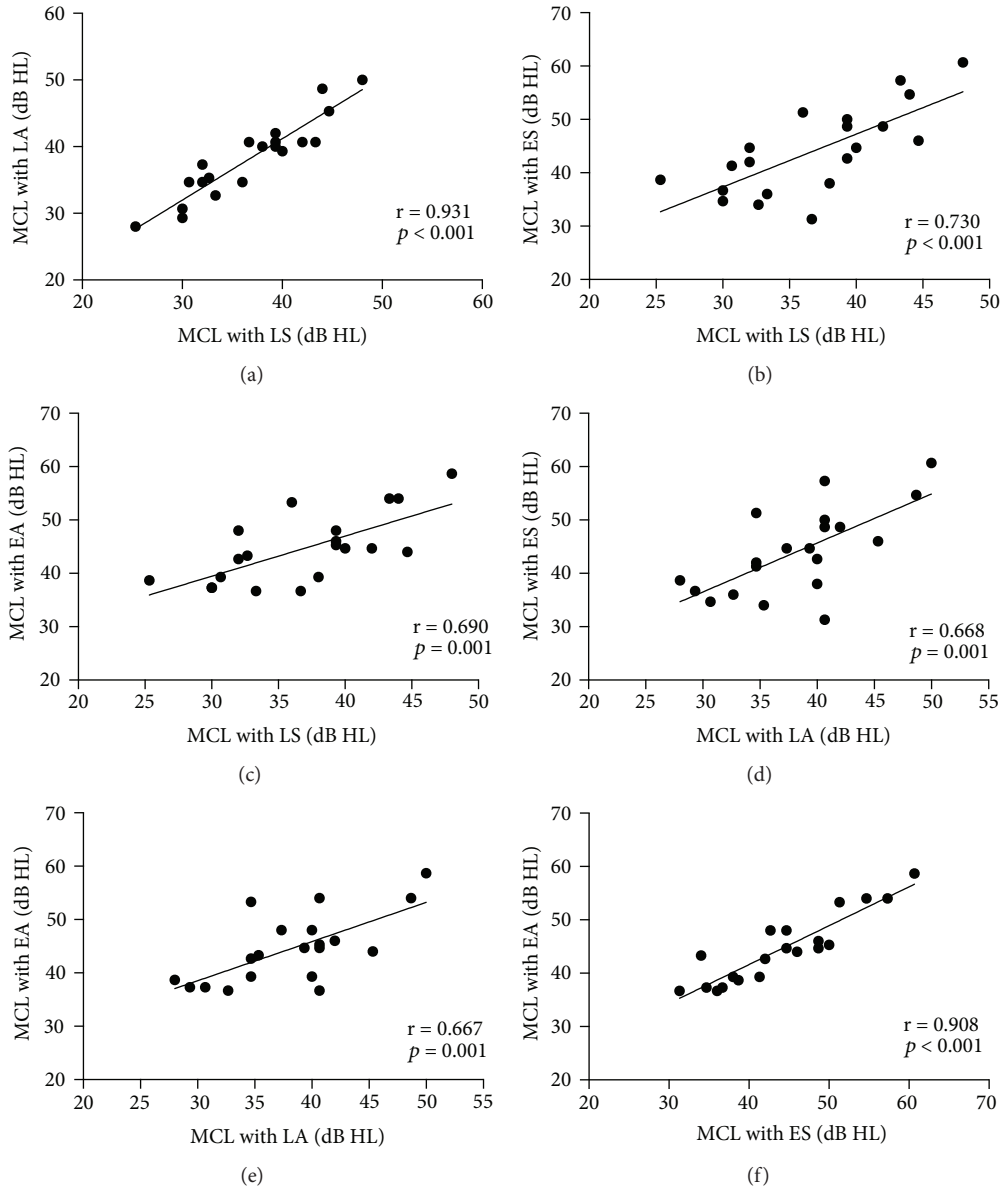

Figure 1: The correlations for MCL between each two methods. A: LS and LA; B: LS and ES; C: LS and EA; D: LA and ES; E: LA and EA; F: ES and EA. The significance level was set $p < 0.05$.

that the MCL was affected by response modes and presentation modes. Second, the results show that the main effect of response modes and presentation modes was different in BNL (response modes [$F = 3.759$; $p = 0.060$] and presentation modes [$F = 8.660$; $p = 0.006$]); the interaction effect of response modes × presentation modes was also not significant ($F = 0.787$; $p = 0.381$). The results indicated that the presentation modes may impact BNL, unlike the response modes. The analysis revealed that the main effect of response modes and presentation modes was not statistically significant for ANL (response modes [$F = 0.191$; $p = 0.665$] and presentation modes [$F = 0.302$; $p = 0.586$]); the interaction effect of response modes × presentation modes was also not significant ($F = 0.008$; $p = 0.931$). Both response modes and presentation modes did not affect ANL values. This showed that the ANL values of different response modes do not change with presentation modes because all the differences for interaction effects are not significant.

3.3. Correlations between MCL and ANL and between BNL and ANL within Each Method. Pearson correlation coefficients were used to observe the relationship between the MCL and ANL and between the BNL and ANL for each test situation. The correlations between MCL-ANL and between BNL-ANL within each method were not significant: coefficients are shown in Table 4.

3.4. Correlations of MCL, BNL, and ANL among Each Method. The correlation results of MCL, BNL, and ANL among each method are displayed in Figures 1, 2, and 3, respectively, and all correlations were significant. The correlations of MCL, BNL, and ANL between any two methods

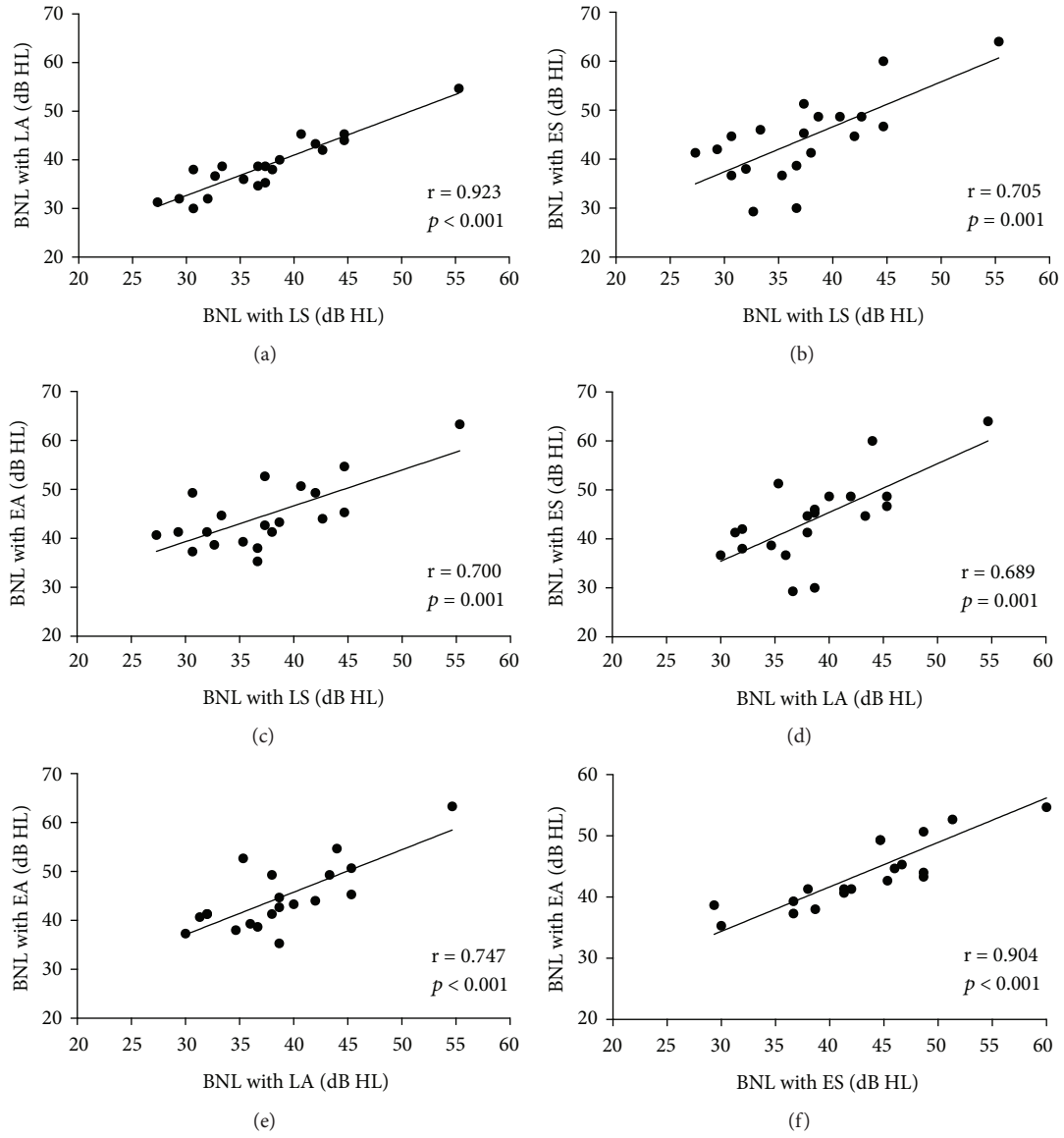

Figure 2: The correlations for BNL between each two methods. A: LS and LA; B: LS and ES; C: LS and EA; D: LA and ES; E: LA and EA; F: ES and EA. The significance level was set $p < 0.05$.

were strongly correlated in this study. Correlation coefficients ranged from 0.667 to 0.931; $p \leq 0.001$.

4. Discussion

This study compared the MCL, BNL, and ANL obtained with the LS, LA, ES, and EA methods in subjects with hearing in normal range. The results initially suggest that the values of MCL and BNL increased and the values of ANL decreased with an increasing number of measurements, except in the EA method. Although ANL value tended to decrease, showing a potential learning effect during this test, and tolerance may influence the ANL tests, the difference of MCL, BNL and ANL values obtained from different measurements within each method was not statistically significant in most situations. And our study also shows that the correlations between ANL, MCL, and BNL obtained from both methods and both measurements were significant. This indicated that the repeatability of the ANL test method was credible. Previous studies [18–21] showed that the Pearson correlations suggested significant correlations between ANL and MCL with a LA method, but the correlations of the current study suggested that ANL values were reliable across testing methods; there were no correlations between ANL and BNL or between ANL and MCL in either method. This means that the ANL did not change with MCL or BNL. ANL may be an intrinsic property for every subject and MCL or BNL could affect ANL in different methods.

The main purpose of this study was to compare the acceptable noise level obtained with a loudspeaker or earphones in Chinese subjects with normal hearing. Clinically, the application of the loudspeaker and earphones is different. Sound field audiometry is used to evaluate the auditory function of the subject in a sound field using the loudspeaker.

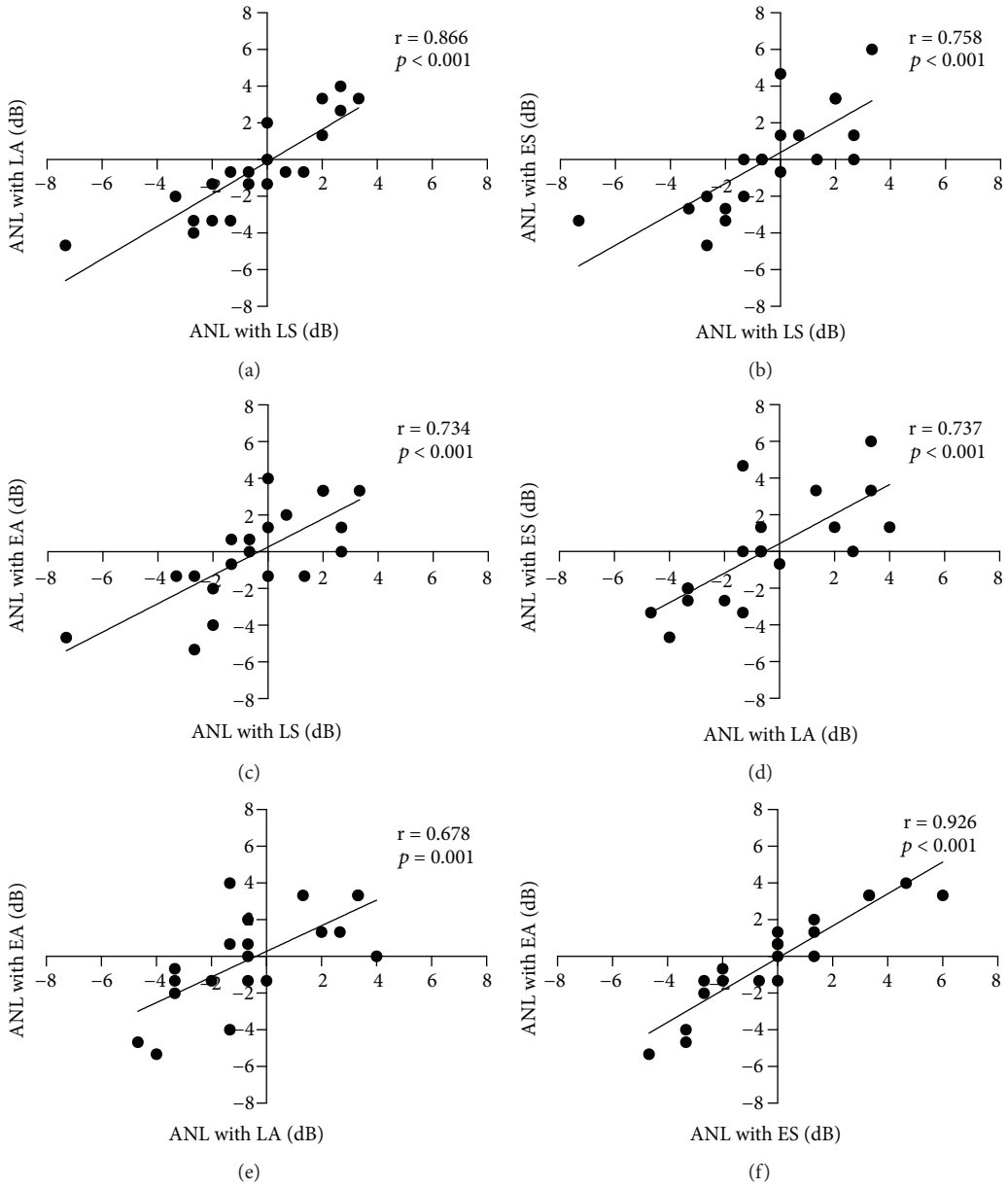

Figure 3: The correlations for ANL between each two methods. A: LS and LA; B: LS and ES; C: LS and EA; D: LA and ES; E: LA and EA; F: ES and EA. The significance level was set $p < 0.05$.

Sound field audiometry has incomparable superiority compared with earphones in children's pure-tone threshold audiometry, hearing aid matching, and evaluation of cochlear implants [22]. When evaluating the effect of the hearing aid, earphones and loudspeakers can be used for the unaided ear, while the patient wearing a hearing aid must be carried out in the sound field through a loudspeaker. Moreover, the results obtained with sound field measurements are more realistic than earphone audiometry. However, sound field audiometry can be easily affected by room size and layout. If the room is too small, subjects may consider it depressing. The capacity for noise isolation and absorption is also important in sound field audiometry. Taken together, the sound field audiometry standards are strict, and the actual operation is complicated. Therefore, it is necessary to conduct ANL testing with earphones and to compare these results with those obtained from earphones and loudspeaker. The results of this study suggest that ANL obtained with earphones is comparable to that obtained with a loudspeaker. Therefore, the hardware requirements and the complexity of the operation could be reduced, which is beneficial to the popularization of ANL tests. For those which do not have sound field conditions and those who are not suitable for sound field audiometry, the ANL obtained from earphones could be used as a reference to that obtained with a loudspeaker in a sound field.

The second main finding of this study compared the acceptable noise level with self-adjusted and audiologist-adjusted levels obtained in Chinese subjects with normal hearing. The ANL tests assess the subject's ability to accept

noise, and the researchers speculate that acceptance of noise may be an intrinsic property of an individual [1]. The loci of control and self-control seem to influence acceptable noise levels [23]. The concept of locus of control was proposed by Rotter [24] and refers to a generalized expectation that the results of events are controlled by oneself (internal control) or external forces (external control). The former is the responsibility for the inherent traits of the individual (such as ability and effort), while the latter is the responsibility attributed to factors beyond their own (such as environmental factors and luck). Garstecki and Erler [25] found that the locus of control tends to be external in women, who are less likely to accept the use of hearing aid. Cox et al. [26] reported that personality characteristic had an impact on the assessment of their hearing aid in a subjective questionnaire. Patients with a high locus of external control are less suited to the noise environment. The ANL test results in our study showed that self-adjusted and audiologist-adjusted tests did not differ in the two types of presentation modes. There were also no significant differences in the interactions between the different presentation modes and response modes. Our results indicated that response modes as factors of external control and internal control may not affect the ANL tests, and the locus of control theory is not consistent with our results. This may be because the subjects who participated were not uniform in personality characteristic. If the subjects were grouped according to their personality characteristic, the ANL tests in our study may be different. Future research requires more detailed analysis.

This study has some weaknesses. First, the age of subjects was 20 to 30, so it is not possible to extrapolate the results to all age populations. Moreover, the younger age of the subjects in this study may cause smaller ANL values than seen in other studies. Secondly, the subjects in this study had a good education, and the influence of knowledge level was not studied in previous studies. Thirdly, our results are from subjects with normal hearing. This conclusion remains to be confirmed in the hearing-impaired subjects. Obviously, larger studies are needed to enable multiple variables to be controlled.

However, our research has several protective measures to minimize other potential limitations. When the same audiologist tested three measurements for the subjects, it is impossible for the audiologist to be completely blind to the previous ANL results. Therefore, we attempted to surmount this limitation by ensuring that there was a minimum of a 30 min gap between the two measurements and scheduling the audiologist to perform at least three further measurements on other subjects before repeating the test on that subject again. Moreover, each subject had at least a 30 min gap between each ANL test in each of the four methods, so that the learning effect had less impact on results.

5. Conclusion

In conclusion, ANL results obtained through a loudspeaker or earphones with the sound levels adjusted by the subjects themselves or by the audiologist are comparable. The results of correlation relationship for ANL under different methods could provide us the possibility of predicting one measurement based on the other. Clinically, the audiologist could select the appropriate method to conduct the ANL tests according to the facilities and the subjects' conditions.

Data Availability

No additional unpublished data are available.

Conflicts of Interest

The authors declare that there is no competing interest relevant to the publication of this paper.

Authors' Contributions

Liang Xia and Jingchun He contributed equally to this paper.

Acknowledgments

This study was supported by grants from the State Key Development Program for Basic Research of China (Grant no. 2014CB541705), the Shanghai Municipal Education Commission/Gaofeng Clinical Medicine Grant Support (Grant no. 20152526), the National Natural Science Foundation of China (Grant no. 81771015), and the Three-year Action Program on Promotion of Clinical Skills/Clinical Innovation for Municipal Hospitals (Grant no. 16CR4027A) to Yanmei Feng.

References

[1] A. K. Nabelek, F. M. Tucker, and T. R. Letowski, "Toleration of background noises: relationship with patterns of hearing aid use by elderly persons," *Journal of Speech and Hearing Research*, vol. 34, no. 3, pp. 679–685, 1991.

[2] K. L. Recker and C. Micheyl, "Speech intelligibility as a cue for acceptable noise levels," *Ear and Hearing*, vol. 38, no. 4, pp. 465–474, 2017.

[3] K. Jonas Brannstrom and S. O. Olsen, "The acceptable noise level and the pure-tone audiogram," *American Journal of Audiology*, vol. 26, no. 1, pp. 80–87, 2017.

[4] H. C. Ho, Y. H. Wu, S. H. Hsiao, E. Stangl, E. J. Lentz, and R. A. Bentler, "The equivalence of acceptable noise level (ANL) with English, Mandarin, and non-semantic speech: a study across the U.S. and Taiwan," *International Journal of Audiology*, vol. 52, no. 2, pp. 83–91, 2012.

[5] E. M. Adams, S. Gordon-Hickey, R. E. Moore, and H. Morlas, "Effects of reverberation on acceptable noise level measurements in younger and older adults," *International Journal of Audiology*, vol. 49, no. 11, pp. 832–838, 2010.

[6] Y. H. Wu, H. C. Ho, S. H. Hsiao, R. B. Brummet, and O. Chipara, "Predicting three-month and 12-month post-fitting real-world hearing-aid outcome using pre-fitting acceptable noise level (ANL)," *International Journal of Audiology*, vol. 55, no. 5, pp. 285–294, 2016.

[7] A. K. Nabelek, J. W. Tampas, and S. B. Burchfield, "Comparison of speech perception in background noise with acceptance of background noise in aided and unaided conditions," *Journal of Speech, Language, and Hearing Research*, vol. 47, no. 5, pp. 1001–1011, 2004.

[8] A. K. Nabelek, M. C. Freyaldenhoven, J. W. Tampas, S. B. Burchfield, and R. A. Muenchen, "Acceptable noise level as a predictor of hearing aid use," *Journal of the American Academy of Audiology*, vol. 17, no. 9, pp. 626–639, 2006.

[9] M. C. Freyaldenhoven, D. Fisher Smiley, R. A. Muenchen, and T. N. Konrad, "Acceptable noise level: reliability measures and comparison to preference for background sounds," *Journal of the American Academy of Audiology*, vol. 17, no. 9, pp. 640–648, 2006.

[10] S. O. Olsen, L. H. Nielsen, J. Lantz, and K. J. Brännström, "Acceptable noise level: repeatability with Danish and non-semantic speech materials for adults with normal hearing," *International Journal of Audiology*, vol. 51, no. 7, pp. 557–563, 2012.

[11] K. Jonas Brännström, J. Lantz, L. H. Nielsen, and S. Ø. Olsen, "Acceptable noise level with Danish, Swedish, and non-semantic speech materials," *International Journal of Audiology*, vol. 51, no. 3, pp. 146–156, 2011.

[12] K. J. Brännström, E. Zunic, A. Borovac, and T. Ibertsson, "Acceptance of background noise, working memory capacity, and auditory evoked potentials in subjects with normal hearing," *Journal of the American Academy of Audiology*, vol. 23, no. 7, pp. 542–552, 2012.

[13] K. J. Brännström, L. Holm, T. Kastberg, and S. Ø. Olsen, "The acceptable noise level: the effect of repeated measurements," *International Journal of Audiology*, vol. 53, no. 1, pp. 21–29, 2013.

[14] D. S. Rogers, A. W. Harkrider, S. B. Burchfield, and A. K. Nabelek, "The influence of listener's gender on the acceptance of background noise," *Journal of the American Academy of Audiology*, vol. 14, no. 7, pp. 372–82; quiz 401, 2003.

[15] A. W. Harkrider and S. B. Smith, "Acceptable noise level, phoneme recognition in noise, and measures of auditory efferent activity," *Journal of the American Academy of Audiology*, vol. 16, no. 8, pp. 530–545, 2005.

[16] S. Gordon-Hickey and R. E. Moore, "Influence of music and music preference on acceptable noise levels in listeners with normal hearing," *Journal of the American Academy of Audiology*, vol. 18, no. 5, pp. 417–427, 2007.

[17] S. Ø. Olsen and K. J. Brännström, "Does the acceptable noise level (ANL) predict hearing-aid use?," *International Journal of Audiology*, vol. 53, no. 1, pp. 2–20, 2013.

[18] J. Chen, H. Zhang, P. N. Plyler, W. Cao, and J. Chen, "Development and evaluation of the Mandarin speech signal content on the acceptable noise level test in listeners with normal hearing in mainland China," *International Journal of Audiology*, vol. 50, no. 6, pp. 354–360, 2011.

[19] C. A. Franklin Jr, J. W. Thelin, A. K. Nabelek, and S. B. Burchfield, "The effect of speech presentation level on acceptance of background noise in listeners with normal hearing," *Journal of the American Academy of Audiology*, vol. 17, no. 2, pp. 141–146, 2006.

[20] A. W. Harkrider and J. W. Tampas, "Differences in responses from the cochleae and central nervous systems of females with low versus high acceptable noise levels," *Journal of the American Academy of Audiology*, vol. 17, no. 9, pp. 667–676, 2006.

[21] M. C. Freyaldenhoven, P. N. Plyler, J. W. Thelin, and M. S. Hedrick, "The effects of speech presentation level on acceptance of noise in listeners with normal and impaired hearing," *Journal of Speech Language and Hearing Research*, vol. 50, no. 4, p. 878, 2007.

[22] G. Walker, H. Dillon, and D. Byme, "Sound field audiometry: recommended stimuli and procedures," *Ear and Hearing*, vol. 5, no. 1, pp. 13–21, 1984.

[23] A. C. Nichols and S. Gordon-Hickey, "The relationship of locus of control, self-control, and acceptable noise levels for young listeners with normal hearing," *International Journal of Audiology*, vol. 51, no. 4, pp. 353–359, 2012.

[24] J. B. Rotter, "Internal versus external control of reinforcement: a case history of a variable," *American Psychologist*, vol. 45, no. 4, pp. 489–493, 1990.

[25] D. C. Garstecki and S. F. Erler, "Hearing loss, control, and demographic factors influencing hearing aid use among older adults," *Journal of Speech, Language, and Hearing Research*, vol. 41, no. 3, pp. 527–537, 1998.

[26] R. M. Cox, G. C. Alexander, and G. Gray, "Personality and the subjective assessment of hearing aids," *Journal of the American Academy of Audiology*, vol. 10, no. 1, pp. 1–13, 1999.

Hindawi
Neural Plasticity
Volume 2018, Article ID 7691473, 9 pages
https://doi.org/10.1155/2018/7691473

Review Article

The Role of Autoimmunity in the Pathogenesis of Sudden Sensorineural Hearing Loss

Guangfei Li,[1] Dan You,[1] Jiaoyao Ma,[1] Wen Li,[1] Huawei Li,[1,2] and Shan Sun[1]

[1]*Key Laboratory of Hearing Medicine of NHFPC, ENT Institute and Otorhinolaryngology Department, Shanghai Engineering Research Centre of Cochlear Implant, Affiliated Eye and ENT Hospital, State Key Laboratory of Medical Neurobiology, Fudan University, Shanghai 200031, China*
[2]*Institutes of Biomedical Sciences and The Institutes of Brain Science and the Collaborative Innovation Center for Brain Science, Fudan University, Shanghai 200032, China*

Correspondence should be addressed to Huawei Li; hwli@shmu.edu.cn and Shan Sun; shansun@fudan.edu.cn

Received 21 March 2018; Accepted 10 May 2018; Published 13 June 2018

Academic Editor: Hai Huang

Sudden sensorineural hearing loss (SSHL) is a clinically common acute symptom in otolaryngology. Although the incidence of SSHL has increased around the world in recent years, the etiology of the disease is still unclear. It has been reported that infections, ototoxic drugs, membrane labyrinth rupture, carcinomas, circulatory system diseases, autoimmune diseases, brain lesions, mental diseases, congenital or inherited diseases, and so on, are all risk factors for SSHL. Here, we discuss the autoimmune mechanisms behind SSHL, which might be induced by type II–IV allergic reactions. We also introduce the main immunosuppressive medications that have been used to treat SSHL, which will help us to identify potential targets for immune therapy.

1. Introduction

Sudden sensorineural hearing loss (SSHL) or "idiopathic sudden sensorineural hearing loss" refers to the sudden, unexplained hearing loss of more than 30 dB across all frequencies. The main clinical symptom is hearing loss, sometimes accompanied by tinnitus, ear blockage, dizziness, nausea, and/or vomiting. The pathogenesis of SSHL involves complex systemic or regional symptoms, and there are as yet no effective treatments. Here, we review our current understanding of SSHL and inner ear structures and cells as the fundamental platform for immune surveillance and responsiveness in hearing loss, and we present a summary of SSHL that results from immune system dysfunction. We think that immune-modulating medications support the clinical findings and suggest some potential targets for therapy in clinics.

2. The Evidence for Autoimmunity in SSHL

The inner ear and brain are traditionally viewed as being immune privileged because there is a blood-labyrinthine barrier that acts in a similar manner as the blood-brain barrier, and only a few macrophages are present in these organs [1]. However, a large number of experimental and clinical cases of SSHL have been identified in which SSHL is a symptom associated with other autoimmune diseases or is the primary symptom of spontaneous systemic autoimmune diseases such as autoimmune hepatitis [2], sympathetic neural hyperalgesia edema syndrome [3], Cogan's syndrome [4, 5], systemic lupus erythematosus [6, 7], multiple sclerosis [8–10], rheumatoid arthritis [11], nodular polyarteritis [12], Crohn's disease [13], and so on. Increasing experimental evidence suggesting an autoimmune component in the pathology of SSHL has emerged since 1979 when McCabe first identified 18 patients with autoimmune-associated SSHL who were effectively medicated with glucocorticoid and vincristine [14]. The presence of antibodies against the inner ear 68 kDa antigen and the recovery of hearing after immunosuppressive therapy have further confirmed the immune-mediated mechanism of hearing loss [15–18]. Immunohistochemistry and other techniques have been used to show that immune cells, including lymphocytes,

Table 1: The main autoimmune target antigens in the inner ear.

Inner ear antigen	Distribution	References
Collagen type II	In the subepithelial layer of the endolymphatic duct and spiral ligament.	[26, 64–68]
HSP-70	Hair cells and supporting cells.	[16, 17, 69–73]
β-Tubulin	Hair cells, supporting cells, the spiral ligament of the stria vascularis, and the spiral ganglion.	[54, 74–78]
Cochlin	In the regions of the fibrocytes of the spiral limbus and the spiral ligament and in the cochlear and vestibular labyrinth.	[52, 53, 79–82]
Beta-tectorin	Hair cells in the basal region of the hair bundle lying over the apical surface of the auditory epithelium, in the basilar papilla, in the clear cells and the cuboidal cells, and in the striolar region of the lagena macula.	[52, 53, 77, 83, 84]
Kresge Hearing Research Institute-3 (KHRI-3)	This is a protein specific to the inner ear and is expressed in the saccular wall cells and transitional epithelial cells in the utricle and ampules, by cells in the endolymphatic sac, and by supporting cells.	[85, 86]

leukocytes, and macrophages, are present in the inner ear as well as to analyze the interactions between these immune cells [19–22]. The following inner ear antigens (see Table 1) are considered to be the main targets of harmful antibodies: 68 kDa protein [23, 24], 30 kDa protein (also called myelin protein zero (P0)) [25], collagen type II [26, 27], tubulin [28], cochlin [29, 30], and inner ear supporting cell antigen [23]. Moscicki et al. have confirmed the clinical relationship between idiopathic SSHL and anti-68 kDa protein antibodies in patient serum [22, 31]. Furthermore, Billings et al. [24] and Bloch et al. [16, 17] have confirmed that the 68 kDa protein is heat shock protein 70 (HSP-70). These studies have provided a basis for the diagnosis and treatment of autoimmune-related SSHL.

3. The Immune Response in the Inner Ear

The immune system plays an important role in protecting the inner ear from damage caused by bacteria, viruses, and other pathogenic microorganisms. However, in the pathogenesis of autoimmune hearing loss, the immune system itself damages the inner ear. Although the exact mechanism of its pathogenesis is not yet fully understood, studies in patients with SSHL and in experimental animal models have identified a number of factors that are involved in autoimmune SSHL. The immune response in the inner ear relies on cytokines, especially IL-1β [32, 33], IL-2, and TNF-α [34], that play important roles in regulating the immune response of the inner ear. Some inflammatory cells in the inner ear are also involved, including macrophages (or microglia-like cells), T lymphocytes, and leukocytes. Our previous work has demonstrated that the ototoxicity of neomycin (an aminoglycoside antibiotic) is mediated through the activation of microglia-like cells that release proinflammatory cytokines that cause damage to the hair cells of the inner ear [35, 36].

3.1. The Physiological Immune Defense in the Inner Ear. The inner ear is fully capable of initiating an immune response to the invasion of external antigens. Previous studies have shown that the lymphatic sac contains several of the immunological components of the immune response and is the primary site of the immune response [37, 38]. The antigens in the inner ear are often used as targets for such immune responses. Recognition of these antigens by the inner ear's innate immune cells (neutrophils, macrophages, dendritic cells, etc.; see Table 2 and Figure 1) stimulates the release of IL-1β, which in turn triggers a series of adaptive immune responses. The cytokines that are released as part of these responses then recruit lymphocytes from the circulatory system into the inner ear where they cause irreversible tissue damage [39].

3.2. Pathological Immunity in the Inner Ear. No lymphocytes are present in the normal endolymphatic sac, and there is no evidence that the lymphocytes present in the cochlea during the immune response are derived from the endolymphatic sac; thus, they must originate mainly from the peripheral circulatory system [40]. Lymphocytes in the circulatory system are predominantly migrating from the spiral vessels and their branches [41]. When they reach the other organs of the body, they initiate the process of antigen absorption, presentation, and degradation. IL-1 plays an important role in regulating the innate immune response, and it acts as an agonist of resting helper T cells and B cells. The helper T cells, once activated by IL-1, will produce IL-2. The secretion of IL-2 results in pluripotent stem cells differentiating into helper T cells, cytotoxic T cells, and suppressor T cells. IL-2 also assists helper T cells in activating B lymphocytes and might play an important role in regulating the immune response in the inner ear [42].

IL-1β and TNF-α are involved in the initiation and amplification of immune responses. IL-1β is mainly expressed in the fibroblasts of the spiral ligament in the case of nonspecific trauma such as surgery or acoustic neuroma, while TNF-α is mainly expressed in infiltrating circulating inflammatory cells or innate immune cells in the endolymphatic sac under the stimulation of external antigens. The release of TNF-α in animal models is a part of the adaptive immune response. When an antigen is injected into the mouse inner ear, both IL-1β and TNF-α are secreted and a normal immune response occurs. However, when the antigen flows from the cerebrospinal fluid to the inner ear and the inner ear is not traumatized, only TNF-α is secreted and only a very weak immune response is initiated. It is

Table 2: The innate immune cells and adaptive immune cells in the inner ear.

Immune cells			Function	Distribution	References
Innate immune cells	Macrophages		Promote the proliferation of T cells and B cells; Process and present antigens and participate in the regulation of adaptive immune responses; Phagocytosis and digestion of pathogenic microorganisms; Mediate and promote inflammatory responses	Endolymphatic sac and subepithelial and endoluminal space and the scala tympani and scala vestibuli.	[37, 38, 87, 88]
	Granulocytes		Anti-inflammatory, release of some inflammatory factors.	In the scala tympani, in the scala vestibuli from the basal turn to the apex, and in the modiolus.	[88–90]
Adaptive immune cells	B cells		Antigen identification and presentation. Activated B cells differentiate into plasma cells that secrete antibodies.	Peripheral circulation system, infiltrating into the endolymph and perilymph of the scala tympani and the scala vestibule and the endolymphatic sac.	[38, 91]
	Helper T cells	Th1 cells	Mediate cellular immunity; Secrete some cytokines, such as IFN-γ.	From the peripheral circulation system, infiltrate into the scala tympani, the scala vestibuli, and the perisaccular connective tissue of the endolymphatic sac and the modiolar vessels.	[20, 21, 52, 54, 82, 87, 91, 92]
		Th2 cells	Mediate humoral immunity; Secrete cytokines IL-4, IL-5, and IL-13.		
		Th17 cells	Secrete inflammatory cytokines IL-17 and IL-22; act as inflammation-initiating cells.		
	Suppressor T cells	$CD4^+/CD25^+$ Th cells	Negative regulator of immune response; $CD4^+CD25^+$ regulatory T cells play an immunosuppressive function in the periphery; iTregs can secrete the suppressive cytokines IL-10 and TGF-β.	From the circulation, infiltrate into the modiolus, the scala tympani, and the perisaccular connective tissue of the endolymphatic sac.	[55, 87, 92, 93]
		Antigen-specific regulatory T cells (inducible regulatory T cells (iTregs))			
	Lymphocytes		Anti-inflammatory	In the scala tympani, in all turns of the cochlea, and in smaller numbers in the scala vestibuli.	[51]

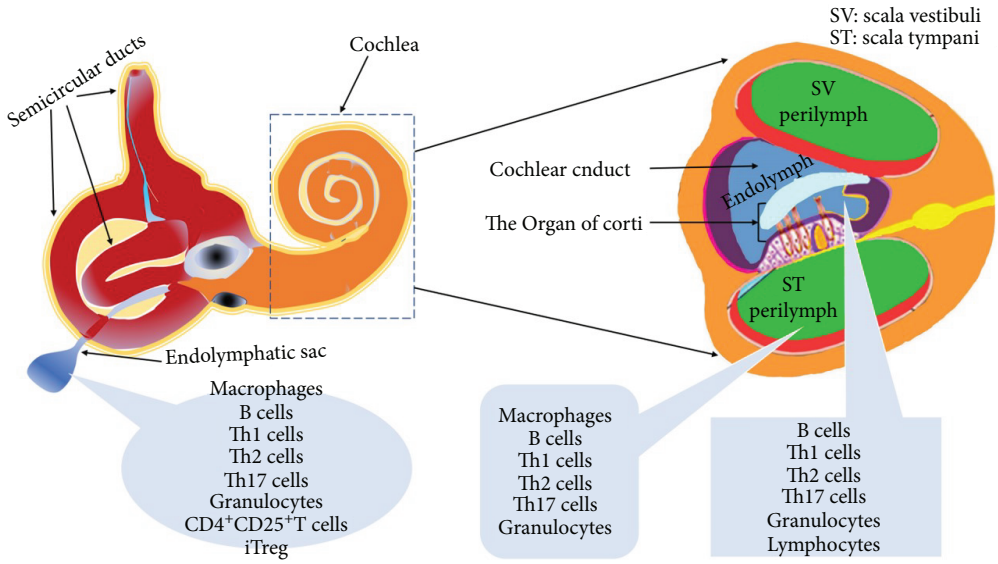

Figure 1: The distribution of immune cells in the inner ear when the immune response is initiated.

worth noting that damage to the cochlea alone can also lead to a slight immune response [43]. These results all show that the nonspecific and specific components of the immune response act synergistically in the inner ear so as to maximize the effect of the immune response.

Therefore, if the cochlea is damaged or antigens are injected into the cochlea (or a patient with an autoimmune disease has immune cells directly attacking the inner ear antigen), both nonspecific and specific immune responses are activated simultaneously, and these can result in simultaneous IL-1β and TNF-α production that amplifies the inflammatory effect and then leads to extensive damage to the inner ear tissue. Animal model experiments have confirmed that the innate immune response predominates in the inner ear until the regulatory immune response produces enough of an inflammatory response to cause damage to the inner ear. Therefore, when innate and specific immune responses are activated at the same time, it might be possible to avoid excessive immune responses by downregulating or inhibiting specific immune responses, particularly those that inhibit the effects of TNF-α.

4. The Immune Pathogenesis of Hearing Loss

Although it is known that immune responses in the inner ear can lead to tissue damage, the exact mechanism behind the injury process remains unclear, and thus we can use other autoimmune diseases as a reference to understand such injury processes in the inner ear. In general, immune response damage is mediated by both humoral and cellular immunity, and autoimmune damage can be classified as type I allergic reactions to type IV allergic reactions. Type I allergic reactions (immediate-type allergic reactions) are mainly caused by the interactions of an antigen with an antibody (usually IgE) on the surface of immune cells that activate the cells and causes them to release active mediators such as histamine and serotonin to induce a rapid immune response. Type II allergic reactions (cytotoxic allergies) are mediated by IgG or IgM, and when the antibody binds to the antigen on the foreign cell surface, the cells are destroyed due to the action of the complement system, phagocytes, or nature killer cells. Type III allergic reactions (immune complex allergies) are caused by the deposition of medium-sized soluble antigen-antibody complexes into capillary walls or tissues, which activates the complement system or leads to the recruitment of leukocytes. Type IV allergic reactions (delayed-type allergies) cause tissue injury that is mediated by T cells. Type I allergic reactions are not associated with autoimmune hearing loss, but types II–IV (see Figure 2) have been shown to be potential mechanisms that lead to inner ear damage in autoimmune SSHL [44], and these are described in the following sections.

4.1. Type II Allergic Reactions (Cytotoxic Allergies). Type II cytotoxic antibody-mediated damage can be confirmed from previous animal studies and clinical studies. Harris [45, 46] injected KLH protein, a metalloprotein extracted from snails, into susceptible guinea pigs. The exposure to KLH resulted in the production of anti-KLH antibodies. Subsequent injection of bovine inner ear antigen into guinea pigs resulted in hearing loss, and circulating antibodies specific to bovine inner ear antigen were found in the serum and perilymph. In patients with SSHL, analysis of antibodies in the inner ear using Western blotting revealed that there were IgG antibodies against the inner ear-specific proteins cochlin and β-tectorin and the nonspecific protein HSP-70. This study revealed that the direct antibody response to inner ear proteins can lead to SSHL and that such antibodies can be used as a marker for disease diagnosis. Using antigen-specific Western blot analysis of patient and healthy sera, it was found that anti-cochlin IgG antibodies were more prevalent in patients with idiopathic sensorineural hearing loss than anti-β-tectorin-specific IgG antibodies, whereas anti-HSP-70 IgG antibodies were more common

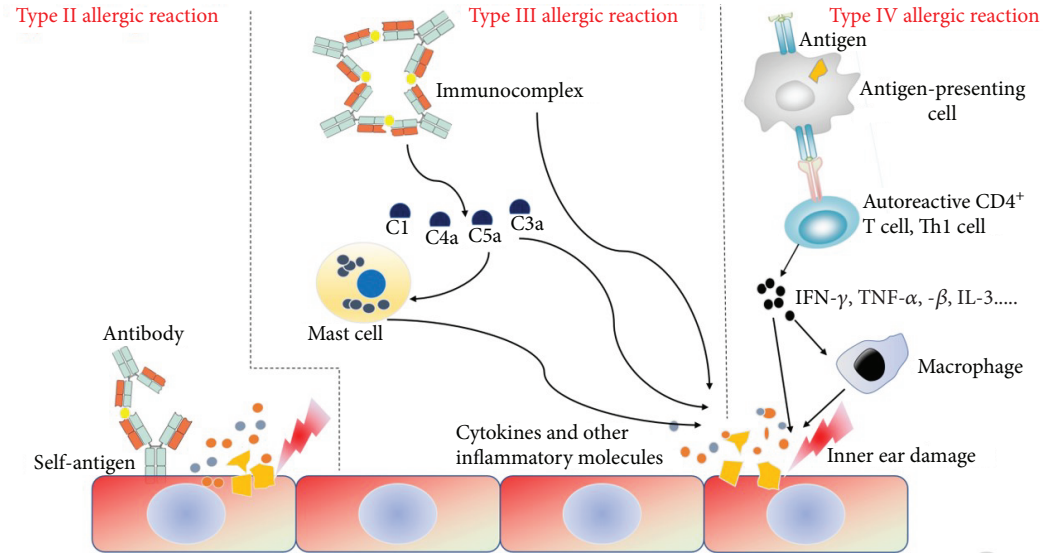

Figure 2: The mechanisms of inner ear damage by the type II–IV allergic reactions.

than anti-cochlin IgG antibodies and anti-β-tectorin-specific IgG antibodies in all of the patients [47]. These animal experiments and clinical studies have provided compelling evidence that in at least some patients with SSHL the pathology is due to antibody-mediated tissue damage in the inner ear.

4.2. Type III Allergic Reactions (Immune Complex Allergies). Type III immunocomplex-mediated hearing loss mechanisms have been identified in animal models of SSHL. Especially in C3H/lpr autoimmune mice with progressive hearing loss, one can find deposition of immunocomplexes in the vascular stria [48], and the deposition of IgM and IgG immunocomplexes can be seen in NZB/kl mice that have high incidences of hearing loss [49]. Trune et al. found the presence of DNA antibodies in the inner ear of MRL/lpr mice, and such anti-DNA or DNA-anti-DNA antibody immunocomplexes result in the destruction of endothelial cell integrity that affects the function of the blood-labyrinthine barrier resulting in SSHL [50]. Although the transfer of findings from animal models to patients is still speculative, the link between systemic autoimmune diseases and SSHL can provide additional evidence for the existence of such a mechanism. Many clinical cases have described hearing loss patients with associated systemic autoimmune disorders, and many of these systemic autoimmune diseases have been confirmed as type III allergic reactions with immunocomplex deposition resulting in tissue damage. For example, a 19-year-old girl with SSHL and mouth ulcers and bleeding under the nails was diagnosed with systemic lupus erythematosus. The histological sections revealed deposition of IgG, C3, C1q, and IgM immunocomplexes, obstruction of the vasculature of the inner ear by the formation of microthrombi, and damage to the organization of the inner ear. This patient's hearing recovered significantly with the use of methylprednisolone and other hormones [6]. Systemic autoimmune diseases such as multiple sclerosis, rheumatoid arthritis, and nodular arteriosclerosis are all associated with SSHL and are believed to form circulating immunocomplexes that deposit in the inner ear's vascular tissue thus causing SSHL.

4.3. Type IV Allergic Reactions (Delayed-Type Allergies): Autoreactive T Cell-Mediated Inflammatory Lesions. SSHL caused by type IV allergic reactions can be observed in animal models. Gloddek et al. used radioactive isotopes of chromium to label lymphocytes in susceptible experimental animals and demonstrated that lymphocytes migrate to the inner ear in response to antigenic stimulation and that infiltrated lymphocytes are found in the basal membrane and in the vestibule of the cochlea [51]. Hearing loss at all frequencies in the auditory brainstem response of mice was observed 5 weeks after immunization with the inner ear-specific protein cochlin 131–150 or β-tectorin in SWXJ mice. Each of the tested peptides activated Th1-like $CD4^+$ T cells with proinflammatory effects as observed by flow cytometry analysis, and after 6 weeks of selective transfer of peptide-activated $CD4^+$ T cells to unimmunized SWXJ mice, the auditory brainstem response threshold was significantly increased. This indicated that T cell-mediated tissue damage can lead to the development of autoimmune hearing loss, and immunocytochemistry analysis showed that the infiltration of leukocytes in the inner ear was associated with the observed hearing loss [52]. Billings also immunized SWXJ mice with cochlin 131–150 and confirmed that $CD45^+$ T cells infiltrate the cochlea and cause autoimmune SSHL [53]. Zhou et al. used the inner ear autoantigen β-tubulin to create a mouse model of experimental spontaneous immune hearing loss. They showed that the response to β-tubulin involves $CD4^+$ T cells producing γ-interferon, whereas T cell-mediated experimental autoimmune hearing loss is primarily caused by the induction of β-tubulin-activated $CD4^+$ T cells in neonatal BALB/c mice and increased auditory brainstem responses were seen in mice in which these cells were activated. Furthermore, a significant decrease in $CD4^+/CD25^+/$

$Foxp3^+$ regulatory T cells was observed in mice immunized with β-tubulin, which inhibited the proliferation of effector $CD4^+/CD25^-$ T cells [54]. Xia et al. used flow cytometry to analyze the clinical T cell subtypes in 17 patients with autoimmune sensorineural hearing loss, 16 patients with noise-induced hearing loss, and 100 individuals with normal hearing. There was no significant difference in the T cell subtypes among the three groups, except that the proportion of $CD4^+$ T cells in the patients with sensorineural hearing loss increased and the function of $CD4^+/CD25^+$ regulatory T cells was absent [55]. The above experimental animal models and clinical cases have confirmed that autoimmune hearing loss can be caused by cytotoxic T cell-mediated organ-specific autoimmune disorders of the inner ear.

5. Immunosuppressive Therapy for SSHL

Glucocorticoids have remained the main stay of treatment over the past four decades since McCabe [14] first treated SSHL with glucocorticoids, and the symptoms of patients were improved significantly. Owing to the systemic side effects of long-term treatment with glucocorticoids, other therapeutic methods also have been investigated. Ruckenstein et al. [56] and Trune et al. [57] used MRL/lpr mice to show that prednisolone can protect against hearing loss. In addition, Satoh et al. [58] and Wang et al. [59] used etanercept, a TNF-α antagonist, to treat SSHL and showed that it can reduce inflammation in the inner ear and prevent hearing loss. Clinically, Xenellis et al. [60] have shown that the intratympanic injection of steroids is a safe and effective method for SSHL treatment, and Haynes et al. [61] have shown that intratympanic injection of dexamethasone can also improve hearing in SSHL patients when systemic medications fail. Furthermore, Battaglia et al. [62] used a combination therapy of intratympanic dexamethasone with high-dose prednisone taper for SSHL and showed that the patients receiving the combination therapy had significant improvements in speech-discrimination score and pure-tone average and recovered their hearing quickly. More recently, azathioprine has been confirmed to maintain the hearing threshold, decrease the risk of relapse, and slow down the rate at which patients relapse [63].

The evidence to date suggests that autoimmune SSHL is mainly mediated by autoantibodies or T cells or by both. As autoimmune reactions are increasingly considered to be a cause of SSHL, animal models and clinical trials have shown that autoimmune processes cause damage to the inner ear through various mechanisms. Humoral immunity and cellular immune-mediated autoimmune damage have both been shown to play a role in the pathogenesis of autoimmune hearing loss. Although the precise diagnosis of autoimmune SSHL is still difficult, the response to immunosuppressive therapy is generally positive for these patients. Therefore, the immune mechanism of SSHL needs further study in order to identify specific antigens of the inner ear and specific diagnostic markers that can provide a more accurate and timely diagnosis and contribute to a more effective treatment plan.

Conflicts of Interest

The authors declare that there is no conflict of interest regarding the publication of this paper.

Authors' Contributions

Guangfei Li and Dan You contributed equally to this work.

Acknowledgments

Funding was provided by the National Key R&D Program of China (nos. 2017YFA0103900 and 2016YFC0905200), the National Natural Science Foundation of China (nos. 81570913 and 81620108005), and the Shanghai Pujiang Talents Plan (18PJ1401700).

References

[1] S. K. Juhn, L. P. Rybak, and S. Prado, "Nature of blood-labyrinth barrier in experimental conditions," *The Annals of Otology, Rhinology, and Laryngology*, vol. 90, no. 2, pp. 135–141, 1981.

[2] M. Düzlü, M. Çolak, İ. K. Önal, H. Tutar, R. Karamert, and Ç. Gökdoğan, "Audiological findings in autoimmune hepatitis: hearing loss at high frequencies," *Gazi Medical Journal*, vol. 28, no. 4, 2017.

[3] J. H. Check, "Sympathetic neural hyperalgesia edema syndrome as a cause of autoimmune hearing loss," *Clinical and Experimental Obstetrics & Gynecology*, vol. 44, no. 1, pp. 133-134, 2017.

[4] S. Montes, S. Rodríguez-Muguruza, V. Soria, and A. Olivé, "Atypical Cogan' syndrome associated with sudden deafness and glucocorticoid response," *Reumatología Clínica*, vol. 10, no. 4, pp. 267-268, 2014.

[5] A. Bacciu, E. Pasanisi, F. di Lella, M. Guida, S. Bacciu, and V. Vincenti, "Cochlear implantation in patients with Cogan syndrome: long-term results," *European Archives of Oto-Rhino-Laryngology*, vol. 272, no. 11, pp. 3201–3207, 2015.

[6] S. Chawki, J. Aouizerate, S. Trad, J. Prinseau, and T. Hanslik, "Bilateral sudden sensorineural hearing loss as a presenting feature of systemic lupus erythematosus: case report and brief review of other published cases," *Medicine*, vol. 95, no. 36, article e4345, 2016.

[7] C. A. Bowman, F. H. Linthicum Jr, R. A. Nelson, K. Mikami, and F. Quismorio, "Sensorineural hearing-loss associated with systemic lupus erythematosus," *Otolaryngology-Head and Neck Surgery*, vol. 94, no. 2, pp. 197–204, 1986.

[8] M. Tanaka and K. Tanaka, "Sudden hearing loss as the initial symptom in Japanese patients with multiple sclerosis and seropositive neuromyelitis optica spectrum disorders," *Journal of Neuroimmunology*, vol. 298, pp. 16–18, 2016.

[9] M. Tekin, G. O. Acar, O. H. Cam, and F. M. Hanege, "Sudden sensorineural hearing loss in a multiple sclerosis case," *Northern Clinics of Istanbul*, vol. 1, no. 2, pp. 109–113, 2014.

[10] M. A. Hellmann, I. Steiner, and R. Mosberg-Galili, "Sudden sensorineural hearing loss in multiple sclerosis: clinical course and possible pathogenesis," *Acta Neurologica Scandinavica*, vol. 124, no. 4, pp. 245–249, 2011.

[11] M. A. Melikoglu and K. Senel, "Sudden hearing loss in a patient with rheumatoid arthritis; a case report and review of

the literature," *Acta Reumatológica Portuguesa*, vol. 38, no. 2, pp. 138-139, 2013.

[12] F. Rubin, N. Tran Khai Hoan, and P. Bonfils, "Sudden bilateral hearing loss revealing polyarteritis nodosa," *European Annals of Otorhinolaryngology, Head and Neck Diseases*, vol. 131, no. 4, pp. 265-266, 2014.

[13] G. Tirelli, P. Tomietto, E. Quatela et al., "Sudden hearing loss and Crohn disease: when Cogan syndrome must be suspected," *American Journal of Otolaryngology*, vol. 36, no. 4, pp. 590–597, 2015.

[14] B. F. McCabe, "Autoimmune sensorineural hearing loss," *The Annals of Otology, Rhinology, and Laryngology*, vol. 88, no. 5, pp. 585–589, 1979.

[15] A. Sismanis, C. Wise, and G. Johnson, "Methotrexate management of immune-mediated cochleovestibular disorders," *Otolaryngology and Head and Neck Surgery*, vol. 116, no. 2, pp. 146–152, 1997.

[16] D. B. Bloch, J. A. Gutierrez, V. Guerriero Jr, S. D. Rauch, and K. J. Bloch, "Recognition of a dominant epitope in bovine heat-shock protein 70 in inner ear disease," *Laryngoscope*, vol. 109, no. 4, pp. 621–625, 1999.

[17] D. B. Bloch, J. E. San Martin, S. D. Rauch, R. A. Moscicki, and K. J. Bloch, "Serum antibodies to heat shock protein 70 in sensorineural hearing loss," *Archives of Otolaryngology–Head & Neck Surgery*, vol. 121, no. 10, pp. 1167–1171, 1995.

[18] L. Xu, C. R. Pfaltz, and W. Arnold, "Human leukocyte antigens in patients with inner ear diseases of unknown etiology," *ORL*, vol. 55, no. 3, pp. 125–134, 1993.

[19] H. Iwai, K. Tomoda, M. Inaba et al., "Evidence of cellular supplies to the endolymphatic sac from the systemic circulation," *Acta Oto-Laryngologica*, vol. 115, no. 4, pp. 509–511, 2009.

[20] H. Iwai, M. Inaba, K. Tomoda, S. Ikehara, K. Sugiura, and T. Yamashita, "T cells infiltrating from the systemic circulation proliferate in the endolymphatic sac," *The Annals of Otology, Rhinology, and Laryngology*, vol. 108, no. 12, pp. 1146–1150, 1999.

[21] B. Gloddek, J. Gloddek, and W. Arnold, "A rat T-cell line that mediates autoimmune disease of the inner ear in the Lewis rat," *ORL*, vol. 61, no. 4, pp. 181–187, 1999.

[22] R. A. Moscicki, J. E. San Martin, C. H. Quintero, S. D. Rauch, Nadol JB Jr, and K. J. Bloch, "Serum antibody to inner ear proteins in patients with progressive hearing loss. Correlation with disease activity and response to corticosteroid treatment," *JAMA*, vol. 272, no. 8, pp. 611–616, 1994.

[23] J. Dhingra and M. Mahalingam, "Antibodies to 68 kd antigen-specific for inner ear disease?," *Laryngoscope*, vol. 107, no. 3, pp. 405-406, 1997.

[24] P. B. Billings, E. M. Keithley, and J. P. Harris, "Evidence linking the 68 kilodalton antigen identified in progressive sensorineural hearing loss patient sera with heat shock protein 70," *The Annals of Otology, Rhinology, and Laryngology*, vol. 104, no. 3, pp. 181–188, 1995.

[25] G. B. Hughes, B. P. Barna, S. E. Kinney, L. H. Calabrese, and N. J. Nalepa, "Clinical diagnosis of immune inner-ear disease," *Laryngoscope*, vol. 98, no. 3, pp. 251–3, 1988.

[26] J. P. Harris, N. K. Woolf, and A. F. Ryan, "A reexamination of experimental type II collagen autoimmunity: middle and inner ear morphology and function," *The Annals of Otology, Rhinology, and Laryngology*, vol. 95, no. 2, pp. 176–180, 1986.

[27] K. C. Campbell and J. J. Klemens, "Sudden hearing loss and autoimmune inner ear disease," *Journal of the American Academy of Audiology*, vol. 11, no. 7, pp. 361–7, 2000.

[28] R. Hallworth, M. McCoy, and J. Polan-Curtain, "Tubulin expression in the developing and adult gerbil organ of Corti," *Hearing Research*, vol. 139, no. 1-2, pp. 31–41, 2000.

[29] M. Komori, Y. Yamamoto, Y. Yaguchi, T. Ikezono, and H. Kojima, "Cochlin-tomoprotein test and hearing outcomes in surgically treated true idiopathic perilymph fistula," *Acta Oto-Laryngologica*, vol. 136, no. 9, pp. 901–904, 2016.

[30] P. Baruah, "Cochlin in autoimmune inner ear disease: is the search for an inner ear autoantigen over?," *Auris Nasus Larynx*, vol. 41, no. 6, pp. 499–501, 2014.

[31] M. Gross, R. Eliashar, A. Ben-Yaakov, R. Ulmansky, and J. Elidan, "Prevalence and clinical significance of anticardiolipin, anti-β_2-glycoprotein-1, and anti-heat shock protein-70 autoantibodies in sudden sensorineural hearing loss," *Audiology & Neuro-Otology*, vol. 13, no. 4, pp. 231–238, 2008.

[32] S. Pathak, E. Goldofsky, E. X. Vivas, V. R. Bonagura, and A. Vambutas, "IL-1β is overexpressed and aberrantly regulated in corticosteroid nonresponders with autoimmune inner ear disease," *Journal of Immunology*, vol. 186, no. 3, pp. 1870–1879, 2011.

[33] S. D. Rauch, "IL-1β inhibition in autoimmune inner ear disease: can you hear me now?," *The Journal of Clinical Investigation*, vol. 124, no. 9, pp. 3685–3687, 2014.

[34] S. Pathak, C. Stern, and A. Vambutas, "*N*-Acetylcysteine attenuates tumor necrosis factor alpha levels in autoimmune inner ear disease patients," *Immunologic Research*, vol. 63, no. 1–3, pp. 236–245, 2015.

[35] S. Sun, H. Yu, H. Yu et al., "Inhibition of the activation and recruitment of microglia-like cells protects against neomycin-induced ototoxicity," *Molecular Neurobiology*, vol. 51, no. 1, pp. 252–267, 2015.

[36] Z. Wang and H. Li, "Microglia-like cells in rat organ of corti following aminoglycoside ototoxicity," *Neuroreport*, vol. 11, no. 7, pp. 1389–1393, 2000.

[37] M. Barbara, G. Attanasio, V. Petrozza, A. Modesti, and R. Filipo, "The endolymphatic sac as the immunocompetent organ of the inner ear," *Annals of the New York Academy of Sciences*, vol. 830, pp. 243–252, 1997.

[38] S. Tomiyama and J. Harris, "The role of the endolymphatic sac in inner ear immunity," *Acta Oto-Laryngologica*, vol. 103, no. 3, pp. 182–188, 1987.

[39] S. Hashimoto, P. Billings, J. P. Harris, G. S. Firestein, and E. M. Keithley, "Innate immunity contributes to cochlear adaptive immune responses," *Audiology and Neuro-Otology*, vol. 10, no. 1, pp. 35–43, 2005.

[40] J. Harris and A. Ryan, "Fundamental immune mechanisms of the brain and inner ear," *Otolaryngology-Head and Neck Surgery*, vol. 112, no. 6, pp. 639–653, 1995.

[41] J. P. Harris, S. Fukuda, and E. M. Keithley, "Spiral Modiolar vein: Its importance in inner ear inflammation," *Acta Oto-Laryngologica*, vol. 110, no. 3-4, pp. 357–364, 1990.

[42] B. Gloddek and J. P. Harris, "Role of lymphokines in the immune response of the inner ear," *Acta Oto-Laryngologica*, vol. 108, no. 1-2, pp. 68–75, 2009.

[43] H. Satoh, G. S. Firestein, P. B. Billings, J. P. Harris, and E. M. Keithley, "Proinflammatory cytokine expression in the endolymphatic sac during inner ear inflammation," *Journal of the*

Association for Research in Otolaryngology, vol. 4, no. 2, pp. 139–147, 2003.

[44] Q. Gopen, E. M. Keithley, and J. P. Harris, "Mechanisms underlying autoimmune inner ear disease," *Drug Discovery Today: Disease Mechanisms*, vol. 3, no. 1, pp. 137–142, 2006.

[45] J. P. Harris, "Immunology of the inner ear: response of the inner ear to antigen challenge," *Otolaryngology-Head and Neck Surgery*, vol. 91, no. 1, pp. 18–23, 1983.

[46] J. P. Harris, "Immunology of the inner ear: evidence of local antibody production," *Annals of Otology, Rhinology & Laryngology*, vol. 93, no. 2, pp. 157–162, 2016.

[47] A. Naumann, J. M. Hempel, and K. Schorn, "Detection of humoral immune response to inner ear proteins in patients with sensorineural hearing loss," *Laryngo- Rhino- Otologie*, vol. 80, no. 5, pp. 237–244, 2001.

[48] D. R. Trune, J. P. Craven, J. I. Morton, and C. Mitchell, "Autoimmune disease and cochlear pathology in the C3H/*lpr* strain mouse," *Hearing Research*, vol. 38, no. 1-2, pp. 57–66, 1989.

[49] H. Nariuchi, M. Sone, C. Tago, T. Kurata, and K. Saito, "Mechanisms of hearing disturbance in an autoimmune model mouse NZB/kl," *Acta Oto-Laryngologica. Supplementum*, vol. 514, pp. 127–131, 1994.

[50] D. R. Trune, J. B. Kempton, S. H. Hefeneider, and R. M. Bennett, "Inner ear DNA receptors in MRL/lpr autoimmune mice: potential 30 and 70 kDa link between autoimmune disease and hearing loss," *Hearing Research*, vol. 105, no. 1-2, pp. 57–64, 1997.

[51] B. Gloddek, A. F. Ryan, and J. P. Harris, "Homing of lymphocytes to the inner ear," *Acta Oto-Laryngologica*, vol. 111, no. 6, pp. 1051–1059, 2009.

[52] C. A. Solares, A. E. Edling, J. M. Johnson et al., "Murine autoimmune hearing loss mediated by $CD4^+$ T cells specific for inner ear peptides," *Journal of Clinical Investigation*, vol. 113, no. 8, pp. 1210–1217, 2004.

[53] P. Billings, "Experimental autoimmune hearing loss," *Journal of Clinical Investigation*, vol. 113, no. 8, pp. 1114–1117, 2004.

[54] B. Zhou, M. H. Kermany, J. Glickstein et al., "Murine autoimmune hearing loss mediated by $CD4^+$ T cells specific for β-tubulin," *Clinical Immunology*, vol. 138, no. 2, pp. 222–230, 2011.

[55] M. Xia, H. B. Zhang, F. Liu, H. Y. Yin, and A. T. Xu, "Impaired $CD4^+CD25^+$ regulatory T cell activity in the peripheral blood of patients with autoimmune sensorineural hearing loss," *European Archives of Oto-Rhino-Laryngology*, vol. 265, no. 9, pp. 1027–1033, 2008.

[56] M. J. Ruckenstein, A. Sarwar, L. Hu, H. Shami, and T. N. Marion, "Effects of immunosuppression on the development of cochlear disease in the MRL-Fas^{lpr} mouse," *Laryngoscope*, vol. 109, no. 4, pp. 626–630, 1999.

[57] D. R. Trune, R. J. Wobig, J. B. Kempton, and S. H. Hefeneider, "Steroid treatment in young MRL.MpJ-*Fas*^{lpr} autoimmune mice prevents cochlear dysfunction," *Hearing Research*, vol. 137, no. 1-2, pp. 167–173, 1999.

[58] H. Satoh, G. S. Firestein, P. B. Billings, J. P. Harris, and E. M. Keithley, "Tumor necrosis factor-α, an initiator, and etanercept, an inhibitor of cochlear inflammation," *Laryngoscope*, vol. 112, no. 9, pp. 1627–1634, 2002.

[59] X. Wang, T. Truong, P. B. Billings, J. P. Harris, and E. M. Keithley, "Blockage of immune-mediated inner ear damage by etanercept," *Otology & Neurotology*, vol. 24, no. 1, pp. 52–57, 2003.

[60] J. Xenellis, N. Papadimitriou, T. Nikolopoulos et al., "Intratympanic steroid treatment in idiopathic sudden sensorineural hearing loss: a control study," *Otolaryngology and Head and Neck Surgery*, vol. 134, no. 6, pp. 940–945, 2016.

[61] B. J. Balough, "Intratympanic dexamethasone for sudden sensorineural hearing loss after failure of systemic therapy," *Yearbook of Otolaryngology-Head and Neck Surgery*, vol. 2008, pp. 45–47, 2008.

[62] A. Battaglia, R. Burchette, and R. Cueva, "Combination therapy (intratympanic dexamethasone + high-dose prednisone taper) for the treatment of idiopathic sudden sensorineural hearing loss," *Otology & Neurotology*, vol. 29, no. 4, pp. 453–460, 2008.

[63] N. Mata-Castro, J. Gavilanes-Plasencia, R. Ramírez-Camacho, A. García-Fernández, and J. R. García-Berrocal, "Azathioprine reduces the risk of audiometric relapse in immune-mediated hearing loss," *Acta Otorrinolaringológica Española*, 2018.

[64] T. J. Yoo, M. A. Cremer, K. Tomoda, A. S. Townes, J. M. Stuart, and A. H. Kang, "Type II collagen-induced autoimmune sensorineural hearing loss and vestibular dysfunction in rats," *Annals of Otology, Rhinology & Laryngology*, vol. 92, no. 3, pp. 267–271, 1983.

[65] T. Yoo, Y. Yazawa, K. Tomoda, and R. Floyd, "Type II collagen-induced autoimmune endolymphatic hydrops in guinea-pig," *Science*, vol. 222, no. 4619, pp. 65–67, 1983.

[66] P. Berger, M. Hillman, M. Tabak, and M. Vollrath, "The lymphocyte transformation test with type II collagen as a diagnostic tool of autoimmune sensorineural hearing loss," *Laryngoscope*, vol. 101, no. 8, pp. 895–899, 1991.

[67] L. F. Bertoli, D. G. Pappas, J. C. Barton, and J. C. Barton, "Serum immunoglobulins in 28 adults with autoimmune sensorineural hearing loss: increased prevalence of subnormal immunoglobulin G1 and immunoglobulin G3," *BMC Immunology*, vol. 15, no. 1, p. 43, 2014.

[68] T. J. Yoo, K. Tomoda, and A. D. Hernandez, "Type II collagen induced autoimmune inner ear lesions in guinea pigs," *Annals of Otology, Rhinology & Laryngology*, vol. 93, Supplement 5, pp. 3–5, 1984.

[69] P. B. Billings, S. O. Shin, and J. P. Harris, "Assessing the role of anti-hsp70 in cochlear impairment," *Hearing Research*, vol. 126, no. 1-2, pp. 210–212, 1998.

[70] C. Ianuale, G. Cadoni, E. de Feo et al., "A systematic review and meta-analysis of the diagnostic accuracy of anti-heat shock protein 70 antibodies for the detection of autoimmune hearing loss," *Otology & Neurotology*, vol. 34, no. 2, pp. 214–219, 2013.

[71] K. Yeom, J. Gray, T. S. Nair et al., "Antibodies to HSP-70 in normal donors and autoimmune hearing loss patients," *Laryngoscope*, vol. 113, no. 10, pp. 1770–1776, 2003.

[72] S. Charchat, L. Lavinsky, E. Cohen, C. A. Muhlen, and C. Bonorino, "Use of HSP70 for diagnosis and treatment of patients of sensorineural autoimmune hearing loss," *Cell Stress & Chaperones*, vol. 5, no. 4, pp. 384–384, 2000.

[73] C. Bonaguri, J. G. Orsoni, L. Zavota et al., "Anti-68 kDa antibodies in autoimmune sensorineural hearing loss - are these autoantibodies really a diagnostic tool?," *Autoimmunity*, vol. 40, no. 1, pp. 73–78, 2007.

[74] T. J. Yoo, X. Ge, O. Sener et al., "Presence of autoantibodies in the sera of Meniere's disease," *Annals of Otology, Rhinology & Laryngology*, vol. 110, no. 5, pp. 425–429, 2001.

[75] T. J. Yoo, H. Tanaka, S. S. Kwon et al., "β-Tubulin as an autoantigen for autoimmune inner ear disease," *International Congress Series*, vol. 1240, pp. 1207–1210, 2003.

[76] T. J. Yoo, X. Du, and S. S. Kwon, "Molecular mechanism of autoimmune hearing loss," *Acta Oto-Laryngologica*, vol. 122, no. 5, pp. 3–9, 2002.

[77] X. Du, T. Yoo, and R. Mora, "Distribution of beta-tubulin in guinea pig inner ear," *ORL*, vol. 65, no. 1, pp. 7–16, 2003.

[78] Q. Cai, X. du, B. Zhou, C. Cai, M. H. Kermany, and T. Yoo, "Induction of tolerance by oral administration of beta-tubulin in an animal model of autoimmune inner ear disease," *ORL*, vol. 71, no. 3, pp. 135–141, 2009.

[79] N. G. Robertson, L. Lu, S. Heller et al., "Mutations in a novel cochlear gene cause DFNA9, a human nonsyndromic deafness with vestibular dysfunction," *Nature Genetics*, vol. 20, no. 3, pp. 299–303, 1998.

[80] N. G. Robertson, B. L. Resendes, J. S. Lin et al., "Inner ear localization of mRNA and protein products of COCH, mutated in the sensorineural deafness and vestibular disorder, DFNA9," *Human Molecular Genetics*, vol. 10, no. 22, pp. 2493–2500, 2001.

[81] T. Ikezono, A. Omori, S. Ichinose, R. Pawankar, A. Watanabe, and T. Yagi, "Identification of the protein product of the Coch gene (hereditary deafness gene) as the major component of bovine inner ear protein," *Biochimica et Biophysica Acta-Molecular Basis of Disease*, vol. 1535, no. 3, pp. 258–265, 2001.

[82] M. J. Baek, H. M. Park, J. M. Johnson et al., "Increased frequencies of cochlin-specific T cells in patients with autoimmune sensorineural hearing loss," *Journal of Immunology*, vol. 177, no. 6, pp. 4203–4210, 2006.

[83] R. Killick, P. K. Legan, C. Malenczak, and G. P. Richardson, "Molecular cloning of chick beta-tectorin, an extracellular matrix molecule of the inner ear," *Journal of Cell Biology*, vol. 129, no. 2, pp. 535–547, 1995.

[84] P. K. Legan, A. Rau, J. N. Keen, and G. P. Richardson, "The mouse tectorins - modular matrix proteins of the inner ear homologous to components of the sperm-egg adhesion system," *Journal of Biological Chemistry*, vol. 272, no. 13, pp. 8791–8801, 1997.

[85] T. S. Nair, D. M. Prieskorn, J. M. Miller, A. Mori, J. Gray, and T. E. Carey, "In vivo binding and hearing loss after intracochlear infusion of KHRI-3 antibody," *Hearing Research*, vol. 107, no. 1-2, pp. 93–101, 1997.

[86] M. Ptok, T. Nair, T. E. Carey, and R. A. Altschuler, "Distribution of KHRI 3 epitopes in the inner ear," *Hearing Research*, vol. 66, no. 2, pp. 245–252, 1993.

[87] M. Takahashi and J. P. Harris, "Analysis of immunocompetent cells following inner ear immunostimulation," *Laryngoscope*, vol. 98, no. 10, pp. 1133–1138, 1988.

[88] M. Takahashi and J. P. Harris, "Anatomic distribution and localization of immunocompetent cells in normal mouse endolymphatic sac," *Acta Oto-Laryngologica*, vol. 106, no. 5-6, pp. 409–416, 1988.

[89] H. F. Schuknecht, "Inner ear pathology in autoimmune disease," *Progress in Human Auditory and Vestibular Histopathology*, Kugler Publications, 1997.

[90] H. F. Schuknecht, "Ear pathology in autoimmune disease," *Advances in Oto-Rhino-Laryngology*, vol. 46, pp. 50–70, 1991.

[91] H. Kawauchi, N. Kaneda, I. Ichimiya, and G. Mogi, "Distribution of immunocompetent cells in the endolymphatic sac," *The Annals of Otology, Rhinology & Laryngology*, vol. 101, Supplement 10, pp. 39–47, 1992.

[92] H. Cantor, F. W. Shen, and E. A. Boyse, "Separation of helper T-cells from suppressor T-cells expressing different Ly components. II. Activation by antigen: after immunization, antigen-specific suppressor and helper activities are mediated by distinct T-cell subclasses," *Journal of Experimental Medicine*, vol. 143, no. 6, pp. 1391–1340, 1976.

[93] A. M. Bilate and J. J. Lafaille, "Induced $CD4^+Foxp3^+$ regulatory T cells in immune tolerance," *Annual Review of Immunology*, vol. 30, no. 1, pp. 733–758, 2012.

Hindawi
Neural Plasticity
Volume 2018, Article ID 6059697, 7 pages
https://doi.org/10.1155/2018/6059697

Clinical Study

The Characteristic and Short-Term Prognosis of Tinnitus Associated with Sudden Sensorineural Hearing Loss

Xiaoqiong Ding,[1] **Xiaoli Zhang**,[2] **Zhichun Huang**,[1] **and Xu Feng**[1]

[1]*Department of Otolaryngology, Head and Neck Surgery, Zhongda Hospital, Southeast University, No. 87 Dingjiaqiao Road, Nanjing 210009, China*
[2]*Department of Otolaryngology, Head and Neck Surgery, Nanjing Drum Tower Hospital, No. 321 Zhongshan Road, Nanjing 210008, China*

Correspondence should be addressed to Zhichun Huang; huang1963618@sohu.com and Xu Feng; fengxu681111@aliyun.com

Received 24 January 2018; Accepted 18 April 2018; Published 13 May 2018

Academic Editor: Geng-lin Li

Tinnitus is believed to result from the maladaptive plasticity of the auditory nervous system; reports regarding its severity and prognosis are conflicting. We evaluated the characteristic and short-term prognosis of tinnitus associated with sudden sensorineural hearing loss (SSNHL). A total of 230 cases were enrolled. The severity and 1-month prognosis of tinnitus (according to the Tinnitus Handicap Inventory (THI)) were assessed in terms of the patients' sex, age, level of hearing loss, type of audiogram results, and so on. According to our statistical analysis, the degree of handicap due to tinnitus was not related to sex, age, or level of hearing loss; the Tinnitus Handicap Inventory indicated that the low-frequency-audiogram group had a low tinnitus handicap ($F = 7.516$, $P = 0.000$). Furthermore, we found that the prognosis of tinnitus was not related to the type of audiogram or level of hearing loss. Recovery from a severe level of hearing loss was, however, found to be associated with a poor tinnitus prognosis ($F = 5.203$, $P = 0.006$). In summary, our study indicates that the association between tinnitus and SSNHL is extremely high. Tinnitus can be ameliorated by the successful treatment of hearing loss. The study was registered in the Chinese Clinical Trial Registry (ChiCTR1800014797).

1. Introduction

Tinnitus, one of the most frequent sensorineural disorders, involves the perception of a fake sound in the absence of a corresponding sound stimulus; it is often considered as the result of maladaptive plasticity in the auditory system [1, 2]. It is reported that 5% to 10% of the population suffer from tinnitus and that it consequently has a negative impact in their life [3, 4]. On the other hand, sudden sensorineural hearing loss (SSNHL) is also a challenging clinical problem. It is reported that the incidence of SSNHL is as high as 5 to 20 per 100,000 people [5]. However, another research suggests a greater incidence of 160 per 100,000 people [6]. The association between tinnitus and SSNHL is extremely high (66% to 93%) [7, 8]. It has not yet been determined whether tinnitus is triggered only by hearing loss or whether the severity of tinnitus is affected by the level of hearing loss. It is also not clear whether the prognosis of hearing loss is associated with the prognosis of tinnitus. Some reports suggest that the prognosis for recovery from tinnitus does not conform with the recovery of hearing in patients with SSNHL. Others have reported that such a recovery is in fact relevant. The presence of tinnitus often has a highly negative impact on patients' lives, sometimes being considered even worse than the discomfort of hearing loss. Neural plasticity has played an important role in recovery from both the hearing loss and tinnitus. Acute tinnitus has been reported to have a high rate of spontaneous recovery; on the other hand, in some cases acute tinnitus has developed into chronic tinnitus, with an associated severely negative impact on patients' lives.

The purpose of the present research was to estimate the characteristics and prognosis of tinnitus associated with SSNHL and discuss the role of neural plasticity in tinnitus.

2. Materials and Methods

2.1. Ethics Statement. This research was approved by the Zhongda Hospital Southeast University Research Ethics Committee (Nanjing, China). Fully informed written consent for publication of clinical data was taken from each patient or from the guardians of the patients who were below 18 years of age.

2.2. Inclusion and Exclusion Criteria. A retrospective study was applied in patients suffering from tinnitus triggered by unilateral SSNHL who were treated at our hospital between January 2015 and July 2017; those with newly developed tinnitus were enrolled in our study. SSNHL was defined as more than 30 dB HL threshold shift in three contiguous frequencies or more in 72 hours. The cause of hearing loss was unknown; enrolled patients suffering from unilateral SSNHL were treated within 14 days of onset. The hearing loss and tinnitus were assessed before treatment and in the following 30 days.

2.3. Treatment. All patients received hyperbaric oxygen therapy, steroid, lidocaine, and ginaton (extract of *Ginkgo biloba* leaves injection, Dr. Willmar Schwabe Pharmaceuticals) administration. They were treated with hyperbaric oxygen therapy for 60 minutes once daily for 10 days, intravenous hydrocortisone sodium succinate (400 mg/day on days 1–3, 200 mg/day on days 4–6, and 100 mg/day on days 7–10), ginaton (87.5 mg/day for 10 days), and lidocaine (100 mg/day for 10 days). Patients with diabetes or hypertension were treated by intratympanic injection of prednol (20 mg/day for 10 days) instead of intravenous hydrocortisone.

2.4. Tinnitus Assessment. The evaluation of the impact of tinnitus on these patients' lives is very important and can be estimated through several questionnaires, the Tinnitus Handicap Inventory (THI) being one of the validated questionnaires. The THI questionnaire consists of three subscales: emotional (9 items), functional (11 items), and catastrophic (5 items). The yes answer to an item gets 4 scores or sometimes 2 scores, and a no gets a zero score. Scores of the total scale range from 0 to 100, with higher scores representing a greater perceived handicap [9, 10]. The severity of tinnitus as measured by the total score is classified as negligible (0–16), mild (18–36), moderate (38–56), severe (58–76), or catastrophic (78–100) [11]. The THI questionnaire was used to estimate the severity of tinnitus before treatment and in the 30-day period after onset. The prognosis of tinnitus was considered as effective if the THI score was improved more than 10 and noneffective if the THI score was improved no more than 10.

2.5. Classification of Level of Hearing Loss. Pure-tone threshold was measured in the affected and nonaffected ears. Pure-tone average thresholds at 0.5, 1, 2, and 4 kHz were assessed as mean pure-tone threshold. When the hearing thresholds of deep losses were not detected, the threshold was considered as the maximum audiometric intensity. Hearing loss was classified into 5 degrees according to the mean pure-tone threshold: mild (26–40 dB HL), moderate (41–55 dB HL), moderately severe (56–70 dB HL), severe (71–90 dB HL), and profound (>90 dB HL). Pure-tone threshold was measured before treatment and during the 30-day period after onset.

2.6. Classification of Audiogram. The audiogram was classified into 4 types by the method reported in[12]. The audiograms were categorized into (1) type A, low-frequency type, hearing loss in low-tone frequencies (250, 500, and 1000 Hz) was at least 15 dB HL more than the other frequencies; (2) type B, flat type, hearing loss is no more than 15 dB HL between low-tone frequencies (250, 500, and 1000 Hz) and high frequencies (above 2000 Hz); (3) type C, high-frequency type, hearing loss in the high frequencies (above 2000 Hz) at least 15 dB HL more than other frequencies; and (4) type D, total deafness, hearing loss of 81 dB HL or more in all frequencies.

2.7. Hearing Recovery Criteria. The following criteria [12] were used to assess hearing recovery: (1) cure: affected frequencies return to within 10 dB of the unaffected ear or normal; (2) obviously effective recovery: affected frequencies are at threshold recovery greater than 30 dB HL at mean; (3) effective recovery: affected frequencies are at threshold recovery greater than 15 dB HL at mean; and (4) no effective: affected frequencies are at threshold recovery no more than 15 dB HL at mean. For purposes of statistical analysis of the data from this study, patients with obviously effective recovery and effective recovery were grouped in the same group, called the "effective group."

2.8. Statistical Methods. Statistical analyses were performed with SPSS software (IBM Corp., version 22). Tests and graphs were based on analysis sets that included all patients. The severity of tinnitus (THI) in terms of patients' sex, age, audiogram type, and hearing loss level was studied by Ridit analysis. The prognosis of tinnitus in terms of audiogram type, level of hearing loss, prognosis of hearing loss, and the severity of tinnitus (THI) was also studied by the same method.

3. Results

Of a total of 283 unilateral SSNHL patients enrolled within 14 days of the onset of acute hearing loss, 252 (89.0%) reported the new development of tinnitus. Of these 252, a total of 22 patients were lost to follow-up. The mean age of the 230 assessed patients was 43.5 years, with a median of 45 years, standard deviation of 15.1; minimum of 15 years and maximum of 70 years. Of those assessed, 136 patients were men (59.1%) and 94 were women (40.9%). There were 22 cases of negligible tinnitus (9.57%), 96 mild cases (41.74%), 86 moderate cases (37.39%), 22 severe cases (9.57%), and 4 catastrophic cases (1.74%).

Sex, age, initial hearing loss level, and audiogram type were reported to be associated with the severity of tinnitus. The degrees of difference in THI in terms of sex and age were compared by Ridit analysis (Table 1). The patients were divided into 5 age groups: 15 to 30 (53 cases, 23.04%), 31 to 40 (38 cases, 16.52%), 41 to 50 (58 cases, 25.22%), 51 to 60 (47 cases, 20.43%), and 61 to 70 (34 cases, 14.78%).

Table 1: The severity of tinnitus in terms of sex and age.

Classifications	No. of cases	Severity of tinnitus (THI)				
		Negligible	Mild	Moderate	Severe	Catastrophic
Sex						
Male	136	12	50	57	15	2
Female	94	10	46	29	7	2
Age						
15–30	53	10	18	17	8	0
31–40	38	5	15	13	3	2
41–50	58	2	27	22	7	0
51–60	47	2	18	24	2	1
61–70	34	3	18	10	2	1

THI, Tinnitus Handicap Inventory. There was no significant difference between males and females ($P = 0.600$) or between age groups ($P = 0.598$).

Table 2: Severity of tinnitus in patients with hearing loss.

Classifications of hearing loss	No. of cases	Severity of tinnitus (THI)				
		Negligible	Mild	Moderate	Severe	Catastrophic
Hearing loss level						
Mild and moderate	71	9	29	26	7	0
Moderately severe	34	3	18	9	4	0
Severe	59	5	23	25	5	1
Profound	66	5	26	26	6	3
Audiogram type						
Type A, low frequency	28	7	18	2	1	0
Type B, flat	83	9	32	34	8	0
Type C, high frequency	65	3	24	30	7	1
Type D, total deafness	54	3	22	20	6	3

THI, Tinnitus Handicap Inventory. In terms of the degree of THI, there was no significant difference among the levels of hearing loss ($F = 0.704$, $P = 0.550$). However, there was a significant difference between different audiograms ($F = 7.516$, $P = 0.000$). The low-frequency-audiogram group had low THI scores compared with others ($P = 0.000$).

Statistically, there was no significant difference between males and females ($P = 0.600$). There was also no significant difference between age groups ($P = 0.598$).

The THI and audiogram scores at different levels of hearing loss were compared by Ridit analysis (Table 2). In terms of the hearing loss, there were 71 mild and moderate cases (30.87%), 34 moderately severe cases (14.78%), 59 severe cases (25.65%), and 66 profound cases (28.70%). There was no significant difference among different hearing loss levels in terms of the THI score ($F = 0.704$, $P = 0.550$). However, there was a significant difference among different audiograms ($F = 7.516$, $P = 0.000$). The low-frequency-audiogram group had a lower score on the THI compared with others.

Tinnitus prognosis was assessed by the THI score. Of the enrolled patients, there were 182 effective cases (79.13%) and 48 noneffective cases (20.87%). The tinnitus prognosis was compared in terms of audiogram result, hearing loss level, hearing prognosis, and THI score. There was no significant difference in tinnitus prognosis among the different audiogram types ($F = 1.640$, $P = 0.181$) (Table 3). However, there was a significant difference among the different hearing prognoses ($F = 5.203$, $P = 0.006$). Patients of the no effective group had a poor tinnitus prognosis compared to the cure group and effective group (Table 4).

The initial level of hearing loss has frequently been considered a prognostic factor for tinnitus. We used one-way orderly Ridit statistical analysis to determine whether there was a correlation between the initial level of hearing loss and the prognosis of tinnitus. There was no significant difference among different hearing loss levels ($F = 0.170$, $P = 0.917$) (Table 5). However, there was a significant difference between the different degrees of THI ($F = 10.623$, $P = 0.000$). The initial degree of THI was also compared with the final degree of THI. Patients with moderate and severe degrees of THI had better tinnitus prognosis than others (Table 6).

4. Discussion

The generation and maintenance of tinnitus are challenging topics of neural research [4, 13]. The mechanism of tinnitus has been studied, and great progress has been made in recent decades. And till now, it has been found that tinnitus is produced in the brain and not in the ear. A study has recently focused on studying how tinnitus might be generated by

Table 3: Tinnitus prognosis and hearing loss curve.

Audiogram type	Tinnitus prognosis	
	Effective group	Noneffective group
Type A, low frequency	25	3
Type B, flat	68	15
Type C, high frequency	46	19
Type D, total deafness	43	11

There was no significant difference among different audiogram types ($F = 1.640$, $P = 0.181$).

Table 4: The prognosis of tinnitus as related to the prognosis of hearing loss.

Hearing prognosis	Tinnitus prognosis	
	Effective group	Noneffective group
Cure group	41	4
Effective group	68	13
No effective group	73	31

There was a significant difference among the different hearing prognoses ($F = 5.203$, $P = 0.006$). Patients of the no effective group had a poor tinnitus prognosis than the cure group ($P = 0.004$) and effective group ($P = 0.021$).

Table 5: Tinnitus prognosis and level of hearing loss.

Level of hearing loss	Tinnitus prognosis	
	Effective group	Noneffective group
Mild to moderate	57	14
Moderately severe	26	8
Severe	48	11
Profound	51	15

There was no significant difference among the different levels of hearing loss ($F = 0.170$, $P = 0.917$).

plasticity and aberrant processing in the peripheral and central auditory system. Much research has been devoted to elucidating the relationship between tinnitus and hearing loss. Acute tinnitus is triggered by cochlear impairment. The reduction signal transduction from the impaired cochlea is considered to reduce lateral inhibition in the brainstem auditory pathway, such as the dorsal cochlear nucleus or inferior colliculus, finally resulting in the high spontaneous activity of auditory neurons around the impaired frequencies [4, 14].

In most patients, tinnitus is associated with hearing loss [8, 15, 16]. The association between tinnitus and SSNHL is extremely high (66 to 93%) [7, 8]. The relationship between tinnitus and hearing loss has also been proved in animal studies [17–20]. Tinnitus in SSNHL was an extremely frequent symptom as reported in the literature and also in our study: 89.0% (252 of 283). Its impact on patients' quality of life was also highly noticeable. However, hearing loss is not always associated to tinnitus. As reported, 7% to 34% patients suffering from SSNHL did not complain of tinnitus [7, 8]. In our study, 11% (31 of 283) of the patients did not complain of tinnitus accompanying SSNHL. In scrutinizing the connection between tinnitus and hearing loss, many researchers' measurements have been based on combined techniques. A recent study showed that subjects with tinnitus as well as hearing loss had better outer hair cell (OHC) function than subjects without tinnitus [21]. When assessed at a higher probe level, the psychophysical tuning lines of the subjects with tinnitus were consistent with those of subjects with normal hearing, implying that OHC damage in subjects with tinnitus might not be as severe as previously thought. Inner hair cell (IHC) damage or auditory nerve fiber dysfunction may play a more important role in the emergence of tinnitus. Auditory brainstem responses of tinnitus subjects with normal audiograms show a significantly decreased amplitude of the wave I potential but normal amplitudes of the wave V. These phenomena have been found in subjects with tinnitus and normal pure-tone hearing threshold [22, 23].

The severity of tinnitus can be influenced by cochlea damage-induced neuronal plasticity throughout the auditory nervous system from the hair cells to the auditory cortex [24] and also by the patient's psychological condition and educational background [25, 26]. Studies have demonstrated that the severity of tinnitus (THI) is not related to sex, age, degree of hearing loss, or audiogram type [27]. We found that the degree of THI was not related to sex or degree of hearing loss, but we did not identify the patients' psychological condition or educational background. We found that the degree of THI was related to the audiogram type and that the low-frequency-audiogram group had a low degree of THI compared with others. Patients with SSNHL and tinnitus ordinarily match the tinnitus pitch to the impaired frequencies or to the audiogram edge [4, 28]. Tinnitus pitch was focused in low frequencies in low-frequency-audiogram SSNHL; this type of tinnitus could easily be covered by environmental noise. Therefore, it may be that the tinnitus of patients with low-frequency-audiogram SSNHL tends to be of lower severity.

It has been found that tinnitus can be treated effectively by treating the concomitant conductive hearing loss [29–31]. Tinnitus was cured when conductive hearing loss was relieved, in more than half of the subjects, and most of the remaining subjects experienced improvement [29, 30]. Tinnitus was improved in more than 80% of the patients who underwent tympanoplasty [31]. Tinnitus can be ameliorated by the use of an artificial cochlear implant and hearing aid [32, 33]. It can also be reduced by treating sensorineural hearing loss [4, 8, 16, 34–36]. Nogueira-Neto et al. have demonstrated that the smaller the THI gain, the greater the degree of hearing recovery [8]. Another study reported that the degree of tinnitus improvement was consistent with SSNHL improvement [16]. Cure of hearing loss and tinnitus were both about three times more frequent in patients with mild to moderate hearing loss than in those with severe to profound categories. It has been found that the pure-tone threshold and speech discrimination score after SSNHL treatment were significantly improved in the patients with significant tinnitus as compared with those whose tinnitus was less severe [35]. Our research has demonstrated that an improvement in tinnitus is associated with the amelioration

Table 6: Tinnitus prognosis and THI.

Tinnitus prognosis	Cases	Severity of tinnitus (THI)				
		Negligible	Mild	Moderate	Severe	Catastrophic
Effective group	182	11	65	81	22	3
No effective group	48	11	31	5	0	1

THI, Tinnitus Handicap Inventory. There was significant difference among different THI degrees ($F = 10.623$, $P = 0.000$). Mild cases had a better prognosis than negligible cases ($P = 0.048$). Moderate cases had a better tinnitus prognosis than negligible and mild cases ($P = 0.000$). Severe cases had a better prognosis than negligible and mild cases ($P = 0.000$).

or cure of SSNHL. There was a significant correlation between tinnitus improvement and hearing recovery after treatment for SSNHL, whereas there was no relation between the degree of hearing loss and the prognosis of tinnitus. Moreover, there is no correlation between initial audiogram types and tinnitus prognosis. This implies that hearing recovery may be a prognostic factor of accompanying tinnitus in SSNHL; that is, the accompanying tinnitus can be improved by the successful treatment of SSNHL.

Our study found that hearing recovery is consistent with a decrease in tinnitus, although the initial level of hearing loss or audiogram type is not a prognostic factor for tinnitus. A study has also shown earlier effects on hearing recovery than on complete tinnitus remission in patients with severe-profound hearing loss [37]. Hearing loss and tinnitus are caused by damage to or dysfunction of the auditory system [38, 39], and there seems to be a difference between the capacity for recovery of afferent input for hearing and for resolution of the perception of tinnitus. The tinnitus recovery mechanism is different from the mechanism for hearing recovery. Many useful methods have been studied to protect the cochlea from damage [40, 41], and several effective methods have been researched to protect the cochlea in vitro [42–46]. However, there were limited methods to treat tinnitus [47]. Generally, sensorineural hearing loss tends to be stable within 3 months of onset, whereas there can be a spontaneous decrease in tinnitus within 5 years of onset. Tinnitus is the result of maladaptive plasticity within the auditory system [1, 14, 18]; the reversal of such changes in plasticity takes longer than the intrinsic cochlear repair mechanisms and may actually depend to some extent on them.

The results of the present study suggest that the association between tinnitus and SSNHL is extremely high. Tinnitus associated with SSNHL has a negative impact on patients' quality of life. The tinnitus was less severe in the low-frequency-audiogram group compared with other types. Tinnitus can be ameliorated by the treatment of SSNHL. Maladaptive plasticity plays an important role in the mechanism of tinnitus. However, the present research reports the short-term prognosis of tinnitus as associated with SSNHL; the longer-term prognosis requires further analysis to assess the neural plasticity of the cochlea and the brain.

Data Availability

The data used to support the findings of this study are available from the corresponding author upon request.

Disclosure

The funders had no role in the study design, data collection and analysis, decision to publish, or preparation of the manuscript.

Conflicts of Interest

The authors declare that there is no conflict of interest regarding the publication of this paper.

Authors' Contributions

Xiaoqiong Ding, Xu Feng, and Zhichun Huang conceived the study, participated in its design, and drafted the manuscript. Xiaoli Zhang participated in the collection of clinical data and data analysis. All authors read and approved the final manuscript. Xu Feng and Zhichun Huang are listed as co-corresponding authors.

Acknowledgments

These investigations were supported by grants from the Fundamental Research Funds of the Central Universities (2242017K40273) and the Nanjing Medical Science and Technology Development Project (YKK16274) to Xiaoqiong Ding. The authors would like to thank LetPub (http://www.letpub.com) for providing linguistic assistance during the preparation of this manuscript.

References

[1] M. J. Guitton, "Tinnitus: pathology of synaptic plasticity at the cellular and system levels," *Frontiers in Systems Neuroscience*, vol. 6, p. 12, 2012.

[2] H. Bartels, M. J. Staal, and F. W. J. Albers, "Tinnitus and neural plasticity of the brain," *Otology & Neurotology*, vol. 28, no. 2, pp. 178–184, 2007.

[3] J. A. Henry, K. C. Dennis, and M. A. Schechter, "General review of tinnitus: prevalence, mechanisms, effects, and management," *Journal of Speech Language and Hearing Research*, vol. 48, no. 5, pp. 1204–1235, 2005.

[4] R. Schaette, "Tinnitus in men, mice (as well as other rodents), and machines," *Hearing Research*, vol. 311, pp. 63–71, 2014.

[5] F. M. Byl Jr., "Sudden hearing loss: eight years' experience and suggested prognostic table," *The Laryngoscope*, vol. 94, no. 5, pp. 647–661, 1984.

[6] E. Klemm, A. Deutscher, and R. Mosges, "A present investigation of the epidemiology in idiopathic sudden sensorineural

hearing loss," *Laryngo- Rhino- Otologie*, vol. 88, no. 8, pp. 524–527, 2009.

[7] E. A. Bogaz, F. A. B. Suzuki, B. A. A. Rossini, D. P. Inoue, and N. . O. Penido, "Glucocorticoid influence on prognosis of idiopathic sudden sensorineural hearing loss," *Brazilian Journal of Otorhinolaryngology*, vol. 80, no. 3, pp. 213–219, 2014.

[8] F. B. Nogueira-Neto, F. P. Gallardo, F. A. B. Suzuki, and N. O. Penido, "Prognostic and evolutive factors of tinnitus triggered by sudden sensorineural hearing loss," *Otology & Neurotology*, vol. 37, no. 6, pp. 627–633, 2016.

[9] C. W. Newman, G. P. Jacobson, and J. B. Spitzer, "Development of the Tinnitus Handicap Inventory," *Archives of Otolaryngology–Head & Neck Surgery*, vol. 122, no. 2, pp. 143–148, 1996.

[10] C. W. Newman, S. A. Sandridge, and G. P. Jacobson, "Psychometric adequacy of the Tinnitus Handicap Inventory (THI) for evaluating treatment outcome," *Journal of the American Academy of Audiology*, vol. 9, no. 2, pp. 153–160, 1998.

[11] A. Dias, R. Cordeiro, and J. E. Corrente, "Tinnitus annoyance assessed by the Tinnitus Handicap Inventory," *Revista de Saúde Pública*, vol. 40, no. 4, pp. 706–711, 2006.

[12] Chinese Sudden Hearing Loss Multi-Center Clinical Study Group, "Prospective clinical multi-center study on the treatment of sudden deafness with different typings in China," *Zhonghua Er Bi Yan Hou Tou Jing Wai Ke Za Zhi*, vol. 48, no. 5, pp. 355–361, 2013.

[13] D. Ryan and C. A. Bauer, "Neuroscience of tinnitus," *Neuroimaging Clinics of North America*, vol. 26, no. 2, pp. 187–196, 2016.

[14] L. E. Roberts, "Neural plasticity and its initiating conditions in tinnitus," *HNO*, vol. 66, no. 3, pp. 172–178, 2018.

[15] P. Ganesan, P. P. Kothandaraman, S. Swapna, and V. Manchaiah, "A retrospective study of the clinical characteristics and post-treatment hearing outcome in idiopathic sudden sensorineural hearing loss," *Audiology Research*, vol. 7, no. 1, p. 168, 2017.

[16] G. Mühlmeier, D. Baguley, T. Cox, M. Suckfüll, and T. Meyer, "Characteristics and spontaneous recovery of tinnitus related to idiopathic sudden sensorineural hearing loss," *Otology & Neurotology*, vol. 37, no. 6, pp. 634–641, 2016.

[17] J. J. Eggermont, "The auditory cortex and tinnitus—a review of animal and human studies," *European Journal of Neuroscience*, vol. 41, no. 5, pp. 665–676, 2015.

[18] J. J. Eggermont and L. E. Roberts, "Tinnitus: animal models and findings in humans," *Cell and Tissue Research*, vol. 361, no. 1, pp. 311–336, 2015.

[19] T. J. Brozoski and C. A. Bauer, "Animal models of tinnitus," *Hearing Research*, vol. 338, pp. 88–97, 2016.

[20] L. Rüttiger, W. Singer, R. Panford-Walsh et al., "The reduced cochlear output and the failure to adapt the central auditory response causes tinnitus in noise exposed rats," *PLoS One*, vol. 8, no. 3, article e57247, 2013.

[21] C. M. Tan, W. Lecluyse, D. McFerran, and R. Meddis, "Tinnitus and patterns of hearing loss," *Journal of the Association for Research in Otolaryngology*, vol. 14, no. 2, pp. 275–282, 2013.

[22] R. Schaette and D. McAlpine, "Tinnitus with a normal audiogram: physiological evidence for hidden hearing loss and computational model," *Journal of Neuroscience*, vol. 31, no. 38, pp. 13452–13457, 2011.

[23] J. W. Gu, B. S. Herrmann, R. A. Levine, and J. R. Melcher, "Brainstem auditory evoked potentials suggest a role for the ventral cochlear nucleus in tinnitus," *Journal of the Association for Research in Otolaryngology*, vol. 13, no. 6, pp. 819–833, 2012.

[24] J. J. Eggermont and L. E. Roberts, "The neuroscience of tinnitus," *Trends in Neurosciences*, vol. 27, no. 11, pp. 676–682, 2004.

[25] P. J. Jastreboff, "Tinnitus retraining therapy," *Progress in Brain Research*, vol. 166, pp. 415–423, 2007.

[26] E. Ooms, S. Vanheule, R. Meganck, B. Vinck, J. B. Watelet, and I. Dhooge, "Tinnitus severity and its association with cognitive and somatic anxiety: a critical study," *European Archives of Oto-Rhino-Laryngology*, vol. 269, no. 11, pp. 2327–2333, 2012.

[27] P. Chen and J. Zhou, "Related factor analysis of the degree of tinnitus in sudden sensorineural hearing loss patients," *Lin Chung Er Bi Yan Hou Tou Jing Wai Ke Za Zhi*, vol. 27, no. 1, pp. 39–41, 2013.

[28] B. C. J. Moore, Vinay, and Sandhya, "The relationship between tinnitus pitch and the edge frequency of the audiogram in individuals with hearing impairment and tonal tinnitus," *Hearing Research*, vol. 261, no. 1-2, pp. 51–56, 2010.

[29] D. Ayache, F. Earally, and P. Elbaz, "Characteristics and postoperative course of tinnitus in otosclerosis," *Otology & Neurotology*, vol. 24, no. 1, pp. 48–51, 2003.

[30] P. G. Sobrinho, C. A. Oliveira, and A. R. Venosa, "Long-term follow-up of tinnitus in patients with otosclerosis after stapes surgery," *The International Tinnitus Journal*, vol. 10, no. 2, pp. 197–201, 2004.

[31] A. da Silva Lima, T. G. Sanchez, M. F. B. Moraes, S. C. B. Alves, and R. F. Bento, "The effect of timpanoplasty on tinnitus in patients with conductive hearing loss: a six month follow-up," *Brazilian Journal of Otorhinolaryngology*, vol. 73, no. 3, pp. 384–389, 2007.

[32] Á. Ramos Macías, J. C. Falcón González, M. Manrique et al., "Cochlear implants as a treatment option for unilateral hearing loss, severe tinnitus and hyperacusis," *Audiology & Neurotology*, vol. 20, Supplement 1, pp. 60–66, 2015.

[33] E. Peltier, C. Peltier, S. Tahar, E. Alliot-Lugaz, and Y. Cazals, "Long-term tinnitus suppression with linear octave frequency transposition hearing AIDS," *PLoS One*, vol. 7, no. 12, article e51915, 2012.

[34] T. Michiba, T. Kitahara, N. Hikita-Watanabe et al., "Residual tinnitus after the medical treatment of sudden deafness," *Auris Nasus Larynx*, vol. 40, no. 2, pp. 162–166, 2013.

[35] Y. C. Rah, K. T. Park, Y. J. Yi, J. Seok, S. I. Kang, and Y. H. Kim, "Successful treatment of sudden sensorineural hearing loss assures improvement of accompanying tinnitus," *The Laryngoscope*, vol. 125, no. 6, pp. 1433–1437, 2015.

[36] S. Sun, M. Sun, Y. Zhang et al., "In vivo overexpression of X-linked inhibitor of apoptosis protein protects against neomycin-induced hair cell loss in the apical turn of the cochlea during the ototoxic-sensitive period," *Frontiers in Cellular Neuroscience*, vol. 8, p. 248, 2014.

[37] M. Suckfuell, G. Lisowska, W. Domka et al., "Efficacy and safety of AM-111 in the treatment of acute sensorineural hearing loss: a double-blind, randomized, placebo-controlled phase II study," *Otology & Neurotology*, vol. 35, no. 8, pp. 1317–1326, 2014.

[38] Y. Wang, J. Li, X. Yao et al., "Loss of CIB2 causes profound hearing loss and abolishes mechanoelectrical transduction in mice," *Frontiers in Molecular Neuroscience*, vol. 10, p. 401, 2017.

[39] Z. He, L. Guo, Y. Shu et al., "Autophagy protects auditory hair cells against neomycin-induced damage," *Autophagy*, vol. 13, no. 11, pp. 1884–1904, 2017.

[40] X. Lu, S. Sun, J. Qi et al., "Bmi1 regulates the proliferation of cochlear supporting cells via the canonical Wnt signaling pathway," *Molecular Neurobiology*, vol. 54, no. 2, pp. 1326–1339, 2017.

[41] L. Liu, Y. Chen, J. Qi et al., "Wnt activation protects against neomycin-induced hair cell damage in the mouse cochlea," *Cell Death & Disease*, vol. 7, no. 3, article e2136, 2016.

[42] M. Waqas, S. Sun, C. Xuan et al., "Bone morphogenetic protein 4 promotes the survival and preserves the structure of flow-sorted Bhlhb5+ cochlear spiral ganglion neurons *in vitro*," *Scientific Reports*, vol. 7, no. 1, article 3506, 2017.

[43] X. Yu, W. Liu, Z. Fan et al., "c-Myb knockdown increases the neomycin-induced damage to hair-cell-like HEI-OC1 cells in vitro," *Scientific Reports*, vol. 7, article 41094, 2017.

[44] G. Sun, W. Liu, Z. Fan et al., "The three-dimensional culture system with Matrigel and neurotrophic factors preserves the structure and function of spiral ganglion neuron *in vitro*," *Neural Plasticity*, vol. 2016, Article ID 4280407, 15 pages, 2016.

[45] W. Yan, W. Liu, J. Qi et al., "A three-dimensional culture system with Matrigel promotes purified spiral ganglion neuron survival and function in vitro," *Molecular Neurobiology*, vol. 55, no. 3, pp. 2070–2084, 2018.

[46] Z. He, S. Sun, M. Waqas et al., "Reduced TRMU expression increases the sensitivity of hair-cell-like HEI-OC-1 cells to neomycin damage in vitro," *Scientific Reports*, vol. 6, no. 1, article 29621, 2016.

[47] S. K. Makar, G. Mukundan, and G. Gore, "Treatment of tinnitus: a scoping review," *The International Tinnitus Journal*, vol. 21, no. 2, pp. 144–156, 2017.

Hindawi
Neural Plasticity
Volume 2018, Article ID 9506387, 6 pages
https://doi.org/10.1155/2018/9506387

Review Article

Potential Application of Electrical Stimulation in Stem Cell-Based Treatment against Hearing Loss

Mingliang Tang,[1,2,3] **Xiaoqian Yan**,[1,2,3] **Qilin Tang**,[4] **Rongrong Guo**,[1,2,3] **Peng Da**,[5] **and Dan Li**[1,2,3]

[1]*Key Laboratory for Developmental Genes and Human Disease, Ministry of Education, Institute of Life Sciences, Southeast University, Nanjing 210096, China*
[2]*Co-Innovation Center of Neuroregeneration, Nantong University, Nantong 226001, China*
[3]*Joint Research Institute of Southeast University and Monash University, Suzhou 215123, China*
[4]*The First Clinical Medical School, Anhui Medical University, 81 Meishan Road, Hefei 230032, China*
[5]*Department of Otolaryngology-Head and Neck Surgery, Affiliated Hospital of Nantong University, Nantong 226001, China*

Correspondence should be addressed to Mingliang Tang; mingliangtang@seu.edu.cn, Peng Da; jdlydap@ntu.edu.cn, and Dan Li; 230169752@seu.edu.cn

Received 23 January 2018; Revised 23 March 2018; Accepted 8 April 2018; Published 8 May 2018

Academic Editor: Geng-lin Li

Deafness is a common human disease, which is mainly caused by irreversible damage to hair cells and spiral ganglion neurons (SGNs) in the mammalian cochlea. At present, replacement of damaged or missing hair cells and SGNs by stem cell transplantation therapy is an effective treatment. However, the survival rate of stem cell transplantation is low, with uncontrollable differentiation hindering its application. Most researchers have focused on biochemical factors to regulate the growth and differentiation of stem cells, whereas little study has been performed using physical factors. This review intends to illustrate the current problems in stem cell-based treatment against deafness and to introduce electric field stimulation as a physical factor to regulate stem cell behavior and facilitate stem cell therapy to treat hearing loss in the future.

1. Introduction

In recent years, with noise, virus infection, ototoxic drug abuse, environmental pollution, and the development and exacerbation of other adverse factors, incidence rates of deafness and hearing loss have gradually increased among the aging population. According to data from the World Health Organization, hearing loss seriously affects the quality of life among 360 million people worldwide, making it a global health problem that cannot be ignored [1]. In general, accumulation of a variety of physicochemical or pathological factors, such as noise and drugs, could ultimately lead to irreversible damage or loss of human inner ear hair cells and/or spiral neuron cells. Therefore, promoting regeneration of hair cells and spiral neurons in order to repair the structure and function of the cochlea has been considered as the best treatment approach. As mammalian hair cells and spiral neurons are not self-regenerative, regenerating damaged cochlear hair cells and spiral neurons, from differentiation of stem cells or progenitor cells, has attracted major research interest in recent years. It was found that supporting cells are a candidate progenitor to replace hair cells in avian cochlea [2]. Since then, there have been increasing investigations conducted on the regeneration of hair cells and spiral neurons in the mammalian inner ear, with the aim to identify intrinsic molecular mechanisms underlying stem cell transplantation, in order to provide a viable clinical approach to treat hearing loss. Many studies have supported the potentials of hearing loss treatment using stem cell transplantation, beginning with a pioneering study by Ito et al. [3]. Furthermore, numerous laboratories have tried to transplant different types of stem cells into the inner

ear [4–7]. For example, the bone marrow-derived mesenchymal stem cells were successfully transplanted into the mouse cochlea and were further differentiated into fibrocyte-like cells [8].

2. Hair Cell and Spiral Ganglion Neuron (SGN) Regeneration Research

Studies have shown that a type of Lgr5-positive cells in the mouse cochlea has the potential to differentiate into hair cells and is therefore considered as potential cochlear stem cells [9, 10]. Many researchers attempted to study the involvement of Wnt and Notch signaling pathways in promoting the proliferation and differentiation of Lgr5-positive cells for hair cell regeneration. Some researchers have focused on growth factors and proteins of signaling pathways necessary for hair cell regeneration and found that insulin-like growth factor 1 could promote synthesis of DNA in chickens [11]. Li et al. have demonstrated that Notch signaling promoted Lgr5-positive progenitor cells to mitotically generate new hair cells and inhibition of Notch activated the canonical Wnt signaling pathway [12]. Both behavioral and physiological studies have shown that hair cell regeneration is able to restore responsive property and vestibular reflex in the vestibular afferent nerve fibers [11, 13, 14]. With advances in mechanistic research in hair cell regeneration, it is increasingly promising to regenerate hair cells from stem cells in the future.

Noise, brain trauma, and a variety of other diseases can cause damage to cochlear spiral ganglion neurons (SGNs), leading to hearing loss. In the mouse model, acute noise-induced damage to SGNs of peripheral nerve endings resulted in loss of hearing [15]. There is an urgent need to repair SGN damage-induced hearing loss. One new therapy is to induce other types of stem cells to differentiate into neurons to replace the damaged SGNs. In this context, there is also evidence indicating that adult mammalian auditory neurons contain neural precursor cells. Rask-Andersen et al. isolated nestin-positive neural stem cells (NSCs) from adult guinea pig helical ganglia [16]. Although adult mammalian cochlear spiral ganglions have regenerative potential, there have been few observations of their regeneration after injury. In addition, although there are indications that human spiral neurons have a slight regenerative capacity, it has no clinical significance [17]. In recent years, NSC transplantation has become a novel approach in the treatment of neurodegenerative diseases including sensorineural deafness [18]. In the past decade, significant progress has been achieved in stem cell replacement therapy using SGNs to treat hearing loss [19, 20]. With the abovementioned profess, increasing studies have been committed to SGN regeneration using stem cell therapy to treat hearing loss.

However, the inability to control the differentiation of transplanted cells *in vivo* has become a serious problem in the treatment against hearing loss. For example, to selectively regenerate hair cells from the inner ear precursors or spiral neurons from the NSCs is still hard to achieve.

3. Stem Cell Transplantation for the Treatment of Hearing Loss

Stem cells, such as adult and embryonic stem cells, are a group of cells with the potential of self-renewal and differentiation [21]. Stem cells have been employed in various fields including tissue engineering [22], regenerative medicine [23], cancer research [24], and various neurological diseases [25]. In particular, Chai et al. have discovered a type of Lgr5-positive cells in the mouse cochlea [9, 10], which could be derived into hair cells and is therefore considered as cochlear stem cells.

Meanwhile, NSCs have been widely used in the treatment of neurodegenerative diseases. It is still challenging to promote the regeneration of neurons from NSCs as well as the functional maturation of newly formed neurons. A stem cell-based approach has been proposed to replace degenerated spiral neurons [26]. Investigations have suggested that differentiation of NSCs into spiral neurons is a viable approach for repairing spiral neuronal damage in the inner ear. NSCs have been reported to have the ability to self-renew and are able to differentiate into neurons, astrocytes, oligodendrocytes, and other major neural tissues. NSCs may differentiate into functional auditory neurons [27]. Due to the self-renewal, pluripotency, migration, good histocompatibility, and low immunogenicity of NSCs, they can be used as excellent seed cells to replace lost spiral neurons to promote their regeneration. For example, studies have demonstrated that adult human mesenchymal-like stem cells isolated from nasal tissues could be employed to restore lost SGCs in cochlear explant culture isolated from neonatal rats following challenge [28].

4. Electric Field (EF) Stimulation Can Regulate Stem Cell Behavior

There is a complex in vivo interaction between stem cells and their surrounding environment, called the niche, which involves biochemical factors, extracellular matrix components, physical factors, and cell-cell interactions [29]. Stem cell niche determines the fate of stem cells; therefore, when the stem cells are studied in vitro, spatial structure of the niche changes, resulting in new obstacles in research. Finding the right factors to regulate the fate of stem cells will greatly improve the development of stem cell therapy. In this context, electric field (EF) stimulation is a common strategy of using physical stimulation to regulate cell behavior both *in vivo* and *in vitro*.

EF stimulation is one of the important guidance cues regulating signaling pathways to induce cellular events such as proliferation and migration in pathological and physiological processes, such as tissue regeneration, embryonic development, and wound healing [11, 30–33]. To date, research on the regulation of cell microenvironment by EF stimulation has mainly focused on using EF to excite receptors and ion channels on the cell membrane to drive depolarization, hyperpolarization, proliferation, migration, and differentiation [34, 35].

Over the past few decades, researches have shifted from using endogenous EFs to promote wound healing to using artificial EF stimulation to excite nerves to induce muscle contraction [36]. Endogenous EFs are known to influence cell migration in vivo. For instance, physiological levels of electrical stimulation applied on OPCs isolated from neonatal Sprague-Dawley rats could affect the in vitro migration of OPCs via β1 integrin [37]. However, the cathodal or anodal electrotaxis is cell-type dependent and most of the cell types are recruited to the cathodal pole of the EF [38–43]. It was reported that neural stem/progenitor cells under physiological EF strength migrated towards the cathode at an increased rate [44]. EF stimulation not only has a significant effect on the migration of stem cells but also has an irreversible effect on their differentiation. A recent study has shown that integrating the conducting carbon nanofibrous scaffold with electrical stimulation enhances NSC functions [45]. These findings indicate that electrical stimulation is indeed an effective physical method to regulate physiological cellular behavior. In a natural situation, the occurrence of an endogenous EF (10–1800 mV/mm) is a prerequisite for normal neuron development in frogs and chick embryos [46]. Direct EFs play a crucial role throughout the development of the nervous system [31, 46]. EFs have profound effects on nerve growth, guidance, and branching during neural construction, where an EF as low as 10 mV/mm was able to frequently turn the growth cones towards the cathode [46]. In the same study, EF was also demonstrated to play a critical role under pathological conditions, where EFs were observed in damaged axons to regenerate axons [46]. In addition, small EFs applied on animal models of spinal cord injury resulted in functional improvements in these central nervous system injury models [47]. Electrical stimulation was also reported to promote NSC differentiation towards nerve regeneration to improve neural circuit reconstruction [48–50].

5. Perspectives

Cochlear implant has become one of the most successful functional artificial organs in modern medicine. It is an electronic device that restores or obtains hearing in individuals with severe hearing loss and even complete deafness. The device converts sound waves into electric signals that directly stimulate spiral nerve cells and auditory nerve fibers, independent of hair cells. With continuous research efforts, cochlear implants have been widely used clinically to treat hearing loss. As the only medical device capable of restoring hearing and speech abilities among deaf patients, cochlear implant has been widely applied since its FDA approval in the mid-1980s. By 2015, over 300,000 patients worldwide have received cochlear implants, with this figure increasing at the rate of tens of thousands every year [51]. In 1995, China introduced multiguided cochlear implant technology, which has been popularized throughout the country and benefited over 100,000 patients.

As mentioned above, stem cell-based therapy has exhibited promising potential for hearing loss treatment. However, it is still a big challenge to construct a more physiologically relevant microenvironment to facilitate basic research and clinical application using different types of materials. The cellular microenvironment directly affects the growth trend of cells and even determines their fates; therefore, constructing a suitable microenvironment for cell growth is crucial for the successful transplantation of stem cells. Stem cells often exhibit different characteristics when they are transplanted into recipients and the traditional culture systems are two dimensional, using multiwell plates, coverslips, and petri dishes [52, 53]. Due to the lack of tissue-specific architecture, mechanical and biochemical cues, and cellular communication in artificial environment, although these traditional two-dimensional cell culture systems are valuable for basic research [54], they are unsuitable for clinical studies demanding a large number of cells for transplantation and regeneration [55]. Therefore, it is crucial to build a three-dimensional (3D) stem cell culture system that mimics the in vivo stem cell microenvironment. 3D culture systems not only preserve the native extracellular matrix structure but also more accurately represent the physiological microenvironment [56]. Due to these excellent features, 3D systems have been widely used in stem cell culturing. Currently, there are two major types of 3D scaffold materials: natural and artificial. Graphene has unique physicochemical properties, such as high specific surface area, high charge mobility, and good mechanical strength, and therefore has been widely used in drug transport [57], stem cell engineering [58], and oncology. For example, human mesenchymal-like stem cells grown on 3D graphene foam scaffold exhibited enhanced differentiation into osteogenic lineages [59]. As an excellent conductive material, graphene has been used as a good neural interface material, which significantly promoted the differentiation of NSCs into neurons [58]. Nevertheless, there are still some limitations to the use of these scaffolds. With the addition of EF stimulation to regulate cell proliferation, differentiation, and migration, combined cochlear and stem cell transplantation may become a new strategy for the treatment against hearing loss.

6. Challenge

It has been reported that electrical stimulation can regulate the differentiation of stem cells, in which special biological materials play an important role [60]. These discoveries have opened a new opportunity for the combined treatment against hearing loss using cochlear implant and stem cells. However, there are still many problems that need to be solved to better implement the treatment against hearing loss with stem cell transplantation and cochlear implant. For example, the strength of electrical stimulation has a crucial effect on the behavior of stem cells. Different intensities of EF stimulation induce differentiation of stem cells into neurons and neuron maturation to different extents [61]. On the other hand, the complex interactions between the substrate materials and the growing cells also influence the behavior of the cultured stem cells. Finding suitable materials, which are biocompatible and conductive, could greatly facilitate stem cell transplantation, meanwhile incorporating electrical stimulation as a regulatory factor. For example, graphene, a new nanomaterial with specific physicochemical properties, has

been reported to be a suitable stem cell scaffold that could deliver electrical stimulation and significantly promote NSC differentiation into neurons [58]. Furthermore, specific molecular events underlying the EF regulation on stem cell behavior are still largely unknown. Further studies are warranted to advance the understanding and treatment on hearing loss using stem cell therapy.

7. Conclusion

Stem cell transplantation technology has greatly benefited deaf patients. On the other hand, there is an urgent need for new physical methods other than biochemistry to solve potential problems in stem cell transplant therapy. EF stimulation is a common strategy of using physical stimulation to regulate cell behavior both *in vivo* and *in vitro*. Prominent research progress has been achieved using electrical stimulation to regulate stem cell behavior. It would be revolutionary to combine electrical stimulation and stem cell transplantation with other biomaterials in the future to improve the treatment of deafness.

Conflicts of Interest

The authors declare no conflicts of interest.

Acknowledgments

This work was supported by grants from the Major State Basic Research Development Program of China (973 Program) (2015CB965000, 2017YFA0104303), the National Natural Science Foundation of China (no. 31571530), the Natural Science Foundation of Jiangsu Province (BK20151404), and the Fundamental Research Funds for the Central Universities (2242017K41042).

References

[1] G. O'Donoghue, "Cochlear implants — science, serendipity, and success," *New England Journal of Medicine*, vol. 369, no. 13, pp. 1190–1193, 2013.

[2] J. T. Corwin and D. A. Cotanche, "Regeneration of sensory hair cells after acoustic trauma," *Science*, vol. 240, no. 4860, pp. 1772–1774, 1988.

[3] J. Ito, K. Kojima, and S. Kawaguchi, "Survival of neural stem cells in the cochlea," *Acta Oto-Laryngologica*, vol. 121, no. 2, pp. 140–142, 2001.

[4] Z. Han, J. M. Yang, F. L. Chi et al., "Survival and fate of transplanted embryonic neural stem cells by Atoh1 gene transfer in guinea pigs cochlea," *Neuroreport*, vol. 21, no. 7, pp. 490–496, 2010.

[5] M. S. Hildebrand, H.-H. M. Dahl, J. Hardman, B. Coleman, R. K. Shepherd, and M. G. de Silva, "Survival of partially differentiated mouse embryonic stem cells in the scala media of the guinea pig cochlea," *Journal of the Association for Research in Otolaryngology*, vol. 6, no. 4, pp. 341–354, 2005.

[6] M. A. Parker, D. A. Corliss, B. Gray et al., "Neural stem cells injected into the sound-damaged cochlea migrate throughout the cochlea and express markers of hair cells, supporting cells, and spiral ganglion cells," *Hearing Research*, vol. 232, no. 1-2, pp. 29–43, 2007.

[7] I. Tateya, T. Nakagawa, F. Iguchi et al., "Fate of neural stem cells grafted into injured inner ears of mice," *Neuroreport*, vol. 14, no. 13, pp. 1677–1681, 2003.

[8] H. Kasagi, T. Kuhara, H. Okada, N. Sueyoshi, and H. Kurihara, "Mesenchymal stem cell transplantation to the mouse cochlea as a treatment for childhood sensorineural hearing loss," *International Journal of Pediatric Otorhinolaryngology*, vol. 77, no. 6, pp. 936–942, 2013.

[9] F. Shi, J. S. Kempfle, and A. S. B. Edge, "Wnt-responsive Lgr5-expressing stem cells are hair cell progenitors in the cochlea," *Journal of Neuroscience*, vol. 32, no. 28, pp. 9639–9648, 2012.

[10] R. Chai, B. Kuo, T. Wang et al., "Wnt signaling induces proliferation of sensory precursors in the postnatal mouse cochlea," *Proceedings of the National Academy of Sciences of the United States of America*, vol. 109, no. 21, pp. 8167–8172, 2012.

[11] J. P. Carey, A. F. Fuchs, and E. W. Rubel, "Hair cell regeneration and recovery of the vestibuloocular reflex in the avian vestibular system," *Journal of Neurophysiology*, vol. 76, no. 5, pp. 3301–3312, 1996.

[12] W. Li, J. Wu, J. Yang et al., "Notch inhibition induces mitotically generated hair cells in mammalian cochleae via activating the Wnt pathway," *Proceedings of the National Academy of Sciences of the United States of America*, vol. 112, no. 1, pp. 166–171, 2015.

[13] C. T. Goode, J. P. Carey, A. F. Fuchs, and E. W. Rubel, "Recovery of the vestibulocolic reflex after aminoglycoside ototoxicity in domestic chickens," *Journal of Neurophysiology*, vol. 81, no. 3, pp. 1025–1035, 1999.

[14] R. Boyle, S. M. Highstein, J. P. Carey, and J. Xu, "Functional recovery of anterior semicircular canal afferents following hair cell regeneration in birds," *JARO - Journal of the Association for Research in Otolaryngology*, vol. 3, no. 2, pp. 149–166, 2002.

[15] S. G. Kujawa and M. C. Liberman, "Adding insult to injury: cochlear nerve degeneration after "temporary" noise-induced hearing loss," *Journal of Neuroscience*, vol. 29, no. 45, pp. 14077–14085, 2009.

[16] H. Rask-Andersen, M. Boström, B. Gerdin et al., "Regeneration of human auditory nerve. In vitro/in video demonstration of neural progenitor cells in adult human and guinea pig spiral ganglion," *Hearing Research*, vol. 203, no. 1-2, pp. 180–191, 2005.

[17] J. B. Nadol Jr, "Patterns of neural degeneration in the human cochlea and auditory nerve: implications for cochlear implantation," *Otolaryngology - Head and Neck Surgery*, vol. 117, no. 3, pp. 220–228, 1997.

[18] C. A. Steiner and J. L. Miller, "Sickle cell disease patients in U.S. hospitals, 2004: statistical brief #21," in *Healthcare Cost and Utilization Project (HCUP) Statistical Briefs*, Agency for Healthcare Research and Quality (US), Rockville (MD), 2006.

[19] M. N. Rivolta, "Developing a stem cell-based therapy for the treatment of hearing loss," *Hearing, Balance and Communication*, vol. 13, no. 4, pp. 148–152, 2015.

[20] F. Shi and A. S. B. Edge, "Prospects for replacement of auditory neurons by stem cells," *Hearing Research*, vol. 297, pp. 106–112, 2013.

[21] L. G. Lajtha, "Stem cell concepts," *Differentiation*, vol. 14, no. 1-3, pp. 23–33, 1979.

[22] P. Bianco and P. G. Robey, "Stem cells in tissue engineering," *Nature*, vol. 414, no. 6859, pp. 118–121, 2001.

[23] J. Ringe, C. Kaps, G.-R. Burmester, and M. Sittinger, "Stem cells for regenerative medicine: advances in the engineering of tissues and organs," *Naturwissenschaften*, vol. 89, no. 8, pp. 338–351, 2002.

[24] H. Clevers, "The cancer stem cell: premises, promises and challenges," *Nature Medicine*, vol. 17, no. 3, pp. 313–319, 2011.

[25] O. Lindvall, Z. Kokaia, and A. Martinez-Serrano, "Stem cell therapy for human neurodegenerative disorders–how to make it work," *Nature Medicine*, vol. 10, no. 7, pp. S42–S50, 2004.

[26] Z. Hu and M. Ulfendahl, "Cell replacement therapy in the inner ear," *Stem Cells and Development*, vol. 15, no. 3, pp. 449–459, 2006.

[27] D. L. Clarke, C. B. Johansson, J. Wilbertz et al., "Generalized potential of adult neural stem cells," *Science*, vol. 288, no. 5471, pp. 1660–1663, 2000.

[28] E. Bas, T. R. Van De Water, V. Lumbreras et al., "Adult human nasal mesenchymal-like stem cells restore cochlear spiral ganglion neurons after experimental lesion," *Stem Cells and Development*, vol. 23, no. 5, pp. 502–514, 2014.

[29] S. Allazetta and M. P. Lutolf, "Stem cell niche engineering through droplet microfluidics," *Current Opinion in Biotechnology*, vol. 35, pp. 86–93, 2015.

[30] R. Nuccitelli, "A role for endogenous electric fields in wound healing," *Current Topics In Developmental Biology*, vol. 58, pp. 1–26, 2003.

[31] R. Nuccitelli, "Endogenous electric fields in embryos during development, regeneration and wound healing," *Radiation Protection Dosimetry*, vol. 106, no. 4, pp. 375–383, 2003.

[32] M. C. Creed, C. Hamani, A. Bridgman, P. J. Fletcher, and J. N. Nobrega, "Contribution of decreased serotonin release to the antidyskinetic effects of deep brain stimulation in a rodent model of tardive dyskinesia: comparison of the subthalamic and entopeduncular nuclei," *Journal of Neuroscience*, vol. 32, no. 28, pp. 9574–9581, 2012.

[33] A. Jahanshahi, L. M. Schönfeld, E. Lemmens, S. Hendrix, and Y. Temel, "In vitro and in vivo neuronal electrotaxis: a potential mechanism for restoration?," *Molecular Neurobiology*, vol. 49, no. 2, pp. 1005–1016, 2014.

[34] R. Babona-Pilipos, I. A. Droujinine, M. R. Popovic, and C. M. Morshead, "Adult subependymal neural precursors, but not differentiated cells, undergo rapid cathodal migration in the presence of direct current electric fields," *PLoS One*, vol. 6, no. 8, article e23808, 2011.

[35] M. J. Sato, H. Kuwayama, W. N. van Egmond et al., "Switching direction in electric-signal-induced cell migration by cyclic guanosine monophosphate and phosphatidylinositol signaling," *Proceedings of the National Academy of Sciences of the United States of America*, vol. 106, no. 16, pp. 6667–6672, 2009.

[36] M. Zhao, "Electrical fields in wound healing—an overriding signal that directs cell migration," *Seminars in Cell & Developmental Biology*, vol. 20, no. 6, pp. 674–682, 2009.

[37] B. Zhu, M. Nicholls, Y. Gu et al., "Electric signals regulate the directional migration of oligodendrocyte progenitor cells (OPCs) via β1 integrin," *International Journal of Molecular Sciences*, vol. 17, no. 11, article 1948, 2016.

[38] J. F. Feng, J. Liu, X. Z. Zhang et al., "Guided migration of neural stem cells derived from human embryonic stem cells by an electric field," *Stem Cells*, vol. 30, no. 2, pp. 349–355, 2012.

[39] F. Lin, F. Baldessari, C. C. Gyenge et al., "Lymphocyte electrotaxis in vitro and in vivo," *The Journal of Immunology*, vol. 181, no. 4, pp. 2465–2471, 2008.

[40] X. T. Meng, M. Arocena, J. Penninger, F. H. Gage, M. Zhao, and B. Song, "PI3K mediated electrotaxis of embryonic and adult neural progenitor cells in the presence of growth factors," *Experimental Neurology*, vol. 227, no. 1, pp. 210–217, 2011.

[41] R. Nuccitelli and C. A. Erickson, "Embryonic cell motility can be guided by physiological electric fields," *Experimental Cell Research*, vol. 147, no. 1, pp. 195–201, 1983.

[42] R. F. Stump and K. R. Robinson, "Xenopus neural crest cell migration in an applied electrical field," *The Journal of Cell Biology*, vol. 97, no. 4, pp. 1226–1233, 1983.

[43] M. Zhao, B. Song, J. Pu et al., "Electrical signals control wound healing through phosphatidylinositol-3-OH kinase-γ and PTEN," *Nature*, vol. 442, no. 7101, pp. 457–460, 2006.

[44] L. Li, Y. H. El-Hayek, B. Liu et al., "Direct-current electrical field guides neuronal stem/progenitor cell migration," *Stem Cells*, vol. 26, no. 8, pp. 2193–2200, 2008.

[45] W. Zhu, T. Ye, S. J. Lee et al., "Enhanced neural stem cell functions in conductive annealed carbon nanofibrous scaffolds with electrical stimulation," *Nanomedicine: Nanotechnology, Biology and Medicine*, 2017.

[46] C. D. McCaig, A. M. Rajnicek, B. Song, and M. Zhao, "Controlling cell behavior electrically: current views and future potential," *Physiological Reviews*, vol. 85, no. 3, pp. 943–978, 2005.

[47] R. B. Borgens, "Stimulation of neuronal regeneration and development by steady electrical fields," *Advances in Neurology*, vol. 47, pp. 547–564, 1988.

[48] C. H. Park, H. F. Rios, Q. M. Jin et al., "Tissue engineering bone-ligament complexes using fiber-guiding scaffolds," *Biomaterials*, vol. 33, no. 1, pp. 137–145, 2012.

[49] H. Wake, P. R. Lee, and R. D. Fields, "Control of local protein synthesis and initial events in myelination by action potentials," *Science*, vol. 333, no. 6049, pp. 1647–1651, 2011.

[50] T. Ishibashi, K. A. Dakin, B. Stevens et al., "Astrocytes promote myelination in response to electrical impulses," *Neuron*, vol. 49, no. 6, pp. 823–832, 2006.

[51] F. G. Zeng, S. J. Rebscher, Q. J. Fu et al., "Development and evaluation of the nurotron 26-electrode cochlear implant system," *Hearing Research*, vol. 322, pp. 188–199, 2015.

[52] T. Hodgkinson, X.-F. Yuan, and A. Bayat, "Adult stem cells in tissue engineering," *Expert Review of Medical Devices*, vol. 6, no. 6, pp. 621–640, 2009.

[53] I. K. Ko, S. J. Lee, A. Atala, and J. J. Yoo, "*In situ* tissue regeneration through host stem cell recruitment," *Experimental & Molecular Medicine*, vol. 45, no. 11, p. e57, 2013.

[54] J. Lee, M. J. Cuddihy, and N. A. Kotov, "Three-dimensional cell culture matrices: state of the art," *Tissue Engineering Part B: Reviews*, vol. 14, no. 1, pp. 61–86, 2008.

[55] A. Birgersdotter, R. Sandberg, and I. Ernberg, "Gene expression perturbation in vitro—a growing case for three-dimensional (3D) culture systems," *Seminars in Cancer Biology*, vol. 15, no. 5, pp. 405–412, 2005.

[56] H. Baharvand, S. M. Hashemi, S. Kazemi Ashtiani, and A. Farrokhi, "Differentiation of human embryonic stem cells into hepatocytes in 2D and 3D culture systems *in vitro*," *The International Journal of Developmental Biology*, vol. 50, no. 7, pp. 645–652, 2006.

[57] K. Yang, S. Zhang, G. Zhang, X. Sun, S. T. Lee, and Z. Liu, "Graphene in mice: ultrahigh in vivo tumor uptake and efficient photothermal therapy," *Nano Letters*, vol. 10, no. 9, pp. 3318–3323, 2010.

[58] S. Y. Park, J. Park, S. H. Sim et al., "Enhanced differentiation of human neural stem cells into neurons on graphene," *Advanced Materials*, vol. 23, no. 36, pp. H263–H267, 2011.

[59] S. W. Crowder, D. Prasai, R. Rath et al., "Three-dimensional graphene foams promote osteogenic differentiation of human mesenchymal stem cells," *Nanoscale*, vol. 5, no. 10, pp. 4171–4176, 2013.

[60] R. Guo, S. Zhang, M. Xiao et al., "Accelerating bioelectric functional development of neural stem cells by graphene coupling: implications for neural interfacing with conductive materials," *Biomaterials*, vol. 106, pp. 193–204, 2016.

[61] Z. Y. Dong, Z. Pei, Z. Li, Y. L. Wang, A. Khan, and X. T. Meng, "Electric field stimulation induced neuronal differentiation of filum terminale derived neural progenitor cells," *Neuroscience Letters*, vol. 651, pp. 109–115, 2017.

Hindawi
Neural Plasticity
Volume 2018, Article ID 8169847, 9 pages
https://doi.org/10.1155/2018/8169847

Research Article

Functional Change in the Caudal Pontine Reticular Nucleus Induced by Age-Related Hearing Loss

Ning Zhao,[1,2] Ana'am Alkharabsheh,[2] Fei Xu,[2,3] and Wei Sun[1,2]

[1]*Department of Otolaryngology–Head and Neck Surgery, The First Affiliated Hospital of China Medical University, Shenyang 110001, China*
[2]*Center for Hearing & Deafness, Department of Communicative Disorders and Science, State University of New York at Buffalo, 3435 Main Street, Buffalo, NY 14214, USA*
[3]*Department of Hearing and Speech Sciences, Zhejiang Chinese Medical University, Hangzhou 310053, China*

Correspondence should be addressed to Wei Sun; weisun@buffalo.edu

Received 28 November 2017; Revised 22 February 2018; Accepted 27 March 2018; Published 26 April 2018

Academic Editor: Renjie Chai

Increased acoustic startle responses (ASR), which represent reduced uncomfortable loudness level in humans, have been reported in middle-aged C57BL/6J mice with sensorineural hearing loss. Although neural plasticity changes in the central auditory system after the peripheral lesions were suggested to underlie this phenomenon, the neurological cause of exaggerated ASR is still not clear. In this study, the local field potentials and firing rates of the caudal pontine reticular nucleus (PnC), which plays a major role in the ASR pathway, were recorded in 2-month- and 6-month-old C57BL/6 J mice. Consistent with our previous studies, the amplitude of ASR increased, and the threshold of ASR decreased in the 6-month-old mice after developing 20–40 dB hearing loss. The PnC response induced by high-frequency stimuli (>20 kHz) decreased in the 6-month group, whereas the PnC response induced by low-frequency stimuli (<12 kHz) showed a significant increase in the 6-month group compared to the 2-month group. The enhancement of PnC response is similar to the ASR increase found in the 6-month-old C57 mice. Our results suggest that the high-frequency hearing loss caused an increase in PnC sensitivity in the C57 mice which may enhance ASRs.

1. Introduction

Age-related hearing loss, one of the most common disorders in the elderly, is predominately associated with sensory receptor cell degeneration. Approximately one in three people in the United States between the ages of 65 and 74 has hearing loss [1]. Age-related hearing loss not only affects the hearing sensitivity but also impairs the central auditory processing the speech signals [2, 3]. Tinnitus and hyperacusis are also commonly found in elderly population which may be due to the progressive increase of age-related hearing loss [4].

Increased acoustic startle responses (ASR) were recorded in animal models of tinnitus induced by high doses of salicylate [5] and noise exposure [6]. ASR is a largely unconscious defensive response to sudden or threatening stimuli recorded in both animals and humans [7, 8]. Recent studies found that ASR amplitude at a given stimulus level increases with decreasing loudness discomfort level (LDL) in human [9]. Therefore, ASR amplitudes may provide an objective indication of LDL, a common audiological evaluation for tinnitus and hyperacusis patients [10].

Enhanced ASRs were reported in C57 mice after they developed moderate high-frequency hearing loss [11, 12]. The loudness augmentation was suggested to be induced by plasticity changes in the central auditory system, for example, possibly by a deficit in centrifugal inhibitory control over the afferent reflex pathways after central neural reorganization [11]. These data suggest that the C57 mouse model may be useful in studying hyperacusis and tinnitus associated with age-related hearing loss. The "startle circuit," which provides an inhibitory pathway to modulate the ASR amplitude, consists of the auditory nerve, cochlear root neurons, caudal pontine reticular nucleus (PnC), motor neurons in the spinal cord, and the central auditory system, including the inferior colliculus (IC) and auditory cortex (AC) [13, 14]. Our recent study measured neurophysiological changes in the IC of 2-,

6-, and 12-month-old C57 mice and detected increase in sound-evoked activity of the IC in 6-month-old mice. Our data suggested that the hyperexcitability in the IC may be related with enhanced ASR amplitudes. However, the functional changes in PnC neurons, a critical nucleus that controls the amplitude and threshold of ASR, in the C57 mouse model have not been reported. In this study, we recorded local field potentials and firing rates of the PnC in young and aged C57 mice to reveal the physiological source of the enhanced ASR.

2. Materials and Methods

2.1. Animals. C57BL/6J mice from Jackson Laboratory (Bar Harbor, ME) were used in this study. Six 2-month-old mice (G-2M group) and six 6-month-old mice (G-6M group) were used for ASR and auditory brainstem-evoked response (ABR) test. Twelve mice (six 2-month-old and six 6-month-old mice) were used for extracellular recordings of PnC neurons.

All protocols were approved by the University at Buffalo Institutional Animal Care and Use Committee (IACUC) and conformed to the guidelines issued by the National Institutes of Health.

2.2. ABR Recording. ABRs were recorded in 2-month- and 6-month-old mice in a soundproof room to evaluate their hearing thresholds (Sun et al.). The mice were anesthetized with a mixture of ketamine (100 mg/kg) and xylazine (10 mg/kg), and ABRs were recorded with stainless steel electrodes. TDT System-3 hardware and software (BioSig, Tucker-Davis Technology, FL, USA) were used for ABR recording. For the differential amplifier input, the vertex was used as noninverting (+), the pinna on the stimulating side was used as inverting (−), and the pinna on the contralateral side was used as the ground. Tone bursts at 4, 8, 16, 24, 32, and 48 kHz (5 ms duration, 0.1 ms rise/fall time) were used to elicit the ABR responses. ABR thresholds were obtained for each animal using a step of 5–10 dB SPL to identify the lowest intensity that elicited a response.

2.3. ASR Recordings. TDT hardware and custom software were used for recording ASR [5, 15]. Briefly, animals were placed in a small, wire mesh cage mounted on a plexiglass base that rested on a sensitive piezoelectric transducer. The wire mesh (0.5 cm × 0.5 cm) cage (4 cm W × 3.5 cm H × 7-8 cm L) restricted the mouse's movement within a calibrated sound field. The output of the piezo transducer was connected to an A/D converter on an RP2 real-time processor (TDT). The ASR was amplified and filtered (0–1000 Hz) using a low-pass filter (LPF-300, World Precision Instruments, Sarasota, FL, USA). The root mean square (RMS) of ASR was calculated using the custom software. Sound stimuli were presented by a loud speaker (FT28D, Madisound Speaker Components Inc., Middleton, WI, USA) located approximately 28 cm above the mouse's head. The ASR-eliciting stimuli consisted of narrowband noise bursts centered at 8, 12, and 20 kHz (bandwidth 2 kHz, 20 ms) presented at intensities from 60 to 100 dB SPL (10 trials on each condition). The intertrial interval (ISI) was randomly varied from 18 to 23 seconds.

2.4. PnC Recordings and Labeling. The PnC neurons were recorded from the mice anesthetized with a mixture of ketamine (100 mg/kg) and xylazine (10 mg/kg, i.p.). The surgical procedure for recording from the PnC was similar to that of the IC recording which has been described in our recent publication [15]. Briefly, the skin over the parietal bone was carefully removed to expose the skull and then treated with 3% hydrogen peroxide (H_2O_2). A head-fixing pole attached to the skull was used to firmly hold the mouse's head during the surgery. A 4 × 4 mm region of the cranial bone overlying the dorsocaudal region of the cerebellum was removed to expose the left IC.

A 16-channel microelectrode (NeuroNexus, A1 × 16-5 mm-100e177, Ann Arbor, MI), mounted on a hydraulic manipulator (FHC Inc., Bowdoinham, ME), was inserted into the lateral side of IC towards the PnC. A broadband noise burst (80–90 dB SPL) was used as a search sound to monitor neural responses. First, we found IC responses emerging from the surface to 2.5 mm depth of the brain and then completely disappearing after 3.5 mm. PnC response reemerged at approximately 4-5 mm depth from the surface. Typically, 3–5 penetrations were used to search for PnC responses in each mouse, starting from the lateral side and moving medially while avoiding major blood vessels. The output of the electrode was connected to a 16-channel preamplifier (RA16PA, TDT), and the preamplifier was connected to a digital signal processing module (RZ5, TDT) connected to a computer. A stainless steel electrode inserted into the neck muscle was used as the ground.

Sound stimuli were generated with the TDT System-3 hardware and presented through a multifield magnetic speaker (MF1, TDT). The rate-level function (RLF), excitatory frequency response area (eFRA) of the firing spikes, and the local field potential (LFP) of the PnC neurons were recorded. Noise bursts (0–100 dB SPL) were used to record the RLF. Tone bursts (0–90 dB SPL, 4 to 42 kHz in 20 logarithmically spaced steps) were used to record eFRA at two different interstimulation intervals (ISI) at 1 and 5 seconds. The sound intensity was calibrated using a sound level meter (824, Larson Davis, Depew, NY) with a 1/4-inch condenser microphone (Larson Davis).

During the testing, the mouse's body temperature was maintained at 37°C using a thermally regulated heating pad system (Harvard Apparatus, Cambridge, MA). The multiunit recording was typically completed in 2-3 h, and the pedal withdrawal reflex of the hind limbs was checked every 45 min to assess the anesthetic depth. Supplemental ketamine and xylazine (~0.1 ml) were given as needed to maintain the proper level of anesthesia.

To confirm the recording site of the brain, DiI staining solution (Invitrogen) was applied on the 16-channel electrode prior to the electrophysiological recordings of the PnC. After completion of the recording, the animal was decapitated; the brain was removed from the skull and fixed in 10% formalin for 2 days. Then, the brain was transferred to 30% sucrose solution for 48 h until the brain tissue sunk.

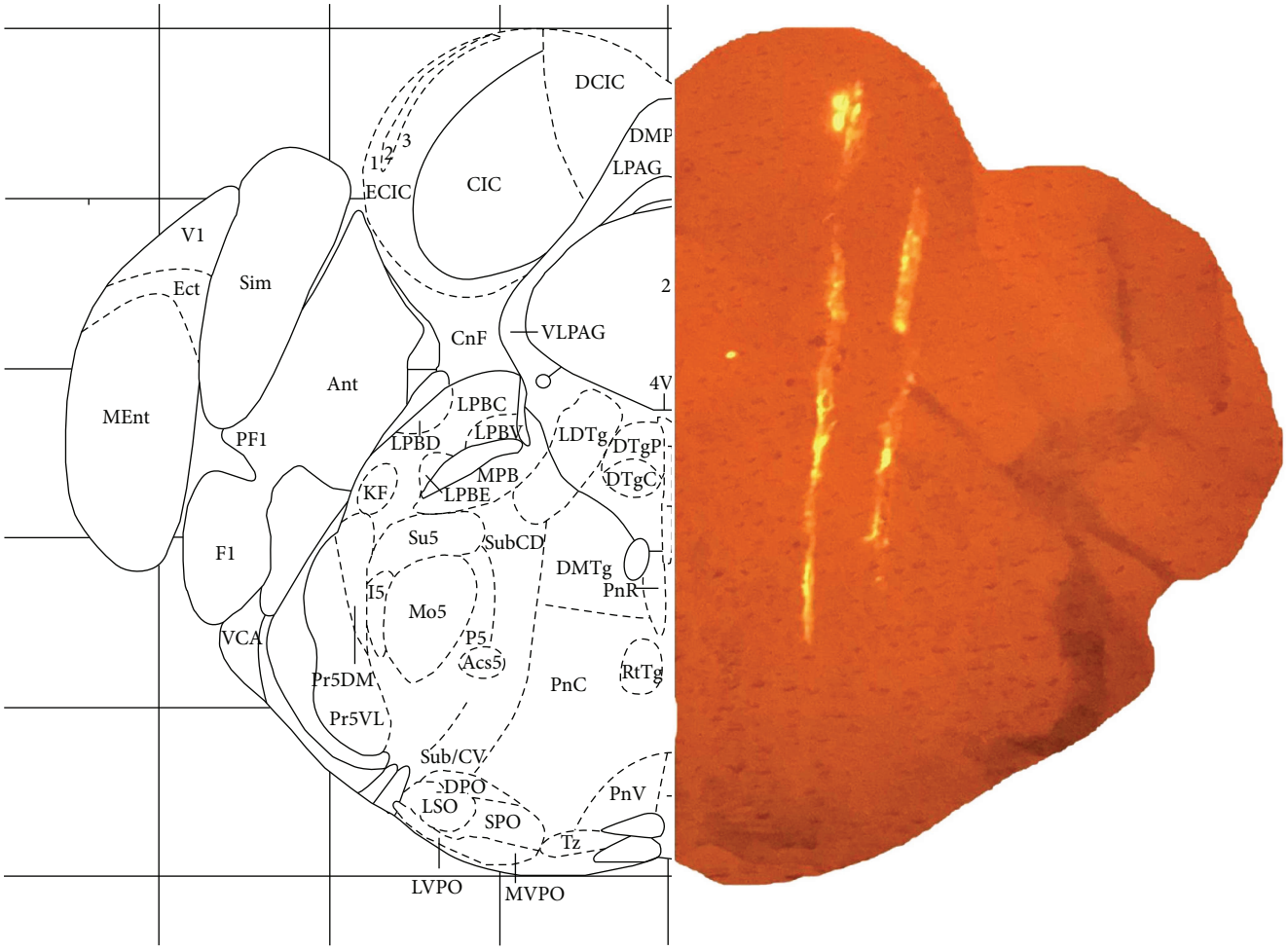

FIGURE 1: The right image shows the16-channel electrode coated with DiI staining on a mouse brain section (yellow fluorescence). The location of PnC recording was confirmed with the left image which shows the same location from the mouse brain atlas (Paxinos & Watson).

Next, the brain was sliced into 40-micron thin sections using a cryostat. DiI-stained electrode insertion was visualized under a fluorescence microscope. Further, DiI-coated electrode tracing of the brain slice (Figure 1) was compared to mouse brain atlas (Paxinos & Watson) to verify the location of the PnC electrophysiological recording.

2.5. Statistical Data Analysis. Graph-Pad Prism software (GraphPad Software, San Diego, CA) was used for plotting and statistical analyses unless otherwise noted. Results were presented as mean ± standard error of the mean (SEM). Two-way ANOVAs and Student's t-tests were used for the neurophysiological data analysis. Student's t-tests were used in the behavioral data analysis. The alpha level was set to $P < 0.05$ for all statistical tests.

3. Results

3.1. The ABR Assessment of Hearing Loss. Age-related cochlear hearing loss was evaluated by measuring the ABR thresholds in 2- and 6-month-old mice. Mean ABR thresholds in the 2-month-old C57BL/6J mice ($n = 6$) was 20–25 dB at 4 to 48 kHz. ABR thresholds deteriorated with age (Figure 2). The threshold increases were greater for the high frequencies (>16 kHz) compared to the low frequencies. The mean ABR thresholds of the aged group (G-6M, $n = 6$) were significantly higher than those of the young group (G-2M, $n = 6$) at all of the tested frequencies (two-way ANOVA, $F = 9.71$, $P < 0.0001$). The age-related hearing loss was consistent with previous findings [11, 15].

3.2. The ASR Changes with Age. To determine the acoustic behavioral consequences of the high-frequency age-related hearing loss, ASR was measured over three consecutive days in different age groups (Figure 3(a)). The RMS values of the ASR amplitude induced by narrowband noise centered at 8, 12, and 20 kHz were measured by a 180 ms window after the onset of sound stimuli (Figures 3(b)–3(d)). The average ASRs as a function of intensity was significantly greater in the 6-month-old mice ($n = 6$) compared to the 2-month group ($n = 6$) at 70 and 80 dB SPL (Student's t-test, $P < 0.05$) but no difference at 90 and 100 dB SPL (Student's t-test, $P > 0.05$, Figures 3(b)–3(d)).

3.3. PnC Response Affected by Age-Related Hearing Loss. To explore the neurophysiological changes in the pathway

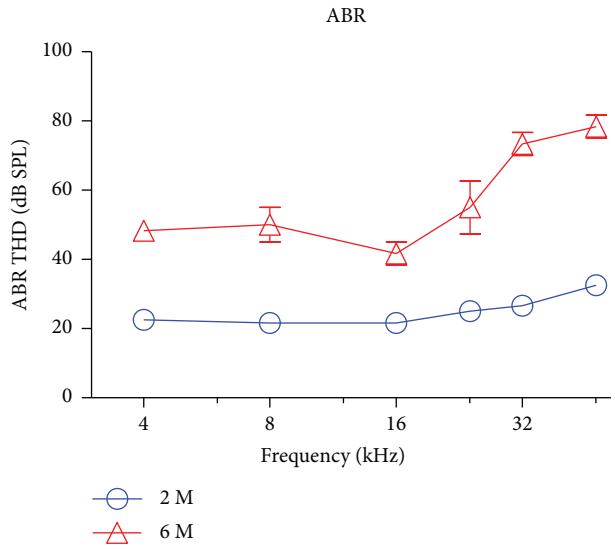

Figure 2: The auditory brainstem response (ABR) thresholds from C57BL/6J mice showed a significant increase with age. The mean ABR thresholds in the 6-month-old group (G-6M, $n = 6$) were significantly higher than those of the 2-month-old group (G-2M, $n = 6$; two-way ANOVA, $P < 0.0001$).

responsible for ASR, PnC neurons were recorded from the 2-month- and 6-month-old mice. To identify the PnC neurons, a multichannel electrode was advanced into the brain from the lateral side of the IC while noise bursts (50 ms, 70–90 dB SPL) were presented. PnC neurons were typically identified in 1-2 mm from the ventral side of the IC neurons (approximately 4-5 mm below the surface of the brain). The recording site again was confirmed with DiI trace and compared to mouse brain atlas after the recording (Figure 1). Figure 4 shows the average LFP (Figure 4(a)) and spike discharge rates (Figure 4(b)) of the PnC induced by noise bursts in the G-2M and G-6M group (ISI = 1 second). The RMS value of the PnC responses (50 ms window after sound onset) for each intensity was calculated and compared from the 2-month group to the 6-month group. The average PnC response ($n = 60$) in the 6-month-old mice was significantly higher than that in the 2-month-old mice ($n = 126$) at above 50 dB SPL (Student's t-test, $P < 0.001$, Figures 4(c) and 4(d)). The LFP and PSTH of PnC neurons elicited by noise bursts at 5-second ISI are shown in Figures 4(e) and 4(f). Similar to the LFP and PSTH recorded with 1-second ISI, the amplitude of PnC responses in the G-6M group was significantly higher than that in the G-2M group (>50 dB SPL) with 5-second ISI. Comparing the LFP and PSTH recorded with 1 s ISI, the response recorded in 5 s ISI showed no significant changes in the G-2M group. However, the LFP and PSTH recorded in the G-6M group with 5-second ISI were significantly higher than those recorded with short ISI (two-way ANOVA, $P < 0.001$). The amplitude of LFP and PSTH increased by 25% and 10%, respectively.

The typical eFRA in the G-2M and G-6M group is shown in Figures 5(a) and 5(b). The threshold of PnC response was 50 dB SPL or above in the G-2M group. For the G-6M group, there were no responses in the PnC neurons at above 20 kHz. However, at 8 and 12 kHz, the threshold of PnC responses in the G-6M group was about 40 dB SPL, slightly lower than the G-2M group. The RLF of PnC neurons elicited by tone bursts at 8, 12, and 20 kHz is shown in Figures 5(c)–5(e). The amplitudes of the PnC LFPs at 50–80 dB SPL in the G-6M group were significantly higher compared to those in the G-2M group at 8 and 12 kHz (Figures 5(c) and 5(d), two-way ANOVA, $P < 0.05$) but significantly lower at 20 kHz at 80 and 90 dB SPL (Figure 5(e), two-way ANOVA, $P < 0.05$).

4. Discussion

The goal of this study was to identify functional changes in the PnC and ASR in age-related hearing loss. There are three major findings of this study: (1) PnC responses recorded in the 6-month-old mice, which showed moderate hearing loss, were significantly higher than those recorded in the 2-month-old mice; (2) the enhancement of PnC response was found predominantly at low frequencies (<12 kHz) which may compensate for the high-frequency hearing loss; and (3) age-related physiological changes of PnC were consistent with the enhancement of ASR and IC function in mice after developing age-related hearing loss [15]. Our results suggest that the sensitivity of PnC neurons at low frequencies increased after developing high-frequency hearing loss, and these physiological changes in the PnC may be directly related to the exaggerated ASR [7].

Typically, the stimulus intensities need to be higher than 70 dB SPL to reliably evoke ASRs [16]. Prepulse inhibition of ASRs is a clinical test for neurological diseases, such as schizophrenia [17], obsessive compulsive disorder [18], and attention deficit/hyperactivity disorder (ADHD) [19]. Recently, ASR amplitude measurement was found to be correlated with reduced LDL in human subjects [9]. ASR may provide an objective indication of LDL since increased ASR amplitudes and decreased thresholds suggest reduced discomfort level to loud sounds. Consistent with previous studies, we found that the 6-month-old C57 mice show enhanced ASR amplitude/reduced threshold after developing hearing loss. These data suggested that decreased loudness discomfort level is correlated with age-related hearing loss which is commonly seen in the elderly [20].

In the startle circuit which is illustrated in Figure 6 (modified from Koch and Schnitzler), PnC neurons are the indispensable sensorimotor interface of the cochleospinal pathway that mediates the ASR. PnC receives direct acoustic input from different nuclei in the central auditory pathway and projects onto the spinal interneurons and motor neurons [13]. Disruption of PnC pathway can dramatically decrease the startle amplitude [21]. Similar to the ASR threshold, PnC neurons also have high firing thresholds and broad frequency tuning indicating that giant PnC neurons have particularly low sensitivity [14]. In this study, we found that PnC thresholds decreased from 70 dB to 50 dB SPL (8 and 12 kHz), and the local field potentials as well as firing rates increased significantly with age. These physiological changes of the PnC neurons were consistent with reduced ASR in age-related hearing loss.

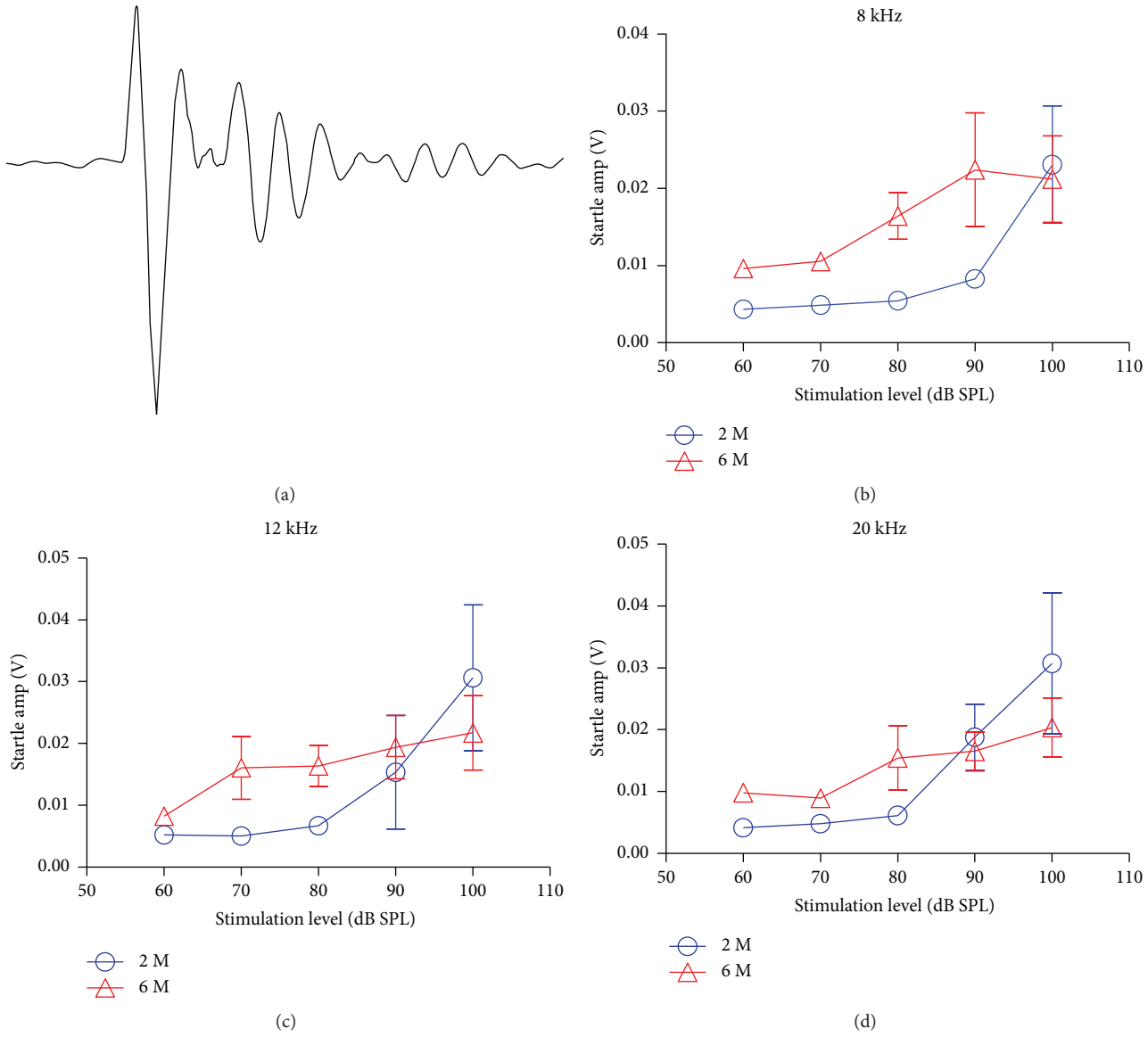

Figure 3: Response of the acoustic startle reflex (ASR) of the 2- and 6-month-old mice elicited by narrowband noise centered at 8, 12, and 20 kHz. (a) A raw startle response recorded from a mouse. (b–d) The startle amplitudes in the 6-month-old mice were significantly larger than those of the 2-month-old mice at 70–80 dB SPL (Student's t-test, $P < 0.05$). At high intensities (90–100 dB SPL), the ASR amplitude was similar in the two groups (Student's t-test, $P > 0.05$).

Previous studies reported that the ASR of C57 mice decreased with the onset of hearing loss and increased at low frequencies at 6 months of age [11]. This delayed exaggeration of the ASR with hearing loss may be caused by the deficit in the centrifugal inhibitory control over the afferent reflex pathways after central neural reorganization [11]. PnC neurons receive neural innervations from the auditory system as well as the limbic systems. For example, the IC neurons, particularly the external cortex, have inhibitory projections to the PnC [14]. Our recent study found that the response in the IC increased in the 6-month C57 mice compared to the young mice [15]. This functional change of the IC neurons may interfere with inhibition of ASR [22, 23]. Lingenhohl and Friauf also detected that the activity of amygdala can enhance the response of PnC [14]. Salicylate exposure which causes enhancement of ASR [5] also affects the response of the amygdala and PnC [24, 25].

The central plasticity changes are commonly induced by hearing loss, and the functional changes are also related to the hearing loss frequency. Parham and Willott and Carlson and Willot reported that the ASR amplitude declined for the high-frequency stimuli, and the biggest increase of ASR was at the edge of the high-frequency hearing loss region, that is, 12 kHz [16, 26]. They suggested that this was induced by the strengthening of neural responses to the still audible sounds which may cause the behavioral sound augmentation as well. The argument of ASR may therefore be contributed to the unmasking effect from the hearing loss region [27, 28]. Our current study demonstrated that age-related hearing loss has a

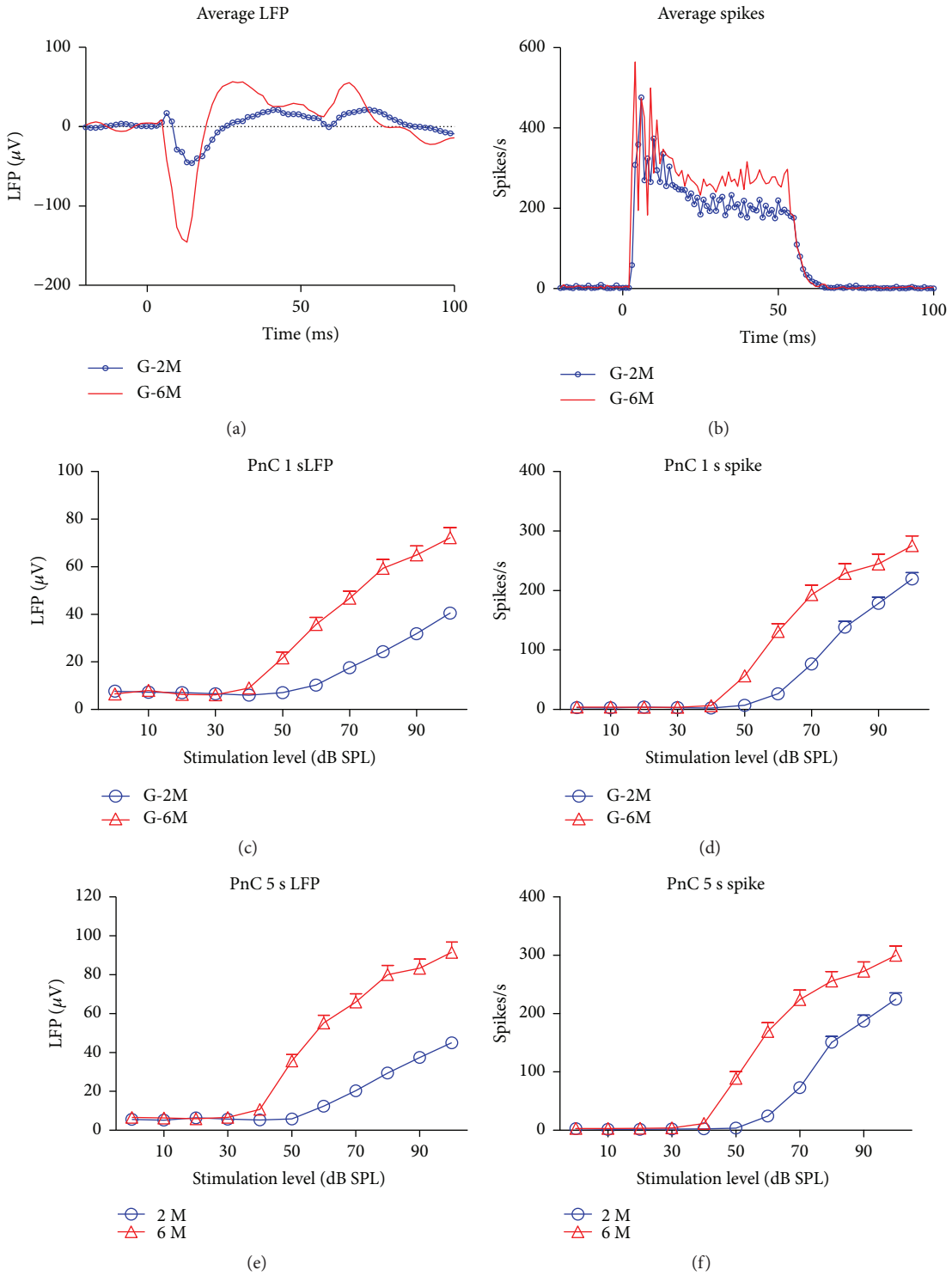

Figure 4: The local field potential (LFP) and spike discharge rates of PnC response elicited by white-noise bursts recorded from the G-2M and G-6M groups. (a) The average LFP at 90 dB SPL recorded from the G-6M group was significantly larger than that from the G-2M group. (b) The average peristimulus time histograms (PSTH, 90 dB SPL) of the 6-month group were also larger than those of the 2 month-old mice. The LFP and firing rate intensity function of the G-6M group were also significantly larger than those of the G-2M group elicited by different interstimulation intervals (ISI) at 1 (c and d) and 5 seconds (e and f) (two-way ANOVA, $P < 0.001$).

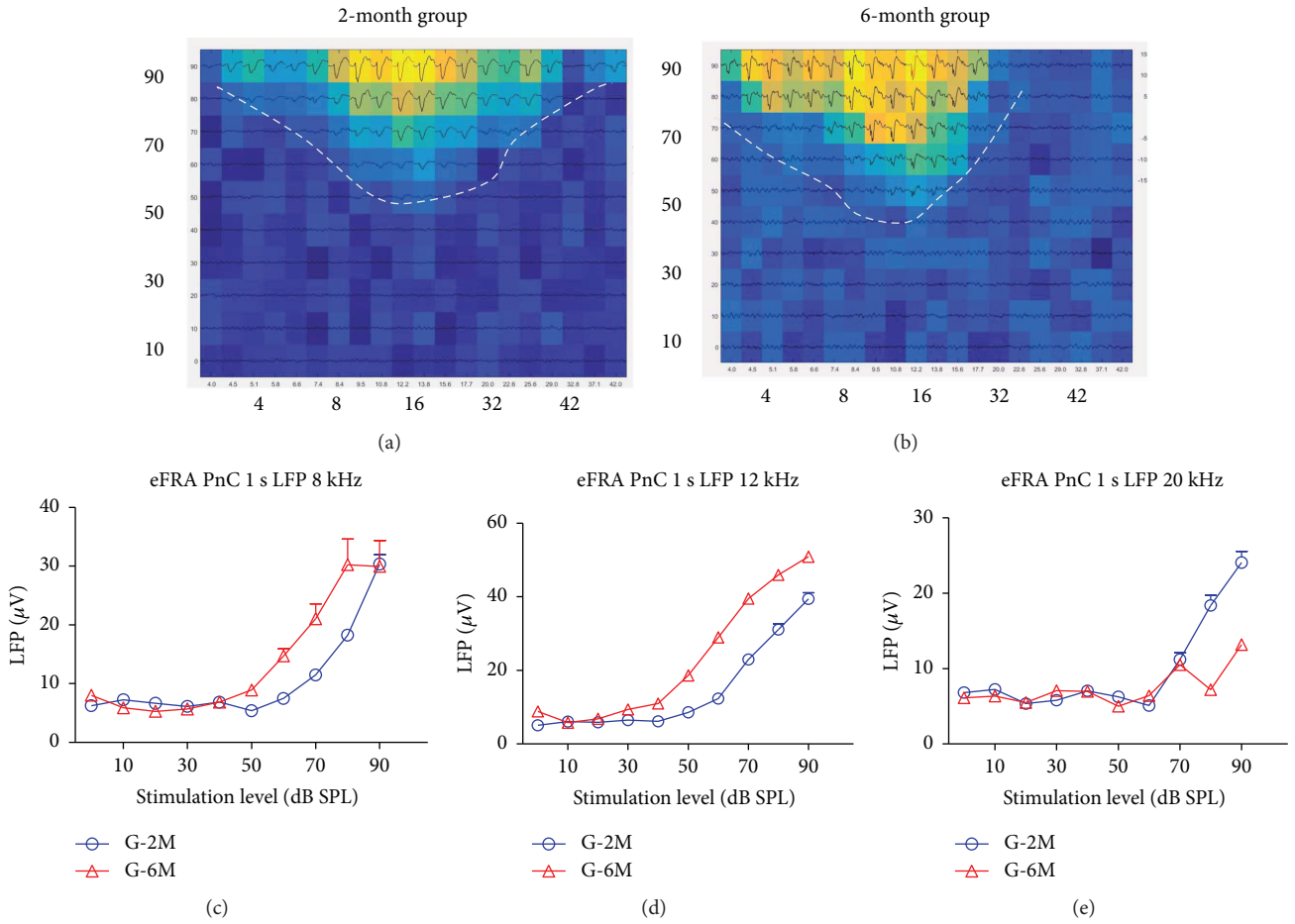

Figure 5: Typical excitatory frequency response area (eFRA) of PnC response in the G-2M and G-6M group (a and b). The threshold of PnC response was about 50–70 dB SPL in the G-2M group. For the 6-month group, there was no response at above 30 kHz. However, at low frequencies (<16 kHz), the threshold of PnC response was slightly lower in the G-6M than in the G-2M group. (c–e) The rate-level function of PnC neurons elicited by tone bursts at 8, 12, and 20 kHz. The amplitude of the PnC response was significantly higher in the G-6M group compared to that in the G-2M group at 8 and 12 kHz at 50–80 dB SPL (Student's t-test, $P < 0.05$), whereas the PnC response at 20 kHz in the G-6M group was significantly lower than that in the G-2M group at 80 and 90 dB SPL (Student's t-tests, $P < 0.05$).

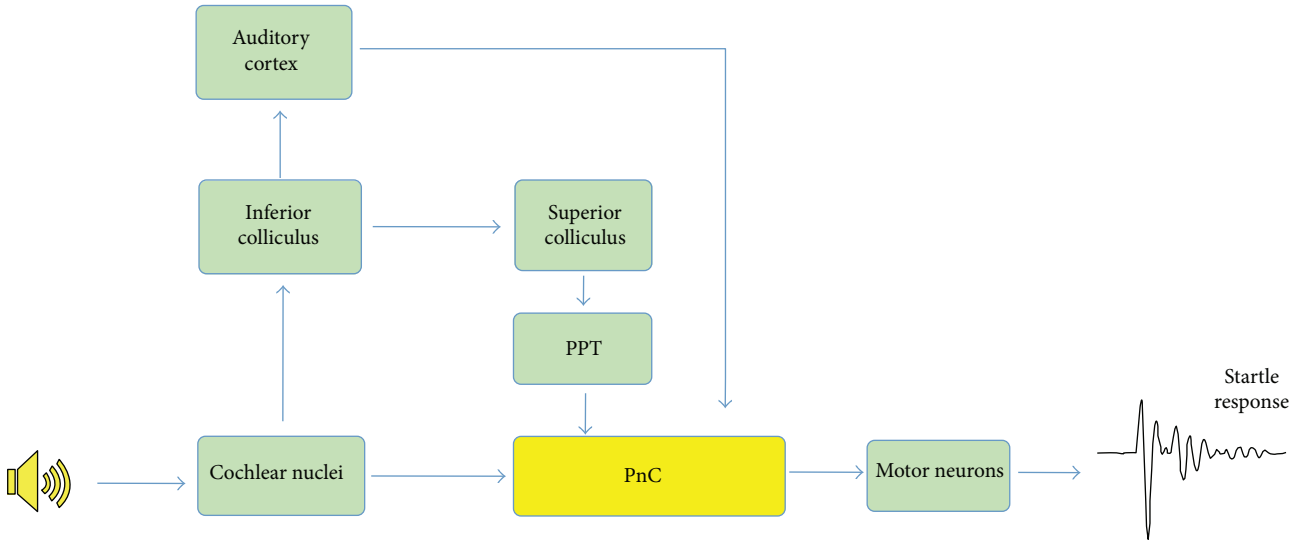

Figure 6: Simplified hypothetical pathway of acoustic startle response and prepulse inhibition (modified from Koch and Schnitzler).

direct effect on the function of PnC neurons which may cause exaggerated ASR and loudness changes.

5. Conclusions

The response of PnC neurons is enhanced with hearing loss in the 6-month-old C57 mice. These findings support the hypothesis that the responses of PnC neurons would reflect the characteristics of the behavioral ASR. The increased response of PnC could be the neural source of enhanced ASR and reduced LDL associated with age-related hearing loss.

Conflicts of Interest

The authors declare that there is no conflict of interest regarding the publication of this paper.

Acknowledgments

The study was supported by the National Natural Science Foundation of China (81528005 to Wei Sun) and Natural Science Foundation of Liaoning Province (20162881 to Ning Zhao).

References

[1] X. Z. Liu and D. Yan, "Ageing and hearing loss," *The Journal of Pathology*, vol. 211, no. 2, pp. 188–197, 2007.

[2] S. F. Tadros, S. T. Frisina, F. Mapes, S. H. Kim, D. R. Frisina, and R. D. Frisina, "Loss of peripheral right-ear advantage in age-related hearing loss," *Audiology and Neurotology*, vol. 10, no. 1, pp. 44–52, 2005.

[3] K. K. Ohlemiller and P. M. Gagnon, "Apical-to-basal gradients in age-related cochlear degeneration and their relationship to "primary" loss of cochlear neurons," *The Journal of Comparative Neurology*, vol. 479, no. 1, pp. 103–116, 2004.

[4] R. J. Longenecker, K. T. Chonko, S. M. Maricich, and A. V. Galazyuk, "Age effects on tinnitus and hearing loss in CBA/CaJ mice following sound exposure," *SpringerPlus*, vol. 3, no. 1, p. 542, 2014.

[5] W. Sun, J. Lu, D. Stolzberg et al., "Salicylate increases the gain of the central auditory system," *Neuroscience*, vol. 159, no. 1, pp. 325–334, 2009.

[6] G. Chen, C. Lee, S. A. Sandridge, H. M. Butler, N. F. Manzoor, and J. A. Kaltenbach, "Behavioral evidence for possible simultaneous induction of hyperacusis and tinnitus following intense sound exposure," *Journal of the Association for Research in Otolaryngology*, vol. 14, no. 3, pp. 413–424, 2013.

[7] L. Li, Y. du, N. Li, X. Wu, and Y. Wu, "Top-down modulation of prepulse inhibition of the startle reflex in humans and rats," *Neuroscience & Biobehavioral Reviews*, vol. 33, no. 8, pp. 1157–1167, 2009.

[8] J. S. Yeomans and P. W. Frankland, "The acoustic startle reflex: neurons and connections," *Brain Research Reviews*, vol. 21, no. 3, pp. 301–314, 1995.

[9] I. M. Knudson and J. R. Melcher, "Elevated acoustic startle responses in humans: relationship to reduced loudness discomfort level, but not self-report of hyperacusis," *Journal of the Association for Research in Otolaryngology*, vol. 17, no. 3, pp. 223–235, 2016.

[10] P. Fournier and S. Hebert, "Gap detection deficits in humans with tinnitus as assessed with the acoustic startle paradigm: does tinnitus fill in the gap?," *Hearing Research*, vol. 295, pp. 16–23, 2013.

[11] J. R. Ison, P. D. Allen, and W. E. O'Neill, "Age-related hearing loss in C57BL/6J mice has both frequency-specific and non-frequency-specific components that produce a hyperacusis-like exaggeration of the acoustic startle reflex," *Journal of the Association for Research in Otolaryngology*, vol. 8, no. 4, pp. 539–550, 2007.

[12] J. F. Willott, J. Kulig, and T. Satterfield, "The acoustic startle response in DBA/2 and C57BL/6 mice: relationship to auditory neuronal response properties and hearing impairment," *Hearing Research*, vol. 16, no. 2, pp. 161–167, 1984.

[13] M. Koch and H. U. Schnitzler, "The acoustic startle response in rats–circuits mediating evocation, inhibition and potentiation," *Behavioural Brain Research*, vol. 89, no. 1-2, pp. 35–49, 1997.

[14] K. Lingenhohl and E. Friauf, "Giant neurons in the rat reticular formation: a sensorimotor interface in the elementary acoustic startle circuit?," *The Journal of Neuroscience*, vol. 14, no. 3, pp. 1176–1194, 1994.

[15] B. Xiong, A. Alkharabsheh, S. Manohar et al., "Hyperexcitability of inferior colliculus and acoustic startle reflex with age-related hearing loss," *Hearing Research*, vol. 350, pp. 32–42, 2017.

[16] K. Parham and J. F. Willott, "Acoustic startle response in young and aging C57BL/6J and CBA/J mice," *Behavioral Neuroscience*, vol. 102, no. 6, pp. 881–6, 1988.

[17] S. Kohl, K. Heekeren, J. Klosterkötter, and J. Kuhn, "Prepulse inhibition in psychiatric disorders–apart from schizophrenia," *Journal of Psychiatric Research*, vol. 47, no. 4, pp. 445–452, 2013.

[18] S. A. Steinman, S. E. Ahmari, T. Choo et al., "Prepulse inhibition deficits only in females with obsessive-compulsive disorder," *Depression and Anxiety*, vol. 33, no. 3, pp. 238–246, 2016.

[19] L. W. Hawk, A. R. Yartz, W. E. Pelham, and T. M. Lock, "The effects of methylphenidate on prepulse inhibition during attended and ignored prestimuli among boys with attention-deficit hyperactivity disorder," *Psychopharmacology*, vol. 165, no. 2, pp. 118–127, 2003.

[20] H. P. Chang and P. Chou, "Presbycusis among older Chinese people in Taipei, Taiwan: a community-based study," *International Journal of Audiology*, vol. 46, no. 12, pp. 738–745, 2007.

[21] M. Davis, D. S. Gendelman, M. D. Tischler, and P. M. Gendelman, "A primary acoustic startle circuit: lesion and stimulation studies," *The Journal of Neuroscience*, vol. 2, no. 6, pp. 791–805, 1982.

[22] K. Parham and J. F. Willott, "Effects of inferior colliculus lesions on the acoustic startle response," *Behavioral Neuroscience*, vol. 104, no. 6, pp. 831–840, 1990.

[23] D. S. Leitner and M. E. Cohen, "Role of the inferior colliculus in the inhibition of acoustic startle in the rat," *Physiology & Behavior*, vol. 34, no. 1, pp. 65–70, 1985.

[24] Y. C. Chen, X. Li, L. Liu et al., "Tinnitus and hyperacusis involve hyperactivity and enhanced connectivity in auditory-limbic-arousal-cerebellar network," *eLife*, vol. 4, 2015.

[25] Y. C. Chen, G. D. Chen, B. D. Auerbach, S. Manohar, K. Radziwon, and R. Salvi, "Tinnitus and hyperacusis: contributions of paraflocculus, reticular formation and stress," *Hearing Research*, vol. 349, pp. 208–222, 2017.

[26] S. Carlson and J. F. Willott, "The behavioral salience of tones as indicated by prepulse inhibition of the startle response: relationship to hearing loss and central neural plasticity in C57BL/6J mice," *Hearing Research*, vol. 99, no. 1-2, pp. 168–175, 1996.

[27] J. Wang, D. Ding, and R. J. Salvi, "Functional reorganization in chinchilla inferior colliculus associated with chronic and acute cochlear damage," *Hearing Research*, vol. 168, no. 1-2, pp. 238–249, 2002.

[28] Y. Niu, A. Kumaraguru, R. Wang, and W. Sun, "Hyperexcitability of inferior colliculus neurons caused by acute noise exposure," *Journal of Neuroscience Research*, vol. 91, no. 2, pp. 292–299, 2013.

Hindawi
Neural Plasticity
Volume 2018, Article ID 1258341, 10 pages
https://doi.org/10.1155/2018/1258341

Research Article

Mechanisms of Hearing Loss in a Guinea Pig Model of Superior Semicircular Canal Dehiscence

Bu-Sheng Tong,[1,2,3,4] Zi-Yu He,[1,3,4] Chen-Ru Ding,[1,3,4] Juan-Mei Yang,[1,3,4] Jing Wang,[1,3,4] Zhao Han,[1,3,4] Yi-Bo Huang,[1,3,4] Na Gao,[1,3,4] Xian-Hao Jia,[1,3,4] Fang-Lu Chi,[1,3,4] and Dong-Dong Ren[1,3,4]

[1]*ENT Institute and Otorhinolaryngology Department, Affiliated Eye and ENT Hospital, Fudan University, Shanghai, China*
[2]*Department of Otorhinolaryngology of the First Affiliated Hospital, Anhui Medical University, Hefei, China*
[3]*Shanghai Auditory Medical Center, Shanghai, China*
[4]*Key Laboratory of Hearing Science, Ministry of Health, Shanghai, China*

Correspondence should be addressed to Fang-Lu Chi; chifanglu@126.com and Dong-Dong Ren; dongdongren@fudan.edu.cn

Received 20 January 2018; Accepted 7 March 2018; Published 24 April 2018

Academic Editor: Jian Wang

Defective acoustic transmission in the cochlea is closely related with various auditory and vestibular symptoms. Among them, semicircular canal dehiscence (SCD) with a defective semicircular bone is typical. Currently, the pathogenesis of SCD is usually explained by the third window hypothesis; however, this hypothesis fails to explain the variability in the symptoms and signs experienced by superior SCD (SSCD) patients. We evaluated the mechanism of hearing loss in a guinea pig model of bony dehiscence with various sizes and locations along the superior semicircular canal. Auditory brainstem responses (ABRs) and laser Doppler velocimetry were used to measure hearing loss and vibration changes before and after fenestration, as well as after restorative patching. ABR thresholds at low frequencies (e.g., 1000 Hz) increased after fenestration and decreased back to the normal range after we repaired the defect. Energy leakage from the surgically introduced third window was detected in the range of 300–1500 Hz, accompanied by increased vibration at the umbo, stapes head, and the dehiscence site, while decreased vibration was observed at the round window membrane in the same frequency range. After the patching procedure, the deviant vibrations were recovered. The degree of postfenestration energy leakage was proportional to the size of fenestration and the proximity of the fenestration site to the oval window. These results suggest that the bony fenestration of the superior semicircular canal mimics the hearing loss pattern of patients with SSCD. The decrease in perilymph wave impedance likely accounts for the auditory changes.

1. Introduction

Superior semicircular canal dehiscence (SSCD), initially reported by Minor et al. in 1998 [1], is a clinical entity associated with vestibular symptoms typically evoked by sound and pressure stimuli. Temporal-bone histopathological studies suggest that the superior canal of 1-2% of the population has abnormally thin overlying bone. Disruption of this thin layer (caused by trauma or pressure from the overlying temporal lobe of the brain) may trigger both symptoms and signs. Dehiscence, being a bone defect, is nearly always diagnosed using a high-resolution CT scan on the temporal bone. Because patients show various clinical symptoms and many of them did not undergo high-resolution CT scans, SSCD is likely to be greatly underdiagnosed [2]. However, some patients also exhibit conductive hearing loss at low frequencies without vestibular symptoms. Most previous investigations have focused on clinical symptoms and treatments [3–5].

Normally, sound is transmitted through the membranes of the oval and round windows, which serve as fluid interface between air in the middle ear and the perilymphatic fluid spaces of the inner ear. The generally accepted hypothesis for the mechanism of the disease is the presence of a third

window in the cochlea, which may cause energy loss during sound transmission in the inner ear. In response to the inward movement of the stapes, the membrane covering the opening is pushed outwards, which reduces the movement of the perilymph and the outward movement of the round window membrane (RWM) [6, 7].

Conductive hearing loss induced by SSCD is presumably due to an increase in air conduction thresholds, concomitant with a decrease in bone conduction thresholds. The effects of SSCD on hearing thresholds have been investigated theoretically using a lumped-element electrical circuit model [6, 8]. Recently, the relationship between the hearing threshold and the size (or location) of dehiscence has been studied to examine the mechanisms of SSCD syndrome and develop protocols for screening SSCD patients [9]. Large air-bone gaps (ABGs) have been shown to accompany SSCD at low frequencies in animal experiments (fat sand rat and chinchilla) [10, 11] and human cadaveric temporal bone studies [12].

A laser Doppler vibrometer is a noncontact, established optical technique that can be used to measure the displacement of the components of the middle ear in response to sound stimulation. This technique has been used to assess the vibration of the RWM, the tympanic membrane (TM), and the stapes footplate in fresh and embalmed cadaveric human temporal bone and animal specimens [13–15]. Over the years, animal models of different diseases have been created to investigate changes in vibration in the ossicular chain and the RWM to explore the potential mechanisms underlying the clinical symptoms of diseases.

To date, there is no *in vivo* animal model that can be used to investigate hearing loss and vibration changes with SSCD through laser Doppler velocimetry (LDV). In this study, we used the guinea pig as an experimental model, and we created dehiscence in the superior semicircular canal to simulate SSCD using a surgical technique. First, we showed that the bony fenestration of the superior semicircular canal in a guinea pig resulted in hearing loss in the low-frequency range, mimicking the characteristic hearing loss pattern in patients with SSCD. Then, we measured vibrations of the RWM, head of the stapes, umbo, and the surgically created dehiscence spot by LDV before and after fenestration, as well as after patching to test the third window hypothesis and clarify the pathogenesis of the hearing loss.

2. Materials and Methods

2.1. Animals. All animal work was approved by the institutional animal care and use committee at the Eye and Ear, Nose, and Throat Hospital, Fudan University, and complied with the National Institutes of Health guide for the care and use of laboratory animals.

In total, 36 healthy albino male guinea pigs with an initial weight of 250–300 g and a positive Preyer reflex were used. All animals were free of middle ear diseases, such as TM perforation or otitis media, as evaluated by otoscopic examination. The identification of preexisting abnormalities of auditory function was made by a prerecruiting auditory brain response (ABR) measurement for each animal. If an abnormal response was found, the animal was excluded from the study.

2.2. Surgical Procedure. All surgeries were performed under anesthesia by applying an anesthetic solution made by mixing 2 ml ketamine (Jiangsu Hengrui Medicine Co. Ltd., serial number 1867-66-9) with 30 mg xylazine powder (Nanjing Pharmaceutical Chemical Factory, serial number 23076-35-9), resulting in a final concentration of 15 mg/ml. The anesthetic solution was injected intramuscularly into the animal at a dose of 1 ml/kg. Supplementary doses were given as necessary, judged by the toe-pinch reflex.

The right ears of the experimental animals underwent surgery to simulate SSCD disorders, and the left ears served as controls. First, we surgically exposed the superior semicircular canal by opening the bulla dorsally; then, the semicircular canal bony wall was removed using a diamond burr until the membranous canals were exposed, presenting as semilucent under the microscope (Figure 1). We divided the animals based on the position of the dehiscence and its size. The individual groups were as follows: (1) a dehiscence with a size of 0.5×1.0 mm, close to the oval window (6 guinea pigs); (2) a dehiscence with a size of 0.5×0.5 mm, close to the oval window (18 guinea pigs); (3) a dehiscence with a size of 0.5×1.0 mm, distal to the oval window (6 guinea pigs); and (4) a dehiscence with a size of 0.5×0.5 mm, distal to the oval window (6 guinea pigs). We defined close to or distal to the oval window as the distances ≤ 1 mm or >3 mm from the superior semicircular canal crista, respectively, for location description.

In each animal, the vibrations of the TM (or umbo; Vu), stapes head (Vs), round window (Vw), and the place of the dehiscence (Vd) were measured (Figure 1(d)) before and after the dehiscence was created and when the dehiscence had been repaired using dental cement.

2.3. ABR Measurements. We have divided the individual groups as follows: (1) a dehiscence with a size of 0.5×1.0 mm, close to the oval window (6 guinea pigs); (2) a dehiscence with a size of 0.5×0.5 mm, close to the oval window (6 guinea pigs); (3) a dehiscence with a size of 0.5×1.0 mm, distal to the oval window (6 guinea pigs); and (4) a dehiscence with a size of 0.5×0.5 mm, distal to the oval window (6 guinea pigs). ABR measurement was performed before and after the dehiscence created in all four groups. ABR measurement was also performed after the dehiscence was repaired with dental cement in groups 1 and 2. After anesthesia, ABRs were tested in a soundproof booth to assess the auditory threshold (Bio-Logic NavPro, 580-NAVPR2, Natus Medical Inc., Pleasanton, CA, USA). ABR was recorded differentially using subcutaneous stainless steel electrodes placed over the rostral to the tragus of the right ear (positive), left ear (negative), and in the middle of the two ears (ground); the inter-electrode impedance was <3 kΩ. Stimulation was presented as tone bursts (5 ms duration, 0.5 ms rise/fall time, Blackman envelope) at a frequency of 0.5, 1, 2, 4, 6, and 8 kHz; the sound-intensity level was decreased in 5 dB steps from 100 to 20 dB SPL, and 1000 response traces at each sound level were recorded and averaged.

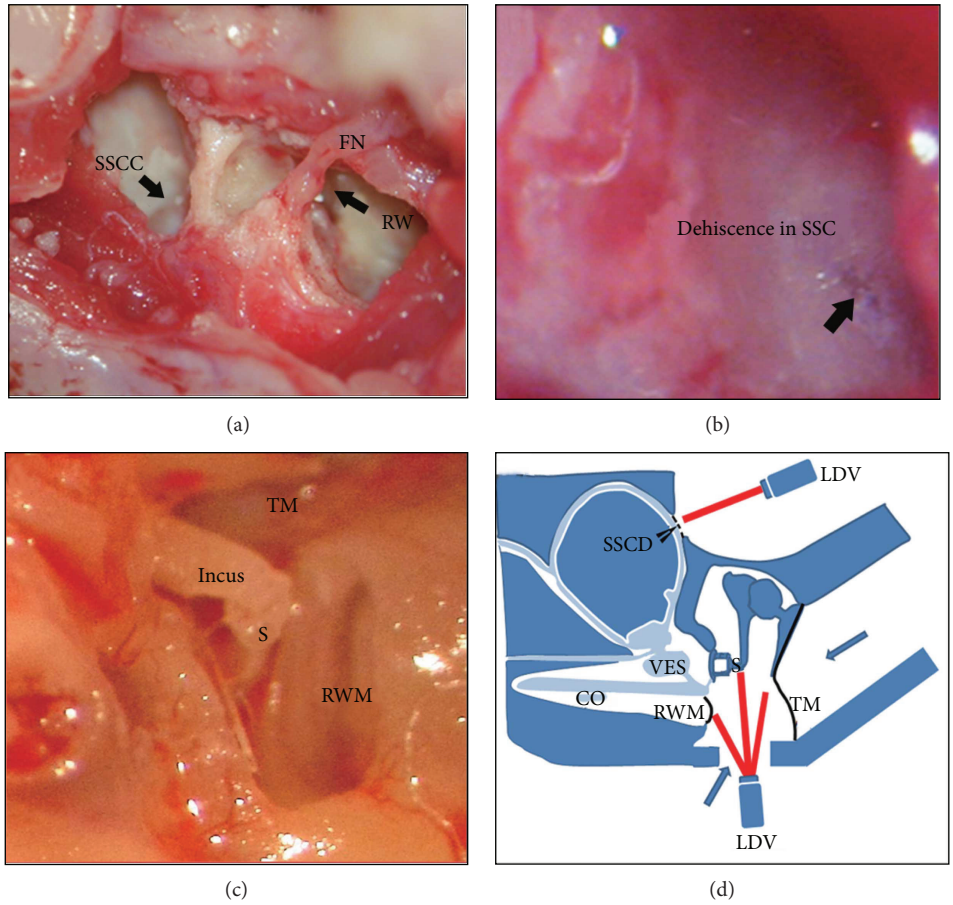

Figure 1: Surgical procedure for the SSCD model and schematic diagram of the laser Doppler vibrometer (LDV) detecting vibration at four locations: (a) anatomical landmarks of the superior semicircular canal (SCC), facial nerve (FN), and round window (RW), viewed from the opened middle ear cavity; (b) dehiscence created in the superior semicircular canal (SCC); (c) the incus, stapes head, round window membrane (RWM), and the medial side of the umbo, viewed from the opened middle ear cavity; (d) diagram of the LDV, as used in four locations to detect vibration.

2.4. Laser Doppler Vibrometer Measurements. The system used in the present study included a laser Doppler vibrometer (Polytec OFV-505, Polytec, Karlsruhe, Germany) coupled with a microscope (OPMI 1-FC, Carl Zeiss, Jena, Germany), a vibrometer controller (OFV-5000, USA), a high-bandwidth backplane (PXIe-1082, NI, USA), a conditioning amplifier (MI-2004, ECON, USA), a micromanipulator (A-HLV-MM30, Polytec, Wurzburg, Germany), and a signal generator (33210A, Agilent, Santa Clara, CA, USA; Figure 1(a)). The intensity of each excitation frequency was calibrated to 100 dB SPL using a sound-level meter (AWA-5661–1B, AiHua, Yiyang city, China). An earphone associated with the microphone (ER-4PT, ER-7C, HLV-SPEC Adapter, Etymotic, Elk Grove Village, IL, USA) was inserted into the osseous external auditory canal to deliver signal stimuli and monitor sound pressure. The distance between the TM and the inserted earphone and microphone was 0.5 mm. The sound stimuli, produced by a closed loudspeaker with a frequency range of 0–10 kHz, with sound level of 100 dB SPL and duration of 320 ms (ER-4PT, USA), were delivered by a plastic tube to the TM. At the same time, a real-time sound monitor was put into the external ear canal to monitor stimulus density and sound waves. The vibration of the target surface was acquired by the system through a reflective beaded foil and recorded by a computer program (LabVIEW SignalExpress, National Instruments, USA) for further analysis. The vibration amplitude of the moving surface was calculated from the voltage output of the vibrometer's velocity decoder. Testing was conducted in a sound-treated booth to achieve a high signal-to-noise ratio. For each stimulus frequency, sound stimuli were repeated at least three times. Traces presenting a good signal-to-noise ratio were averaged during offline data analysis.

2.5. Section Processing and Hematoxylin and Eosin Staining. Six guinea pigs were used in this part. The right ears of three animals underwent successful surgery to simulate SSCD disorders with a thin endosteum in the dehiscence. Surgeries on the other three animals failed resulting in fistula in SSCD. Intracardiac perfusion was performed with 150 ml 0.2 M PBS, followed by 4% paraformaldehyde, and then the temporal bone was removed and fixed in 4% paraformaldehyde (pH = 7.4) for more than 24 h at 4°C. The temporal bones were decalcified in ethylenediaminetetraacetic acid. Samples

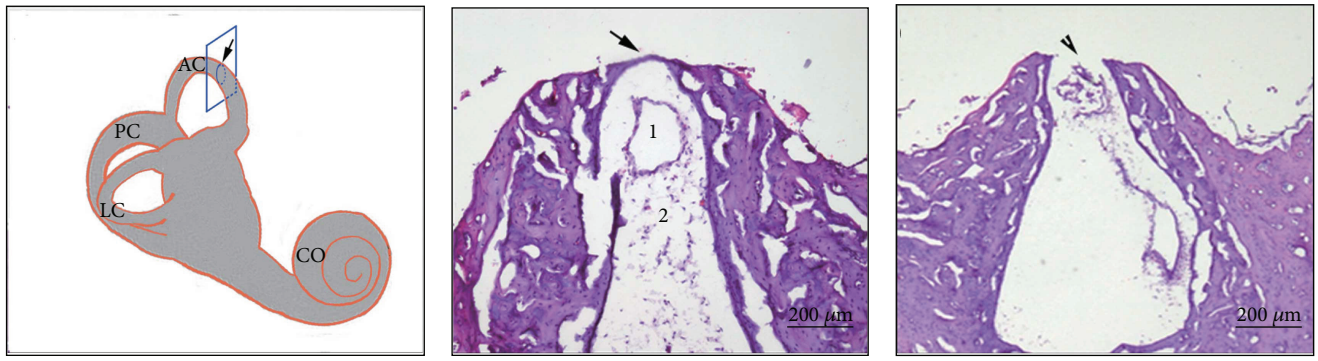

Figure 2: Successful SSCD model, confirmed by sectioning and hematoxylin and eosin (H&E) staining. (a) shows the schematic diagram of the section plane (blue pane) of the fenestration (arrow) in SCD. The section shows a successful SSCD model in the plane perpendicular to the superior semicircular canal dehiscence with H&E staining showing the thin endosteum in the dehiscence ((a) 1 = endolymph fluid space, 2 = perilymph fluid space) and a failed SSCD model with a large fistula (b).

were saturated in 15% sucrose for 4 h and then 30% for 4 h, embedded in optimum cutting temperature (OCT) compound, and sectioned serially at 10 μm in the plane perpendicular to the SCD (Leica CM1830). The sections were stained with hematoxylin and eosin (H&E) and then were observed under a light microscope (6030116204, Carl Zeiss, Jena, Germany).

2.6. Statistical Analysis. Data are presented as mean ± standard error. All analyses were performed using SPSS software (ver. 19.0; IBM, USA). Two-tailed Student's *t*-tests were used to determine the confidence interval for comparison between two groups. P values < 0.05 were considered statistical significance.

3. Results

3.1. Observation of Tissue Sections of Surgically Induced SSCD in Guinea Pigs. To understand the successful surgeries that created dehiscence in the superior semicircular canal, we observed the sections after H&E staining. In the right ear of the animal, we created dehiscence close (1 mm) to the oval window with a size of 0.5 × 0.5 mm (Figure 1(b)). Under the light microscope, we observed that the membranous canal was exposed and appeared semilucent (Figure 1(b)). The criterion for success in the dehiscence model was a thin endosteum in the dehiscence (seen in the schematic diagram of the section plane (Figure 2(a)) and H&E staining; Figure 2(b)), demonstrating clearly the fluid areas of the endolymph and perilymph. A surgeon should refrain from removing too much bone from the superior semicircular canal, which could result in a large fistula (e.g., Figure 2(c)) and false measurement of lymph pressure. In the supplemental material, we have done the whole-mount immunostaining with phalloidin (green), peripherin (red), and Ctbp2 (blue) in the apical (S1: A, D, and G), middle (S1: B, E, and H), and midbasal (S1: C, F, and I) turns of the cochlear in the surgically prepared guinea pigs (dehiscence close to the oval window with a size of 0.5 × 0.5 mm), which showed the normal structure of hair cells, neural nerves, and synapses.

3.2. Effects of SSCD and Its Repair on ABR Response. In this experiment, the animals underwent surgeries to create dehiscence close to the oval window and distal to the oval window, with a size of 1.0 × 0.5 mm and 0.5 × 0.5 mm, within 1 mm or more than 3 mm from the superior semicircular canal crista. ABR threshold measurements were performed before and after the dehiscence was created in the four groups; ABR measurement was also performed after the dehiscence was repaired with dental cement with the dehiscence close to the oval window.

The results of the ABR threshold before the operation, in the SSCD model, and after patching the dehiscence are listed in Figure 3. The means and standard errors of all groups were recorded. The elevation of the ABR threshold was observed in ears associated with dehiscence in the superior semicircular canal in the four groups ($n = 6$ in each group) at low frequencies of 250, 500, 1000, and 2000 Hz (Figure 3(a)). Student's *t*-tests showed that at 250, 500, and 1000 Hz, the mean ABR threshold in the SSCD model (0.5 × 1.0 mm, close to the oval window) was significantly higher than it was before the operation ($P < 0.05$, indicated by the asterisks in Figures 3(a) and 3(b)). In the SSCD model (0.5 × 0.5 mm close to the oval window), the mean ABR threshold in 1000 Hz was significantly higher than it was before the operation. ($P < 0.05$, indicated by the asterisks in Figures 3(a) and 3(c)). There were no significant ABR threshold elevation in the dehiscence far away from the oval window. After the dehiscence close to the oval window was repaired, the ABR thresholds were decreased at frequencies of 250, 500, 1000, and 2000 Hz (Figures 3(b) and 3(c)). Student's *t*-tests revealed that the mean ABR threshold in the dehiscence close to the oval window after patching showed no difference compared to the group before the operation ($P > 0.05$).

3.3. Effects of SSCD and Its Repair on Movement of the Umbo, Stapes Head, and RWM and the Effects of Location of Dehiscence according to LDV Measurements. In this experiment, the animals used were the same as those for the ABR threshold measurements, with dehiscence close

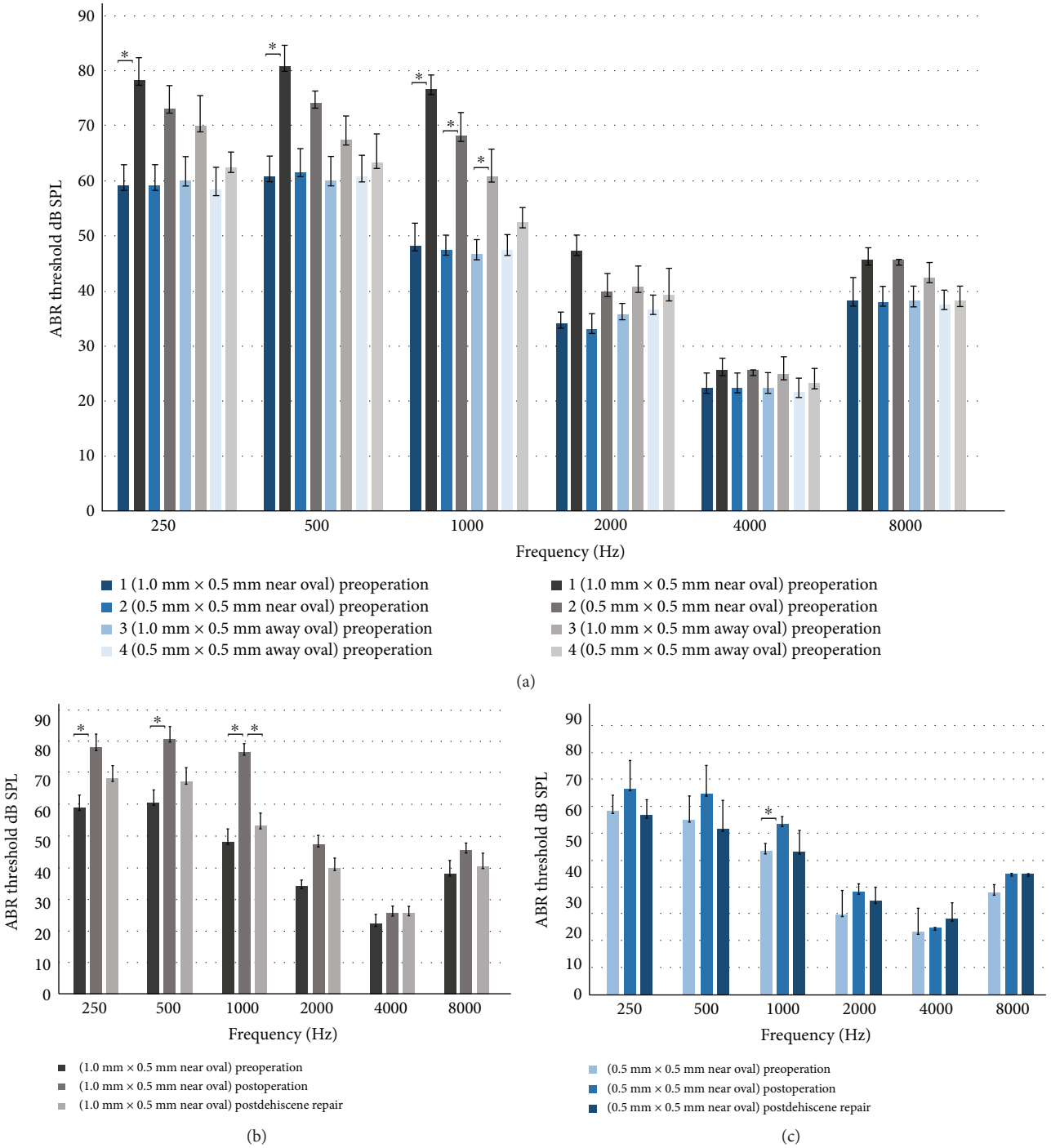

Figure 3: ABR threshold in different groups at frequencies of 0.25, 0.5, 1, 2, 4, and 8 kHz. (a) shows the ABR thresholds in four groups (1: 1×0.5 mm near the oval ($n = 6$), 2: 0.5×0.5 mm near the oval ($n = 6$), 3: 1×0.5 mm far away from the oval ($n = 6$), and 4: 0.5×0.5 mm far away from the oval ($n = 6$)) at frequencies of 0.25, 0.5, 1, 2, 4, and 8 kHz. ABR threshold in all frequencies increased after the dehiscence was created in group 1 and group 2, with a statistically significant difference at the frequency of 250, 500, and 1000 Hz ($^*P < 0.05$) in group 1 ($^*P < 0.05$) and 1000 Hz in group 2 ($^*P < 0.05$). (b) and (c) show ABR threshold presurgery, postsurgery SSCD, and postdehiscence repair at frequencies of 0.25, 0.5, 1, 2, 4, and 8 kHz in groups 1 and 2. The ABR thresholds at the low frequencies 250, 500, 1000, and 2000 Hz increased notably after the dehiscence (1×0.5 mm near the oval and 0.5×0.5 mm near the oval) was created, with a statistically significant difference at the frequency of 250, 500, and 1000 Hz in group1 ($^*P < 0.05$) and 1000 Hz in group 2 ($^*P < 0.05$), which was offset after the dehiscence was repaired.

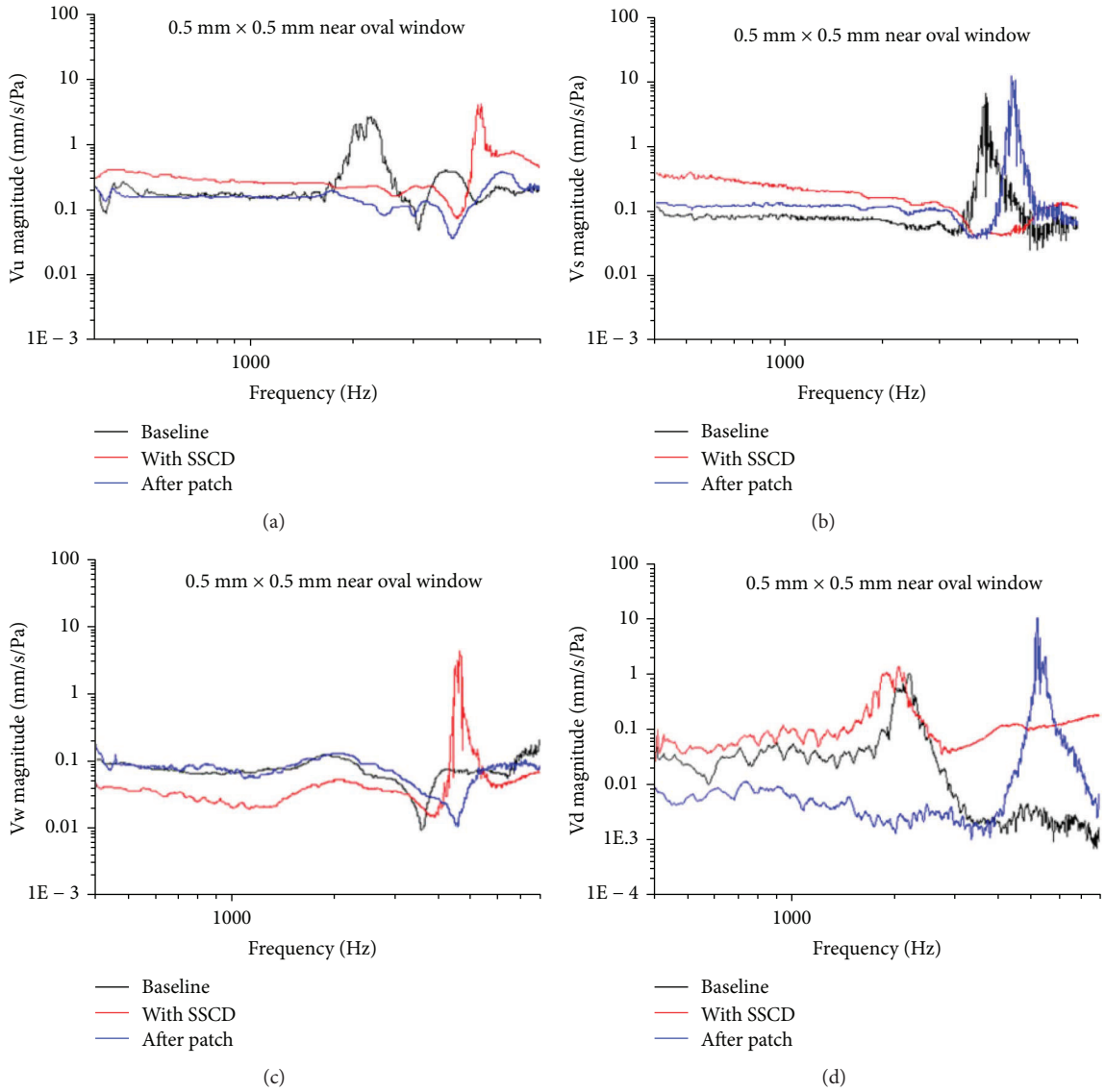

Figure 4: Vibration of the tympanic membrane (a), stapes head (b), round window (c), and the dehiscence (d), detected by LDV presurgery (black baseline) and postsurgery (red line) and after the dehiscence was repaired (blue line) ($n = 6$). (a) The presence of dehiscence (red line) statistically significantly ($P < 0.006$) increased the vibration of the tympanic membrane, in the range of 300–1500 Hz. The increase showed an offset after the dehiscence was repaired after surgery (blue line). (b) The presence of the dehiscence (red line) increased the vibration of the staples head, whereas it decreased the inner ear impedance statistically significantly ($P < 0.001$) in the range of 300–3000 Hz. This increase showed an offset after the dehiscence was repaired. (c) The presence of the dehiscence (red line) decreased vibration in the round window membrane statistically significantly ($P < 0.001$), in the range of 300–3000 Hz, which was offset after the dehiscence was repaired (blue line). (d) The vibration of the dehiscence located at the superior semicircular canal increased statistically significantly ($P < 0.001$) after the dehiscence was created, in the range of 300–2000 Hz. This increase showed an offset after the dehiscence was repaired.

to the oval window, with a size of 0.5×0.5 mm ($n = 6$). After ABR threshold measurement, the animals underwent LDV measurement.

A laser vibrometer was used to measure the target vibration. Vu, Vs, Vw, and Vd were detected (Figures 1(c) and 1(d)). During the measurements, a foil with reflective beads was attached to the target position to gain robust signals. To determine the SSCD influence, we measured and compared vibrations at the four different locations before and after the dehiscence was created as well as after the dehiscence was repaired with dental cement.

There was some energy leakage from the created third window, in the range of frequencies from 300 to 1500 Hz in the animal model, which presented as increased Vu (Figure 4(a)) and Vs (Figure 4(b)). In Figure 4(a), it can be seen that in comparison with the baseline (black line), the presence of dehiscence (red line) resulted in increased Vu significantly ($P < 0.006$), in the frequency range of 300–1500 Hz. The increase showed an offset after the dehiscence was repaired after surgery (blue line). In Figure 4(b), the presence of the dehiscence resulted in increased Vs, whereas it led to significantly decreased inner ear impedance ($P < 0.001$), in

the range of 300–3000 Hz. This increase showed an offset after the dehiscence was repaired.

The decreased Vw (Figure 4(c)) resulted in statistically significantly decreased ($P < 0.001$) inner ear impedance, in the range of 300–3000 Hz. The decrease showed an offset after patching.

Vd, located at the superior semicircular canal (Figure 4(d)), increased significantly ($P < 0.001$) after the dehiscence was created, in the range of 300–2000 Hz. This increase showed an offset after the dehiscence was repaired. The energy leakage was improved after the dehiscence was repaired.

3.4. Effects of SSCD with Varied Sizes and Locations on Movement of the Umbo, Stapes Head, and RWM, Assessed by LDV Measurements. In this part, the two dehiscence sizes were 0.5×0.5 mm and 0.5×1.0 mm, while the two locations were near the oval window (less than 1 mm between the superior semicircular canal crista) and away from it (3 mm from the superior semicircular canal crista). Vu, Vs, and Vw were measured before and after the dehiscence were created ($n = 6$ in each group).

Vu in the group with the larger dehiscence (1.0×0.5 mm; red line) was stronger than in the group with the smaller dehiscence (0.5×0.5 mm; black line), in the range of 500–1000 Hz ($P < 0.05$; Figure 5(a)). Vs in the group with the larger dehiscence (1.0×0.5 mm; red line) was stronger than in the group with the smaller dehiscence (0.5×0.5 mm; black line), in the range of 400–1000 Hz ($P < 0.05$; Figure 5(b)). Vw in the group with the larger dehiscence (1.0×0.5 mm; red line) was weaker than in the group with the smaller dehiscence (0.5×0.5 mm; black line), in the range of 400–2000 Hz ($P < 0.001$; Figure 5(c)).

Vu in the group with the large dehiscence (1.0×0.5 mm; red line in Figure 5(d)) near the oval window was stronger than in the group with the smaller dehiscence (0.5×0.5 mm; black line in Figure 5(d)) near the oval window, in the range of 500–1000 Hz ($P < 0.05$). Vu in the group with the smaller dehiscence (0.5×0.5 mm; black line in Figure 5(d)) near the oval window was stronger than in the group with the smaller dehiscence (0.5×0.5 mm; blue line in Figure 5(d)) and the larger dehiscence (1.0×0.5 mm; green line in Figure 5(d)) far from the oval window, in the range of 400–800 Hz ($P < 0.05$). There were no statistically significant differences ($P > 0.05$) between the groups with different size dehiscences located far from the oval window (blue and green lines in Figure 5(d)).

Generally, the impedance of the inner ear in the group with a dehiscence of 1.0×0.5 mm located close to the oval window had larger decreases than the group with a dehiscence of 0.5×0.5 mm located at the same site in the frequency range of 500–1000 Hz. The vibration coming from the group with a dehiscence close to the oval window decreased more than the others in the frequency range of 400–800 Hz.

4. Discussion

This is, to the best of our knowledge, the first report on the measurement of movements of the umbo, stapes head, and RWM *in vivo* in a guinea pig SSCD model using an LDV. The LDV has become a popular device for measuring sound-induced TM velocity in healthy ears and ears with conductive hearing loss for diagnostic purposes in the clinic [16, 17]. In experimental settings, LDV is also used to measure other membranous movements. For example, the vibration of the RWM associated with acute otitis media is significantly decreased compared to that in the healthy ears of guinea pigs [15]. However, no prior study has reported dynamic behavioral changes in the umbo, the stapes head, and the RWM in association with the SSCD animal model *in vivo*.

Previous studies have suggested a third window hypothesis for the SSCD syndrome. Briefly, the vibration of the stapes footplate would induce motion of the endolymph in the bony semicircular canal when a third window exists [6, 18]. Although the third-window hypothesis is useful for explaining our experimental results and many symptoms observed in patients with SSCD syndrome, it is unclear how it resolves the vast variability in symptoms in SSCD patients mechanistically. Some SSCD patients show debilitating vestibular symptoms, such as a severe sound-induced or pressure-induced vertigo with normal hearing; others have hearing loss, such as conductive, sensorineural, or mixed, with no significant vestibular symptoms; and some patients seem to have a combination of vestibular and auditory symptoms [3, 6–8, 19, 20]. What is the mechanistic basis for these different clinical symptoms? Are the varying sizes and locations of the dehiscences in SCD responsible for the different hearing and vestibular symptoms? A clinical study found no significant association between the size or location of the dehiscence and the audiogram pattern or individual findings in 27 patients (34 ears) [21]. However, Yuen et al. reported that an ABG was seen consistently at low frequencies when the dehiscence was larger than 3 mm and that the size of the average ABG correlated with the size of the dehiscence [22]. Sone et al. evaluated five ears with pathological third-window lesions. Contrast-enhanced magnetic resonance imaging (MRI) revealed that four had endolymphatic hydrops (EH), which might create auditory or vestibular symptoms [23].

To clarify this phenomenon, dehiscences of various sizes and locations along the superior semicircular canal were made in guinea pigs. Then, at various locations in the ear, we measured the vibration resulting from application stimuli of various frequencies using LDV. In our experiment, we found that animals with larger dehiscences (0.5×1.0 mm) showed larger effects on inner ear impedance than those with smaller dehiscences (0.5×0.5 mm). In investigating the effects of dehiscence location on the symptoms, we found that a dehiscence close to the oval window produced more effects on the inner ear system than a dehiscence that was further away. This result is similar to that of a previous three-dimensional finite-element model of a human ear study, which showed the importance of the width of the dehiscence closest to the oval window [24]. In clinical SSCD patients, various circumstances affect hearing and vestibular symptoms, not only the size and location of the dehiscence. Furthermore, in our guinea pig SSCD model, there was some energy leakage from the third window created, in the

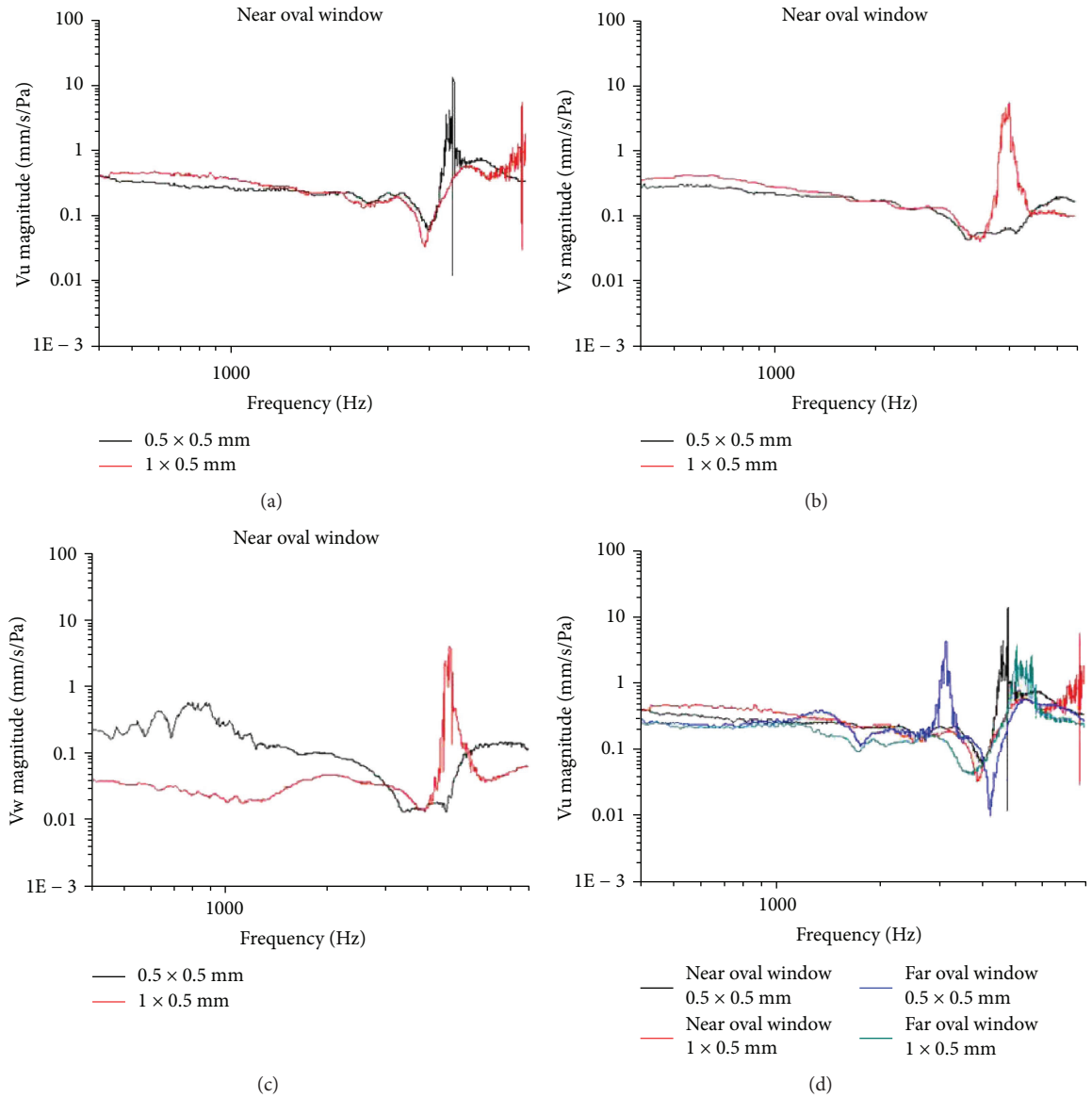

Figure 5: Effects of SSCD with different sizes and locations on the movement of the tympanic membrane, stapes head, and RWM by LDV measurements presurgery and postsurgery SSCD. (a) Vibration of the tympanic membrane (Vu) in the groups with different sizes of dehiscence (0.5 × 0.5 mm and 1.0 × 0.5 mm) near the oval window. Vu in the group with the larger dehiscence (1.0 × 0.5 mm; red line) was stronger than in the group with the smaller dehiscence (0.5 × 0.5 mm; black line), in the range of 500–1000 Hz ($P < 0.05$). (b) Vibration of the stapes head (Vs) in groups with different sizes of dehiscence (0.5 × 0.5 mm and 1.0 × 0.5 mm) near the oval window. Vs in the group with the larger dehiscence (1.0 × 0.5 mm; red line) was stronger than in the group with the smaller dehiscence (0.5 × 0.5 mm; black line), in the range of 400–1000 Hz ($P < 0.05$). (c) Vibration of the round window (Vw) in groups with different sizes of dehiscence (0.5 × 0.5 mm and 1.0 × 0.5 mm) near the oval window. Vw in the group with the larger dehiscence (1.0 × 0.5 mm; red line) was weaker than in the group with the smaller dehiscence (0.5 × 0.5 mm; black line), in the range of 400–2000 Hz ($P < 0.001$). (d) Vibration of the tympanic membrane in the groups with different sizes of dehiscence located at different points ($n = 6$ in each group). Vibration in the group with the larger dehiscence (1.0 × 0.5 mm; red line) was stronger than in the group with the smaller dehiscence (0.5 × 0.5 mm; black line) near the oval window ($P < 0.05$) in the range of 500–1000 Hz. Vibration in the group with the smaller dehiscence (0.5 × 0.5 mm; black line) near the oval window was stronger than in the groups with larger (green line) or small dehiscences (blue line) far from the oval window ($P < 0.05$) in the range of 400–800 Hz. There were no statistically significant differences between the groups with different sized dehiscences away from the oval window ($P > 0.05$).

range of frequencies of 300–1500 Hz, which presented as increased Vu, Vs, and Vd, as well as decreased Vw, resulting in a decreased inner ear impedance in the range of 300–3000 Hz, consistent with the hypothesis that a dehiscence acts as a mobile third window, in addition to the oval and round windows, providing a pathway through which a fluid-motion wave can be shunted away from the cochlea into the SSC. After patching the fenestration, the increased

Vu, Vs, and Vd showed offsets, and simultaneously, Vw increased back to almost normal. One limitation of our study is that we did not measure changes in vestibular function in this model with fenestration and after patching the fenestration. Our aim is to further explore the hearing loss mechanism *in vivo* in this animal model and determine whether it is related to the decrease in inner ear impedance. Furthermore, it remains difficult to evaluate and quantify vestibular symptoms fully using present devices with this animal model.

According to clinical auditory symptoms, many studies have concluded that typical patients demonstrate low-frequency conductive hearing loss, which can be rectified after surgery [3, 9, 17, 25–27]. Our *in vivo* SSCD model demonstrated the same phenomenon. In our experiment, we also found that the ABR thresholds increased after the dehiscence was created at low frequencies, namely, 250, 500, 1000, and 2000 Hz, and particularly at 250, 500, and 1000 Hz with the dehiscence 1.0×0.5 mm and at 1000 Hz with the dehiscence 1.0×0.5 mm close to the oval window (significant increase). These ABR threshold increases all showed offsets after the fenestrations close to the oval window were repaired surgically. This could be explained by the presence of a third window with decreased cochlear impedance due to energy leakage. After the fenestration of the SSC was patched, the third window was eliminated and the fluid motion in the SSC reverted to normal.

In conclusion, the presence of SSCD, behaving as a third window in the inner ear, could cause energy leakage during sound transmission, thus lowering inner ear impedance, resulting in corresponding cochlear symptoms. The size and location of the dehiscence appear to be important in producing differential effects in the pathology.

Conflicts of Interest

The authors declare no conflicts of interest.

Authors' Contributions

Bu-Sheng Tong and Zi-Yu He contributed equally to this work.

Acknowledgments

The authors are thankful to other lab members for their continued support and encouragement. This study was supported by the National Natural Science Foundation of China (NSFC) Grant nos. 81420108010, 81771077, 81570920, 81370022, and 81000413 and the Key Project of Chinese National Programs (2016YFC0905200, 2016YFC0905202), and Dong-Dong Ren was supported by the Training Program of the Excellent Young Talents of the Shanghai Municipal Health System (Grant no. XYQ2013084) and the "Zhuo-Xue Plan" of Fudan University. Ya-Sheng Yuan was supported by the Training Program of Outstanding Academic Leaders of Shanghai Municipal System of Health and Family Planning(Grant no. 2017BR057). Dr Ya-Sheng Yuan performed the experiment and revised the manuscript.

Supplementary Materials

S1: whole-mount immunostaining of cochlear basement membrane in the surgically prepared guinea pigs (dehiscence close to the oval window with a size of 0.5×0.5 mm), with phalloidin (green), peripherin (red), and Ctbp2 (blue) in the apical (A, D, and G), middle (B, E, and H), and mid-basal (C, F, and I) turns of the cochlear, which showed the normal structure of hair cells, neural nerves, and synapses. *(Supplementary Materials)*

References

[1] L. B. Minor, D. Solomon, J. S. Zinreich, and D. S. Zee, "Sound- and/or pressure-induced vertigo due to bone dehiscence of the superior semicircular canal," *Archives of Otolaryngology – Head & Neck Surgery*, vol. 124, no. 3, pp. 249–258, 1998.

[2] J. P. Carey, L. B. Minor, and G. T. Nager, "Dehiscence or thinning of bone overlying the superior semicircular canal in a temporal bone survey," *Archives of Otolaryngology – Head & Neck Surgery*, vol. 126, no. 2, pp. 137–147, 2000.

[3] A. A. Mikulec, M. J. McKenna, M. J. Ramsey et al., "Superior semicircular canal dehiscence presenting as conductive hearing loss without vertigo," *Otology & Neurotology*, vol. 25, no. 2, pp. 121–129, 2004.

[4] S. N. Merchant, J. J. Rosowski, and M. J. McKenna, "Superior semicircular canal dehiscence mimicking otosclerotic hearing loss," *Advances in Oto-Rhino-Laryngology*, vol. 65, pp. 137–145, 2007.

[5] A. Wenzel, B. K. Ward, E. K. Ritzl et al., "Intraoperative neuromonitoring for superior semicircular canal dehiscence and hearing outcomes," *Otology & Neurotology*, vol. 36, no. 1, pp. 139–145, 2015.

[6] J. J. Rosowski, J. E. Songer, H. H. Nakajima, K. M. Brinsko, and S. N. Merchant, "Clinical, experimental, and theoretical investigations of the effect of superior semicircular canal dehiscence on hearing mechanisms," *Otology & Neurotology*, vol. 25, no. 3, pp. 323–332, 2004.

[7] S. N. Merchant and J. J. Rosowski, "Conductive hearing loss caused by third-window lesions of the inner ear," *Otology & Neurotology*, vol. 29, no. 3, pp. 282–289, 2008.

[8] J. E. Songer and J. J. Rosowski, "A mechano-acoustic model of the effect of superior canal dehiscence on hearing in chinchilla," *The Journal of the Acoustical Society of America*, vol. 122, no. 2, pp. 943–951, 2007.

[9] G. P. Rajan, M. R. Leaper, L. Goggin, M. D. Atlas, R. Boeddinghaus, and R. K. Eikelboom, "The effects of superior semicircular canal dehiscence on the labyrinth: does size matter?," *Otology & Neurotology*, vol. 29, no. 7, pp. 972–975, 2008.

[10] J. Attias, B. I. Nageris, R. Shemesh, J. Shvero, and M. Preis, "Superior canal dehiscence effect on hearing thresholds: animal model," *Otolaryngology and Head and Neck Surgery*, vol. 145, no. 4, pp. 648–653, 2011.

[11] J. E. Songer and J. J. Rosowski, "A superior semicircular canal dehiscence-induced air-bone gap in chinchilla," *Hearing Research*, vol. 269, no. 1-2, pp. 70–80, 2010.

[12] M. E. F. Niesten, C. Stieger, D. J. Lee et al., "Assessment of the effects of superior canal dehiscence location and size on intracochlear sound pressures," *Audiology & Neuro-Otology*, vol. 20, no. 1, pp. 62–71, 2015.

[13] R. L. Goode, G. Ball, S. Nishihara, and K. Nakamura, "Laser Doppler vibrometer (LDV)–a new clinical tool for the otologist," *The American Journal of Otology*, vol. 17, no. 6, pp. 813–822, 1996.

[14] K. R. Whittemore Jr, S. N. Merchant, B. B. Poon, and J. J. Rosowski, "A normative study of tympanic membrane motion in humans using a laser Doppler vibrometer (LDV)," *Hearing Research*, vol. 187, no. 1-2, pp. 85–104, 2004.

[15] R. Z. Gan, D. Nakmali, and X. Zhang, "Dynamic properties of round window membrane in guinea pig otitis media model measured with electromagnetic stimulation," *Hearing Research*, vol. 301, pp. 125–136, 2013.

[16] A. Jakob, M. Bornitz, E. Kuhlisch, and T. Zahnert, "New aspects in the clinical diagnosis of otosclerosis using laser Doppler vibrometry," *Otology & Neurotology*, vol. 30, no. 8, pp. 1049–1057, 2009.

[17] J. J. Rosowski, H. H. Nakajima, and S. N. Merchant, "Clinical utility of laser-Doppler vibrometer measurements in live normal and pathologic human ears," *Ear and Hearing*, vol. 29, no. 1, pp. 3–19, 2008.

[18] W. L. Bi, R. Brewster, D. Poe et al., "Superior semicircular canal dehiscence syndrome," *Journal of Neurosurgery*, vol. 127, no. 6, pp. 1268–1276, 2017.

[19] F. L. Chi, D. D. Ren, and C. F. Dai, "Variety of audiologic manifestations in patients with superior semicircular canal dehiscence," *Otology & Neurotology*, vol. 31, no. 1, pp. 2–10, 2010.

[20] E. O. Teixeira and M. T. Fonseca, "Superior semicircular canal dehiscence syndrome without vestibular symptoms," *International Archives of Otorhinolaryngology*, vol. 18, no. 2, pp. 210–212, 2014.

[21] A. Pfammatter, V. Darrouzet, M. Gärtner et al., "A superior semicircular canal dehiscence syndrome multicenter study: is there an association between size and symptoms?," *Otology & Neurotology*, vol. 31, no. 3, pp. 447–454, 2010.

[22] H. W. Yuen, R. Boeddinghaus, R. H. Eikelboom, and M. D. Atlas, "The relationship between the air-bone gap and the size of superior semicircular canal dehiscence," *Otolaryngology and Head and Neck Surgery*, vol. 141, no. 6, pp. 689–694, 2009.

[23] M. Sone, T. Yoshida, K. Morimoto, M. Teranishi, T. Nakashima, and S. Naganawa, "Endolymphatic hydrops in superior canal dehiscence and large vestibular aqueduct syndromes," *Laryngoscope*, vol. 126, no. 6, pp. 1446–1450, 2016.

[24] N. Kim, C. R. Steele, and S. Puria, "Superior-semicircular-canal dehiscence: effects of location, shape, and size on sound conduction," *Hearing Research*, vol. 301, pp. 72–84, 2013.

[25] L. B. Minor, J. P. Carey, P. D. Cremer, L. R. Lustig, S. O. Streubel, and M. J. Ruckenstein, "Dehiscence of bone overlying the superior canal as a cause of apparent conductive hearing loss," *Otology & Neurotology*, vol. 24, no. 2, pp. 270–278, 2003.

[26] C. J. Limb, J. P. Carey, S. Srireddy, and L. B. Minor, "Auditory function in patients with surgically treated superior semicircular canal dehiscence," *Otology & Neurotology*, vol. 27, no. 7, pp. 969–980, 2006.

[27] L. B. Minor, "Clinical manifestations of superior semicircular canal dehiscence," *Laryngoscope*, vol. 115, no. 10, pp. 1717–1727, 2005.

Hindawi
Neural Plasticity
Volume 2018, Article ID 9425725, 6 pages
https://doi.org/10.1155/2018/9425725

Research Article

Autosomal Recessive Congenital Sensorineural Hearing Loss due to a Novel Compound Heterozygous PTPRQ Mutation in a Chinese Family

Xia Wu,[1] Shan Wang,[2] Sen Chen,[1] Ying-ying Wen,[1] Bo Liu,[1] Wen Xie,[1] Dan Li,[1] Lin Liu,[2] Xiang Huang,[3] Yu Sun,[1] and Wei-jia Kong[1,3,4]

[1]*Department of Otorhinolaryngology, Union Hospital, Tongji Medical College, Huazhong University of Science and Technology, Wuhan 430022, China*
[2]*Department of Obstetrics and Gynecology, Union Hospital, Tongji Medical College, Huazhong University of Science and Technology, Wuhan 430022, China*
[3]*Institute of Otorhinolaryngology, Union Hospital, Tongji Medical College, Huazhong University of Science and Technology, Wuhan 430022, China*
[4]*Hubei Medical Center of Otorhinolaryngology-Head and Neck, Wuhan 430022, China*

Correspondence should be addressed to Yu Sun; sunyu@hust.edu.cn and Wei-jia Kong; entwjkong@hust.edu.cn

Received 23 January 2018; Accepted 31 March 2018; Published 19 April 2018

Academic Editor: Hai Huang

PTPRQ gene, encoding protein tyrosine phosphatase receptor Q, is essential for the normal maturation and function of hair bundle in the cochlea. Its mutations can cause the defects of stereocilia in hair cell, which lead to nonsyndromic sensorineural hearing loss. Using next-generation sequencing and Sanger sequencing method, we identified a novel compound heterozygous missense mutation, c.4472C>T p.T1491M (maternal allele) and c.1973T>C p.V658A (paternal allele), in PTPRQ gene. The two mutations are the first reported to be the cause of recessively inherited sensorineural hearing loss. Hearing loss levels and progression involved by PTPRQ mutations among the existing cases seem to be varied, and the relationship between genotypes and phenotypes is unclear. Our data here further prove the important role of PTPRQ in auditory function and provide more information for the further mechanism research of PTPRQ-related hearing loss.

1. Introduction

Hearing loss is one of the most common sensory disabilities in humans. According to the latest data of WHO, there are 360 million people—over 5% of the world's population—suffering from hearing loss, with 32 million are children (http://www.who.int/mediacentre/factsheets/fs300/en/). Genetic factors are the major cause of congenital sensorineural hearing loss (SNHL). Approximately 80% of nonsyndromic genetic hearing loss is autosomal recessive inheritance [1]. Currently, 64 genes for autosomal recessive nonsyndromic SNHL have been mapped (http://hereditaryhearingloss.org).

PTPRQ gene, encoding protein tyrosine phosphatase receptor Q, is one of the latest identified causes accounting for nonsyndromic SNHL. It is assigned DFNB84 locus on chromosome 12q21.31 and comprised of 58 exons [2]. The PTPRQ protein, localized in the basal region of the stereocilia membrane, is one of the membrane proteins which composed of 2299 amino acids. It has been reported that PTPRQ may have key roles in hair cells: establishing the membrane at the base of the stereocilia, regulating actin dynamics, and tethering the stereocilia membrane to the cytoskeleton with Myosin VI [3–5]. It is known to be required for the development of hair bundles, regulation of normal maturations, and formation of shaft connectors [6].

To date, there are eight families with inherited recessive mutations of PTPRQ which have been published [2, 7–10]. Identifications of PTPRQ mutations could be helpful to establish a better understanding of the relationship between PTPRQ and SNHL. Here, we present a Chinese family with congenital SNHL caused by a novel compound heterozygous PTPRQ mutation.

2. Materials and Methods

2.1. Family Description. This Chinese family, named Family 1, is a two-generation family associated with autosomal recessive nonsyndromic SNHL (Figure 1). The affected member II1, a 4-year and 2-month-old child, was diagnosed with congenital SNHL. The other individuals (I1, I2, and II2) had no history of hearing impairment. The child who was born in Hubei Province failed the newborn hearing screening and was diagnosed as congenital sensorineural hearing loss.

2.2. Audiological Examination. Visual reinforcement audiometry (VRA) was performed after the patient underwent otoscopic examination in our department. Degree of hearing loss was assessed by using pure tones. The stimuli were produced in the frequencies of 0.25, 0.5, 1, 2, 4, and 6 kHz. By using the stimulus-reply-visual reinforcement conditioning, the minimum response level was obtained in the lowest intensity which the child responded.

2.3. DNA Preparation. Peripheral venous blood samples from all the family members were obtained for genetic analysis. Genomic DNA was extracted from the blood samples using QIAamp DSP DNA Blood Mini Kit (61104, Qiagen Inc., Germany) according to kit's protocol.

2.4. Next-Generation Sequencing + Sanger Sequencing. The target deafness-related gene capture and next-generation sequencing + Sanger sequencing were performed by MyGenostics Inc. (Beijing, China). First, the genomic DNA was fragmented to special size about 350–400 base pair for library construction. End-repair and Illumina adapter ligation were taken according to the Illumina protocols. After PCR amplification, target DNA fragments were captured with biotinylated single-strand DNA capture probe (MyGenostics, MD, USA) by hybridization. The target gene fragments were enriched, and then high-throughput sequencing was performed using Illumina HiSeq2000 Analyzer for automated cycles per read. Primary data were generated using TrimGalore software (version 0.4.3). Reads were matched to NCBI37/hg19 using BWA program. Previously identified SNPs were annotated using CCDS, human genome database (HG19), and dbSNP (v138). SIFT and POLYPHEN2 were utilized to predict the function of SNP-affected protein.

2.5. Structural-Based Model Building and Analysis. The molecular homology modeling of the human wild type and mutations was built up by SWISS-MODEL (http://www.swissmodel.expasy.org/). The complete protein sequence of human PTPRQ is available in the NCBI GenBank (NP_001138498.1). Data were showed by JavaScript Protein Viewer.

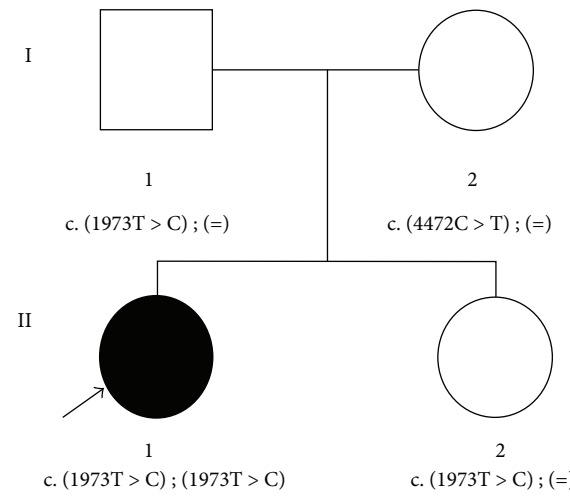

Figure 1: Pedigree of the affected Family 1 with congenital SNHL. Sanger sequencing analysis showed that patient II1 had the compound heterozygous mutation (c.[1973T>C]; c.[4472C>T]), and the parents and sister had the heterozygous mutation. The patient is denoted in black. [=] means wild type.

3. Results

3.1. Mutation Detection and Analysis. Mutations in mitochondria and miRNA regions were excluded. After aligning to the human reference genome (GRCh37/hg19), these mutations corresponded to c.4472C>T and c.1973T>C, occurring in exon26 and exon13 of PTPRQ. The c.4472C>T leads to a single substitution within the fibronectin type III (FNIII) domain, from threonine to methionine (p.T1491M), and the other, c.1973T>C, leads to a single substitution (valine to alanine; p.V658A) within the FNIII domain. SIFT (http://sift.jcvi.org/) and POLYPHEN2 (http://genetics.bwh.harvard.edu/pph2/) were used to analyze the amino acid substitutions of p.T1491M and p.V658A. Both programs predicted these two mutations to be deleterious, which means they probably damage and affect protein functions. The sequencing results showed that the two parents were heterozygous carriers of c.4472C>T (maternal allele) and c.1973T>C (paternal allele), which demonstrated the compound heterozygous cosegregating mutation with the phenotype in II1 (Figure 2). The frequency of c.4472C>T mutation is 0.0016 in the East Asian population of EXAC database as well as 0.0002 in 1000 Genome Project. The c.1973T>C mutation rate accounts for 0.0222 in 1000 Genome Project. The frequency of c.1973T>C mutation was not found in the East Asian population of EXAC database.

3.2. Structure Modeling. Protein tertiary structures were modelling with SWISS-MODEL (http://www.swissmodel.expasy.or-g/), which predict the sequence homology. The p.T1491M protein model, covering the target sequence (residues 1163–1564), was constructed based on the receptor-type protein tyrosine phosphatase S (PDB ID: 4pbx.1.A).

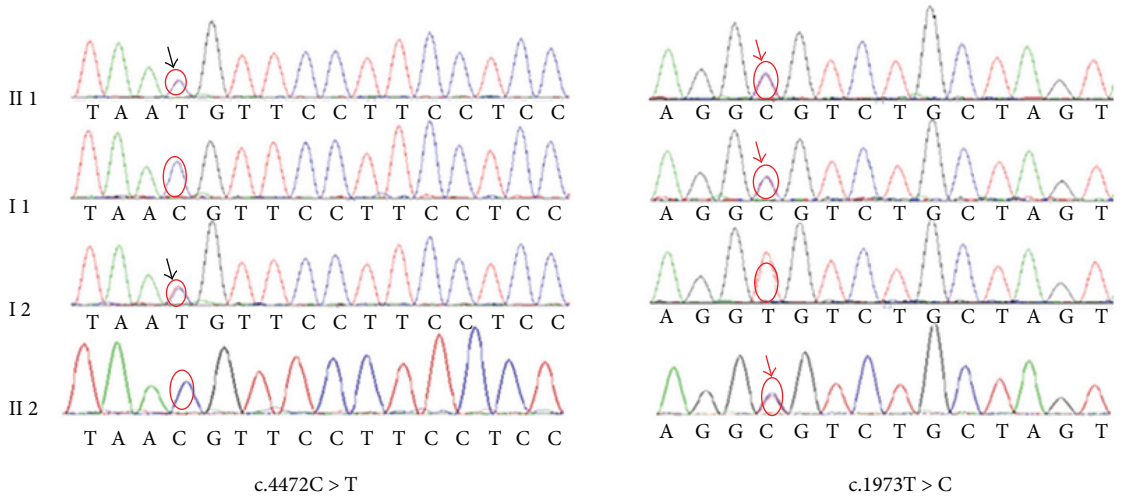

Figure 2: Electropherogram analysis of PTPRQ in Family 1. Electropherogram analysis showed that compound heterozygous mutations (c.4472C>T, black arrows and c.1973T>C, red arrows) cosegregate with the phenotype.

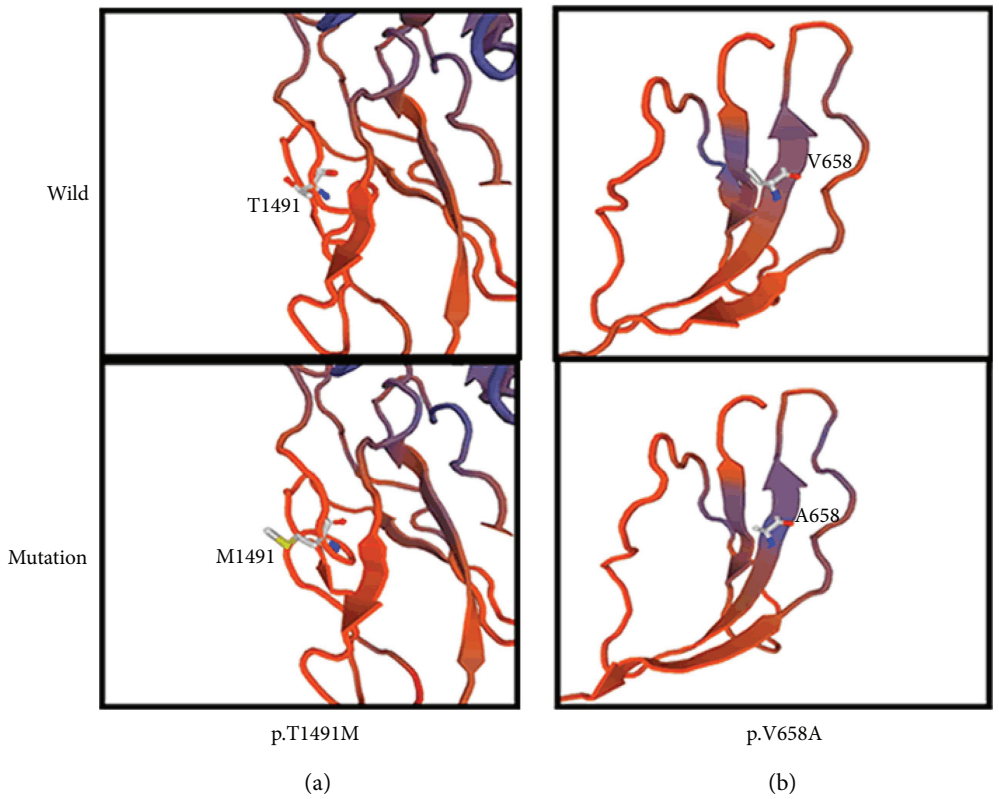

Figure 3: Protein molecular models of wild types and PTPRQ mutations. (a) The mutation protein M1491 has a different side chain to the wild-type protein T1491. (b) The wild-type protein has a longer side chain than the mutation protein A658.

Sequence identity between the target and template was 25.78%. As shown in Figure 3(a), the mutation probably affected the amino acid side chain through the substitution of threonine acid to methionine. The p.V658A protein model, covering the target sequence (residues 618–880), was constructed based on the receptor-type protein tyrosine phosphatase delta (PDB ID: 4yh7.1.A). Sequence identity between the target and template was 28.69%. As shown in Figure 3(b), it predicted that the mutation affected the amino acid side chain by the substitution of valine acid to alanine.

3.3. Clinical Data. Patient II1 is a 4-year and 2-month-old girl. Newborn hearing screening was failed at the age of 42 days. She had been referred to the Department of Otorhinolaryngology, Wuhan Union Hospital, for hearing

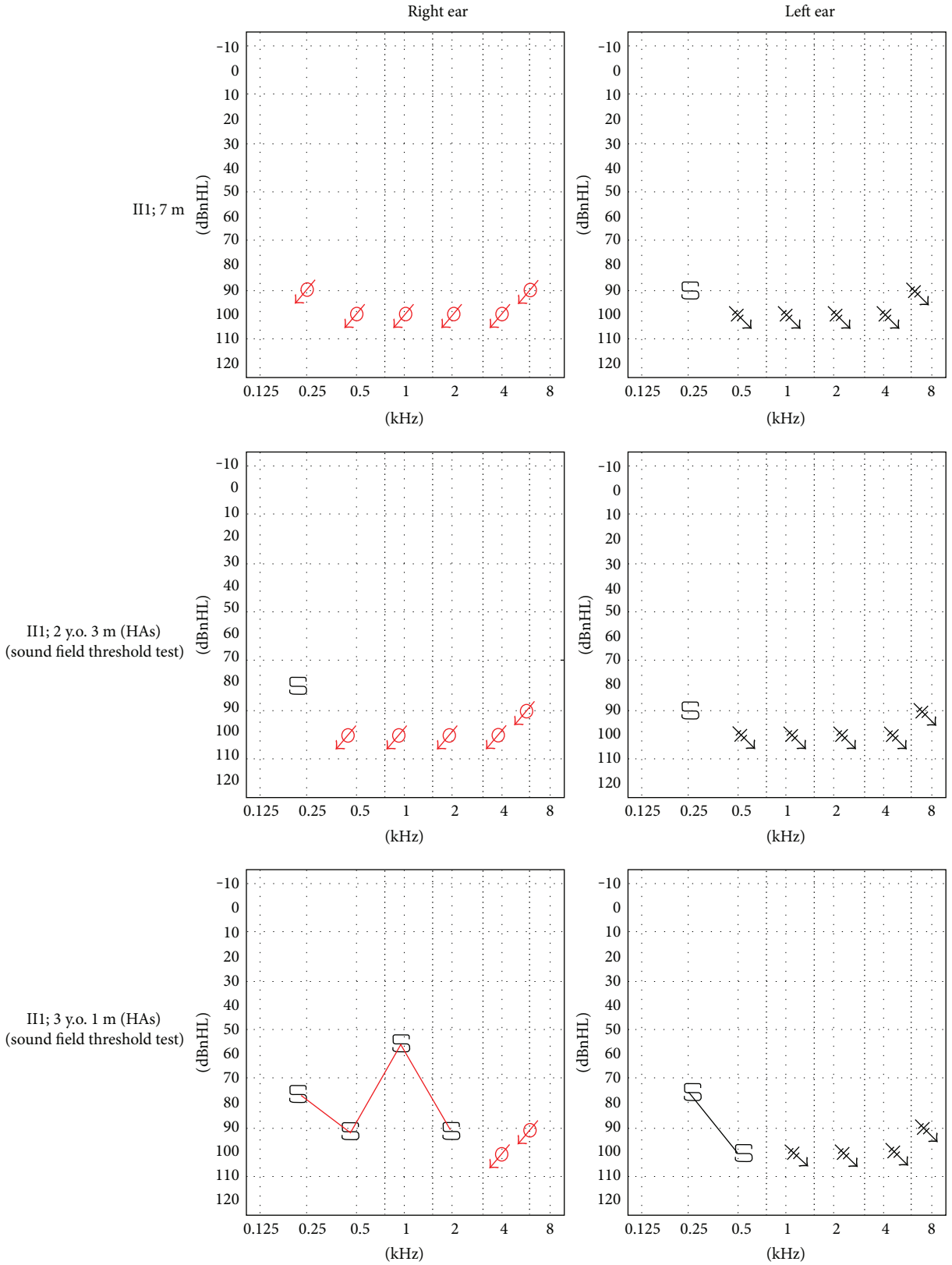

Figure 4: Pure tone audiometry. Visual reinforcement audiometry showed severe-profound SNHL at month 7. After hearing aids (HAs), sound field threshold test showed improvement of hearing levels.

examinations when 3 months. 40 Hz auditory steady-state evoked potential showed that the thresholds were 85 dBnHL at 500 Hz and 100 dBnHL at 1000 Hz of the left ear and 95 dB at 500 Hz and 95 dB at 1000 Hz of the right ear. Auditory brainstem audiometry (ABR) showed that reproducible wave cannot be elicited at 105 dBnHL bilaterally. The diagnosis of congenital severe-profound sensorineural hearing loss (SNHL) was made. Her parents took her for the hearing compensation in our hospital after four months. A visual reinforcement audiometry (VRA), computed tomography (CT) scan of temporal bone, and magnetic resonance (MR) imaging were performed. The VRA showed no response of both ears in all frequencies (Figure 4). The CT showed narrow of both internal auditory canal without any malformation of middle ear and osseous labyrinth. The MR showed that bilateral cochlear nerves cannot be identified well, considering a neurological maldevelopment, while there was no abnormality of the membranous labyrinth. She was consequently fitted for bilateral hearing aids. Her hearing was followed up in the following years (Figure 4). VRA revealed response of 90 dBnHL at 250 Hz of the left ear and 80 dBnHL at 250 Hz of the right ear at age 2 years and 3 months old. Acoustic immittance testing was within the normal limit. When she was 3 years and 1 month old, VRA showed response of 75 dBnHL at 250 Hz of the left ear and 60 dBnHL at 1000 Hz of the right ear. She had no balance manifestation, tinnitus, or vertigo.

4. Discussion

Hair cells are the essential sound receptors of auditory system. The hair bundle, comprised of about 100 actin-filled stereocilia, on the top of hair cells can help the sound transduction from mechanical signal to electrical signal. PTPRQ is a stereociliar membrane protein which belongs to the type III receptor-like protein tyrosine phosphatase (PTPase). It has three domains: the fibronectin type III-(FNIII-) like extracellular domain, the transmembrane domain, and the cytosolic PTPase domain, which have phosphatidylinositol phosphatase activity [11]. The PTPRQ mutant mice showed malformation of shaft connectors and immaturation of cochlear hair bundles which lead to deafness [12]. Here, we identified a novel compound heterozygous cosegregating mutation in the PTPRQ gene, c.4472C>T p.T1491M (maternal allele) and c.1973T>C p.V658A (paternal allele), as a probable cause of autosomal recessive congenital SNHL in a Chinese population by using an approach of next-generation sequencing and Sanger sequencing method. These two mutations have never been reported in previous studies.

There are 9 mutation variants of PTPRQ gene causing SNHL reported until now. They have been identified in different ethnic groups and countries, including c.1285C>T in Palestinian [7]; c.1491T>A in Dutch [2]; c1369A>G in Moroccan [2]; c3125A>G and c.5981A>G in Chinese [8]; c.166C>G, c4046T>C, and c.1261C>T in Japanese [9]; and c.16_17insT and c.2714delA in a Kazakh family of China [10]. Here, novel compound heterozygous mutations in PTPRQ, c.4472C>T and c.1973T>C, were identified by next-generation sequencing + Sanger sequencing method in patient II1. These two substitutions both occur within the extracellular FNIII domains, which can bind ligands like extracellular molecules and proteins [13, 14]. The mutations were predicted to perturb the amino acid side chain, which may interfere FNIII function and the interactions with other molecules and residues. Furthermore, based on the calculation results of SIFT and POLYPHEN2, the substitutions are deleterious and probably damage the protein functions. Although the c.1973T>C mutation rate is a little higher in normal population, which suggests that the pathogenicity is questionable, we cannot rule out the pathogenesis of the compound heterozygous mutations. Further experiments are needed to confirm our findings.

In this study, the patient II1 did not pass the examinations of newborn hearing screening when she was 42 days. In subsequent hearing tests, she went on to exhibit to a series of severe-profound sensorineural hearing loss symptoms. In the past studies, the affected patients had different hearing levels from moderate to profound and different progressions from stable to progressive. In our case, the patient had a severe-profound degree of hearing loss and a stable progression. Based on the results of existing PTPRQ mutation reports, we suspect that there is no obvious correlation between genotype and phenotype. PTPRQ mutation appeared to be liable for the vestibular dysfunction. The patients with PTPRQ mutations always had vertigo or dizziness. Consistent with this manifestation, the $Ptprq^{-/-}$ mice showed defects in the hair bundles of the saccule and ampullae [15]. However, patient II1 in our study had no experience of vestibular dysfunction, which is the same as case 1 reported in Japan [9]. When patient II1 got to be 7 months, the CT and MR revealed a neurological maldevelopment of bilateral cochlear nerves. The relationship between the cochlear nerves abnormality and hearing loss is still not clear. These uncertainties need to be investigated further in animal models. In our case, the patient II1 received bilateral hearing aids at the age of 7 months. Her hearing threshold levels were advanced partly after hearing compensation using hearing aids. Consistent with our result, the hearing level of another patient with PTPRQ mutation was also improved after implantation at the age of 19 [9]. We speculated that hearing therapy might be helpful to the patients with PTPRQ mutations.

In summary, our findings suggest that the novel compound heterozygous PTPRQ mutations, c.4472C>T (p.T1491M) and c.1973T>C (p.V658A), are the cause of congenital SNHL in this family. The identification of additional mutations here further confirms the key role of PTPRQ in hearing function. More precise mechanism researches are needed for a better understanding of the gene.

Ethical Approval

All procedures followed were in accordance with the ethical standards of the responsible committee on human experimentation (Tongji Medical College, Huazhong University

of Science and Technology) and with the Helsinki Declaration of 1975, as revised in 2000 (5).

Consent

Informed consent was obtained from all patients for being included in the study.

Conflicts of Interest

Xia Wu, Shan Wang, Sen Chen, Ying-ying Wen, Bo Liu, Wen Xie, Dan Li, Lin Liu, Xiang Huang, Yu Sun, and Wei-jia Kong declare that they have no conflict of interest.

Authors' Contributions

Xia Wu and Shan Wang contributed equally to this work.

Acknowledgments

The authors thank their families for the participation in this study. This work was supported by the National Nature Science Foundation of China (81470696, 81570923, 81500795, 81500793, and 81000408).

References

[1] C. C. Morton and W. E. Nance, "Newborn hearing screening–a silent revolution," *The New England Journal of Medicine*, vol. 354, no. 20, pp. 2151–2164, 2006.

[2] M. Schraders, J. Oostrik, P. L. M. Huygen et al., "Mutations in *PTPRQ* are a cause of autosomal-recessive nonsyndromic hearing impairment DFNB84 and associated with vestibular dysfunction," *American Journal of Human Genetics*, vol. 86, no. 4, pp. 604–610, 2010.

[3] H. Sakaguchi, J. Tokita, M. Naoz, D. Bowen-Pope, N. S. Gov, and B. Kachar, "Dynamic compartmentalization of protein tyrosine phosphatase receptor Q at the proximal end of stereocilia: implication of myosin VI-based transport," *Cell Motility and the Cytoskeleton*, vol. 65, no. 7, pp. 528–538, 2008.

[4] T. Takenawa and T. Itoh, "Phosphoinositides, key molecules for regulation of actin cytoskeletal organization and membrane traffic from the plasma membrane," *Biochimica et Biophysica Acta (BBA) - Molecular and Cell Biology of Lipids*, vol. 1533, no. 3, pp. 190–206, 2001.

[5] M. Hirono, C. S. Denis, G. P. Richardson, and P. G. Gillespie, "Hair cells require phosphatidylinositol 4,5-bisphosphate for mechanical transduction and adaptation," *Neuron*, vol. 44, no. 2, pp. 309–320, 2004.

[6] A. Oganesian, M. Poot, G. Daum et al., "Protein tyrosine phosphatase RQ is a phosphatidylinositol phosphatase that can regulate cell survival and proliferation," *Proceedings of the National Academy of Sciences of the United States of America*, vol. 100, no. 13, pp. 7563–7568, 2003.

[7] H. Shahin, M. Rahil, A. A. Rayan et al., "Nonsense mutation of the stereociliar membrane protein gene *PTPRQ* in human hearing loss *DFNB84*," *Journal of Medical Genetics*, vol. 47, no. 9, pp. 643–645, 2010.

[8] X. Gao, Y. Su, Y. L. Chen et al., "Identification of two novel compound heterozygous PTPRQ mutations associated with autosomal recessive hearing loss in a Chinese family," *PLoS One*, vol. 10, no. 4, article e0124757, 2015.

[9] N. Sakuma, H. Moteki, H. Azaiez et al., "Novel *PTPRQ* mutations identified in three congenital hearing loss patients with various types of hearing loss," *Annals of Otology, Rhinology & Laryngology*, vol. 124, Supplement 1, pp. 184S–192S, 2015.

[10] Q. Sang, H. Mei, A. Kuermanhan et al., "Identification of a novel compound heterozygous mutation in *PTPRQ* in a DFNB84 family with prelingual sensorineural hearing impairment," *Molecular Genetics and Genomics*, vol. 290, no. 3, pp. 1135–1139, 2015.

[11] M. B. Wright, C. Hugo, R. Seifert, C. M. Disteche, and D. F. Bowen-Pope, "Proliferating and migrating mesangial cells responding to injury express a novel receptor protein-tyrosine phosphatase in experimental mesangial proliferative glomerulonephritis," *The Journal of Biological Chemistry*, vol. 273, no. 37, pp. 23929–37, 1998.

[12] R. J. Goodyear, P. K. Legan, M. B. Wright et al., "A receptor-like inositol lipid phosphatase is required for the maturation of developing cochlear hair bundles," *The Journal of Neuroscience*, vol. 23, no. 27, pp. 9208–9219, 2003.

[13] I. D. Campbell and C. Spitzfaden, "Building proteins with fibronectin type III modules," *Structure*, vol. 2, no. 5, pp. 333–337, 1994.

[14] D. Craig, M. Gao, K. Schulten, and V. Vogel, "Tuning the mechanical stability of fibronectin type III modules through sequence variations," *Structure*, vol. 12, no. 1, pp. 21–30, 2004.

[15] R. J. Goodyear, S. M. Jones, L. Sharifi, A. Forge, and G. P. Richardson, "Hair bundle defects and loss of function in the vestibular end organs of mice lacking the receptor-like inositol lipid phosphatase PTPRQ," *The Journal of Neuroscience*, vol. 32, no. 8, pp. 2762–2772, 2012.

Hindawi
Neural Plasticity
Volume 2018, Article ID 5616930, 13 pages
https://doi.org/10.1155/2018/5616930

Research Article

Specific Influences of Early Acoustic Environments on Cochlear Hair Cells in Postnatal Mice

Aoshuang Chang,[1,2] **Peng Chen**,[1] **Shasha Guo**,[1] **Nana Xu**,[1] **Wenlu Pan**,[1] **Hongzheng Zhang**,[3] **Cuixian Li**,[1,4] **and Jie Tang**[1,4]

[1]*Department of Physiology, School of Basic Medical Sciences, Southern Medical University, Guangzhou, China*
[2]*School of Basic Medical Sciences, Guizhou Medical University, Guiyang, China*
[3]*Department of Otolaryngology Head and Neck Surgery, Zhujiang Hospital, Southern Medical University, Guangzhou, China*
[4]*Institute of Mental Health, Southern Medical University, Guangzhou, China*

Correspondence should be addressed to Cuixian Li; licxian@smu.edu.cn and Jie Tang; jietang@smu.edu.cn

Received 22 January 2018; Revised 5 March 2018; Accepted 21 March 2018; Published 16 April 2018

Academic Editor: Renjie Chai

The auditory function develops and matures after birth in many mammalian species. After hearing onset, environmental sounds exert profound and long-term effects on auditory functions. However, the effects of the acoustic environment on the functional development of the peripheral auditory system, especially the cochlear sensory hair cells, are still unclear. In the present study, we exposed mouse pups to frequency-enriched acoustic environments in postnatal days 0–14. The results indicated that the acoustic environment significantly decreased the threshold of the auditory brainstem response in a frequency-specific manner. Compared with controls, no difference was found in the number and alignment of inner and outer hair cells or in the length of hair bundles after acoustic overstimulation. The expression and function of prestin, the motor protein of outer hair cells (OHCs), were specifically increased in OHCs activated by acoustic stimulation at postnatal days 7–11. We analyzed the postnatal maturation of ribbon synapses in the hair cell areas. After acoustic stimulation, the number of ribbon synapses was closer to the mature stage than to the controls. Taken together, these data indicate that early acoustic exposure could promote the functional maturation of cochlear hair cells and the development of hearing.

1. Introduction

Acoustic information carried by sound waves is transduced into electric signals by cochlear hair cells (HCs) and transmitted to spiral ganglion neurons (SGNs) and central auditory nuclei. In many mammalian species, auditory function develops and matures after birth. In rodents, the spikes of cortical neurons in response to acoustic stimulation are initially observed after postnatal days 10 to 12 (P10–P12), which is defined as the "hearing onset" [1–3]. During a brief postnatal period around the hearing onset, the structure and function of the cochlea and central auditory system undergo marked changes [3–5]. The auditory system is susceptible to environmental sounds during this short period. Early exposure to an acoustic environment can quickly change the sensitivity and frequency selectivity of neurons at many levels along the auditory pathway [3, 5]. Early exposure to environmental sounds modulates the innervations and response properties of neurons in the auditory pathway [5–9]. It is well recognized that these neuronal mechanisms are involved in the plasticity induced by early exposure to environmental sounds in the auditory system. As all input signals for neural activity originated from HCs, which are the peripheral sensory cells of the auditory system, any inference on HCs may have a major effect on the development of the auditory function. However, little is known about whether early experience influences the development of cochlear HCs.

The maturation of the cochlea, which is the peripheral auditory system, is also completed after birth. The mechanoelectrical transduction (MET), electromotility, and synapse transmission are fundamental functions of HCs and are

critical for normal hearing [10]. In murines, the pattern of hair bundles is formed before postnatal day 6 [11–14]. The functional development of MET is completed at the same age [4, 11]. The electromotility of outer hair cells (OHCs) are first detected at P6 and are gradually developed after that [15, 16]. Meanwhile, the maturation of both efferent and afferent innervations is also established after birth [17]. These findings imply that the HCs have the capability of responding to sound signals at the early postnatal stage. We are curious about whether the sound environment could elicit any morphological or functional changes of hair cells during this period.

In the present study, we aimed to clarify whether the environmental sound can regulate the developmental processes of these HC functions. We applied sound exposure at different frequencies to stimulate the mouse pups starting at P0–P14 and found that the auditory brainstem responses (ABRs) were enhanced by acoustic stimulation in a frequency-specific manner. No change was observed in the development of stereocilia in the HCs. The sound enhanced the expression and function of prestin, a motor protein on the outer hair cells, and the refinement of ribbon synapses of the inner hair cells (IHCs). Our results suggest that early exposure to acoustic environments could promote the functional maturation of cochlear HCs and the development of hearing.

2. Material and Methods

All experiments were performed in accordance with the Chinese Prevention of Cruelty to Animals Act, and approval was obtained from the Southern Medical University Laboratory Animal Center.

2.1. Animal Care and Early Acoustic Stimulation. Adult C57BL/6 mice of equal sex and pups ranging in age from P0 to P14 were used in this study. The control animals were housed in a normal sound environment (with environmental sound level of 40–50 dB sound pressure level (SPL)) under a 12 h light/dark schedule and had free access to water and a standard diet. For the treated group, litters of P0 and their mothers were housed in a soundproof chamber for 14 days. A 12 h light/dark schedule was established in the soundproof chamber. For each litter, one of three different acoustic environments was used to stimulate the mouse pups: narrow band (0–2 kHz) noise burst, 16 kHz, and 32 kHz tone bursts. The sounds were delivered by a loudspeaker (ES1, Tucker-Davis Technologies, Alachua, FL, USA) placed on the ceiling of the chamber, ~40 cm away from the animals. The mouse litters were subjected to an alternation of 250 ms long noise or tone bursts and 250 ms quiet intervals 24 h/day for 14 days at a sound level of 70 dB SPL. The stimulus and environmental sound levels were calibrated by a B&K measuring amplifier through a B&K 4135 microphone placed in the center of the chamber. No distortion or significant harmonic signal was found in the chamber when a stimulus was delivered. Compared with the control group, no obvious weight loss was observed in the sound-stimulated litters, indicating normal lactation.

2.2. Auditory Brainstem Response (ABR) Recording. Animals were anesthetized with an intraperitoneal injection of sodium pentobarbital (22 mg/kg for pups and 30 mg/kg for adults) and subsequently placed on an antivibration table in a soundproof room. During ABR recording, a heating pad was used to maintain the animal's body temperature at 37.5°C. By using fine scissors, a 1-2 mm incision ventroposterior to the external pinna was made to place the indifference or ground electrode. A subdermal needle electrode (recording electrode) was located over the skull vertex. Tone bursts (1 ms rise/fall, 3 ms plateau) of various frequencies (1, 2, 4, 8, 16, 24, and 32 kHz) and intensities (0–90 dB SPL at 5 dB intervals) were delivered using a loudspeaker (ES1, Tucker-Davis Technologies, Alachua, FL, USA) placed 10 cm in front of the animal. The sound levels were calibrated by a B&K measuring amplifier through a B&K 4135 microphone placed 10 cm in front of the speaker. The tone bursts with different frequency and amplitude were controlled by TDT System 3 (Tucker-Davis Technologies, Alachua, FL, USA) and were delivered in a randomized sequence. Each frequency-amplitude combination was repeated 256 times at a rate of 10 bursts/s. The ABR signals were amplified, filtered (100–1000 Hz), averaged using TDT System 3, and recorded using BioSigRP software (Tucker-Davis Technologies, Alachua, FL, USA). Hearing thresholds were defined as the minimum sound intensity at which averaged waveform II could be detected. Data were stored for offline analysis. The entire recording for one animal spanned over approximately 60 min.

2.3. Tissue Dissection and Immunostaining. After physiological experiments, the mouse was sacrificed using CO_2 and the skull was opened along the sagittal midline. The brain was removed and the inner ears were isolated from the temporal bones and transferred into a Petri dish filled with ice-cold L-15 medium (Invitrogen, Carlsbad, CA, USA). Under the dissection microscope, the bony capsule of the cochlea was removed. The organ of Corti and associated stria vascularis were unwrapped from the modiolus. By holding the basal portion of the stria vascularis, the organ of Corti was separated from the stria vascularis completely by unwinding slowly from base-to-apex. The apical, middle, and basal turns of the organ of Corti were cut by using fine scissors. The segments of the organ of Corti were fixed in 4% paraformaldehyde for 4 h and decalcified in 6% ethylenediaminetetraacetic acid (EDTA) for 3 additional days. Tissues were blocked with 10% goat serum at 27°C for 30 min after permeabilization using 0.3% Triton X-100 in phosphate-buffered saline (PBS) for 30 min. After incubation with anti-prestin antibody (1 : 100, Santa Cruz Biotech, Santa Cruz, CA, USA) or anti-CtBP2 antibody (1 : 500, Proteintech, Chicago, IL, USA) overnight at 4°C, the tissues were subsequently incubated with Alexa Fluor 488-conjugated Goat Anti-rabbit IgG (1 : 600, Invitrogen, Carlsbad, CA, USA) at 27°C for 1 h. After washing with PBS, rhodamine fluorescence phalloidin (1 : 200, Sigma, St. Louis, MO, USA) was used to label the hair bundles. The segments were mounted with ProLong Gold antifade Mountant reagent (Invitrogen, Carlsbad, CA, USA) on a glass slide. The fluorescence images were

acquired using a confocal microscope (A1+, Nikon, Japan). To quantify ribbon synapses, fluorescence images were acquired using z-scan, with a step of 0.8–1.2 μm between each plane.

2.4. Scanning Electron Microscopy (SEM). The cochleae of P3–P14 animals were collected after ABR measurements and were fixed for 2 h in glutaraldehyde (3% in PBS). The round window and apex of the cochlea were opened to provide access to the fixative. After decalcification in 10% EDTA for 2 d, the specimens were rinsed with PBS and fixed again in osmium tetroxide (1% in PBS) for 1 h at 27°C. The bony wall of the cochlea was removed to expose the organ of Corti. Subsequently, gradient alcohol was used for dehydration (15 min). After critical point drying and coating with gold, the specimens were imaged by using SEM (H-3400, Hitachi, Tokyo, Japan). The length of the OHC and IHC stereocilia was measured at different postnatal ages.

2.5. Western Blotting. The segments of the dissected organs of Corti were collected and homogenized with ultrasonic cell crushers (VCX150, Sonic, Newtown, CT, USA). The supernatants of the homogenates were subjected to 8% sodium dodecyl sulfate polyacrylamide gel electrophoresis and transferred to nitrocellulose blotting membranes (Millipore, Bedford, MA, USA). After blocking with 5% nonfat milk in TBS-T (20 mM Tris, 137 mM NaCl, and 0.1% Tween 20, pH 7.6) for 1 h at 27°C, the membranes were incubated with anti-prestin or anti-GAPDH antibodies overnight at 4°C, followed by horseradish peroxidase-conjugated secondary antibodies for 1 h at 27°C. The immunobands were detected by a chemiluminescence detection system (GE Healthcare, Chicago, IL, USA) and visualized using the Amersham Imager 600 (AI600, GE Healthcare, Chicago, IL, USA). The intensity of the immunobands was quantified using Multi-Gauge software (GE Healthcare, Chicago, IL, USA). Data were obtained from four independent experiments.

2.6. Quantitative Polymerase Chain Reaction (qPCR) Assay. After ABR measurements, the apical segments of the cochlear basal membrane were quickly peeled and total RNA was extracted using TRIzol reagent (Invitrogen, Carlsbad, CA, USA). The purity and completeness of the extracted RNA were evaluated to obtain high-quality RNA. Subsequently, cDNA was synthesized with the PrimeScript RT master mix kit (RRO36A, Takara). The reverse transcription (RT)-qPCR assay of prestin was carried out using the ABI Real-Time PCR system (StepOnePlus, Thermo Fisher Scientific, Waltham, MA, USA); GAPDH was used as the internal reference. Two pairs of primers (Invitrogen, Carlsbad, CA, USA) were used [18]: Prestin, forward: 52032-CGACTTGTATAGCAGCGCTTTAAA -3′, reverse: 5′-TTCTTCTCGCTCCCATAATGAGT-3′; GAPDH, forward: 5′-CTTCGATGCCGGGGCTGGCATT-3′, reverse: 5′-TGT TGGGGGCCGAGTTGGGATAGG-3′. Data were obtained from four independent experiments.

2.7. Nonlinear Capacitance (NLC) Measurement of OHCs. The NLC recording of isolated OHCs was performed as described in our recent study [19]. The dissected segments of the organ of Corti were digested using collagenase IV for 5 min (2 mg/ml, Sigma, St. Louis, MO, USA). After gentle pipetting, the OHCs were isolated from the organ of Corti and were transferred into a small plastic chamber filled with enzyme-free L-15 medium (pH 7.35 and 300 mOsm). Healthy looking OHCs were selected for whole-cell patch clamp recording. The recording electrode was pulled using a pipette puller (P97, Sutter, Sacramento, CA, USA) and filled with intracellular solution (120 mM CsCl, 2 mM $MgCl_2$, 10 mM EGTA, and 10 mM HEPES, 300 mOsm, pH 7.3). Typically, the impedance of patch pipette was 5–8 MΩ in bath solution (L-15). Classical whole-cell patch clamp recording was performed using an Axopatch 700B amplifier and a 1440 A/D converter (Molecular Devices, San Jose, CA, USA). A two sine-wave voltage stimulus protocol was generated by using jClamp 32 (Scisoft, CT, USA) to measure the membrane capacitance of OHCs at different membrane voltages. Data were stored and analyzed by the jClamp software offline. The capacitance can be fitted with a two-state Boltzmann function and can reflect the nonlinear charge movements to membrane voltage [20]. The Boltzmann function for capacitance fitting is calculated as follows:

$$C_m = C_{\text{lin}} + \frac{Q_{\max}\alpha}{\exp[\alpha(V_m - V_{1/2})](1 + \exp[-\alpha(V_m - V_{1/2})])^2}, \quad (1)$$

where C_m is the membrane capacitance, C_{lin} is the linear capacitance which is related to the surface area of the cell membrane, $Q_{\max}$ the maximum charge transfer across the membrane, $V_{1/2}$ (or V_h) is the membrane voltage at which the maximum charge movement occurs, or, equivalently, the peak of the capacitance-voltage function, and α represents the slope of the voltage dependence ($\alpha = ze/kT$, where k is the Boltzmann constant, T is the absolute temperature, z is the valence of the charge movement, and e is the electron charge). To compare the magnitude values of the NLC obtained from OHCs with various cell sizes, we normalized NLC and $Q_{\max}$ and C_{lin}.

2.8. Statistical Analysis. Excel and SPSS software were used for the calculations, analysis, and plotting. The t-test was used to examine the significance between different data groups. The significance between different NLC responses was examined by repeated ANOVA, mixed linear model. Significance was defined as $p < 0.05$.

3. Results

The ABR was examined first in postnatal mice in the control group. During the first few days after birth, no ABR was detectable until P7. At P7, the ABR was elicited only by high-frequency tone bursts at high sound level, whereas no ABR was detectable for mid- and low-frequency tone bursts (Figure 1(a)). In the following days, the frequency range of ABR extended gradually from high frequency to low frequency. At P11, robust ABRs could be measured in response to all tested frequencies. At P14, the ABR amplitudes were

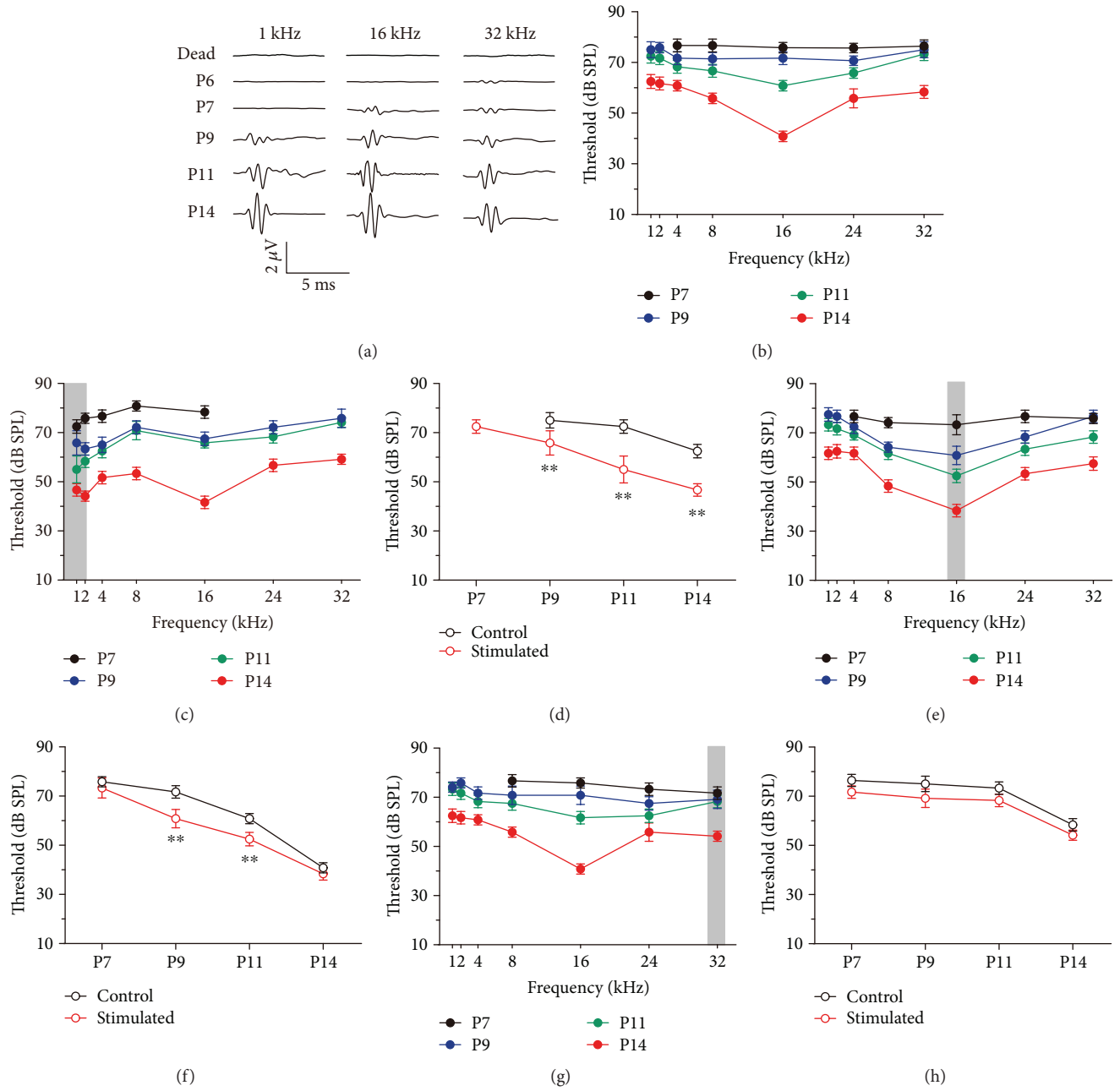

Figure 1: Effects of acoustic stimulation on ABR responses at different postnatal ages. (a) Representative ABR waveforms in response to 1 kHz, 16 kHz, and 32 kHz tone bursts (80 dB SPL) at different postnatal ages. The traces recorded from dead animals show that no stimulation artifact was observed. (b) The ABR threshold frequency-tuning curves at different postnatal ages (P7, $N = 7$; P9, $N = 7$; P11, $N = 6$; P14, $N = 6$). The color code in (b) applies for (c), (e), and (g). (c) The ABR threshold frequency-tuning curves at different postnatal ages after low-frequency sound environment stimulation. The grey area indicates the stimulation frequency used for the sound environment (P7, $N = 6$; P9, $N = 7$; P11, $N = 6$; P14, $N = 6$). (d) The changes in ABR threshold in response to a 1 kHz tone burst during postnatal development for those animals in (c) (red) and control animals in (b) (black). (e) The ABR threshold frequency-tuning curves at different postnatal ages after 16 kHz sound environment stimulation (P7, $N = 6$; P9, $N = 6$; P11, $N = 6$; P14, $N = 6$). (f) The changes in ABR threshold in response to a 16 kHz tone burst during postnatal development for those animals in (e) (red) and control animals in (b) (black). (g) The ABR threshold frequency-tuning curves at different postnatal ages after 32 kHz sound environment stimulation (P7, $N = 6$; P9, $N = 6$; P11, $N = 6$; P14, $N = 6$). (h) The changes in ABR threshold in response to a 32 kHz tone burst during postnatal development for those animals in (g) (red) and control animals in (b) (black). All data points represent the mean ± standard deviation. $^{**}p < 0.01$. ABR: auditory brainstem response; N: number; P: postnatal day.

comparable with those of adult animals. As shown in Figure 1(b), the ABR thresholds decreased with postnatal age, indicating that auditory function of mice pups developed between P7 and P14. Hearing in mice started from a high-frequency range and extended later to low frequency. In the present study, we raised mice in controlled-sound environments. Low-frequency noise (0–2 kHz) was used to stimulate the mice pups (gray area in Figure 1(c)); the frequency threshold-tuning curve was measured based on recorded ABR data. Compared with the control group, the ABR thresholds decreased significantly in response to the stimulus frequency (1 kHz). Moreover, the first day at which the ABR in response to 1 kHz tones appeared preceded from P9 to P7 (Figure 1(d)). Similar effects on ABR development by 16 kHz and 32 kHz acoustic environments were observed, as shown in Figures 1(e)–1(h). However, these influences were only observed in mice pups younger than P14. The acoustic environments have no effect on the ABR thresholds of adult animals (i.e., the mothers; data not shown). These results suggest that pups were more sensitive to low-frequency sound environments. Therefore, the effects of low-frequency sounds were investigated. Consistent with our previous study [21], waves IV to VII were absent in the ABR waveforms recorded from pups in the present study. This observation may reflect the immature function of the central auditory system. These data suggest that the sound environment changed the function of the peripheral auditory system during early development. Since the responses of cochlear HCs and spiral ganglion neurons contribute greatly to the ABR waves I and II [10], we further examined the impact of the environment enriched by low-frequency noise burst on the morphology and function of HCs.

Figure 2(a) depicts the HCs located in the apical segment of the basilar membrane of the cochlea, the segment corresponding to low frequencies. The OHCs were clearly lined up in three rows and IHCs in one row in both the control group and the group treated with 14-day exposure to low-frequency sounds (Figure 2(a)). No observable difference was identified between the two groups. Further examination of the OHC/IHC hair bundles was made based on SEM images as shown in Figure 2(b). Compared with the control group, no significant change in the length of stereocilia was observed after early sound stimulation both in OHCs and IHCs (Figures 2(c) and 2(d)). For mice raised in low-frequency sound environments, the HCs in the middle and basal locations of the cochlea received less sound stimulation than those HCs in the control group. Their morphology and development were also examined (Figure 3(a)). Together with the measurements of the stereocilia length (Figures 3(b) and 3(c)), our data indicated that low-frequency sound environments have no effect on the growth of HC stereocilia during development, regardless of the location of HCs in the cochlea.

Both IHCs and OHCs convert sound vibration into electrical signals. Moreover, OHCs generate motion by changing their cell length with acoustic stimulation [22]. This motion was driven by prestin, the motor protein on the lateral membrane of OHCs. The immunostaining results showed that the expression of prestin starts in the control group at P7 in OHCs of the basal cochlea (Figure 4). No prestin-related fluorescence was detected before P9 in the OHCs of the apical cochlea. Under a low-frequency sound environment, detectable prestin fluorescence was observed at P7 in the apical OHCs. Furthermore, compared with the control group at the same postnatal ages, the prestin fluorescence was more pronounced from P7 to P14. To evaluate the expression level of prestin, Western blot and qPCR assays were performed in the apical and basal in the organ of Corti. As shown in Figure 5(a), in the apical turn of the cochlea, the expression level of prestin increased with the postnatal ages. Under a low-frequency sound environment, the expression level of prestin was significantly increased from P7 to P11. However, no difference in the prestin level was found in the basal turn of the cochlea, except a slight decrease at P7 (Figure 5(b)). The increase of prestin expression in the apical cochlea was further confirmed by the qPCR results. The prestin mRNA levels were significantly increased by low-frequency sound exposure from P5 to P11 (Figure 5(c)).

We also applied whole-cell patch clamp technology to determine the function of prestin expressed on the OHCs. In OHCs, NLC and electromotility are typically coupled [20, 23]. The NLC can be easily measured and precisely reflects the electrophysiological function of prestin. Therefore, NLC was first measured in OHCs isolated from apical cochlea at different postnatal ages. Figure 6(a) depicts the NLCs of apical OHCs at different postnatal ages. No NLC was found in response to the changes of membrane voltage before P7. Subsequently, the NLC membrane potential curves changed with the postnatal ages. Low-frequency sound environment increased the capacitance of OHCs compared with the control group. The NLC amplitude ($\mathrm{NLC}/C_{\mathrm{lin}}$) and the moving charge density ($Q_{\mathrm{max}}/C_{\mathrm{lin}}$) were increased by sound stimulation before P14, while the peak of the capacitance-voltage function ($V_{1/2}$) and the shape of the NLC curves (reflected by the z value) remained largely unchanged (Figures 6(b)–6(e)). NLC was then measured in OHCs isolated from the basal cochlea. As shown in Figure 6(f), no significant difference was observed between control and low-frequency-exposed groups ($p > 0.05$, repeated ANOVA test).

The sound elicited by the vibration of the basilar membrane is amplified by the OHCs and was converted into electrical signals in the IHCs. These signals are transferred to SGNs via ribbon synapses, which are the afferent synapses between IHCs and SGNs. To analyze the postnatal maturation of afferent synapses in the IHC areas, we examined the number of ribbon synapses by evaluating CtBP2, a specific ribbon synaptic marker, in the cochlear sensory epithelium at P9, P11, and P14 (Figure 7(a)). Consistent with previous studies [17, 24, 25], the number of ribbon synapses in IHCs decreased during postnatal development, indicating the refinement of the connections between IHCs and SGNs. As shown in Figure 7(b), the number of CtBP2 clusters per IHC (mean ± standard error of the mean) decreased from 22.2 ± 1.4 at P9 to 13.9 ± 1.4 (mean ± SEM) at P14 in the apical region. Under the administration of low-frequency sound stimulation, the number of CtBP2 clusters per IHC changed from 18.7 ± 1.3 in the controls to 16.4 ± 1.6 at P11 ($p < 0.05$, t-test). In the middle region of the cochlea, early

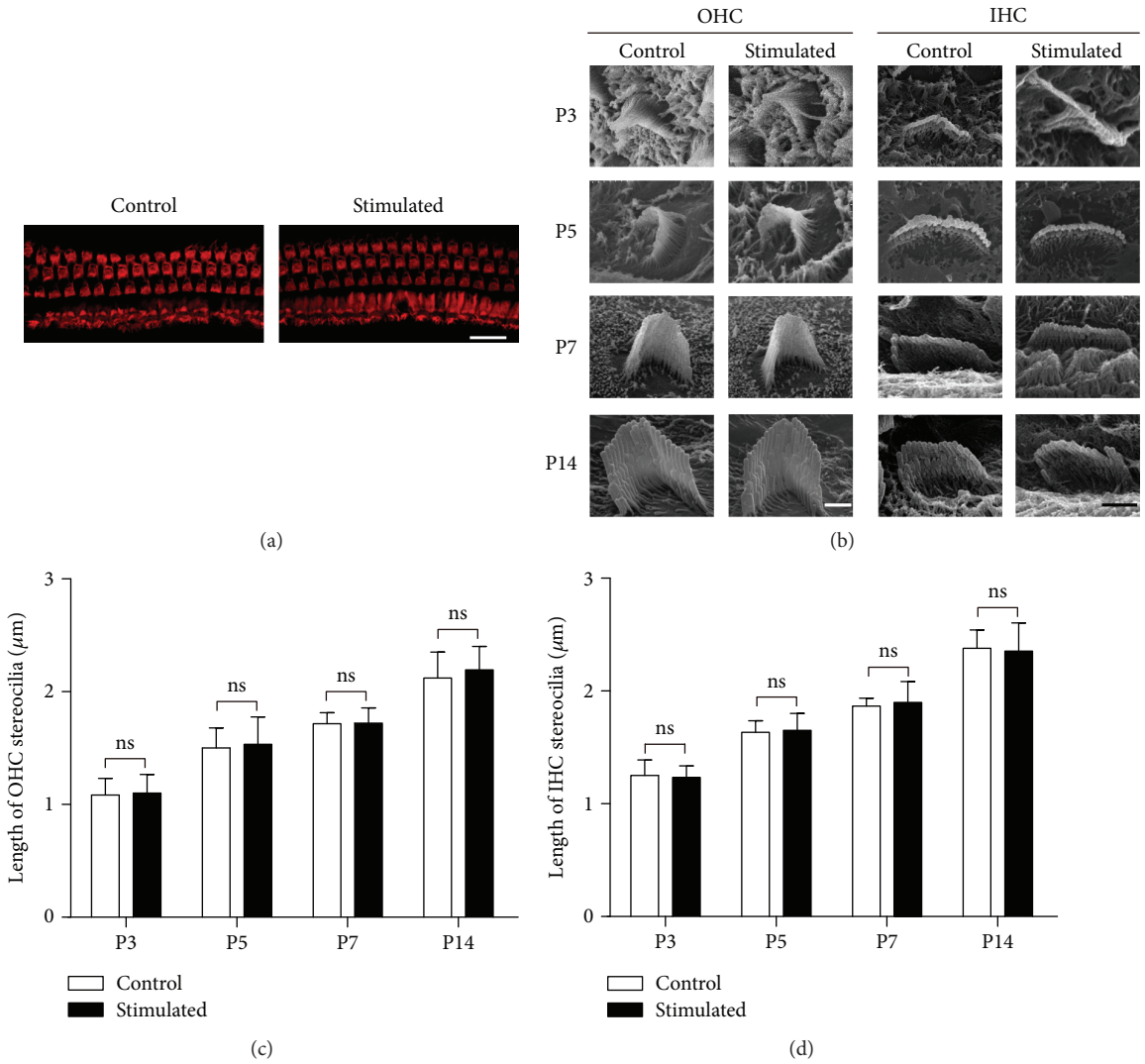

Figure 2: Low-frequency sound environment did not change the alignment and the growth of hair bundles in hair cells in the apical turn of the cochleae. (a) Three rows of OHCs and one row of IHCs (labeled with rhodamine-phalloidin (red)) were observed in both acoustic-stimulated and control groups at P14. Scale bar = 20 μm. (b) Scanning electron microscope images of the hair bundles of OHCs and IHCs in the apical turns of the cochleae at different postnatal ages. Scale bar = 1 μm for OHCs. Scale bar = 2 μm for IHCs. (c) and (d) depict the length of OHC (c) and IHC (d) stereocilia at different postnatal ages. At least six cells from six cochleae were measured for each column. All data points represent as mean ± standard deviation. INC: inner hair cell; ns: no significance; OHC: outer hair cell; P: postnatal day.

sound exposure resulted in no change in the number of CtBP2 clusters. In contrast, in the basal region of the cochlea, low-frequency sound stimulation increased the number of CtBP2 clusters per IHC from 16.0 ± 0.9 in the controls to 17.9 ± 1.1 at P11 ($p < 0.05$, t-test).

4. Discussion

Life experience and environmental factors markedly affect animal perception, including the hearing function. Although plasticity could be observed throughout the lifespan of animals, this experience-dependent plasticity is extreme during development. Sound stimulation in early life can change the sensitivity and frequency selectivity of the animal's auditory system, by shaping the architecture of the auditory system and modulating the maturation of the auditory function. Many studies have demonstrated that the sound stimulation modulated the innervations of auditory neurons and refined the synaptic functions in the auditory cortex [1–3, 5]. For example, the balance between the excitatory and inhibitory inputs of primary auditory cortical neurons is facilitated by sound stimulation applied to rats younger than P20 [5, 8]. There is no doubt that the plasticity of the auditory central nervous system contributes greatly to the profound and persistent adaption to the sound environment during a brief postnatal epoch. However, the influence of early sound stimulation on the development of the peripheral auditory system has not been elucidated. In the present study, the ABRs of mice pups were examined to determine whether the early exposure to a sound environment could modify the function of the cochlea. In adult mice, ABR usually exhibits 5 to7 peaks generated by distinct nuclei along

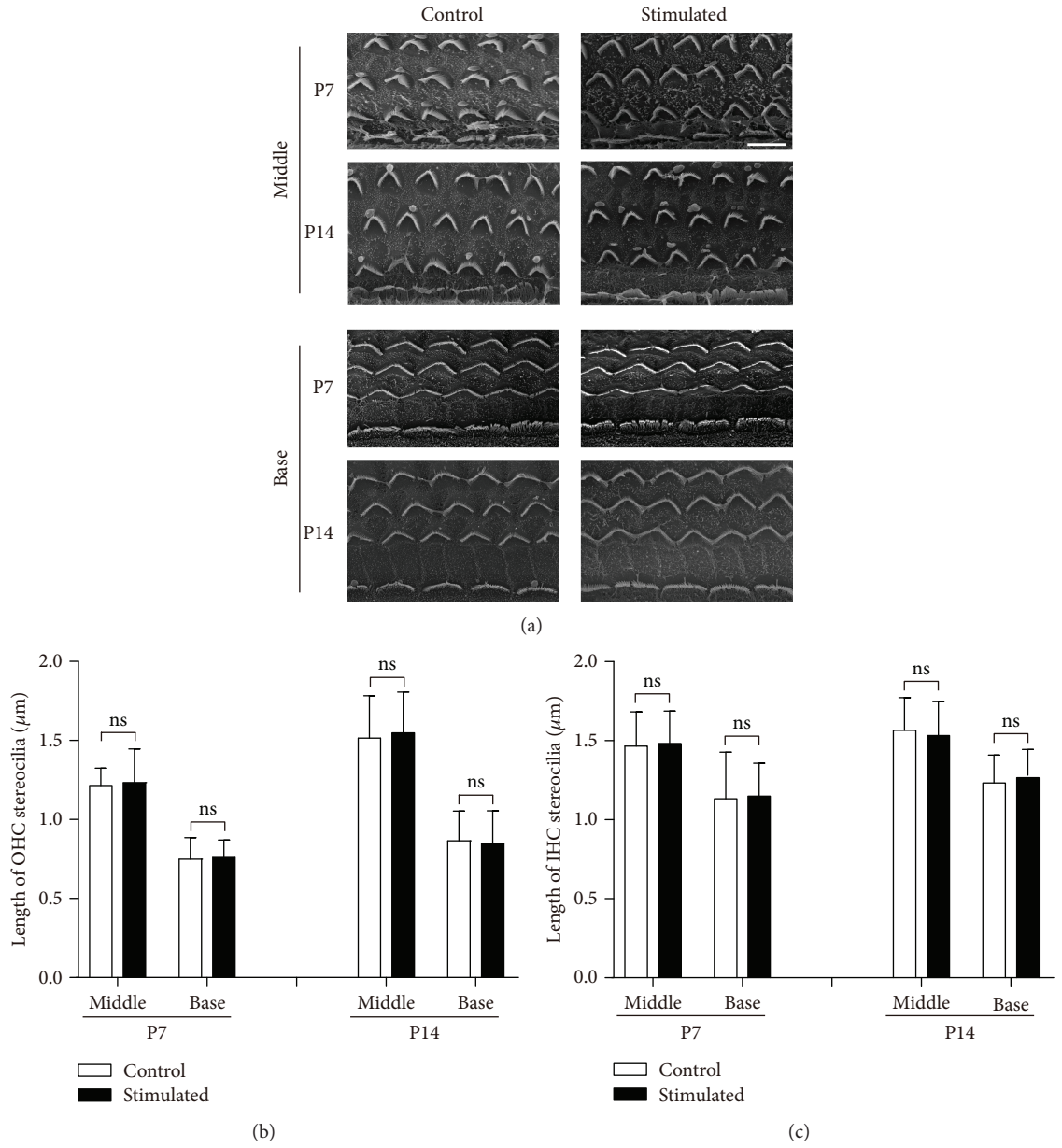

Figure 3: Low-frequency sound environment did not change the alignment and the growth of hair bundles in hair cells in the middle and basal turns. (a) Scanning electron microscope images show the hair bundles of OHCs and IHCs in the middle and basal turns at different postnatal ages. Scale bar = 10 μm. (b and c) The length of OHC (b) and IHC (c) stereocilia at different postnatal ages, compared between low-frequency sound environment-stimulated and control groups. At least six cells from six cochleae were measured for each column. All data points represent the mean ± standard deviation. INC: inner hair cell; ns: no significance; OHC: outer hair cell; P: postnatal day.

the ascending pathway of the auditory system. As reported in our previous study, only waves I to III of the ABR waveforms were observed in mice pups before P14 [21]. The absence of later ABR waveforms implies the weak activity of higher stages of auditory nuclei in the early postnatal epoch. The continuous improvement of ABR waveforms and thresholds after hearing onset may imply the maturation of the central auditory system [26]. It is generally accepted that waves I and II of ABR waveforms represent the response of cochlear sensory cells and the auditory nerve [10]. We found that sound stimulation specifically changed the ABR threshold in a frequency-dependent manner, indicating that sound can modulate the function of the cochlear sensory cells (Figure 1).

The morphological and functional maturation of HCs occurs after birth in rodents. The maturation of hair bundles, MET function, electromotility of OHCs, and ribbon synapses is not completed until P10–P14, which is defined as the "onset" of hearing [4, 27, 28]. Any change in these items may greatly influence the function of HCs, resulting in changes in the maturation of the auditory functions. In the present study, we first examined the morphology of hair bundles under the sound environment. The sound-induced deflection of stereocilia in the hair bundles opens the MET

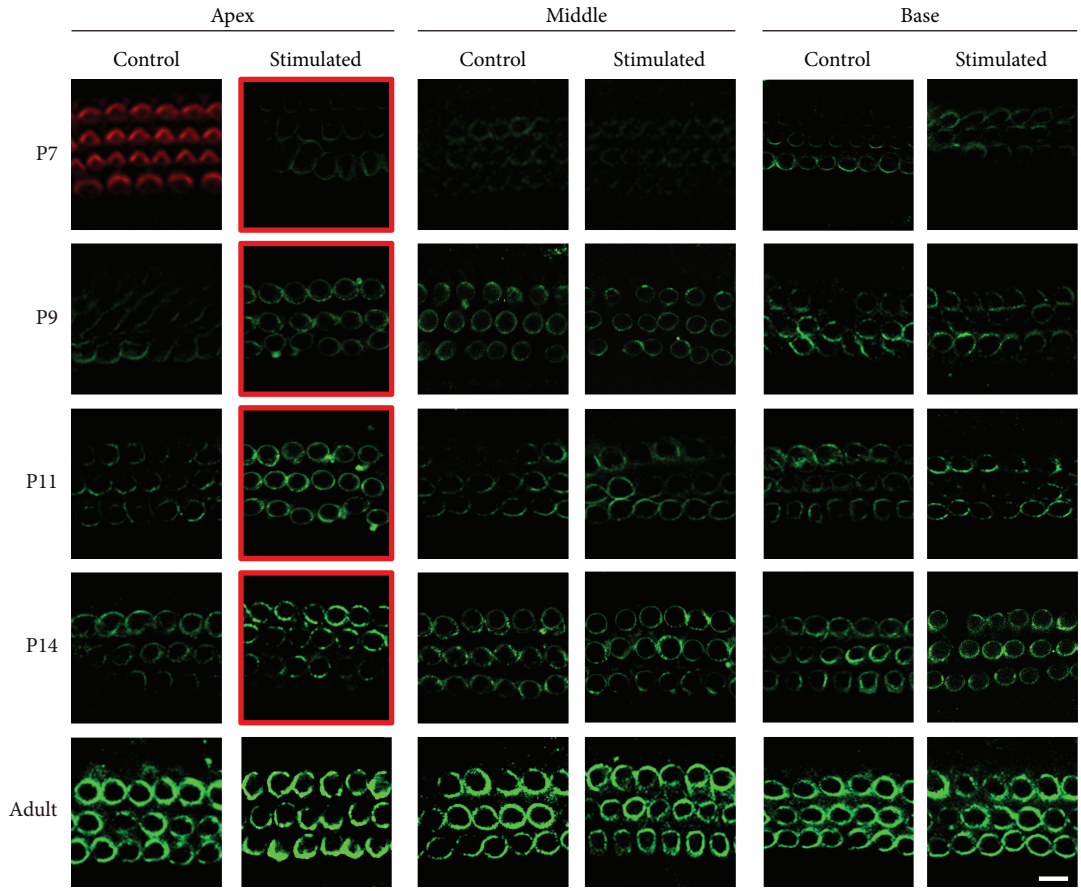

Figure 4: Confocal images indicate that a low-frequency sound environment increases the expression of prestin in apical OHCs during postnatal development. Prestin (green) was labeled in three segments (apex, middle, and base) along the cochlea in P7, P9, P11, P14, and adult mice. For P7 apical turns, no green fluorescence was detected. The hair bundles of hair cells were labeled with rhodamine-phalloidin (red) to indicate the location of the hair cells. The red borders mark the postnatal ages at which prestin expression level was higher in the sound-stimulated group. Scale bar = 10 μm. OHC: outer hair cell; P: postnatal day.

channels located on the top of the stereocilia. Normal length and arrangement of stereocilia are required to generate normal MET currents and convert sound waves to electrical signals. Our results indicated that early exposure to the enriched acoustic environment does not change the features of hair bundles during development, including the shape, length, and the arrangement of stereocilia neither in IHCs nor OHCs (Figures 2 and 3). Although we did not measure the MET currents directly, our results suggested that the hair bundle functions may remain unchanged by early sound exposure.

The mammalian OHCs can change the length of their cell body at the frequency of sound signals. This process is termed electromotility and is powered by prestin, the motor protein expressed on the membrane surface of OHCs [29, 30]. Driven by the receptor potential, intracellular chloride moves in and out of prestin and triggers prestin to switch between a long and short conformation, resulting in the elongation and shortening of OHCs [22, 29]. The expression of prestin starts in the OHCs at the basal cochlea at approximately P5 and spreads to apical OHCs in the following days [21, 31]. We found that low-frequency sound environment specifically increased the expression of prestin in apical OHCs, as evidenced by the Western blotting and qPCR data (Figures 4 and 5). Furthermore, the NLC of apical OHCs was also potentiated by low-frequency sound environment at P7–P11, indicating that the electromotility of these OHCs was enhanced (Figure 6). However, such effects could not be obtained in the basal OHCs, although a slightly decreased prestin expression was observed at P7 (Figures 4–6). The changes in the expression and function of prestin can increase the sensitivity to low-frequency sounds and may be, at least partially, responsible for augmented ABR in response to low-frequency sound. However, these changes could only be observed in the period between P7 and P14. No difference was observed in mice older than P14. Therefore, the early exposure to sound can only accelerate the expression of prestin during development but cannot induce the overexpression of prestin in OHCs. It has been reported that the prestin expression level and function were enhanced in residual noise-exposed OHCs. One possible modulating source is the central feedback. The activity of OHCs is modulated by an efferent pathway through an acetylcholine alpha-9/10 receptor. It is not likely that early sound exposure modulates the expression of prestin through this mechanism, because the efferent pathway is not well

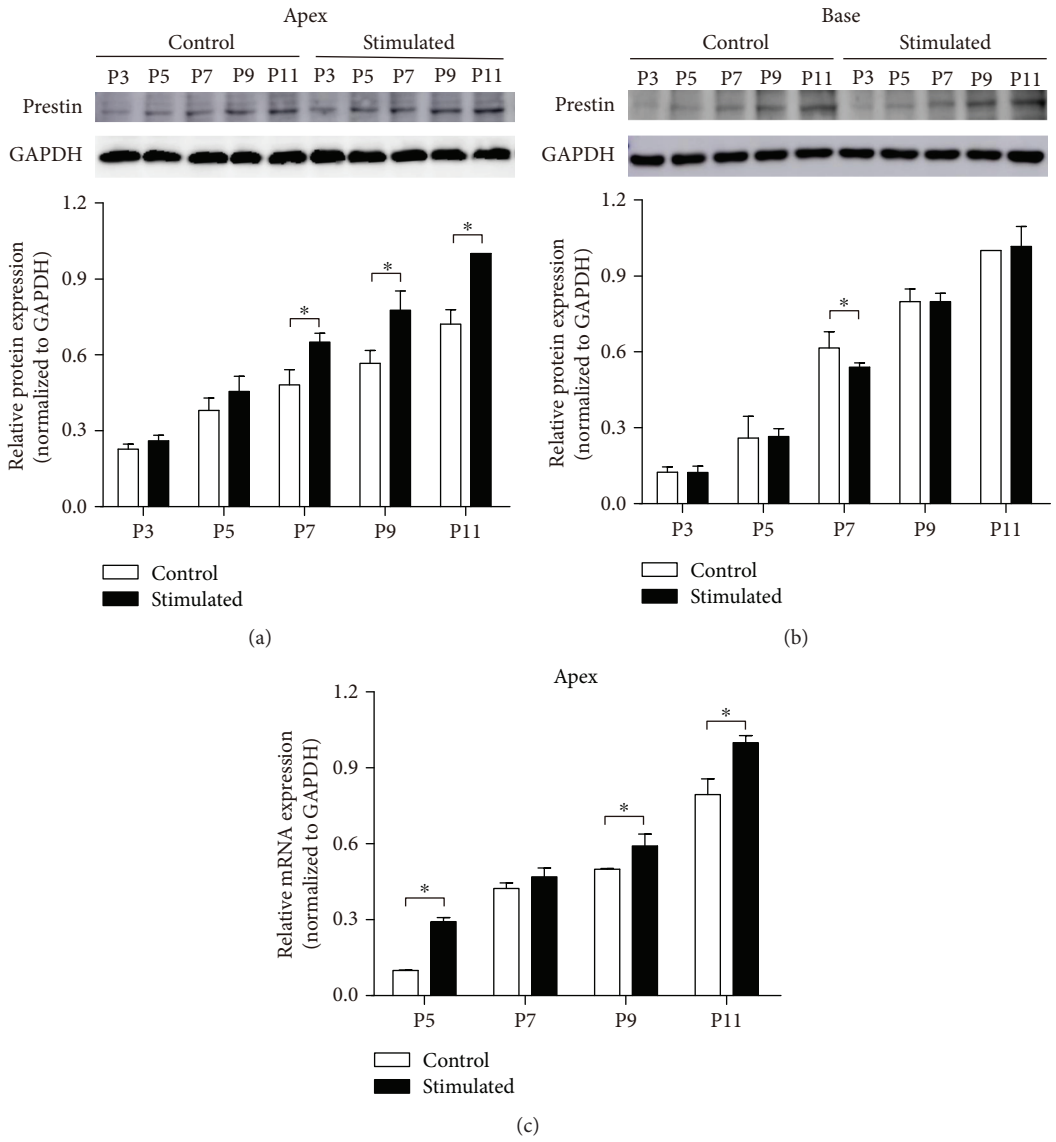

Figure 5: Low-frequency sound environment enhances the expression of prestin in OHCs in the apical turns. (a) Prestin protein expression is increased in the apical organ of Corti after low-frequency sound environment stimulation. Upper panel: immunobands of prestin from the apical organ of Corti at different postnatal ages. Lower panel: normalized prestin expression level. (b) Prestin protein expression is unchanged in the basal organ of Corti after sound environment stimulation. Upper panel: immunobands of prestin at different postnatal ages. Lower panel: normalized prestin expression level. (c) Normalized prestin mRNA level is increased in the apical organ of Corti after sound stimulation. All data points represent the mean ± standard deviation. $^{*}p < 0.05$. OHC: outer hair cell.

developed before the onset of hearing [32–34]. The prestin level can be regulated by the thyroid hormone, retinoid nuclear transcription factor, GATA-3, and Pou4f3 during development [35–37]. Further studies are still needed to determine the exact mechanism underlying the impact of early sound exposure on prestin expression in OHCs.

The HC responses are transmitted to SGNs through glutamatergic synapses, which are known as ribbon synapses. Proper number and size of ribbon synapses at the bottom region of HC are critical for the effective transmission of electrical signals from IHCs to SGNs [24, 32, 33]. During the early developmental epoch, the number of ribbon synapses decreased with postnatal age in IHCs at all locations along the cochlea (Figure 7). This result is consistent with previous findings [17, 24, 25]. We found that low-frequency sound environment selectively decreased ribbon synapses in apical IHCs and increased ribbon synapses in basal IHCs, indicating that the neural transmission was also influenced by early sound exposure (Figure 7). Similar to the changes in the expression of prestin, these changes could not be observed after P14.

Although the functional maturation of cochlea occurs considerably faster than that for more central parts of the auditory system, immaturity of conductive factors may limit the efficiency of cochlear responses. The ear canal is closed and the ossicular ossification is incomplete before the hearing onset in rodents [38]. One may raise the question about how sound is transmitted to the cochlea and influence the

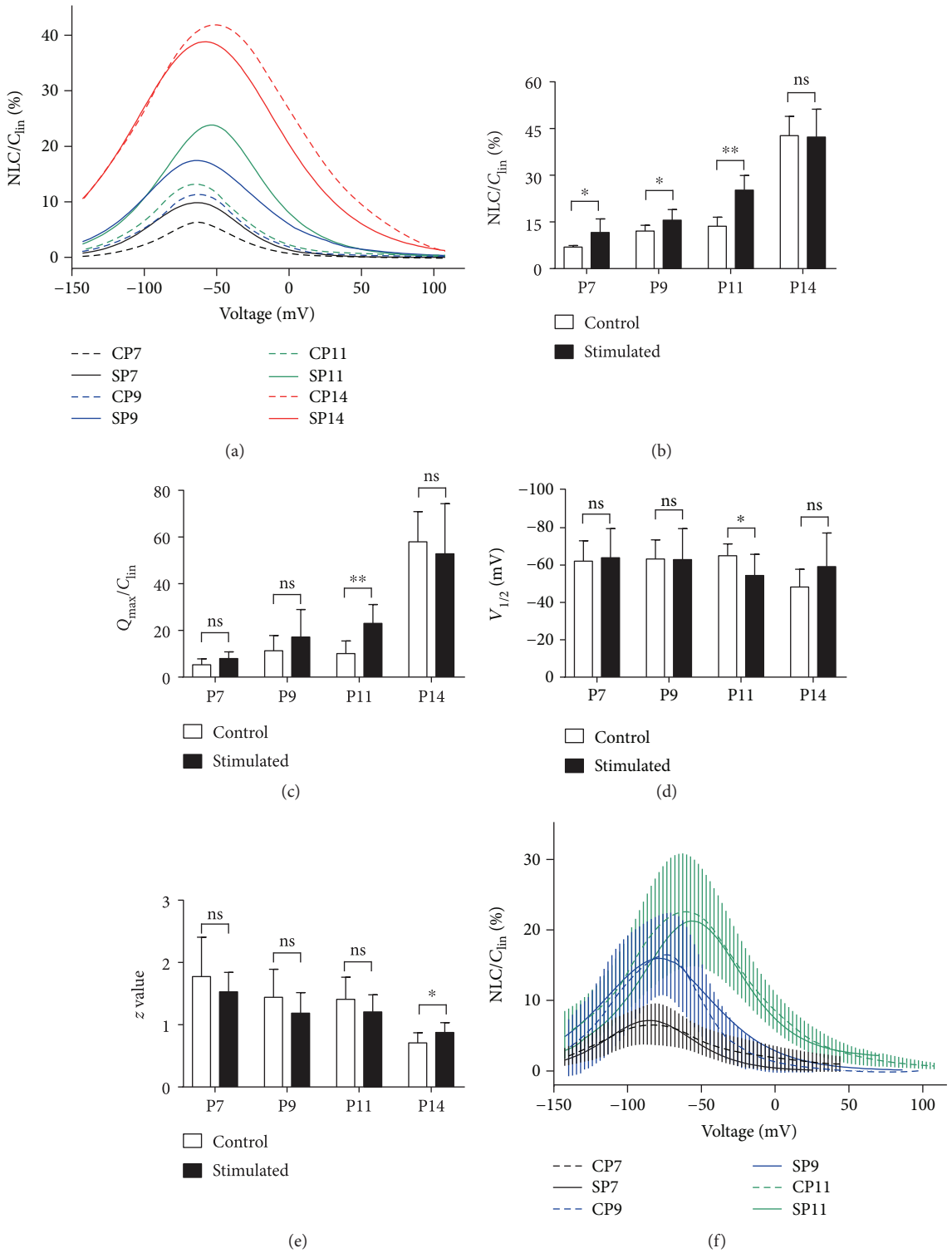

Figure 6: Low-frequency sound environment stimulation enhances the NLC response of OHCs from the apical turns of the cochleae. (a) Means of NLC from low-frequency noise-stimulated (SP, solid lines) and control (CP, dashed lines) OHCs in apical cochlea at P7 (SP7, $n = 8$; CP7, $n = 5$), P9 (SP9, $n = 9$; CP9, $n = 8$), P11 (SP11, $n = 12$; CP11, $n = 9$), and P14 (SP14, $n = 13$; CP14, $n = 10$). The mean capacitance-voltage responses were fitted with the Boltzmann function. (b–e) Four parameters obtained from curve fitting using the Boltzmann function. All data points represent the mean ± standard deviation. $^{*}p < 0.05$; $^{**}p < 0.01$; NLC: nonlinear capacitance; ns: no significance; OHC: outer hair cell; P: postnatal day. (f) Means of NLC from low-frequency noise-stimulated (SP, solid lines) and control (CP, dashed lines) OHCs in basal cochlea at P7 (SP7, $N = 5$; CP7, $N = 12$), P9 (SP9, $N = 4$; CP9, $N = 9$), and P11 (SP11, $N = 4$; CP11, $N = 8$). The mean capacitance-voltage responses were fitted with the Boltzmann function. The SDs of mean NLCs are indicated by the vertical bars for the controls. No significant difference was found between the two groups ($p > 0.05$, repeated ANOVA).

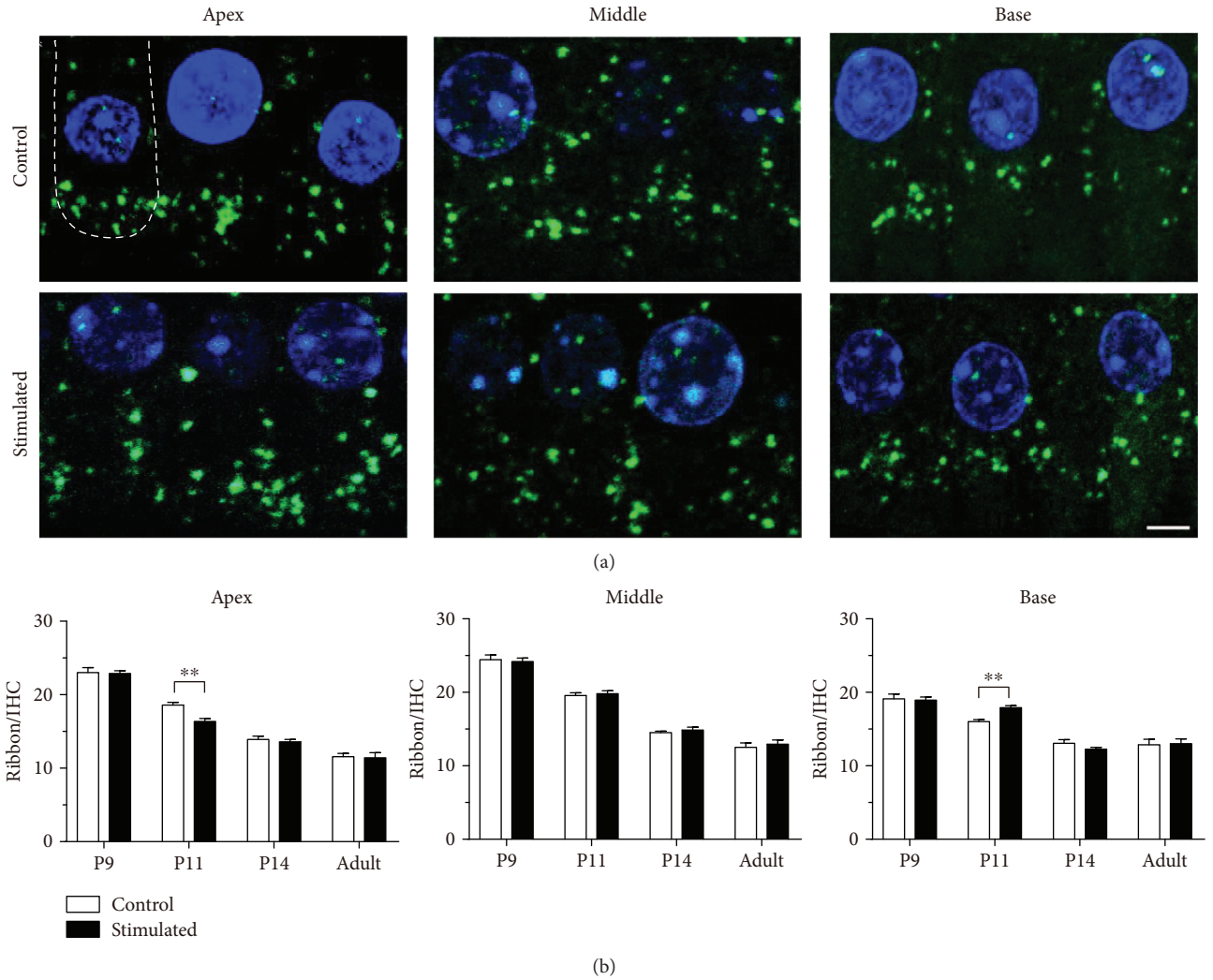

Figure 7: Low-frequency sound environment stimulation influences the changes in ribbon synapses during postnatal development. (a) Representative maximum projections of confocal Z stacks of IHCs in the apical, middle, and basal turns of the cochleae at P11. Anti-CtBP2 and DAPI were used to visualize the IHCs ribbons (green) and nuclei (blue), respectively. The white line in the first image indicates the bottom of an IHC. Scale bar = 5 μm. (b) The number of ribbon synapses per IHC from different locations along the cochlea at different postnatal ages. At least 15 IHCs from 3–5 cochleae were measured for each column. All data points represent the mean ± standard error of the mean. $^{**}p < 0.01$. DAPI: 4′,6-diamidino-2-phenylindole; IHC: inner hair cell; P: postnatal day.

development of hair cells. The air-filled middle ear cavity and clearance of the auditory canal are not ready for air-0conducted stimulation in the first two weeks after birth. However, ABR to bone-conducted auditory stimuli could be recorded from neonatal rats at age of P7 [38]. We propose that the over sound exposure in the present study is transmitted to the cochlea via the bone conduction and influence the sensorineural development before the hearing onset. This suggestion is supported by the results that high-intensity sound stimuli evoke ABR and behavior response before hearing onset [21, 39]. In our study, low-frequency sound exerted stronger effects on the maturation of HCs than high-frequency sound. This may have two possible explanations. First, the maturation of the basal HCs, which is responsive to high-frequency sound stimuli, occurs earlier than the maturation of apical HCs, which is responsive to low-frequency sound stimuli. This difference in the timing of development allows a longer period for low-frequency sound environments to induce more profound effects on apical HCs. Second, in contrast to the adult middle ear, which is filled with air, the middle ear of pups younger than P11 is filled with liquid. As more energy is attenuated by the liquid and soft ossicular chain in the case of high-frequency sounds, than the low-frequency sound, the latter is more effectively conducted to the inner ear.

Our study suggested that early exposure to sound can enhance the function of HCs and accelerate the development of the peripheral auditory system. However, early exposure to sound environment induced effects on the cochlea that were different from the plasticity in the central auditory nervous system during development. The changes in HCs observed in the present study are not persistent. After P14, most HCs features showed no differences between the control- and sound-exposed groups, implying that peripheral HC

development is largely controlled by intrinsic genetic makeup. The early exposure to sound accelerates the development of HCs by so far unknown factors. Compared with the control group, pups exposed to low-frequency sound received less stimulation at high frequency. In addition, the development of HCs in the basal cochlea was delayed under the exposure to the low-frequency sound environment as evidenced by the Western blotting and ribbon synapse staining results (Figures 5 and 7). These results suggest that sound plays a role in modulating the development of inner ear sensory cells. However, in the present study, the effect of the sound environment on HCs occurred before the hearing onset (approximately at P10). This implies that the development of the central neural system requires matured HCs to provide proper input signals. Thus, although the modulation in HCs is not as profound as the plasticity in central neurons during development, the effects of early sound exposure on HC functions may result in persistent changes in the whole auditory system by altering the input signals. Our findings provide a new strategy to modulate the function of cochlear sensory cells during development. This approach is safer and easier to apply than drug and gene therapies.

5. Conclusions

In conclusion, our results indicate that acoustic exposure significantly decreased the ABR thresholds of neonatal mice in a frequency-specific manner. The expression and function of prestin, the motor protein of OHCs, were specifically increased by acoustic stimulation. The number of ribbon synapses in the hair cell areas was also promoted by early acoustic stimulation.

Conflicts of Interest

The authors declare that they have no competing interests.

Acknowledgments

This work was supported by the 973 Program of China (Grant no. 2014CB943002), the National Natural Science Foundation of China (Grant nos. 11534013 and 31500841), and the Guangdong Natural Science Foundation (Grant no. 2017A030313178).

References

[1] L. I. Zhang, S. Bao, and M. M. Merzenich, "Persistent and specific influences of early acoustic environments on primary auditory cortex," *Nature Neuroscience*, vol. 4, no. 11, pp. 1123–1130, 2001.

[2] E. de Villers-Sidani, E. F. Chang, S. Bao, and M. M. Merzenich, "Critical period window for spectral tuning defined in the primary auditory cortex (A1) in the rat," *The Journal of Neuroscience*, vol. 27, no. 1, pp. 180–189, 2007.

[3] D. H. Sanes and S. Bao, "Tuning up the developing auditory CNS," *Current Opinion in Neurobiology*, vol. 19, no. 2, pp. 188–199, 2009.

[4] J. Waguespack, F. T. Salles, B. Kachar, and A. J. Ricci, "Stepwise morphological and functional maturation of mechanotransduction in rat outer hair cells," *The Journal of Neuroscience*, vol. 27, no. 50, pp. 13890–13902, 2007.

[5] R. C. Froemke and B. J. Jones, "Development of auditory cortical synaptic receptive fields," *Neuroscience and Biobehavioral Reviews*, vol. 35, no. 10, pp. 2105–2113, 2011.

[6] E. Caminos, C. Vale, R. Lujan, J. R. Martinez-Galan, and J. M. Juiz, "Developmental regulation and adult maintenance of potassium channel proteins (Kv 1.1 and Kv 1.2) in the cochlear nucleus of the rat," *Brain Research*, vol. 1056, no. 2, pp. 118–131, 2005.

[7] I. Fukui and H. Ohmori, "Developmental changes in membrane excitability and morphology of neurons in the nucleus angularis of the chicken," *The Journal of Physiology*, vol. 548, no. 1, pp. 219–232, 2003.

[8] A. L. Dorrn, K. Yuan, A. J. Barker, C. E. Schreiner, and R. C. Froemke, "Developmental sensory experience balances cortical excitation and inhibition," *Nature*, vol. 465, no. 7300, pp. 932–936, 2010.

[9] Y. J. Sun, G. K. Wu, B. H. Liu et al., "Fine-tuning of pre-balanced excitation and inhibition during auditory cortical development," *Nature*, vol. 465, no. 7300, pp. 927–931, 2010.

[10] R. A. Møler and A. R. MøLler, *Hearing:Anatomy, Physiology, and Disorders of the Auditory System*, Academic, San Diego, CA, USA, 2006.

[11] M. C. Kelly and P. Chen, "Development of form and function in the mammalian cochlea," *Current Opinion in Neurobiology*, vol. 19, no. 4, pp. 395–401, 2009.

[12] A. K. Groves and D. M. Fekete, "Shaping sound in space: the regulation of inner ear patterning," *Development*, vol. 139, no. 2, pp. 245–257, 2012.

[13] A. Dabdoub, M. J. Donohue, A. Brennan et al., "Wnt signaling mediates reorientation of outer hair cell stereociliary bundles in the mammalian cochlea," *Development*, vol. 130, no. 11, pp. 2375–2384, 2003.

[14] P. C. G. Rida and P. Chen, "Line up and listen: planar cell polarity regulation in the mammalian inner ear," *Seminars in Cell & Developmental Biology*, vol. 20, no. 8, pp. 978–985, 2009.

[15] D. Z. Z. He, B. N. Evans, and P. Dallos, "First appearance and development of electromotility in neonatal gerbil outer hair cells," *Hearing Research*, vol. 78, no. 1, pp. 77–90, 1994.

[16] T. Abe, S. Kakehata, R. Kitani et al., "Developmental expression of the outer hair cell motor prestin in the mouse," *The Journal of Membrane Biology*, vol. 215, no. 1, pp. 49–56, 2007.

[17] L. D. Liberman and M. C. Liberman, "Postnatal maturation of auditory-nerve heterogeneity, as seen in spatial gradients of synapse morphology in the inner hair cell area," *Hearing Research*, vol. 339, pp. 12–22, 2016.

[18] A. Xia, Y. Song, R. Wang et al., "Prestin regulation and function in residual outer hair cells after noise-induced hearing loss," *PLoS One*, vol. 8, no. 12, article e82602, 2013.

[19] M. Fu, M. Chen, X. Yan, X. Yang, J. Xiao, and J. Tang, "The effects of urethane on rat outer hair cells," *Neural Plasticity*, vol. 2016, Article ID 3512098, 11 pages, 2016.

[20] J. Santos-Sacchi, "Reversible inhibition of voltage-dependent outer hair cell motility and capacitance," *The Journal of Neuroscience*, vol. 11, no. 10, pp. 3096–3110, 1991.

[21] J. Hang, W. Pan, A. Chang et al., "Synchronized progression of prestin expression and auditory brainstem response during

postnatal development in rats," *Neural Plasticity*, vol. 2016, Article ID 4545826, 10 pages, 2016.

[22] P. Dallos, B. N. Evans, and R. Hallworth, "Nature of the motor element in electrokinetic shape changes of cochlear outer hair cells," *Nature*, vol. 350, no. 6314, pp. 155–157, 1991.

[23] K. Homma and P. Dallos, "Evidence that prestin has at least two voltage-dependent steps," *The Journal of Biological Chemistry*, vol. 286, no. 3, pp. 2297–2307, 2011.

[24] T. M. Coate and M. W. Kelley, "Making connections in the inner ear: recent insights into the development of spiral ganglion neurons and their connectivity with sensory hair cells," *Seminars in Cell & Developmental Biology*, vol. 24, no. 5, pp. 460–469, 2013.

[25] R. Kalluri and M. Monges-Hernandez, "Spatial gradients in the size of inner hair cell ribbons emerge before the onset of hearing in rats," *Journal of the Association for Research in Otolaryngology*, vol. 18, no. 3, pp. 399–413, 2017.

[26] Y. Zhang, R. H. Dyck, S. E. Hamilton, N. M. Nathanson, and J. Yan, "Disrupted tonotopy of the auditory cortex in mice lacking M1 muscarinic acetylcholine receptor," *Hearing Research*, vol. 201, no. 1-2, pp. 145–155, 2005.

[27] J. A. Kaltenbach, P. R. Falzarano, and T. H. Simpson, "Postnatal development of the hamster cochlea. II. Growth and differentiation of stereocilia bundles," *The Journal of Comparative Neurology*, vol. 350, no. 2, pp. 187–198, 1994.

[28] J. Defourny, F. Lallemend, and B. Malgrange, "Structure and development of cochlear afferent innervation in mammals," *American Journal of Physiology Cell Physiology*, vol. 301, no. 4, pp. C750–C761, 2011.

[29] P. Dallos, "Cochlear amplification, outer hair cells and prestin," *Current Opinion in Neurobiology*, vol. 18, no. 4, pp. 370–376, 2008.

[30] J. Zheng, W. Shen, D. Z. Z. He, K. B. Long, L. D. Madison, and P. Dallos, "Prestin is the motor protein of cochlear outer hair cells," *Nature*, vol. 405, no. 6783, pp. 149–155, 2000.

[31] I. A. Belyantseva, H. J. Adler, R. Curi, G. I. Frolenkov, and B. Kachar, "Expression and localization of prestin and the sugar transporter GLUT-5 during development of electromotility in cochlear outer hair cells," *The Journal of Neuroscience*, vol. 20, no. 24, article RC116, 2000.

[32] D. D. Simmons, "Development of the inner ear efferent system across vertebrate species," *Journal of Neurobiology*, vol. 53, no. 2, pp. 228–250, 2002.

[33] A. C. Meyer and T. Moser, "Structure and function of cochlear afferent innervation," *Current Opinion in Otolaryngology & Head and Neck Surgery*, vol. 18, no. 5, pp. 441–446, 2010.

[34] L. Delacroix and B. Malgrange, "Cochlear afferent innervation development," *Hearing Research*, vol. 330, Part B, pp. 157–169, 2015.

[35] T. Weber, U. Zimmermann, H. Winter et al., "Thyroid hormone is a critical determinant for the regulation of the cochlear motor protein prestin," *Proceedings of the National Academy of Sciences of the United States of America*, vol. 99, no. 5, pp. 2901–2906, 2002.

[36] J. Gross, K. Stute, J. Fuchs, M. Angerstein, N. Amarjargal, and B. Mazurek, "Effects of retinoic acid and butyric acid on the expression of prestin and Gata-3 in organotypic cultures of the organ of Corti of newborn rats," *Developmental Neurobiology*, vol. 71, no. 7, pp. 650–661, 2011.

[37] J. Gross, M. Angerstein, J. Fuchs, K. Stute, and B. Mazurek, "Expression analysis of prestin and selected transcription factors in newborn rats," *Cellular and Molecular Neurobiology*, vol. 31, no. 7, pp. 1089–1101, 2011.

[38] M. Geal-Dor, S. Freeman, G. Li, and H. Sohmer, "Development of hearing in neonatal rats: air and bone conducted ABR thresholds," *Hearing Research*, vol. 69, no. 1-2, pp. 236–242, 1993.

[39] N. Rybalko, T. Chumak, Z. Bures, J. Popelar, D. Suta, and J. Syka, "Development of the acoustic startle response in rats and its change after early acoustic trauma," *Behavioural Brain Research*, vol. 286, pp. 212–221, 2015.

Hindawi
Neural Plasticity
Volume 2018, Article ID 7272308, 6 pages
https://doi.org/10.1155/2018/7272308

Research Article

A Novel p.G141R Mutation in *ILDR1* Leads to Recessive Nonsyndromic Deafness DFNB42 in Two Chinese Han Families

Xueling Wang,[1,2,3] **Longhao Wang**,[1,2,3] **Hu Peng**,[1,2,3,4] **Tao Yang**,[1,2,3] **and Hao Wu**[1,2,3]

[1]*Department of Otorhinolaryngology-Head and Neck Surgery, Shanghai Ninth People's Hospital, Shanghai Jiao Tong University School of Medicine, Shanghai, China*
[2]*Ear Institute, Shanghai Jiao Tong University School of Medicine, Shanghai, China*
[3]*Shanghai Key Laboratory of Translational Medicine on Ear and Nose Diseases, Shanghai, China*
[4]*Department of Otolaryngology-Head and Neck Surgery, Changzheng Hospital, Second Military Medical University, Shanghai, China*

Correspondence should be addressed to Tao Yang; yangtfxl@sina.com and Hao Wu; wuhao622@sina.cn

Received 25 January 2018; Accepted 27 February 2018; Published 16 April 2018

Academic Editor: Renjie Chai

Genetic hearing impairment is highly heterogeneous. In this study, targeted next-generation sequencing (NGS) in two Chinese Han families identified a novel p.G141R homozygous mutation in *ILDR1* as the genetic cause of the deafness. Consistent with the recessive inheritance, cosegregation of the p.G141R variant with the hearing loss was confirmed in members of both families by PCR amplification and Sanger sequencing. SNP genotyping analysis suggested that those two families were not closely related. Our study showed that targeted NGS is an effective tool for diagnosis of genetic deafness and that p.G141R in *ILDR1* may be a relatively frequent mutation for DFNB42 in Chinese Hans.

1. Introduction

Approximately one in every thousand children suffers congenital or early-onset deafness. In more than half of such cases the hearing impairment can be attributed to genetic causes [1]. To date, more than 100 genes and 150 loci have been identified to be associated with nonsyndromic hearing impairment (Hereditary Hearing Loss Homepage) (http://hereditaryhearingloss.org), with approximately 80% of cases being autosomal recessive [2].

Mutations in the *ILDR1* gene (OMIM 609739) lead to autosomal recessive nonsyndromic deafness DFNB42. *ILDR1* encodes the immunoglobulin-like domain containing receptor 1, a predicted type 1 transmembrane protein. It is widely expressed in a variety of tissues including prostate, testes, pancreas, and kidney. In 2011, Borck et al. first reported several loss-of-function mutations in *ILDR1* resulting in autosomal recessive hearing impairment DFNB42 [3]. *Ildr1* was found expressing in hair cells and supporting cells of the developing mouse cochlea and vestibule [3]. In *Ildr1* knockout mice, hair cells undergo postnatal degeneration. At P35, all knockout mice had profound sensorineural hearing loss associated with a complete loss of outer hair cells and a disorganization of most stereocilia in inner hair cells [4]. Evidence suggested that IDLR1 functions as a water barrier at the tricellular tight junction [5].

To date, only a limited number (less than 20) of *ILDR1* mutations have been reported for DFNB42 in selected ethnic groups in Asia [3, 6–14]. In the present study, we identify a novel missense mutation in *ILDR1* in two Chinese families with DFNB42.

2. Materials and Methods

2.1. Subjects and Clinical Evaluations. This study included two small Chinese recessive deaf families: family 1 (Figure 1(a)) and family 2 (Figure 1(b)). All affected individuals were clinically evaluated in the Department of Otolaryngology-Head and Neck Surgery, Shanghai Ninth People's Hospital, Shanghai, China. The evaluation included

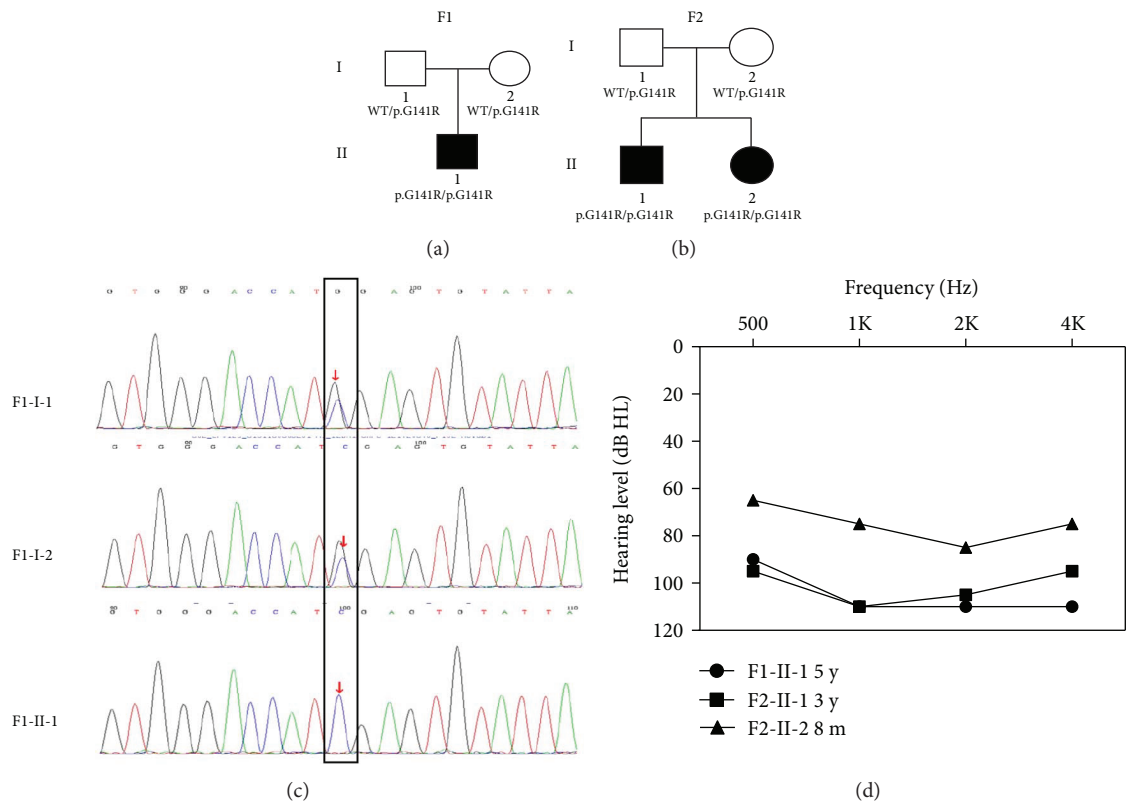

Figure 1: Pedigree and sequencing results of families F1 and F2. (a) Pedigree of family F1. (b) Pedigree of family F2. (c) Representative chromatograms showing the heterozygous (F1-I-1 and F1-I-2) and homozygous (F1-II-1) p.G141R mutation in *ILDR1*. (d) Audiograms of affected members.

a complete medical history interview and a detailed physical examination to rule out possible environmental or syndromic hearing impairment. Auditory evaluations were performed including otoscopic examination, otoacoustic emission (OAE), and pure tone audiometry (PTA). Hearing thresholds of subjects were determined by the air-conduction pure-tone average thresholds ranging from 250 to 8000 Hz. Hearing level was classified as normal (<20 dB), mild (20–40 dB), moderate (41–70 dB), severe (71–90 dB), and profound (>90 dB). Hearing thresholds reported in this study were averages of the right and left ears. Romberg testing and tandem gait were performed for vestibular function examination. Computerized tomography (CT) scan of the temporal bone was carried out for excluding inner-ear anomalies.

2.2. Mutation Identification. Informed consent was obtained from all participants or from parents of the young subjects according to a protocol approved by the ethics committee of the Shanghai Ninth People's Hospital, Shanghai Jiao Tong University School of Medicine. Genomic DNA was extracted from peripheral blood samples using a blood DNA kit (TIANGEN Biotech Inc., Beijing, China). Targeted next-generation sequencing was performed in probands of family 1 and family 2 as previously described. Briefly, exon and flanking intron sequences of 159 known deafness genes (Supplementary Table 1) were captured by a customized capture array (NimbleGen, Roche) and sequenced on the Illumina HiSeq2000 analyzer. Data analysis and bioinformatics processing were performed following the standard operation procedure of Illumina. The minor allele frequencies (MAF) of the variants were determined using the gnomAD database (http://gnomad.broadinstitute.org/) and the in-house sequencing data of 200 Chinese Han normal hearing controls. Nonsynonymous variants with an MAF of 0.005 or less and consistent with the autosomal recessive inheritance were considered as candidate pathogenic mutations. Cosegregation of the disease phenotype and the detected variants were confirmed in all family members by PCR amplification and Sanger sequencing. Potential pathogenic effects of the candidate mutations were evaluated by the PolyPhen-2 [15], SIFT [16], and MutationTaster [17] programs.

3. Results

3.1. Clinical Features. For the three affected individuals in both families (F1-II-1, F2-II-1, and F2-II-2), the hearing impairment was prelingual and bilateral, and the severity ranged from moderate (F1-II-1) to profound (F2-II-1 and F2-II-2) (Figure 1(d)). Speech perception ability was severely impaired in patients F1-II-1 and F2-II-2. No predisposing factors were revealed from their medical and family history. All affected individuals failed the automated auditory brainstem response testing during the neonatal hearing screening and were diagnosed with sensorineural hearing loss. Hearing impairment appeared to be nonsyndromic,

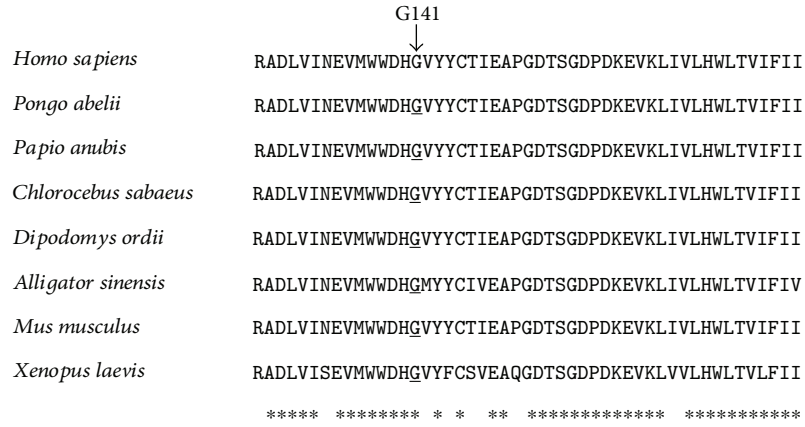

Figure 2: Multispecies sequence alignment of ILDR1 showing the evolutionarily conserved G141 residue.

Table 1: Genotype of SNPs in chromosome 3 for probands F1-II-1 and F2-II-1.

dbSNP	Chromosome	Position	Gene	Genotype		MAF in Chinese Hans
				F1-II-1	F2-II-1	
rs78962087	3p13	70014199	*MITF*	C/A	C/C	0.0021
rs2306522	3p21.31	45542083	*LARS2*	T/T	T/C	0.1413
rs11549809	3p21.31	45557707	*LARS2*	G/A	G/G	0.1413
rs10578999	3p21.31	46751073	*TMIE*	TAAG/T	T/T	0.7314
p.G141R	3q13.33	121720670	*ILDR1*	G/G	G/G	0
rs2877561	3q13.33	121712051	*ILDR1*	C/C	A/A	0.6304
rs16846663	3q25.1	150658264	*CLRN1*	G/A	G/G	0
rs187218889	3q25.1	150690487	*CLRN1*	G/T	G/G	0.0057
rs3796240	3q25.1	150690566	*CLRN1*	T/T	C/C	0.0630
rs188384	3q28	191074873	*CCDC50*	G/G	C/C	0.6435
rs11542549	3q28	191075902	*CCDC50*	C/T	C/C	0.1652
rs2028573	3q28	191093080	*CCDC50*	A/A	G/G	0.1500
rs4677728	3q28	191093310	*CCDC50*	A/G	A/A	0.0783
rs4677729	3q28	191093384	*CCDC50*	A/A	G/G	0.0152
rs188384	3q28	191094873	*CCDC50*	G/G	C/C	0.6434
rs34031057	3q28	191097928	*CCDC50*	G/G	G/GT	0.0109
rs7624750	3q29	193334991	*OPA1*	G/A	G/G	0.2457
rs166850	3q29	193355074	*OPA1*	C/C	T/T	0.6739
rs10451941	3q29	193355102	*OPA1*	T/C	T/T	0.2000
rs9851685	3q29	193374964	*OPA1*	T/C	T/T	0.2326
rs3772393	3q29	193336639	*OPA1*	T/C	T/T	0.2000

and no congenital anomalies, facial dysmorphisms, or intellectual disabilities were reported by the families or detected during physical examination. No vestibular symptoms were recorded.

3.2. Identification and Verification of the p.G141R Mutation in ILDR1. Targeted next-generation sequencing of 159 known deafness genes in probands F1-II-1 and F2-II-1 identified a total of 8 and 6 variants, respectively (Supplementary Table 2). In both cases, a homozygous c.421G>C (p.G141R) variant in *ILDR1* (NM_001199799) was the only candidate variant consistent with the possible recessive inheritance. Sanger sequencing confirmed cosegregation of this mutation and the hearing impairment in family 1 and family 2, with all affected individuals being homozygous and all parents of the affected being heterozygous (Figure 1). The p.G141R mutation changed codon GGU to GCU in exon 4, substituting an evolutionarily conserved amino acid arginine with histidine in the immunoglobulin superfamily domain of ILDR1 (Figure 2). This mutation was predicted to be pathogenic by programs PolyPhen-2, SIFT, and MutationTaster. It has a minor allele frequency of 0.00009 in gnomAD and was not seen in 200 Chinese Han normal hearing controls. The F1 and F2 families originated from Jiangsu and Zhejiang provinces, respectively, two distinct regions of China. Neither of the families were from

Table 2: Summary of mutations in *ILDR1* that are associated with DFNB42.

Mutation (protein)	Affected domains	Hearing phenotype	Ethnic group	Reference
p.Met1Ile*ext*+136	Signal peptide and extracellular domain	Moderate to profound	Pakistan	[3]
p.Gly20_Thr31del	Signal peptide and extracellular domain	Moderate to profound	Iranians	[3]
p.V28SfsX31	Extracellular, transmembrane, and intracellular domains	N/A	Pakistan	[3]
p.Pro69His	Extracellular domain	Postlingual onset and partial deafness	Korean	[11]
p.Arg97Gln	Extracellular domain	N/A	Pakistan	[3]
p.Val102Glu	Extracellular domain	Severe to profound	Iranian	[10]
p.Asn109_Pro111dup	Extracellular domain	Moderate to profound	Saudi Arabian	[9]
p.Trp137CysfsX25	Extracellular domain	N/A	Pakistan	[3]
p.G141R	Extracellular domain	Moderate to profound	Chinese	This study
p.Tyr143Cys	Extracellular domain	Moderate to profound	Iranians	[15]
p.Trp168LysfsTer47	Transmembrane and intracellular domains	Severe	Pakistan	[3]
p.Gln195X	Intracellular domain	Severe to profound	Iranians	[3]
p.Glu269ArgfsTer47	Intracellular domain	Severe to profound	United Arab Emirates	[13]
p.Q274X	Intracellular domain	N/A	Iranian	[8]
p.C314X	Intracellular domain	N/A	Iranian	[7]
p.Thr345ProfsX20	Intracellular domain	Severe	Pakistan	[3]
p.Glu379X	Intracellular domain	Severe to profound	Pakistan	[3]
p.Glu394SerfsX15	Intracellular domain	Severe	Pakistan	[3]
p.S406X	Intracellular domain	Moderate to profound	Iranian	[10]
p.Arg453Gln	Intracellular domain	Severe to profound	Pakistan	[3]

consanguineous marriage. Based on sequencing results of *ILDR1* and other deafness genes in chromosome 3, F1-II-1 and F2-II-1 has a distinct genotype for a number of SNPs (Table 1), suggesting that those two probands were not closely related.

4. Discussion

In this study, we reported a novel p.G141R mutation in *ILDR1* as the likely genetic cause for the autosomal recessive sensorineural hearing loss (ARSNHL) in two Chinese Han families. Evidence supporting the pathogenic roles of the p.G141R mutation includes: (1) Homozygous p.G141R mutation was identified in all three affected individuals (F1-II-1, F2-II-1, and F2-II-2), and the intrafamilial segregation pattern is consistent with the recessive inheritance (Figure 1). (2) Targeted NGS of 159 known deafness genes identified p.G141R as the only likely pathogenic mutation in probands of both families (Supplementary Table 2). (3) The p.G141R has an extremely low MAF of 0.00009 in 277,128 alleles in the gnomAD database and was absent in 200 ethnically matched normal hearing controls. (4) The p.G141R mutation changes an evolutionarily conserved amino of ILDR1 (Figure 2) and is unanimously predicted to be pathogenic by computational analysis tools PolyPhen-2, SIFT, and MutationTaster. (5) Based on the ACMG guideline [18], the p.G141R variant should be defined as likely pathogenic as it meets with 1 PS4 (the prevalence of the variant in affected individuals is significantly increased compared with the prevalence in controls) and 1 PM2 (extremely low frequency in controls if recessive) criteria.

To date, only 19 *ILDR1* mutations have been reported. Interestingly, most mutations were identified from populations in south and west Asia (Table 2). To our knowledge, our study is the first report of *ILDR1* mutations in Chinese Hans. The two families with the *ILDR1* mutations were identified by targeted NGS of 162 sporadic deaf probands with likely recessive inheritance. The incidence of the pathogenic *ILDR1* variants, therefore, is estimated to be approximately 1.2% in Chinese Han deaf patients. Since homozygous p.G141R mutations were identified in both nonconsanguineous families in the current study and our SNP genotyping analysis suggested that families F1 and F2 were unlikely to be closely related (Table 1), the p.G141R mutation in *ILDR1* may be relatively frequent in Chinese Hans and deserve further screening in expanded studies of deaf patients in China.

Of the 19 previously reported *ILDR1* mutations, the majority were nonsense mutations, indels, and stop-codon mutations that significantly truncates or alters the protein structure of ILDR1 (Figure 3, top). Interestingly, 5 of the 6 missense mutations in *ILDR1* including p.G141R were within the extracellular immunoglobulin (Ig) superfamily domain (Figure 3, bottom), suggesting that this domain may have a critical role in relation to the hearing function. On the other hand, the onset and severity of hearing impairment associated with DFNB42 are diverse and there is no clear

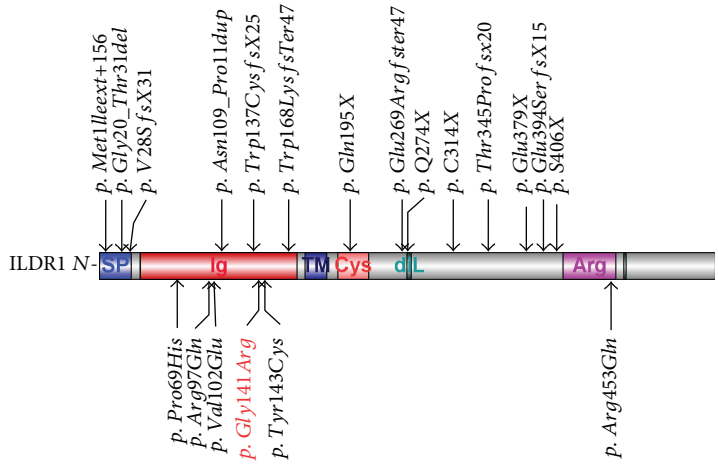

Figure 3: Schematic representation of the functional domains of ILDR1 and the locations of *ILDR1* mutations. The nonmissense and missense mutations are listed above and under the domain structure, respectively.

genotype-phenotype correlation between the missense and nonmissense mutations (Table 2). Our results further verified this point as the affected individuals of families F1 and F2 had moderate and profound hearing impairment, respectively.

Our results also showed that targeted NGS is a powerful tool for the identification of the genetic causes of rare, heterogeneous disorders such as hearing impairment. The implication of this method should be recommended especially when the mutation is rare and the family size is limited, in which cases other methods such as an association study or linkage analysis will not be available.

5. Conclusions

The novel p.G141R mutation in *ILDR1* is the likely genetic cause for the hearing impairment in two unrelated Chinese Han DFNB42 families. Targeted NGS is recommended for mutation identification of the rare deafness genes in small families or sporadic cases.

Conflicts of Interest

The authors declare no conflicts of interests.

Authors' Contributions

Xueling Wang, Longhao Wang, and Hu Peng contributed equally to this work.

Acknowledgments

This research was supported by grants from the National Key R&D Program of China (2017YFC1001800 to HW), National Science Foundation of China (81700899 to XW, 81570930 to TY, and 81702643 to HP), Shanghai Municipal Science and Technology Commission (14DZ2260300 to HW and 16YF1403400 to HP), Shanghai Municipal Commission of Health and Family Planning Foundation (201740005 to XW and 201540173 to HP), China Postdoctoral Science Foundation (2017M611586 to HP) and Shanghai Municipal Education Commission—Gaofeng Clinical Medicine Grant (20152519 to TY).

Supplementary Materials

Supplementary Table 1: 159 deafness genes targeted for the next-generation sequencing. Supplementary Table 2: candidate variants identified by targeted NGS for probands F1-II-1 and F2-II-1. *(Supplementary Materials)*

References

[1] N. E. Morton, "Genetic epidemiology of hearing impairment," *Annals of the New York Academy of Sciences*, vol. 630, no. 1 Genetics of H, pp. 16–31, 1991.

[2] P. D'Adamo, V. I. Guerci, A. Fabretto et al., "Does epidermal thickening explain GJB2 high carrier frequency and heterozygote advantage?," *European Journal of Human Genetics*, vol. 17, no. 3, pp. 284–286, 2009.

[3] G. Borck, A. U. Rehman, K. Lee et al., "Loss-of-function mutations of *ILDR1* cause autosomal-recessive hearing impairment DFNB42," *American Journal of Human Genetics*, vol. 88, no. 2, pp. 127–137, 2011.

[4] T. Higashi, T. Katsuno, S. Kitajiri, and M. Furuse, "Deficiency of Angulin-2/ILDR1, a tricellular tight junction-associated membrane protein, causes deafness with cochlear hair cell degeneration in mice," *PLoS One*, vol. 10, no. 3, article e0120674, 2015.

[5] Y. Gong, N. Himmerkus, A. Sunq et al., "ILDR1 is important for paracellular water transport and urine concentration mechanism," *Proceedings of the National Academy of Sciences of the United States of America*, vol. 114, no. 20, pp. 5271–5276, 2017.

[6] M. Aslam, M. Wajid, M. H. Chahrour et al., "A novel autosomal recessive nonsyndromic hearing impairment locus (DFNB42) maps to chromosome 3q13.31-q22.3," *American Journal of Medical Genetics Part A*, vol. 133A, no. 1, pp. 18–22, 2005.

[7] G. Bademci, J. Foster, N. Mahdieh et al., "Comprehensive analysis via exome sequencing uncovers genetic etiology in autosomal recessive nonsyndromic deafness in a large multiethnic cohort," *Genetics in Medicine*, vol. 18, no. 4, pp. 364–371, 2016.

[8] O. Diaz-Horta, D. Duman, J. Foster et al., "Whole-exome sequencing efficiently detects rare mutations in autosomal recessive nonsyndromic hearing loss," *PLoS One*, vol. 7, no. 11, article e50628, 2012.

[9] K. Ramzan, K. Taibah, A. I. Tahir et al., "*ILDR1*: novel mutation and a rare cause of congenital deafness in the Saudi Arabian population," *European Journal of Medical Genetics*, vol. 57, no. 6, pp. 253–258, 2014.

[10] Z. Mehrjoo, M. Babanejad, K. Kahrizi, and H. Najmabadi, "Two novel mutations in *ILDR1* gene cause autosomal recessive nonsyndromic hearing loss in consanguineous Iranian families," *Journal of Genetics*, vol. 94, no. 3, pp. 483–487, 2015.

[11] N. K. D. Kim, T. Higashi, K. Y. Lee et al., "Downsloping high-frequency hearing loss due to inner ear tricellular tight junction disruption by a novel *ILDR1* mutation in the Ig-like domain," *PLoS One*, vol. 10, no. 2, article e0116931, 2015.

[12] F. Talebi, F. G. Mardasi, J. M. Asl, and M. Sayahi, "Next-generation sequencing identifies three novel missense variants in *ILDR1* and *MYO6* genes in an Iranian family with hearing loss with review of the literature," *International Journal of Pediatric Otorhinolaryngology*, vol. 103, pp. 103–108, 2017.

[13] A. Tlili, A. Fahd al Mutery, M. Mahfood, W. Kamal Eddine Ahmad Mohamed, and K. Bajou, "Identification of a novel frameshift mutation in the *ILDR1* gene in a UAE family, mutations review and phenotype genotype correlation," *PLoS One*, vol. 12, no. 9, article e0185281, 2017.

[14] M. Dokmanovic-chouinard, W. K. Chung, J. C. Chevre et al., "Positional cloning of "Lisch-Like", a candidate modifier of susceptibility to type 2 diabetes in mice," *Plos Genetics*, vol. 4, no. 7, p. e1000137, 2008.

[15] I. A. Adzhubei, S. Schmidt, L. Peshkin et al., "A method and server for predicting damaging missense mutations," *Nature Methods*, vol. 7, no. 4, pp. 248-249, 2010.

[16] P. Kumar, S. Henikoff, and P. C. Ng, "Predicting the effects of coding non-synonymous variants on protein function using the SIFT algorithm," *Nature Protocols*, vol. 4, no. 7, pp. 1073–1081, 2009.

[17] J. M. Schwarz, D. N. Cooper, M. Schuelke, and D. Seelow, "MutationTaster2: mutation prediction for the deep-sequencing age," *Nature Methods*, vol. 11, no. 4, pp. 361-362, 2014.

[18] S. Richards, N. Aziz, S. Bale et al., "Standards and guidelines for the interpretation of sequence variants: a joint consensus recommendation of the American College of Medical Genetics and Genomics and the Association for Molecular Pathology," *Genetics in Medicine*, vol. 5, no. 17, pp. 405–424, 2015.

Hindawi
Neural Plasticity
Volume 2018, Article ID 4610592, 10 pages
https://doi.org/10.1155/2018/4610592

Research Article

The Benefits of Residual Hair Cell Function for Speech and Music Perception in Pediatric Bimodal Cochlear Implant Listeners

Xiaoting Cheng,[1,2] Yangwenyi Liu,[1,2] Bing Wang,[1,2] Yasheng Yuan,[1,2] John J. Galvin III,[3] Qian-Jie Fu,[4] Yilai Shu,[1,2] and Bing Chen[1,2]

[1]*Department of Otology and Skull Base Surgery, Eye and Ear, Nose, Throat Hospital of Fudan University, Shanghai, China*
[2]*Key Laboratory of Hearing Medicine, National Health and Family Planning Commission, Shanghai, China*
[3]*House Ear Institute, Los Angeles, CA, USA*
[4]*Department of Head and Neck Surgery, David Geffen School of Medicine, UCLA, Los Angeles, CA, USA*

Correspondence should be addressed to Yilai Shu; yilai_shu@fudan.edu.cn and Bing Chen; bingchen@fudan.edu.cn

Received 27 December 2017; Accepted 13 March 2018; Published 15 April 2018

Academic Editor: Geng-lin Li

Objective. The aim of this study was to investigate the benefits of residual hair cell function for speech and music perception in bimodal pediatric Mandarin-speaking cochlear implant (CI) listeners. *Design*. Speech and music performance was measured in 35 Mandarin-speaking pediatric CI users for unilateral (CI-only) and bimodal listening. Mandarin speech perception was measured for vowels, consonants, lexical tones, and sentences in quiet. Music perception was measured for melodic contour identification (MCI). *Results*. Combined electric and acoustic hearing significantly improved MCI and Mandarin tone recognition performance, relative to CI-only performance. For MCI, performance was significantly better with bimodal listening for all semitone spacing conditions ($p < 0.05$ in all cases). For tone recognition, bimodal performance was significantly better only for tone 2 (rising; $p < 0.05$). There were no significant differences between CI-only and CI + HA for vowel, consonant, or sentence recognition. *Conclusions*. The results suggest that combined electric and acoustic hearing can significantly improve perception of music and Mandarin tones in pediatric Mandarin-speaking CI patients. Music and lexical tone perception depends strongly on pitch perception, and the contralateral acoustic hearing coming from residual hair cell function provided pitch cues that are generally not well preserved in electric hearing.

1. Introduction

For cochlear implant (CI) users, access to residual acoustic hearing in the contralateral ear can greatly benefit speech and music performance. Residual acoustic hearing provides detailed low-frequency information that can greatly benefit CI users under challenging listening condition. Bimodal listening—electric stimulation in one ear and acoustic stimulation (aided or unaided) in the contralateral ear—has been shown to significantly improve speech and music performance over the CI alone [1–26].

Most previous bimodal CI studies have been conducted with English-speaking CI users. For tonal languages such as Mandarin Chinese, the perception of lexical tones depends strongly on fundamental frequency (F0) cues [27]. The coarse spectral resolution provided by the CI is not sufficient to support complex pitch perception, which is needed for difficult listening tasks such as music perception, F0 perception, and speech understanding in noise [28]. Despite the weak F0 cues, Mandarin-speaking CI users are able to achieve moderately good tone recognition performance [20, 29–34], most likely due to perception of amplitude contour and duration cues that covary with F0 in naturally uttered Chinese tones [29, 34]. For patients with some amount of residual acoustic hearing, combining a hearing aid (HA) with the CI may represent the best opportunity to improve CI users' Chinese tone recognition. Aided acoustic hearing may provide the F0 cues necessary for tone recognition in addition to amplitude and duration cues available with the CI.

Previous studies with Chinese-speaking CI users have shown significant benefits for bimodal listening over the CI alone. Yuen et al. [24] measured tone and disyllable word

recognition in quiet and in noise in 15 Mandarin-speaking pediatric bimodal CI listeners aged 5 to 14 years old. Head shadow benefits in noise, tone, and disyllable word recognition were significantly better with bimodal than CI-only listening. Li et al. [35] found significantly better tone, vowel, and consonant recognition with bimodal listening (relative to CI-only) in 12 Mandarin-speaking CI users aged 16 to 24 years old. Interestingly, the bimodal benefit for tone recognition in quiet was significantly correlated with CI experience, suggesting that bimodal CI users learn to better combine the low-frequency spectrotemporal cues from acoustic hearing with the temporal envelope cues from electric hearing over time. Chang et al. [36] measured Mandarin tone, syllable, and vowel recognition in 15 prelingually deaf Mandarin-speaking bimodal CI users aged 10 to 20 years old. Tone and syllable recognition significantly improved with bimodal listening, while vowel recognition did not. Correlation analyses revealed that the bimodal benefits could not be predicted by acoustic hearing thresholds in the nonimplanted ear or by demographic variables of the participants. Yang and Zeng [37] measured bimodal benefits in 13 Mandarin-speaking bimodal listeners aged 5 to 46 years old (mean: 15.3 years old). There was a significant bimodal benefit for word recognition, largely due to better consonant and tone recognition.

Taken together, these previous studies demonstrated bimodal benefits in adult and pediatric Mandarin-speaking CI users for some listening tasks and conditions. However, the bimodal benefits varied across studies, and the number of subjects in each study was relatively small (4–15 subjects, depending on the study and conditions). Previous studies have also shown that Mandarin-speaking pediatric CI users have difficulty with pitch-related music perception, such as melodic contour identification (MCI; [20]). Crew et al. [5] showed that combined acoustic and electric hearing provides significantly better MCI recognition performance when comparing to CI-only conditions in English-speaking CI adults. Mandarin-speaking pediatric CI users may similarly benefit from combined acoustic and electric hearing for melodic pitch perception, but this has yet to be tested.

In this study, bimodal benefits for music and speech perception were studied in a large cohort of Mandarin-speaking pediatric CI users ($n = 35$). Music perception was measured using an MCI task, and Mandarin speech perception in quiet was measured using vowel, consonant, tone, and sentence recognition tasks. Performance was measured with the CI-only or with the CI + HA. Bimodal and CI-only performances were compared to various demographic variables, and music and speech perception was compared to one another to observe potential contributions of pitch cues to the different listening tasks.

2. Materials and Methods

2.1. Ethics Statement. The study and the informed consent procedures were approved by the local ethics committee (Ethics Committee of the Eye, Ear, Nose, and Throat Hospital, Fudan University, approval number: KY2012-009), and written informed consent was obtained from children's parents before participation.

2.2. Subjects. Thirty-five (10 females and 25 males) Mandarin-speaking pediatric CI patients were recruited from the Shanghai Rehabilitation Center, Shanghai, China. The inclusion criteria were that all pediatric participants used a CI in one ear and a HA in the contralateral ear for at least 6 months. The exclusion criteria were formal music training experience, as well as any cognitive, visual, and intelligence disorders. Across all CI subjects, the mean age at testing was 6.5 years (range: 4.9–12.3 years), the mean age at implantation was 2.9 years (range: 0.9–7.0 years), the mean CI experience was 3.5 years (range: 0.6–8.1 years), and the mean HA experience was 2.7 years (range: 0.5–9.0 years). Demographic information is shown in Table 1.

2.3. Audiometric Thresholds. Aided thresholds with the CI-only and the HA-only were measured in sound field using warble tones and using subjects' clinical settings for the CI and HA. All subjects were tested in a sound-treated booth and seated directly facing a single loudspeaker positioned 1 m away from the subject. Unaided thresholds were collected using pure tone with headphones. Pure-tone average (PTA) thresholds across 0.5, 1.0, and 2.0 kHz are shown for each subject in Table 1.

2.4. Music and Speech Perception. All stimuli were presented in sound field at 65 dBA. Music and speech perception was measured with the CI-only and with the CI + HA; subjects were tested using the clinical settings for each device, which were not changed throughout the study. All stimuli were presented, and responses were collected using custom software (Mandarin Angel Sound software; freely available at http://mast.emilyfufoundation.org); performance was scored in terms of percent correct.

2.4.1. Music Stimuli and Test Procedures. MCI stimuli were similar to those in previous studies (Galvin et al. [38, 39]) and consisted of nine melodic contours (rising, rising-flat, rising-falling, flat-rising, flat, flat-falling, falling-rising, falling-flat, or falling), composed of five notes of equal duration (250 ms, with 50 ms of silence between each note). The lowest note in any contour was C4 (262 Hz). The spacing between successive notes in each contour was varied to be 1, 2, 3, or 5 semitones. The instrument used for the contour was a piano sample, as in Galvin et al. [39]. Thus, the stimulus set consisted of 36 stimuli (9 melodic contours × 4 semitone spacing), and all 36 stimuli were presented during each test run.

MCI was measured using a 9-alternative forced choice (9-AFC) procedure. Prior to formal testing, a practice session was conducted to familiarize subjects with the stimuli, task, and procedures. During testing, a contour would be randomly selected from the stimulus set and presented to the subject, who responded by clicking on one of the response boxes shown on the computer screen.

2.4.2. Mandarin Tone Recognition in Quiet. Mandarin tone stimuli consisted of 4 tonal patterns produced by two males and two females, taken from the Standard Chinese Database

Table 1: CI subject demographic information.

Subject	Etiology	Gender	Age at testing (yrs)	Age at CI (yrs)	Dur deaf (yrs)	CI exp (yrs)	HA exp (yrs)	CI device	CI strategy	Aided PTA dB HL	Unaided PTA dB HL
S1	Unknown	F	9.2	4.0	4.0	5.2	1.00	AB HiRes 90K	F120	36.7	70.0
S2	Unknown	M	7.3	3.1	3.1	4.2	3.80	Cochlear N-24	ACE	45.0	70.0
S3	LVAS	F	5.0	3.0	2.0	1.0	2.00	Cochlear N-24	ACE	40.0	73.3
S4	Unknown	M	10.0	5.0	5.0	5.0	9.00	Cochlear N-24	ACE	53.3	73.3
S5	Unknown	M	5.9	1.3	1.3	4.6	4.00	AB HiRes 90K	F120	33.3	75.0
S6	LVAS	F	8.0	2.3	2.3	5.7	6.00	MED-EL Pulsar	FSP	38.3	80.0
S7	LVAS	F	5.0	2.0	3.0	3.0	3.00	MED-EL Pulsar	FSP	40.0	83.3
S8	LVAS	M	7.2	5	2	2.2	2.00	AB HiRes 90K	F120	41.7	83.3
S9	Unknown	M	5.8	1.0	1.0	4.8	5.00	Cochlear N-24	ACE	35.0	88.3
S10	LVAS	M	6	1.5	1.5	4.5	3.30	AB HiRes 90K	F120	46.7	88.3
S11	LVAS	M	5.3	4.7	4.7	0.6	4.70	AB HiRes 90K	F120	35.0	90.0
S12	Unknown	M	8.1	7.0	2.0	1.1	3.00	MED-EL Pulsar	FSP	38.3	90.0
S13	LVAS	F	6.1	3.5	1.2	2.6	3.80	MED-EL Pulsar	FSP	48.3	91.7
S14	Unknown	M	5.9	3.1	3.1	2.8	1.00	MED-EL Pulsar	FSP	45.0	93.3
S15	LVAS	M	5.5	2	1	3.5	4.50	MED-EL Pulsar	FSP	40.0	96.7
S16	Unknown	F	5.6	2.1	2.1	3.5	2.00	Cochlear N-24	ACE	46.7	96.7
S17	Unknown	M	6.5	2.3	2.3	4.2	0.50	Cochlear N-24	ACE	53.3	96.7
S18	Unknown	F	5.2	1	1	4.2	1.00	MED-EL Pulsar	FSP	45.0	98.3
S19	Unknown	M	12.3	5.6	5.6	6.7	2.50	Cochlear N-24	ACE	56.7	98.3
S20	Unknown	M	5.8	3.3	3.3	2.5	1.00	Cochlear N-24	ACE	50.0	98.3
S21	Unknown	M	5.2	2.8	2.8	2.4	1.00	MED-EL Pulsar	FSP	36.7	98.3
S22	Unknown	M	5.2	3.1	3.1	2.1	5.00	MED-EL Pulsar	FSP	63.3	100.0
S23	LVAS	M	8.4	3.1	3.1	5.3	0.50	AB HiRes 90K	F120	56.7	105.0
S24	Unknown	F	5	1	4	3	4.00	Cochlear N-24	ACE	56.7	105.0
S25	Unknown	F	7.0	6.0	6.0	1.0	3.00	MED-EL Pulsar	FSP	58.3	106.7
S26	Unknown	M	5.2	1	1	4.2	0.60	MED-EL Pulsar	FSP	75.0	108.3
S27	Unknown	M	10.0	1.9	1.9	8.1	7.00	Cochlear N-24	ACE	70.0	108.3
S28	Unknown	M	5.2	3.0	3.0	2.2	1.50	Cochlear N-24	ACE	46.7	108.3
S29	Unknown	M	4.9	0.9	0.9	4	4.00	Cochlear N-24	ACE	65.0	110.0
S30	Unknown	M	6	2.6	2.6	3.4	1.00	MED-EL Pulsar	FSP	46.7	110.0
S31	Unknown	M	5.9	3.4	3.4	2.5	1.00	Cochlear N-24	ACE	60.0	110.0
S32	Unknown	M	6.8	2	2	4.8	1.00	Cochlear N-24	ACE	63.3	111.7
S33	Unknown	F	7.8	5.8	5.8	2.0	0.50	Cochlear N-24	ACE	61.7	111.7
S34	Unknown	M	5.1	0.9	0.9	4.2	1.00	MED-EL Pulsar	FSP	95.0	115.0
S35	Unknown	M	5.0	4.0	4.0	5.2	1.00	Cochlear N-24	ACE	66.7	115.0
AVE			6.5	2.9	2.7	3.5	2.7			51.1	96.0
SE			0.3	0.3	0.2	0.3	0.4			2.3	2.3

LAVS = large vestibular aqueduct syndrome; F = female; M = male; age at CI = age at cochlear implantation; dur deaf = duration of deafness; CI exp = CI experience; HA exp = HA experience; N-24 = Nucleus 24; AB = Advanced Bionics; ACE = advanced combination encoder; F120 = Fidelity 120; FSP=fine-structure processing; PTA = pure-tone average threshold across 0.5, 1.0, and 2.0 kHz. AVE = average; SE = standard error.

recorded at University of Science and Technology of China [40]. The four tonal patterns included tone 1 (high-level), tone 2 (high-rising), tone 3 (falling-rising), and tone 4 (high-falling), produced for 4 monosyllables (b/a/, b/o/, b/u/, and b/i/). Thus, the stimulus set consisted of 64 stimuli (4 tones × 4 monosyllables × 4 talkers), and all 64 stimuli were presented during each test run. During testing, a stimulus would be randomly selected from the stimulus set and presented to the subject, who responded by clicking on one of the 4 response boxes (labelled according to tone number) shown on the computer screen. No trial-by-trial feedback or training was provided.

2.4.3. Vowel Recognition in Quiet. Vowel stimuli were monosyllabic words produced by one male and one female talker, taken from the same Standard Chinese Database as tone stimuli. Vowel stimuli consisted of six groups of 4 vowels each; the initial consonant for each group was the same. The six groups of vowel stimuli included (1) yá, yáng, yú, yíng, (2) mò, mù, mèi, miè, (3) qiú, qué, qín, qún, (4) guī, gōu, gēn, gōng, (5) shé, shí, sháo, shéng, and (6) chá, chái, chán, chún. Thus, there were 24 vowel stimuli in the stimulus set. During testing, a group would be randomly selected, and a vowel stimulus would be randomly selected from within the group and presented to the subject, who responded by clicking on one of the 4 response choices labelled according to the vowels in the selected group. No trial-by-trial feedback or training was provided. All 24 stimuli were presented during the test run.

2.4.4. Consonant Recognition in Quiet. Consonant stimuli were monosyllabic words produced by one male and one female talker, taken from the same Standard Chinese Database as tone stimuli. Similar to the vowel stimuli, consonant stimuli consisted of six groups of 4 consonants each; the final vowel for each group was the same. The six groups of consonant stimuli included (1) jì, rì, cì, sì, (2) pí, lí, qí, xí, (3) fù, tù, nù, bù, (4) gǔ, hǔ, zhǔ, wǔ, (5) gǒu, kǒu, shǒu, zǒu, and (6) māo, dāo, chāo, yāo. Thus, there were 24 consonant stimuli in the stimulus set. During testing, a group would be randomly selected, and a consonant stimulus would be randomly selected from within the group and presented to the subject, who responded by clicking on one of the 4 response choices labelled according to the consonants in the selected group. No trial-by-trial feedback or training was provided. All 24 stimuli were presented during the test run.

2.4.5. Sentence Recognition in Quiet. Sentence recognition was measured using sentences from the Mandarin speech perception (MSP) test, which consisted of 10 lists of 10 sentences, each sentence with 7 syllables [41, 42]. Sentence recognition was measured using an open-set paradigm. During testing, a list was randomly selected, and a sentence was randomly selected from the list and presented to the subject, who repeated as many words as possible. The experimenter scored the correctly identified words. One MSP list was presented for each test session, and no lists were repeated within test subjects.

3. Results

Figure 1 shows boxplots of MCI scores with the CI-only and with CI + HA. Mean MCI performance improved from 47% correct with the CI-only to 58% correct with CI + HA. A two-way RM ANOVA with listening condition (CI, CI + HA) and semitone spacing (1, 2, 3, and 5) as factors showed a significant effect for listening condition [$F(1,102) = 30.9$, $p < 0.001$], but not for semitone spacing [$F(3,102) = 2.2$, $p = 0.098$]; there was no significant interaction [$F(3,102) = 0.9$, $p = 0.427$]. Post hoc Bonferroni pairwise comparisons showed that MCI performance was significantly better with CI + HA than with the CI-only for all semitone spacing conditions ($p > 0.05$ in all cases).

Figure 2 shows boxplots of tone recognition scores with the CI-only and with CI + HA. A two-way RM ANOVA with listening condition and lexical tone (1, 2, 3, and 4) as factors showed significant effects for listening condition [$F(1,102) = 4.9$, $p = 0.034$] and lexical tone [$F(3,102) = 11.9$, $p < 0.001$]; there was a significant interaction [$F(3,102) = 3.2$, $p = 0.028$]. Post hoc Bonferroni pairwise comparisons showed that performance was significantly better with CI + HA only for tone 2 ($p < 0.05$). With the CI + HA, performance was significantly poorer with tone 3 than with tone 1 or tone 4 ($p < 0.05$ in both cases). With the CI-only, performance was significantly better tones 1 and 4 than with tones 2 and 3 ($p < 0.05$ in all cases).

Figure 3 shows boxplots of vowel, consonant, tone, and sentence recognition scores with the CI-only and CI + HA. Note that due to time constraints, vowel and consonant recognition was measured in only 17 subjects; tone and sentence recognition was measured in all 35 subjects. Mean vowel recognition improved from 88% correct with the CI-only to 90% correct with CI + HA. A one-way RM ANOVA showed no significant difference between CI-only and CI + HA [$F(1,16) = 1.1$, $p = 0.302$]. Mean consonant recognition improved from 84% correct with the CI-only to 91% correct with CI + HA. A one-way RM ANOVA showed no significant difference between CI-only and CI + HA [$F(1,16) = 3.0$, $p = 0.103$]. Mean tone recognition improved from 87% correct with the CI-only to 91% correct with CI + HA. A one-way RM ANOVA showed that performance was significantly better with the CI + HA than with the CI-only [$F(1,34) = 4.9$, $p = 0.033$]. Mean sentence recognition improved from 79% correct with the CI-only to 82% correct with CI + HA. A one-way RM ANOVA showed no significant difference between CI-only and CI + HA [$F(1,34) = 1.7$, $p = 0.203$].

Demographic variables age at testing, age at cochlear implantation, duration of deafness, CI experience, HA experience, aided PTA threshold, and unaided PTA thresholds were compared to MCI, vowel recognition, consonant recognition, mean tone recognition, and sentence recognition with the CI-only or the CI + HA using Pearson correlations. Note that for the correlations for MCI, tone, and sentence recognition, $n = 35$; for vowel and consonant recognition, $n = 17$. The results are shown in Table 2. There were no significant correlations between any of the demographic variables and MCI or vowel recognition performance with the CI-only or

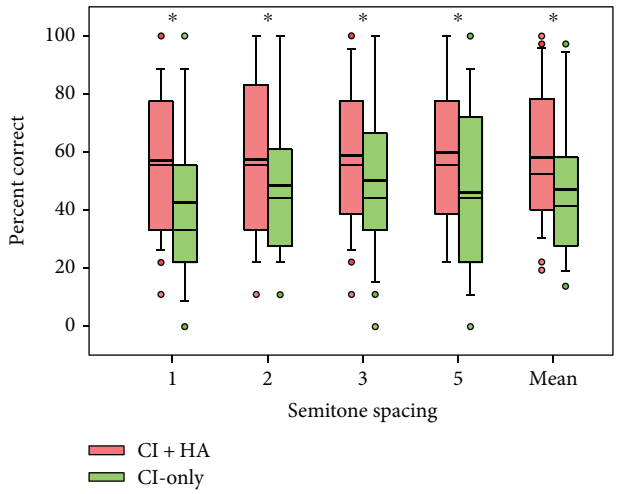

Figure 1: Box plots of MCI scores for different semitone spacing and across all semitone spacing with the CI-only and with the CI + HA. The boxes show the 25th and 75th percentiles, the error bars show the 5th and 95th percentiles, the circles show outliers, the thin solid line shows the median, the thick solid line shows the mean, and the asterisks indicate significant differences between CI + HA and CI-only performance.

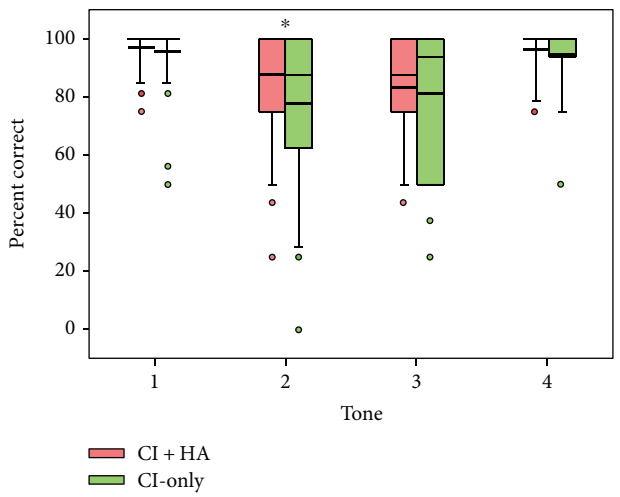

Figure 2: Box plots of tone recognition scores for the different lexical tones with the CI-only and with the CI + HA. The boxes show the 25th and 75th percentiles, the error bars show the 5th and 95th percentiles, the circles show outliers, the thin solid line shows the median, the thick solid line shows the mean, and the asterisks indicate significant differences between CI + HA and CI-only performance.

with the CI + HA ($p > 0.05$ in all cases). Consonant recognition with the CI-only or with the CI + HA was negatively correlated with age at CI and duration of deafness ($p < 0.05$ in all cases); consonant recognition with the CI-only was also correlated with CI experience ($p < 0.05$). Tone recognition with the CI-only or with the CI + HA was correlated with CI experience ($p < 0.05$ in both cases); tone recognition with the CI + HA was negatively correlated with age at cochlear implantation

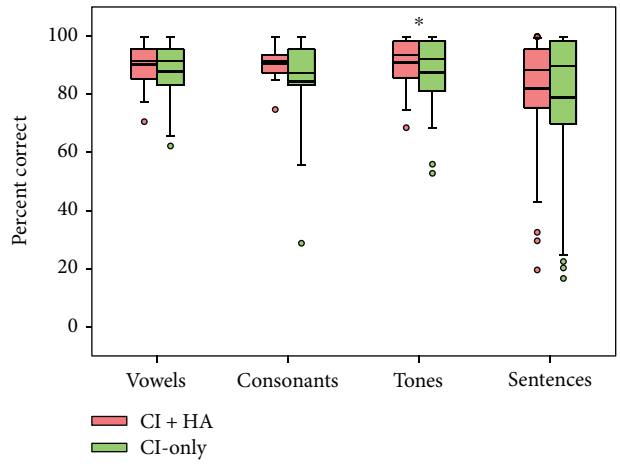

Figure 3: Box plots of vowel, consonant, tone (averaged across all 4 lexical tones), and sentence recognition scores with the CI-only and with the CI + HA. The boxes show the 25th and 75th percentiles, the error bars show the 5th and 95th percentiles, the circles show outliers, the thin solid line shows the median, the thick solid line shows the mean, and the asterisks indicate significant differences between CI + HA and CI-only performance.

($p < 0.05$). Sentence recognition with the CI-only was negatively correlated with age at cochlear implantation and duration of deafness ($p < 0.05$ in both cases) and correlated with CI experience and bimodal experience ($p < 0.05$ in both cases). Sentence recognition with the CI + HA was correlated with unaided PTA thresholds ($p < 0.05$).

Pearson correlation analyses were also performed among the various music and speech tests. With the CI-only or with the CI + HA, there were no significant correlations between MCI and any of the speech tests ($p > 0.05$ in all cases). With the CI-only or with the CI + HA, there were significant correlations among all the speech tests ($p < 0.05$ in all cases).

4. Discussion

The present data show that combined acoustic and electric hearing can significantly improve Mandarin-speaking pediatric CI patients' music and Mandarin tone perception, two listening tasks in which pitch cues are important. However, there was no significant bimodal benefit for vowel, consonant, or sentence recognition in quiet. Speech performance with the CI-only or with the CI + HA was significantly correlated with age at implantation and duration of deafness, underscoring the benefit of early implantation. Tone recognition was significantly correlated with all other speech measures, underscoring the strong contribution of lexical tone perception to Mandarin speech perception. Below, we discuss the results in greater detail.

4.1. CI-Only Music and Speech Performance

4.1.1. Music Perception. Mean MCI performance was generally poor (47% correct) and highly variable (range: 17–97% correct). Mean MCI performance was significantly better ($p < 0.001$) than the 23% correct reported in Tao et al. [20],

Table 2: Pearson correlations between demographic variables and music and speech perception.

		MCI		Vowel		Consonant		Tone		Sentence	
		r	*p*	*r*	*p*	*r*	*p*	*r*	*p*	*r*	*p*
CI-only	Age test	−0.02	0.904	−0.05	0.763	0.14	0.581	0.38	0.137	0.04	0.827
	Age CI	−0.08	0.669	−0.25	0.148	−0.50	*0.039**	−0.36	0.153	−0.43	*0.009**
	Dur deaf	−0.06	0.735	−0.32	0.059	−0.50	*0.039**	−0.32	0.208	−0.44	*0.008**
	CI exp	0.03	0.863	0.17	0.327	0.55	*0.023**	0.70	*0.002**	0.44	*0.008**
	HA exp	0.13	0.470	−0.07	0.686	−0.10	0.697	−0.05	0.848	0.20	0.239
	Bimodal exp	0.14	0.428	0.09	0.615	0.27	0.301	0.43	0.0878	0.38	*0.024**
	Aided PTA	0.17	0.351	0.17	0.522	0.24	0.362	0.09	0.603	0.01	0.977
	Unaided PTA	−0.02	0.911	−0.13	0.454	−0.19	0.476	−0.10	0.693	−0.33	0.055
CI + HA	Age test	−0.04	0.807	−0.14	0.440	−0.12	0.635	0.15	0.563	<0.01	0.997
	Age CI	−0.05	0.796	−0.21	0.234	−0.67	*0.003**	−0.50	*0.039**	−0.32	0.058
	Dur deaf	−0.18	0.327	−0.26	0.138	−0.66	*0.004**	−0.41	0.099	−0.33	0.056
	CI exp	<0.01	0.984	0.06	0.729	0.43	0.083	0.58	*0.014**	0.30	0.077
	HA exp	0.26	0.148	0.00	0.980	0.23	0.376	0.17	0.519	0.30	0.079
	Bimodal exp	0.23	0.206	0.06	0.752	0.37	0.149	0.43	0.087	0.3	0.082
	Aided PTA	0.02	0.914	−0.08	0.635	0.07	0.785	−0.02	0.932	−0.08	0.645
	Unaided PTA	−0.11	0.529	−0.15	0.399	0.13	0.618	−0.09	0.735	−0.39	*0.023**

The italics and asterisks indicate significant correlations ($p < 0.05$). MCI = melodic contour identification; age test = age at testing; age CI = age at cochlear implantation; dur deaf = duration of deafness; CI exp = cochlear implant experience; HA exp = hearing aid experience; PTA = pure-tone average threshold.

but comparable ($p = 0.11$) to the 34% correct reported in Fu et al. [43]; both studies were conducted with Chinese CI users. CI-only performance was also comparable to that in previous studies with adult English-speaking CI users [6, 38, 39]. In this study, there was no significant effect of semitone spacing, consistent with Tao et al. [20], who showed no significant differences among semitone spacing, except for between 1 and 6 semitones. Differences in subject age, duration of deafness, and previous acoustic hearing experience may have also contributed to differences in MCI performance observed between this and previous studies.

4.1.2. Speech Perception. Mean tone recognition with the CI-only was 87% correct, and recognition of tones 2 and 3 was significantly poorer than recognition of tones 1 and 4. While mean tone recognition score was comparable to the 81% correct reported in Tao et al. [20], recognition of individual tones differed between these studies even though the test materials and procedures were exactly the same. In Tao et al. [20], recognition of tone 2 was significantly poorer than that of tones 1, 3, and 4, and recognition of tone 4 was significantly better than that of the tones 1, 2, and 3. Recognition of tone 1 in this study was significantly poorer than that of Tao et al. [20] ($p < 0.05$), with no significant difference in between studies in recognition of tones 2, 3, and 4. Note that while significant, performance differences were generally small across these studies.

Mean baseline MSP sentence recognition was 79% correct, comparable to the 85% correct reported by Su et al. [44] for pediatric CI patients, but much higher than the 59% correct reported by Li et al. [45] for adult CI patients. Mean vowel (87% correct) and consonant (84% correct) recognition scores in quiet were much higher than reported in Li et al. [45] (58.9% and 45.8% correct for vowels and consonants, resp.). It is possible that differences in age at testing and duration of deafness may have contributed to the discrepancies in sentence recognition across studies. In Li et al. [45], adult subjects were tested; in China, adult CI users often experience a longer duration of hearing loss before implantation than children. Note also that phoneme recognition was measured using a 20-AFC procedure in Li et al. [45], compared to the 4-AFC procedure with multiple subsets of stimuli in this study.

4.2. Bimodal Benefits for Music and Speech Perception

4.2.1. Music Perception. Relative to CI-only, bimodal MCI performance improved by 11 percentage points. Mean bimodal MCI performance (58% correct) was poorer than the 72% correct reported for English-speaking adult bimodal listeners in Crew et al. [6]; in both studies, CI-only performance was comparable. Interestingly, bimodal performance was slightly poorer than HA-only performance in Crew et al. [6], suggesting that there was little bimodal benefit over the HA alone. In this study, HA-only performance was not measured. It is possible that the HA may have similarly carried MCI perception with bimodal listening; if so, it is unclear whether the present bimodal subjects experienced interference between acoustic and electric hearing. Alternatively, performance with the HA might have been poorer than that observed in Crew et al. [6]. Note that a slightly higher base note (the lowest note in a contour) was used in this study (C4 or 262 Hz) than in Crew et al. [5] (A3 or 220 Hz). Depending on the amount of aided acoustic hearing, some notes in the contours may have been near the limits of aided acoustic hearing. Finally, differences between postlingual

adults in Crew et al. [6] and the present prelingual pediatric CI users may have contributed to differences in bimodal MCI performance.

Bimodal MCI performance was significantly better than CI-only performance, in agreement with previous studies that showed a bimodal advantage for music perception [5, 10, 11, 13, 19, 46, 47]. Previous studies have shown that adding low-frequency acoustic hearing in the contralateral ear can improve CI users' pitch perception ([46, 48, 49]). Chen et al. [48] also found a significant correlation between HA experience and bimodal pitch perception in pediatric CI users, suggesting that HA experience before and/or implantation may help to develop pitch pattern perception. However, other studies have not shown significant bimodal advantages for music perception. Prentiss et al. [50] found a significant bimodal advantage for music chord perception, but not for musical timbre perception. Bartov and Most [51] found a bimodal advantage for song identification when listeners were presented with simple, tonal representations, but not for full arrangements, a cappella versions, or melodic and rhythmic versions. Thus, bimodal benefits may differ according to the amount of acoustic hearing in the contralateral ear, the amount of HA and/or bimodal listening experience, subject age, status of hearing loss (prelingual or postlingual), and the musical listening task.

4.2.2. Speech Perception. The present results showed a small but significant bimodal benefit for tone recognition (largely due to improved recognition of tone 2), consistent with previous findings ([35, 36]). However, there was no significant bimodal benefit for vowel, consonant, or sentence recognition in quiet, consistent with some previous studies [18, 35]. Li et al. [35] found a significant bimodal benefit for vowel recognition in quiet in adult Mandarin-speaking CI users, but not for tone or vowel recognition in quiet. Rathna-Kumar et al. [18] found a bimodal benefit for speech understanding in noise in India-speaking pediatric CI users, but not for speech understanding in quiet. Note that the variability in performance was reduced with the CI + HA, relative to CI-only.

One limit for bimodal benefits may have been ceiling performance for the speech perception measures in quiet. With the CI-only, mean tone, vowel, consonant, and sentence recognition performance was 87.3%, 87.7%, 84.3%, and 79.4% correct, respectively. With the CI + HA, mean tone, vowel, consonant, and sentence recognition performance improved by 3.8, 2.4, 6.4, and 3.1 percentage points, respectively. Most previous studies have shown bimodal benefits for speech understanding in noise (e.g., [3, 5, 6, 8, 9, 13, 18, 25, 26]). Although HA-only performance was not measured in the present study, there was likely a strong performance asymmetry between the HA and CI ears in the present subjects. Yoon et al. [23] showed a greater bimodal benefit when the performance asymmetry between ears was reduced. While it is likely that the present group of prelingual Mandarin pediatric CI users might have received a bimodal benefit in noise, this should be tested in a similarly large cohort.

4.3. Correlational Analyses. With the CI-only, consonant, tone, and sentence recognition was significantly correlated with CI experience. Consonant and sentence recognition was negatively correlated with age at implantation and duration of deafness. Taken together, these correlations underscore the benefit of early implantation for pediatric CI users. Interestingly, CI-only sentence recognition was significantly correlated with bimodal listening experience. It is possible that previous acoustic hearing or listening with the combined acoustic and electric hearing may have strengthened CI-only speech pattern recognition performance.

With the CI + HA, consonant and tone recognition was significantly correlated with age at implantation, and consonant recognition was significantly correlated with duration of deafness. While there were no significant correlations between sentence recognition and age at implantation ($r = -0.32$; $p = 0.058$), duration of deafness ($r = -0.33$; $p = 0.056$), CI experience ($r = 0.30$; $p = 0.077$), or HA experience ($r = 0.30$; $p = 0.079$), the relationship between sentence recognition and these demographic variables approached significance. Interestingly, unaided (rather than aided) PTA thresholds were significantly correlated with bimodal sentence recognition. The unaided PTA thresholds may reflect (to some degree) the health of the nonimplanted ear, with higher thresholds indicating poorer nerve survival. Aiding better ears may have required less amplification, compression, and overall signal distortion; broader auditory filters with greater hearing loss may have exacerbated distortion to the signal associated with the HA processing.

Significant correlations were observed among vowel, consonant, tone, and sentence recognition with the CI-only and with CI + HA, underscoring the importance of tone perception for sentence recognition [52]. Somewhat surprisingly, there were no correlations between MCI and any speech performance measures with the CI-only or with CI + HA. Given that pitch cues are important for both listening tasks, one might expect that better pitch perception would benefit both MCI and tone recognition. Tao et al. [20] also found no significant correlation between MCI and tone recognition in young Mandarin-speaking CI users. In both studies, ceiling performance for tone recognition in quiet most likely limited correlations. Tone recognition in noise might reduce ceiling performance effects and possibly show a relationship between MCI and tone recognition. Note that pitch cues in the MCI task occurred within a 1500 ms contour, while pitch cues for tone recognition occurred within a 300 ms syllable. Also, CI users were able to make use of duration and amplitude cues for tone recognition which may have contributed to ceiling performance effects; for MCI, duration and amplitude cues were kept constant within the contours.

5. Conclusions

Music and Mandarin speech perception was measured in 35 pediatric Chinese CI users with the CI alone and with the CI + HA (bimodal listening). Key findings include the following:

(1) Performance was significantly better with bimodal listening than with the CI-only for MCI and tone

perception in quiet. There was no significant bimodal advantage for vowel, consonant, or sentence recognition in quiet.

(2) With the CI-only, significant correlations were observed between CI experience and consonant, tone, and sentence recognition, between age at implantation and consonant and tone recognition, and between duration of deafness and consonant and tone recognition, underscoring the benefit of early implantation for Mandarin-speaking pediatric CI users.

(3) With the CI + HA, significant correlations were observed between age at implantation and consonant and tone recognition and between duration of deafness and consonant recognition. While not significant, notable relationships were observed between sentence recognition and age at implantation, duration of deafness, CI experience, and HA experience, suggesting that early implantation may benefit combined acoustic and electric hearing.

(4) There were significant correlations among all speech measures, underscoring the importance of tone perception to Mandarin sentence recognition. Despite the importance of pitch cues to both listening tasks, there was no correlation between MCI and tone recognition, most likely due to ceiling performance effects associated with tone recognition in quiet.

Conflicts of Interest

The authors declare that there is no conflict of interests regarding the publication of this paper.

Acknowledgments

The authors thank the subjects for their participation in this study. This work was partly supported by the National Institutes of Health (Grant no. R01-DC 004792), Joint project of key disease of health system in shanghai (2014ZYJB0005), and the National Natural Science Foundation of China (Grant nos. 81570914).

References

[1] M. Armstrong, P. Pegg, C. James, and P. Blamey, "Speech perception in noise with implant and hearing aid," *The American Journal of Otology*, vol. 18, Supplement 6, pp. S140–S141, 1997.

[2] S. Berrettini, S. Passetti, M. Giannarelli, and F. Forli, "Benefit from bimodal hearing in a group of prelingually deafened adult cochlear implant users," *American Journal of Otolaryngology*, vol. 31, no. 5, pp. 332–338, 2010.

[3] C. A. Brown and S. P. Bacon, "Achieving electric-acoustic benefit with a modulated tone," *Ear and Hearing*, vol. 30, no. 5, pp. 489–493, 2009.

[4] T. Y. Ching, P. Incerti, and M. Hill, "Binaural benefits for adults who use hearing aids and cochlear implants in opposite ears," *Ear and Hearing*, vol. 25, no. 1, pp. 9–21, 2004.

[5] J. D. Crew, J. J. Galvin 3rd, and Q. J. Fu, "Perception of sung speech in bimodal cochlear implant users," *Trends in Hearing*, vol. 20, article 233121651666932, 2016.

[6] J. D. Crew, J. J. Galvin 3rd, D. M. Landsberger, and Q.-J. Fu, "Contributions of electric and acoustic hearing to bimodal speech and music perception," *PLoS One*, vol. 10, no. 3, article e0120279, 2015.

[7] H. E. Cullington and F. G. Zeng, "Comparison of bimodal and bilateral cochlear implant users on speech recognition with competing talker, music perception, affective prosody discrimination, and talker identification," *Ear and Hearing*, vol. 32, no. 1, pp. 16–30, 2011.

[8] M. F. Dorman and R. H. Gifford, "Combining acoustic and electric stimulation in the service of speech recognition," *International Journal of Audiology*, vol. 49, no. 12, pp. 912–919, 2010.

[9] M. F. Dorman, R. H. Gifford, A. J. Spahr, and S. A. McKarns, "The benefits of combining acoustic and electric stimulation for the recognition of speech, voice and melodies," *Audiology & Neuro-Otology*, vol. 13, no. 2, pp. 105–112, 2008.

[10] F. El Fata, C. J. James, M. L. Laborde, M.-L. Laborde, and B. Fraysse, "How much residual hearing is 'useful' for music perception with cochlear implants?," *Audiology & Neurotology*, vol. 14, Supplement 1, pp. 14–21, 2009.

[11] K. E. Gfeller, C. Olszewski, C. Turner, B. Gantz, and J. Oleson, "Music perception with cochlear implants and residual hearing," *Audiology & Neurotology*, vol. 11, Supplement 1, pp. 12–15, 2006.

[12] J. H. Heo, J. H. Lee, and W. S. Lee, "Bimodal benefits on objective and subjective outcomes for adult cochlear implant users," *Korean Journal of Audiology*, vol. 17, no. 2, pp. 65–73, 2013.

[13] Y. Y. Kong, G. S. Stickney, and F. G. Zeng, "Speech and melody recognition in binaurally combined acoustic and electric hearing," *The Journal of the Acoustical Society of America*, vol. 117, no. 3, pp. 1351–1361, 2005.

[14] V. Looi, H. McDermott, C. McKay, and L. Hickson, "The effect of cochlear implantation on music perception by adults with usable pre-operative acoustic hearing," *International Journal of Audiology*, vol. 47, no. 5, pp. 257–268, 2008.

[15] X. Luo, Y. P. Chang, C. Y. Lin, and R. Y. Chang, "Contribution of bimodal hearing to lexical tone normalization in Mandarin-speaking cochlear implant users," *Hearing Research*, vol. 312, pp. 1–8, 2014.

[16] M. J. Polonenko, S. Giannantonio, B. C. Papsin, P. Marsella, and K. A. Gordon, "Music perception improves in children with bilateral cochlear implants or bimodal devices," *The Journal of the Acoustical Society of America*, vol. 141, no. 6, pp. 4494–4507, 2017.

[17] L. G. Potts, M. W. Skinner, R. A. Litovsky, M. J. Strube, and F. Kuk, "Recognition and localization of speech by adult cochlear implant recipients wearing a digital hearing aid in the nonimplanted ear (bimodal hearing)," *Journal of the American Academy of Audiology*, vol. 20, no. 6, pp. 353–373, 2009.

[18] S. B. Rathna-Kumar, P. Mohanty, and S. G. Prakash, "Speech recognition performance in children with cochlear implants using bimodal stimulation," *Indian Journal of Otolaryngology and Head & Neck Surgery*, vol. 62, no. 4, pp. 342–345, 2010.

[19] C. M. Sucher and H. J. McDermott, "Bimodal stimulation: benefits for music perception and sound quality," *Cochlear Implants International*, vol. 10, Supplement 1, pp. 96–99, 2009.

[20] D. Tao, R. Deng, Y. Jiang, J. J. Galvin III, Q. J. Fu, and B. Chen, "Melodic pitch perception and lexical tone perception in

Mandarin-speaking cochlear implant users," *Ear and Hearing*, vol. 36, no. 1, pp. 102–110, 2015.

[21] R. S. Tyler, A. J. Parkinson, B. S. Wilson, S. Witt, J. P. Preece, and W. Noble, "Patients utilizing a hearing aid and a cochlear implant: speech perception and localization," *Ear and Hearing*, vol. 23, no. 2, pp. 98–105, 2002.

[22] Y. S. Yoon, Y. Li, and Q. J. Fu, "Speech recognition and acoustic features in combined electric and acoustic stimulation," *Journal of Speech, Language, and Hearing Research*, vol. 55, no. 1, pp. 105–124, 2012.

[23] Y. S. Yoon, Y. R. Shin, J. S. Gho, and Q. J. Fu, "Bimodal benefit depends on the performance difference between a cochlear implant and a hearing aid," *Cochlear Implants International*, vol. 16, no. 3, pp. 159–167, 2015.

[24] K. C. Yuen, K. L. Cao, C. G. Wei, L. Luan, H. Li, and Z. Y. Zhang, "Lexical tone and word recognition in noise of Mandarin-speaking children who use cochlear implants and hearing aids in opposite ears," *Cochlear Implants International*, vol. 10, Supplement 1, pp. 120–129, 2009.

[25] T. Zhang, M. F. Dorman, and A. J. Spahr, "Information from the voice fundamental frequency (F0) region accounts for the majority of the benefit when acoustic stimulation is added to electric stimulation," *Ear and Hearing*, vol. 31, no. 1, pp. 63–69, 2010.

[26] T. Zhang, A. J. Spahr, and M. . F. Dorman, "Frequency overlap between electric and acoustic stimulation and speech-perception benefit in patients with combined electric and acoustic stimulation," *Ear and Hearing*, vol. 31, no. 2, pp. 195–201, 2010.

[27] M. C. Lin, "The acoustic characteristics and perceptual cues of tones in standard Chinese," *Chinese Yuwen*, vol. 204, pp. 182–193, 1988.

[28] R. V. Shannon, Q. J. Fu, and J. J. Galvin 3rd, "The number of spectral channels required for speech recognition depends on the difficulty of the listening situation," *Acta Oto-Laryngologica*, vol. 124, pp. 50–54, 2004.

[29] Q. J. Fu, C. J. Hsu, and M. J. Horng, "Effects of speech processing strategy on Chinese tone recognition by Nucleus-24 cochlear implant users," *Ear and Hearing*, vol. 25, no. 5, pp. 501–508, 2004.

[30] T. S. Huang, N. M. Wang, and S. Y. Liu, "Tone perception of Mandarin-speaking postlingually deaf implantees using the Nucleus 22-channel cochlear mini system," *The Annals of Otology, Rhinology & Laryngology Supplement*, vol. 166, pp. 294–298, 1995.

[31] X. Luo, Q. J. Fu, C. G. Wei, and K.-L. Cao, "Speech recognition and temporal amplitude modulation processing by Mandarin-speaking cochlear implant users," *Ear and Hearing*, vol. 29, no. 6, pp. 957–970, 2008.

[32] W. I. Wei, R. Wong, Y. Hui et al., "Chinese tonal language rehabilitation following cochlear implantation in children," *Acta Oto-Laryngologica*, vol. 120, no. 2, pp. 218–221, 2000.

[33] J. L. Wu and H. M. Yang, "Speech perception of Mandarin Chinese speaking young children after cochlear implant use: effect of age at implantation," *International Journal of Pediatric Otorhinolaryngology*, vol. 67, no. 3, pp. 247–253, 2003.

[34] N. Zhou, J. Huang, X. Chen, and L. Xu, "Relationship between tone perception and production in prelingually deafened children with cochlear implants," *Otology & Neurotology*, vol. 34, no. 3, pp. 499–506, 2013.

[35] Y. Li, G. Zhang, J. J. Galvin, and Q. J. Fu, "Mandarin speech perception in combined electric and acoustic stimulation," *PLoS One*, vol. 9, no. 11, article e112471, 2014.

[36] Y. P. Chang, R. Y. Chang, C. Y. Lin, and X. Luo, "Mandarin tone and vowel recognition in cochlear implant users: effects of talker variability and bimodal hearing," *Ear and Hearing*, vol. 37, no. 3, pp. 271–281, 2016.

[37] H. I. Yang and F. G. Zeng, "Bimodal benefits in Mandarin-speaking cochlear implant users with contralateral residual acoustic hearing," *International Journal of Audiology*, vol. 56, Supplement 2, pp. S17–S22, 2017.

[38] J. J. I. I. I. Galvin, Q. J. Fu, and G. Nogaki, "Melodic contour identification by cochlear implant listeners," *Ear and Hearing*, vol. 28, no. 3, pp. 302–319, 2007.

[39] J. J. Galvin 3rd, Q. J. Fu, and R. V. Shannon, "Melodic contour identification and music perception by cochlear implant users," *Annals of the New York Academy of Sciences*, vol. 1169, no. 1, pp. 518–533, 2009.

[40] R. H. Wang, *The Standard Chinese Database. University of Science and Technology of China, Internal Materials*, Standards Press of China, Beijing, 1993.

[41] Q. J. Fu, M. Zhu, and X. Wang, "Development and validation of the Mandarin speech perception test," *The Journal of the Acoustical Society of America*, vol. 129, no. 6, pp. EL267–EL273, 2011.

[42] M. Zhu, X Wang, and Q.J. Fu, "Development and validation of the Mandarin disyllable recognition test," *Acta otolaryngologica*, vol. 132, no. 8, pp. 855–861, 2012.

[43] Q. J. Fu, J. J. Galvin 3rd, X. Wang, and J. L. Wu, "Benefits of music training in mandarin-speaking pediatric cochlear implant users," *Journal of Speech, Language, and Hearing Research*, vol. 58, no. 1, pp. 163–169, 2015.

[44] Q. Su, J. J. Galvin, G. Zhang, Y. Li, and Q. J. Fu, "Effects of within-Talker Variability on Speech Intelligibility in Mandarin-Speaking Adult and Pediatric Cochlear Implant Patients," *Trends in hearing*, 2016.

[45] Y Li, S Wang, Q Su, J. J. Galvin, and Q. J. Fu, "Validation of List Equivalency for Mandarin Speech Materials to Use with Cochlear Implant Listeners," *International journal of audiology*, vol. 56, Supplement 2, pp. S31–S40, 2017.

[46] N. Peterson and T. R. Bergeson, "Contribution of hearing aids to music perception by cochlear implant users," *Cochlear Implants International*, vol. 16, Supplement 3, pp. S71–S78, 2015.

[47] S. Shirvani, Z. Jafari, M. Motasaddi Zarandi, S. Jalaie, H. Mohagheghi, and M. R. Tale, "Emotional perception of music in children with bimodal fitting and unilateral cochlear implant," *Annals of Otology, Rhinology & Laryngology*, vol. 125, no. 6, pp. 470–477, 2016.

[48] J. K. Chen, A. Y. Chuang, C. McMahon, T.-H. Tung, and L. P.-H. Li, "Contribution of nonimplanted ear to pitch perception for prelingually deafened cochlear implant recipients," *Otology & Neurotology*, vol. 35, no. 8, pp. 1409–1414, 2014.

[49] V. D. Driscoll, A. E. Welhaven, K. Gfeller, J. Oleson, and C. P. Olszewski, "Music perception of adolescents using electro-acoustic hearing," *Otology & Neurotology*, vol. 37, no. 2, pp. e141–e147, 2016.

[50] S. M. Prentiss, D. R. Friedland, J. J. Nash, and C. L. Runge, "Differences in perception of musical stimuli among acoustic, electric, and combined modality listeners," *Journal of the American Academy of Audiology*, vol. 26, no. 5, pp. 494–501, 2015.

[51] T. Bartov and T. Most, "Song recognition by young children with cochlear implants: comparison between unilateral, bilateral, and bimodal users," *Journal of Speech, Language, and Hearing Research*, vol. 57, no. 5, pp. 1929–1941, 2014.

[52] Q. J. Fu, F. G. Zeng, R. V. Shannon, and S. D. Soli, "Importance of tonal envelope cues in Chinese speech recognition," *The Journal of the Acoustical Society of America*, vol. 104, no. 1, pp. 505–510, 1998.

Hindawi
Neural Plasticity
Volume 2018, Article ID 6890613, 8 pages
https://doi.org/10.1155/2018/6890613

Research Article

Contralateral Suppression of DPOAEs in Mice after Ouabain Treatment

Jieying Li,[1,2] Yan Chen,[1,2] Shan Zeng,[1,2] Chuijin Lai,[1,2] Yanping Zhang,[1,2] Liting Zhang,[3] Yuxuan Shi,[1] Tianyu Zhang,[1,2] Huawei Li,[1,2,4,5] and Peidong Dai[1,2]

[1]*ENT Institute and Otorhinolaryngology Department of Affiliated Eye and ENT Hospital, State Key Laboratory of Medical Neurobiology, Fudan University, Shanghai 200031, China*
[2]*Key Laboratory of Hearing Medicine of NHFPC, Shanghai 200031, China*
[3]*Department of Cardiology, Shandong Provincial Hospital Affiliated to Shandong University, 324 Jing Wu Road, Shandong, China*
[4]*Institutes of Biomedical Sciences, The Institutes of Brain Science and the Collaborative Innovation Center for Brain Science, Fudan University, Shanghai 200032, China*
[5]*Shanghai Engineering Research Centre of Cochlear Implant, Shanghai 200031, China*

Correspondence should be addressed to Huawei Li; hwli@shmu.edu.cn and Peidong Dai; daipeidongent@163.com

Received 5 September 2017; Revised 25 January 2018; Accepted 27 February 2018; Published 10 April 2018

Academic Editor: Geng-lin Li

Medial olivocochlear (MOC) efferent feedback is suggested to protect the ear from acoustic injury and to increase its ability to discriminate sounds against a noisy background. We investigated whether type II spiral ganglion neurons participate in the contralateral suppression of the MOC reflex. The application of ouabain to the round window of the mouse cochlea selectively induced the apoptosis of the type I spiral ganglion neurons, left the peripherin-immunopositive type II spiral ganglion neurons intact, and did not affect outer hairs, as evidenced by the maintenance of the distorted product otoacoustic emissions (DPOAEs). With the ouabain treatment, the threshold of the auditory brainstem response increased significantly and the amplitude of wave I decreased significantly in the ouabain-treated ears, consistent with the loss of type I neurons. Contralateral suppression was measured as reduction in the amplitude of the $2f_1-f_2$ DPOAEs when noise was presented to the opposite ear. Despite the loss of all the type I spiral ganglion neurons, virtually, the amplitude of the contralateral suppression was not significantly different from the control when the suppressor noise was delivered to the treated cochlea. These results are consistent with the type II spiral ganglion neurons providing the sensory input driving contralateral suppression of the MOC reflex.

1. Introduction

In the cochlea, the neurons of the spiral ganglion emit peripheral processes that extend to the organ of Corti and have central processes that project to the cochlear nuclei via the auditory nerve. There are two types of spiral ganglion neurons (SGNs): (1) myelinated type I spiral ganglion cells, which innervate the inner hair cells and represent 90%–95% of the population; (2) unmyelinated type II ganglion cells, which innervate the outer hair cells (OHCs) and represent 5%–10% of the population. The scarcity and small caliber axons of the type II SGNs make them difficult to study. In consequence, there has been little experimental research into the physiology of the type II spiral SGNs [1].

To magnify low-intensity sounds and compress the dynamic intensity range, cochlear outer hair cells amplify the basilar membrane vibrations in a nonlinear, intensity-dependent pattern. Instantaneous waveform distortion is produced in this process, generating new sound frequencies that are absent from the original stimulation. These distortion products can be detected in the ear canal as otoacoustic emissions. The "cochlear amplifier" can be evaluated by measuring the distortion product otoacoustic emissions (DPOAEs) [2].

Medial olivocochlear (MOC) fibers projecting to the cochlea originate on both sides of the medial portion of the superior olivary complex, where they form synapses with the outer hair cells (OHCs). By hyperpolarizing the OHCs, the MOC efferents inhibit the electromotility of the OHCs, thereby reducing the gain of the cochlear amplifier, which manifests as a reduction in the DPOAEs. The MOC reflex includes both contralateral suppression and ipsilateral suppression. The contralateral suppression is commonly detected with a suppressor sound contralateral to the DPOAE test ear [3]. With an intact olivocochlear bundle, the amplitude of DPOAEs decrease quickly after the contralateral noise is turned on. After this "rapid onset adaptation," the response returns to a value similar to that before the contralateral noise [3]. MOC efferent feedback is suggested to protect the ear from acoustic injury and to increase its ability to discriminate sounds against a noisy background [3].

However, the sensory input that drives the MOC efferent reflex has not been identified. A recent study [4], based on a peripherin (*Prph*) knockout mouse model, proposed that the type II SGNs drive the MOC reflex. Peripherin is strongly expressed in type II (but not type I) SGNs [5]. In the transgenic mouse model, the outer spiral bundle of type II SGNs is largely absent in $Prph^{-/-}$ cochleae [4]. The study found that both contralateral suppression and ipsilateral suppression were almost totally lost in the $Prph^{-/-}$ ears compared with $Prph^{+/+}$ ears. On the contrary, another report suggested that type II SGNs are not the sensory limb of the cochlear efferent reflex [6]. That study showed that peripherin is also expressed in MOC fibers and that the inactivation of the MOC reflex observed in the peripherin knockout mice could be interpreted as the loss of the MOC function [6]. Therefore, in this study, an ouabain-treated mouse model was used, in which the apoptosis of the type I SGNs was induced, while the type II SGNs remained intact [7–9], to explore whether the type II SGNs play a role in the MOC reflex.

2. Materials and Methods

2.1. Animal Groups and Surgery. The cold method was used to prepare poloxamer 407 gels [10]. Poloxamer 407 was slowly added to cold distilled water to prepare a 20% (weight/weight) stock solution. The ouabain solution was prepared by dissolving ouabain powder in distilled water to produce a 10 mM stock solution. The stock solution was diluted with cold distilled water to produce a solution containing 18% (weight/weight) poloxamer 407 and 2 mM ouabain. This formulation is in a fluid state at room temperature and in the gel state at the body temperature of mice. The gel promotes the prolonged release of ouabain.

The experiments were performed on eight 4-week-old male C57BL/6 mice. The animals were anesthetized with pentobarbital sodium (50 mg/kg, intraperitoneally (i.p.)). One-third of the initial dose of anesthetic was given when needed. A posteroinferior skin incision was made in the retroauricular area of the right ear. To expose the bulla, the nearby muscles and facial nerve were separated. A small opening was made in the bulla to expose the round window. A 2.5 μl Hamilton syringe was used to apply the ouabain gel described above (1.6 μl) to the round window membrane. Sham operations were conducted in another group of 4-week-old C57BL/6 mice as controls ($n = 8$). The bulla was covered with bone wax, and a nonabsorbable suture was used to close the incision. The animal was placed on a homeothermic blanket for recovery. Electrophysiological tests of cochlear function were conducted 2 weeks after the surgeries. All the procedures were approved by the Institutional Animal Care and Use Committee of the Eye and ENT Hospital of Fudan University, China.

2.2. Cochlear Function Tests. An auditory-evoked potential and DPOAE workstation (TDT system 3 with RX6 and RX6-2 signal processors; Tucker Davis Technologies, Fort Lauderdale, FL, USA) was used to conduct the cochlear function tests, with the BioSig32 software. The auditory brainstem responses (ABRs) and DPOAEs were recorded as per previous study [4]. The amplitude of the $2f_1–f_2$ (cubic) distortion products and the surrounding noise floor were recorded. The mice were anesthetized with ketamine (100 mg/kg, i.p.) and xylazine (10 mg/kg, i.p.). The threshold for ABR was determined as the lowest intensity at which a repeatable ABR waveform could be identified. The wave I component was identified and the peak-to-peak amplitude computed by off-line analysis of stored waveforms. In the DPOAE recordings, the frequency ratio f_2/f_1 was 1.2 and the intensity of f_1 and f_2 was the same, increasing together in 5 dB steps (from 20 dB SPL to 80 dB SPL). The amplitude of the $2f_1–f_2$ distortion products and the surrounding noise floor were recorded. The DPOAE thresholds were determined based on when the cubic ($2f_1–f_2$) distortion product reached 5 dB above the noise floor, as the tone intensity increased, as previously described [4].

The contralateral suppression was measured after DPOAE test without dismounting the DPOAE-measuring probe from the untreated ear. The parameter setting for contralateral suppression was optimized based on prior studies [11, 12]. The right ears (after surgeries) of ouabain-treated mice were exposed to 76 dB SPL, 13–20 kHz broadband suppressor noise (continuous for 15 s, closed field), whereas the DPOAEs were elicited in the left ears (without surgeries) with 60 dB SPL, 16 kHz primary tones. Sham-operated mice without ouabain treatment served as controls. Three measurements were averaged (4/s) for each recording. The DPOAEs were monitored before and after the suppression noise to obtain the baseline DPOAE measurement. The amplitude of the $2f_1–f_2$distortion products relative to the noise floor was recorded before, during, and after the noise stimulation. The broadband noise was generated with the Cool Edit Pro software (Adobe Systems, San Jose, CA, USA). The stimulus was delivered as closed field using MF1 Multi-Field Magnetic Speakers (Tucker-Davis Technologies), with a customized coupler. To address the effect of the cross talk to contralateral suppression, we measured contra-noise effects before and after mechanical destruction of the contralateral cochlea (right ears) by opening the cochlear basal turn ($n = 6$). As shown in the

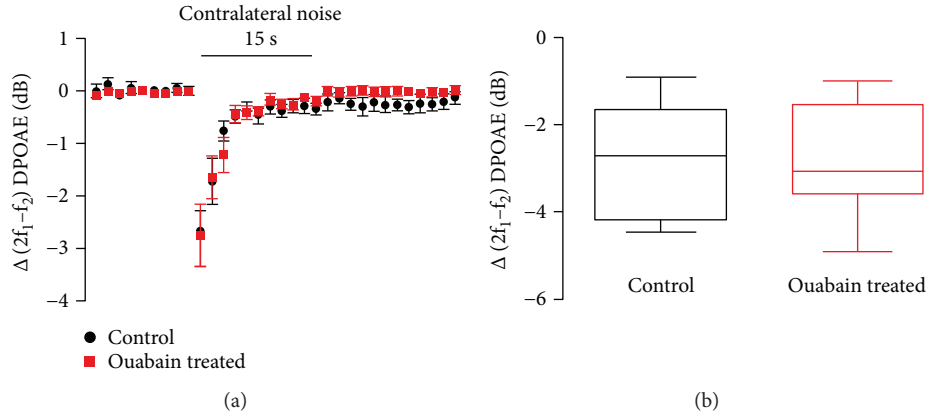

Figure 1: Ouabain treatment did not significantly alter contralateral suppression. (a) The time course of contralateral suppression showed no significant difference between the control and ouabain-treated groups. $N = 8$, data were shown as the mean ± SEM. (b) The amplitude of the peak suppression of the control and ouabain-treated groups. Fifteen seconds of 76 dB SPL. 13–20 kHz noise produced a similar reduction in the amplitude of the $2f_1-f_2$ DPOAE (60 dB SPL 16 kHz) in the control and ouabain-treated ears. Data in (b) showed the amplitude of the peak suppression which is from the first measurement after noise onset relative to the average of the prenoise baseline. $N = 8$, the boundaries indicated 25th and 75th percentile; solid line indicated median; error bars indicated the maximum and minimum.

Supplemental Figure 1, the destruction completely eliminated the contralateral suppression.

2.3. Immunofluorescence Staining. Immediately after the dissection of the cochlea, 4% paraformaldehyde in phosphate-buffered saline (PBS) was perfused through the round window and oval window. The cochlea was immersed in the same solution for 2 h at 4°C. For frozen sectioning, the cochlea was decalcified (0.1 M ethylenediaminetetraacetic acid (EDTA)) and cryoprotected in 30% sucrose at 4°C overnight prior to embedding in optimal cutting temperature compound (OCT). Then, the sections were made and mounted on slides for immunofluorescence staining. Immunostaining began with blocking buffer (10% donkey serum in PBS) for 2 h at room temperature. The sections were then incubated at 4°C overnight in a combination of the following primary antibodies: (1) mouse anti-tubulin $\beta 3$ (Tuj1, BioLegend), diluted 1 : 300; (2) rabbit antiperipherin (Prph, Abcam), diluted 1 : 500. The samples were then incubated at 4°C overnight with a species-appropriate secondary antibody (Alexa Fluor 488-labeled anti-mouse IgG antibody, Alexa Fluor 594-labeled anti-rabbit IgG antibody). The images were captured using fluorescence microscope (NIKON ECLIPSE Ni U, Nikon Instruments Inc., Japan), and Photoshop CS5 software (Adobe Systems, San Jose, CA, USA) was used to adjust contrast and brightness of images.

2.4. SGN Counting. Tubulin $\beta 3$- (Tuj1-) positive and peripherin- (Prph-) positive neurons in 12 serial midmodiolar sections of the cochlear (120 μm thickness in total) were counted [13]. The sectional area of Rosenthal's canal was calculated from the images with the Photoshop CS5 software (Adobe Systems, San Jose, CA, USA) as the literature [13] described; an image of a standard slide was used to calibrate the scale, which was converted from pixels to micrometers; the outline of Rosenthal's canal was circumscribed in every section; the total number of pixels for Rosenthal's canal was calculated and converted into square micrometers. In Rosenthal's canal, Tuj1-positive and Prph-negative cells were defined as type I SGNs; Tuj1-positive and Prph-positive cells were defined as type II SGNs. The total number of each type of SGN was then divided by the two-dimensional area to obtain the density of SGNs per square millimeter [14].

2.5. Statistical Analysis. Data are expressed as the population mean ± standard errors of the means (SEM) except for the data in Figure 1(b). The statistical analysis was performed with SPSS 11.5 (SPAA Inc., Chicago, IL, USA). Two-way ANOVA was used to compare the thresholds of ABR and DPOAE and the amplitudes of the $2f_1-f_2$ distortion products at 16 kHz and the amplitude of wave I between the ouabain-treated and control groups [4]. Two-way ANOVA was also used to compare contralateral suppression between the ouabain-treated and control groups [4]. One-way ANOVA was used to compare the peak amplitudes of the rapid contralateral suppression between the ouabain-treated and control groups and to compare the numbers of type I and type II SGNs between the ouabain-treated and control groups.

3. Results

3.1. Cochlear Function Tests. To explore whether type II spiral ganglion neurons participate in the contralateral suppression of the MOC reflex, ouabain was applied to the right cochlea at the round window to eliminate the type I spiral ganglion neurons. This application of ouabain selectively induced the apoptosis of the type I spiral ganglion neurons, but left the type II spiral ganglion neurons intact as reported previously [8]. The sham-operated mice without ouabain treatment were used as controls. Cochlear function was tested after the ouabain treatment. Two weeks after the application of ouabain, the ABR threshold increased significantly compared with that in the control ear ($P < 0.01$ at 8, 12, 16, 20, and 24 kHz; Figure 2(a)). The ABR thresholds increased by 30–45 dB SPL at all frequencies after ouabain treatment.

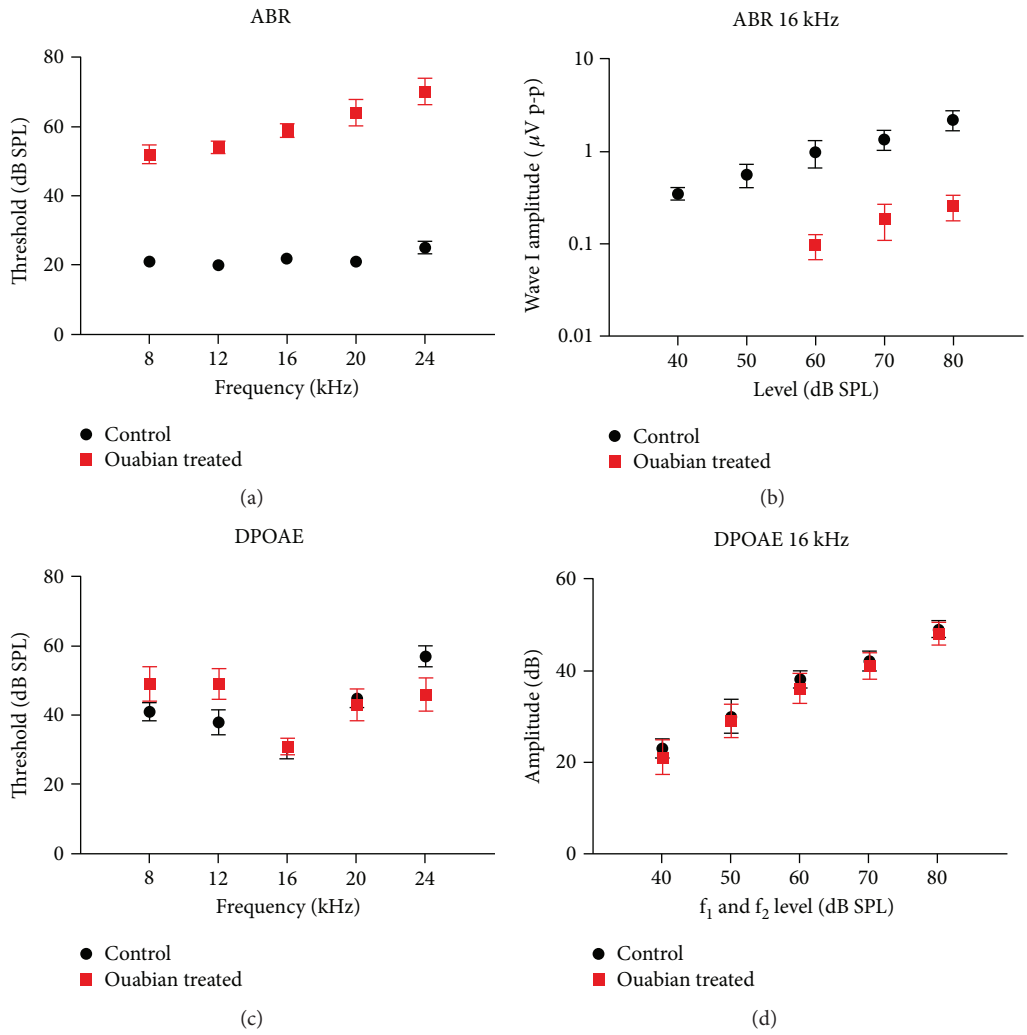

Figure 2: ABR and DPOAE results of the control and ouabain-treated ears. (a) ABR thresholds for the control ears ($n = 8$) versus ouabain-treated ears ($n = 8$) at 2 weeks after the application of ouabain. (b) Mean amplitudes of ABR wave I at 16 kHz for the animals shown in (a). (c) DPOAE thresholds for the animals shown in (a). (d) Mean amplitudes versus level functions at $f_2 = 16$ kHz for the animals shown in (a). $N = 8$, data were shown as the mean ± SEM.

Besides, the amplitude of wave I at 16 kHz decreased significantly compared with the control group ($P < 0.01$ at 60, 70, and 80 dB SPL, Figure 2(b)). However, ouabain treatment had no significant effect on the threshold and amplitude of DPOAEs at 16 kHz compared with the control ears (Figures 2(c) and 2(d)), indicating that the cochlear outer hair cells remained intact 2 weeks after the application of ouabain.

3.2. Cochlear Histopathology. We immunostained frozen sections of the whole cochleae for two marker proteins: (1) tubulin β3 (Tuj1), which is expressed in both type I and type II SGNs, and (2) peripherin (Prph), a type III intermediate filament, whose immunoreactivity is restricted to the soma and processes of type II SGNs in the mature cochlea. Figures 3(a) and 3(d) showed that after ouabain treatment, there was a nearly complete elimination of type I SGCs. Figures 3(b) and 3(e) show that nearly all of peripherin-positive type II SGCs remained, which were detected in both the control cochleae and the experimental cochleae 2 weeks after treatment with ouabain.

3.3. SGN Counting. The type I SGNs (Tuj1-positive and Prph-negative) and type II SGNs (Tuj1-positive and Prph-positive) were counted in 12 midmodiolar sections of the ouabain-treated and control cochleae. In the control group, the average densities of type I and type II SGNs were $1898 \pm 103/\text{mm}^2$ and $202 \pm 58/\text{mm}^2$, respectively. After ouabain treatment, about 99% of the type I SGNs were eliminated and the density of the remaining type I neurons was $10 \pm 6/\text{mm}^2$ ($P < 0.01$). Meanwhile, the average density of surviving type II SGNs was $190 \pm 62/\text{mm}^2$. The density of type II SGNs has no significant difference between the control and ouabain treatment groups ($P = 0.97$). These data indicate that there was no loss of type II neurons and almost total loss of type I neurons after the application of ouabain. These results also suggest that about 9.59% ± 0.39% of the SGNs in the normal mouse ear were type II.

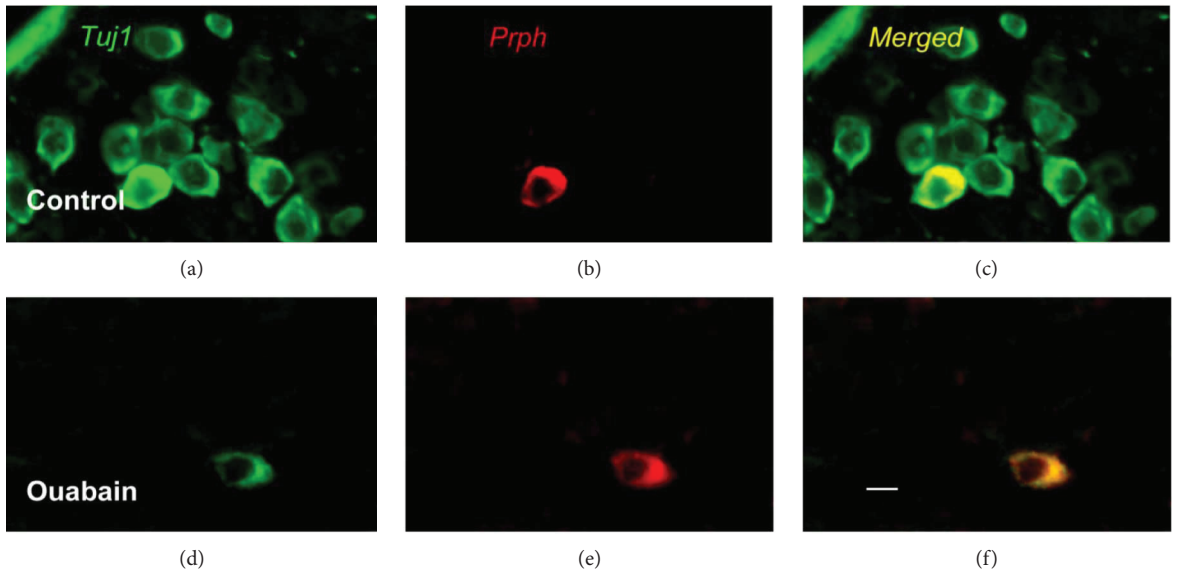

Figure 3: Images of spiral ganglion neurons in control and ouabain-treated ears. (a–c) Representative image of Tuj1 and Prph immunostaining in spiral ganglion cells of the control group. Prph, a marker of type II spiral ganglion cells, was detected with Alexa Fluor 594 (red). Tuj1, a marker of type I and type II neurons, was detected with Alexa Fluor 488 (green). (d–f) Representative image of Tuj1 and Prph immunostaining in spiral ganglion cells of the ouabain-treated group. Nearly, all type I spiral ganglion cells were lost, whereas Prph-positive type II neurons survived after ouabain exposure. Scale bar = 20 μm.

3.4. Contralateral Suppression in Mice of Control and Ouabain-Treated Groups. The functional effect of the MOC reflex, evident as contralateral suppression, was evaluated as a reduction in $2f_1$–f_2 DPOAEs induced by suppressor noise in the ear opposite to that which the DPOAE was measured in. With an intact olivocochlear bundle, the amplitude of distortion products decreased quickly after the contralateral noise was turned on. Thus, wideband noise was delivered to the ouabain-treated ears (right ears) and the DPOAEs were recorded in the left ears as the previous study reported [15]. Sham-operated mice without ouabain treatment served as controls. Both in the control and ouabain-treated groups, suppression was obvious from the onset of the contralateral noise, and the maximal reduction in the DPOAEs occurred within 1 s (Figure 1(a)). The suppression displayed near-complete adaptation after the noise had been presented for 10 s. The ouabain-treated ears showed similar contralateral suppression time course to that in the control group (Figure 1(a), $P = 0.35$). The amplitude of the peak suppression in the ouabain-treated ears (2.88 ± 0.46 dB, $n = 8$) did not differ significantly from that in the control group (2.86 ± 0.46 dB, $n = 8$, Figure 1(b), $P = 0.77$). The peak suppression in both the control and ouabain-treated ears occurred within 1 s after the onset of the contralateral noise. The control and ouabain-treated ears showed similar rates of shift in their DPOAEs.

4. Discussion

The afferents of the MOC reflex must originate from either the type I SGNs and/or the type II SGNs. A recent report [4] proposed that the type II neurons drive the MOC reflex. A peripherin knockout mouse model lacking type II innervation of the cochlea was used in that study. Peripherin is strongly expressed in type II but not type I SGNs [5]. The contralateral and ipsilateral suppression of the MOC reflex was nearly eliminated in the $Prph^{-/-}$ ears compared with that in the $Prph^{+/+}$ ears. On the contrary, another report suggested that peripherin is also expressed in some MOC fibers. The loss of MOC function in the peripherin knockout mice can be interpreted as the inactivation of contralateral suppression and ipsilateral suppression [6]. Besides the type II neurons, the function of other peripheral neurons is probably affected in $Prph^{-/-}$ mice because peripherin is widely expressed in the peripheral nervous system. To study the function of type II neurons, an animal model that separates type I and type II neurons without affecting other neurons is required. Therefore, in this study, we used a mouse model in which ouabain was applied unilaterally to the cochlear round window, which induced the apoptosis of type I SGNs but left the type II SGNs intact in the ouabain-treated ear. The MOC fibers in the other ear (in which DPOAE were elicited) were not affected by ouabain. Contralateral suppression was used to evaluate the inhibition of cochlear amplification by the MOC reflex.

Several previous studies [7, 8, 16, 17] have shown that the application of ouabain to the round window causes the nearly complete elimination of the type I SGNs but leaves the type II SGNs intact, with no obvious loss of or damage to the hair cells. The results of our electrophysiological tests of cochlear function and cochlear histopathology in the ouabain-treated ears are consistent with those of the previous studies. Ouabain treatment significantly elevated the ABR threshold and decreased the amplitude of wave I, with no significant shift in the DPOAE threshold or amplitude (Figure 2). Moreover, the immunofluorescence

staining further confirmed that the application of ouabain selectively causes the death of type I neurons, without damaging type II neurons (Figure 3).

After ouabain exposure, the amplitude of contralateral suppression was not significantly different from that in the control group. Because the application of ouabain to the round window of the cochlea induces the apoptosis of type I SGNs but leaves the type II SGNs intact [7–9, 16], the pathway from the inner hair cells and their type I SGNs to the brain is almost silenced in the ouabain-treated ears. Therefore, the responses of these ears to sound are attributed to an alternative mechanism of auditory sensing in which the outer hair cells and type II SGNs probably participate. The afferents of the MOC suppression reflex must either be type I SGNs and/or type II SGNs. Our results support the hypothesis that type II SGNs exclusively drive the MOC contralateral suppression reflex.

Recent studies suggest that type II SGNs act as cochlear nociceptors, functioning only when the OHCs are damaged [18, 19]. Cochlear type II afferents and somatosensory C-fiber nociceptors share anatomical features, physiological properties, and protein expression [19]. Maison et al. [6] proposes that this finding contradicts the hypothesis that the type II SGNs drive the MOC contralateral suppression reflex, because nociceptors respond to traumatically high sound levels, whereas cochlear efferents respond near the hearing threshold. However, Flores et al. speculates that instead of pain, auditory nociception might elicit an axon reflex, an autonomic reaction, or an efferent response, like MOC reflex, to protect the inner ear from further damage [19].

There is only a 10–20 dB difference between the thresholds of MOC neurons and type I neurons [20], and type II neurons must be similarly sensitive to sound if they act as the afferents of this reflex. Recent electrophysiological experiments in isolated rat organs of Corti support this hypothesis. The integration of synaptic input from multiple OHCs by type II SGNs was identified [21]. The length constants of type II SGNs imply that synaptic inputs can sum effectively through the processes of the type II neurons [21]. Experimental records and the computational model both imply that the extended dendrites of the type II neurons can integrate these inputs. It is speculated that the small synaptic inputs elicited by the neurotransmitters released by individual OHCs will sum approximately linearly across the many tens of OHCs innervated by each of the type II SGN neurites. In the computation model, six synchronous synaptic inputs are required to generate a spike. Because the probability of transmitter release by OHCs is low, the simultaneous stimulation of 24 OHCs is required for action potential in the model of type II SGNs. This number is in the range of OHCs connected to type II neurons, estimated in the previous studies [22].

Some studies have reported that type II SGNs are insensitive to sound [23–25]. However, the antidromic stimulation used in those studies may not reflect the physical electrical features of type II SGNs. Moreover, the sample sizes in those studies were small, with only 1, 19, and 8 long-latency neurons studied by Robertson [23], Brown [24], and Robertson et al. [25], respectively. According to Robertson et al. [25], in both Robertson's [23] and Brown's [24] studies, it is possible that during the process of recording the SGNs, the opening of the cochlea may have selectively affected the OHCs and thus changed the response of the type II neurons. Robertson et al. and Brown were also unable to successfully fill all the neurons with horseradish peroxidase. Consequently, they could not ensure that the neurons were actually type II SGNs [25]. Another line of evidence inconsistent with our observation is that the antidromic response latencies of type II neurons to brainstem shocks are 6-7 ms and are therefore longer than the sound-evoked latencies of MOC efferents, which are 4.5 ms [26]. However, the point of antidromic activation of the central processes can greatly affect latency. For example, the stimulating electrode used by Brown was inserted into the cochlear nucleus, yet the electrode used by Robertson was set on the auditory nerve [25]. As a result, the mean latency for the long-latency neurons recorded by Brown was nearly five times greater than that recorded by Robertson.

Our results support the hypothesis that type II SGNs drive the MOC contralateral suppression reflex. However, the ouabain-exposed mouse model has limitations. Although the morphological evidence showed that there were nearly no type I SGNs in 12 consecutive midmodiolar sections of the ouabain-exposed cochlea, it is possible that the few remaining type I SGNs were able to drive the MOC contralateral suppression reflex. An animal model in which the type II neurons can be manipulated selectively is required for the further exploration of their physiological functions.

5. Conclusions

After ouabain exposure, the amplitude of the contralateral suppression was not significantly different from that of the control group. Almost no type I spiral ganglion neurons remained in the ouabain-treated cochleae. Thus, the type II spiral ganglion neurons are almost certainly the afferents responsible for contralateral suppression. Our study helps resolve the controversy about whether type II afferents are driving medial olivocochlear (MOC) efferent fibers [4] or not [6].

Abbreviations

MOC: Medial olivocochlear
SGNs: Spiral ganglion neurons
OHCs: Outer hair cells
DPOAEs: Distortion product otoacoustic emissions
Prph: Peripherin gene
PBS: Phosphate-buffered saline
EDTA: Ethylenediaminetetraacetic acid
OCT: Optimal cutting temperature compound
Tuj1: Tubulin $\beta 3$
Prph: Peripherin protein
ANOVA: Analysis of variance.

Conflicts of Interest

The authors declare that they have no conflicts of interest.

Authors' Contributions

Jieying Li and Yan Chen contributed equally to this work.

Acknowledgments

This work was supported by grants from the National Natural Science Foundation of China (81270687, 81570911, 81230019, 81570934, and 81771010), the National Key R&D Program of China (2017YFA0103900, 2016YFC0905200), and National Science and Technology Support Program (2015BAK31B00).

Supplementary Materials

Supplemental Table 1: ABR threshold of the sham-operated and ouabain-treated groups (dB SPL). Supplemental Table 2: peak-to-peak amplitude of wave I at 16 kHz in ABR test (μV). Supplemental Table 3: DPOAE threshold of the control group and the surgery group. Supplemental Table 4: amplitude of $2f_1-f_2$ distortion products at 16 kHz (dB SPL). Supplemental Table 5: density of type I and type II spiral ganglion neurons. Figure S1: contra-noise suppression of DPOAEs disappears after contralateral cochlear destruction (CCD). The right ears were destroyed by opening the cochlear basal turn and then exposed to 76 dB SPL, 13–20 kHz broadband noise (continuous for 15 s, closed field), whereas the DPOAEs were elicited in the left ears with 60 dB SPL, 16 kHz primary tones. All the experimental parameters are the same as we described in the method of the manuscript. $N = 6$, data are presented as the mean ± SEM. *(Supplementary Materials)*

References

[1] B. A. Nayagam, M. A. Muniak, and D. K. Ryugo, "The spiral ganglion: connecting the peripheral and central auditory systems," *Hearing Research*, vol. 278, no. 1-2, pp. 2–20, 2011.

[2] P. Avan, B. Buki, and C. Petit, "Auditory distortions: origins and functions," *Physiological Reviews*, vol. 93, no. 4, pp. 1563–1619, 2013.

[3] J. J. Guinan Jr, "Olivocochlear efferents: anatomy, physiology, function, and the measurement of efferent effects in humans," *Ear and Hearing*, vol. 27, no. 6, pp. 589–607, 2006.

[4] K. E. Froud, A. C. Y. Wong, J. M. E. Cederholm et al., "Type II spiral ganglion afferent neurons drive medial olivocochlear reflex suppression of the cochlear amplifier," *Nature Communications*, vol. 6, no. 1, p. 7115, 2015.

[5] A. Hafidi, "Peripherin-like immunoreactivity in type II spiral ganglion cell body and projections," *Brain Research*, vol. 805, no. 1-2, pp. 181–190, 1998.

[6] S. Maison, L. D. Liberman, and M. C. Liberman, "Type II cochlear ganglion neurons do not drive the olivocochlear reflex: re-examination of the cochlear phenotype in peripherin knock-out mice," *eNeuro*, vol. 3, no. 4, 2016.

[7] H. Lang, B. A. Schulte, and R. A. Schmiedt, "Ouabain induces apoptotic cell death in type I spiral ganglion neurons, but not type II neurons," *Journal of the Association for Research in Otolaryngology*, vol. 6, no. 1, pp. 63–74, 2005.

[8] Y. Yuan, F. Shi, Y. Yin et al., "Ouabain-induced cochlear nerve degeneration: synaptic loss and plasticity in a mouse model of auditory neuropathy," *Journal of the Association for Research in Otolaryngology*, vol. 15, no. 1, pp. 31–43, 2014.

[9] H. Lang, M. Li, L. A. Kilpatrick et al., "Sox2 up-regulation and glial cell proliferation following degeneration of spiral ganglion neurons in the adult mouse inner ear," *Journal of the Association for Research in Otolaryngology*, vol. 12, no. 2, pp. 151–171, 2011.

[10] G. Dumortier, J. L. Grossiord, F. Agnely, and J. C. Chaumeil, "A review of poloxamer 407 pharmaceutical and pharmacological characteristics," *Pharmaceutical Research*, vol. 23, no. 12, pp. 2709–2728, 2006.

[11] X. Zhu, O. N. Vasilyeva, S. Kim et al., "Auditory efferent feedback system deficits precede age-related hearing loss: contralateral suppression of otoacoustic emissions in mice," *The Journal of Comparative Neurology*, vol. 503, no. 5, pp. 593–604, 2007.

[12] R. D. Frisina, S. R. Newman, and X. Zhu, "Auditory efferent activation in CBA mice exceeds that of C57s for varying levels of noise," *Journal of the Acoustical Society of America*, vol. 121, no. 1, pp. El29–El34, 2007.

[13] C. P. Richter, G. Kumar, E. Webster, S. K. Banas, and D. S. Whitlon, "Unbiased counting of neurons in the cochlea of developing gerbils," *Hearing Research*, vol. 278, no. 1-2, pp. 43–51, 2011.

[14] A. E. Schettino and A. M. Lauer, "The efficiency of design-based stereology in estimating spiral ganglion populations in mice," *Hearing Research*, vol. 304, pp. 153–158, 2013.

[15] S. F. Maison, H. Usubuchi, D. E. Vetter, A. B. Elgoyhen, S. A. Thomas, and M. C. Liberman, "Contralateral-noise effects on cochlear responses in anesthetized mice are dominated by feedback from an unknown pathway," *Journal of Neurophysiology*, vol. 108, no. 2, pp. 491–500, 2012.

[16] R. A. Schmiedt, H. O. Okamura, H. Lang, and B. A. Schulte, "Ouabain application to the round window of the gerbil cochlea: a model of auditory neuropathy and apoptosis," *Journal of the Association for Research in Otolaryngology*, vol. 3, no. 3, pp. 223–233, 2002.

[17] H. Lang, B. A. Schulte, J. C. Goddard et al., "Transplantation of mouse embryonic stem cells into the cochlea of an auditory-neuropathy animal model: effects of timing after injury," *Journal of the Association for Research in Otolaryngology*, vol. 9, no. 2, pp. 225–240, 2008.

[18] C. Liu, E. Glowatzki, and P. A. Fuchs, "Unmyelinated type II afferent neurons report cochlear damage," *Proceedings of the National Academy of Sciences of the United States of America*, vol. 112, no. 47, pp. 14723–14727, 2015.

[19] E. N. Flores, A. Duggan, T. Madathany et al., "A non-canonical pathway from cochlea to brain signals tissue-damaging noise," *Current Biology*, vol. 25, no. 5, pp. 606–612, 2015.

[20] M. C. Brown, S. G. Kujawa, and M. L. Duca, "Single olivocochlear neurons in the guinea pig. I. Binaural facilitation of responses to high-level noise," *Journal of Neurophysiology*, vol. 79, no. 6, pp. 3077–3087, 1998.

[21] C. J. C. Weisz, E. Glowatzki, and P. A. Fuchs, "Excitability of type II cochlear afferents," *Journal of Neuroscience*, vol. 34, no. 6, pp. 2365–2373, 2014.

[22] C. J. C. Weisz, M. Lehar, H. Hiel, E. Glowatzki, and P. A. Fuchs, "Synaptic transfer from outer hair cells to type II

afferent fibers in the rat cochlea," *Journal of Neuroscience*, vol. 32, no. 28, pp. 9528–9536, 2012.

[23] D. Robertson, "Horseradish peroxidase injection of physiologically characterized afferent and efferent neurones in the guinea pig spiral ganglion," *Hearing Research*, vol. 15, no. 2, pp. 113–121, 1984.

[24] M. C. Brown, "Antidromic responses of single units from the spiral ganglion," *Journal of Neurophysiology*, vol. 71, no. 5, pp. 1835–1847, 1994.

[25] D. Robertson, P. M. Sellick, and R. Patuzzi, "The continuing search for outer hair cell afferents in the guinea pig spiral ganglion," *Hearing Research*, vol. 136, no. 1-2, pp. 151–158, 1999.

[26] M. C. Brown, R. K. de Venecia, and J. J. Guinan, "Responses of medial olivocochlear neurons - specifying the central pathways of the medial olivocochlear reflex," *Experimental Brain Research*, vol. 153, no. 4, pp. 491–498, 2003.

Hindawi
Neural Plasticity
Volume 2018, Article ID 7513217, 7 pages
https://doi.org/10.1155/2018/7513217

Research Article

Modulation of Glucose Takeup by Glucose Transport on the Isolated OHCs

Xiao-ting Cheng,[1,2] Feng-bo Yang,[1,3] Qing-qing Jiang,[1] Rong Zhang,[2] Shi-ming Yang,[1] and Ning Yu[1]

[1]*Department of Otorhinolaryngology Head and Neck Surgery and Institute of Otorhinolaryngology, The PLA General Hospital, Beijing 100853, China*
[2]*Department of Otorhinolaryngology Head and Neck Surgery, The First Affiliated Hospital of Fujian Medical University, Fujian 350005, China*
[3]*Department of Otolaryngology, Affiliated Hospital of North Sichuan Medical College, Nanchong 637100, China*

Correspondence should be addressed to Ning Yu; yuning12@sina.com

Received 21 January 2018; Accepted 3 March 2018; Published 5 April 2018

Academic Editor: Renjie Chai

Glucose is a fundamental source of energy for mammalian cells; however, whether glucose is taken up through the lateral walls of cochlear outer hair cells (OHCs) is unknown. The OHC lateral wall is complex, composed of a plasma membrane, cortical lattice, and subsurface cisternae. This study assessed the uptake of glucose by OHCs using live-cell microscopy and examined the distribution of glucose transporter isoforms by immunohistochemistry. We found that glucose transporter-4 was mostly expressed on the lateral wall of OHCs. Glucose crossed the lateral walls of OHCs via glucose transporters-4 mainly, and this process could be modulated. These results suggest that the lateral walls are involved in modulating energy transport into OHCs.

1. Introduction

The length of cochlear OHCs can change at a very high frequency when they receive acoustic signals [1, 2]. Although electromotility is not directly dependent on ATP or other chemical intermediates [3, 4], these rapid changes in body length must consume a great deal of energy. The complex lateral cortex of an OHC is composed of three distinct layers, namely, the subsurface cisternae (SSC), cortical cytoskeletal lattice (CL), and plasma membrane (PM) [5]. The SSC is a specialized and substantial fraction of the endoplasmic membrane within OHCs; in guinea pigs, as many as twelve ordered layers line the lateral cytoplasmic surface of the PM [6]. The cortical lattice is an unusual protein skeleton associated with the outermost surface of the lateral cisternae beneath the PM. The outermost PM contains a high density of integral membrane proteins. One of these, prestin, a specialized electromotor protein, is expressed on the outer PM [7]. The relationship between glucose transporters and prestin is unclear [8, 9].

The functions of OHC lateral walls are understudied. How glucose is transported across the three membrane structures, whether they participate in energy transport, and whether glucose transporters are related to electromotility are unknown. Here, we assessed the cytoplasmic uptake of glucose by OHCs using live-cell microscopy and examined the subcellular localization of glucose transporter (GLUT) isoforms by immunohistochemistry. We observed that glucose crossed the membrane via glucose transporters and that this process could be controlled; further, we found that GLU-4 was expressed on the subcellular localization. These results imply that the lateral walls of cochlear OHCs are involved in controlling energy transport.

2. Materials and Methods

2.1. Animal Preparation and Cochlear Cell Isolation. Cochlear cells were freshly isolated from adult guinea pigs (250–300 g) [10, 11]. Briefly, guinea pigs were anesthetized

with an overdose of chloral hydrate (0.3 ml/100 g), and otic capsules were removed after decapitation. The otic capsules were dissected, and the isolated cochleas were put in normal extracellular solution (142 mM NaCl, 5.37 mM KCl, 1.47 mM $MgCl_2$, 2 mM $CaCl_2{\cdot}2H_2O$, and 10 mM HEPES; 300 mOsm; pH 7.2). After removal of the bone and stria vascularis, the sensory epithelium (organ of Corti) was collected using a sharpened needle and further dissociated with trypsin (0.5 mg/ml) for 2-3 min with shaking. Cochlear cells were then transferred to a recording dish. All experimental procedures were performed at room temperature (23°C). The animals were purchased from Vital River Laboratory Animal Technology Co. Ltd. (Beijing, China). All animal experiments were approved by the Institutional Animal Care and Use Committee of the Chinese PLA General Hospital (Beijing, China).

2.2. Experimental Agents. Adenosine 5′-triphosphate (ATP) disodium salt solution (cat. no. A6559-25UMO), indinavir (cat. no. Y-0000788), and WZB-117 (SML0621-5MG) were purchased from Sigma (St. Louis, MO). Antibodies against 4-[[[[4-(1,1-dimethylethyl)phenyl]sulfonyl]amino]methyl]-N-3-pyridinylbenzamide (STF-31; cat. no. SC-364692) and prestin (H-294; cat. no. sc-30163) were purchased from Santa Cruz Biotechnology (Santa Cruz, CA). The dyes di-8-ANEPPS (D3167), Hoechst 33342 (R37605), and 2-NBDG (N13195) were purchased from Molecular Probes (Eugene, OR). Antibodies against GLUT-1 (ab652) and GLUT-4 (ab654) were purchased from LifeSpan BioSciences Inc. (Seattle, WA). A perfusion system was used to apply reagents to cells. The animals were anesthetized for all procedures with an intraperitoneal injection of chloral hydrate.

2.3. Immunohistochemistry. Dissociated cochlear cells were fixed with 4% paraformaldehyde for 30 min. After three washes with 0.01 M PBS, the cells were incubated in blocking solution (10% goat serum in PBS with 0.25% Triton X-100) for 30 min. The cells were then incubated with anti-GLUT or anti-prestin antibodies (1 : 100–250) in blocking solution at room temperature (23°C) for 2 h. In control experiments, the primary antibody was omitted. After three washes with PBS, the cells were incubated with Alexa Fluor 488-conjugated donkey anti-rabbit IgG (1 : 200; cat. no. A21206, Molecular Probes) or Alexa Fluor 568-conjugated donkey anti-goat IgG (1 : 200; cat. no. A11057, Molecular Probes) in blocking solution at room temperature for 1 h. For costaining with di-8-ANEPPS to visualize the PM and cytoplasmic membranous organelles, the cells were further incubated in 30 μM di-8-ANEPPS (D-3167; Molecular Probes) for 20 min after secondary antibody incubation. After completely washing out the dye with 0.01 M PBS, staining was observed under a confocal microscope.

Cell nuclei were stained with Hoechst 33342 (R37605; Molecular Probes). Following incubation with the secondary antibody, pieces of dissociated cells were incubated with a dilution of Hoechst 33342 stock solution (2 drops per ml) at room temperature for 15–30 min and washed three times with PBS.

2.4. Live-Cell Imaging, Image Processing, and Statistical Analysis. Live-cell imaging was performed using an Applied Precision DeltaVision microscope (GE Healthcare, Issaquah, WA), and data were acquired and processed with the accompanying software. Fluorescence intensity was measured using ImageJ. All data are expressed as the mean ± standard deviation (SD). Data were analyzed using an unpaired *t*-test (Student's *t*-test) for two groups and a one-way ANOVA with Bonferroni post hoc tests for multiple comparisons, as noted in the figure legends (SPSS 13.0 software; SPSS Inc., Chicago, IL). Differences with $p < 0.05$ were deemed statistically significant. Error bars in the figures represent the SD.

3. Results

3.1. 2-NBDG Is Transported into the Cytoplasm of OHCs. 2-NBDG is a novel fluorescent derivative of glucose that is useful for assessing glucose uptake activity [12]. A good viability of isolated OHCs can be sustained for two hours in normal extracellular solution [13], and the procedure for acquiring isolated OHCs in this experiment only need 15 minutes. As shown in Figure 1, following 20 min of exposure to 2-NBDG (1 mM), the OHCs from the basal and apical turn displayed intracellular fluorescence, indicating uptake (Figures 1(b) and 1(d)). Control OHCs without perfusion with 2-NBDG had minimal cellular fluorescence, indicating relatively little autofluorescence (data was not shown here). Hence, the OHCs appeared to take up 2-NBDG rapidly and retain it on the lateral wall and within the cytoplasm (Figures 1(b) and 1(d)).

Then we examined the concentration and time dependency of 2-NBDG uptake by OHCs. We perfused a series of 2-NBDG concentrations (0.1 mm/l, 0.5 mm/l, 1 mm/l, and 2 mm/l) to the OHCs that were isolated from all turns of the cochlea. The normalized fluorescence intensity (NFI) on the lateral wall and cytoplasm at each concentration was divided by the initial concentration (0.1 mm/l) (Figure 1(e)). The NFI increased with the increase of 2-NBDG concentration. Similarly, fluorescence was normalized by dividing the value by that at time zero. The uptake of 2-NBDG increased gradually over time until reaching a plateau (Figure 1(f)). The results suggested that 2-NBDG uptake by OHCs depended on the concentration and time.

3.2. GLUT-1 and GLUT-4 Expression in OHCs. Despite the above results showing that 2-NBDG is taken up by OHCs, little is known about the expression and localization of glucose transporters in these cells. Previous studies have shown GLUT-1, GLUT-3, GLUT-4, GLUT-5, GLUT-8, GLUT-10, and GLUT-12 expressions in both the stria vascularis and the spiral ligament [14]. We examined the relative distribution of GLUT isoforms in OHCs by immunohistochemistry (Figure 2; some data was not shown). Staining for all glucose transporters except GLUT-4 was punctate and mostly close to the edge of the cell; GLUT-4 was distributed evenly along the lateral cell edges, similar to previous observations of prestin distribution [7]. We also observed the expression of transporters on the cuticular plate, which has not been previously reported and is consistent with our observation of 2-NBDG

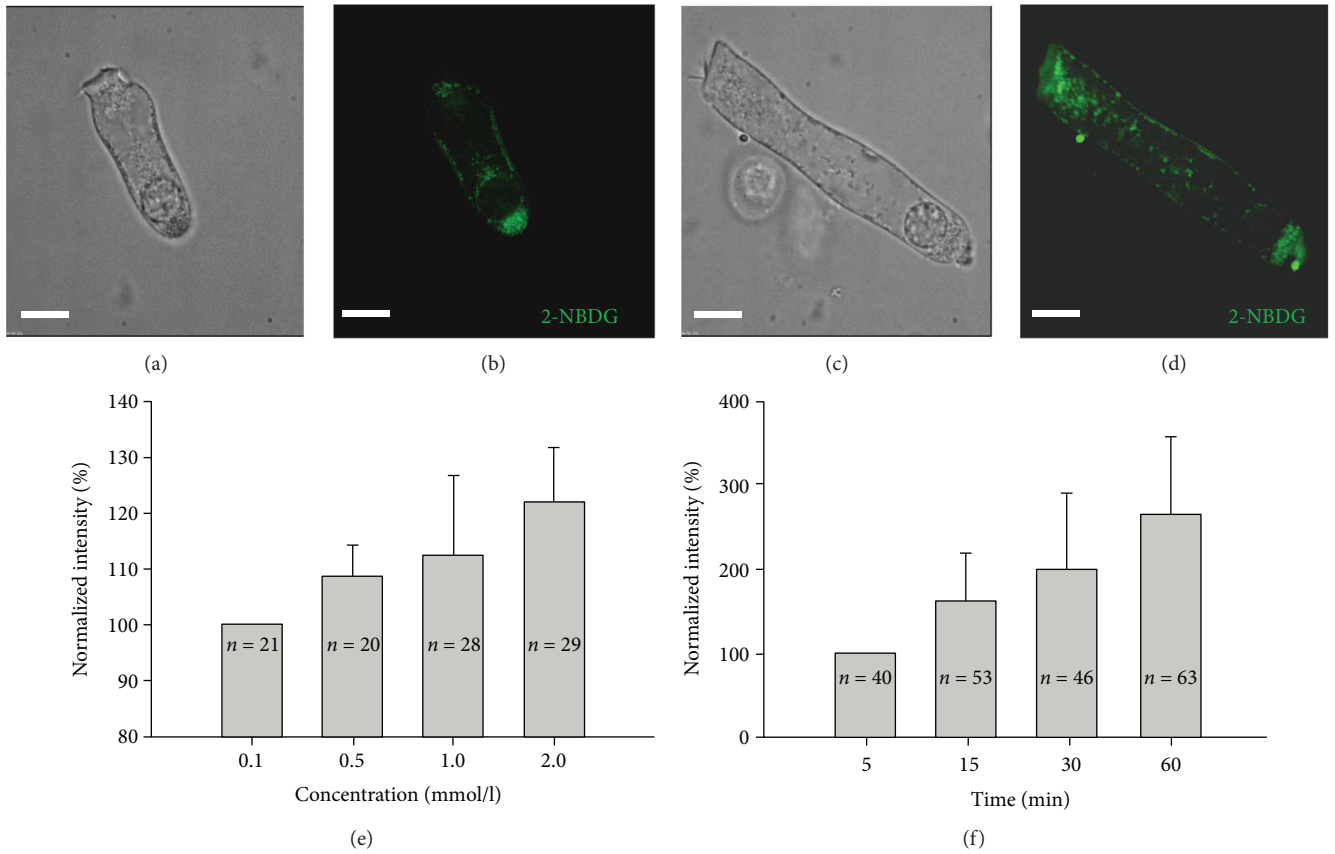

Figure 1: Uptake of 2-NBDG into OHCs and concentration or time-dependent uptake of 2-NBDG by OHCs. (a and c) Nomarski images. (b and d) Guinea pig OHCs of various lengths following exposure to 2-NBDG (1 mM for 20 min; cells were imaged after a 10 min washout; green, 2-NBDG). (e) Normalized fluorescence intensity of 2-NBDG at varying concentrations. The concentration was measured at 20 min after giving the 2-NBDG. (f) Normalized fluorescence intensity of 2-NBDG over time. The concentration of 2-NBDG used was 1 mM/l. Scale bars, 10 μm.

uptake by OHCs through the cuticular plate using live-cell imaging (data not shown). While previous reports indicated that OHCs did not express GLUT-5 [9], we observed that the outer hair cells expressed GLUT-5 scatteredly (data was not shown). These findings strongly suggest that a number of GLUT isoforms participate in glucose transport in OHCs.

3.3. OHC Uptake of 2-NBDG Is Modulated by GLUT-1 and GLUT-4 Antagonists. We next examined the effect of glucose antagonists on the uptake of 2-NBDG (Figure 3; all data are relative to untreated cells). STF-31 and WZB117 are GLUT-1 antagonists [15, 16] and decreased the uptake of 2-NBDG to 0.9308 ± 0.0909 and 0.9561 ± 0.1095, respectively, though the reductions were small. Indinavir (50 μmol/l) [17, 18] is a GLUT-4 antagonist and decreased the uptake of 2-NBDG to 0.5907 ± 0.0649.

3.4. Comparison Dye or Antibody Staining Localization between GLUT-4 and Di-8-ANEPPS. In addition to the lateral walls, some GLUT-4 labeling was observed at the basal PM, though the staining was weak (Figures 2(d), 4(a), and 5(c)). To determine whether the basal staining resulted from GLUT-4 antibody penetration through the PM into the cytoplasm, we costained cells with di-8-ANEPPS, a membrane-impermeable dye that labels the phospholipid bilayer (Figure 4(b)).

Di-8-ANEPPS labeled the PM as well as other cell membranous structures, including the SSC, and overlapped with GLUT-4 labeling at the basolateral wall (Figures 4(a)–4(c)). To clarify the localization of GLUT-4, we colabelled cells using anti-prestin antibodies. Prestin was expressed only in OHCs at the outermost layer of the PM along the lateral wall. High-magnification images (inset in Figure 5(b)) revealed that the two proteins did not colocalize; prestin was confined to the outermost PM layer, while GLUT-4 was just inside, likely at the SSC.

We next examined the effect of receptor P2X7 agonists on the uptake of 2-NBDG (Figure 6; all data are relative to untreated cells). Intracochlear ATP is an important mediator in the regulation of hearing, and it affects the transmembrane potential in OHCs [19, 20]. The ATP receptor P2X7 is expressed on the lateral wall of OHCs [10, 11], similar to the distribution of GLUT-4 (data below). Thus, we examined the effect of ATP on 2-NBDG uptake by OHCs. ATP increased the uptake of 2-NBDG significantly to 1.7582 ± 0.5625.

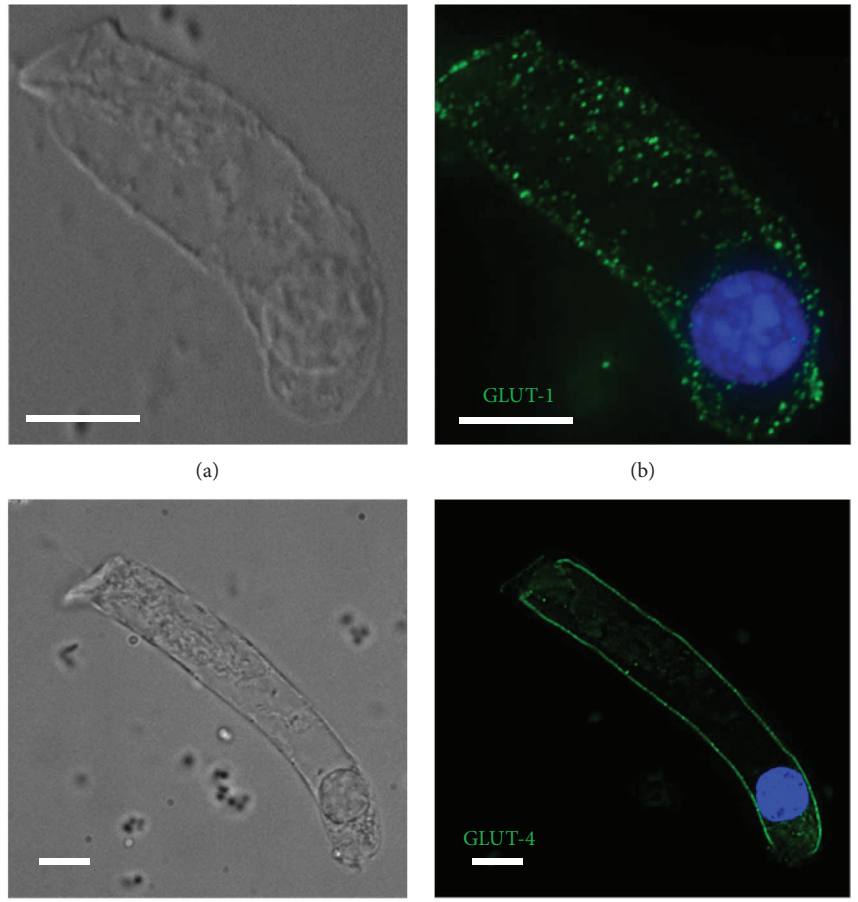

Figure 2: Subcellular distribution of GLUT isoforms in OHCs. Deconvoluted images of OHCs labeled with antibodies specific for various glucose transporters (green). (b) GLUT-1 and (d) GLUT-4. Blue staining corresponds to Hoechst 33342 (nuclei). (a) and (c) are Nomarski images. Scale bar, 10 μm.

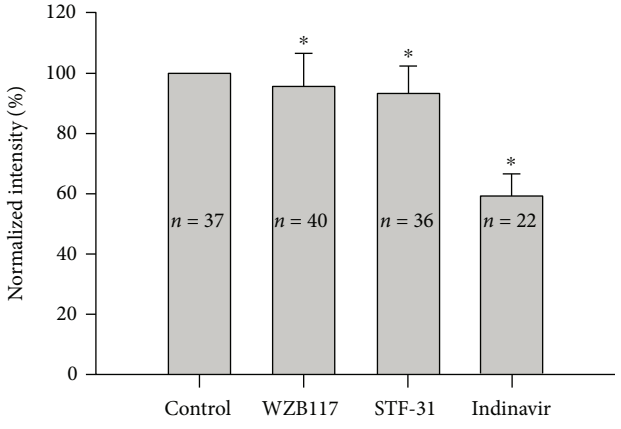

Figure 3: The antagonists of GLUT-1 and GLUT-4 alter the uptake of 2-NBDG. WZB117 and STF-31 are GLUT-1 antagonists and indinavir is a GLUT-4 antagonist. Error bars represent the standard error. $*$ indicates $p < 0.05$ by a paired t-test.

4. Discussion

In this study, we demonstrated the uptake of 2-NBDG by OHCs. We further demonstrated that the uptake was time- and concentration-dependent and regulated by ATP receptors and glucose transporters.

Our examination of the distribution of GLUT isoforms using specific antibodies identified the expression of glucose transporters on the cuticular plate, in accordance with our live-cell imaging results showing glucose uptake at this location (data not shown). GLUT-1 expressed on all parts of OHCs scatteredly; it was not only in the cytoplasma but also on the cell membranes. The GLUT-1 inhibitors STF-31 and WZB117 [15, 21] inhibited the uptake of 2-NBDG, indicating that glucose are transported through GLUT-1. There is no study showing the GLUT expression in the OHCs; only some studies elucidate GLUT expression in the stria vascularis and the spiral ligament. Takeuchi and Ando [22] and Ando et al. [23] showed that GLUT-1 was expressed in the stria vascularis, whereas in basal cells and not marginal cells, the studies indicated that GLUT-1 might contribute to the transcellular glucose takeup pathway. Edamatsu et al. [14] showed that GLUT-1, GLUT-3, GLUT-5, GLUT-8, GLUT-

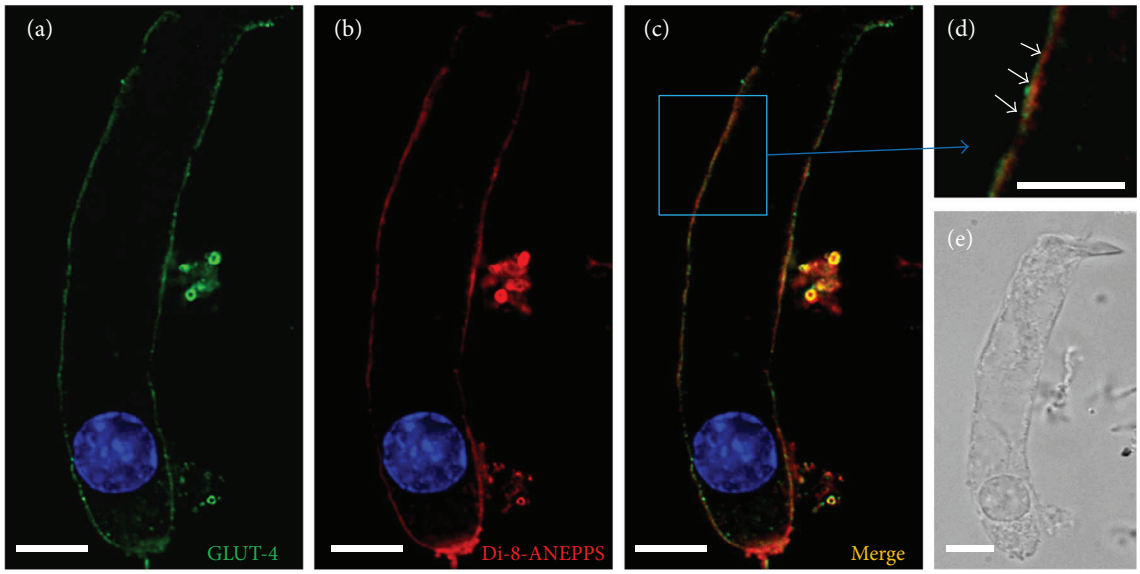

Figure 4: Basal staining for GLUT-4 may result from intracellular penetration of the antibody. OHCs were costained using anti-GLUT-4 antibodies and di-8-ANEPPS: (a) GLUT-4 staining; (b) di-8-ANEPPS staining; (c) merged image; (d) high magnification; (e) Nomarski image. Scale bar, 10 μm in all images except the inset (2 μm).

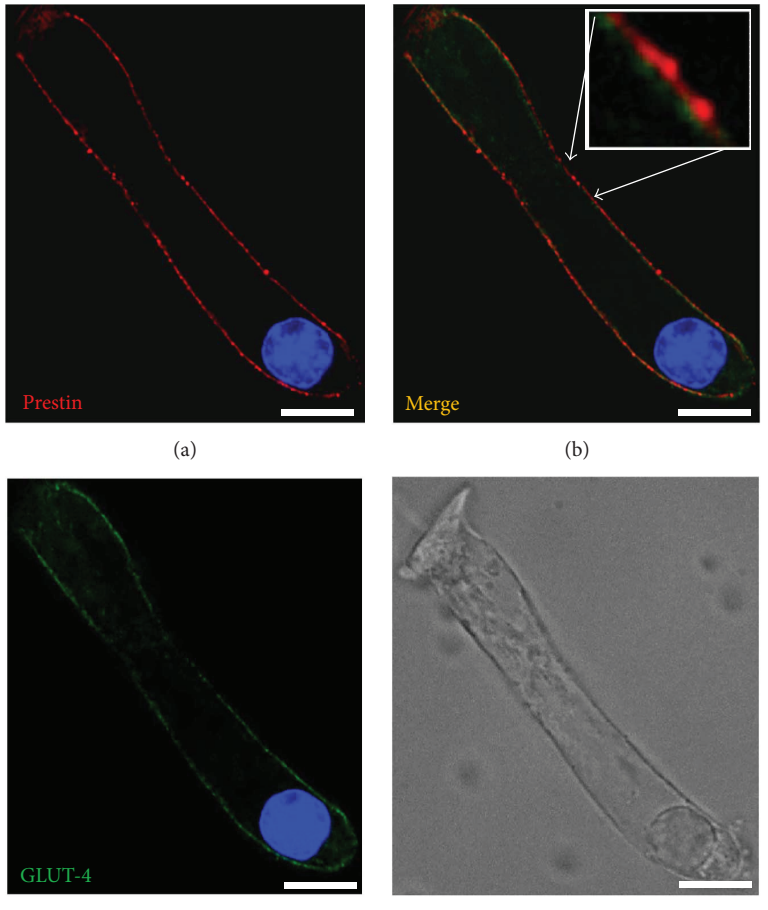

Figure 5: GLUT-4 colocalizes with prestin in the lateral, but not the basal, wall of OHCs. OHCs were costained for GLUT-4 and prestin. (a) Prestin and (b) merged image. Inset: high-magnification image revealing the separation of GLUT-4 and prestin. (c) GLUT-4 and (d) Nomarski image in the same field. Scale bar, 10 μm in all images except the inset (2 μm).

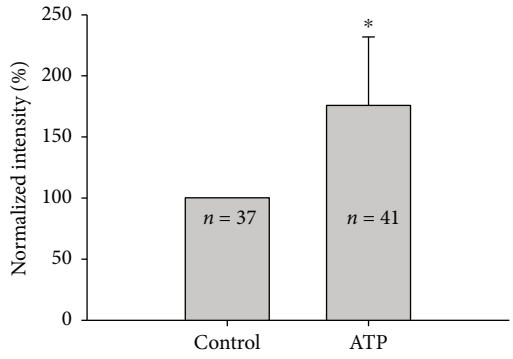

Figure 6: P2X7 receptor agonist alters the uptake of 2-NBDG. ATP is a P2X7 receptor agonist that could increase the uptake of 2-NBDG obviously. Error bars represent the standard error. * indicates $p < 0.05$ by a paired t-test.

10, and GLUT-12 were detected in both the stria vascularis and the spiral ligament and revealed that there were significant differences between the stria vascularis and the spiral ligament of GLUT-1, GLUT-4, GLUT-5, and GLUT-10 isoforms, which indicated GLUT-1, GLUT-4, GLUT-5, and GLUT-10 isoforms involved in glucose transport in the stria vascularis and the spiral ligament.

In this study, we observed that the outer hair cells expressed GLUT-5 scatteredly (data was not shown), which was consistent to the results of Belyantseva et al. [24]. They found that GLUT-5 and prestin were highly expressed in the lateral membrane of OHCs, indicating that GLUT-5 might be involved in the control of cochlear electromotility, whereas the results were different from Wu et al. [9] which showed that GLUT-5 was not detected in the OHCs and GLUT-5 was not necessary for OHC motility or cochlear amplification. The discrepancy may due to the different types of experimental animals. Our observation of GLUT-4 expression along the entire lateral wall of OHCs suggests that it is responsible for most glucose transport in these cells. Then we used the GLUT-4 antagonist indinavir to exam the function of GLUT-4 and we observed that the uptake of 2-NBDG decreased when the indinavir was applied. Through these results, we can suggest that GLUT-4 mainly relates with glucose transport in OHCs.

At the same time, we observed that GLUT-4 was localized to a layer just inside the membrane where prestin was expressed, namely, the inner SSC of the OHC lateral wall [7]. Ning et al. [25] showed that the distribution of the P2X7 receptor overlapped with the prestin expression. Thus, the subcellular distribution of GLUT-4 in OHCs also resembled that of P2X7. Prestin is a unique ATP- and Ca^{2+}-independent motor protein of the outer hair cell, involved in the electromotility and cochlear amplification [26–28]. The process needs a lot of energy consumption provided by ATP, which is also the P2X7 receptor agonist [29, 30]. This study showed that the uptake of 2-NBDG increased after the application of ATP. ATP enhanced glucose uptake, suggesting that GLUT-4 and P2X7 may participate in electromotility. The distribution of GLUT-4 also suggests that it is related to electromotility; however, more evidence is needed to verify this hypothesis.

Diabetes is a known risk reason for hearing loss, and some previous studies suggest that GLUT-4 mutations are linked to diabetes. GLUT-4 plays an important role in the pathophysiology of T2DM, and its defective expression will hinder the entrance of glucose into the cell for energy production [31–33]. Altered insulin sensitivity may influence the expression of GLUT-4, leading to the death of OHCs because of glucose deficiency. Our observation that GLUT-4 was the most strongly expressed GLUT isoform in OHCs may explain why diabetes can cause deafness. Degerman et al. [34] found that the sensory epithelium of human saccule expressed insulin-sensitive glucose transporter (GLUT-4), which also exhibited expression of the insulin receptor, insulin receptor substrate 1, and protein kinase B, indicating that those proteins might have a role in mechanism between diabetes and hearing loss. Thus, GLUT-4 may participate in the mechanism of hearing impairment of diabetes.

In summary, glucose is transported into OHCs across the lateral membrane via glucose transporters 1 and 4 mainly, and this transport is regulated by ATP and glucose antagonists. GLUT-4 is expressed on the inner OHC lateral walls, suggesting that it is related to electromotility. In conclusion, the lateral walls of cochlear OHCs are involved in controlling energy transport.

Conflicts of Interest

The authors declare that they have no conflicts of interest.

Authors' Contributions

Xiao-ting Cheng and Feng-bo Yang contributed equally to this work.

Acknowledgments

This project was supported by the National Basic Research Program of China (973 Program) (2014CB943002), the National Natural Science Foundation of China (nos. 81470700 and 81528005, http://www.nsfc.gov.cn), and Noise Grant (BWS14J045). The authors thank Ms. Can Xie and Dr. Hai-long Wang for the technical support. The English in this document has been checked by Dr. Anping Xia and at least two professional editors, both native speakers of English. For a certificate, please see http://www.textcheck.com/certificate/b5FiuP.

References

[1] B. Kachar, W. E. Brownell, R. Altschuler, and J. Fex, "Electrokinetic shape changes of cochlear outer hair cells," *Nature*, vol. 322, no. 6077, pp. 365–368, 1986.

[2] J. Ashmore, "Cochlear outer hair cell motility," *Physiological Reviews*, vol. 88, no. 1, pp. 173–210, 2008.

[3] S. Ramamoorthy and A. L. Nuttall, "Outer hair cell somatic electromotility in vivo and power transfer to the organ of Corti," *Biophysical Journal*, vol. 102, no. 3, pp. 388–398, 2012.

[4] Y. Zhu, C. Liang, J. Chen, L. Zong, G. D. Chen, and H. B. Zhao, "Active cochlear amplification is dependent on supporting cell gap junctions," *Nature Communications*, vol. 4, p. 1786, 2013.

[5] K. Saito, "Fine structure of the sensory epithelium of guinea-pig organ of Corti: subsurface cisternae and lamellar bodies in the outer hair cells," *Cell and Tissue Research*, vol. 229, no. 3, pp. 467–481, 1983.

[6] L. Song and J. Santos-Sacchi, "An electrical inspection of the subsurface cisternae of the outer hair cell," *Biophysical Journal*, vol. 108, no. 3, pp. 568–577, 2015.

[7] N. Yu, M. L. Zhu, and H. B. Zhao, "Prestin is expressed on the whole outer hair cell basolateral surface," *Brain Research*, vol. 1095, no. 1, pp. 51–58, 2006.

[8] X. Wu, B. Currall, T. Yamashita, L. L. Parker, R. Hallworth, and J. Zuo, "Prestin–prestin and prestin–GLUT5 interactions in HEK293T cells," *Developmental Neurobiology*, vol. 67, no. 4, pp. 483–497, 2007.

[9] X. D. Wu, X. Wang, J. G. Gao et al., "Glucose transporter 5 is undetectable in outer hair cells and does not contribute to cochlear amplification," *Brain Research*, vol. 1210, pp. 20–28, 2008.

[10] H. B. Zhao, N. Yu, and C. R. Fleming, "Gap junctional hemichannel-mediated ATP release and hearing controls in the inner ear," *Proceedings of the National Academy of Sciences of the United States of America*, vol. 102, no. 51, pp. 18724–18729, 2005.

[11] N. Yu and H. B. Zhao, "ATP activates P2x receptors and requires extracellular Ca^{++} participation to modify outer hair cell nonlinear capacitance," *Pflügers Archiv - European Journal of Physiology*, vol. 457, no. 2, pp. 453–461, 2008.

[12] K. Yoshioka, H. Takahashi, T. Homma et al., "A novel fluorescent derivative of glucose applicable to the assessment of glucose uptake activity of *Escherichia coli*," *Biochimica et Biophysica Acta (BBA) - General Subjects*, vol. 1289, no. 1, pp. 5–9, 1996.

[13] Z. Su, "Techniques for isolating hair cells from guinea pig cochlea," *Zhonghua Er Bi Yan Hou Ke Za Zhi*, vol. 27, no. 3, pp. 133–135, 1992.

[14] M. Edamatsu, Y. Kondo, and M. Ando, "Multiple expression of glucose transporters in the lateral wall of the cochlear duct studied by quantitative real-time PCR assay," *Neuroscience Letters*, vol. 490, no. 1, pp. 72–77, 2011.

[15] D. A. Chan, P. D. Sutphin, P. Nguyen et al., "Targeting GLUT1 and the Warburg effect in renal cell carcinoma by chemical synthetic lethality," *Science Translational Medicine*, vol. 3, no. 94, article 94ra70, 2011.

[16] K. R. Boheler, S. Bhattacharya, E. M. Kropp et al., "A human pluripotent stem cell surface N-glycoproteome resource reveals markers, extracellular epitopes, and drug targets," *Stem Cell Reports*, vol. 3, no. 1, pp. 185–203, 2014.

[17] I. Igbe, E. K. Omogbai, and A. O. Oyekan, "Renal effects of glucose transporter 4 in Nω-nitro-L-arginine/ /high salt-induced hypertensive rats," *Bratislava Medical Journal*, vol. 116, no. 1, pp. 57–63, 2015.

[18] C. Wilson, A. Contreras-Ferrat, N. Venegas et al., "Testosterone increases GLUT4-dependent glucose uptake in cardiomyocytes," *Journal of Cellular Physiology*, vol. 228, no. 12, pp. 2399–2407, 2013.

[19] S. G. Kujawa, C. Erostegui, M. Fallon, J. Crist, and R. P. Bobbin, "Effects of adenosine 5′-triphosphate and related agonists on cochlear function," *Hearing Research*, vol. 76, no. 1-2, pp. 87–100, 1994.

[20] D. J. B. Muñoz, P. R. Thorne, G. D. Housley, T. E. Billett, and J. M. Battersby, "Extracellular adenosine 5′-triphosphate (ATP) in the endolymphatic compartment influences cochlear function," *Hearing Research*, vol. 90, no. 1-2, pp. 106–118, 1995.

[21] Y. Liu, Y. Cao, W. Zhang et al., "A small-molecule inhibitor of glucose transporter 1 downregulates glycolysis, induces cell-cycle arrest, and inhibits cancer cell growth in vitro and in vivo," *Molecular Cancer Therapeutics*, vol. 11, no. 8, pp. 1672–1682, 2012.

[22] S. Takeuchi and M. Ando, "Marginal cells of the stria vascularis of erbils take up glucose via the facilitated transporter GLUT: application of autofluorescence," *Hearing Research*, vol. 114, no. 1-2, pp. 69–74, 1997.

[23] M. Ando, M. Edamatsu, S. Fukuizumi, and S. Takeuchi, "Cellular localization of facilitated glucose transporter 1 (GLUT-1) in the cochlear stria vascularis: its possible contribution to the transcellular glucose pathway," *Cell and Tissue Research*, vol. 331, no. 3, pp. 763–769, 2008.

[24] I. A. Belyantseva, H. J. Adler, R. Curi, G. I. Frolenkov, and B. Kachar, "Expression and localization of prestin and the sugar transporter GLUT-5 during development of electromotility in cochlear outer hair cells," *The Journal of Neuroscience*, vol. 20, no. 24, article RC116, 2000.

[25] Y. Ning, Z. Hong-bo, Y. Shi-ming, and Z. Suo-qiang, "Distribution of P2 receptors on outer hair cell membrane," *Journal of Otology*, vol. 6, pp. 441–441, 2008.

[26] J. Zheng, W. Shen, D. Z. Z. He, K. B. Long, L. D. Madison, and P. Dallos, "Prestin is the motor protein of cochlear outer hair cells," *Nature*, vol. 405, no. 6783, pp. 149–155, 2000.

[27] M. C. Liberman, J. G. Gao, D. Z. Z. He, X. D. Wu, S. P. Jia, and J. Zuo, "Prestin is required for electromotility of the outer hair cell and for the cochlear amplifier," *Nature*, vol. 419, no. 6904, pp. 300–304, 2002.

[28] P. Dallos and B. Fakler, "Prestin, a new type of motor protein," *Nature Reviews Molecular Cell Biology*, vol. 3, no. 2, pp. 104–111, 2002.

[29] M. Kukley, P. Stausberg, G. Adelmann, I. P. Chessell, and D. Dietrich, "Ecto-nucleotidases and nucleoside transporters mediate activation of adenosine receptors on hippocampal mossy fibers by $P2X_7$ receptor agonist 2′-3′-*O*-(4-benzoylbenzoyl)-ATP," *The Journal of Neuroscience*, vol. 24, no. 32, pp. 7128–7139, 2004.

[30] S. F. Moore and A. B. Mackenzie, "Species and agonist dependent zinc modulation of endogenous and recombinant ATP-gated $P2X_7$ receptors," *Biochemical Pharmacology*, vol. 76, no. 12, pp. 1740–1747, 2008.

[31] M. Sato, N. Dehvari, A. I. Oberg et al., "Improving type 2 diabetes through a distinct adrenergic signaling pathway involving mTORC2 that mediates glucose uptake in skeletal muscle," *Diabetes*, vol. 63, no. 12, pp. 4115–4129, 2014.

[32] J. S. Hansen, X. Zhao, M. Irmler et al., "Type 2 diabetes alters metabolic and transcriptional signatures of glucose and amino acid metabolism during exercise and recovery," *Diabetologia*, vol. 58, no. 8, pp. 1845–1854, 2015.

[33] S. T. Yan, C. L. Li, H. Tian et al., "MiR-199a is overexpressed in plasma of type 2 diabetes patients which contributes to type 2 diabetes by targeting GLUT4," *Molecular and Cellular Biochemistry*, vol. 397, no. 1-2, pp. 45–51, 2014.

[34] E. Degerman, U. Rauch, S. Lindberg, P. Caye-Thomasen, A. Hultgårdh, and M. Magnusson, "Expression of insulin signalling components in the sensory epithelium of the human saccule," *Cell and Tissue Research*, vol. 352, no. 3, pp. 469–478, 2013.

Hindawi
Neural Plasticity
Volume 2018, Article ID 5898025, 8 pages
https://doi.org/10.1155/2018/5898025

Research Article

Three *MYO15A* Mutations Identified in One Chinese Family with Autosomal Recessive Nonsyndromic Hearing Loss

Fengguo Zhang,[1,2] Lei Xu,[1,2] Yun Xiao,[1,2] Jianfeng Li,[1,2] Xiaohui Bai,[1,2] and Haibo Wang[1,2]

[1]*Department of Otorhinolaryngology Head and Neck Surgery, Shandong Provincial Hospital Affiliated to Shandong University, Jinan, China*
[2]*Shandong Provincial Key Laboratory of Otology, Jinan, China*

Correspondence should be addressed to Xiaohui Bai; sphbaixiaohui@163.com and Haibo Wang; whboto11@163.com

Received 27 September 2017; Accepted 3 December 2017; Published 5 April 2018

Academic Editor: Hai Huang

Hearing impairment is one of the most common sensory disease, of which more than 50% is attributed to a genetic etiology. The goal of this research is to explore the genetic cause of a Chinese deafness pedigree who was excluded of *GJB2*, *SLC26A4*, or *MtDNA12SrRNA* variants. Three variants, c.3971C>A (p.A1324D), c.4011insA (p.Q1337Qfs*22), and c.9690+1G>A, in the *MYO15A* gene were identified by targeted capture sequencing and Sanger sequencing, and the first two of them were novel. These variants were cosegregated with the disease in this family and absent in 200 normal hearing persons. They were concluded to be pathogenic mutations by phylogenetic analysis and structure modeling. Thus, the combined use of SNPScan assay and targeted capture sequencing is a high-efficiency and cost-effective screening procedure for hereditary hearing loss. Genetic counseling would be important for this family, and our finding would be a great supplement to the mutation spectrum of *MYO15A*.

1. Introduction

Hearing impairment is a common sensorineural disease, affecting about one in 500–1000 children, and more than 50% congenital hearing loss is attributable to genetic origins [1]. Approximately, 70% of the deafness without other symptoms is known as nonsyndromic hearing loss (NSHL). Hereditary deafness can be classified as autosomal dominant, autosomal recessive, mitochondrial, and X-linked. Autosomal recessive nonsyndromic hearing loss (ARNSHL) is the most frequent hereditary pattern [2, 3].

Since *GJB2* was identified as the responsible gene for hereditary hearing loss [4], over 80 genes and 2000 mutations have been identified causing NSHL till now (http://deafnessvariationdatabase.org). *MYO15A* gene was revealed to be the disease-causing gene of ARNSHL [5]. Since then, more and more studies on *MYO15A* gene have focused on the mutational analysis. Usually, pathogenic mutations of *MYO15A* gene can cause congenital severe to profound hearing loss in all frequencies [6, 7], whereas some patients are noted to have residual hearings at low frequencies [8].

MYO15A gene consisting of 66 exons encodes a protein myosin XVA with 3530 amino acid. Myosin XVA can be classified into two isoforms: class 1 and class 2 [9]. They both contain six same domains: motor, MyTH, IQ, FERM, SH3, and PDZ. In addition, the class 1 isoform also has an N-terminal domain [10–12]. Both two isoforms can be found in the human inner ear [9].

Myosin XVA, expressed at the tips of stereocilia in the cochlea hair cells, is essential for the function of mechanotransduction apparatus [13], which is proved by a myosin XVA-deficient mouse model study [14].

Here, we report a consanguineous Chinese family affected by profound sensorineural hearing loss. We used SNPscan assay and targeted capture sequencing to identify the gene responsible for the deafness in the family. The results identified three compound heterozygous mutations, c.3971C>A (p.A1324D), c.4011insA (p.Q1337Qfs*22), and

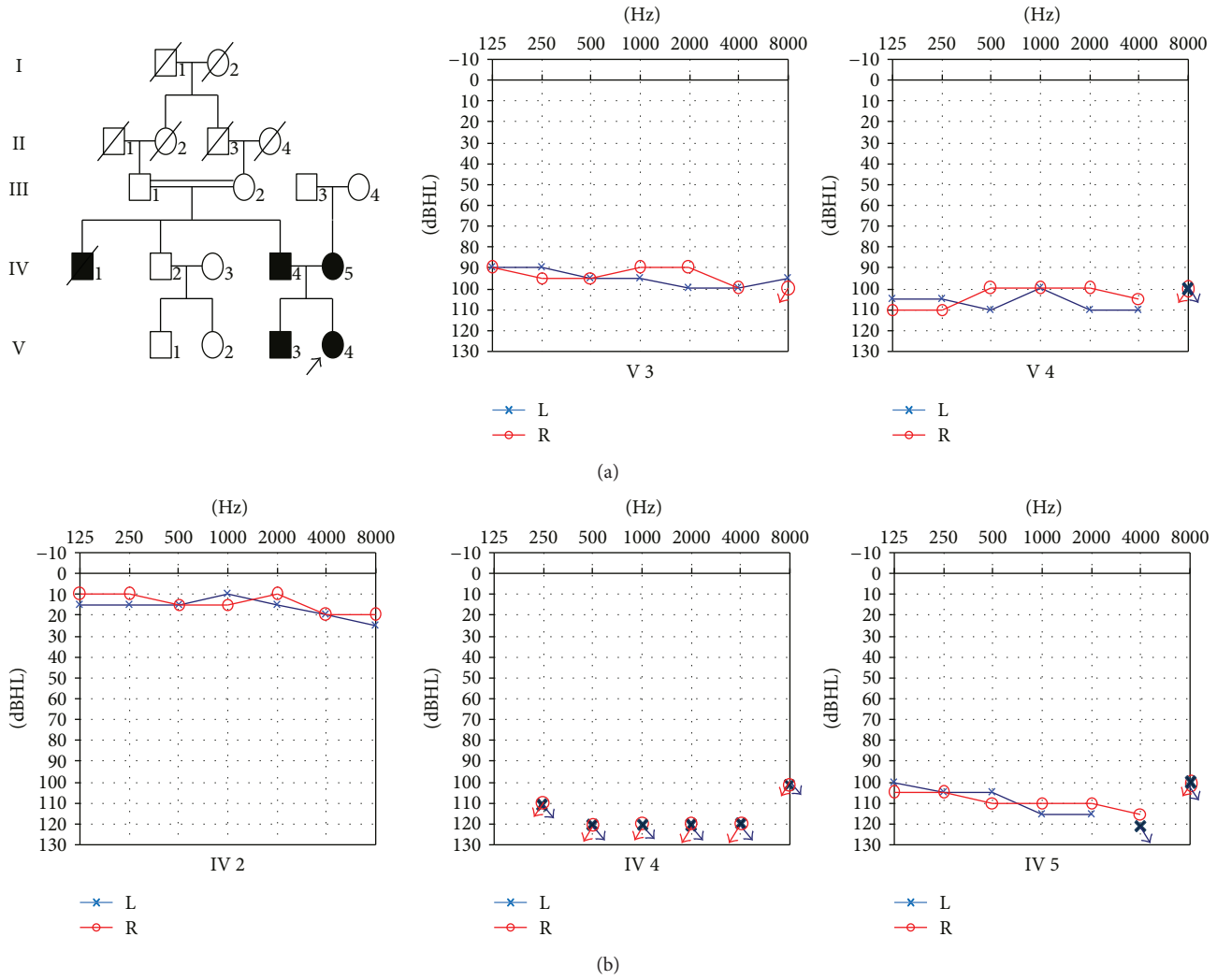

Figure 1: Clinical phenotype presentations of the pedigree. (a) Disease presentation of the family members and the pedigree map. All living members participated in the study, and V-3, V-4, and IV-2 were sequenced using capture gene sequencing. (b) Pure-tone audiograms of the family. Frequency in hertz (Hz) is plotted on the *x*-axis and the hearing level in decibels (dBHL) on the *y*-axis. The arrows in blue or red mean that the pure tones are not elicited at this point.

c.9690+1G>A, in the *MYO15A* gene, and the first two of them were novel. Our finding would be a great supplement for the *MYO15A* pathogenic mutations and would make the genetic counseling available for this family.

2. Materials and Methods

2.1. Subjects. This work was carried out with the permission of Shandong University ethical committee (number 014). All participants involved in the project signed written informed consent. A Chinese family affected by ARNSHL was recruited. The living family members consisted of four patients (V:3, V:4, IV:4, and IV:5, Figure 1(a)) and eight healthy persons. All affected members showed a bilateral congenital hearing loss. 200 normal persons were collected. All audiometric tests and physical examinations were evaluated at Shandong Provincial Hospital.

2.2. Clinical Evaluations. Audiometric assessments consist of auditory brainstem response, pure tone audiometry, distortion product otoacoustic emission, tympanometry, and acoustic stapedial reflex. The classification of deafness was based on the pure tone average (PTA) [15]. Hearing level was sorted into normal hearing (<25 dBHL), mild deafness (>25 and <40 dBHL), moderate deafness (>40 and <60 dBHL), severe deafness (>61 and <80 dBHL), and profound deafness (>80 dBHL) [16].

2.3. DNA Samples. A DNA extraction kit (AXYGEN) was employed to extract genomic DNA of all family members and 200 controls. Agarose gel electrophoresis was performed for evaluating the quality and quantity of DNA samples according to the routine protocol,

excluding common deafness genes.

In order to exclude mutations of *GJB2*, *SLC26A4*, and *MtDNA12SrRNA* genes, a "SNPscan assay" was employed.

Table 1: Clinical features of the family.

Subjects	Age	Age onset	Hearing loss	ABR	DPOAE	AR	MRI
IV-2	57 yr	–	Normal	–	–	–	Normal
IV-4	50 yr	0	Profound	95 dB	+	+	Normal
IV-5	47 yr	0	Profound	95 dB	+	+	Normal
V-3	19 yr	0	Profound	90 dB	+	+	Normal
V-4	17 yr	0	Profound	90 dB	+	+	Normal

+: presence; –: absence.

This SNPscan assay from Genesky Biotechnologies Inc. (Shanghai, China) was designed to capture a total of 115 mutations of the three common deafness-causing genes [17, 18]. It was carried out according to the detailed protocol described previously [19].

2.4. Targeted Capture Sequencing of Deafness Genes. After excluding common mutations, the targeted deafness gene capture was conducted by BGI Inc. (Wuhan, China). All exons, splicing sites, and flanking intron sequences of 127 hearing loss-related genes (Supplement Material: Table S1) were captured. The workflow was (1) the fragmentization of Genomic DNA into 200–300 base pairs, (2) the construction of the genomic library, (3) the capture of targeted DNA fragments by hybridization to the capture array, (4) sequencing on Illumina HiSeq2000 Analyzers, and (5) data collection and bioinformatics analysis. The SOAPsnp software and the GATK IndelGenotyper were used to identify SNPs and indels, respectively. The NCBI dbSNP, 1000 Genomes, and the in-house database were also involved to filter SNPs [20].

2.5. Direct Sanger Sequencing. Using targeted capture sequencing, we identified three candidate mutations. In order to determine whether these variants were cosegregated with hearing loss in the family, the PCR and Sanger sequencing were employed. Therefore, the following primers were synthesized: 5′-GATTGCCTGGTACCTC TGGG-3′ and 5′-AGCCTCCTCATCTTCCTGGT-3′ for human *MYO15A* c.3971C>A and c.4011insA mutations and 5′-TCAGAGGATTGTGCGCCTTT-3′ and 5′-ATGC TCAGTCTTCCTGGCAC-3′ for human *MYO15A* c.9690 +1G>A mutation (BGI Inc., China). The PCR and amplification were performed according to a previous protocol [15]. Sequence alignment of *MYO15A* was performed using the DNASTAR software.

2.6. Functional Prediction. Next, phylogenetic analysis of different sequence alignments was performed by BioEdit. The included sequences were NP_057323.3 (human), XP_001077498.1 (rat), XP_015149897.1 (chicken), XP_009430930.1 (chimpanzee), XP_014974242.1 (monkey), XP_015323568.1 (cattle), and XP_015293218.1 (macaque).

2.7. Structure Modeling. Lastly, three-dimensional (3D) structure of the mutant and wild-type motor domain of *MYO15A* (NP_057323.3) was constructed by I-TASSER. These 3D models were visualized by Swiss-Pdb Viewer 4.01.

3. Result

3.1. Subjects and Clinical Findings. Four affected patients (V-3, V-4, IV-4, and IV-5) and eight unaffected members (V-1, V-2, IV-2, IV-3, III-1, III-2, III-3, and III-4) in the consanguineous Chinese family with ARNSHL participated in this study (Figure 1(a)). The proband was 17 years old and suffered from congenital deafness. As shown in Figure 1(b), all patients were affected with bilateral profound deafness with a flat audiogram revealed by PTA.

Clinical evaluations and otoscopy tests showed no abnormalities. Type A tympanograms were obtained from acoustic immittance tests, and there was no inner ear anomaly in patients revealed by MRI. ABR test revealed that the hearing loss of patients were all above 90 dBHL, and DPOAE were absent bilaterally from all patients. The clinical features of this family were summarized in Table 1.

3.2. Targeted Deafness Gene Capture Sequencing. All 127 hearing loss-related genes were sequenced in V-3, V-4, and IV-2 family members. Three mutations, c.3971C>A (p.A1324D), c.4011insA (p.Q1337Qfs*22), and c.9690 +1G>A, were detected in *MYO15A* gene (NM_016239), which were cosegregated with the disease, suggesting that these mutations may be the etiology of deafness in this ARNSHL family.

3.3. Confirmation of the Three Variants. The three *MYO15A* variants were confirmed by direct sequencing in all participating persons. The homozygous *MYO15A* mutation c.9690 +1G>A was detected in the affected patient IV-4. The compound heterozygous *MYO15A* variants c.3971C>A and c.4011insA were detected in the affected patient IV-5. The compound heterozygous c.3971C>A & c.9690+1G>A and c.4011insA & c.9690+1G>A were identified in the affected siblings, respectively (V-3, V-4) (Figure 2(a)). The other unaffected family members either carried only one heterozygous mutation or had a wild-type genotype (Table 2). However, these variants were absent in two hundred ethnically matched control persons. To our knowledge, c.3971C>A and c.4011insA variants were all considered as the first report and that three mutations identified in one family was quite rare.

The mutation c.3971C>A of *MYO15A*, a missense mutation, leads to an alternation of an alanine with an aspartic at amino acid position 1324 (p.A1324D). The protein structure change caused by this mutation is predicted next. The mutation c.4011insA is an insertion mutation predicting to lead to a reading frame shift at position 1337 and a stop codon (p.Q1337Qfs*22) and truncate the translation of mRNA resulting in lack of its complete length. The mutation c.9690 +1G>A was a splicing-site mutation resulting in a G to A transition at the donor splice site of intron 59. Thus, this mutation impaired the normal processing of mRNA formation.

The alignment of *MYO15A* from different species of human, rat, chicken, chimpanzee, monkey, cattle, and macaque was analyzed (Figure 2(b)). The result proved that p.A1324 and p.Q1337 were conservative among multiple species, which powerfully suggesting that these residues are important for the proper protein function.

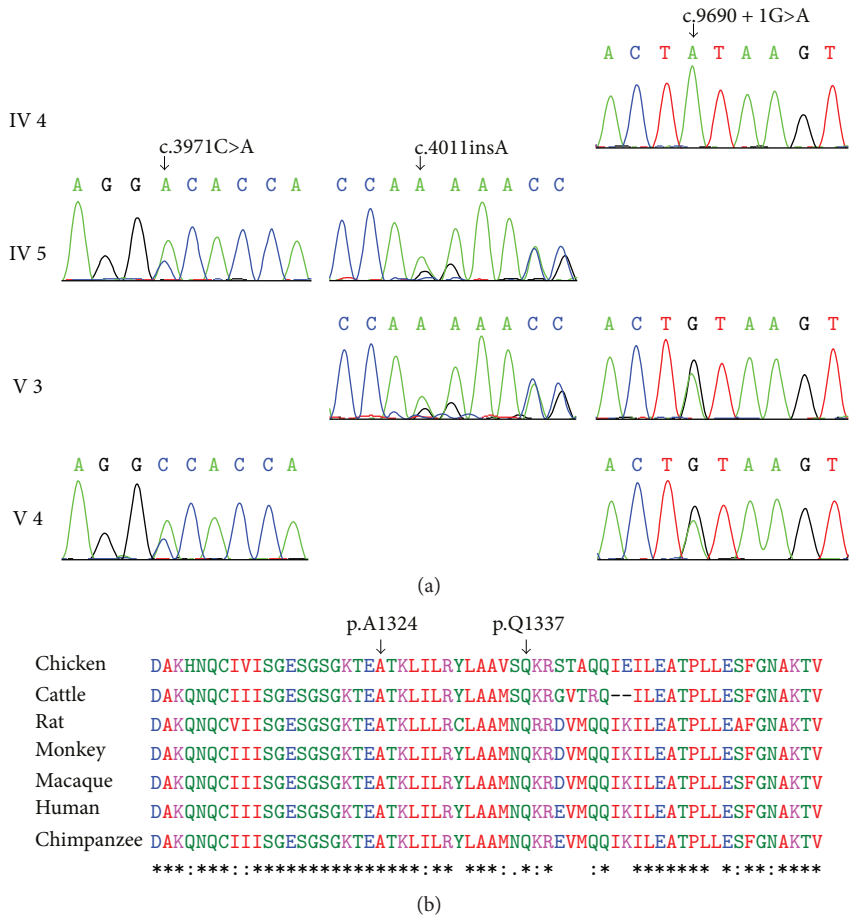

Figure 2: Sequence chromatograms and protein alignment. (a) The sequences of *MYO15A* at 3971, 4011, and 9690 + 1 of four family members. (b) The conservation of the p.A1324 and p.Q1337 residues (shown with black arrows) in healthy human, rat, chicken, chimpanzee, monkey, cattle, and macaque.

Table 2: Genotypes of all family members.

Family member	Genotype		Zygosity
	Variant 1	Variant 2	
III-1	c.9690+1G>A		Heterozygous
III-2	c.9690+1G>A		Heterozygous
III-3	c.4011insA		Heterozygous
III-4	c.3971C>A		Heterozygous
IV-2	c.9690+1G>A		Heterozygous
IV-3			Wild
IV-4	c.9690+1G>A		Homozygous
IV-5	c.3971C>A	c.4011insA	Compound heterozygous
V-1	c.9690+1G>A		Heterozygous
V-2			Wild
V-3	c.3971C>A	c.9690+1G>A	Compound heterozygous
V-4	c.4011insA	c.9690+1G>A	Compound heterozygous

3.4. Structural Modeling of p.A1324D in the Motor Domain of MYO15A. A 3D simulative structure (PDB ID:1g8xA) of *MYO15A* motor domain was built, which contained the myosin XVA protein residues 1261–1887. The sequence identity between the template and target was 44% which was higher than the average 25%. We used Swiss-Pdb Viewer 4.1 software to analyze the mutated and wild structures of motor domain (Figure 3). The variant was speculated to

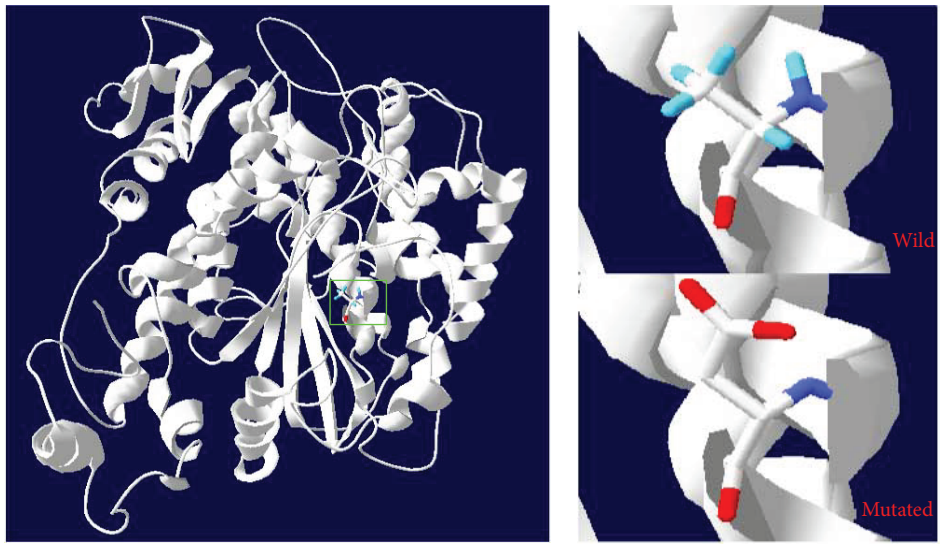

(a) (b)

Figure 3: Structure modeling of wild-type and mutated MYO15A motor domain. (a) Green box shows the complete MYO15A motor domain. (b) The detailed structure of wild and mutated p.A1324 residue.

affect the side chain because of the missense change. The prediction uncovered that this mutation caused damage to the protein function by means of the change of protein structure.

4. Discussion

Changes in the *MYO15A* gene are known to be responsible for DFNB3 deafness. DFNB3 is the third pathogenic locus responsible for severe to profound ARNSHL. This report performed targeted capture sequence of 127 known deafness genes to describe genetic causes of a Chinese ARNSHL family. We identified three disease-causing *MYO15A* mutations finally. Multiple novel gene mutations revealed in one NSHL family are quite rare in the previous studies.

Our finding revealed that the variants p.A1324D and p.Q1337Qfs*22 are located at myosin XVA motor domain. This region containing actin- and ATP-binding sites can produce the force that transports actin filaments in vitro [21]. The mutation p.A1324D is a missense change leading to an amino acid substitution, and p.Q1337Qfs*22 results in a frameshift insertion and introduces a stop codon in the *MYO15A* open reading frame. A truncated protein is generated caused by the frameshift mutation. We estimate that the truncated protein is likely to be misexpressed or mislocated in the inner ear. Similarly to human DFNB3 hearing loss, a mouse model with homozygous variant in the myosin XVA motor domain exhibits profound hearing loss [22]. Many mutations were reported in this domain [8, 23] and were proposed probably to have deleterious effects on protein function.

Another mutation c.9690+1G>A was first reported in 2015 [24]. It is a splicing-site mutation resulting in a G to A transition at the donor site and is predicted to locate between the junctional region of the posterior MyTH4 domain and the FERM domain in myosin XVA. Similarly to the myosin VIIA MyTH4-FERM domain, this region is important for the localization to the stereocilia tips [25, 26], which is essential for the normal function of the stereocilia tips. Therefore, we speculate that this mutation could weaken the MyTH4-FERM interface that leads to the disease.

To date, a number of mutations in *MYO15A* gene have been identified in hereditary hearing loss (Figure 4). Interestingly, the mutation spectrum of *MYO15A* varies among different ethnic populations. For example, a relatively low frequency of 0.89% (10/1120) was reported in a study of Japanese deafness cohort [27]. A mutational frequency of 3.3% was revealed in the Middle and South Asian areas [28]. In another genetic analysis study, 4% (5/125) was found in a Chinese ethnic population preexcluding common mutations [29]. Furthermore, a frequency of 5% was found in a Pakistani recessively inherited severe to profound hearing loss population [30]. And a higher frequency of 5.71% was reported in an Iranian population preexcluding GJB2 mutations [31]. Therefore, for every country, consummating its own *MYO15A* mutation spectrum is essential for the diagnosis and prevention of hearing loss.

In this family, we identified three novel mutations in *MYO15A* gene causing profound hearing loss. Exactly as literatures state, *MYO15A* variants have usually been regarded as the cause of congenital severe to profound deafness [6, 7]. However, recently, some families suffering from less severe hearing impairment were also diagnosed a genetic cause of *MYO15A* mutations. We find those mutations leading to less severe hearing loss are usually located in the N-terminal domain in reported literatures. We estimate that the defect caused by the mutations in the N-terminal domain other than the rest of the domains might be compensated by the existence of class 2 isoform which has no N-terminal domain. The N-terminal

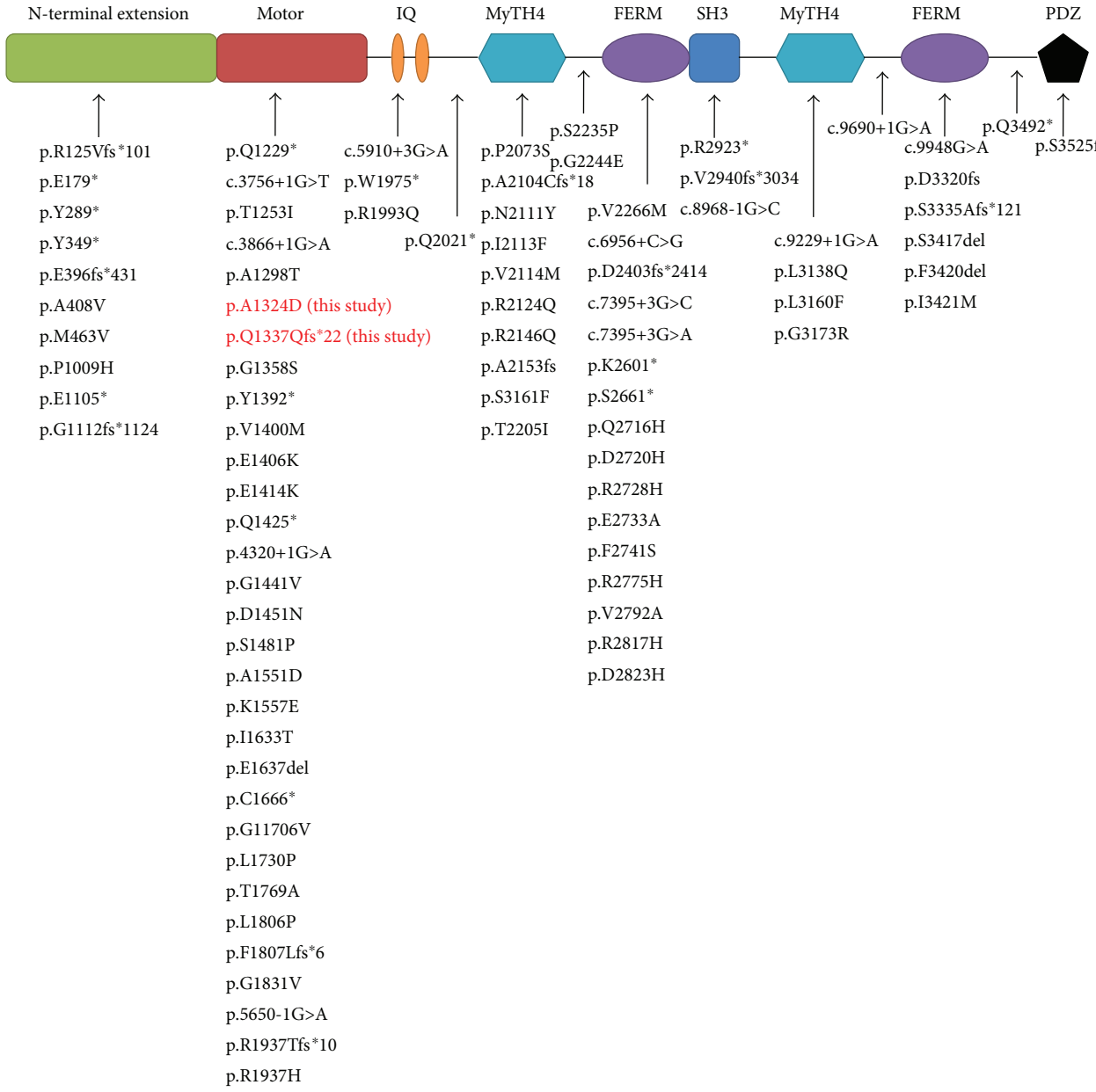

Figure 4: Reported mutations of *MYO15A* gene and their locations in the protein structure. The red characters refer to novel mutations identified in this study.

extension domain plays a less important role than the other parts of the gene in the protein function. Chang et al.'s study in 2015 took the same ground [8].

In conclusion, three variants in *MYO15A* were identified using SNPscan assay and targeted capture sequencing: c.3971C>A (p.A1324D), c.4011insA (p.Q1337Qfs*22), and c.9690+1G>A, and the first two of them were novel. All these mutations were cosegregated with the severe to profound deafness and were predicted to be pathogenic mutations. The present results also demonstrated that the combined application of SNPscan assay and targeted capture sequencing is a valuable and cost-saving molecular diagnostic strategy for ARNSHL. Our findings further extended the pathogenic variants of *MYO15A* gene in the ARNSHL group and would have a positive implication in genetic counseling for hearing loss families.

Conflicts of Interest

The authors declare that there is no conflict of interests to report.

Acknowledgments

This work was supported by grants from the National 973 Basic Research Program of China (2014CB541703), grants from the National Natural Science Foundation of China (81670932, 81470704, and 81670942), and grants from

Shandong Provincial Natural Science Foundation, China (ZR2014HM022 and 2016GSF201226).

Supplementary Materials

Table S1: summary of the 127 targeted deafness genes. *(Supplementary Materials)*

References

[1] D. Yan, M. Tekin, S. Blanton, and X. Z. Liu, "Next-generation sequencing in genetic hearing loss," *Genetic Testing and Molecular Biomarkers*, vol. 17, no. 8, pp. 581–587, 2013.

[2] F. Cengiz, D. Duman, A. Sirmaci et al., "Recurrent and private *MYO15A* mutations are associated with deafness in the Turkish population," *Genetic Testing and Molecular Biomarkers*, vol. 14, no. 4, pp. 543–550, 2010.

[3] H. Xia, X. Huang, Y. Guo et al., "Identification of a novel *MYO15A* mutation in a Chinese family with autosomal recessive nonsyndromic hearing loss," *PLoS One*, vol. 10, no. 8, article e0136306, 2015.

[4] D. P. Kelsell, J. Dunlop, H. P. Stevens et al., "Connexin 26 mutations in hereditary non-syndromic sensorineural deafness," *Nature*, vol. 387, no. 6628, pp. 80–83, 1997.

[5] A. Wang, Y. Liang, R. Fridell et al., "Association of unconventional myosin *MYO15* mutations with human nonsyndromic deafness *DFNB3*," *Science*, vol. 280, no. 5368, pp. 1447–1451, 1998.

[6] Z. Brownstein, L. Friedman, H. Shahin et al., "Targeted genomic capture and massively parallel sequencing to identify genes for hereditary hearing loss in Middle Eastern families," *Genome Biology*, vol. 12, no. 9, article R89, 2011.

[7] X. Gao, Q. Zhu, Y. Song et al., "Novel compound heterozygous mutations in the *MYO15A* gene in autosomal recessive hearing loss identified by whole-exome sequencing," *Journal of Translational Medicine*, vol. 11, no. 1, p. 284, 2013.

[8] M. Chang, A. Kim, N. K. Kim et al., "Identification and clinical implications of novel *MYO15A* mutations in a non-consanguineous Korean family by targeted exome sequencing," *Molecules and Cells*, vol. 38, no. 9, pp. 781–788, 2015.

[9] Y. Liang, A. Wang, I. Belyantseva et al., "Characterization of the human and mouse unconventional myosin XV genes responsible for hereditary deafness *DFNB3* and shaker 2," *Genomics*, vol. 61, no. 3, pp. 243–258, 1999.

[10] J. Berg, B. Powell, and R. Cheney, "A millennial myosin census," *Molecular Biology of the Cell*, vol. 12, no. 4, pp. 780–794, 2001.

[11] B. Garcia-Alvarez, J. de Pereda, D. Calderwood et al., "Structural determinants of integrin recognition by talin," *Molecules and Cells*, vol. 11, no. 1, pp. 49–58, 2003.

[12] M. Krendel and M. Mooseker, "Myosins: tails (and heads) of functional diversity," *Physiology*, vol. 20, no. 4, pp. 239–251, 2005.

[13] I. Belyantseva, E. Boger, and T. Friedman, "Myosin XVa localizes to the tips of inner ear sensory cell stereocilia and is essential for staircase formation of the hair bundle," *Proceedings of the National Academy of Sciences of the United States of America*, vol. 100, no. 24, pp. 13958–13963, 2003.

[14] L. Beyer, H. Odeh, F. Probst et al., "Hair cells in the inner ear of the pirouette and shaker 2 mutant mice," *Journal of Neurocytology*, vol. 29, no. 4, pp. 227–240, 2000.

[15] F. Zhang, X. Bai, Y. Xiao et al., "Identification of a novel mutation in *SLC26A4* gene in a Chinese family with enlarged vestibular aqueduct syndrome," *International Journal of Pediatric Otorhinolaryngology*, vol. 85, pp. 75–79, 2016.

[16] J. Carioli and A. Teixeira, "Use of hearing AIDS and functional capacity in middle-aged and elderly individuals," *International Archives of Otorhinolaryngology*, vol. 18, no. 03, pp. 249–254, 2014.

[17] F. Zhang, Y. Xiao, L. Xu et al., "Mutation analysis of the common deafness genes in patients with nonsyndromic hearing loss in Linyi by SNPscan assay," *BioMed Research International*, vol. 2016, Article ID 1302914, 7 pages, 2016.

[18] Y. Ma, Y. Xiao, X. Bai et al., "*GJB2*, *SLC26A4*, and mitochondrial *DNA12S rRNA* hot-spots in 156 subjects with non-syndromic hearing loss in Tengzhou, China," *Acta Oto-Laryngologica*, vol. 136, no. 8, pp. 800–805, 2016.

[19] W. Du, J. Cheng, H. Ding, Z. Jiang, Y. Guo, and H. Yuan, "A rapid method for simultaneous multi-gene mutation screening in children with nonsyndromic hearing loss," *Genomics*, vol. 104, no. 4, pp. 264–270, 2014.

[20] X. Wei, X. Ju, X. Yi et al., "Identification of sequence variants in genetic disease-causing genes using targeted next-generation sequencing," *PLoS One*, vol. 6, no. 12, article e29500, 2011.

[21] M. Redowicz, "Myosins and deafness," *Journal of Muscle Research & Cell Motility*, vol. 20, no. 3, pp. 241–248, 1999.

[22] F. Probst, R. Fridell, Y. Raphael et al., "Correction of deafness in shaker-2 mice by an unconventional myosin in a BAC transgene," *Science*, vol. 280, no. 5368, pp. 1444–1447, 1998.

[23] H. Woo, H. Park, J. Baek et al., "Whole-exome sequencing identifies *MYO15A* mutations as a cause of autosomal recessive nonsyndromic hearing loss in Korean families," *BMC Medical Genetics*, vol. 14, no. 1, p. 72, 2013.

[24] Y. Chen, Z. Wang, Z. Wang et al., "Targeted next-generation sequencing in Uyghur families with non-syndromic sensorineural hearing loss," *PLoS One*, vol. 10, no. 5, article e0127879, 2015.

[25] L. Wu, L. Pan, Z. Wei, and M. Zhang, "Structure of MyTH4-FERM domains in myosin VIIa tail bound to cargo," *Science*, vol. 331, no. 6018, pp. 757–760, 2011.

[26] R. Chai, G. Li, J. Wang, and J. Zou, "Hearing Loss: Reestablish the Neural Plasticity in Regenerated Spiral Ganglion Neurons and Sensory Hair Cells," *Neural Plasticity, article*, vol. 1807581, 2017.

[27] M. Miyagawa, S. Nishio, M. Hattori et al., "Mutations in the *MYO15A* gene are a significant cause of nonsyndromic hearing loss: massively parallel DNA sequencing-based analysis," *Annals of Otology Rhinology & Laryngology*, vol. 124, 1_suppl, pp. 158S–168S, 2015.

[28] N. Nal, Z. Ahmed, E. Erkal et al., "Mutational spectrum of *MYO15A*: the large N-terminal extension of myosin XVA is required for hearing," *Human Mutation*, vol. 28, no. 10, pp. 1014–1019, 2007.

[29] T. Yang, X. Wei, Y. Chai, L. Li, and H. Wu, "Genetic etiology study of the non-syndromic deafness in Chinese Hans by targeted next-generation sequencing," *Orphanet Journal of Rare Diseases*, vol. 8, no. 1, p. 85, 2013.

[30] R. Bashir, A. Fatima, and S. Naz, "Prioritized sequencing of the second exon of *MYO15A* reveals a new mutation segregating in a Pakistani family with moderate to severe hearing loss," *European Journal of Medical Genetics*, vol. 55, no. 2, pp. 99–102, 2012.

[31] Z. Fattahi, A. Shearer, M. Babanejad et al., "Screening for *MYO15A* gene mutations in autosomal recessive nonsyndromic, *GJB2* negative Iranian deaf population," *American Journal of Medical Genetics Part A*, vol. 158A, no. 8, pp. 1857–1864, 2012.

Hindawi
Neural Plasticity
Volume 2018, Article ID 2160854, 9 pages
https://doi.org/10.1155/2018/2160854

Research Article

Hollow Mesoporous Silica@Zeolitic Imidazolate Framework Capsules and Their Applications for Gentamicin Delivery

Xiaoxiang Xu,[1] Heyin Chen,[2] Xia Wu,[1] Sen Chen,[1] Jing Qi,[2] Zuhong He,[1] Shengyu Zou,[1] Le Xie,[1] Kai Xu,[1] Haitao Yuan,[2] Yu Sun,[1] Haoquan Zheng,[2] and Weijia Kong[1]

[1]*Department of Otorhinolaryngology, Union Hospital, Tongji Medical College, Huazhong University of Science and Technology, Wuhan 430020, China*
[2]*Key Laboratory of Applied Surface and Colloid Chemistry, Ministry of Education, School of Chemistry and Chemical Engineering, Shaanxi Normal University, Xi'an 710119, China*

Correspondence should be addressed to Yu Sun; sunyu@hust.edu.cn, Haoquan Zheng; zhenghaoquan@snnu.edu.cn, and Weijia Kong; entwjkong@hust.edu.cn

Received 16 November 2017; Accepted 27 December 2017; Published 5 April 2018

Academic Editor: Renjie Chai

We have synthesized hollow mesoporous silica (HMS) at a zeolitic imidazolate framework (ZIF) capsule that can be used as a drug delivery system for gentamicin (GM). The GM is first loaded into HMS. Then, the outer surface of the GM/HMS is coated with uniformed ZIF nanoparticles (denoted as GM/HMS@ZIF). The GM/HMS@ZIF has been successfully prepared and acts as a capsule for GM. The GM/HMS@ZIF shows a good biocompatibility and a good cellular uptake in House Ear Institute-Organ of Corti 1 (HEI-OC1) cells. The GM is released slowly within 10 h under acidic conditions, which is used to simulate the pH of the endosome and lysosome compartments. The *in vivo* assay shows that the signal from fluorescein isothiocyanate (FITC) can be observed after 15 days, when the mice were injected with FITC/HMS@ZIF. This opens new opportunities to construct a delivery system for GM via one controlled low dose and sustained release for the therapy of Ménière's disease.

1. Introduction

Ménière's disease is a common inner ear disorder [1]. The clinical observation of Ménière's disease includes episodic vertigo, fluctuating hearing loss, tinnitus, and aural fullness, which negatively impacts the patient's life both physically and psychosocially. The gentamicin (GM) administration has been widely used for the treatment of Ménière's disease and has demonstrated to be effective in clinical applications. To avoid the systemic effect of aminoglycoside, Schuknecht developed a technique to deliver streptomycin intratympanically, which could control vertigo admirably [2]. Although intratympanic injection proves to be efficient, the high dose of the gentamicin in the local area of ears causes ototoxicity [3]. Despite that gentamicin is a very effective aminoglycoside, its potential ototoxicity which is of irreversible nature makes it a challenge and limits its application [4–13]. The use of low-dose and less frequent intratympanic gentamicin injection could solve this problem. More recently, controllable delivery systems for GM via sustained release have attracted many scientists' attentions. This kind of delivery system could deliver a precise and consistent amount of medicine to the round window due to continuous release of low-dose drug [14]. However, it is still challenging to construct a designable drug delivery system that can continuously release gentamicin and allow the control of the administration of the drug.

In the present study, the potential of nanomaterials as a neural interfacing material for drug release, neural repair, and regeneration has been widely explored [15–17]. More recently, metal-organic frameworks (MOFs) constructed by the coordination of metal ions or clusters with organic ligands have been developed [18–28]. MOFs have been used as a controlled delivery system for functional molecules, such as DNA, enzyme, fluorescein, and drugs [29–35]. Zeolitic imidazolate framework- (ZIF-) 8 is built from Zn ions and

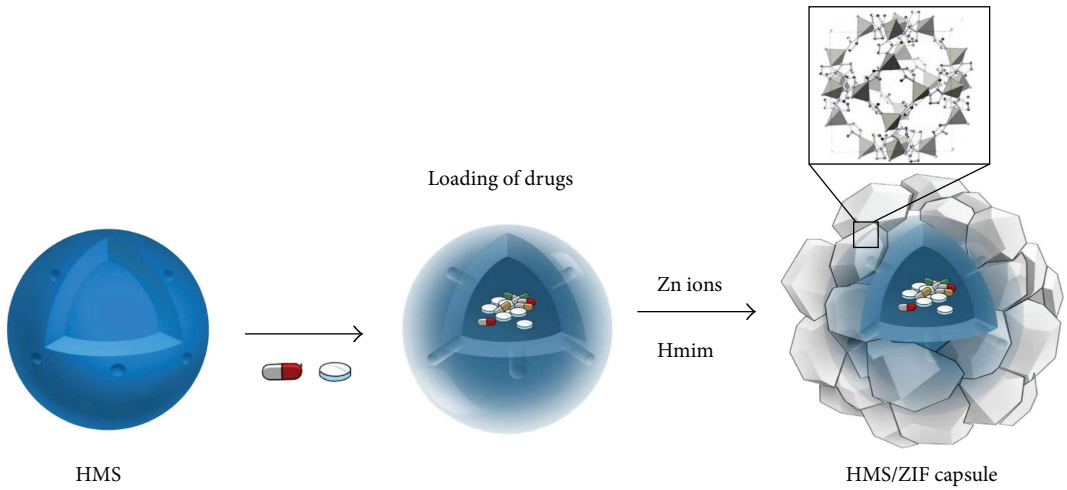

Figure 1: HMS/ZIF capsule for gentamicin.

2-methylimidazole (Hmim), which is a nontoxic and biocompatible ZIF [36–44]. However, the size of most drugs is larger than that of the pore opening of ZIF-8 (3.4 Å). It is difficult to load drugs by a postloading method. A one-pot synthetic route to encapsulate drugs in ZIF-8 nanoparticles has been developed [37]. A sustained release of drugs from the drug-loaded ZIF-8 has been achieved due to the decomposition of the ZIF framework under acidic conditions. However, the loading of drugs in ZIF is limited to 20 wt%. The use of high dose of ZIF carriers would give rise to the cytotoxicity due to the necrosis, which is caused by the nano-sized particle and unprogrammed cell death [34, 35, 45]. Therefore, a ZIF-based drug delivery system with a higher loading of drugs and a controlled release manner is still of high demand.

Here, we have synthesized hollow mesoporous silica (HMS) at a ZIF capsule as a carrier for GM (Figure 1). The nanocarriers improve the existing treatment, since they can alter biodistribution profiles and pharmacokinetics. HMS has huge inner cavities and radially oriented mesochannels, which are useful for drug storage and delivery [46–50]. The mesochannels are perpendicular to the surface connecting the outer environment and the inner cavity. The GM is loaded in the inner cavities of the HMSs. The loading of GM can reach up to 38 wt% in GM/HMS@ZIF due to the big volume of the inner cavity. We demonstrate the sustained release of GM from the GM/HMS@ZIF capsule by *in vitro* and *in vivo* assays.

2. Materials and Methods

2.1. Synthesis of the HMSs. Typically, 60 mL of ethanol, 100 mL of H_2O, and 2 mL of concentrated ammonia aqueous solution (25 wt% NH_3) were added into a 250 mL flask. 0.3 g of CTAB was dissolved in ethanolic solution [51]. The mixture was then heated to 35°C, and tetraethyl orthosilicate (TEOS, 2 mL) was rapidly added under vigorous stirring. The solid mesoporous silica nanospheres were dispersed in distilled water (320 mL) at 100°C for 48 h and washed again with ethanol and dried under high vacuum. The surfactants were removed by calcination at 550°C for 6 h.

2.2. Synthesis of GM/HMS@ZIF Capsules. 30 mg of HMS was suspended in 5 mL of ethanolic solution containing 70 mg GM. The suspension was conducted at 45°C under vacuum to remove the solvent. The obtained powder was dried by freezing-drying under vacuum. Then, 0.1 g of GM/HMS was added to 10 mL aqueous solution containing 1.89 g Hmim. Subsequently, a solution of 0.0975 g $Zn(NO_3)_2$ in 1 mL H_2O was added. The mixture was stirred at room temperature for 5 min, followed by centrifugation and washing with deionized water. The GM/HMS@ZIF capsule was then obtained. The same synthesis approach was applied to prepare fluorescein isothiocyanate (FITC)/HMS@ZIF. Part of GM/HMS@ZIF was dissolved in HCl solution. The amount of GM in the supernatant was determined by high-performance liquid chromatography (HPLC). The detection of GM was carried out at 280 nm. The loading of GM was calculated as loading of GM (wt%) = m_{GM}/m_{total}.

2.3. Confocal Microscopy. House Ear Institute-Organ of Corti 1 (HEI-OC1) cells were seeded at a concentration of 1×10^6 cells per well onto the surface of coverslips placed in plates and precultured for 24 h at 37°C. Then, the medium was removed, and fresh medium that contained FITC/HMS@ZIF ($2\,mg{\cdot}L^{-1}$) was added. After 2, 8, or 24 h of incubation, the cells were washed twice with PBS and then fixed with 4% paraformaldehyde in PBS for 15 min at RT. The cells were then stained with $2.5\,mg{\cdot}L^{-1}$ of 4′,6-diamidino-2-phenylindole (DAPI) for 10 min and mounted with ProLong Gold antifade mounting medium. The stained samples were examined at excitation/emission wavelengths of 405/461 nm for DAPI and 490/530 nm for FITC.

2.4. MTT Assays in Breast Cancer. The Michigan Cancer Foundation- (MCF-) 7 cells were seeded at 1×10^5 cells per well onto 96-well plates and were cultured in media containing 10% fetal calf serum. The suspensions of

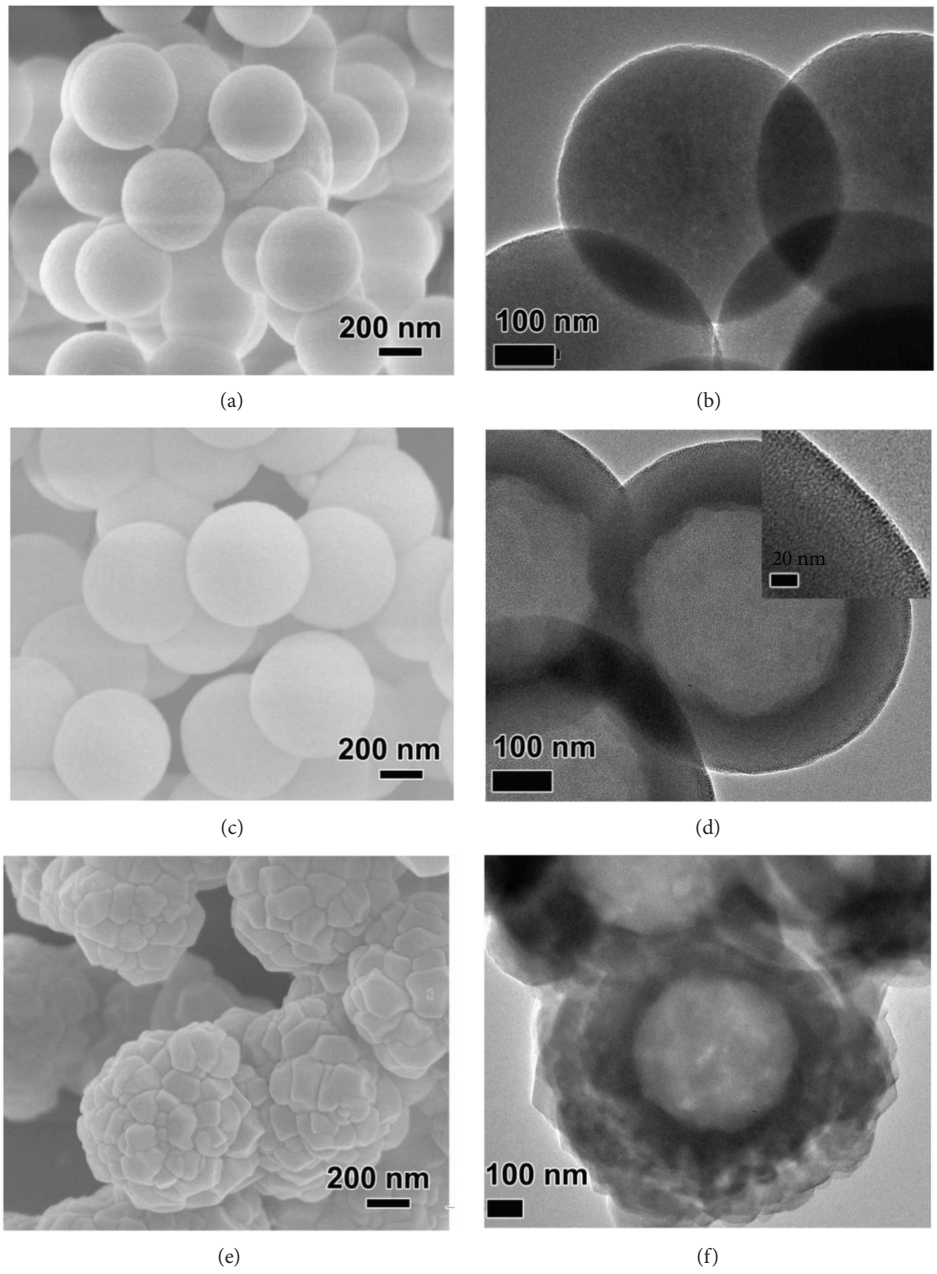

Figure 2: SEM images and TEM images of solid MS (a, b), HMS (c, d), and GM/HMS@ZIF (e, f), respectively.

samples at various concentrations were added and cultivated at 37°C for 24 h. 10 μL of MTT (3-(4,5,-dimethylthiazol-2-yl)-2,5-diphenyltetrazolium bromide) was added to each well after 24 h. The MCF-7 cells were further incubated for another 4 h. The MTT medium was removed, and then DMSO was added to each well. The absorbance at 570 nm was determined with a plate reader.

2.5. A Stepped Release of GM from GM/HMS@ZIF. 10 mg of the GM/HMS@ZIF capsule was tested in a 20.0 mL buffer solution (pH 7.4) of 10% (*v*/*v*) FBS at 37°C. The pH of the solution was then adjusted to 5 with diluted HCl (0.6 M). The release percentages of GM were calculated according to the formula (release percentage (%) = mr/ml, in which mr is the amount of released GM while ml is the total amount of loaded GM). The amount of GM was determined by HPLC. When using FITC/HMS@ZIF, the amount of FITC was determined by a fluorescence spectrophotometer. The FITC was examined at excitation/emission wavelengths of 490/520 nm.

2.6. In Vivo Imaging of FITC/HMS@ZIF in a Rat Model. KM mice, 4-5 weeks old, were used. Mice were randomly assigned to three groups ($n = 6$): group 1 for PBS solutions as control, group 2 for free FITC solution, and group 3 for FITC/HMS@ZIF. 50 μL of PBS solution, 50 μL of free FITC

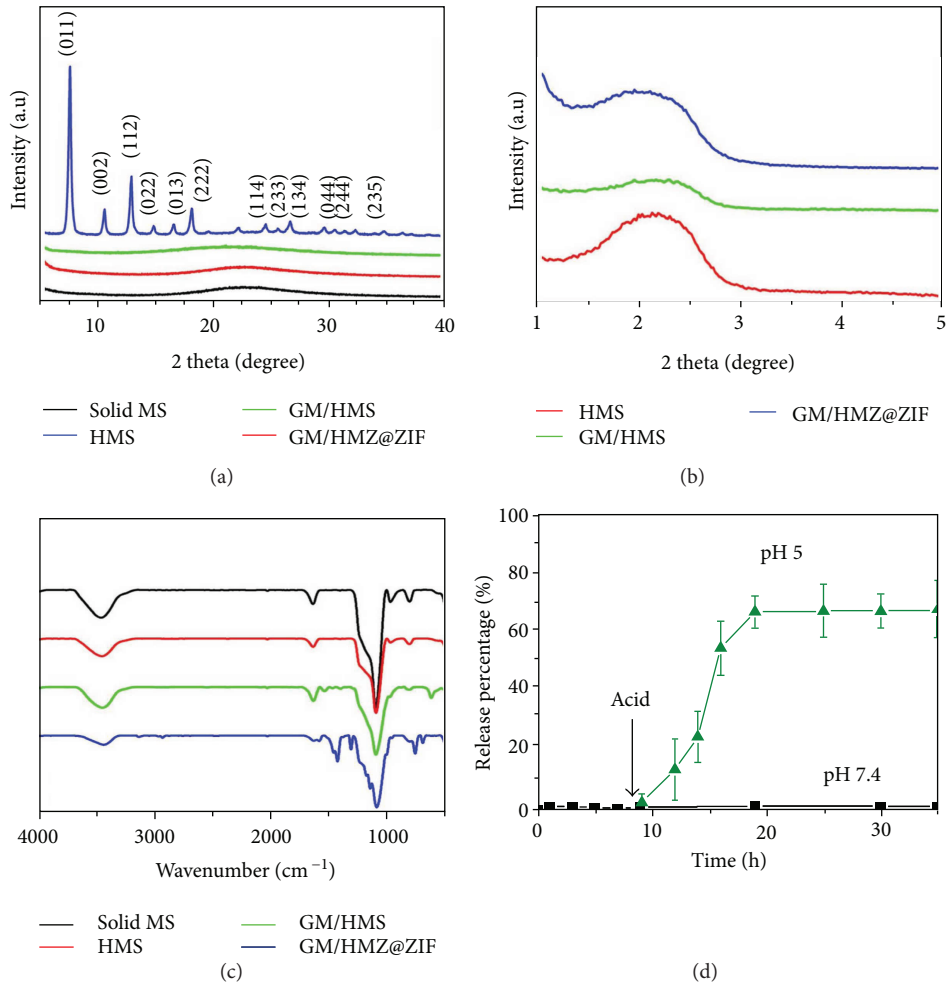

Figure 3: Wide-angle PXRD patterns (a), small-angle PXRD patterns (b), and FTIR spectra (c) of solid MS, HMS, GM/HMS, and GM/HMS@ZIF. (d) Release profiles of GM from GM/HMS@ZIF capsules by stepwise acidification.

(5 mg·mL^{-1}), or 50 μL of FITC/HMS@ZIF (10 mg·mL^{-1}) was subcutaneously injected by postauricular hypodermic injections of mice. The images of mice were taken after treatment for 1, 3, 5, 8, 12, and 15 days. The mice were anesthetized by a mixed anesthesia of ketamine and chlorpromazine. The release of FITC in the ear after subcutaneous injection was monitored continuously by an in vivo imaging device. The samples were examined at excitation/emission wavelengths of 490/530 nm.

3. Results

The HMS was synthesized by two steps. The solid mesoporous silica (denoted as solid MS) was first generated by a surfactant assembly sol-gel process. A scanning electron microscopy (SEM) image showed that the solid MS had a particle size of 550 nm (Figures 2(a) and 2(b)). The solid MS was then incubated in H_2O at 100°C for 48 h. The hydrothermal treatment changed the spontaneous morphology to the desired hollow structure, which was demonstrated by the difference between the hollow and the shell (Figures 2(c) and 2(d)). The mesopores in the shell enable the efficient mass transfer between the outside environment and the inner core (Figure 2(d), inset). As shown in Figure S1, the morphology of the GM-loaded HMS (denoted as GM/HMS) did not change. The powder X-ray diffraction (PXRD) patterns of solid MS, HMS, and GM/HMS showed a broad peak at 20°, which was attributed to the amorphous framework of the silica (Figures 3(a) and 3(b)). The Fourier-transform infrared spectroscopy (FTIR) showed the relative intensity of Si-O bending bands at 960 cm^{-1} in HMS and GM/HMS (Figure 3(c)). The infrared vibrations around 1350–1500 cm^{-1} were then assigned to the C-H vibrations of the GM in GM/HMS, demonstrating the successful loading of GM in HMS.

The mesopores in the shell are still accessible in GM/HMS. As shown in Figure 2(e), after coating ZIF-8 on the outer surface, HMS was completely covered by ZIF-8 nanoparticles. These nanoparticles present rhombic dodecahedral shapes with 50–200 nm in size. The hollow structure was not affected by the ZIF-8 coating. The sharp diffraction peaks of GM/HMS@ZIF fitted well with the previously reported peaks of ZIF-8, which implied the high crystallinity of ZIF-8. FTIR spectrum also demonstrated the formation of ZIF-8. N_2 adsorption/desorption isotherms of GM/HMS@ZIF was shown in Figure S2.

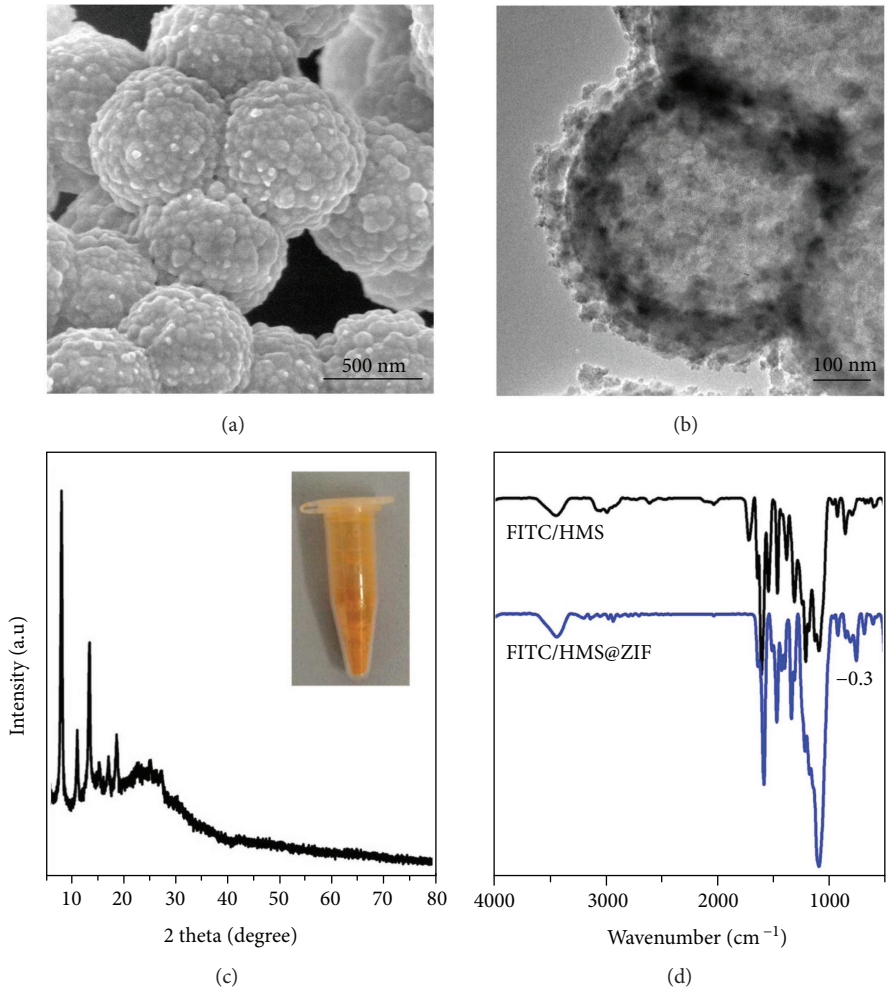

Figure 4: SEM image (a), TEM image (b), PXRD pattern (c), photograph (inset), and FTIR spectrum (d) of the FITC/HMS@ZIF capsule.

The capillary condensation in the range of p/p0 at 0.2-0.3, which can be attributed to the mesopores in the shell, disappeared. The mesopores were fully capped by ZIF-8 nanoparticles, and the GM/HMS@ZIF thus acted as a capsule and stored GM in the inner cavity. GM loading in the GM/HMS@ZIF was calculated to be 38 wt%. We tested the dynamic light scattering (DLS) of GM/HMS@ZIF (Figure S3). GM/HMS@ZIF had a narrow particle size distribution in the aqueous solution of 0.9% NaCl. These nanoparticles were highly dispersed, as a result of its high ζ potential of +30.1. There was no release of GM from GM/HMS@ZIF at pH 7.4 for 15 days, which demonstrated the safe storage of GM before passing the endosome and lysosome compartments (Figures 3(d) and S4) [52, 53].

We further studied the potential of the HMS@ZIF as a drug delivery system for GM. The cell assays showed that the viability of cells was higher than 95% after the treatment of MCF-7 cells with HMS@ZIF for 24 h. This result indicated that our material had a good biocompatibility (Figure S5). FITC was a modeling fluorescence and was used as a labelling agent in biomedicine. We chose FITC to replace GM for further investigation of the cellular uptake of our material. An SEM image showed that FITC/HMS@ZIF had a similar morphology to GM/HMS@ZIF (Figure 4(a)). As shown in Figure 4(b), the HMS was completely covered by nanocrystals. The PXRD demonstrated that these nanocrystals were ZIF nanocrystals (Figure 4(c)), while the FTIR spectra demonstrated the successful loading of FITC and the formation of ZIF in FITC/HMS@ZIF (Figure 4(d)). Confocal microscopy was then used to investigate the uptake of FITC/HMS@ZIF into HEI-OC1 cells (Figure 5). After the incubation with HEI-OC1 cells for 2, 8, and 24 h, the FITC/HMS@ZIF exhibited efficient intracellular uptake. The FITC/HMS@ZIF nanoparticles are located mainly in the cytoplasm and accumulated around the cell nuclei, which showed that the GM/HMS@ZIF nanocapsules had pass through the cell membrane. The transfer between the circulation in the bloodstream and the endosome and lysosome compartments (pH 5-6) was mimicked by a stepped release system. About 75% of GM were released slowly from the GM/HMS@ZIF within 10 h at pH 5.0. Therefore, a sustained release of GM from GM/HMS@ZIF can be achieved using this designable drug delivery system.

We took the *in vivo* images of mice after administration of free FITC and FITC/HMS@ZIF after several days (Figure 6). The mice were treated with free FITC or FITC/

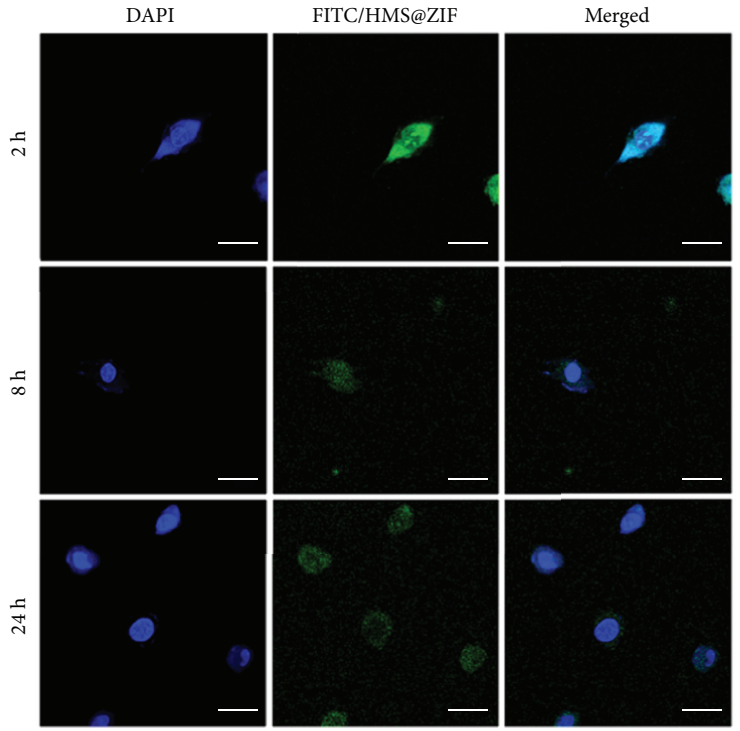

Figure 5: The cellular uptake study of the FITC/HMS@ZIF capsule in HEI-OC1 cells by the confocal microcopy images. The scale bar = 5 μm.

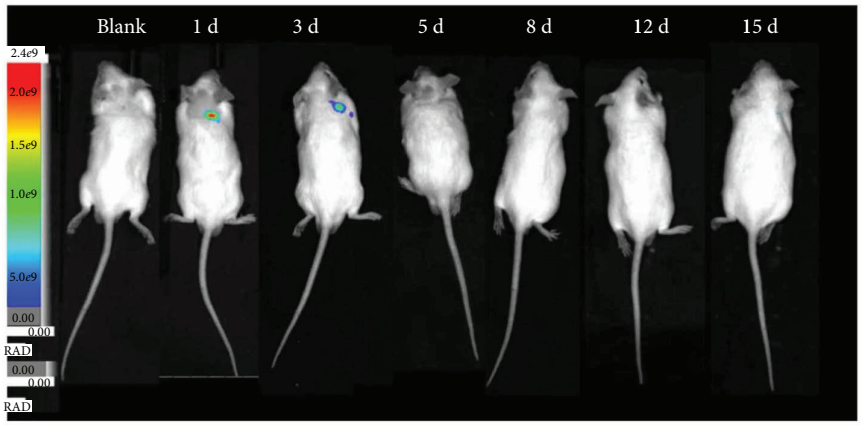

(a)

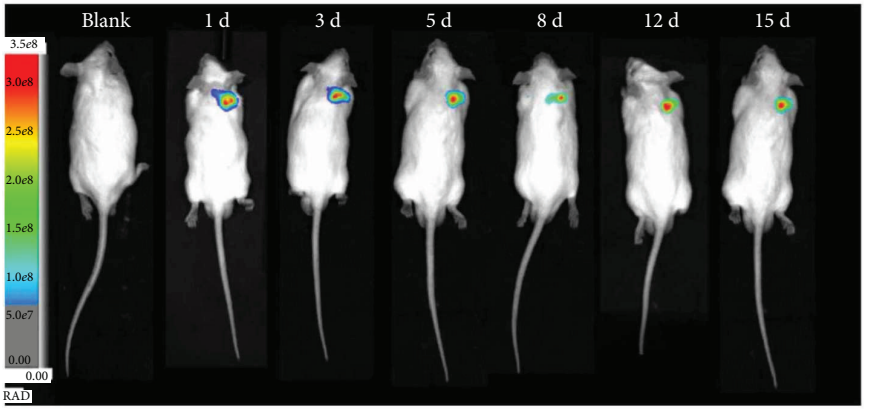

(b)

Figure 6: *In vivo* imaging of mice after administration of free FITC (a) and FITC/HMS@ZIF (b) at 1, 3, 5, 8, 12, and 15 days.

HMS@ZIF by postauricular hypodermic injections. When free FITC was used, no signal from FITC could be observed after 3 days. The signal with high intensity was observed from the mice injected with FITC/HMS@ZIF even after a long period of 15 days, demonstrating a continuous and sustained release of FITC form FITC/HMS@ZIF. Compared with free drug, the nanocarriers of HMS@ZIF may change both the pathways to the circulation due to the nanosize. Furthermore, the drug-eliminated half-life of GM might also change due to the freshly released GM at each subtle time period. Therefore, it is possible to construct an efficient delivery system with a controlled release manner. This novel delivery system for GM would make the treatment dosage of the GM precise and can be used to prevent the side effects of the GM, especially ototoxicity, during the treatments of Ménière's disease in clinical applications.

4. Discussion

We have synthesized HMS@ZIF capsule that can be used as controlled drug delivery system for GM. The GM has been first loaded into HMS. Then, the obtained GM/HMS has been coated with uniformed ZIF nanoparticles on the outer surface. The GM/HMS@ZIF has been successfully prepared and acts as a capsule. The GM/HMS@ZIF shows a good biocompatibility and a good cellular uptake in HEI-OC1 cells and is located in the cytoplasm. The GM is released slowly within 10 h under acidic conditions, which is used to simulate the pH of the endosome and lysosome compartments. The *in vivo* assay shows that the signal from FITC can be observed after 15 days from the mice that were injected with FITC/HMS@ZIF. This opens new opportunities to construct a delivery system for GM via one controlled low dose and sustained release for the therapy of Ménière's disease.

Conflicts of Interest

The authors declare that they have no conflicts of interest.

Acknowledgments

This work was supported by the National Natural Science Foundation of China (nos. 81230021, 81570923, and 21601118) and the Major State Basic Research Development Program of China (973 program; no. 2011CB504504).

Supplementary Materials

Figure S1: the HRTEM image of HMS (a) and TEM image of GM/HMS (b). Figure S2: N_2 adsorption/desorption isotherms of HMS and GM/HMS@ZIF. Figure S3: size distributions of GM/HMS@ZIF in 0.9% NaCl solution. Figure S4: release profiles of GM from GM/HMS@ZIF capsules at pH 7.4 for 15 days. Figure S5: the function of mitochondria in the MCF-7 cells treated for 24 h. *(Supplementary Materials)*

References

[1] S. S. da Costa, L. C. A. de Sousa, and M. R. de Toledo Piza, "Meniere's disease: overview, epidemiology, and natural history," *Otolaryngologic Clinics of North America*, vol. 35, no. 3, pp. 455–495, 2002.

[2] H. F. Schuknecht, "Ablation therapy for the relief of Meniere's disease," *The Laryngoscope*, vol. 66, no. 7, pp. 859–870, 1956.

[3] G. Sam, D. W. Chung, R. van der Hoeven, S. Verweij, and M. Becker, "The effect of intratympanic gentamicin for treatment of Ménière's disease on lower frequency hearing," *International Journal of Clinical Pharmacy*, vol. 38, no. 4, pp. 780–783, 2016.

[4] W. Ni, S. Zeng, W. Li et al., "Wnt activation followed by Notch inhibition promotes mitotic hair cell regeneration in the postnatal mouse cochlea," *Oncotarget*, vol. 7, no. 41, pp. 66754–66768, 2016.

[5] Z. He, L. Guo, Y. Shu et al., "Autophagy protects auditory hair cells against neomycin-induced damage," *Autophagy*, vol. 13, no. 11, pp. 1884–1904, 2017.

[6] E. I. Draz, A. A. Abdin, N. I. Sarhan, and T. A. Gabr, "Neurotrophic and antioxidant effects of silymarin comparable to 4-methylcatechol in protection against gentamicin-induced ototoxicity in guinea pigs," *Pharmacological Reports*, vol. 67, no. 2, pp. 317–325, 2015.

[7] C. Cheng, L. Guo, L. Lu et al., "Characterization of the transcriptomes of Lgr5+ hair cell progenitors and Lgr5- supporting cells in the mouse cochlea," *Frontiers in Molecular Neuroscience*, vol. 10, no. 122, 2017.

[8] X. Yu, W. Liu, Z. Fan et al., "c-Myb knockdown increases the neomycin-induced damage to hair-cell-like HEI-OC1 cells in vitro," *Scientific Reports*, vol. 7, article 41094, 2017.

[9] M. Guan, Q. Fang, Z. He et al., "Inhibition of ARC decreases the survival of HEI-OC-1 cells after neomycin damage *in vitro*," *Oncotarget*, vol. 7, no. 41, pp. 66647–66659, 2016.

[10] M. Waqas, S. Zhang, Z. He, M. Tang, and R. Chai, "Role of Wnt and Notch signaling in regulating hair cell regeneration in the cochlea," *Frontiers of Medicine*, vol. 10, no. 3, pp. 237–249, 2016.

[11] Z. He, S. Sun, M. Waqas et al., "Reduced TRMU expression increases the sensitivity of hair-cell-like HEI-OC-1 cells to neomycin damage in vitro," *Scientific Reports*, vol. 6, no. 1, p. 29621, 2016.

[12] L. Liu, Y. Chen, J. Qi et al., "Wnt activation protects against neomycin-induced hair cell damage in the mouse cochlea," *Cell Death & Disease*, vol. 7, no. 3, article e2136, 2016.

[13] S. Sun, M. Sun, Y. Zhang et al., "*In vivo* overexpression of X-linked inhibitor of apoptosis protein protects against neomycin-induced hair cell loss in the apical turn of the cochlea during the ototoxic-sensitive period," *Frontiers in Cellular Neuroscience*, vol. 8, p. 248, 2014.

[14] B. Liu, Y.-m. Leng, H. Shi et al., "Modified titration intratympanic gentamicin injection for unilateral intractable Ménière's disease," *Journal of Huazhong University of Science and Technology [Medical Sciences]*, vol. 35, no. 5, pp. 747–751, 2015.

[15] R. Guo, S. Zhang, M. Xiao et al., "Accelerating bioelectric functional development of neural stem cells by graphene coupling: implications for neural interfacing with conductive materials," *Biomaterials*, vol. 106, pp. 193–204, 2016.

[16] Z. He, S. Zhang, Q. Song et al., "The structural development of primary cultured hippocampal neurons on a graphene substrate," *Colloids and Surfaces B: Biointerfaces*, vol. 146, pp. 442–451, 2016.

[17] Y. Zha, R. Chai, Q. Song et al., "Characterization and toxicological effects of three-dimensional graphene foams in rats

in vivo," *Journal of Nanoparticle Research*, vol. 18, no. 5, p. 122, 2016.

[18] N. Ding, H. Li, X. Feng et al., "Partitioning MOF-5 into confined and hydrophobic compartments for carbon capture under humid conditions," *Journal of the American Chemical Society*, vol. 138, no. 32, pp. 10100–10103, 2016.

[19] E. D. Bloch, W. L. Queen, R. Krishna, J. M. Zadrozny, C. M. Brown, and J. R. Long, "Hydrocarbon separations in a metal-organic framework with open iron(II) coordination sites," *Science*, vol. 335, no. 6076, pp. 1606–1610, 2012.

[20] N. L. Rosi, J. Eckert, M. Eddaoudi et al., "Hydrogen storage in microporous metal-organic frameworks," *Science*, vol. 300, no. 5622, pp. 1127–1129, 2003.

[21] J.-R. Li, J. Sculley, and H.-C. Zhou, "Metal–organic frameworks for separations," *Chemical Reviews*, vol. 112, no. 2, pp. 869–932, 2011.

[22] J. Lee, O. K. Farha, J. Roberts, K. A. Scheidt, S. T. Nguyen, and J. T. Hupp, "Metal–organic framework materials as catalysts," *Chemical Society Reviews*, vol. 38, no. 5, pp. 1450–1459, 2009.

[23] W. Tingting, J. Yanyuan, C. Qiang et al., "A new luminescent metal-organic framework for selective sensing of nitroaromatic explosives," *Science China Chemistry*, vol. 59, no. 8, pp. 959–964, 2016.

[24] M. D. Allendorf, C. A. Bauer, R. K. Bhakta, and R. J. T. Houk, "Luminescent metal–organic frameworks," *Chemical Society Reviews*, vol. 38, no. 5, pp. 1330–1352, 2009.

[25] H. A. Patel, T. Islamoglu, Z. Liu et al., "Noninvasive substitution of K^+ sites in cyclodextrin metal–organic frameworks by Li^+ ions," *Journal of the American Chemical Society*, vol. 139, no. 32, pp. 11020–11023, 2017.

[26] Z. Li, A. W. Peters, V. Bernales et al., "Metal–organic framework supported cobalt catalysts for the oxidative dehydrogenation of propane at low temperature," *ACS Central Science*, vol. 3, no. 1, pp. 31–38, 2017.

[27] P. Li, J. A. Modica, A. J. Howarth et al., "Toward design rules for enzyme immobilization in hierarchical mesoporous metal-organic frameworks," *Chem*, vol. 1, no. 1, pp. 154–169, 2016.

[28] L. Shang, Y. Yu, W. Gao et al., "Bio-inspired anisotropic wettability surfaces from dynamic ferrofluid assembled templates," *Advanced Functional Materials*, vol. 28, no. 7, article 1705802, 2018.

[29] M.-X. Wu and Y.-W. Yang, "Metal–organic framework (MOF)-based drug/cargo delivery and cancer therapy," *Advanced Materials*, vol. 29, no. 23, article 1606134, 2017.

[30] P. Horcajada, R. Gref, T. Baati et al., "Metal–organic frameworks in biomedicine," *Chemical Reviews*, vol. 112, no. 2, pp. 1232–1268, 2011.

[31] K. Liang, R. Ricco, C. M. Doherty et al., "Biomimetic mineralization of metal-organic frameworks as protective coatings for biomacromolecules," *Nature Communications*, vol. 6, no. 1, p. 7240, 2015.

[32] J. Deng, K. Wang, M. Wang, P. Yu, and L. Mao, "Mitochondria targeted nanoscale zeolitic imidazole framework-90 for ATP imaging in live cells," *Journal of the American Chemical Society*, vol. 139, no. 16, pp. 5877–5882, 2017.

[33] J. Guan, Y. Hu, Y. Wang et al., "Controlled encapsulation of functional organic molecules within metal–organic frameworks: in situ crystalline structure transformation," *Advanced Materials*, vol. 29, no. 12, article 1606290, 2017.

[34] J. Della Rocca, D. Liu, and W. Lin, "Nanoscale metal–organic frameworks for biomedical imaging and drug delivery," *Accounts of Chemical Research*, vol. 44, no. 10, pp. 957–968, 2011.

[35] P. Horcajada, T. Chalati, C. Serre et al., "Porous metal–organic-framework nanoscale carriers as a potential platform for drug delivery and imaging," *Nature Materials*, vol. 9, no. 2, pp. 172–178, 2010.

[36] H. Ren, L. Zhang, J. An et al., "Polyacrylic acid@zeolitic imidazolate framework-8 nanoparticles with ultrahigh drug loading capability for pH-sensitive drug release," *Chemical Communications*, vol. 50, no. 8, pp. 1000–1002, 2014.

[37] J. Zhuang, C.-H. Kuo, L.-Y. Chou, D.-Y. Liu, E. Weerapana, and C.-K. Tsung, "Optimized metal–organic-framework nanospheres for drug delivery: evaluation of small-molecule encapsulation," *ACS Nano*, vol. 8, no. 3, pp. 2812–2819, 2014.

[38] X.-C. Huang, Y.-Y. Lin, J.-P. Zhang, and X.-M. Chen, "Ligand-directed strategy for zeolite-type metal–organic frameworks: zinc(II) imidazolates with unusual zeolitic topologies," *Angewandte Chemie International Edition*, vol. 45, no. 10, pp. 1557–1559, 2006.

[39] K. S. Park, Z. Ni, A. P. Cote et al., "Exceptional chemical and thermal stability of zeolitic imidazolate frameworks," *Proceedings of the National Academy of Sciences of the United States of America*, vol. 103, no. 27, pp. 10186–10191, 2006.

[40] C.-Y. Sun, C. Qin, X.-L. Wang et al., "Zeolitic imidazolate framework-8 as efficient pH-sensitive drug delivery vehicle," *Dalton Transactions*, vol. 41, no. 23, pp. 6906–6909, 2012.

[41] R. Röder, T. Preiß, P. Hirschle et al., "Multifunctional nanoparticles by coordinative self-assembly of His-tagged units with metal–organic frameworks," *Journal of the American Chemical Society*, vol. 139, no. 6, pp. 2359–2368, 2017.

[42] S. Wuttke, M. Lismont, A. Escudero, B. Rungtaweevoranit, and W. J. Parak, "Positioning metal-organic framework nanoparticles within the context of drug delivery – a comparison with mesoporous silica nanoparticles and dendrimers," *Biomaterials*, vol. 123, pp. 172–183, 2017.

[43] D. J. Levine, T. Runčevski, M. T. Kapelewski et al., "Olsalazine-based metal–organic frameworks as biocompatible platforms for H_2 adsorption and drug delivery," *Journal of the American Chemical Society*, vol. 138, no. 32, pp. 10143–10150, 2016.

[44] X. Zheng, L. Wang, Q. Pei, S. He, S. Liu, and Z. Xie, "Metal–organic framework@porous organic polymer nanocomposite for photodynamic therapy," *Chemistry of Materials*, vol. 29, no. 5, pp. 2374–2381, 2017.

[45] H. Zheng, Y. Zhang, L. Liu et al., "One-pot synthesis of metal–organic frameworks with encapsulated target molecules and their applications for controlled drug delivery," *Journal of the American Chemical Society*, vol. 138, no. 3, pp. 962–968, 2016.

[46] Z. Teng, X. Su, Y. Zheng et al., "A facile multi-interface transformation approach to monodisperse multiple-shelled periodic mesoporous organosilica hollow spheres," *Journal of the American Chemical Society*, vol. 137, no. 24, pp. 7935–7944, 2015.

[47] Y. Chen, H. Chen, L. Guo et al., "Hollow/rattle-type mesoporous nanostructures by a structural difference-based selective etching strategy," *ACS Nano*, vol. 4, no. 1, pp. 529–539, 2010.

[48] M. Wu, Q. Meng, Y. Chen et al., "Large pore-sized hollow mesoporous organosilica for redox-responsive gene delivery

and synergistic cancer chemotherapy," *Advanced Materials*, vol. 28, no. 10, pp. 1963–1969, 2016.

[49] N. Lu, P. Huang, W. Fan et al., "Tri-stimuli-responsive biodegradable theranostics for mild hyperthermia enhanced chemotherapy," *Biomaterials*, vol. 126, pp. 39–48, 2017.

[50] J. Zhang, L. Weng, X. Su et al., "Cisplatin and doxorubicin high-loaded nanodrug based on biocompatible thioether- and ethane-bridged hollow mesoporous organosilica nanoparticles," *Journal of Colloid and Interface Science*, vol. 513, pp. 214–221, 2018.

[51] Z. Teng, X. Su, Y. Zheng et al., "Mesoporous silica hollow spheres with ordered radial mesochannels by a spontaneous self-transformation approach," *Chemistry of Materials*, vol. 25, no. 1, pp. 98–105, 2013.

[52] H. Zheng, L. Xing, Y. Cao, and S. Che, "Coordination bonding based pH-responsive drug delivery systems," *Coordination Chemistry Reviews*, vol. 257, no. 11-12, pp. 1933–1944, 2013.

[53] L. Xing, H. Zheng, Y. Cao, and S. Che, "Coordination polymer coated mesoporous silica nanoparticles for pH-responsive drug release," *Advanced Materials*, vol. 24, no. 48, pp. 6433–6437, 2012.

Hindawi
Neural Plasticity
Volume 2018, Article ID 2062346, 10 pages
https://doi.org/10.1155/2018/2062346

Research Article

Identification of Binding Partners of Deafness-Related Protein PDZD7

Haibo Du,[1,2] Rui Ren,[1,2] Panpan Chen,[1,2] Zhigang Xu,[1,2,3] and Yanfei Wang[1,2]

[1]*Shenzhen Research Institute of Shandong University, Shenzhen, Guangdong 518057, China*
[2]*Shandong Provincial Key Laboratory of Animal Cells and Developmental Biology, School of Life Sciences, Shandong University, Jinan, Shandong 250100, China*
[3]*Co-Innovation Center of Cell Biology, Shandong Normal University, Jinan, Shandong 250014, China*

Correspondence should be addressed to Zhigang Xu; xuzg@sdu.edu.cn and Yanfei Wang; wang_yf@sdu.edu.cn

Received 2 December 2017; Revised 24 January 2018; Accepted 14 February 2018; Published 28 March 2018

Academic Editor: Renjie Chai

PDZD7 is an important deafness gene, whose mutations are associated with syndromic and nonsyndromic hearing loss. PDZD7 contains multiple PDZ domains that are essential for organizing various proteins into protein complex. Several PDZD7-binding proteins have been identified, including usherin, ADGRV1, whirlin, harmonin, SANS, and MYO7A, all belonging to USH proteins. Here, we report the identification of novel PDZD7-binding partners through yeast two-hybrid screening using the first two PDZ domains of PDZD7 as bait. Eleven proteins were identified, most of which have not been reported as PDZD7-binding partners before. Among the identified proteins, ADGRV1, gelsolin, and β-catenin have been shown to play important roles in hearing, whereas the functions of other proteins in the inner ear remain elusive. We confirmed the expression of one candidate PDZD7-binding protein, CADM1, in the mouse inner ear and evaluated the auditory function of *Cadm1* knockout mice by performing auditory brainstem response (ABR) measurement. Unexpectedly, *Cadm1* knockout mice show normal hearing threshold, which might be explained by the possible compensation by its homologs that are also expressed in the inner ear. Taken together, our work identified several novel PDZD7-binding proteins, which will help us to further understand the role of PDZD7 in hearing transduction.

1. Introduction

Usher syndrome (USH) is the most frequent form of inherited sensory deaf-blindness that is characterized by hearing loss and vision defect [1, 2]. According to the severity of hearing loss as well as the presence or absence of balancing problems, USH is clinically classified into three subtypes, namely, USH1, USH2, and USH3, with USH1 as the most severe one. At present, ten genes have been associated with USH, including *MYO7A*, *USH1C*, *CDH23*, *PCDH15*, *USH1G*, *CIB2*, *USH2A*, *ADGRV1*, *WHRN*, and *CLRN-1* [3–15]. Mutations of *USH* genes are also responsible for nonsyndromic hearing loss. USH proteins have been shown to interact with one another and form multiprotein complexes and play important roles in the development, maintenance, and function of stereocilia and synapses in the inner ear sensory hair cells [16].

Recently, *PDZD7* was suggested to be a USH modifier and a contributor to digenic USH [17]. Meanwhile, mutations in human *PDZD7* gene are also associated with nonsyndromic hearing loss DFNB57 [18–20]. Similar to harmonin (USH1C) and whirlin (USH2D), full-length PDZD7 contains three PDZ domains, a harmonin-N like (HNL) domain, and a proline-rich (PR) region. Shorter PDZD7 isoforms containing the first two PDZ domains were also detected in the inner ear [17, 18, 21]. In mice, loss of PDZD7 was shown to result in stereocilia disorganization as well as mechanotransduction deficits [21].

As a PDZ domain-containing scaffold protein, PDZD7 plays important roles in organizing protein complex. PDZD7 has been shown to bind the three known USH2 proteins usherin (USH2A), ADGRV1 (USH2C), and whirlin (USH2D), forming the so-called ankle-link complex at the ankle region of hair cell stereocilia [17, 21–23]. In *Pdzd7*

knockout mice, the localization of the three USH2 proteins at the ankle links was interrupted, suggesting that PDZD7 plays a pivotal role in organizing the ankle-link complex [21]. Moreover, PDZD7 was also shown to interact with USH1 proteins MYO7A (USH1B), harmonin (USH1C), and SANS (USH1G) [18, 24, 25].

At present, little is known about other non-USH PDZD7-binding partners. In the present work, yeast two-hybrid screening was performed using the first two PDZ domains as bait to identify new PDZD7-binding partners that are expressed in the inner ear. Identification of PDZD7-binding proteins will help us to further understand the role of PDZD7 in hearing transduction.

2. Materials and Methods

2.1. DNA Constructs. Mouse cDNA encoding PDZD7 short isoform (amino acids 1–557) was inserted into pBD-GAL4 Cam vector (Stratagene) to express the bait protein for yeast two-hybrid screen. The same cDNA was inserted into pmCherry-N1 or pMYC-C2 (modified pEGFP-C2 with EGFP-coding sequence replaced by Myc-coding sequence) to express PDZD7-mCherry or Myc-PDZD7 fusion protein. Full-length cDNAs encoding mouse β-catenin and CADM1, as well as cDNA encoding chicken AMOT (amino acids 311–910), were inserted into pEGFP-C2 to express EGFP-fusion proteins.

2.2. Yeast Two-Hybrid Screen. The yeast two-hybrid screen was performed as previously described [26–28]. Briefly, yeast strain AH109 (Clontech) was sequentially transformed with the bait plasmid and a chicken cochlear cDNA library in the HybriZAP two-hybrid vector [29]. A total of 2.4×10^6 transformants were screened using *HIS3* as the primary reporter gene with the presence of 2.5 mM of 3-amino-1,2,4-triazole (3-AT). The positive colonies were further examined using two other reporter genes *ADE2* and *lacZ*. The prey vectors in triple-positive yeast colonies were recovered, and the sequence of cDNA inserts was determined by sequencing.

2.3. Colocalization Assay. COS-7 cells were grown on gelatin-coated glass cover slips and transfected with vectors that express target proteins fused to EGFP or mCherry. Twenty-four hours after transfection, cells were fixed with 4% paraformaldehyde (PFA) in PBS for 15 minutes, then permeabilized and blocked with PBT1 (0.1% Triton X-100, 1% BSA, 5% heat-inactivated donkey serum in PBS, pH 7.3) for 30 minutes. For nuclei staining, cells were incubated with DAPI (Gen-View Scientific Inc.) for 15 minutes, then mounted in glycerol/PBS (1 : 1). The subcellular localization of target proteins was examined with a confocal microscope (LSM 700, Zeiss).

2.4. Coimmunoprecipitation (co-IP) and Western Blot. HEK293T cells were transfected with vectors that express target proteins fused to EGFP or Myc epitope. Twenty-four hours after transfection, cells were washed with PBS and lysed in ice-cold lysis buffer consisting of 150 mM NaCl, 50 mM Tris at pH 7.5, 1% (vol/vol) Triton X-100, 1 mM PMSF, and 1x protease inhibitor cocktail (Roche). After centrifugation at 4°C, the supernatant was incubated with immobilized anti-Myc antibody (Sigma-Aldrich, Cat. number E6654) at 4°C for 2 hours. Immunoprecipitated proteins were separated by polyacrylamide gel electrophoresis (PAGE), then transferred to PVDF membrane. After blocking in PBS containing 5% BSA and 0.1% Tween-20, the membrane was incubated with anti-Myc (Abmart, Cat. number M20002) or anti-GFP (Abmart, Cat. number M20004) antibody at 4°C overnight, followed by incubation with HRP-conjugated secondary antibody (Bio-Rad, Cat. number 170-6516) at room temperature for an hour. The signals were detected with the ECL system (Cell Signaling Technology, Danvers, MA).

2.5. Reverse Transcription-Polymerase Chain Reaction (RT-PCR). Total RNA of different tissues was extracted using RNeasy Micro Kits (Qiagen) according to the manufacturer's protocol. Reverse transcription (RT) was carried out at 42°C for 1 hour in a 20 μl reaction mixture containing 1 μg of total RNA, 10 pmol of oligo-dT, and 200 units of SuperScript III reverse transcriptase (Invitrogen). Polymerase chain reaction (PCR) was performed using the cDNA as template with the following primers: *Cadm1*: forward primer CGA CAT GGC GAG TGC TGT, reverse primer CCG AAT GAG CCT TTC CCA CT (986 bp); *Cadm2*: forward primer GGC TGC TTC AAA AAG TAA AGT CA, reverse primer GCT GCT AAC GGT GAA GGT CT (523 bp); *Cadm3*: forward primer GCC AAG TCC CTT GTC ACT GT, reverse primer CGC CTT CTG CGT TGA TGA TG (799 bp); *Cadm4*: forward primer TGA AGG ACG AGC GAT TCC AG, reverse primer GTC AGC ACC AGA GTG TCT CC (517 bp); *Necl5*: forward primer TCA CCC TCC TGG ACG AAT CT, reverse primer TGA CAA CGT GGA ATT CGG CA (871 bp); and *β-actin*: forward primer CTC CAT CCT GGC CTC GCT GT, reverse primer GCT GTC ACC TTC ACC GTT CC (268 bp). To obtain the optimal sensitivity and specificity, cycle lengths for different PCR reaction sets were adjusted between 23 and 38 cycles, and annealing temperatures were adjusted between 56 and 64°C. The PCR products were separated by electrophoresis on agarose gel.

2.6. Quantitative Real-Time PCR (Q-PCR). Q-PCR was carried out using SYBR® Premix Ex Taq™ system (Perfect Real Time, Takara) according to the manufacturer's protocol. Amplification and detection were run in a Sequence Detection System SLA-3296 (Bio-Rad) in triplicate with an initial cycle of 95°C for 10 seconds followed by 40 cycles of 95°C for 5 seconds, 60°C for 30 seconds, and 72°C for 20 seconds. Negative control samples (without template) were processed in the same way. The specificity of the amplifications was verified by melting curve analysis. The sequences of primers are as follows: *Cadm1*: forward primer GTG ATC CAG CTC CTG AAC CC, reverse primer CGT GTA GAG CTG GCA GAA GT and *β-actin*: forward primer CTC CAT CCT GGC CTC GCT GT, reverse primer GCT GTC ACC TTC ACC GTT CC. Relative quantization of *Cadm1* expression normalized to *β-actin* was calculated according to the $2^{-\Delta\Delta}$CT method.

2.7. X-Gal Staining of Mouse Inner Ear. Mouse inner ear temporal bones were dissected and fixed with 4% PFA containing 2 mM $MgCl_2$, 5 mM EGTA, and 0.02% NP-40 at 4°C overnight. After rinsing three times with washing buffer (0.1 M PBS, 2 mM $MgCl_2$, 0.01% NP-40, and 0.01% sodium deoxycholate), the samples were incubated with staining buffer (0.1 M PBS, 5 mM $K_3[Fe(CN)_6]$, 5 mM $K_4[Fe(CN)_6]$, 2 mM $MgCl_2$, 1 mg/ml X-gal, and 0.01% NP-40) at 37°C overnight. The samples were washed three times with PBS, then the basilar membranes together with the modiolus were dissected out and imaged with a light microscope (Nikon YS100, Japan).

2.8. Animal Maintenance and Auditory Brainstem Response (ABR) Measurement. Cadm1 knockout mice (number RBRC04063) were obtained from RIKEN BioResource Center. Generation and characterization of *Cadm1* knockout mice have been described elsewhere [30, 31]. All animal experiments were approved by the Ethics Committee of Shandong University School of Life Sciences and conducted accordingly. For ABR measurement, mice were anesthetized with 5% chloral hydrate (0.5 ml/100 g body weight). Electrodes were inserted subcutaneously at the vertex, pinna, and near the tail. A RZ6 workstation and BioSig software (Tucker Davis Technologies Inc.) were used for the stimulus generation, presentation, ABR acquisition, and data management. Specific acoustic stimuli were generated using high-frequency transducers, and ABR thresholds were obtained by reducing the stimulus intensity in 10 dB SPL steps to identify the lowest intensity at which all ABR waves were detectable. For noise exposure, mice were exposed to 2–8 kHz noise at 96 dB SPL (Crown, CD i1000) for 2 hours, and ABR thresholds were measured preexposure and at various post-exposure time points. For each genotype, at least three animals were used, and data were shown as means ± standard errors. Student's *t*-test was used for statistical analysis, and $p < 0.05$ was considered statistically significant.

3. Results

3.1. Identification of Potential PDZD7-Binding Partners through Yeast Two-Hybrid Screening. In order to identify new PDZD7-binding partners, we performed yeast two-hybrid screening of a chicken cochlear cDNA library using PDZD7 short isoform as bait. This isoform contains the first two PDZ domains of PDZD7. Around thirty positive clones were obtained that activate all the three reporter genes, representing eleven candidate PDZD7-binding proteins (Table 1). Among the proteins identified, ADGRV1 (USH2C) is a known PDZD7-binding partner, whereas the interactions between PDZD7 and the other proteins have not been reported. The most frequently encountered two proteins are β-catenin and ADGRV1, both of which contain a type I PDZ-binding interface (PBI) at their C-termini. Six candidate PDZD7-binding proteins (gelsolin, TRIM35, CADM1, AMOT, Golgin45, and Numb) contain a type II PBI at their C-termini. Three candidates (KCTD10, CCDC27, and TRIP11) do not have a predictable C-terminal PBI.

Table 1: Potential PDZD7-binding partners identified from yeast two-hybrid screening. Fragment containing the first two PDZ domains of PDZD7 was used as bait to screen a chicken cochlear cDNA library.

GenBank accession number	Protein	Prey redundancy	PBI
NM_205081	β-Catenin	13	-DTDL
XM_015280551	ADGRV1 (VLGR1)	4	-DTHL
NM_204934	Gelsolin	2	-DVDV
XM_004935864	TRIM35	1	-DVPV
XM_015298217	CADM1	1	-EYFI
XM_004940799	Angiomotin (AMOT)	1	-EYLI
XM_416590	Golgin45 (BLZF1)	1	-LIAL
XM_015286934	Numb	1	-EIEL
XM_004945619	KCTD10	2	
XM_015297094	CCDC27	2	
XM_421324	TRIP11 (GMAP210)	1	

Three candidate proteins β-catenin, AMOT, and CADM1 were picked to test the specificity of the interactions by introducing the bait plasmid and prey plasmids back to the reporter yeast strain AH109. Gal4 BD-PDZD7, Gal4 AD-β-catenin, Gal4 AD-AMOT, or Gal4 AD-CADM1 alone did not activate the reporter gene *HIS3*. However, when Gal4 BD-PDZD7 was present, Gal4 AD-β-catenin, Gal4 AD-AMOT, or Gal4 AD-CADM1 activated *HIS3* expression, suggesting that these proteins specifically interact with PDZD7 (Figures 1(a)–1(c)).

3.2. PDZD7 Colocalizes with β-Catenin, AMOT, and CADM1 When Overexpressed in COS-7 Cells. Next, we examined the subcellular localization of PDZD7 in the presence of these candidate binding partners in cultured cells. When overexpressed in COS-7 cells, PDZD7-mCherry localized in the cytoplasm as well as on the plasma membrane (Figure 2(a)), whereas EGFP-β-catenin mainly localized in the nuclei in a punctate pattern (Figure 2(b)). Noticeably, when expressed together with EGFP-β-catenin, PDZD7-mCherry translocated into the nuclei and colocalized with EGFP-β-catenin (Figure 2(c)), in consistent with the potential interaction between these two proteins.

Colocalization was also observed between PDZD7 with AMOT and CADM1. EGFP-AMOT localized as perinuclear aggregates in transfected COS-7 cells (Figure 3(a)). When coexpressed, PDZD7-mCherry colocalized with EGFP-AMOT (Figure 3(b)). Similarly, PDZD7-mCherry colocalized with EGFP-CADM1 in the cytoplasm (Figures 4(a) and 4(b)). Taken together, the colocalization results are consistent with the yeast two-hybrid results, confirming that β-catenin, AMOT, and CADM1 are PDZD7-binding partners.

3.3. Cadm1 Expression in the Mouse Inner Ear. Among the identified candidate PDZD7-binding partners, CADM1 attracted our most attention. The interaction between CADM1 and PDZD7 was further confirmed by co-IP of

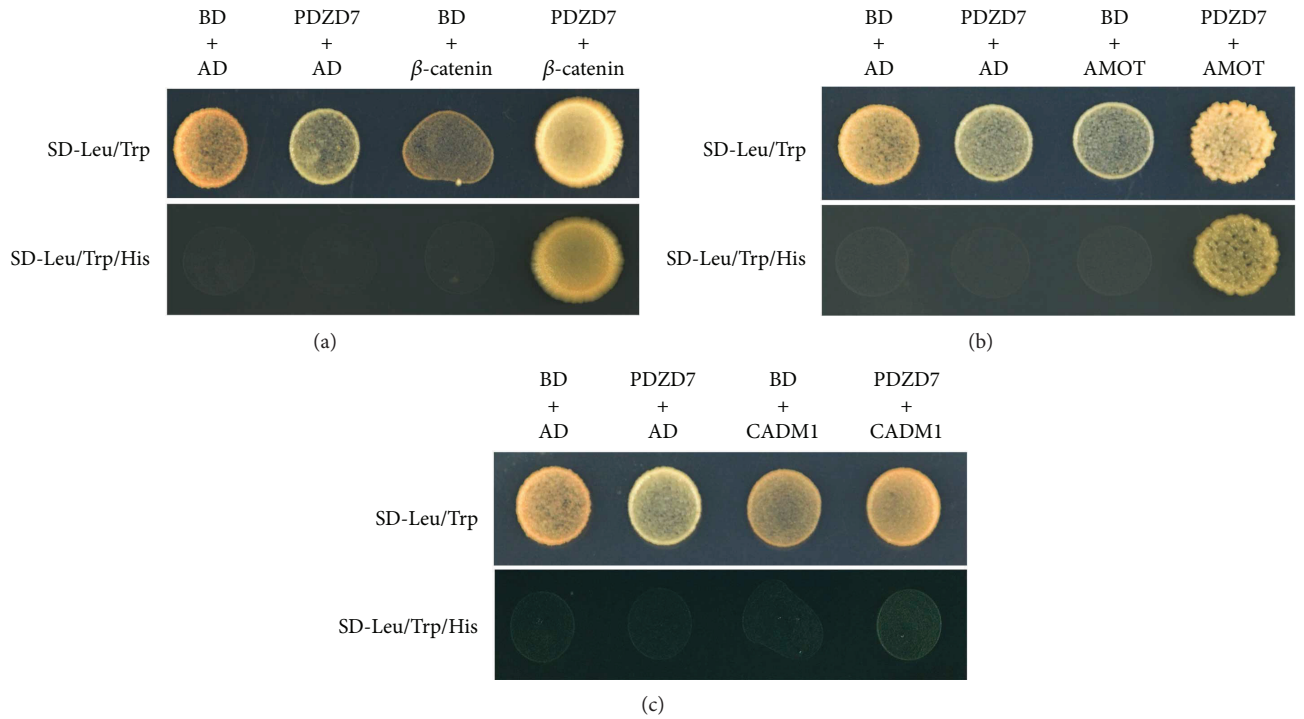

Figure 1: Verification of protein interactions by performing yeast two-hybrid experiments. AH109 yeast cells containing either Gal4 BD/Gal4 AD, Gal4 BD-PDZD7/Gal4 AD, Gal4 BD/Gal4 AD-β-catenin, Gal4 BD/Gal4 AD-AMOT, Gal4 BD/Gal4 AD-CADM1, Gal4 BD-PDZD7/Gal4 AD-β-catenin, Gal4 BD-PDZD7/Gal4 AD-AMOT, or Gal4 BD-PDZD7/Gal4 AD-CADM1 were plated on nonselective (–Leu/Trp) and selective (–Leu/Trp/His) plates with the presence of 2.5 mM 3-AT and incubated at 30°C for 3 days.

epitope-tagged proteins (Figures 4(c)). RT-PCR results showed that *Cadm1* is highly expressed in the spiral ganglion and weakly expressed in the basilar membrane (Figure 5(a)). The expression of *Cadm1* in the developing inner ear was examined by performing quantitative real-time PCR (Q-PCR), which showed that *Cadm1* was detected in all developmental stages examined, peaking at around postnatal day 9 (P9) (Figure 6(a)).

The expression pattern of *Cadm1* in the cochlea was further examined using a mouse model whose exon 1 of *Cadm1* gene was replaced by *lacZ* reporter gene cassette [30, 31]. X-gal staining of P7 $Cadm^{+/-}$ inner ear suggested that *Cadm1* is abundantly expressed in the spiral ganglion. At this stage, the expression of *Cadm1* in the basilar membrane was relatively weak and mainly enriched in supporting cells (Figures 6(b)–6(e)).

3.4. Cadm1 Knockout Mice Have Normal Hearing Threshold. We then evaluated the effect of *Cadm1* disruption on mouse auditory function by performing ABR measurement. The result showed that hearing thresholds of 1-month-old to 4-month-old $Cadm1^{-/-}$ mice were comparable to those of wild-type or $Cadm1^{+/-}$ mice, suggesting that CADM1 is not indispensable for hearing transduction (Figure 7(a)). To investigate whether $Cadm1^{-/-}$ mice show increased acoustic vulnerability, we exposed P45 mice to 2–8 kHz noise at 96 dB SPL for 2 hours. ABR thresholds were measured before and after the noise exposure, which did not reveal any significant difference between $Cadm1^{-/-}$ and $Cadm1^{+/-}$ or wild-type mice (Figure 7(b)). Taken together, our results suggested that the auditory function of $Cadm1^{-/-}$ mice is normal.

The normal hearing threshold of *Cadm1* knockout mice promoted us to look for possible explanations. It has been suggested that the loss of specular protein might be compensated for by its homologous protein(s). As an immunoglobulin- (Ig-) like cell adhesion molecule (CAM), CADM1 belongs to nectin-like molecule (Necl) family, which contains five members (CADM1, CADM2, CADM3, CADM4, and Necl5) [32, 33]. We examined the expression of Necl family members in mouse inner ear by performing RT-PCR. The results showed that all members are expressed in the mouse inner ear (Figure 5(a)), whereas none of them is upregulated in *Cadm1* knockout mice (Figure 5(b)).

4. Discussion

PDZD7 is an important deafness gene, whose mutations contribute to syndromic as well as nonsyndromic hearing loss [17–20]. PDZD7 is a scaffold protein containing three PDZ domains, a HNL domain, and a PR region. Scaffold proteins are important for organizing multiple proteins into protein complex. At present, only a few PDZD7-binding proteins have been reported, including usherin, ADGRV1, whirlin, harmonin, SANS, and MYO7A [17, 18, 21–25]. In this work, we used yeast two-hybrid screening to identify new PDZD7-binding proteins, which will help us to learn more about the role of PDZD7 in hearing transduction.

Among the potential PDZD7-binding partners identified in this work, β-catenin is the most frequently encountered

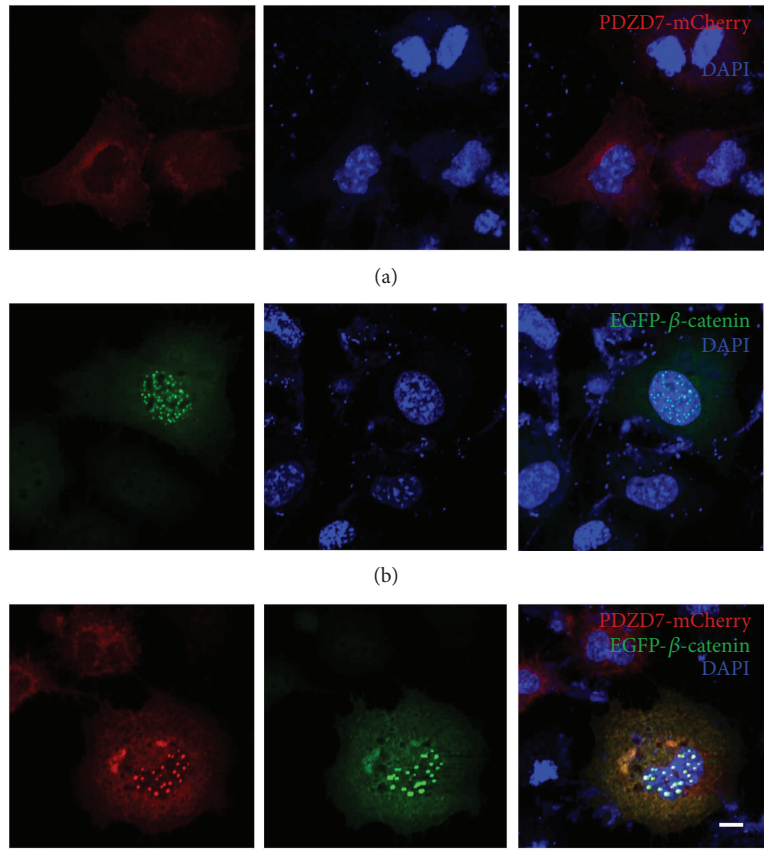

Figure 2: Colocalization of PDZD7 with β-catenin in COS-7 cells. Expression vectors were transfected into COS-7 cells, and the subcellular localization of target proteins was determined using confocal microscopy. (a) PDZD7-mCherry localized in the cytoplasm as well as on the plasma membrane. (b) EGFP-β-catenin mainly localized in the nuclei in a punctate pattern. (c) When expressed together, PDZD7-mCherry colocalized with EGFP-β-catenin in the nuclei. Scale bar: 10 μm.

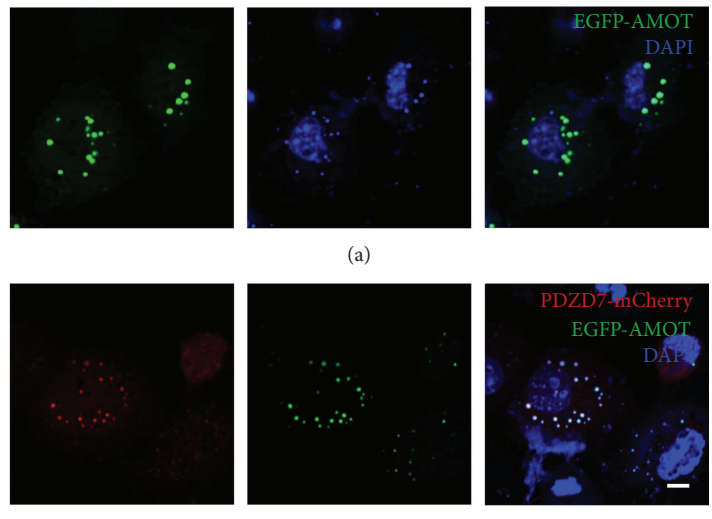

Figure 3: Colocalization of PDZD7 with AMOT in COS-7 cells. Expression vectors were transfected into COS-7 cells, and the subcellular localization of target proteins was determined using confocal microscopy. (a) EGFP-AMOT localized as perinuclear aggregates when expressed alone in COS-7 cells. (b) When expressed together, PDZD7-mCherry colocalized with EGFP-AMOT. Scale bar: 10 μm.

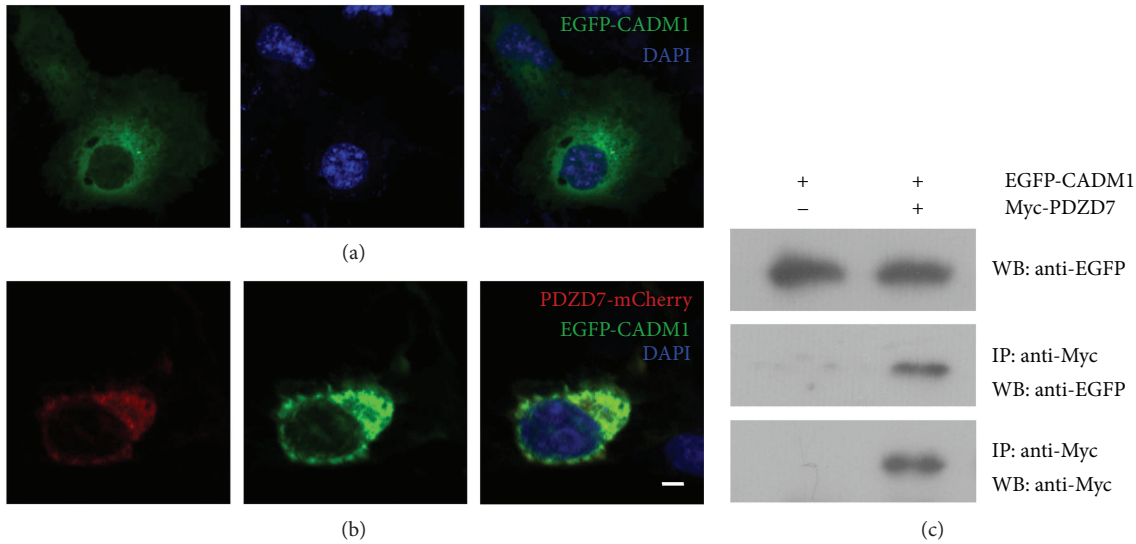

Figure 4: Interaction of PDZD7 with CADM1 in transfected cells. Expression vectors were transfected into COS-7 cells, and the subcellular localization of target proteins was determined using confocal microscopy. (a) EGFP-CADM1 localized in the cytoplasm of COS-7 cells. (b) When expressed together, PDZD7-mCherry colocalized with EGFP-CADM1. Scale bar: 10 μm. (c) Western blots showed that CADM1 was coimmunoprecipitated with PDZD7. Expression vectors were transfected into HEK293T cells to express epitope-tagged PDZD7 and CADM1 proteins, and cell lysates were subjected to immunoprecipitation. IP indicates antibody used for immunoprecipitation, and WB indicates antibody used for detection.

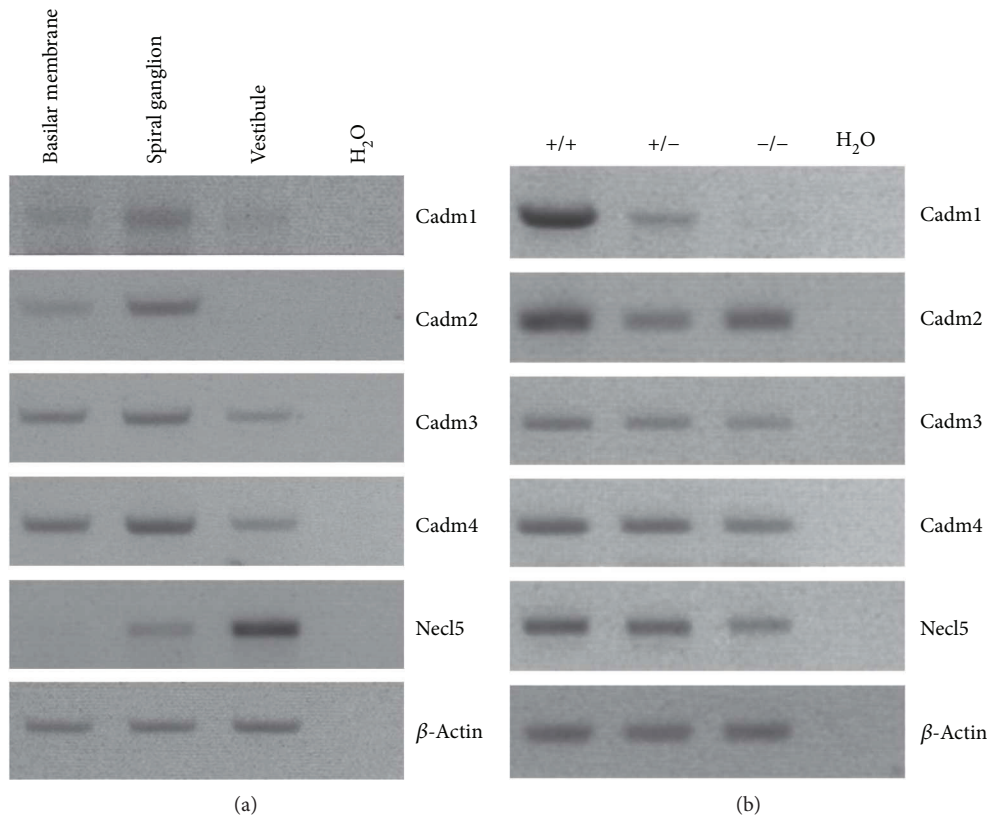

Figure 5: Expression of Necl family members in mouse inner ear. Total RNA from postnatal day 2 (P2) mice was extracted and reverse-transcribed into cDNA, which was then used as PCR template to examine the expression of Necl family members. (a) Expression of Necl family members in basilar membrane, spiral ganglion, and vestibule of wild-type mice was examined through RT-PCR. (b) Expression of Necl family members in the inner ear of *Cadm1* knockout mice was examined through RT-PCR. *β-Actin* was included as internal control.

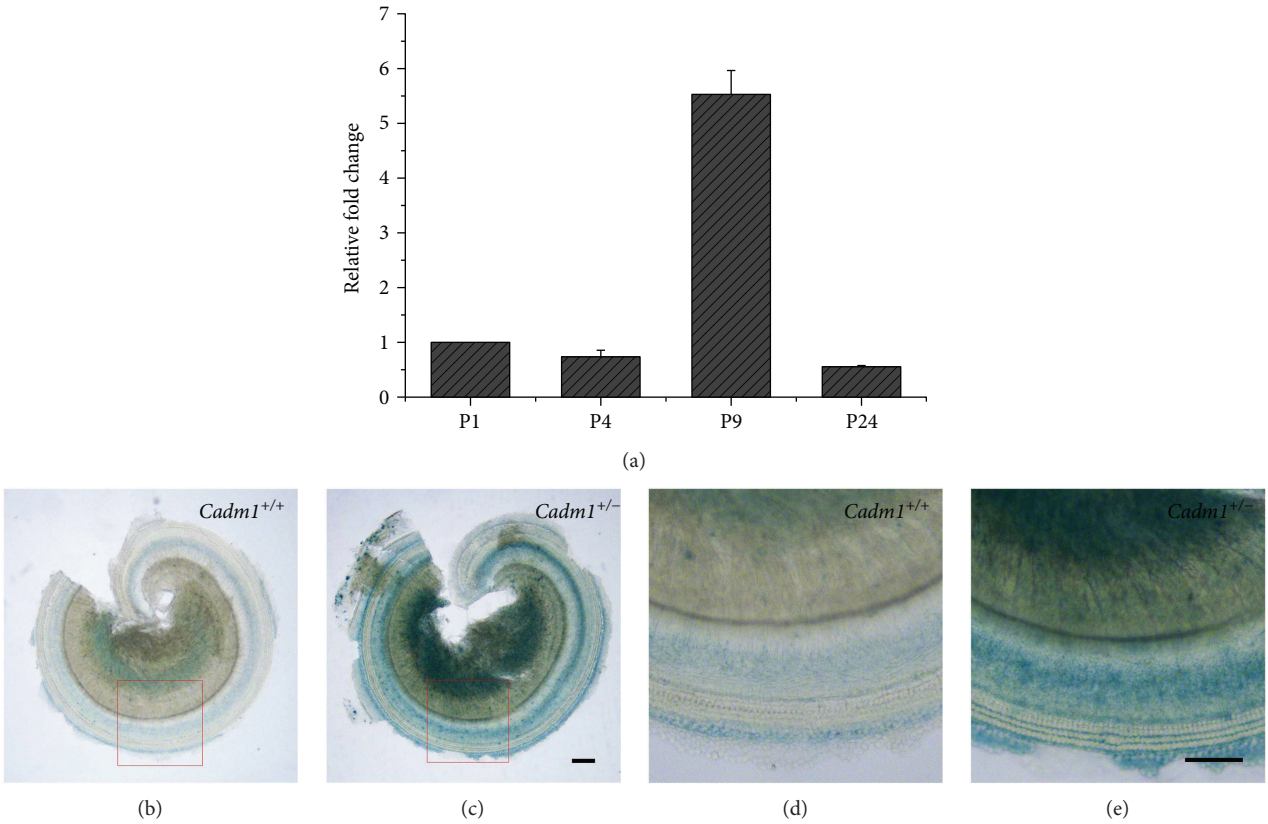

Figure 6: Expression pattern of *Cadm1* in mouse inner ear. (a) Expression of *Cadm1* in different developmental stages of mouse inner ear examined by Q-PCR. The bar graphs show quantification of the PCR results with each value representing the mean ± standard error. (b) LacZ activity in the basilar membrane and spiral ganglion of P7 $Cadm1^{+/+}$ mice. (c) LacZ activity in the basilar membrane and spiral ganglion of P7 $Cadm1^{+/-}$ mice. (d) Higher-magnification image from the insect of (b). (e) Higher-magnification image from the insect of (c). Scale bars, 100 μm.

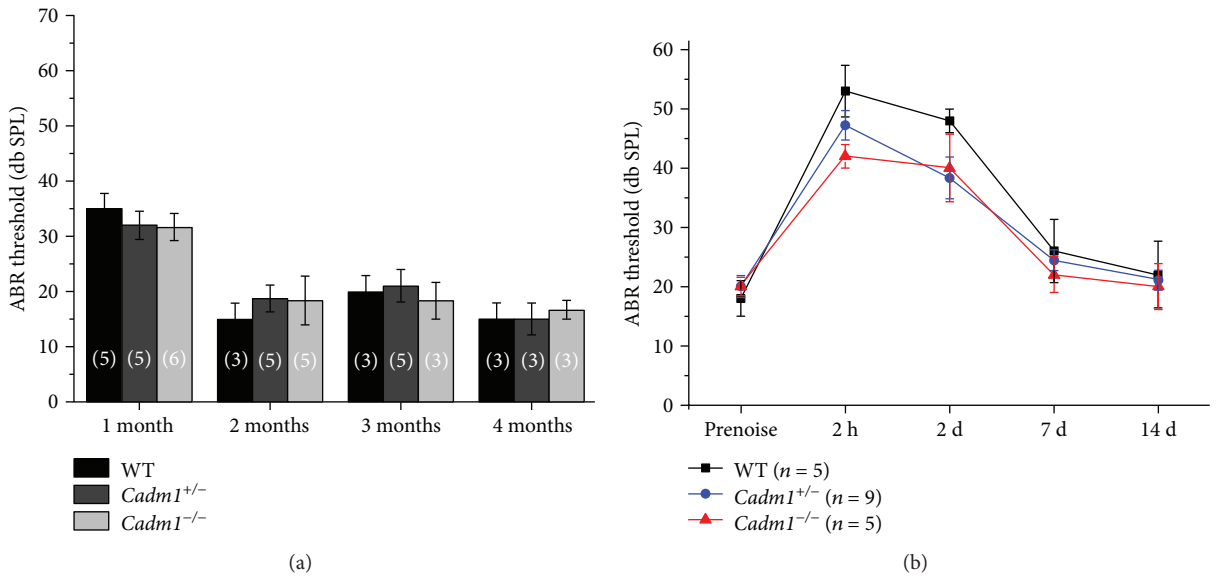

Figure 7: Auditory brainstem response (ABR) measurements show normal auditory function of *Cadm1* knockout mice. (a) ABR thresholds of wild-type, $Cadm1^{+/-}$, and $Cadm1^{-/-}$ mice to click stimuli were measured at different ages as indicated. (b) Wild-type, $Cadm1^{+/-}$, and $Cadm1^{-/-}$ mice at P45 were subjected to 2–8 kHz noise at 96 dB DSL for 2 hours, and ABR thresholds were measured preexposure and at different postexposure time points as indicated. Variance bars indicate standard error. No significant differences were observed between genotypes. The numbers of animals for each group used in the experiments are indicated.

one. Wnt/β-catenin signaling pathway plays pivotal roles in development, tissue homeostasis, and so on [34]. It has been suggested that Wnt/β-catenin signaling regulates proliferation of sensory precursors in the postnatal mouse cochlea [35, 36]. β-Catenin could upregulate the expression of Atoh1, a transcription factor that is critical for hair-cell differentiation [37]. Consistently, loss of β-catenin inhibited hair-cell differentiation from sensory progenitors [38], whereas forced stabilization of β-catenin in supporting cells resulted in proliferation of supporting cells and generation of hair cells [39]. Our data show that PDZD7 interacted with β-catenin and that PDZD7 translocated into the nuclei together with β-catenin in transfected cells, suggesting a potential role of PDZD7 in regulating β-catenin pathway. Further investigation is needed to fully understand the significance and the mechanism of this interaction.

Gelsolin is a calcium-activated actin-binding protein and plays important roles in F-actin severing, capping, and nucleation [40, 41]. It has been shown that gelsolin binds p55 and localizes to the tips of shorter stereocilia of outer hair cells (OHCs) [42]. In mice lacking gelsolin, stereocilia in the apex of the cochlea became long and straggly, suggesting that gelsolin is involved in the regulation of stereocilia elongation [42, 43]. Our data suggested that PDZD7 might interact with gelsolin, hence might play a role in stereocilia development and/or maintenance. Consistent with this hypothesis, OHC stereocilia disorganization has been observed in *Pdzd7* knockout mice [21].

Numb is an evolutionary conserved protein with multiple functions such as asymmetric cell division control, cell fate determination, endocytosis, cell adhesion, cell migration, ubiquitination of specific substrates, and a number of signaling pathways [44]. It has been reported that Numb was expressed in rat cochlear sensory epithelium, and overexpression of Numb upregulated the expression of *Atoh1* in cochlear whole mount cultures [45]. The potential interaction of PDZD7 with Numb raises the possibility that PDZD7 might regulate the function of Numb, which awaits further investigation.

Unlike ADGRV1, β-catenin, gelsolin, and Numb, the other PDZD7-binding proteins identified in the present work have not been reported to function in the inner ear. Genes encoding some of the proteins including CADM1, AMOT, Golgin45, and KCTD10 have been detected in mouse cochlea by RNA transcriptome sequencing (SHIELD, https://shield.hms.harvard.edu) [46]. Among these proteins, CADM1 attracted most our attention. CADM1 is an immunoglobulin (Ig) superfamily protein that contains extracellular Ig-like domains, a single transmembrane domain, and a small intracellular C-terminal tail. CADM1 can bind either transhomophilically or transheterophilically with other nectins or Necls [47, 48]. CADM1 plays important roles in modulating synapse development and plasticity, and mutations in *CADM1*/*Cadm1* gene have been associated with autism spectrum disorder [49–51]. We show here that CADM1 interacts with PDZD7 and *Cadm1* is abundantly expressed in mouse inner ear. However, our data did not reveal any auditory deficit in *Cadm1* knockout mice, suggesting that CADM1 is dispensable for hearing function in mice. Alternatively, other Necl family members might compensate for the loss of CADM1 in the inner ear. Similar scenario has been observed in the neuromuscular junction (NMJ) of *Cadm1* knockout mice, where the loss of CADM1 was compensated for by CADM4 [52].

In conclusion, our present work identified several novel inner ear-expressed PDZD7-binding partners, which will help us to learn more about the role of PDZD7 in hearing. Further investigation is needed to fully understand the biological significance of these interactions.

Conflicts of Interest

The authors declare that there is no conflict of interests regarding the publication of this paper.

Acknowledgments

This work is supported by grants from the Innovation Commission of Shenzhen Municipality (JCYJ2016033 1174108379) and the National Natural Science Foundation of China (81771001).

References

[1] J. A. Boughman, M. Vernon, and K. A. Shaver, "Usher syndrome: definition and estimate of prevalence from two high-risk populations," *Journal of Chronic Diseases*, vol. 36, no. 8, pp. 595–603, 1983.

[2] B. J. B. Keats and D. P. Corey, "The usher syndromes," *American Journal of Medical Genetics*, vol. 89, no. 3, pp. 158–166, 1999.

[3] D. Well, S. Blanchard, J. Kaplan et al., "Defective myosin VIIA gene responsible for Usher syndrome type IB," *Nature*, vol. 374, no. 6517, pp. 60-61, 1995.

[4] J. D. Eudy, M. D. Weston, S. Yao et al., "Mutation of a gene encoding a protein with extracellular matrix motifs in Usher syndrome type IIa," *Science*, vol. 280, no. 5370, pp. 1753–1757, 1998.

[5] M. Bitner-Glindzicz, B. Glaser, K. J. Lindley et al., "A recessive contiguous gene deletion causing infantile hyperinsulinism, enteropathy and deafness identifies the Usher type 1C gene," *Nature Genetics*, vol. 26, no. 1, pp. 56–60, 2000.

[6] E. Verpy, M. Leibovici, I. Zwaenepoel et al., "A defect in harmonin, a PDZ domain-containing protein expressed in the inner ear sensory hair cells, underlies Usher syndrome type 1C," *Nature Genetics*, vol. 26, no. 1, pp. 51–55, 2000.

[7] Z. M. Ahmed, S. Riazuddin, S. L. Bernstein et al., "Mutations of the protocadherin gene *PCDH15* cause Usher syndrome type 1F," *The American Journal of Human Genetics*, vol. 69, no. 1, pp. 25–34, 2001.

[8] K. N. Alagramam, H. Yuan, M. H. Kuehn et al., "Mutations in the novel protocadherin *PCDH15* cause Usher syndrome type 1F," *Human Molecular Genetics*, vol. 10, no. 16, pp. 1709–2603, 20011718, 2001.

[9] H. Bolz, B. von Brederlow, A. Ramírez et al., "Mutation of *CDH23*, encoding a new member of the cadherin gene family, causes Usher syndrome type 1D," *Nature Genetics*, vol. 27, no. 1, pp. 108–112, 2001.

[10] J. M. Bork, L. M. Peters, S. Riazuddin et al., "Usher syndrome 1D and nonsyndromic autosomal recessive deafness DFNB12

are caused by allelic mutations of the novel cadherin-like gene *CDH23*," *The American Journal of Human Genetics*, vol. 68, no. 1, pp. 26–37, 2001.

[11] T. Joensuu, R. Hämäläinen, B. Yuan et al., "Mutations in a novel gene with transmembrane domains underlie Usher syndrome type 3," *The American Journal of Human Genetics*, vol. 69, no. 4, pp. 673–684, 2001.

[12] D. Weil, A. el-Amraoui, S. Masmoudi et al., "Usher syndrome type I G (USH1G) is caused by mutations in the gene encoding SANS, a protein that associates with the USH1C protein, harmonin," *Human Molecular Genetics*, vol. 12, no. 5, pp. 463–471, 2003.

[13] M. D. Weston, M. W. J. Luijendijk, K. D. Humphrey, C. Möller, and W. J. Kimberling, "Mutations in the *VLGR1* gene implicate G-protein signaling in the pathogenesis of Usher syndrome type II," *The American Journal of Human Genetics*, vol. 74, no. 2, pp. 357–366, 2004.

[14] I. Ebermann, H. P. N. Scholl, P. Charbel Issa et al., "A novel gene for Usher syndrome type 2: mutations in the long isoform of whirlin are associated with retinitis pigmentosa and sensorineural hearing loss," *Human Genetics*, vol. 121, no. 2, pp. 203–211, 2007.

[15] S. Riazuddin, I. A. Belyantseva, A. P. J. Giese et al., "Alterations of the CIB2 calcium- and integrin-binding protein cause Usher syndrome type 1J and nonsyndromic deafness DFNB48," *Nature Genetics*, vol. 44, no. 11, pp. 1265–1271, 2012.

[16] P. Mathur and J. Yang, "Usher syndrome: hearing loss, retinal degeneration and associated abnormalities," *Biochimica et Biophysica Acta (BBA) - Molecular Basis of Disease*, vol. 1852, no. 3, pp. 406–420, 2015.

[17] I. Ebermann, J. B. Phillips, M. C. Liebau et al., "*PDZD7* is a modifier of retinal disease and a contributor to digenic Usher syndrome," *The Journal of Clinical Investigation*, vol. 120, no. 6, pp. 1812–1823, 2010.

[18] E. Schneider, T. Märker, A. Daser et al., "Homozygous disruption of *PDZD7* by reciprocal translocation in a consanguineous family: a new member of the Usher syndrome protein interactome causing congenital hearing impairment," *Human Molecular Genetics*, vol. 18, no. 4, pp. 655–666, 2009.

[19] K. T. Booth, H. Azaiez, K. Kahrizi et al., "*PDZD7* and hearing loss: more than just a modifier," *American Journal of Medical Genetics Part A*, vol. 167A, no. 12, pp. 2957–2965, 2015.

[20] B. Vona, S. Lechno, M. A. H. Hofrichter et al., "Confirmation of *PDZD7* as a nonsyndromic hearing loss gene," *Ear and Hearing*, vol. 37, no. 4, pp. e238–e246, 2016.

[21] J. Zou, T. Zheng, C. Ren et al., "Deletion of *PDZD7* disrupts the Usher syndrome type 2 protein complex in cochlear hair cells and causes hearing loss in mice," *Human Molecular Genetics*, vol. 23, no. 9, pp. 2374–2390, 2014.

[22] M. Grati, J. B. Shin, M. D. Weston et al., "Localization of PDZD7 to the stereocilia ankle-link associates this scaffolding protein with the Usher syndrome protein network," *The Journal of Neuroscience*, vol. 32, no. 41, pp. 14288–14293, 2012.

[23] Q. Chen, J. Zou, Z. Shen, W. Zhang, and J. Yang, "Whirlin and PDZ domain-containing 7 (PDZD7) proteins are both required to form the quaternary protein complex associated with Usher syndrome type 2," *The Journal of Biological Chemistry*, vol. 289, no. 52, pp. 36070–36088, 2014.

[24] C. P. Morgan, J. F. Krey, M.'. Grati et al., "PDZD7-MYO7A complex identified in enriched stereocilia membranes," *eLife*, vol. 5, article e18312, 2016.

[25] J. Zou, Q. Chen, A. Almishaal et al., "The roles of USH1 proteins and PDZ domain-containing USH proteins in USH2 complex integrity in cochlear hair cells," *Human Molecular Genetics*, vol. 26, no. 3, pp. 624–636, 2017.

[26] H. Nie, Y. Liu, X. Yin et al., "Plasma membrane targeting of protocadherin 15 is regulated by the golgi-associated chaperone protein PIST," *Neural Plasticity*, vol. 2016, Article ID 8580675, 9 pages, 2016.

[27] C. Liu, X. Zhai, B. Zhao, Y. Wang, and Z. Xu, "Cyclin I-like (CCNI2) is a cyclin-dependent kinase 5 (CDK5) activator and is involved in cell cycle regulation," *Scientific Reports*, vol. 7, article 40979, 2017.

[28] Y. Liu, H. Nie, C. Liu et al., "Angulin proteins ILDR1 and ILDR2 regulate alternative pre-mRNA splicing through binding to splicing factors TRA2A, TRA2B, or SRSF1," *Scientific Reports*, vol. 7, no. 1, p. 7466, 2017.

[29] S. Heller, C. A. Sheane, Z. Javed, and A. J. Hudspeth, "Molecular markers for cell types of the inner ear and candidate genes for hearing disorders," *Proceedings of the National Academy of Sciences of the United States of America*, vol. 95, no. 19, pp. 11400–11405, 1998.

[30] E. Fujita, Y. Kouroku, S. Ozeki et al., "Oligo-astheno-teratozoospermia in mice lacking RA175/TSLC1/SynCAM/IGSF4A, a cell adhesion molecule in the immunoglobulin superfamily," *Molecular and Cellular Biology*, vol. 26, no. 2, pp. 718–726, 2006.

[31] E. Fujita, Y. Tanabe, T. Hirose et al., "Loss of partitioning-defective-3/isotype-specific interacting protein (par-3/ASIP) in the elongating spermatid of RA175 (IGSF4A/SynCAM)-deficient mice," *The American Journal of Pathology*, vol. 171, no. 6, pp. 1800–1810, 2007.

[32] Y. Takai, J. Miyoshi, W. Ikeda, and H. Ogita, "Nectins and nectin-like molecules: roles in contact inhibition of cell movement and proliferation," *Nature Reviews Molecular Cell Biology*, vol. 9, no. 8, pp. 603–615, 2008.

[33] K. Mandai, Y. Rikitake, M. Mori, and Y. Takai, "Nectins and nectin-like molecules in development and disease," *Current Topics in Developmental Biology*, vol. 112, pp. 197–231, 2015.

[34] C. Y. Logan and R. Nusse, "The Wnt signaling pathway in development and disease," *Annual Review of Cell and Developmental Biology*, vol. 20, no. 1, pp. 781–810, 2004.

[35] R. Chai, B. Kuo, T. Wang et al., "Wnt signaling induces proliferation of sensory precursors in the postnatal mouse cochlea," *Proceedings of the National Academy of Sciences of the United States of America*, vol. 109, no. 21, pp. 8167–8172, 2012.

[36] F. Shi, J. S. Kempfle, and A. S. B. Edge, "Wnt-responsive Lgr5-expressing stem cells are hair cell progenitors in the cochlea," *The Journal of Neuroscience*, vol. 32, no. 28, pp. 9639–9648, 2012.

[37] F. Shi, Y. F. Cheng, X. L. Wang, and A. S. B. Edge, "β-catenin up-regulates *Atoh1* expression in neural progenitor cells by interaction with an *Atoh1* 3′ enhancer," *The Journal of Biological Chemistry*, vol. 285, no. 1, pp. 392–400, 2010.

[38] F. Shi, L. Hu, B. E. Jacques, J. F. Mulvaney, A. Dabdoub, and A. S. B. Edge, "β-Catenin is required for hair-cell differentiation in the cochlea," *The Journal of Neuroscience*, vol. 34, no. 19, pp. 6470–6479, 2014.

[39] F. Shi, L. Hu, and A. S. B. Edge, "Generation of hair cells in neonatal mice by β-catenin overexpression in Lgr5-positive cochlear progenitors," *Proceedings of the National Academy*

of Sciences of the United States of America, vol. 110, no. 34, pp. 13851–13856, 2013.

[40] L. Spinardi and W. Witke, "Gelsolin and diseases," *Subcellular Biochemistry*, vol. 45, pp. 55–69, 2007.

[41] G. H. Li, P. D. Arora, Y. Chen, C. A. McCulloch, and P. Liu, "Multifunctional roles of gelsolin in health and diseases," *Medicinal Research Reviews*, vol. 32, no. 5, pp. 999–1025, 2012.

[42] P. Mburu, M. R. Romero, H. Hilton et al., "Gelsolin plays a role in the actin polymerization complex of hair cell stereocilia," *PLoS One*, vol. 5, no. 7, article e11627, 2010.

[43] J. Olt, P. Mburu, S. L. Johnson et al., "The actin-binding proteins eps8 and gelsolin have complementary roles in regulating the growth and stability of mechanosensory hair bundles of mammalian cochlear outer hair cells," *PLoS One*, vol. 9, no. 1, article e87331, 2014.

[44] A. Gulino, L. Di Marcotullio, and I. Screpanti, "The multiple functions of Numb," *Experimental Cell Research*, vol. 316, no. 6, pp. 900–6, 2010.

[45] Z. Gao, F. L. Chi, Y. B. Huang, J. M. Yang, N. Cong, and W. Li, "Expression of Numb and Numb-like in the development of mammalian auditory sensory epithelium," *Neuroreport*, vol. 22, no. 2, pp. 49–54, 2011.

[46] J. Shen, D. I. Scheffer, K. Y. Kwan, and D. P. Corey, "SHIELD: an integrative gene expression database for inner ear research," *Database*, vol. 2015, article bav071, 2015.

[47] C. J. Chan, D. M. Andrews, and M. J. Smyth, "Receptors that interact with nectin and nectin-like proteins in the immunosurveillance and immunotherapy of cancer," *Current Opinion in Immunology*, vol. 24, no. 2, pp. 246–251, 2012.

[48] Y. Rikitake, K. Mandai, and Y. Takai, "The role of nectins in different types of cell–cell adhesion," *Journal of Cell Science*, vol. 125, no. 16, pp. 3713–3722, 2012.

[49] Y. Zhiling, E. Fujita, Y. Tanabe, T. Yamagata, T. Momoi, and M. Y. Momoi, "Mutations in the gene encoding CADM1 are associated with autism spectrum disorder," *Biochemical and Biophysical Research Communications*, vol. 377, no. 3, pp. 926–929, 2008.

[50] E. Fujita, H. Dai, Y. Tanabe et al., "Autism spectrum disorder is related to endoplasmic reticulum stress induced by mutations in the synaptic cell adhesion molecule, CADM1," *Cell Death & Disease*, vol. 1, no. 6, article e47, 2010.

[51] Y. Takayanagi, E. Fujita, Z. Yu et al., "Impairment of social and emotional behaviors in Cadm1-knockout mice," *Biochemical and Biophysical Research Communications*, vol. 396, no. 3, pp. 703–708, 2010.

[52] Y. Tanabe, E. Fujita, Y. K. Hayashi et al., "Synaptic adhesion molecules in Cadm family at the neuromuscular junction," *Cell Biology International*, vol. 37, no. 7, pp. 731–736, 2013.

Hindawi
Neural Plasticity
Volume 2017, Article ID 8941537, 9 pages
https://doi.org/10.1155/2017/8941537

Research Article

Effects of Various Extents of High-Frequency Hearing Loss on Speech Recognition and Gap Detection at Low Frequencies in Patients with Sensorineural Hearing Loss

Bei Li, Yang Guo, Guang Yang, Yanmei Feng, and Shankai Yin

Department of Otolaryngology Head and Neck Surgery, Shanghai Jiao Tong University Affiliated Sixth People's Hospital, No. 600, Yishan Road, Xuhui District, Shanghai 200233, China

Correspondence should be addressed to Yanmei Feng; feng.yanmei@126.com and Shankai Yin; yinshankai@china.com

Received 29 August 2017; Accepted 7 November 2017; Published 27 December 2017

Academic Editor: Hai Huang

This study explored whether the time-compressed speech perception varied with the degree of hearing loss in high-frequency sensorineural hearing loss (HF SNHL) individuals. 65 HF SNHL individuals with different cutoff frequencies were recruited and further divided into mildly, moderately, and/or severely affected subgroups in terms of the averaged thresholds of all frequencies exhibiting hearing loss. Time-compressed speech recognition scores under both quiet and noisy conditions and gap detection thresholds within low frequencies that had normal thresholds were obtained from all patients and compared with data from 11 age-matched individuals with normal hearing threshold at all frequencies. Correlations of the time-compressed speech recognition scores with the extents of HF SNHL and with the 1 kHz gap detection thresholds were studied across all participants. We found that the time-compressed speech recognition scores were significantly affected by and correlated with the extents of HF SNHL. The time-compressed speech recognition scores also correlated with the 1 kHz gap detection thresholds except when the compression ratio of speech was 0.8 under quiet condition. Above all, the extents of HF SNHL were significantly correlated with the 1 kHz gap thresholds.

1. Introduction

In ENT clinical, patients with high-frequency sensorineural hearing loss (HF SNHL) always complain about the intelligibility of the fast speech. Sensorineural hearing loss (SNHL) is very commonly encountered in the clinic. Researches showed that compared to the normal-hearing (NH) individuals, the ability to comprehend speech in noise decreased in the SNHL individuals [1–3]. Low-intensity signals masked in speech cannot be perceived by those with SNHL, rendering poor speech recognition. Although speech contains a wide range of frequencies [4], according to Ardoint and Lorenzi [5], the most important frequency range in terms of speech perception is 1-2 kHz. Usually, the SNHL begins at high frequencies and slowly spreads to lower frequencies. Once SNHL extends into the low-frequency region (1-2 kHz), the speech recognition ability of SNHL individuals becomes even worse.

Of all those with SNHL, even individuals with only HF SNHL usually complain about the intelligibility of fast speech, especially in noise. Accumulated evidence shows that the speech recognition scores of HF SNHL patients with normal low-frequency hearing are poorer than those of NH individuals, even when speech stimuli are limited to low frequencies [6–10]. Age also played an important role in speech perception [11]. Leigh-Paffenroth and Elangovan [12] found significant poorer temporal processing in the low-frequency regions (with normal thresholds) in middle-aged individuals even without HF SNHL, compared to the younger individuals. Fullgrabe et al. [13] found declines in speech perception in older persons compared to the youth persons, even the audiometric sensitivities of both were

within normal ranges. It is necessary to exclude the influence of age and hearing differences in low-frequency region to study the impact of HF SNHL in speech perception in low frequencies. After auditory sensitivity and age were controlled, research suggested that suprathreshold temporal processing deficits did exist [6, 14]. Others showed that noise-induced HF SNHL affected low-frequency temporal resolution in guinea pigs, even though the thresholds in the low-frequency region were within normal ranges [15, 16]. In this point of view, the speech perception difficulties that many SNHL individuals experienced probably consist of not only SNHL of the high-frequency region but also the temporal processing disability in the low-frequency region.

Previous studies found that speech recognition ability varied among individuals with different extents of SNHL [12, 17–20]. Andrade et al. [18] reported that the speech recognition thresholds correlated with the extents of SNHL in individuals with nonflat audiograms. Also, self-assessed scores of hearing disability were associated with the pure-tone thresholds [17, 19, 20]. Notably, Dobie [19] explored the relationships between pure-tone averages (at 0.5, 1, 2, and 3 kHz) and self-assessed hearing disability scores of 1001 patients and found no correlation between self-assessed scores and pure-tone averages in patients whose pure-tone averages were below 25 dB HL. However, a linear correlation was evident between the self-assessed hearing disability scores and pure-tone averages in patients whose pure-tone averages were above 25 dB HL [19].

However, whether and how HF SNHL affects low-frequency speech perception and temporal resolution remains largely unknown. In the present work, we grouped patients by cutoff frequency (1, 2, and 4 kHz) of HF SNHL. Thus, the thresholds at and below each cutoff frequency were within normal ranges, and the thresholds beyond the cutoff frequencies were higher than 25 dB HL. And gap detection tasks were used to evaluate the temporal resolution of low-frequency region. Speech recognition scores upon delivery of time-compressed sentences under both quiet and noisy conditions and gap detection thresholds were measured and compared between HF SNHL groups with the same cutoff frequency but various degrees of HF SNHL and age-matched NH group.

2. Materials and Methods

2.1. Participants. A total of 76 individuals were recruited, including 65 HF SNHL patients and 11 NH individuals. All HF SNHL participants were recruited from the Department of Otolaryngology Head and Neck Surgery at Shanghai Jiao Tong University Affiliated Sixth People's Hospital, and NH individuals from the staff of the same hospital. No neurological, psychiatric, or other disorders that would undermine speech recognition ability were identified in all participants including the HF SNHL participants. The program was approved by the Ethics Committee of Shanghai Jiao Tong University Affiliated Sixth People's Hospital. All participants gave written informed consent prior to study commencement.

All participants were native Mandarin-speaking Chinese. All NH individuals had pure-tone thresholds 25 dB HL or less at all octave frequencies between 250 and 8000 Hz, in both ears. HF SNHL patients were rigorously selected according to the following criteria: (1) symmetrical SNHL, with threshold differences of 15 dB or less (at all frequencies) between both ears for more than 6 months; (2) pure-tone thresholds of 25 dB HL or less, both at and below the cutoff frequencies; (3) pure-tone thresholds > 25 dB HL above the cutoff frequencies; and (4) type A or Ad type tympanograms.

HF SNHL patients were grouped by the HF SNHL cutoff frequencies evident on audiograms (e.g., 1, 2, and 4 kHz). In each of these three groups, patients were further subdivided into those with mild (25–40 dB HL), moderate (41–60 dB HL), and severe (>60 dB HL) HF SNHL subgroups, defined by the means of averaged pure-tone threshold across frequencies higher than the cutoff frequency. Thus, finally, we formed eight HF SNHL groups, including mild, moderate, and severe groups with cutoff frequencies at 1 and 2 kHz and mild and moderate groups with cutoff frequency at 4 kHz, and one NH group. The means and standard deviations of the auditory thresholds of the tested ears for all groups are shown in Figure 1. Demographic data of all groups are shown in Table 1.

2.2. Stimuli and Procedure. The gap detection task was measured in a three-interval forced-choice procedure. For the gap marker, white noise was low-pass filtered at cutoff frequencies of 1, 2, and 4 kHz, respectively, via 3000th-order finite impulse response filter with an approximately −116 dB/octave filter slope.

In brief, a three-interval forced-choice program had been run on MATLAB software (version 7.0). Three buttons were presented on a monitor to the participant who was asked to indicate which one of the three stimuli was different (i.e., which of the three stimuli was inserted with a gap). As each of the three stimuli playing, the corresponding button was highlighted in red (from left to right). Participant was instructed to click one of the three buttons with the mouse as a response after each presentation of three signals. The next trial was initiated after an answer was given. All subjects were trained to be familiar with the procedure before formal test. The training would last until their performances reached platforms, respectively. No feedback was given to the subject throughout the test. The gap varying in size from 20 to 1 ms was embedded in the middle of one of the three noise bursts (total duration: 1000 ms for each). The gap was shaped using a 1 ms, raised cosine envelope. Each test, commenced with a gap of 20 ms, was followed by a down sequence (in 2 ms steps) until the first erroneous answer was recorded. The two-down, one-up procedure was then adopted (with a gap step size of 1 ms) until the appointed reversals were reached. In gap detection tests, the frequency spectra of the gap markers tested in the HF SNHL groups differed. For example, 4 kHz group members were tested separately with 1, 2, and 4 kHz gap markers. Those of the 2 kHz groups were tested using 1 and 2 kHz gap markers. For those of the 1 kHz groups, only the 1 kHz gap marker test was tested.

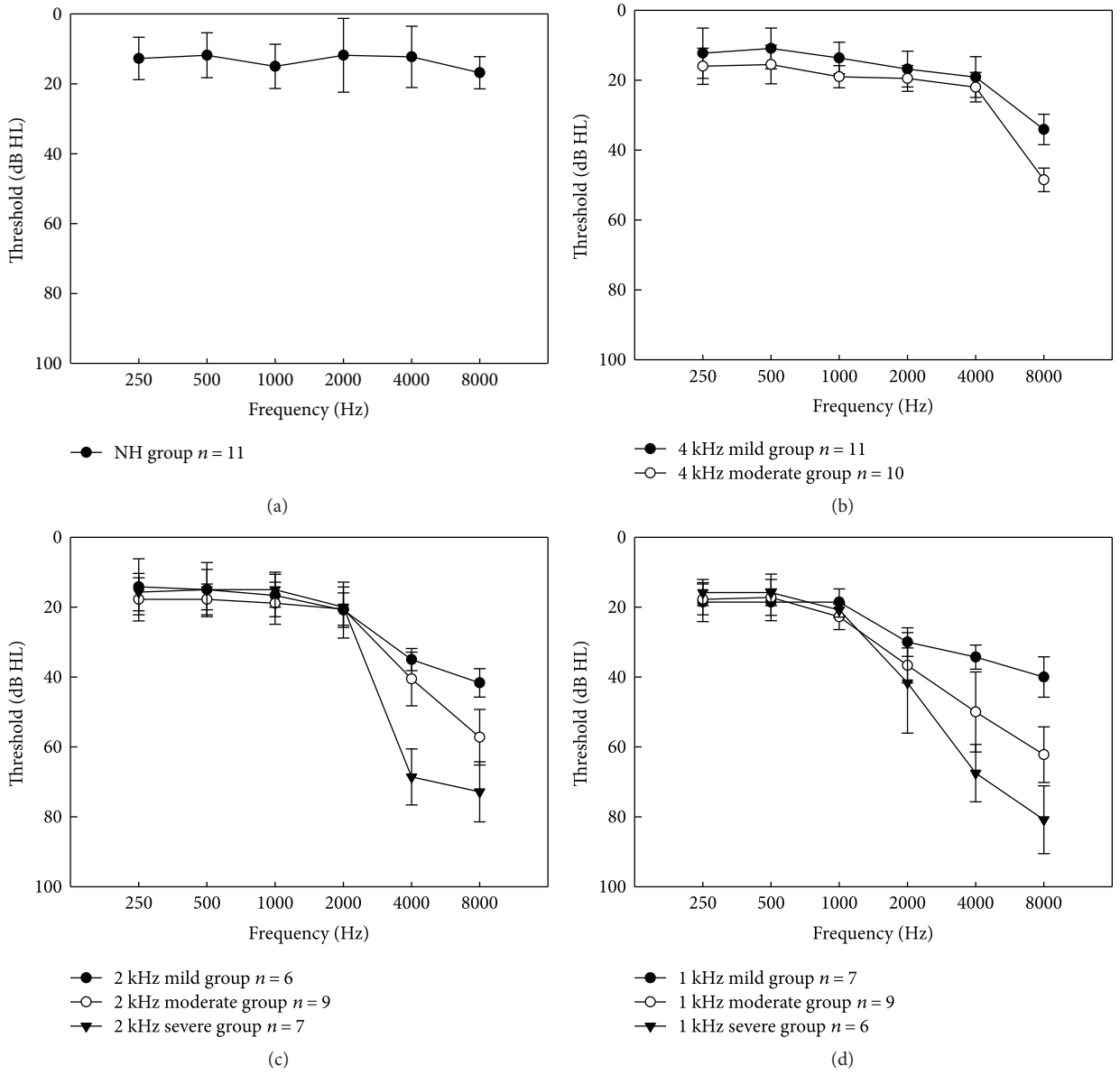

Figure 1: Mean audiometric thresholds (dB HL), with standard deviations, for each group. The audiometric thresholds of the tested ears for the normal hearing (NH) and 4, 2, and 1 kHz HF SNHL groups are shown in (a), (b), (c) and (d), respectively.

Table 1: Demographic data for the NH group and HF SNHL subgroups.

Group	Male	Female	Age mean ± SD (yrs)
NH	2	9	45.6 ± 13.5
4 kHz mild	5	6	51.2 ± 8.5
4 kHz moderate	5	5	48.3 ± 5.3
2 kHz mild	3	3	52.0 ± 5.4
2 kHz moderate	3	6	46.4 ± 7.9
2 kHz severe	3	4	52.9 ± 11.3
1 kHz mild	3	4	42.6 ± 8.2
1 kHz moderate	4	5	52.7 ± 13.4
1 kHz severe	3	3	51.0 ± 8.6

NH: normal hearing; SD: standard deviation.

Speech perception was assessed using the Mandarin version of the Hearing in Noise Test (MHINT) of the House Ear Institute [21], representing a daily and communicative style of speech, which could be easily understood by native Mandarin-speaking listeners with various degrees of education. Speech was time-compressed using Praat software (version 5.3), without any significant change in the power spectrum [22]. We used three compression ratios: 0.6, 0.8, and 1.0 that of the normal speech rate (the compression ratio of 1.0, namely, was normal speech rate). Speech recognition tests were run under both quiet and noisy [signal-to-noise ratio (SNR): −5 dB] conditions.

All test signals were presented at 75 dB SPL under both quiet and noisy conditions and were delivered monaurally through Sennheiser HD580 headphones. Only right ears were tested, and a 40 dB SPL speech-shaped noise was

conducted to the left ears as masker all along the tests. To create noisy conditions, a speech-shaped noise of the same spectrum as that of the MHINT sentence was presented with SNR at −5 dB. The noise began 500 ms before the sentence and continued for 500 ms after the sentence had concluded. A complete set of tests required approximately 30 min. Practice was conducted before each test, and feedback was provided. After practice, each participant achieved stable recognition scores. During a speech recognition test, each sentence was played only once, and no feedback was given. The same methods were also applied by Feng et al. [14].

3. Results

3.1. Age Matching and Pure-Tone Thresholds of the NH and HF SNHL Groups. One-way analysis of variance (ANOVA) showed that the mean ages of all nine groups did not differ significantly ($F_{(8,75)} = 1.097$, $p = 0.376$).

Comparisons of the averaged thresholds across the frequencies with normal thresholds in all groups showed that the thresholds of frequencies exhibiting normal hearing did not differ significantly among the groups ($F_{(8,75)} = 1.899$, $p = 0.075$).

3.2. Gap Detection Task. The gap thresholds of groups varying in terms of gap marker cutoff frequency are shown in Figure 2. The gap thresholds of the gap markers with different cutoff frequencies for the same listener group were compared firstly. Paired *t*-tests showed that the gap thresholds of 1 kHz gap marker were significantly higher than those of 2 kHz gap marker for 2 kHz mild HF SNHL group ($t = 5.349$, $p = 0.003$), 2 kHz moderate HF SNHL group ($t = 10.639$, $p < 0.001$), and 2 kHz severe HF SNHL group ($t = 7.22$, $p < 0.001$). One-way repeated ANOVA showed significant main effects of cutoff frequencies of gap marker on gap thresholds of 4 kHz mild HF SNHL group ($F_{(2,20)} = 19.334$, $p < 0.001$), 4 kHz moderate HF SNHL group ($F_{(2,18)} = 21.063$, $p < 0.001$), and NH group ($F_{(2,20)} = 57.133$, $p < 0.001$); the post hoc analyses (LSD tests) revealed that gap thresholds of 1 kHz gap marker, 2 kHz gap marker, and 4 kHz gap marker differed from each other significantly for the three groups, respectively. Generally, the gap thresholds of all groups gradually decrease as cutoff frequencies of the gap marker increase gradually.

Then, data derived from different groups with the same gap marker frequency were analyzed by one-way ANOVA. There was a significant difference when the cutoff frequency of gap marker is 1 kHz ($F_{(8,75)} = 2.189$, $p = 0.039$); the post hoc analysis (LSD test) revealed that the gap thresholds of the NH group and 4 kHz mild HF SNHL group were significantly lower than those of the 1 kHz mild HF SNHL group, 1 kHz moderate HF SNHL group, and 1 kHz severe HF SNHL group. And there was also a significant difference when the cutoff frequency of gap marker is 4 kHz ($F_{(2,31)} = 3.515$, $p = 0.043$); the post hoc analysis (LSD test) revealed that the gap thresholds of the NH group were significantly lower than those of the 4 kHz moderate HF SNHL group with 4 kHz gap marker. However, no difference was evident with 2 kHz gap marker ($F_{(5,53)} = 0.231$, $p = 0.947$).

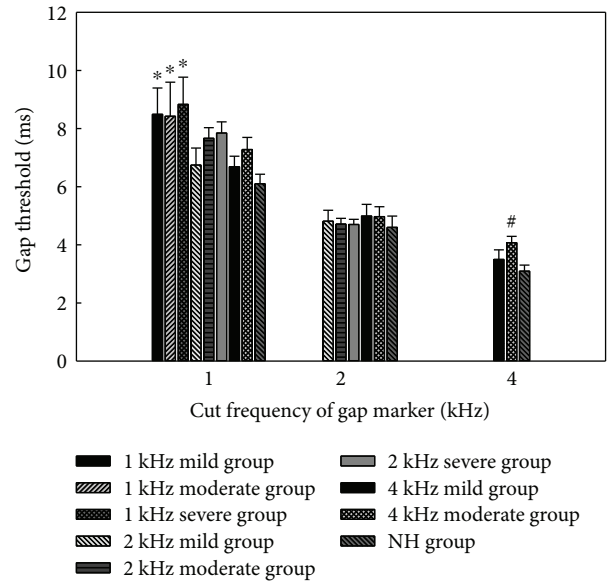

Figure 2: The mean gap thresholds in the high-frequency sensorineural hearing loss (HF SNHL) groups and normal-hearing (NH) group. The error bars indicate standard errors. * indicates gap thresholds of the 1 kHz mild, moderate, and severe HF SNHL groups with 1 kHz gap marker which were significantly higher than those of the NH group and the 4 kHz mild HF SNHL group; # indicates gap thresholds of the 4 kHz moderate HF SNHL group which were significantly higher than those of the NH group for 4 kHz gap marker.

When presented with gap marker of the same cutoff frequency, in general, the gap thresholds of various groups tended to be higher if the range of HF SNHL was wider or the degrees of hearing impairment were higher.

3.3. Time-Compressed Speech Recognition. The original scores under quiet and noisy conditions are shown in Figures 3 and 4, respectively. Overall, the speech recognition scores of all groups decreased as the time compression ratio fell from 1.0 (normal speech rate) to 0.6 and the scores were lower under noisy conditions than those under quiet conditions at the same time compression ratio.

Before analysis, all speech recognition scores were arcsine-transformed to avoid ceiling or floor effects. Data from the NH and eight HF SNHL groups in quiet were subjected to two-way repeated-measures ANOVA to test the effects of group and time compression ratio on speech recognition. The effects of group and compression ratio were both significant: $F_{\text{group}(8,67)} = 5.368$, $p < 0.001$ and $F_{\text{compression}(2,134)} = 114.028$, $p < 0.001$. There was a statistically significant two-way interaction between group and time compression ratio ($F_{(16,134)} = 2.130$, $p = 0.010$). The LSD method was applied in post hoc comparisons, to explore the effect of the extent of HF SNHL on speech recognition scores in quiet. When speech compression ratio was 0.6, all HF SNHL groups scored significantly lower than the NH group except the 2 kHz mild and severe HF SNHL groups and 4 kHz mild HF SNHL group; when speech compression ratio was 0.8, the NH group scored significantly higher than the 1 kHz moderate and severe HF SNHL groups and 4 kHz

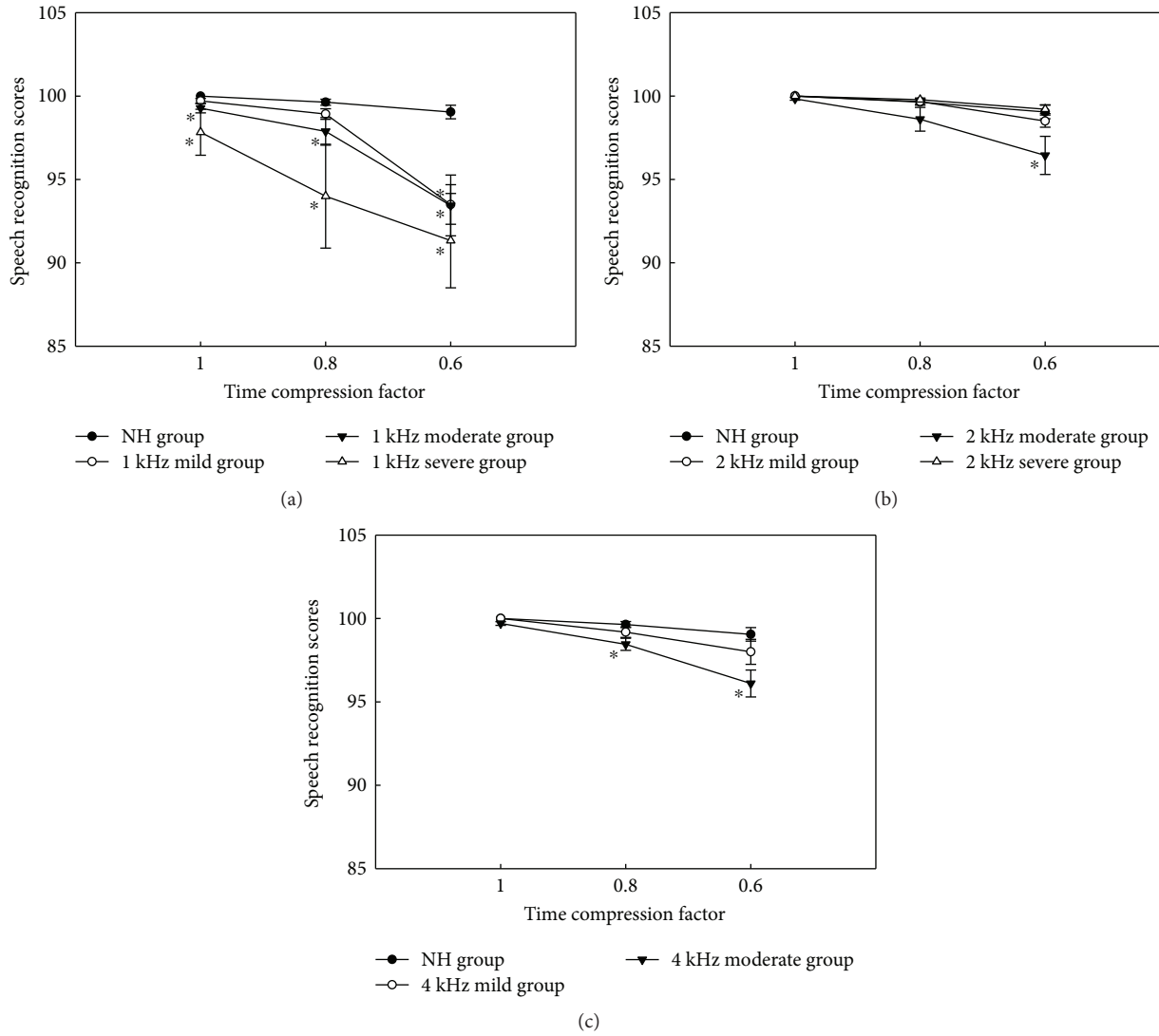

Figure 3: Speech recognition scores under quiet conditions for the normal-hearing (NH) and high-frequency sensorineural hearing loss (HF SNHL) groups, as a function of the time compression ratio. The scores for the 1, 2, and 4 kHz HF SNHL groups are shown in (a), (b), and (c), respectively. The error bars indicate standard errors. ∗ indicates significant difference of speech recognition scores when compared with that of the NH group at the same time compression factor.

moderate HF SNHL group, while the NH group scored significantly higher than the 1 kHz moderate and severe HF SNHL groups when speech compression ratio was 1.0. The differences among the 1 kHz mild, moderate, and severe HF SNHL groups were not statistically significant when speech compression ratio was 0.6 or 1.0, but the scores of the 1 kHz mild HF SNHL groups were significantly higher than the 1 kHz severe HF SNHL groups when speech compression ratio was 0.8; the differences among the 2 kHz mild, moderate, and severe HF SNHL groups and the differences between the 4 kHz mild and moderate HF SNHL groups were not statistically significant for all three speech compression ratios.

A two-way repeated-measures ANOVA was used to evaluate the effects of group and time compression ratio on speech recognition in noise. The effects of group and compression ratio were both significant: $F_{\text{group}(8,67)} = 11.541$, $p < 0.001$ and $F_{\text{compression}(2,134)} = 144.785$, $p < 0.001$. There was a statistically significant two-way interaction between group and time compression ratio ($F_{(16,134)} = 4.434$, $p \leq 0.001$). The LSD method was used in post hoc comparisons to explore the effect of the extent of HF SNHL on speech recognition scores in noise. When speech compression ratio was 0.8 and 1.0, the differences between scores of the NH group and all HF SNHL groups were significant; when speech compression ratio was 0.6, the NH group scored significantly higher than all HF SNHL groups except the 2 kHz mild HF SNHL group. The differences among the 1 kHz mild, moderate, and severe HF SNHL groups were not statistically significant when speech compression ratio was 0.6 or 0.8, but the scores of the 1 kHz mild HF SNHL groups were significantly higher than those of 1 kHz severe HF SNHL groups when speech compression ratio was 1.0; the 2 kHz mild HF SNHL group scored significantly higher

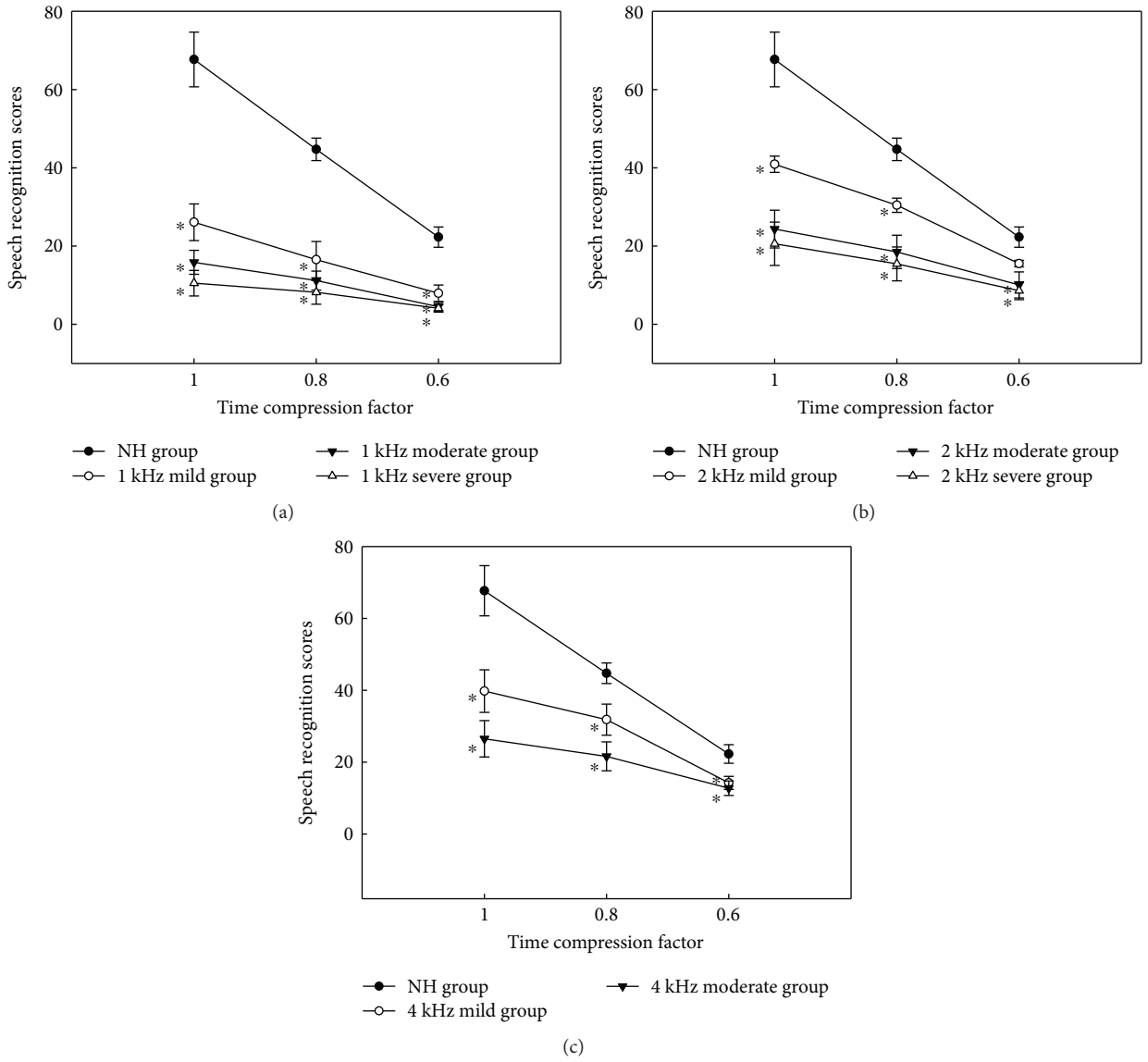

Figure 4: Speech recognition scores under noisy conditions (SNR = −5 dB) for the normal-hearing (NH) and high-frequency sensorineural hearing loss (HF SNHL) groups, as a function of the time compression ratio. The scores for the 1, 2, and 4 kHz HF SNHL groups are shown in (a), (b), and (c), respectively. The error bars indicate standard errors. ∗ indicates significant difference of speech recognition scores when compared with that of the NH group at the same time compression factor.

than the 2 kHz moderate and severe HF SNHL groups when speech compression ratio was 0.6 and 0.8, and the 2 kHz mild HF SNHL group scored significantly higher than the 2 kHz severe HF SNHL group when speech compression ratio was 1.0. The differences between the 4 kHz mild and moderate HF SNHL groups were not statistically significant for all three speech compression ratios.

As a whole, at the same time compression ratio, the scores of the NH group were better than those of any HF SNHL group, and the scores of those with HF SNHL decreased as the degree of HF SNHL increased, which was more obvious under noisy conditions.

3.4. Correlation Analysis. We explored relationships between time-compressed speech recognition scores, pure-tone HF averages, and gap detection thresholds, by calculating *Pearson* correlations as follows: (1) between pure-tone HF averages (for NH groups, the average was calculated across 2, 4, and 8 kHz; for HF SNHL groups, the average was calculated across frequencies where exhibited hearing loss) and time-compressed speech recognition scores; (2) between pure-tone HF averages and the 1 kHz gap detection thresholds; and, (3) between the time-compressed speech recognition scores and the 1 kHz gap detection thresholds (all participants underwent 1 kHz gap detection testing). As shown in Table 2, the pure-tone HF averages were significantly correlated with time-compressed speech recognition scores at compression ratios of both 0.6 and 0.8, and normal speech recognition scores (all p values < 0.05), under both quiet and noisy conditions. What is noteworthy is that pure-tone

Table 2: Correlation analysis between pure-tone averages of high-frequency hearing loss and speech recognition scores with different compression and different test backgrounds.

	Compression ratio of speech in quiet			Compression ratio of speech in noise		
	1	0.8	0.6	1	0.8	0.6
Pearson correlation	−0.279	−0.269	−0.329	−0.694	−0.627	−0.536
p value	0.015*	0.019*	0.004*	<0.001*	<0.001*	<0.001*

For NH groups, the average was calculated across 2, 4, and 8 kHz; for HF SNHL groups, the average was calculated across frequencies where exhibited hearing loss. * indicates p values smaller than 0.05.

Table 3: Correlation analysis between 1 kHz gap thresholds and speech recognition scores with different compression ratios under different test backgrounds.

	Compression ratio of speech in quiet			Compression ratio of speech in noise		
	1	0.8	0.6	1	0.8	0.6
Pearson correlation	−0.231	−0.185	−0.427	−0.388	−0.394	−0.381
p value	0.045*	0.109	<0.001*	0.001*	<0.001*	0.001*

* indicates p values smaller than 0.05.

HF averages were significantly correlated with the 1 kHz gap detection thresholds (*Pearson* correlation = 0.367, $p = 0.001$). In Table 3, the results showed that 1 kHz gap thresholds were significantly correlated with the speech recognition scores at all compression ratios under noisy conditions (all p values ≤ 0.001). This was also true under quiet conditions for both normal speech and that at a 0.6 compression ratio ($p_{0.6\text{compression}} \leq 0.001$, $p_{\text{normal speed}} = 0.045$).

4. Discussion

Our primary purpose in the present study was to explore whether and how HF SNHL affected time-compressed speech perception and gap detection in low-frequency region with normal auditory threshold. We found that the time-compressed speech recognition scores of the HF SNHL group were poorer than those of the NH group and decreased as the extent of HF SNHL increased in patients with the same cutoff frequency. Generally, the recognition scores of patients with severe HF SNHL were poorer than the scores of those with moderate HF SNHL, which in turn were poorer than those of patients with mild HF SNHL at the same cutoff frequencies, under both quiet and noisy conditions (Figures 3 and 4).

As shown in Table 2, pure-tone averages of HF SNHL were significantly correlated with the time-compressed speech recognition scores. These results suggested that the ability to recognize time-compressed speech was affected by HF SNHL and correlated with the extent of HF SNHL. These results are similar to those of our previous study and indeed extend our earlier work [14]. We previously showed that the time-compressed speech recognition scores of the HF SNHL subjects were poorer than those of NH individuals [14]. However, the effect of the extent of HF SNHL on speech recognition was not explored in detail. Therefore, in the present study, we focused on the effect of varying levels of HF SNHL on time-compressed speech recognition abilities.

Indeed, the extent of HF SNHL affects the ability of speech recognition. Moore [23] found that, in individuals with cochlear hearing loss of up to approximately 45 dB, a change in audibility was the single most important contributor to speech perception problems. However, when the extent of hearing loss was greater, poor discrimination of suprathreshold stimuli also became of major importance. Nimitbunnasarn et al. [24] examined tonal identification in Thai speakers with normal hearing and different extents of SNHL. Identification ability was affected by SNHL per se and the extent thereof [24]. Jerger et al. [25] explored correlations among speech recognition performance, the pure-tone hearing level, and the age of individuals with SNHL. The relationship between the extent of hearing loss and speech recognition score was strongest in older individuals with SNHL. Other studies sought correlations between self-assessed hearing inventories and individual pure-tone thresholds [12, 17, 19] or between speech reception and pure-tone thresholds [20]. All data suggested that the extents of SNHL correlated with the speech recognition scores. Our results are consistent with such findings and suggest that the extents of HF SNHL are also correlated with the time-compressed speech recognition scores. Similar hearing configurations that vary in the extent of hearing loss may impact speech recognition differently, especially when speech is fast. More severe speech disruption is evident as the severity of hearing loss rises.

It is worth noting that the pure-tone averages of HF SNHL correlated with the 1 kHz gap thresholds significantly, which indicates that the HF SNHL could impair the temporal resolution of the low-frequency region. This is in line with our previous research results, which suggests that HF SNHL exerted an off-channel effect on temporal processing ability in the low-frequency region of the auditory system, whether in guinea pigs or humans [14, 15]. This off-channel effect may contribute to the difficulty, which is experienced by patients with normal hearing in low frequencies but suffered from HF SNHL, of perceiving the time-compressed speech [14] and temporal fine structure speech [6].

The relationship between speech recognition and temporal resolution, another focus of the present study, remains unclear. Previous studies suggested that temporal resolution

played an important role in speech recognition [26–29]. However, no influence of any temporal processing ability, such as gap detection, on speech perception, has been conclusively shown [11].

To determine whether the gap detection threshold correlated with time-compressed speech recognition ability, we carefully controlled for age and the extent of HF SNHL. As shown in Table 3, the gap thresholds with 1 kHz-low-pass-filtered noise were negatively correlated with the time-compressed speech recognition scores, suggesting that speech recognition ability was also affected by temporal resolution of the low-frequency region, even whose auditory sensitivity was normal.

5. Conclusions

Even when age was controlled, the extent of HF SNHL impacted the ability to recognize compressed speech. The greater the extent of HF SNHL was, the poorer the speech recognition ability was. The significant correlation between the extents of HF SNHL and gap detection thresholds implied that there was probable off-channel mechanism underlying. The decrease of time-compressed speech recognition ability may be partly attributable to the increased thresholds in gap detection task, which signified the deterioration of suprathresholdly temporal resolution.

Conflicts of Interest

The authors declare that there is no competing interest relevant to the publication of this paper.

Authors' Contributions

Bei Li and Yang Guo contributed equally to this paper.

Acknowledgments

The study was supported by a grant from the National Natural Science Foundation of China (81771015), Shanghai Municipal Education Commission—Gaofeng Clinical Medicine Grant Support (20152526), and Three-Year Action Program on Promotion of Clinical Skills and Clinical Innovation for Municipal Hospitals (16CR4027A) to Yanmei Feng and a grant from the National Natural Science Foundation of China (81530029) to Shankai Yin.

References

[1] J. R. Dubno, D. D. Dirks, and D. E. Morgan, "Effects of age and mild hearing loss on speech recognition in noise," *The Journal of the Acoustical Society of America*, vol. 76, no. 1, pp. 87–96, 1984.

[2] A. R. Needleman and C. C. Crandell, "Speech recognition in noise by hearing-impaired and noise-masked normal-hearing listeners," *Journal of the American Academy of Audiology*, vol. 6, no. 6, pp. 414–424, 1995.

[3] A. J. Klein, J. H. Mills, and W. Y. Adkins, "Upward spread of masking, hearing loss, and speech recognition in young and elderly listeners," *The Journal of the Acoustical Society of America*, vol. 87, no. 3, pp. 1266–1271, 1990.

[4] B. C. J. Moore, "The role of temporal fine structure processing in pitch perception, masking, and speech perception for normal-hearing and hearing-impaired people," *Journal of the Association for Research in Otolaryngology*, vol. 9, no. 4, pp. 399–406, 2008.

[5] M. Ardoint and C. Lorenzi, "Effects of lowpass and highpass filtering on the intelligibility of speech based on temporal fine structure or envelope cues," *Hearing Research*, vol. 260, no. 1-2, pp. 89–95, 2010.

[6] B. Li, L. Hou, L. Xu et al., "Effects of steep high-frequency hearing loss on speech recognition using temporal fine structure in low-frequency region," *Hearing Research*, vol. 326, pp. 66–74, 2015.

[7] A. C. Leger, D. T. Ives, and C. Lorenzi, "Abnormal intelligibility of speech in competing speech and in noise in a frequency region where audiometric thresholds are near-normal for hearing-impaired listeners," *Hearing Research*, vol. 316, pp. 102–109, 2014.

[8] A. C. Léger, B. C. J. Moore, and C. Lorenzi, "Abnormal speech processing in frequency regions where absolute thresholds are normal for listeners with high-frequency hearing loss," *Hearing Research*, vol. 294, no. 1-2, pp. 95–103, 2012.

[9] C. Lorenzi, L. Debruille, S. Garnier, P. Fleuriot, and B. C. J. Moore, "Abnormal processing of temporal fine structure in speech for frequencies where absolute thresholds are normal," *The Journal of the Acoustical Society of America*, vol. 125, no. 1, pp. 27–30, 2009.

[10] V. Summers, M. J. Makashay, S. M. Theodoroff, and M. R. Leek, "Suprathreshold auditory processing and speech perception in noise: hearing-impaired and normal-hearing listeners," *Journal of the American Academy of Audiology*, vol. 24, no. 4, pp. 274–292, 2013.

[11] A. Strouse, D. H. Ashmead, R. N. Ohde, and D. W. Grantham, "Temporal processing in the aging auditory system," *The Journal of the Acoustical Society of America*, vol. 104, no. 4, pp. 2385–2399, 1998.

[12] E. D. Leigh-Paffenroth and S. Elangovan, "Temporal processing in low-frequency channels: effects of age and hearing loss in middle-aged listeners," *Journal of the American Academy of Audiology*, vol. 22, no. 7, pp. 393–404, 2011.

[13] C. Fullgrabe, B. C. Moore, and M. A. Stone, "Age-group differences in speech identification despite matched audiometrically normal hearing: contributions from auditory temporal processing and cognition," *Frontiers in Aging Neuroscience*, vol. 6, p. 347, 2014.

[14] Y. Feng, S. Yin, M. Kiefte, and J. Wang, "Temporal resolution in regions of normal hearing and speech perception in noise for adults with sloping high-frequency hearing loss," *Ear and Hearing*, vol. 31, no. 1, pp. 115–125, 2010.

[15] Y. Feng, S. Yin, and J. Wang, "Deterioration of cortical responses to amplitude modulations of low-frequency carriers after high-frequency cochlear lesion in guinea pigs," *International Journal of Audiology*, vol. 49, no. 3, pp. 228–237, 2010.

[16] S. K. Yin, Y. M. Feng, Z. N. Chen, and J. Wang, "The effect of noise-induced sloping high-frequency hearing loss on the gap-response in the inferior colliculus and auditory cortex of guinea pigs," *Hearing Research*, vol. 239, no. 1-2, pp. 126–140, 2008.

[17] C. H. Chien, T. Y. Tu, A. S. Shiao et al., "Prediction of the pure-tone average from the speech reception and auditory brainstem response thresholds in a geriatric population," *ORL*, vol. 70, no. 6, pp. 366–372, 2008.

[18] K. C. Andrade, P. L. Menezes, A. T. Carnauba, R. G. Rodrigues, M. C. Leal, and L. D. Pereira, "Non-flat audiograms in sensorineural hearing loss and speech perception," *Clinics*, vol. 68, no. 6, pp. 815–819, 2013.

[19] R. A. Dobie, "The AMA method of estimation of hearing disability: a validation study," *Ear and Hearing*, vol. 32, no. 6, pp. 732–740, 2011.

[20] S. Coren and A. R. Hakstian, "The development and cross-validation of a self-report inventory to assess pure-tone threshold hearing sensitivity," *Journal of Speech and Hearing Research*, vol. 35, no. 4, pp. 921–928, 1992.

[21] L. L. Wong, S. D. Soli, S. Liu, N. Han, and M. W. Huang, "Development of the Mandarin hearing in noise test (MHINT)," *Ear and Hearing*, vol. 28, 2 Supplement, pp. 70S–74S, 2007.

[22] P. Boersma and D. Weenink, "Praat: Doing phoenetics by computer [computer program]," in *Version 4.3.14 Amsterdam*, Institute of Phonetic Sciences, University of Amsterdam; 2005, Netherlands, 2008.

[23] B. C. Moore, "Perceptual consequences of cochlear hearing loss and their implications for the design of hearing aids," *Ear and Hearing*, vol. 17, no. 2, pp. 133–161, 1996.

[24] C. Nimitbunnasarn, P. Amatyakul, J. Gandour, A. Carney, C. Nimitbunnasarn, and P. Amatyakul, "Tonal confusions in Thai patients with sensorineural hearing loss," *Journal of Speech and Hearing Research*, vol. 27, no. 1, pp. 89–97, 1984.

[25] J. Jerger, S. Jerger, and F. Pirozzolo, "Correlational analysis of speech audiometric scores, hearing loss, age, and cognitive abilities in the elderly," *Ear and Hearing*, vol. 12, no. 2, pp. 103–109, 1991.

[26] R. Drullman, J. M. Festen, and R. Plomp, "Effect of temporal envelope smearing on speech reception," *The Journal of the Acoustical Society of America*, vol. 95, no. 2, pp. 1053–1064, 1994.

[27] K. W. Grant and T. C. Walden, "Understanding excessive SNR loss in hearing-impaired listeners," *Journal of the American Academy of Audiology*, vol. 24, no. 4, pp. 258–273, 2013.

[28] B. R. Glasberg, B. C. Moore, and S. P. Bacon, "Gap detection and masking in hearing-impaired and normal-hearing subjects," *The Journal of the Acoustical Society of America*, vol. 81, no. 5, pp. 1546–1556, 1987.

[29] R. S. Tyler, Q. Summerfield, E. J. Wood, and M. A. Fernandes, "Psychoacoustic and phonetic temporal processing in normal and hearing-impaired listeners," *The Journal of the Acoustical Society of America*, vol. 72, no. 3, pp. 740–752, 1982.